ISTANBUL TECHNICAL UNIVERSITY ★ GRADUATE SCHOOL OF SCIENCE ENGINEERING AND TECHNOLOGY

IMPROVEMENT OF THE CYCLIC FLEXURAL CAPACITY OF RC COLUMNS WITH FRP REINFORCEMENT

Ph.D. THESIS

Engin Cüneyt SEYHAN

Civil Engineering Department

Structural Engineering Program

SEPTEMBER 2016

ISTANBUL TECHNICAL UNIVERSITY ★ GRADUATE SCHOOL OF SCIENCE ENGINEERING AND TECHNOLOGY

IMPROVEMENT OF THE CYCLIC FLEXURAL CAPACITY OF RC COLUMNS WITH FRP REINFORCEMENT

Ph.D. THESIS

Engin Cüneyt SEYHAN
(501062005)

Civil Engineering Department

Structural Engineering Program

Thesis Advisor: Prof. Dr. Alper İLKİ

SEPTEMBER 2016

İSTANBUL TEKNİK ÜNİVERSİTESİ ★ FEN BİLİMLERİ ENSTİTÜSÜ

LİFLİ POLİMER DONATILAR KULLANILARAK BETONARME KOLONLARIN ÇEVRİMSEL YÜKLER ALTINDA EĞİLME KAPASİTELERİNİN ARTIRILMASI

DOKTORA TEZİ

Engin Cüneyt SEYHAN
(501062005)

İnşaat Mühendisliği Anabilim Dalı

Yapı Mühendisliği Programı

Tez Danışmanı: Prof. Dr. Alper İLKİ

EYLÜL 2016

Engin Cüneyt SEYHAN, a Ph.D. student of ITU Graduate School of Science Engineering and Technology 501062005, successfully defended the thesis/dissertation entitled "IMPROVEMENT OF THE CYCLIC FLEXURAL CAPACITY OF RC COLUMNS WITH FRP REINFORCEMENT", which he prepared after fulfilling the requirements specified in the associated legislations, before the jury whose signatures are below.

Thesis Advisor :	**Prof. Dr. Alper İLKİ** İstanbul Technical University	.....
Jury Members :	**Prof. Dr. Zekai CELEP** Fatih Sultan Mehmet University	.....
	Prof. Dr. Metin AYDOĞAN İstanbul Technical University	.....
	Prof. Dr. Mustafa ZORBOZAN Yıldız Technical University	.....
	Prof. Dr. Şevket ÖZDEN Okan University	.....

Date of Submission : 29 April 2016
Date of Defense : 30 September 2016

To my spouse and child,

FOREWORD

I would like to thank Prof. Dr. Alper İLKİ for his guidence and endless support during my academic life since I was an undergraduate. His knowledge, experience, willingness and enthusiasm encouraged me to overcome every challenge I have faced as a student.

I would like to thank to Prof. Dr. Zekai CELEP and Prof.Dr. Şevket ÖZDEN for their valuable contributions during the thesis.

I am grateful to Res.Assist. Çağlar GÖKSU for her valuable support and contributions in all steps of this thesis. This thesis would not be completed without her great efforts during the experimental phase.

I would like to thank to Ergün BİNBİR (M.Sc.), Res.Assist. İlyas SARIBAŞ and Ahmet UZUNHASANOĞLU (M.Sc.) for their significant contribution during the experimental phase of this thesis.

I would like to thank to the staff of Structural and Earthquake Engineering Laboratory, Ahmet ŞAHİN, Mahmut ŞANLI and Hakan SARUHAN (M.Sc.) for their hard work and technical assistances.

I am grateful to my company BASF Construction Chemicals Turkey for financial support and my dear collegues Talat SİVRİOĞLU (M.Sc.) and Ahmet TOPALBEBEK for their valuable supports during the experimental phase of this thesis.

I would like to thank to OTS Construction&Engineering, Art-Yol Engineering, Teknomak Machinery and Akgün Engineering Companies for their contributions during the experimental phase of this thesis.

Special thanks to my dear parents (Coşkun SEYHAN and Şule SEYHAN) for their warm support throughout my whole life.

Special thanks to my dear wife (Elif YAZICI SEYHAN) for her supports and patience since I left her helpless with our newborn baby (Mete SEYHAN) to complete this study.

April 2016 Engin Cüneyt SEYHAN

TABLE OF CONTENTS

Page

ABBREVIATIONS

ACI	**:** American Concrete Institute
AFRP	**:** Aramid Fiber Reinforced Polymer
ASTM	**:** American Society of Testing Materials
CFRP	**:** Carbon Fiber Reinforced Polymer
DSE	**:** Deep Surface Embedded
EBR	**:** Externally Bonded Reinforcement
FRP	**:** Carbon Fiber Reinforced Polymer
GC	**:** Collapsing Limit
GFRP	**:** Glass Fiber Reinforced Polymer
GPa	**:** Kilonewton per square milimeter
GV	**:** Safety Limit
MN	**:** Minimum Damage Limit
MPa	**:** Newton per square milimeter
NSM	**:** Near Surface Mounted
RC	**:** Reinforced Concrete
SRM	**:** Structural Repair Mortar
TML	**:** Tokyo Measuring Instruments Laboratory Co., Ltd
TRM	**:** Textile Reinforced Mortar

SYMBOLS

$a_1^{(i)}$	: Modal acceleration at (i)th step at the first mode
A_{frp}	: Cross-section area of the FRP anchor reinforcement
A_{fv}	: Area of FRP shear reinforcement
A_g	: Gross area of the column section
A_u	: Cross-sectional area of the transverse reinforcing bar
A_v	: Area of shear reinforcement spacing s
A_0	: Effective ground acceleration coefficient
A(T)	: Spectral acceleration coefficient
b	: Width of compression face of member, short side dimension of compression member of prismatic cross section
b_w	: Web width of the column
C_E	: Environmental reduction factor according to ACI 440-2R-08 2008
C_{R1}	: Spectral displacement amplification factor for the first mode of the building for an earthquake in "x" directio
d	: Distance from extreme compression fiber through centroid of tension steel reinforcement
$d_1^{(i)}$	: Modal displacement
d_{fv}	: Effective depth of FRP shear reinforcement
e	: Eccentricity due to horizontal displacement of the column
E_f	: Tensile modulus of elasticity of FRP reinforcement
E_s	: Modulus of elasticity of steel reinforcement
f'_c	: Design compressive strength of concrete
f_{ck}	: Characteristic compressive strength of concrete
f_{cc}	: Compressive strength of the confined concrete
f_{cm}	: Compressive strength of the unconfined concrete
f_l	: Confinement pressure created by FRP wrap around the column
f_{max}	: Tensile strength of longitudinal and transverse reinforcing bar
f_y	: Specified yield strength of longitudinal steel reinforcing bar
f_{yt}	: Design yield strength of transverse reinforcement
F_{bond}	: Bond capacity of epoxy grout on AFRP reinforcement
F_{frp}	: Tensile strength of FRP
H	: Height of the column
h	: Effective length of cross-section of column in bending
h_i	: Distance between the center of the respective part and the tip of the column
I	: Building importance factor
κ_a	: Efficiency factor for FRP reinforcement in determination of confined concrete compressive strength (based on geometry of cross section)
l_{db}	: Embedment length
l_i	: Length of the respective part of the column
L_p	: Plastic hinge length
m_n	: Lumped story mass

M : Experimental moment capacity
M_o : Theoretical moment capacity calculated by fiber analysis approach
$M_{x1}^{(i)}$: Effective modal mass for the first mode for an earthquake in "x" direction
M_1 : Effective modal mass for the first mode for an earthquake in "x" direction
n : Number of plies of FRP sheet
N : Axial load applied the column
N_u : Factored axial load normal to cross-section (to be taken as positive for compression)
P : Applied lateral load
P_0 : Nominal axial strength at zero eccentricity
r_c : Radius of edges of a prismatic cross section confined with FRP
R_{y1} : Load reduction factor for the first mode for an earthquake in "x" direction
s : Spacing of shear reinforcement measured in a direction parallel to the longitudinal reinforcement
s_f : Spacing of FRP reinforcement plies
$S(T)$: Spectrum coefficient
S_{ae1} : Elastic spectral acceleration for the first mode for an earthquake in "x" direction
S_{de1} : Linear elastic spectral displacement for the first mode for an earthquake in "x" direction
S_{di1} : Nonlinear spectral displacement for the first mode for an earthquake in "x" direction
T : Period of the building
T_A, T_B : Soil characteristic spectral periods
$T_1^{(1)}$: Period of the building at the first mode or an earthquake in "x" direction
t_f : Nominal thickness of one ply of FRP reinforcement
u : Perimeter of the FRP anchor
$U_{xN1}^{(i)}$: Top displacement in x direction
V_c : Nominal shear strength provided by concrete
V_s : Nominal shear strength provided by shear reinforcement
V_n : Nominal shear strength
$V_{r\text{-}frp}$: Nominal shear strength (with the contribution of FRP)
V_f : FRP contribution to shear strength
$V_{x1}^{(i)}$: Base shear force at $(i)^{th}$ step for the first mode
w_f : Width of FRP reinforcement plies
δ_t : Top displacement of the column
δ_{res} : Residual displacement of the column
δ_{un} : Target displacement of the column
θ_p : Plastic rotation
$\phi_{N1}^{(i)}$: N^{th} component of the mode shape vector for the first mode
Φ_{xN1} : Mode shape vector for the first mode at N^{th} story at the $(i)^{th}$ step in the x direction
ε_{co} : Axial strain corresponding to unconfined concrete strength
ε_{cc} : Axial strain corresponding to confined concrete strength
ε_f : Strain level in the FRP reinforcement
ε_{fe} : Effective strain of FRP sheet attained at failure

ε_{fu} : Design rupture strain of FRP reinforcement

ε_{fu}^* : Ultimate rupture strain of FRP reinforcement declared by manufacturer

ε_s : Strain of longitudinal steel reinforcement

ρ_f : FRP reinforcement ratio (used for confinement)

ρ_s : Existing volumetric ratio of transverse reinforcement of columns

ρ_{sm} : Required volumetric ratio of transverse reinforcement of columns

τ_b : Uniform bond strength along the anchorage length

χ_i : Curvature of the respective part of the column

χ_p : Curvature of the plastic part of the column

χ_T : Total curvature demand of the column

Ψ_f : FRP strength reduction factor

Γ_{x1} : Participation factor for the first mode

ω_1 : Circular frequency for the first mode

LIST OF TABLES

Page

LIST OF FIGURES

Page

IMPROVEMENT OF THE CYCLIC FLEXURAL CAPACITY OF RC COLUMNS WITH FRP REINFORCEMENT

SUMMARY

A significant part of the existing building stock of the world was constructed right after the Second World War with restricted budgets. Many of these reinforced concrete structures were constructed with substandard characteristics. Poor quality concrete, wrong transverse reinforcement details and insufficient flexural strength are among the most common deficiencies. While consistent structures are in need of retrofitting, particularly in seismic areas, problems such as high costs and disturbance to occupants are major obstacles for retrofit interventions. Fiber reinforced polymers can provide feasible retrofit solutions with minimum disturbance to occupants. In this study, the basic aim is to investigate the flexural seismic performance of substandard reinforced concrete columns retrofitted with embedded longitudinal fiber reinforced polymer reinforcement without increasing the original dimensions of the columns.

Fiber reinforced polymers (FRP) have been utilized to improve the load bearing capacities of the structures more than two decades, while the technical and academic researches started a decade earlier than practical applications. Although, FRPs are widely used in several industry sectors today, there are still missing application areas, which is avoided by national and international reinforced concrete building design codes. The most relevant avoided application seems to be improving the flexural capacity of the columns subjected to seismic loading by utilizing additional longitudinal FRP reinforcement. Even though, FRP confinement improves the flexural capacity and the ductility of the reinforced concrete columns, the increase in the flexural load bearing capacity is not significant when compared to the demand under seismic loading. Moreover, large plastic deformations enabled by FRP confinement does not allow further usage of the building after severe earthquakes. This also means that FRP confinement could be utilized to save human lives up to a certain level while significant economic loss is inevitable. In this case, concrete and steel jacketing are described for improving the flexural capacity of the buildings but it should be noted that there are unavoidable obstacles for practical application of traditional jacketing. This is an important common problem confronted in developing countries located on seismically active areas. Most of the time relocating the occupants of the buildings during the long, heavy retrofitting period is practically impossible and FRPs stand as the only retrofitting solution without major disturbance to the occupants and eliminate the relocation needs. Due to these facts, there is a strong need for utilizing FRPs for remarkable improvement of the flexural capacity of the reinforced concrete columns and enhance them to overcome extensive seismic loading even in elastic limits. In other words, retrofitted buildings should be kept in immediate occupancy performance level defined by TSDC (2007) and ASCE/SEI 41/06 (2007) even after severe earthquakes. This behavior will not only save human lives but also will contribute to

economy remarkably. The very first starting point of this study was based on the described strong need for efficient flexural retrofitting with keeping the structures in their elastic deformation limits and lack of efficient methods for utilizing FRPs as additional longitudinal reinforcement for reinforced concrete columns. Externally bonded (EBR) FRPs and near surface mounted (NSM) FRPs are the two available methods to increase the flexural capacity, which are described in relevant design codes. Both application methods are bond crictical and require a sound concrete substrate with sufficient tensile strength, which is not the case for consistent structures with severe corrosion and low quality concrete. Besides, there are very few studies available in the literature to improve the cyclic flexural capacity of the RC columns by utilizing FRPs through NSM method, while these studies considered medium or relatively high quality concrete, which do not bring any solution to the existing problem with the consistent buildings with low strength concrete. In the light of these facts, a new method tried to be developed in this study.

Carbonation of low quality concrete over the years induces a uniform corrosion of the steel reinforcement, which results with full debonding of the carbonated cover concrete and loss of structural integrity of the reinforcement. The proposed technique in this study requires full replacement of the carbonated, deteriorated cover concrete with high strength structural repair mortar and embedment of the longitudinal FRP reinforcement (pultruded bars and strips) with high strength polymeric adhesives. Eventually, final FRP confinement provides the sufficient shear strength, prevention of buckling of longitudinal FRP reinforcement and improved overall ductility. Additionally, structural repair mortar (SRM) guarantees a strong substrate with sufficient tensile strength for proper adhesion and a physical protective barrier around the FRP reinforcement. Furthermore, the high compressive strength of the SRM also contributes to improvement of flexural strength of the column. Similar to the corrosion damages some buildings also have structural problems due to the several reasons such as experienced earthquakes, wrong construction practices and wrong usage. These type of buildings are also require repair applications up to certain extend prior to the retrofitting applications. Therefore, a proper repair method is inevitable for efficient retrofitting technique needed for consistent buildings. The proposed application method for FRP reinforcement will be called by the author as deep surface embedded (DSE).

In this thesis, an experimental and analytical study is carried out for investigating the seismic performance of the consistent RC columns after retrofitting with structural repair mortar and fibre reinforced polymer reinforcement. Eleven consistent RC column were constructed with low quality concrete and plain rebars. These specimens were splitted into three different groups for investigating the impact of the different parameters on the efficiency of the proposed retrofitting technique. Investigating efficiency of the different anchorage methods for the longitudinal FRP reinforcement was the main aim with the first group specimens. Investigating the effect of the hybrid usage of the different type of longitudinal FRP reinforcing bars on the flexural behavior of the columns when loaded in their strong direction was aimed with second group specimens. The impact of the pre-damage conditions of the columns were investigated with third group specimens.

First specimen was tested in its strong direction and under constant 120 kN axial load (20 % - 13 % of the axial load capacity of the columns) without any replacement of the cover concrete and retrofitting application to reveal the actual condition of the specimens as a reference specimen. Afterwards, the cover concrete of the 3 specimens

were replaced with cement based SRM to represent the common corrosion repairs, which is often needed in case of low quality concrete and poor cover concrete. Following the representative repair application, these specimens were retrofitted in their strong direction by using surface mounted aramid fiber reinforced polymer strips with three different connection methods to the footing and investigated experimentally to determine the most efficient anchorage technique. After determining the most efficient anchorage technique, second group of specimens were repaired with same technique used in first group of specimens and afterwards retrofitted in their strong direction by using different combinations of deep surface embedded aramid, carbon and glass fiber reinforced polymer bars with the selected connecting method to the footing. Two columns in the third group of specimens were tested first in their weak direction without replacement of the cover concrete and retroftting untill reaching to pre-defined damage states under 20 % axial load. These pre-damaged samples were repaired by utilizing SRM and retrofitted in their weak direction by using deep surface embedded aramid fiber reinforced polymer bars and tested under the same parameters with pre-damage tests. The remaining two columns of the third group of specimens were repaired and retrofitted in their weak direction by using different combinations of surface mounted aramid and glass fiber reinforced polymer bars and tested under same level of axial load with previous specimens.

A significant enhancement was obtained in lateral flexural strength through the proposed retrofitting method (38 % - 207 %). Furthermore, it was observed that the cyclic lateral drift capacities of the retrofitted columns were minimum 3 % in case of AFRP strips and bars while it reached up to 8 % in the specimens, in which GFRP bars utilized. Nevertheless, achieved drift ratios could be deemed as quite satisfactory against seismic actions. The comparison of the experimental data including strain profiles with analytical calculations revealed that a conventional design approach assuming composite action between concrete and fiber reinforced polymer reinforcement could be used for flexural retrofit design. Experimental results also demonstrated that strain limit for longitudinal FRP reinforcement should be remarkably lower in case of reversed cyclic loading conditions when compared to the strain limits stated by design codes for the similar applications.

LİFLİ POLİMER DONATILAR KULLANILARAK BETONARME KOLONLARIN ÇEVRİMSEL YÜKLER ALTINDA EĞİLME KAPASİTELERİNİN ARTIRILMASI

ÖZET

Dünya üzerindeki yapı stoğunun önemli bir bölümü ikinci dünya savaşının büyük yıkımı sonrasında, acil ihtiyaçlar göz önünde bulundurularak hızlı bir şekilde ve son derece kısıtlı maddi imkanlar ile inşaa edilmiştir. Bu yapıların bir çoğunun inşaası sırasında kendi dönemlerine ait inşaat yönetmelikleri gözetilmemiş, eksik ve/veya yanlış detaylarla yapım gerçekleştirilmiştir. Gelişmiş ülkelerde savaş sonrasında inşaat sektöründe bu olumsuzluklar yaşanırken gelişmemiş ülkelerde ise savaşın getirdiği ekonomik yıkım büyük iç ve dış göçleri tetiklemiş ve bu da şehirlerde çarpık yapılaşmayı kontrol edilemez boyutlara taşımıştır. Çarpık yapılaşma doğal olarak beraberinde yapı yönetmeliklerine uymayan, son derece düşük malzeme ve işçilik kalitesine sahip devasa bir yapı stoğunu oluşturmuştur. Sismik olarak aktif olmayan bölgelerde bu tip zayıf yapılar kısa ve orta vadede ileri boyutta bir soruna neden olmazken aktif deprem kuşağında yer alan bölgelerde ciddi riskler doğurmaktadır. Bu yapıların tamamen yıkılarak güncel yönetmeliklere uygun, belirli bir şehir planının parçası olarak kaliteli malzeme ve işçilik ile yeniden inşaa edilecek yapılar ilk etapta kalıcı ve etkin bir çözüm olarak düşünülebilir. Ancak yüksek risk taşıyan yapı stoğunun ulaştığı devasa boyutlar düşünüldüğünde yeniden yapımın gerektirdiği maddi ve fiziki koşulları karşılamak için sahip olunan imkanların son derece yetersiz olduğu gerçeği ile karşılaşılmaktadır. Tüm yapı stoğunu yenilenmesi için gereken zaman, para, malzeme ve iş gücü gibi kaynaklar özellikle de gelişmemiş ülkeler için astronomik boyutlara ulaşmakta, maddi kaynak yaratılsa bile fiziksel olarak yeterli iş gücünün sağlanması imkansıza yakın olarak durmaktadır.

Yapısal olarak yetersiz olan bu binaların farklı yöntemler kullanılarak onarılması ve güçlendirilmesi ile sahip oldukları güvenlik seviyeleri yükseltilebilir ve olası deprem senaryolarında can kaybı tahminleri dramatik şekilde azaltılabilir. Bu gerçekten yola çıkılarak geride bıraktığımız yüzyılda betonarme yapıların ana bileşenleri olan beton ve çelik kullanılarak betonarme mantolama tekniği geliştirilmiş ve yaygın olarak kullanılmıştır. Betonarme mantolomaya paralel olarak taşıyıcı elemanlara dışarıdan yapıştırılarak veya kaynaklayarak eklenen çelik levhalar ile yine zayıf yapıların güçlendirilmesi amaçlanmış ve yaygın olarak bu metodlar dünya genelinde kullanılmıştır. Malzeme teknolojilerinde kaydedilen gelişmeler ve üretim tekniklerinin ilerlemesi kompozit malzemelerin geliştirilmesini tetiklemiş, savunma, uzay ve havacılık gibi yüksek teknolojli sektörlerde kompozit malzemelerin kullanımı yaygınlaşmıştır. Zaman içerisinde üretim maliyetlerinin azalması kompozit malzemelerin farklı sektörlerde de kullanım alanları bulmasına neden olmuş, bu gelişmenin bir parçası olarak inşaat sektörü de kompozit malzemeler için bir kullanım alanı açmıştır. Literatürde lifli polimer olarak adlandırılan, tamamen sentetik olarak elde edilen, çok hafif ve çok yüksek dayanımlı, dayanıklılığı yüksek, karbon, aramid, cam gibi farklı kimyasal öze sahip malzemeler yine polimer esaslı yüksek performanslı reçineler ile birlikte kullanılarak çok yüksek dayanımlı kompozit malzemeler elde

edilmiştir. Bu malzemelerin çelik gibi geleneksel güçlendirme malzemelerine oranla çok hafif olmaları, kesitlerinin ince olması sayesinde yapının mevcut mimari özelliklerini fazla bozmamaları ve çok hızlı, kolay uygulanabilmeleri ile yapıların işlevlerini bozmadan güçlendirme imkanı tanımaları neticesinde bir anda çok güçlü bir alternatif güçlendirme sistemi olarak pazarda yer almaya başlamıştır. Lifli polimer malzemeler kumaş, şetir, çubuk ve profil gibi farklı biçimlerde üretilmekte ve bu sayede farklı tip güçlendirme uygulamalarına imkan tanımaktadırlar. Sismik güçlendirme uygulamalarında genellikle lifli polimer kumaşlar kullanılarak betonarme kolonlar sargılanmakta, bu şekilde kısıtlı da olsa bir miktar eğilme dayanımı artırılmakta ve esas olarak ileri düzeyde süneklik artırılarak yapıların enerji yutma kapasiteleri geliştirilmektedir. Aynı zamanda kolonların zayıf enine donatı detaylarından kaynaklanan düşük kayma dayanımları da ileri düzeyde artırılmakta ve kayma hasarları engellenmektedir. Bu şekilde yapıların sismik hareketlerden daha az etkilenmesi amaçlanmaktadır. Kolonlara benzer şekilde kirişler de sargılanarak kayma kapasiteleri artırılmakta, hasarların elemanlar üzerine yayılarak kolon-kiriş düğüm noktalarında yoğunlaşması engellenmek istenmektedir. Aynı lifli polimer kumaşlar ve şeritler taşıyıcı olmayan bölme duvarların yüzeylerine çapraz olarak yapıştırılmak suretiyle binaların rijitliği ve yatay yük kapasiteleri arttırılarak toptan göçmenin engellenmesi böylece olası can kayıplarının en aza indirilmesi amaçlanmaktadır. Döşemelerde ve kirişlerde ise çekme bölgelerine lifli polimer kumaşlar veya şeritler yapıştırılarak düşey yükler altında bu elemanların taşıma kapasiteleri arttırılmaktadır. Yaygın olarak kullanılan bu tekniklerin yanı sıra son dönemlerde literatürde NSM (near surface mounted) adı verilen teknik ile lifli polimer çubuklar betonarme elemanların yüzeyine sonradan açılan dar kanallar içerisinde epoksi esaslı yapıştırıcılar kullanılarak yerleştirilmekte ve bu şekilde betonarme elemanın düşey yükler altında eğilme kapasitesi artırılmaya çalışılmaktadır.

1980'li yıllardan başlayarak yapılan bilimsel araştırmalar ışığında lifli polimerlerin betonarme yapıların güçlendirilmesinde kullanımı üzerine ciddi bilgi birikimine ulaşılmış ve bir çok gelişmiş ülke bu konuda kendi yönetmeliklerini oluşturmuştur. Bu yönetmeliklerde lifli polimerler kullanılarak betonarme elemanların kayma dayanımlarının artırılması, sargılama tekniği ile sünekliklerinin artırılması, düşey yükler altında eğilme dayanımlarının artırılması gibi bazı ana konular detaylı olarak ele alınmış ve tasarım esasları belirtilmiştir. Ancak çok ama çok önemli bir konu, yani betonarme elemanların sismik yükler altında eğilme kapasitelerinin artırılması yönetmelikler tarafından kapsam dışı bırakılmıştır. Lifli polimer malzemelerin sadece çekme gerilmeleri altında yüksek performans gösterirken basınç gerilmeleri altında kolayca burkulmaları ve yük taşımamaları bu malzemelerin çevrimsel yükler altında kullanımlarının kısıtlanmasını getirmektedir. Böylece en kritik noktalardan birisi olan sismik etkiler altındaki elemanların boyuna doğrultuda lifli polimerlerle güçlendirilmesi, üzerinde birçok soru işareti barındıran bir konu olarak yeni bir araştırma alanı yaratmıştır.

Bu tez kapsamında, standartlara uymayan zayıf betonarme kolonların onarıldıktan sonra lifli polimerler kullanılarak güçlendirilerek sismik performanslarının incelendiği deneysel ve analitik çalışma yapılmıştır. Deneysel çalışma kapsamında standartlara uymayacak şekilde detaylandırılmış, düşük beton dayanımına sahip, nervürsüz boyuna donatıların kullanıldığı, dikdörtgen kesitli 11 adet betonarme kolon üretilmiştir. Bu numunelerden ilki herhangi bir onarım ve güçlendirme uygulamasına tabi tutulmadan, % 20 sabit eksenel yük seviyesinde, çevrimsel tekrarlı yatay yüklere maruz bırakılarak test edilmiştir. Bu deney ile numunelerin mevcut eğilme kapasiteleri tespit edilmeye

çalışılmıştır. Daha sonra 3 adet numune boyuna donatılar üzerindeki zayıf beton örtüsü uzaklaştırılıp, çimento esaslı, yüksek dayanımlı yapısal tamir harcı ile donatıları yüzeysel olarak kapatacak kalınlıkta onarım uygulaması yapılmıştır. Ardından aramid lifli polimer şeritler yüksek dayanımlı, macun kıvamında epoksi esaslı yapıştırıcı ile kolonun güçlü doğrultusundaki her iki yüzeye de yapıştırılmıştır. Boyuna doğrultuda ilave donatı olarak kullanılmak istenen bu aramid lifli polimer şeritlerin kolon üzerinde taşıyacakları yükleri temele aktarmaları için etkili olacak ankraj tekniğini bulmak için her üç numunede de farklı bir bir ankraj detayı kullanılmıştır. Bu numunelerden birinde lifli polimer şeritler temel üzerinde 30 cm derinliğinde konik kesitli olacak şekilde açılmış ankraj çukuruna doğrudan indirilmiş ve yine epoksi esaslı yüksek dayanımlı akışkan bir harç ile ankraj çukurları doldurulmuştur. İkinci numunede lifli polimer şeritler ilk numunedeki gibi ankraj çukurlarına doğrudan indirilirken bu bölgeyi güçlendirmek için ilave olarak aynı miktarda lifli polimer şerit 50 cm'si kolon yüzeyinde, 30 cm'si ankraj çukurunda kalacak şekilde ilave ankraj donatısı olarak yerleştirilmiştir. Üçüncü numunede ise lifli polimer şerit tıpkı ilk numunede olduğu gibi ilave bir ankraj donatısı olmaksızın ankraj çukuruna indirilmiştir. Ancak burada diğer numunelerden farklı olarak kolon – temel birleşim yüzeyinde yoğunlaşması beklenen şekil değiştirmeleri daha geniş bir aralığa dağıtmak ve deformasyonların yığılması nedeniyle meydana gelecek olası kopmayı engellemek için kolon – temel birleşim düzleminden başlayarak ankraj çukuruna doğru lifli polimer şeritler üzerindeki 10 cm'lik bir bölüm ayırıcı bantlar ile izole edilmiştir. Bu şekilde, ankraj için kullanılan epoksi harcın FRP şerit üzerinde yalıtılmış bölgede yapışmaması ve böylece şekilde değiştirmelerin noktasal olarak yığılmadan bu bölgede serbestçe dağılması amaçlanmıştır. Boyuna doğrultuda yapıştırılan lifli polimer donatıların ankraj uygulamaları bittikten sonra yine aynı yapısal tamir harcı kullanılarak bu donatıların yüzeyleri kapatılmış ve kolonlar orijinal kesit ölçülerine ulaşacak şekilde tamir harcı ile nihai beton örtüsü oluşturulmuştur. Güçlendirilmiş kolonların eğilme kapasitelerinde meydana gelecek artışa bağlı olarak maruz kalacakları büyük kayma kuvvetlerinin güvenle taşınabilmesi ve boyuna doğrultudaki lifli polimer donatıların burkulmalarının engellenmesi için her üç numune de karbon lifli polimer kumaşlarla iki kat olarak sarıgılanmıştır. Bu detaylarla güçlendirilen numuneler % 20 sabit eksenel yük altında, güçlü doğrultuda ve çevrimsel yatay yükler altında test edilmiştir. Test sonuçlarına bağlı olarak ilk numunede uygulanan, herhangi bir ilave ankraj olmaksızın boyuna doğrultudaki lifli polimer şeritlerin doğrudan ankraj çukuruna uzatıldığı ankraj teknik etkin ve pratik yöntem olarak tespit edilmiş ve kalan numunelerin tamamında temele ankraj için bu teknik kullanılmıştır. İkinci grup numune olarak seçilen 3 numune yine önceki numuneler gibi onarılmış, ardından güçlü doğrultuda ancak bu sefer aramid, karbon ve cam lifli polimer çubuklar farklı miktarlarda birlikte kullanılarak güçlendirilmiştir. Güçlendirilen bu numuneler ilk grup numuneler gibi % 20 sabit eksenel yük etkisi ve çevrimsel yatay yükler altında test edilmiştir. Üçüncü grup numunelere ait 2 kolon herhangi bir onarım ve güçlendirme uygulaması olmaksızın zayıf doğrutuda, % 20 eksenel yük seviyesinde farklı hasar seviyelerine ulaşacak şekilde çevrimsel yatay yükler altında test edilmiştir. Ön hasar verilen bu numuneler, daha sonra önceki numunelerdekine benzer olarak yapısal tamir harçları ile onarılmış, zayıf doğrultuda aramid lifli polimer çubuklar kullanılarak güçlendirilmiş ve ardından aynı eksenel yükler altında, zayıf doğrultuda test edilmişlerdir. Aynı grup içerisinde yer alan diğer 2 numune ise birinci ve ikinci gruptaki güçlendirilmiş numunelerde olduğu gibi ilk olarak onarılmış ardından zayıf doğrultuda aramid ve cam lifli polimer çubuklar kullanılarak güçlendirilmiştir.

Güçlendirilen numuneler 120 kN sabit eksenel yük altında (kolon kapasitesinin yaklaşık olarak %20 - % 13'ü) ve çevrimsel yatay yükler altında test edilmiştir.

Deneylerin tamamında göçme, eğilme kapasitesine ulaşılması şekilde gerçekleşmiş, hedeflendiği gibi herhangi bir kayma problemine rastlanmamıştır. Güçlendirilen numunelerin tamamında yatay yük taşıma kapasitesinde ciddi artışlar elde edilmiştir (% 38 - % 207). Bu numunelerde ayrıca enerji yutma kapasiteleri ciddi oranlarda artmış, yatay ötelemeler % 3'ün altına düşmemek kaydıyla bazı numunelerde % 6'yı geçmiş hatta % 8'e ulaşmıştır. Deprem etkileri düşünüldüğünde bu öteleme oranları ciddi bir iyileştirmenin de göstergesi olmaktadır. Deneysel olarak elde edilen sonuçlar teorik hesaplarla karşılaştırıldığında beton ve çelik arasındaki kusursuz aderans kabülü üzerine kurulu geleneksel taşıma gücü metodunun bu numunelerde kullanılan güçlendirme tekniğinin tasarımında da geçerli olduğu sonucuna varılmaktadır. Bu noktada dikkat edilmesi gereken en önemli nokta boyuna doğrultuda kullanılan lifli polimer donatıların şekil değiştirme kapasitelerinin çevrimsel yükler ve eksenel yük etkisi altında ciddi olarak azaldığıdır. Ayrıca numune davranışları incelendiğinde lifli polimer donatıların kimyasal yapısının çevrimsel yükler altındaki davranışını etkilediği açık bir şekilde tespit edilmiştir. Şekilde değiştirme ölçerlerde tespit edilen değerler incelendiğinde en yüksek şekil değiştirme değerlerine cam lifli polimer donatıların ulaştığı ve bu donatıların hibrid olarak kullanıldığı numunelerde enerji yutma kapasitelerinin iler boyutlara ulaştığı görülmüştür.

Bu çalışmanın ana amacı deney sonuçlarının değerlendirilmesi ile önemli miktarda veri elde etmek ve standartlara uymayan zayıf taşıyıcı elemanların lifli polimer kompozit malzemeler ile güçlendirilerek deprem performanslarının artırılmasını sağlayacak, gerektiğinde yapıyı TSDC (2007) tarafından ortaya konulan hemen kullanım performans seviyesine taşıyarak deprem sonrasında da binaların güvenle kullanılmasına imkan verecek yöntemler geliştirmektir.

1. INTRODUCTION

Many of existing reinforced concrete structures were constructed with substandard characteristics. Low quality concrete, poor transverse reinforcement details and insufficient flexural strength are among the most common deficiencies. High costs and disturbance to occupants are major obstacles for retrofit interventions for these substandard structures when traditional strengthening methods are considered. Fiber reinforced polymers (FRPs) can provide feasible retrofit solutions with minimum disturbance to occupants and comparable costs.

There are several techniques, which have been developed to overcome the deficiencies as low quality concrete, insufficient shear and flexural strength and insufficient ductility are already defined by several national codes on use of FRPs in retrofitting applications. On the other hand, enhancing the flexural strength of the columns under seismic loading is achievable only with traditional retrofitting techniques as concrete or steel jacketing. The most relevant design codes and guidelines e.g. ACI 440.2R-08 (2008), Eurocode 8-3 (2005), CEB-FIB (2001), TSDC (2007), CNR-DT 200/2004 (2004) do not allow utilization of the fiber reinforced polymers to increase the flexural capacity of the vertical structural members under seismic loading.

Seven chapters, a list of references, and 3 appendices are included in the thesis.

In chapter one, the scope of the thesis is described with a general introduction, previous analytical and experimental studies on retrofitting reinforced concrete (RC) members by using fiber reinforced polymers in the literature are introduced. In chapter two, the characteristics of specimens, and the test setup with its instrumentation are introduced. In chapter three, the manufacturing of specimens is introduced. Construction of the columns, replacing the cover concrete with high strength structural repair mortars, embedding the relevant FRP reinforcement into the column cross section and anchorage to the footing and eventually the FRP confinement of the columns are described in this chapter with details.

In chapter four, test results of material and column specimens with the evaluation of lateral load-displacement relationships, moment-curvature relationships and strain distributions are reported. In chapter five, the comparison of all specimens with each other are reported. In chapter six, an analytical study is done on the utilization of the proposed method in real scale building. In chapter seven, overall assessment of the test results and analytical study are summarized with conclusions.

1.1 Purpose of Thesis

In this study, the basic aim is to investigate the flexural seismic performance of substandard reinforced concrete columns retrofitted with embedded longitudinal FRP reinforcement without increasing the original dimensions of the columns. In addition to basic aim of increasing the flexural strength, it is also targeted to bring the buildings into elastic deformation region for achieving immediate occupancy structural safety level defined by ASCE/SEI 41-06 (2006) and TSDC (2007).

1.2 Literature Review

Many substandard reinforced concrete structures are required to be seismically retrofitted to reduce their vulnerabilities against seismic actions. Financial constraints, disturbance to the occupants and disruption of functions of the structures are the main obstacles for proper seismic retrofitting of these substandard existing structures. Traditional retrofitting techniques as concrete jacketing and steel jacketing are not feasible in many cases due to high disturbance to occupants, long return to service time, which is very crictical for commercial and industrial buildings. In recent years, use of FRPs in construction industry has become quite common. They offer feasible and innovative solutions for seismic retrofitting due to their lightweight, high tensile strength and noncorrosive character (CEB-FIB, 2001; Pessiki et al. 2001; Bakis et al. 2002; Lam and Teng 2003; ACI440-2R-08, 2008; Bank 2013). While there are many studies on external confinement of columns or joints (Seible et al. 1997; Sheikh and Yau 2002; Antonopoulos and Triantafillou, 2003; Iacobucci et al 2003; Xiao, 2004; Prota et al. 2004; Bousias et al. 2004; Chang et al. 2004; Memon and Sheikh, 2005; Tsonos, 2007; Ilki et al. 2009; Garcia et al. 2010; Ilki et al. 2011; Wang et al. 2011; Jirawattanasomkul et al. 2013; Parvin and Brighton, 2014; Demir et al. 2015), and on flexural retrofit with near surface mounted (NSM) FRP bars or pultruded strips under

monotonic loading conditions (Nanni et al. 1999; De Lorenzis and Nanni, 2002; De Lorenzis et al. 2004; Hassan and Rizkalla, 2004; El-Hacha and Rizkalla, 2004; Barros et al. 2006; Nordin and Täljsten, 2006; Liu et al. 2006; Teng et al. 2006; De Lorenzis and Teng, 2006; Seracino et al. 2007; Castro et al. 2007; Chikh et al. 2008; El-Maaddawy and El-Dieb, 2011; Sharaky et al. 2013; Bilotta et al. 2015), only few studies are available on flexural retrofitting by using FRPs under repeated loading conditions (Sena Cruz et al. 2006; Badawi and Soudki, 2009; Ceroni, 2010). Reversed cyclic flexural behavior of RC members strengthened with longitudinal FRP reinforcement was studied for the first time by Ilki and Kumbasar (2002). More recently, Barros et al. (2006), Perrone et al. (2009), Bournas and Triantafillou (2009), Goksu et al. (2012), Fahmy and Wu (2012), Vrettos et al. (2013), Li et al. (2013), Faustino and Chastre (2015) and Kaya et al. (2016) also studied this type of behavior.

Barros et al. (2008) reported a retrofitting technique based on NSM CFRP strips installed into the grooves opened on the cover concrete to increase the flexural capacity of columns subjected to flexural and axial loading. Two series of reinforced concrete columns, subjected to axial compression and lateral cyclic loading, showed a significant increase in the load carrying capacity by using NSM technique. As expected, the columns with less steel reinforcement (4 ϕ10) reported with more load carrying capacity increase (92 %), where the columns with more steel reinforcement (4 ϕ12) had just an increase in load carrying capacity with 34 %. In the study, the amount of the NSM FRPs used for strengthening, was limited to avoid from de-bonding failures and provide to use full strength of the FRP's, which resulted with failure of some CFRP strips in the base of columns. Since the partial replacement of the cover concrete with epoxy mortar did not show a significant confinement effect, energy absorption capacity of the tested RC columns was not improved by NSM FRP technique. Barros et al. (2008) also implemented a fibrous model in a computational code based on finite element techniques to simulate the behaviour reinforced concrete columns strengthened with NSM FRP technique. It is reported by the authours that a fibrous model with cyclic constitutive laws for concrete and steel reinforcement was implemented in a computational code based on finite element techniques. This computational model can simulate the reversed cyclic behaviour in compression and in tension of unconfined and confined concrete.

Bournas and Triantafillou (2009) presented the results of a large-scale experimental program aiming to study the behavior of reinforced concrete columns under simulated seismic loading, strengthened in flexure with different types and configurations of near-surface-mounted (NSM) reinforcing materials including FRPs. Eleven large-scale RC column specimens with the same geometry were constructed by casting concrete with average ultimate compressive strength of 26 MPa. Test parameters were type of NSM reinforcement (CFRP strips, GFRP bars, and stainless steel reinforcing bars), configuration of NSM reinforcement, geometrical reinforcing ratio of NSM or internal reinforcement ratio, type of adhesive for bonding NSM reinforcement and NSM reinforcement with or without local jacketing at the member ends. Bournas and Triantafillou (2009) preformed the grooves, where NSM reinforcement would be embedded, by mounting plastic rods at proper positions on the molds to simplify the retrofitting process. Direct anchoring of the NSM reinforcement to the foundation was utilized to contionus transfer of the loads. Anchorage holes in 25 mm wide and 300 mm deep, were drilled on the footing anchorage of the NSM reinforcement. NSM reinforcement were embedded into the grooves and anchorage holes by using epoxy adhesive in all specimens except two specimens retrofitted with stainless steel, which were placed by using cementitious mortar. In 3 specimens, textile reinforced mortar (TRM) jacketing was utilized to prevent the buckling of the NSM reinforcement and enhance the ductility of the column specimens. For TRM application, a commercially available textile with bi-directional carbon rovings was applied 4 layers by using a smooth cementitious mortar.

The retrofitted columns were subjected to lateral cyclic loading under a constant axial load, corresponding to 20 % of the members' compressive strength. The performance and failure mode of all tested specimens were controlled by flexure, as expected due to their design characteristics. All retrofitted specimens performed considerably higher (from approximately 25 % up to approximately 90 %) flexural strength compared to the reference column in exception with one specimen. The stainless steel bars were more effective, resulting in a strength increase between 64 % to 90 %. The respective values for FRPs were lower (26 % for CFRP and 22 % for GFRP) due to failure of the FRP reinforcing elements at strains less than those corresponding to ultimate strains in monotonic loading as a result of cyclic loading. A clear negative impact of the cyclic loading on the strength enhancement of the retrofitted samples with FRP reinforcement

was revealed by the test results. All types of FRP NSM reinforcement, which were bonded with epoxy adhesive, reached large strains; however, due to the effect of cycling loading, those strains were well below (27 % - 67 %) the ultimate strains declared by manufacturers (Bournas and Triantafillou, 2009).

However, in all cases, except the studies of Perrone et al. (2009) and Goksu et al. (2012), it is difficult to perceive the performance of either NSM or DSE FRP system and anchoring of these reinforcement into the footing in case of low strength concrete.

In the study of Perrone et al. (2009) cyclic flexural behavior and the energy dissipation capacity of the substandard (starter steel rebars with insufficient lap splice; 260 mm and ϕ6 / 250 transverse reinfocement) RC columns with low strength concrete (except one column with moderate concrete quality) were investigated. A total of 8 specimens we constructured with the same geometry but with four different size of internal deformed steel reinforcing bars (4 ϕ10, 4 ϕ12 ve 4 ϕ16). Concrete strength was measured 8 MPa in 28 days for 7 specimens and 29 MPa for the last specimen. 3 of these columns were assigned as reference specimens and tested (up to 1.5 % drift ratio) without retrofitting. After testing, these control specimens were repaired, retrofitted and retested (up to 3 % drift ratio) to observe the effect of pre-damage. Remaining 5 specimens were retrofitted and tested afterwards. In the retrofitting procedure, longitudinal NSM CFRP strips were installed in to the pre-cut grooves on the column surfaces, which would be subjected to the tension/compression stresses by using an epoxy paste. To anchor the CFRP strips to the column's footing, holes were drilled with a depth that ranged between 120 mm and 150 mm. These anchorage holes were filled with the same epoxy adhesive, which was used to install the CFRP strips into the grooves on the columns surfaces. In order to increase the ductility and energy dissipation capacity specimens were wrapped with CFRP sheets after NSM FRP application. Starting from the footing 430 mm height of the columns were wrapped with two layers (except one specimen, which was wrapped with 3 layers) of CFRP sheets. The remaining part of the specimen (over the first 430 mm) was wrapped by using 150 mm wide CFRP fabrics with a spacing of 110 mm, which matches the area between the existing steel stirrups.

All columns were tested under constant 120 kN axial load (7 % - 24 % of the axial capacity) and reversed cyclic lateral loading. In the specimens, which had 8 MPa concrete compressive strength, the used technique provided an increase of about

67 % and 46 % in lateral load carrying capacity, when applied to undamaged and pre-damaged columns, respectively. In the specimen with moderate concrete compressive strength (29 MPa), the used technique was even more effective, since, when compared to the maximum lateral capacity of the corresponding strengthened column of 8 MPa of average compressive strength, an increase of 39 % was achieved. In terms of energy dissipation capacity, the increase ranged between 40 % – 96 % in the undamaged columns compared to reference specimens with low strength concrete. In specimen with moderate concrete strength 109 % increase in engery dissipation capacity was obtained comparing to corresponded pre-damaged retrofitted specimen with low strength concrete. On the other hand, due to the very low concrete strength, the increase in the energy dissipation capacities of the retrofitted pre-damaged columns compared to corresponding reference columns were marginal.

In the study of Goksu et al. (2012), which was the precursor of this experimental study, the possibility of using carbon FRP (CFRP) longitudinal (bar, strip, sheet) and transverse (sheet) reinforcement for the flexural seismic retrofit of low strength RC members under reversed cyclic loading conditions was investigated. Five symmetrically reinforced cantilever RC columns were designed to be flexural critical and identical. These specimens were constructed by using plain reinforcing bars and low strength concrete with an average compressive strength of 9.3 MPa at the time of testing (after 180 days of age) to represent the existing substandard structures. Two of the specimens were tested without retrofitting, as control specimens, while the remaining 3 specimens were retrofitted before testing. Since these columns are representing old structures with substandard elements, loose cover concrete was replaced by cement based structural repair mortar to simulate the typical corrosion repairs and afterwards they were retrofitted by utilizing longitudinal CFRP bars, and pultruded CFRP strips in different configurations. Replacing the poor cover concrete and reprofilling the column surfaces with high strength structural repair mortar (SRM) forms a sound substrate for strong adhesion of CFRP reinforcement and eliminates the risk of premature debonding failures of the longitudinal FRP reinforcement. After finishing the curing of the repair mortar, CFRP reinforcement bonded on the columns surfaces in the longitudinal direction by using a high strength epoxy paste and the entire columns surfaces reprofilled again with the same structural repair mortar to achieve the original dimensions of the specimens. After placement of longitudinal

CFRP reinforcement and reformation of concrete cover, CFRP sheets were wrapped around the members in transverse direction to enhance the ductility and to avoid potential shear failure caused by increased flexural strength.

Different anchorage types were applied during the retrofitting applications in the study of Goksu et al. (2012). In two specimens, longitudinal CFRP reinforcement were not embedded into the footing while additional anchorages were manufactured out of CFRP sheets and embedded 200mm deep holes dug in the footings. These anchorages made from CFRP sheets were also bonded on the longitudinal CFRP reinforcement with fluid epoxy adhesive. In the third specimen, the longitudinal CFRP reinforcement were directly embedded into the anchorage holes and additionally same amount of CFRP bars were installed into the holes as additional anchorages to avoid premature failures in the anchorage zone.

All specimens were tested under reversed cyclic lateral loading. The first two specimens, in which CFRP sheets were used as anchorage reinforcement sustained maximum lateral load up to 1.5 % and 2.0 % drift ratios until premature failure of the CFRP anchorage sheets occurred. Unlikely to these specimens, the third specimen, which was retrofitted by using CFRP bars as additional anchorages did not show any premature failure in anchoring region until 6 % drift ratio and then fractured together with the longitudinal CFRP reinforcement at the column – footing interface. The increase in the lateral load capacity was reported as approximately 100 % for the first two specimens comparing to control specimens, while they reached only 57 % of their theoretical capacity due to premature anchorage fail in relatively small drift ratios. The third specimen achieved an increase of 370 % in lateral load capacity when compared to control specimens and approximately 130 % of its theoretical capacity. By using the proposed retrofitting technique in the study of Goksu et al. (2012), buckling and debonding of CFRP reinforcement and shear damages could be avoided until large cyclic drifts are achieved. It was revealed that anchorage of longitudinal CFRP reinforcement to the footing appeared to be a significant obstacle for effective utilization of CFRP reinforcement in flexural retrofitting.

In the light of existing studies, it should be concluded that, despite the significant improvement in the flexural behaviour of the RC columns by utilizing NSM FRP retrofitting technique, while these studies (except Goksu et al., 2012 and Perrone et al., 2009) considered medium or relatively high quality concrete, which do not bring

any solution to the existing problem with the consistent buildings with low strength concrete. In the light of these facts, a new method tried to be developed in this study

1.3 Hypothesis

The aim of flexural retrofitting by using FRP reinforcement, mainly in the longitudinal direction, is to obtain flexural strength enhancement under reversed cyclic loading, since many existing structures, among other deficiencies, suffer from lack of sufficient flexural strength in case of seismic loading. Furthermore, it is very important not to sacrifice from drift capacity, since drift capacity is as important as strength in case of earthquake. Although, FRP confinement increases the ductility and contributes to flexural strength enhancement of the RC columns under seismic loading, due to the extensive plastic deformations, the structure could be no longer used in accordance with the strict deformation limits of design codes, e.g. ASCE/SEI 41-06 (2006) and TSDC (2007).

By using proper types and kinds of FRP reinforcement in longitudinal direction with proper anchorage details and additional transverse FRP reinforcement around the columns, after replacing poor cover concrete it would be possible to increase the flexural strength and ductility of the substandard columns significantly in case of seismic loading. Furthermore, it would be possible with keep the the structures in their elastic deformation limits in accordance with ASCE/SEI 41-06 (2006) and TSDC (2007) to achieve an immediate occupany performance level even after severe seismic loading. This performance level does not only guarantee saving human lives but also brings a significant positive impact on the deomestic economy, which is crucial for developing countries.

2. EXPERIMENTAL DESIGN

2.1 Description of Test Specimens

The specimens represent typical low strength RC columns with poor detailing, which is common for the majority of the old buildings in Turkey and many other undedevelop countries. These buildings are carrying a significant risk of collapse under seismic actions due to not only substandard detailing and low strength concrete, but also suffering from active corrosion, which compromises the structural integrity of the reinforcing bars in the concrete matrix and decreases the tensile strength of the rebars. Although the specimens designed with poor detailing, they are constructed with sufficient lap splice to avoid the potential problems related with insufficient lap splice and focus on enhancement of the flexural strength of the columns.

A total of 11 large-scale reinforced concrete columns were manufactured and retrofitted with variety combinations of different kind of longitudinal and transverse FRP reinforcement for investigating the utilization of FRPs to increase the flexural capacity under reversed cyclic loading and decrease the plastic deformations significantly that structure could conform the immediate occupancy performance level stated by ASCE/SEI 41/06 (2007) and TSDC (2007) even after severe earthquakes. All columns were identical (before retrofitting) and flexure-critical. The geometry of the columns are presented in Figure 2.1 and the details of reinforcing cage are presented in Appendix A.

The cross-section dimensions of columns were 200×300 mm, height was 1950 mm and a footing of size 720×720×550 mm supported the columns. The average compressive strengths of the concrete was 10.3 MPa at the time of testing (after 28 – 34 days) first group of specimens (4 columns) and 15.2 MPa at the time of testing (after 750 - 1260 days) second and third groups of specimens. Clear cover was 20 mm from the transverse bars. The geometric longitudinal steel reinforcement ratio was 1 % and the volumetric ratio of transverse bars in x and y directions were 0.55 % and 0.33 % respectively. Four steel reinforcing bars with 14 mm diameter, which are continuous through the height of the columns without any lap splice, used as

longitudinal reinforcement. They were selected as S220 plain steel bars with average yield strength of approximately 296 MPa. Transverse bars were also selected as S220 plain steel bars with a diameter of 10 mm, which had average yield strength of approximately 315 MPa. The spacing of transverse bars inside and outside the main testing region are 200 mm and 100 mm, respectively.

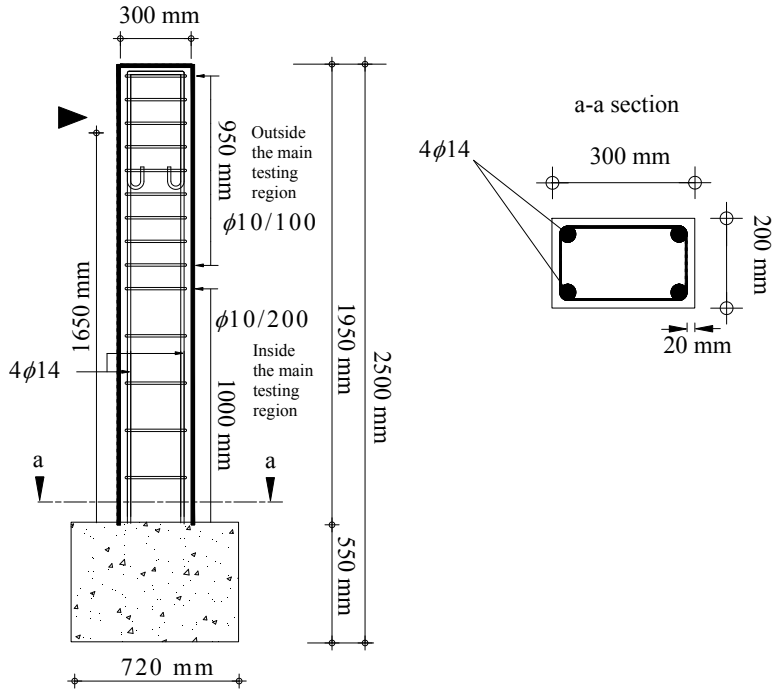

Figure 2.1 : The geometry of the columns.

The behavior of concrete members strengthened or retrofitted with FRP systems is highly dependent on a sound concrete substrate and proper preparation and profiling of the concrete surface. Applications can be categorized as bond-critical or contact-critical. Bond-critical applications, such as flexural or shear strengthening of beams, slabs, columns, or walls, require an adhesive bond between the FRP system and the concrete (ACI 440.2R-08, 2008). Deteriorated concrete and corrosion damages are the most common diagnosis made in the on site assessment of the substandard structures. Due to this fact, structural repair of concrete becomes an important part of the retrofitting procedure. Although the specimens were not damaged, poor concrete cover was removed from the entire column surfaces for all specimens and the steel reinforcement exposed, as they would be coated against corrosion in order to secure the structural integrity of both internally and externally applied FRP system. Afterwards, steel reinforcement was covered by using a thin layer of cementitious structural repair mortar and surfaces were levelled for proper application of

longitudinal FRP reinforcement. A high strength epoxy adhesive was used to bond the FRP reinforcement on to the column surfaces, which were selected depending on the lateral loading direction. A second layer of the structural repair mortar was applied onto the columns surfaces and levelled carefully to bring the specimens into to their original dimensions (300x200 mm). In order to increase ductility and eliminate the risk of shear failure due to the increased flexural strength, all retrofitted specimens were confined externally in transverse direction with two layers of CFRP sheets as the final step of the strengthening.

Specimens were named depending on the test parameters and their retrofitting characteristics. For the sake of simplicity, some secondary parameters were represented with the selected notations only for the relevant specimens and were not included in the names of other specimens. The meanings of the notations of the specimens are shown in Table 2.1.

Table 2.1 : Notations used for the specimens.

Notation	Notation	Represent	Graphic
Loading Direction	S	Strong	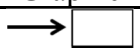
	W	Weak	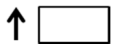
Axial Load	N1	120 kN	
FRP Reinforcement	AR	Aramid Bar	
	ARS	Aramid Strip	
	G	Glass Bar	
	C	Carbon Bar	
Damage History	P1	Pre-damage: Medium	-
	P2	Pre-damage: Heavy	-
Anchorage Type	PB	Partially Bonded	-
Specimen Type	REF	Reference	-

2.1.1 First group specimens

Anchorage of longitudinal CFRP reinforcement to the footing was appeared to be a significant obstacle for effective utilization of CFRP reinforcement in flexural retrofitting in the study of Goksu et al. (2012). Therefore, 3 specimens were retrofitted with additional longitudinal FRP reinforcement with different anchorage technique to find out the most effective anchoring method, which would be utilized in remaining specimens. Main features of the specimens are shown in the Table 2.2.

The specimen called SD-N1-REF was tested in the strong direction, without any repair or retrofitting application in order to evaluate the current condition of the columns. The remaining 3 specimens were retrofitted by embedding 2 AFRP strips on both surfaces in stong direction and afterwards, confined by 2 layers of transverse continuous CFRP sheet through the height of the columns.

Table 2.2 : Properties of the first group specimens.

Specimen	Concrete compressive strength of columns (MPa)	Longitudinal and transverse steel reinforcement	Type of FRP reinforcement	Quantity of FRP reinforcement
SD-N1-REF	10	S220	-	-
SD-N1-2ARS	10	S220	AFRP strips	2x2 (each 42mm x 1.4mm)
SD-N1-4ARS	10	S220	AFRP strips	4*x2 (each 42mm x 1.4mm)
SD-N1-2ARS-PB	10	S220	AFRP strips	2x2 (each 42mm x 1.4mm)

Retrofitting and anchorage details are shown in Figure 2.2.

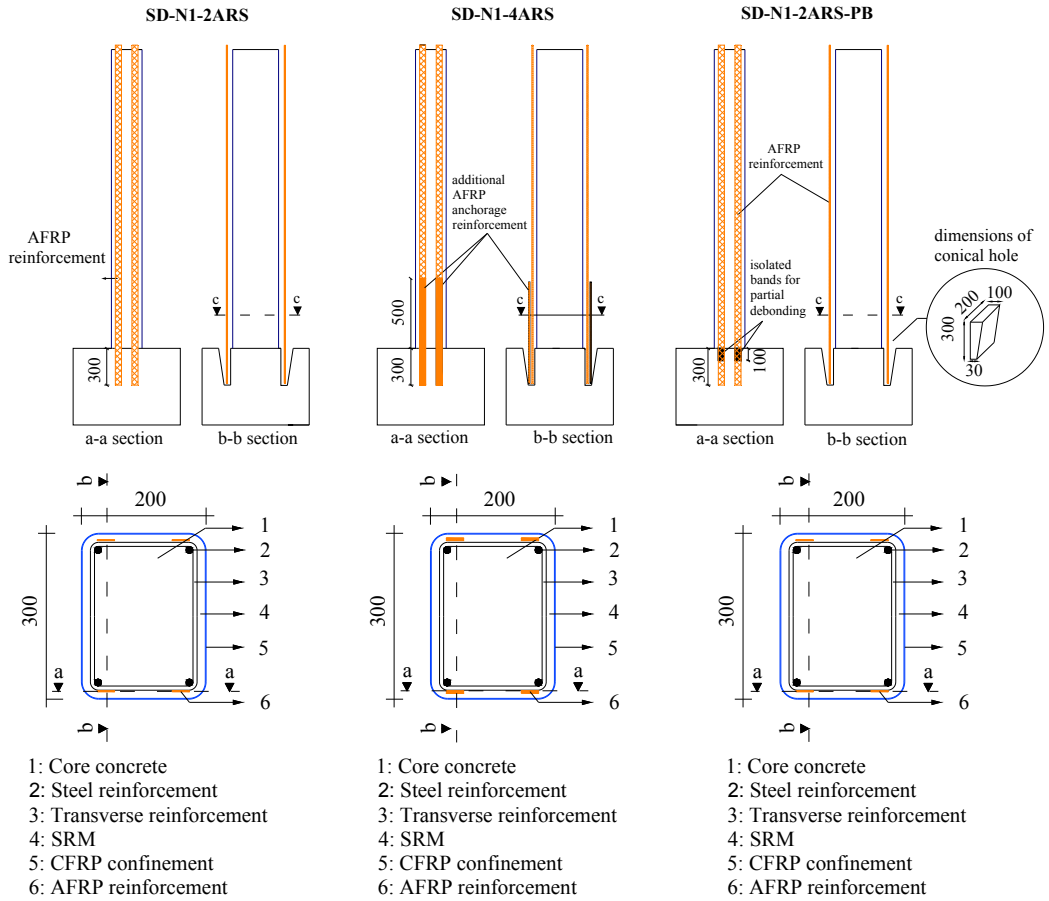

Figure 2.2 : Retrofitting and anchorage details of first group specimens.

An adhesive tape was used to create an isolated section on the AFRP strips, which would be stayed debonded in the anchorage hole for the specimen SD-N1-2ARS-PB.

The aim was to form an unbonded section just at the column – footing intersection, which could distribute the strains in a wide area on the AFRP strip and avoid the premature fracture due to concentrated deformations at the column-footing intersection. Conical holes were dug on the footings to anchor the longitudinal AFRP reinforcement.

In the specimens SD-N1-2ARS and SD-N1-4ARS, longitudinal AFRP reinforcement were directly embedded into the anchorage holes directly by using an epoxy grout without any debonded section. In order to enhance the anchorage performance, 2 additional AFRP strips in the same geometry with longitudinal AFRP reinforcement were embedded into the anchorage holes in the specimen SD-N1-4ARS differently than SD-N1-2ARS, Figure 2.2.

2.1.2 Second group specimens

Direct embedment of the longitudinal reinforcement, which was utilized in specimen SD-N1-2ARS, was determined as the most effective anchoring technique after analyzing the test results of the first group of specimens. Therefore, this anchoring method was used for the all remaining specimens. In order to investigate the effect of the different types of the FRP reinforcement, bars were used in this group of specimens and the remaining specimens tested as third group. Additionally, hybrid usage of the FRP reinforcement was also investigated in this group of specimens. Three specimens were retrofitted with different kinds of longitudinal FRP reinforcement in different configuration. Contrary to the first group specimens concrete strength was measured as 15 MPa around the day of testing (750 days). However, it was only 10 MPa at 28 days. This long term strength development was also considered in the theoretical assessment and the retrofit design of the specimens (second and third groups) tested after 750 – 1260 days. Main features of the specimens are shown in Table 2.3.

Table 2.3 : Properties of the second group specimens.

Specimen	Concrete compressive strength of columns (MPa)	Longitudinal and transverse steel reinforcement	Type of FRP reinforcement	Quantity of FRP reinforcement
SD-N1-3AR	15	S220	AFRP bars	3x2 (ϕ10)
SD-N1-1AR5G	15	S220	AFRP and GFRP bars	1x2 (ϕ10)AFRP 5x2 (ϕ8)GFRP
SD-N1-1AR1C1G	15	S220	AFRP, CFRP and GFRP bars	1x2 (ϕ10)AFRP 1x2 (ϕ8)CFRP 1x2 (ϕ8)GFRP

Three longitudinal AFRP reinforcing bars were installed on short sides of the specimen SD-N1-3AR to retrofit it in the strong direction. In the specimen SD-N1-1AR5G, 1 AFRP and 5 GFRP reinforcing bars were combined for retrofitting in the strong direction. Differently from the first two specimens, 1 additional CFRP bar was combined with 1 AFRP and 1 GFRP bars to retrofit the specimen SD-N1-1AR1C1G. It should be noted that, despite the significant increase in the concrete compressive strength at the day of testing, axial load was kept as 120 kN during the tests. Retrotiffing details of the second group specimens are shown in Figure 2.3

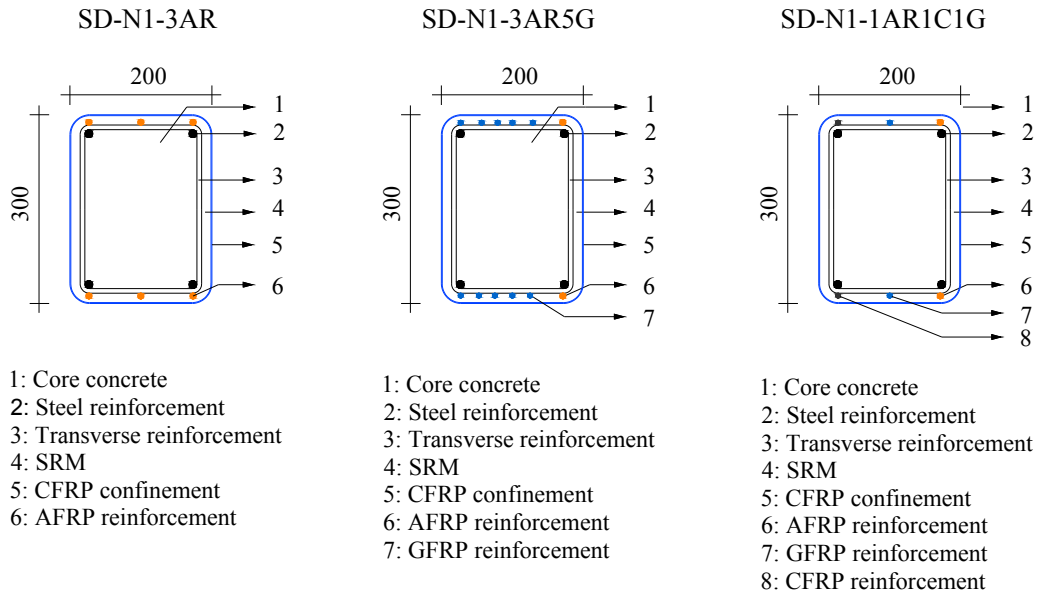

Figure 2.3 : Retrofitting details of the second group specimens.

2.1.3 Third group specimens

Some structures stand sound even after large earthquakes, while many other structures suffer from different level of damages due to several deficiencies. Depending on the damage level, some buildings are demolished and some are decided to be refurbished and/or retrofitted. Especially after major earthquakes such as Kobe 1995 or Kocaeli 1999, huge number of structures can be reported for demolishing or retrofitting for the public safety. Demolishing and re-construction costs could reach to astronomic levels, which could shake the whole economy of a country. In this case, safe retrofitting of medium and heavily damaged buildings could soften the negative economical impact of the earthquakes. Therefore, repairing and retrofitting of the pre-damaged structures has a key importance for both developing and underdeveloped countries.

In order to investigate the effect of different pre-damage conditions of the columns on the applicability and efficiency of the selected retrofitting technique, 2 columns were tested to achive a certain level of damage, repaired and retrofitted afterwards and re-tested under same conditions. In order to make a comprehensive assessment on the retrofitting of the pre-damaged columns, 2 specimens were strengthened without any pre-damage and tested under same conditions. The aim was to evaluate the efficiency of the proposed retrofitting technique on pre-damaged columns compared to non-damaged columns. Main features of the specimens are shown in the Table 2.4.

Table 2.4 : Properties of the third group specimens.

Specimen	Concrete compressive strength of columns (MPa)	Longitudinal and transverse steel reinforcement	Type of FRP reinforcement	Quantity of FRP reinforcement
WD-N1-P1	15	S220	-	-
WD-N1-P2	15	S220	-	-
WD-N1-2AR-P1	15	S220	AFRP bars	2x2 (ϕ10)
WD-N1-2AR-P2	15	S220	AFRP bars	2x2 (ϕ10)
WD-N1-2AR	15	S220	AFRP bars	2x2 (ϕ10)
WD-N1-1AR2G	15	S220	AFRP and GFRP bars	1x2 (ϕ10)AFRP 2x2 (ϕ8)GFRP

Specimens WD-N1-P1 was tested untill achieving ±2 % drift ratio, while the specimen WD-N1-P2 was tested untill ±4 % which could be counted as heavy damage. After pre-damage testing, these two specimens were repaired by using same SRM and retrofitted by installing 2 AFRP bars on the surfaces in weak direction and re-tested under same conditions up to a drift ratio of ±8 % like retrofitted sample of first group and second group specimens. Retrotiffing details of the third group specimens are shown in Figure 2.4.

The specimen WD-N1-2AR was strengthened identically with the retrofitted pre-damaged specimens and tested under same conditions, while specimen WD-N1-1AR2G was retrofitted by using 1 AFRP and 2 GFRP bars in the weak direction to further investigate the flexural behavior of columns with hybrid utilization of FRP reinforcement when compared to pre-damaged columns retrofitted homogenously with only AFRP reinforcement. It should be noted that, similar to the despite the significant increase in the concrete compressive strength at the day of testing, axial load was kept as 120 kN during the tests as done with second group specimens.

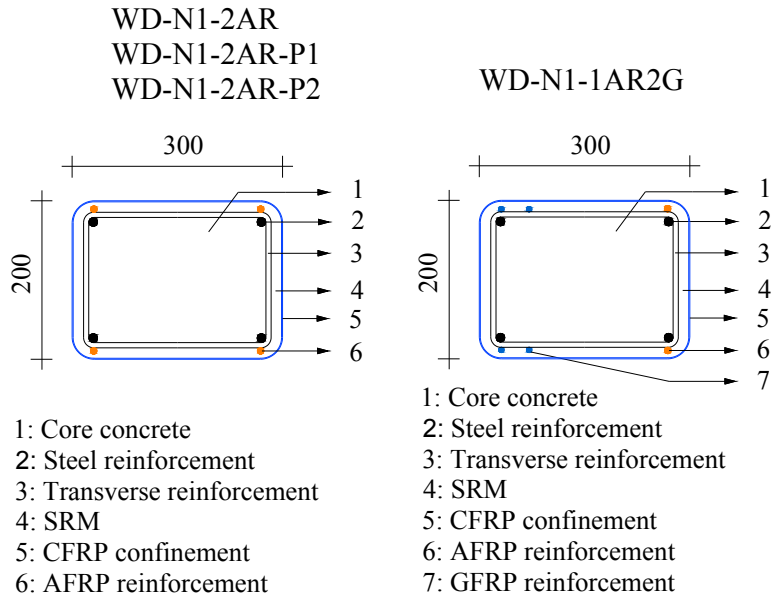

Figure 2.4 : Retrofitting details of the third group specimens.

2.1.4 Concrete

A low strength concrete was designed for the specimens to represent the existing substandard columns common in Turkey and other similar developing countries. In order to achieve a realistic behavior, the same poor concrete was used to cast both columns and the footing. The stress-strain relationship of concrete was obtained by performing compressive strength tests on standard 150×300 mm cylinder specimens. Concrete cylinders were kept under same conditions with the column specimens until the day of testing. Compressive strength values were obtained as 10.3 MPa and 15.2 MPa for 28 days and 750 days respectively. The increase in the strength value over the time was considered in calculating the theoretical capacities of the relevant specimens. Concrete mix constituents for the specimens are shown in Table 2.5.

Table 2.5 : Concrete mix constituents for the specimens.

Constituents	(kg/m^3)	Properties
Crushed sand	705	0-4 mm
Coarse Aggregate No.1	870	4-16 mm
Natural sand	408	0-1 mm
Cement	185	CEM2 32.5R
Water	180	
TOTAL	2348	

2.1.5 Reinforcing steel bar

S220 type plain steel bars were used as longitudinal (ϕ14) and transverse reinforcement (ϕ10) in all specimens with the same geometry. In order to avoid premature failure,

which could occur in the footing, S420 deformed bars were used as longitudinal and transverse reinforcement in costruction of footings. Stress-strain relationships of reinforcing bars of S220 longitudinal bars and transverse bars are shown in Table 2.6.

Table 2.6 : Properties of S220 steel reinforcement.

Steel Reinforcement	f_y (MPa)	f_{max} (MPa)	E_s (GPa)
ϕ10	315	400	201.3
ϕ14	296	399	198.6

Stress-strain relationships of reinforcing bars of S220 longitudinal bars and transverse bars used in columns are shown in Figure 2.5.

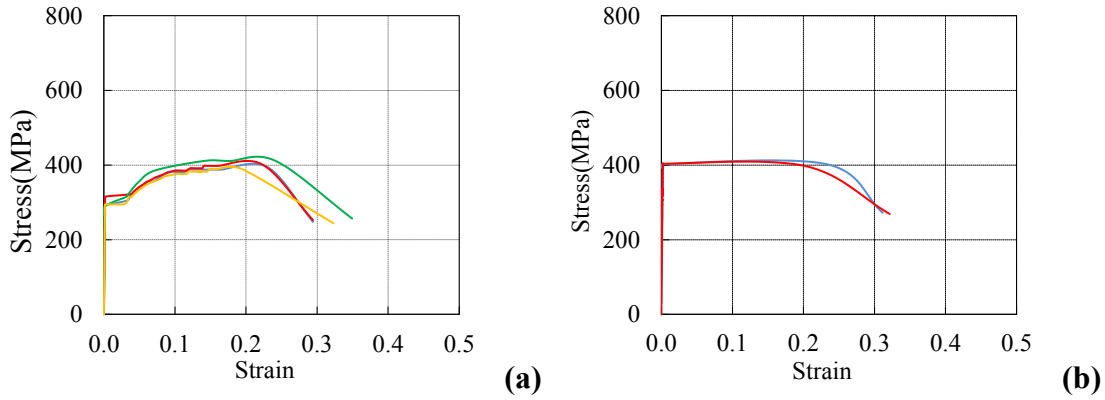

Figure 2.5 : Stress-strain relationships of S220 steel: (a)Longitudinal bars, ϕ14. (b)Transverse bars, ϕ10.

Stress-strain relationships of reinforcing bars of S420 longitudinal bars and transverse bars used in footing are shown in Figure 2.6.

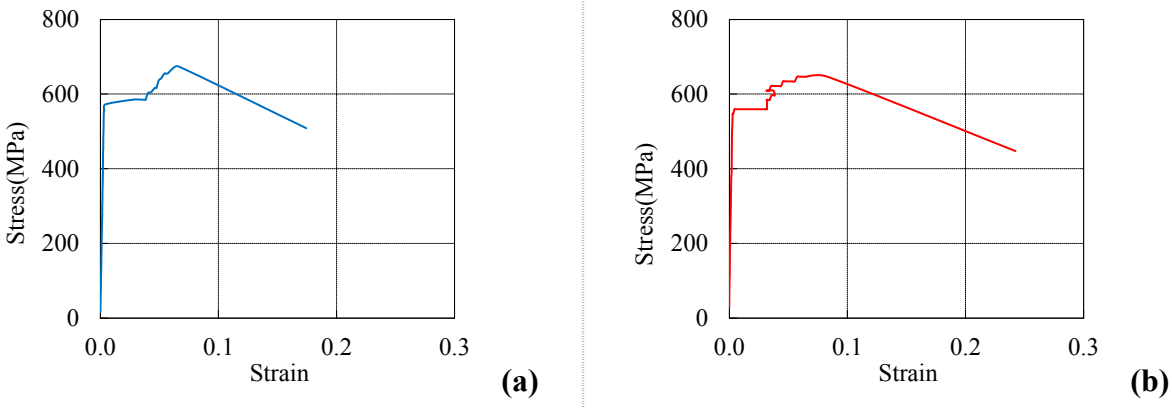

Figure 2.6 : Stress-strain relationships of S420 steel: (a)Longitudinal bars, ϕ14. (b)Transverse bars, ϕ10.

2.1.6 Structural repair mortar

MasterEmaco S 488, which is one component, cement based, shrinkage compensated, fibre reinforced (with polyacrylonitrile fibres), and high strength structural repair mortar was selected for replacing the poor concrete cover and forming a sound substrate for longitudinal FRP reinforcement and CFRP transverse reinforcement. MasterEmaco S 488 is certified as an R4 class structural repair mortar according to EN 1504-3 (2005). Technical properties, which is provided by the manufacturer BASF Construction Chemicals, are shown in Table 2.7.

Table 2.7 : Properties of structural repair mortar, MasterEmaco S 488.

Compressive strength[1] (MPa)	Modulus of elasticity[1] (Gpa)	Adhesion to concrete[2] (MPa)
50 (7 days)	>20 (7 days)	>2 (7 days)
60 (28 days)	>20 (28 days)	>2 (28 days)

[1] Mean values obtained by using 4x4x16cm prism test samples according to EN 196-1.
[2] Minimum values obtained by testing according to EN 1542.

2.1.7 FRP reinforcement and adhesives

Aramid bars and strips, glass bars and carbon bars were used as longitudinal FRP reinforcement during the retrofitting applications. Additionally, carbon FRP fabric was used for confinement of the specimens to increase the shear capacity and ductility. It should be noted that, unlikely to steel reinforcement, FRPs behave linear elastic until they reach to their elongation capacity. Technical properties, which is provided by the manufacturer BASF Construction Chemicals, are shown in Table 2.8. Visual appearance of the CFRP sheet is shown in Figure 2.7.

Table 2.8 : Properties of FRP reinforcement.

FRP	Modulus of elasticity, E_f (MPa)	Diameter, d_b (mm)	Thickness, t_f (mm)	Width, w_f (mm)	Ultimate rupture strain ε^*_{frpult}
AFRP (strip)	60,000	-	1.400	42	0.023
AFRP (bar)	70,000	10	-	-	0.024
CFRP (bar)	165,000	8	-	-	0.015
GFRP (bar)	40,000	8	-	-	0.028
CFRP (sheet)	230,000	-	0.166	500	0.015

* Manufacturer's declared values.

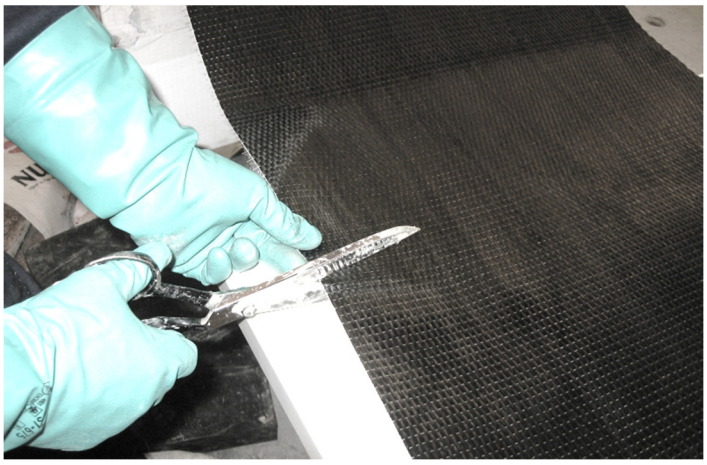

Figure 2.7 : High strength type, uni-directional CFRP woven fabric.

In order to ensure the perfect load transfer, FRP reinforcement were bonded on to the surfaces by using high performance adhesives, which are recommended as a part of MasterBrace FRP retrofitting system by BASF Construction Chemicals. Properties of the adhesives used in retrofitting application are shown in Table 2.9.

Table 2.9 : Properties of of adhesives used in retrofitting.

Materials	Product Name	Compressive Strength[1] (MPa)
Epoxy adhesive used for bonding longitudinal FRP reinforcement	MasterBrace ADH 4000	75
Epoxy mortar used for embedding FRP anchorage reinforcement	MasterFlow 402	80
Epoxy adhesive used for bonding repair mortar on to the longitudinal FRP reinforcement	MasterBrace ADH 1420	80
Epoxy adhesive used for bonding transverse FRP reinforcement	MasterBrace SAT 4500	60

[1] Obtained by using 4x4x16cm prism test samples according to EN 196-1

High build, thixotrophic epoxy adhesive, MasterBrace ADH 4000 was used to bond longitudinal FRP reinforcement to bond on to the columns. To guarantee the proper bond between longitudinal FRP reinforcement and the covering final repair mortar layer, a high performance epoxy primer and adhesive, which is called MasterBrace ADH 1420 was used as creating a structural bonding bridge. This adhesive is CE certified according to EN-1504-4 (2004). Longitudinal FRP reinforcement were anchored to the footing by using a three component, flowable epoxy mortar called MasterFlow 402. This mortar is CE certified according to EN 1504-6 (2005) as anchoring mortar. As a final step of the retrofitting procedure, CFRP sheets were

wrapped around the columns by using low viscous, fluid epoxy adhesive MasterBrace SAT 4500.

2.2 Design of Specimens

The theoretical strength and local deformation characteristics were determined through moment-curvature relationships obtained by fiber analysis approach. The effect of axial load was considered while obtaining the moment-curvature relationships. In the moment-curvature analysis, longitudinal steel rebars were assumed to behave in an elasto-plastic manner with strain hardening. Longitudinal FRP reinforcement were taken into account as linear elastic material in both tension and compression. Findings of Mallick (1988), Wu (1990) and Ehsani (1993) were used to determine the compression behavior of the FRP reinforcement. According to Mallick (1988) and Ehsani (1993), the compressive modulus of elasticity for AFRP, CFRP and GFRP reinforcement are 100 %, 85 % and 80 % of their tensile modulus of elasticity respectively. Additionally, Mallick (1988) and Wu (1990) reported that compressive strengths of AFRP, CFRP and GFRP reinforcement were obtained as 20 %, 78 % and 55 % of ther tensile strengths respectively. Buckling and debonding of FRP reinforcement during cyclic loading was assumed to be prevented by structural repair mortar and CFRP confinement. Since the retrofitted specimens, thereby the FRP applications, were exposed to laboratory conditions for a very short time prior to testing, the environmental reduction factor, C_E, was taken as 1.0. In other words, the design rupture strain of AFRP reinforcement (ε_{fu}) was assumed equal to ε_{fu}*, which was the manufacturer declared ultimate strain of FRP reinforcement in the equation (2.1).

$$\varepsilon_{fu} = C_E \cdot \varepsilon^*_{fu} \tag{2.1}$$

Existing studies in the literature reveal that longitudinal FRP reinforcement could not reach to their declared ultimate strain under reversed cyclic loading. Bournas and Triantafillou (2009) reported maximum strains on longitudinal FRP reinforcement, which had been measured by straingauges during the reversed cyclic loading, varied between 27 % and 67 % of the ultimate strain. In the study of Vrettos et al. (2013), where the longitudinal CFRP fabrics were used for flexural retrofitting of RC columns, the measured maximum strains were also far behind ultimate strains declared by the

manufacturer. The average of the maximum strains, which were calculated through analysis of the cross-section at the column base by using conventional RC force equilibrium, strain compatibility, and material constitutive relationships based on the test results, was 38 % of the ultimate strain stated by manufacturer. Perrone et al. (2009) came up with similar results on the measured maximum strains on the longitudinal FRP reinforcement. The average measured strain at fracture of the FRP reinforcement was 41 % of the declared ultimate strain. In the light of these recent studies, it could be concluded that the rupture strains of the longitudinal FRP reinforcement vary in a wide range, which prevents to make general assumptions for design rupture strain under cyclic flexural loading. In order to calculate the therotecial load – deformation behavior of the retrofitted samples more accurately, each specimen was considered individually. The maximum values measured by strain gagues were assumed as design rupture strains of longitudinal FRP reinforcement for the relevant specimen, in which FRP reinforcement were ruptured during the tests. On the other hand, manufacturer's declared strain values were assumed as design rupture strains for the FRP reinforcement, which were not ruptured. Design modulus of elasticities and design rupture strains are given in Table 2.10.

Table 2.10 : Design parameters for FRP reinforcement.

FRP	Specimen	Compression		Tension	
		E_f (MPa)	ε_{fu}	E_f (MPa)	ε_{fu}
AFRP (strip)	SD-N1-2ARS	60,000	-0.0031	60,000	0.0104
AFRP (strip)	SD-N1-2ARS-PB	60,000	-0.0027	60,000	0.0125
AFRP (strip)	SD-N1-4ARS	60,000	-0.0079	60,000	0.0104
AFRP (bar)	SD-N1-3AR	70,000	-0.0055	70,000	0.0152
AFRP (bar)	SD-N1-1AR5G	70,000	-0.0087	70,000	0.0089
AFRP (bar)	SD-N1-1AR1C1G	70,000	-0.0054	70,000	0.0081
AFRP (bar)	WD-N1-2AR	70,000	-0.0056	70,000	0.0098
AFRP (bar)	WD-N1-1AR2G	70,000	-0.0094	70,000	0.0128
AFRP (bar)	WD-N1-2AR-P1	70,000	-0.0067	70,000	0.0090
AFRP (bar)	WD-N1-2AR-P2	70,000	-0.0051	70,000	0.0114
GFRP (bar)	SD-N1-1AR5G	32,000	-0.0193	40,000	0.0280
GFRP (bar)	SD-N1-1AR1C1G	32,000	-0.0193	40,000	0.0280
GFRP (bar)	WD-N1-1AR2G	32,000	-0.0193	40,000	0.0280
CFRP (bar)	SD-N1-1AR1C1G	140,250	-0.0129	165,000	0.0150

The model proposed by Ilki et al. (2008) was used to obtain the stress-strain relationship of CFRP confined concrete. The stress-strain relationship of CFRP confined concrete was obtained for two different parts of the confined cross-section (for core concrete confined by transverse steel bars and external CFRP sheet, and for SRM as concrete cover confined by only external CFRP sheet). It should be considered

that the moment-curvature analysis for the retrofitted specimens was terminated when longitudinal FRP reinforcement ruptures.

After obtaining the moment-curvature relationships through fiber analysis approach with summarized assumptions, the total top displacements (δ_t) of the specimens were determined considering the elastic and inelastic deformations. It should be noted that the shear deformations were neglected since they were very small with respect to contribution of flexure. As a first step, for calculating the yield displacements (δ_y) of the columns using equation 2.2, the columns were discretized into 10 elements (5 through the plastic hinge length at the bottom of the column and 5 outside of the plastic hinge lenth) for considering effective flexural stiffness, rather than the gross cross-sectional stiffness, at different heights of the column as a function of bending moment when the longitudinal reinforcing bars yield at the critical maximum moment region as shown in Figure 2.8.

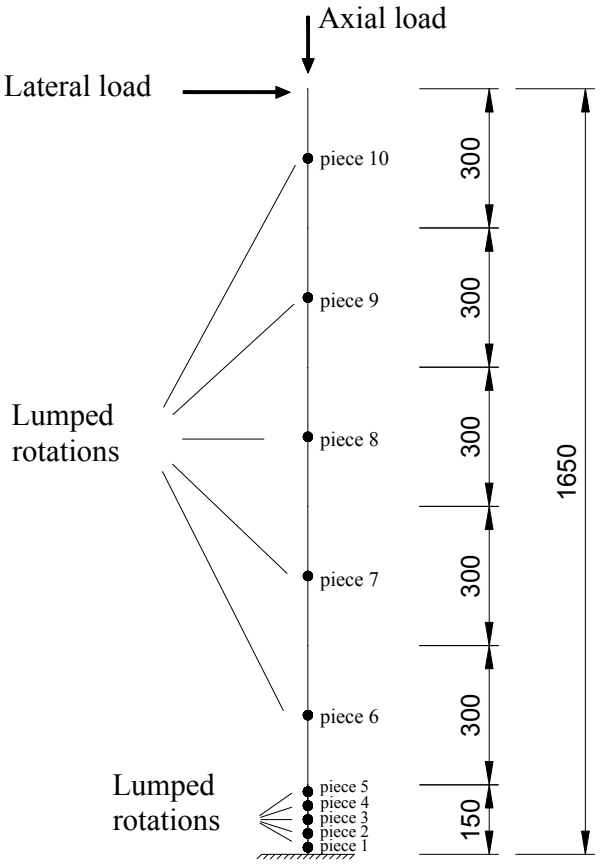

Figure 2.8 : The locations of lumped rotations.

In equation 2.2, χ_i is the elastic curvature (corresponding to respective bending moment on that discretized part), l_i is the length of the respective part, and h_i is the

distance between the center of the respective part and the tip of the column, where the lateral load is applied.

$$\delta_y = \sum_{i=1}^{5} \chi_i \cdot l_i \cdot h_i \tag{2.2}$$

$$\delta_p = \chi_p \cdot l_p \cdot (H - \frac{l_p}{2}) \tag{2.3}$$

$$\delta_t = \delta_y + \delta_p \tag{2.4}$$

Conventional plastic hinge approach was used for calculating the plastic component of the total top displacements (δ_p) of the specimens as it is given in equation 2.3. χ_p is the plastic curvature at the plastic hinge of the column, l_p is the plastic hinge length, H is the distance between the interface of the column and the footing and the point of application of the lateral load. The length of plastic hinge (l_p) of the column was assumed as h/2 according to TSDC (2007), where h refers to the depth of the cross-section of the column. Finally, the total top displacements (δ_t) of the columns were determined using equation (2.4. The theoretical lateral load-displacement relationships were then obtained and compared with the experimental load-displacement relationships in the section "Overall Evaluation of Test Results".

2.2.1 Reference specimens

The cyclic behavior of the column specimens was dominated by flexure. In order to ensure the flexural behavior axial load level of the columns is assumed around 20 % of their capacity. Axial load capacity of the reference columns is calculated by equation (2.5).

$$P_0 = f'_{ck} \cdot \mathrm{b} \cdot \mathrm{h} \tag{2.5}$$

The average moment capacities of the reference specimen SD-N1-REF and the unretrofitted pre-damaged specimens WD-N1-P1 and WD-N1-P2 are calculated using XTRACT, cross section analysis computer programme by using Mander Model for confined concrete (only transverse steel reinforcement), are shown in Figure 2.9 and Figure 2.10.

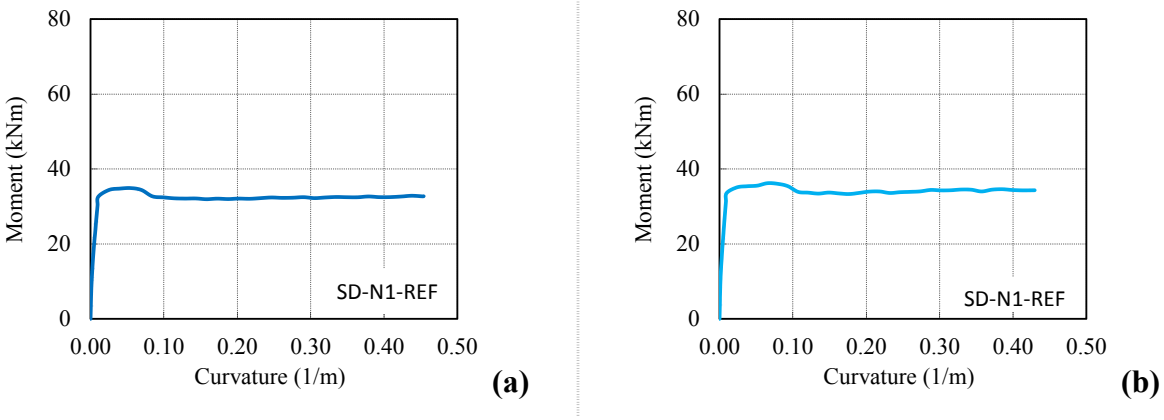

Figure 2.9 : Theoretical moment-curvature relationships of reference specimens in strong direction: (a)f'_c=10.3 MPa, N=120 kN. (b)f'_c=15.2 MPa, N=120 kN.

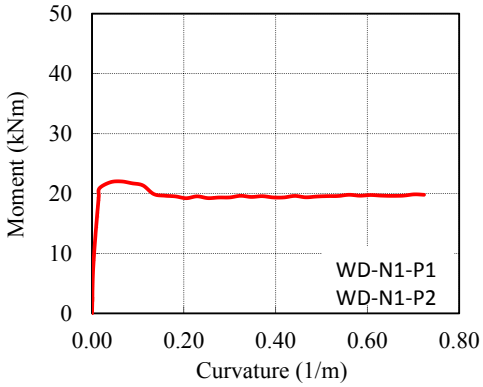

Figure 2.10 : Theoretical moment-curvature relationships of reference specimen in weak direction: f'_c=15.2 MPa, N=120 kN.

According to ACI 318M-14 (2014), the shear strength of reference specimens (the ones with 10.3 MPa compressive strength and tested in strong direction), which includes contributions of concrete and transverse reinforcement, can be calculated using equation 2.6, equation 2.7 (units are in MPa) and equation 2.8. In these equations, V_s is the nominal shear strength provided by transverse steel reinforcement, A_v is the area of the transverse reinforcement, f_{yt} is the characteristic yield strength of transverse reinforcement, d is the effective depth, s is the spacing of transverse reinforcement, V_c is the nominal shear strength provided by concrete, N_u is the factored axial load normal to cross-section (to be taken as positive for compression), A_g is the gross area of the column section, f'_c is the characteristic compressive strength of concrete and b_w is the width of the column.

$$V_s = \frac{A_v \cdot f_{yt} \cdot d}{s} \tag{2.6}$$

$$V_c = 0.166\left(1 + \frac{N_u}{14A_g}\right) \cdot \sqrt{f'_c} \cdot b_w \cdot d \tag{2.7}$$

$$V_n = V_c + V_s \tag{2.8}$$

Shear strengths of the all columns are calculated by using equation 2.6, equation 2.7 and equation 2.8 and the results are given in Table 2.11. Lateral load capacities of the specimens are calculated based on their moment capacities and compared with shear capacities. As it could be derived from the theoretical capacities shown in Table 2.11, with the present design and reinforcement detailing, flexure was expected to be the dominant behavior for reference specimens during cyclic reversed loading.

Table 2.11 : Lateral load and shear capacities of the reference specimens.

Specimen	Maximum Lateral Load Capacity (kN)	Shear Capacity (kN)
SD-N1-REF[1]	20.4	97.1
SD-N1-REF[2]	21.1	104.0
WD-N1-REF	12.8	76.5

[1] Compressive strength was assumed as 10.3 MPa.
[2] Compressive strength was assumed as 15.2 MPa.

2.2.2 First group specimens

The cyclic behavior of the first group retrofitted column specimens are dominated by flexure. The moment capacities of the retrofitted specimens in strong direction are calculated using XTRACT. Moment - curvature relationships calculated at the bottom 20 mm are shown in Figure 2.11.

Contributions of CFRP confinement and structural repair mortar to the flexural strength of the retrofitted specimens are considered while modelling the column cross sections in the XTRACT computer programme. SRM is assumed as one to one replacement of the cover concrete but with much higher compressive strength and this is taken into account while calculating the forces in the compression zone of the cross section. Furthermore, the confinement effect of the transverse CFRP reinforcement is considered on the ultimate strength and deformation capacity of the SRM and core concrete. This approach was followed for all retrofitted specimens in this study.

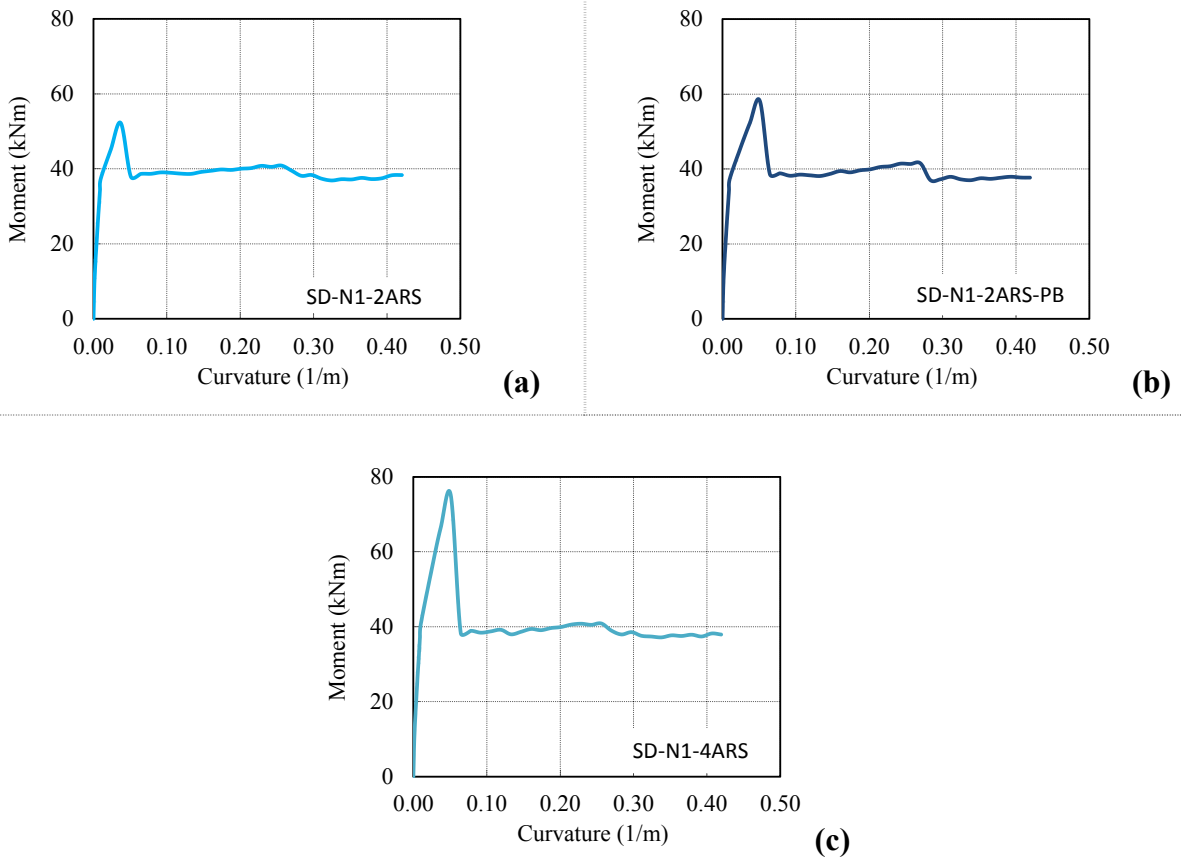

Figure 2.11 : Theoretical moment-curvature relationships of first group specimens: (a)SD-N1-2ARS.(b) SD-N1-2ARS-PB. (c)SD-N1-4ARS.

According to ACI-440-2R-08 (2008), the contribution of FRP reinforcement to shear strength can be obtained using equation (2.9) and equation (2.10).

$$V_f = \frac{A_{fv} \cdot \varepsilon_{fe} \cdot E_f \cdot d_{fv}}{s_f} \tag{2.9}$$

$$A_{fv} = 2\mathrm{n} \cdot t_f \cdot w_f \tag{2.10}$$

In these equations, V_f is the nominal shear strength provided by transverse FRP reinforcement, A_{fv} is the area of the transverse FRP reinforcement, ε_{fe} is effective strain of transverse FRP reinforcement attained at failure, which is assumed to be 0.004 as recommended by ACI-440-2R-08 (2008). E_f is the tensile modulus of elasticity of transverse FRP reinforcement, d_{fv} is effective depth for transverse FRP reinforcement, s_f is spacing of transverse FRP reinforcement, n is the number of the transverse FRP reinforcement plies, ω_f is the width of transverse FRP reinforcement.

According to ACI-440-2R-08 (2008), the total shear strength of the column with contributions of concrete, steel stirrups and tranverse FRP reinforcement, can be obtained by using equation (2.11).

$$V_n = V_c + V_s + \psi_f V_f \tag{2.11}$$

ψ_f is the FRP strength reduction factor and was assumed to be 0.95 as recommended by ACI-440-2R-08 (2008) for fully wrapped sections, which resist to shear forces. The contribution of structural repair mortar to the shear resistance was neglected due to the marginal impact on the total shear strength of the retrofitted specimens. This approach was applied to the all retrofitted specimens in this study.

Shear strengths of the all columns are calculated by using equation 2.9, equation 2.10 and equation 2.11 and the results are given in Table 2.12.

Table 2.12 : Lateral load and shear capacities of the retrofitted first group specimens.

Specimen	Maximum Lateral Load Capacity (kN)	Shear Capacity (kN)
SD-N1-2ARS	30.5	271.2
SD-N1-2AR-PB	34.1	271.2
SD-N1-4ARS	43.4	271.2

As it is seen in the Table 2.12, with the current design and reinforcement detailing, flexure was expected to be the dominant behaviour for retrofitted speciemens during cyclic reversed loading.

2.2.3 Second group specimens

The cyclic behavior of the second group retrofitted column specimens are dominated by flexure. The moment capacities of the retrofitted specimens in strong direction are calculated using XTRACT. Moment - curvature relationships are shown in Figure 2.12.

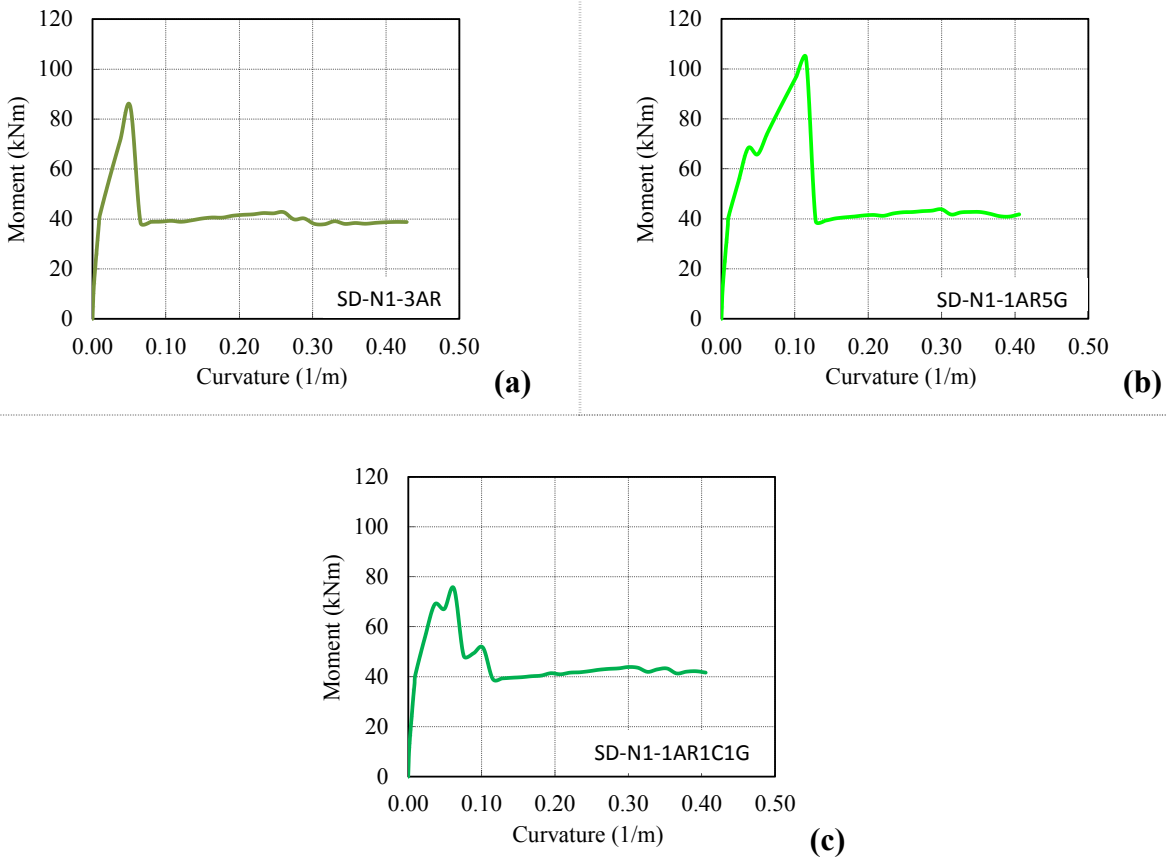

Figure 2.12 : Theoretical moment-curvature relationships of second group specimens: (a)SD-N1-3AR. (b)SD-N1-1AR5G. (c)SD-N1-1AR1C1G.

Shear strengths of the all columns were calculated by using equation 2.9, equation 2.10 and equation 2.11 and the results are given in Table 2.13.

Table 2.13 : Lateral load and shear capacities of the second group specimens.

Specimen	Maximum Lateral Load Capacity (kN)	Shear Capacity (kN)
SD-N1-3AR	49.4	278.1
SD-N1-1AR5G	61.4	278.1
SD-N1-1AR1C1G	45.2	278.1

As it is seen in Table 2.13, similar to the first group retrofitted specimens, with the current design and reinforcement detailing, flexure was expected to be the dominant behavior for second group specimens during the test.

2.2.4 Third group specimens

Third group specimens were both retrofitted and tested in their weak direction. The average moment capacities of the retrofitted specimens in weak direction are

calculated using XTRACT. Moment - curvature relationships of the retrofitted specimens are shown in Figure 2.13.

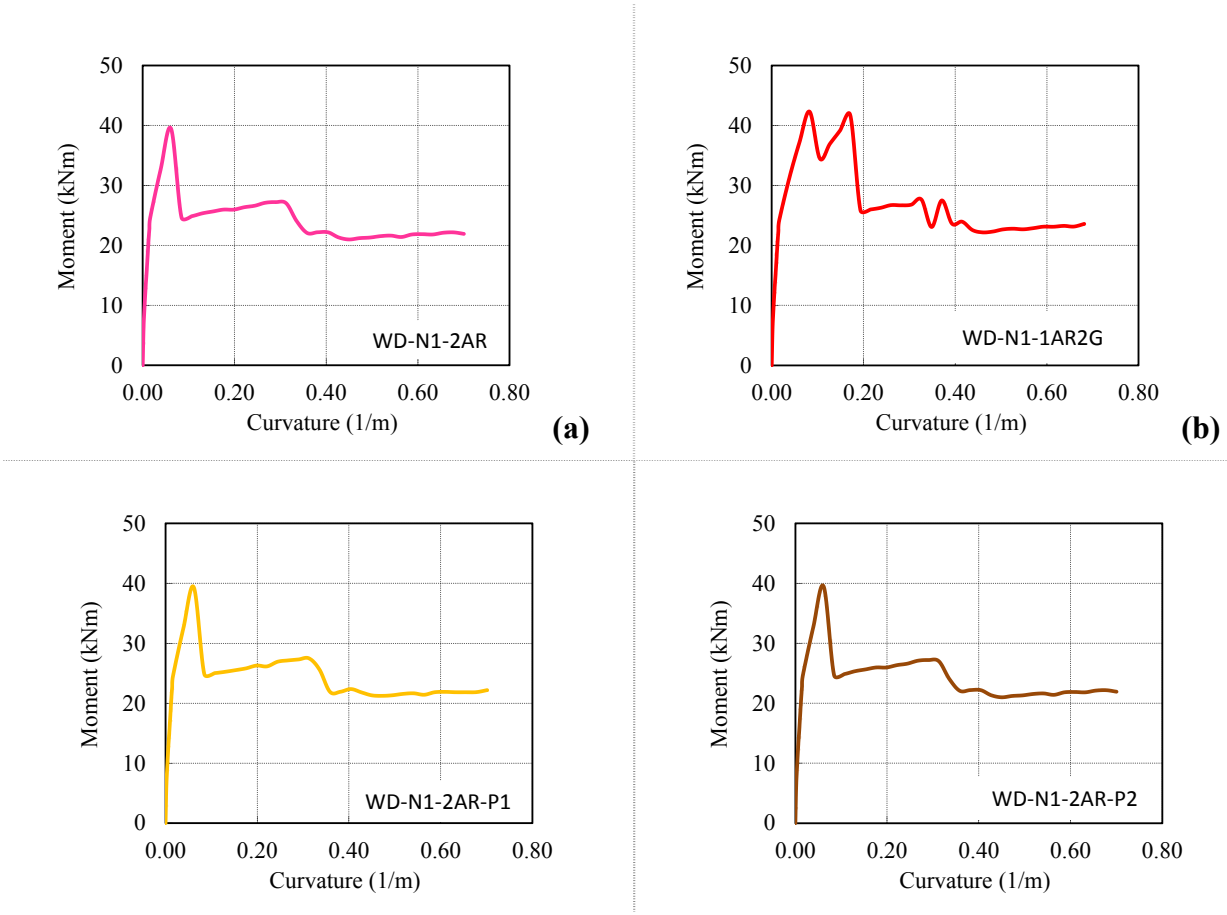

Figure 2.13 : Theoretical moment-curvature relationships of third group specimens: (a)WD-N1-2AR. (b)WD-N1-1AR2G. (c)WD-N1-2AR-P1. (d)WD-N1-2AR-P2.

Shear strengths of the all columns are calculated by using equation 2.9, equation 2.10 and equation 2.11 and the results are given in Table 2.14.

Table 2.14 : Lateral load and shear capacities of the retrofitted third group specimens.

Specimen	Maximum Lateral Load Capacity (kN)	Shear Capacity (kN)
WD-N1-2AR-P1	23.0	192.6
WD-N1-2AR-P2	23.5	192.6
WD-N1-2AR	23.0	192.6
WD-N1-1AR2G	25.6	192.6

As it is seen in the Table 2.14, similar to the first and second group retrofitted specimens, with the current design and reinforcement detailing, flexure is expected to be the dominant behavior for the third group specimens during the test.

2.2.5 Anchorage design

The failure of FRP reinforcement was desired to be due to rupture of the reinforcement at the critical cross section rather than pull-out, concrete splitting, concrete cone and spacing and edge cone failures, which have been listed as five primary anchorage failure modes in ACI 355.1R-91 (1991). Among these failures, the possibility of concrete splitting, concrete cone and edge cone failures are significantly reduced due to the constraining effect of steel rebars in the footing, where the conical anchor holes were dug in. Therefore, only possibilities of pullout failure and fracture of FRP reinforcement were taken into account by comparing the tensile strength of FRP reinforcement and the adhesion between concrete and epoxy grout in equation (2.12) and equation (2.13).

$$F_{bond} = \tau_b \cdot l_{db} \cdot u \tag{2.12}$$

$$F_{frp} = E_f \cdot \varepsilon^*_{fu} \cdot A_{frp} \tag{2.13}$$

In these equations, F_{bond} is the bond capacity, τ_b is the uniform bond strength along the anchorage length, l_{db} is the embedment length, while u is the perimeter of anchorage hole, F_{frp} is the tensile capacity of the FRP reinforcement, ε^*_{fu} is the ultimate rupture strain of FRP reinforcement declared by manufacturer, and A_{frp} is the cross-sectional area of the FRP reinforcement. In the light of previous studies (Perrone et al., 2009; Bournas and Triantafillou, 2009; Goksu et al., 2012; Fahmy and Wu, 2012; Vrettos et al., 2013; Li et al., 2013; and Faustino and Chastre, 2015), embedment length was selected as 300 mm due to the reported premature anchorage failures when depth of the anchorage hole is less than 150 mm. The dimensions of the conical anchorage holes in mm are presented in Figure 2.14.

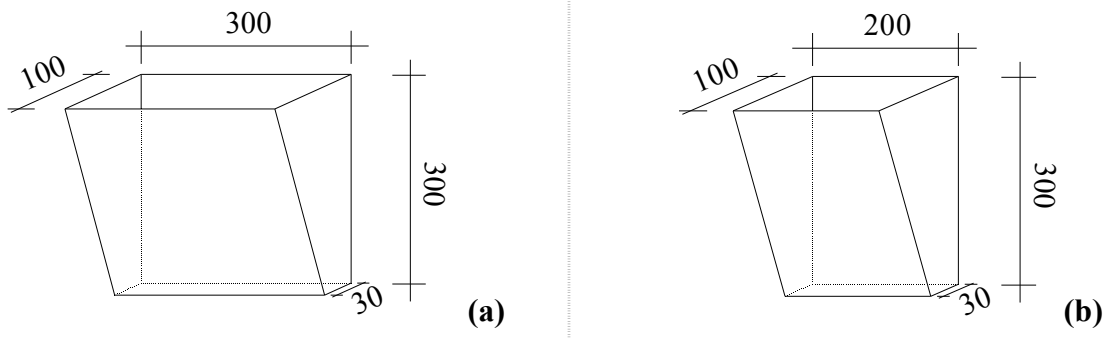

Figure 2.14 : Geometric properties of anchorage holes: (a)Specimens retrofitted in weak direction. (b)Specimens retrofitted in strong direction.

ACI 355.1R-91 (1993) assumes a uniform bond stress distribution along the anchorage length and a bond strength in the order of 9 MPa. This bond strength is accepted for a concrete with compressive strength of 21 MPa and an embedment length of nine anchor diameters. Since ACI 355.1R-91 (1993) states that bond strength increases approximately with the square root of the concrete strength, τ_b is calculated to be 6.3 MPa based on a simple correlation between concrete strengths 10.3 MPa and 21 MPa. While calculating tensile load capacity of FRP anchorage reinforcement, environmental reduction factor is neglected. Besides, in order to keep the design in the safe side, strength reduction factor is also neglected and the ultimate rupture strain declared by the manufacturer is considered. F_{frp} is calculated for the specimens only, which has a different amount of FRP reinforcement. The theoretical pull out load capacity of the anchorage holes and the maximum tensile load capacities of the FRP reinforcement are given in Table 2.15.

Table 2.15 : Pull out force and the maximum tensile load can be carried by the FRP reinforcement of the specimens.

Specimen	F_{bond} (kN)	F_{frp} (kN)
SD-N1-2ARS	1,012	162
SD-N1-4ARS	1,012	325
SD-N1-3AR	1,012	396
SD-N1-1AR1C1G	1,012	313
SD-N1-1AR5G	1,012	413
WD-N1-2AR	1,395	264
WD-N1-1AR2G	1,395	245

Moreover, test results of the retrofitted columns also confirm that the embedment length of FRP reinforcement is sufficient. No debonding problem or damages resulting from concrete cone, concrete splitting, edge cone and pullout failures were observed during the tests.

2.3 Test Setup

2.3.1 Testing procedure

All specimens were constructed and tested at Istanbul Technical University, Civil Engineering Faculty, Structural and Earthquake Engineering Laboratory and Building Materials Laboratory. The experimental test setup is shown in Figure 2.15.

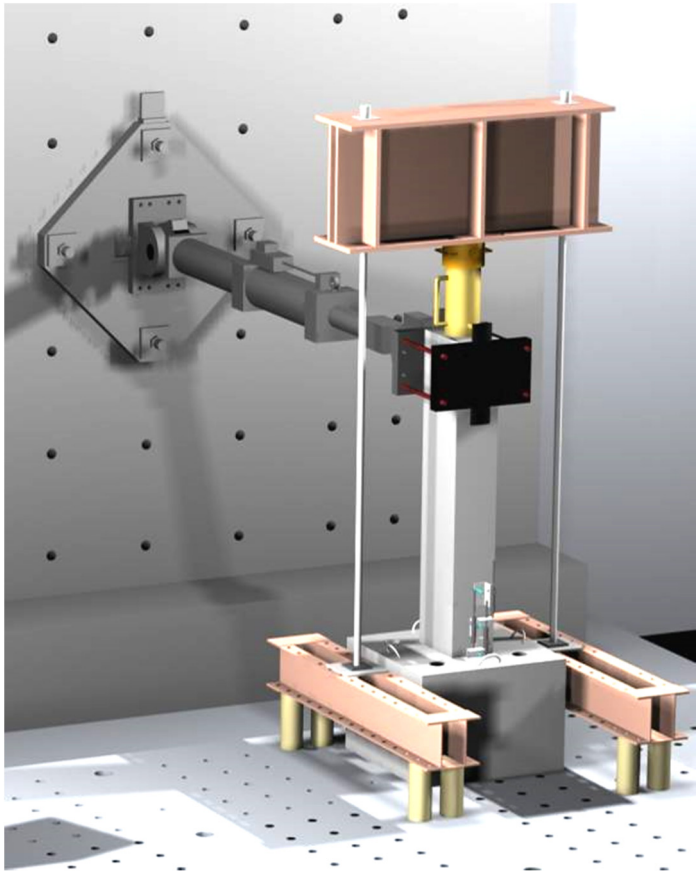

Figure 2.15 : Test setup (Demirtaş, 2008).

The lateral load was applied at the tip of the specimen, approximately at 1700 mm height from the base of the column with an MTS hydraulic actuator of 250 kN capacity. An axial load of 120 kN (20 % of column axial load capacity for 1st group specimens and 13 % for the 2nd and 3rd group specimens) was applied through a jack at the top of the columns. It should be noted that the contribution of the steel reinforcement to the axial load capacity is neglected. The axial load was applied via two 6-wire-strand post tensioning steel tendons. The tendons passed through a rigid steel beam, which are fixed to the strong foundation to transfer the axial loads. At the top of the column, the tendons were attached to another rigid steel beam which allowed the tendons to be loaded by a centrally located hydraulic jack. Applied axial load was measured by load cell, which was centrally located on the hydraulic jack. The specimens were tested under constant axial load and reversed cyclic lateral load.

Once the specimen was transported to the testing port, where actuator was located, it was fixed to the adaptor foundation by using 4 high strength rods by screwing tightly through the holes left on the foundation of the specimens during the construction process. Eight mm diameter holes were drilled at 20 mm, 150 mm and 300 mm above

the footing for mounting the LVDTs, which were used to measure the displacement and afterwards calculate the moment-curvature relationships.

2.3.2 Instrumentation

A combination of TML transducers, YFLA–5–3L, FLA-3-11-3L type straingauges, TML load cell were used for instrumentation of the specimens. Additionally interior load cell and interior displacement transducer of MTS actuator were used as important components of testing instrumentation. The data of these instruments were collected by using TML TDS 303 data logger through a TML ASW-50C switch box.

2.3.2.1 LVDTs

For measuring the lateral displacement of the specimen, two LVDTs were placed horizontally at the mid (CDP100) and tip (SDP200 or SDP300) of the column height. For obtaining the average curvature values of the columns over different gage lengths, six LVDTs were placed vertically parallel to the column measuring in 20 mm, 150 mm and 300 mm gage lengths. Two of six LVDTs, which were placed in 20 mm, were CDP50, while the remaining four LVDTs were CDP25 type. Two LVDTs were placed on the footing for measuring the possible rotations, and one additional LVDT was placed horizontally at the mid height of the footing to measure any movement of the footing. The locations of the LVDTs are shown in Figure 2.16.

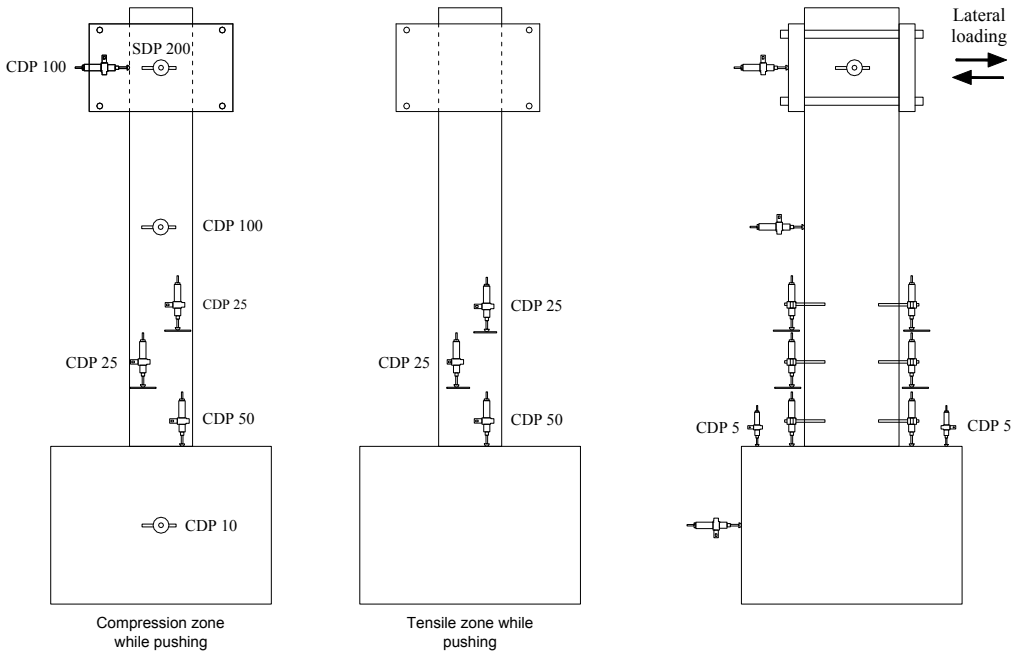

Figure 2.16 : Position of LVDTs.

2.3.2.2 Straingauges

Straingauges were used to measure strains and to obtain the strain profiles in the longitudinal and transverse steel reinforcement and longitudinal FRP reinforcement. The straingauges were installed on the reinforcing cage of the specimens before casting concrete. The surfaces of the steel reinforcing bars were grinded with grindstone to remove the rust, and then cleaned with acetone. In case of longitudinal FRP reinforcement, grindstones were used to remove irregularities (e.g. sand on the aramid and glass FRP bars, which was spread to improve the adhesion) on the surfaces and create a smooth substrate to fix straingauges properly. Straingauges were bonded to these smooth and clean surfaces with ultra fast setting acrylate based adhesive. N-1, which is a water resistant sealant, was applied on the straingauges prior to wrapping with VM-tape isolation strap and one ply of insulation tape. Each straingauge was labelled with stickers which shows the location and the type of the straingauges at the tip of the cables of the straingauges. The location of the straingauges at the longitudinal and transverse steel bars are shown in Figure 2.17.

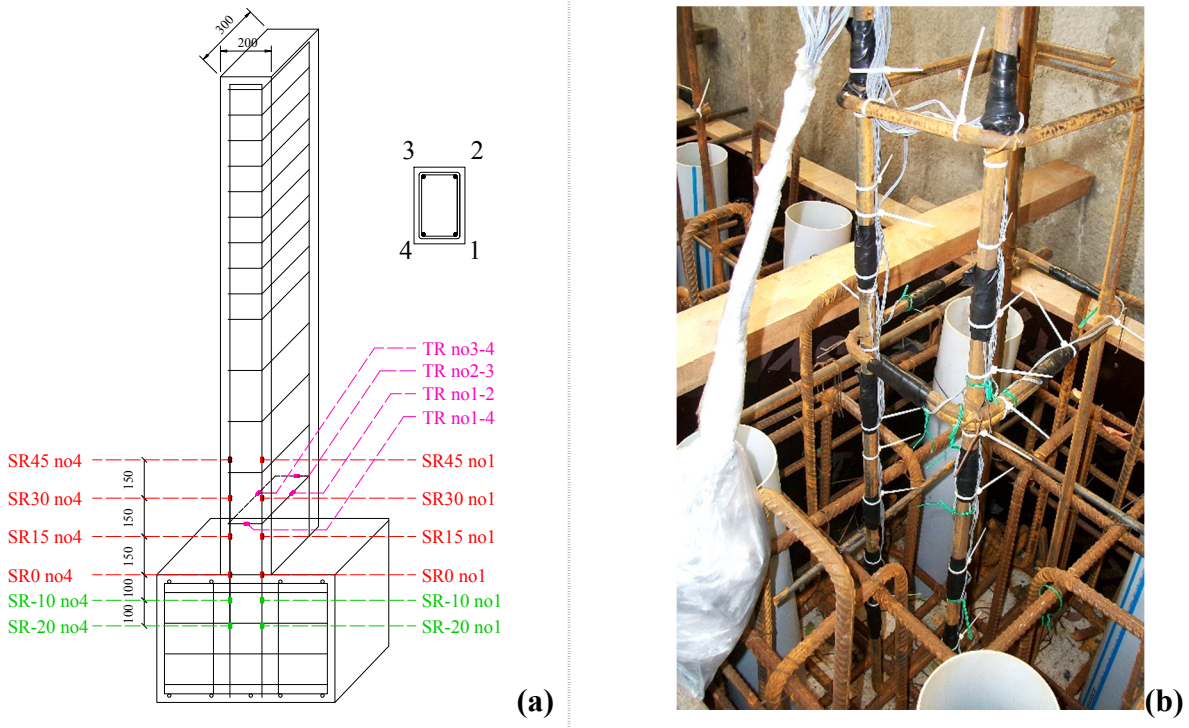

Figure 2.17 : Positions of the straingauges: (a)Scheme. (b)Application.

Six straingauges were glued on each longitudinal steel bar, located in front face of the column in strong direction, where two of six straingauges are located in footing and four straingauges were glued on the transverse bars in all specimens.

Properties of straingauges used on longitudinal and transverse steel reinforcement are presented in Table 2.16 and Table 2.17, respectively.

Table 2.16 : Properties of straingauges on longitudinal steel reinforcement

Straingauges	Type of straingauge	Reinforcement position	Straingauge position	Gage factor
SR45 no1	YFLA-5-3L	Short side - right	45 cm over footing	2.11±2 %
SR30 no1	YFLA-5-3L	Short side - right	30 cm over footing	2.11±2 %
SR15 no1	YFLA-5-3L	Short side - right	15 cm over footing	2.11±2 %
SR0 no1	YFLA-5-3L	Short side - right	Right on footing	2.11±2 %
SR-10 no1	YFLA-5-3L	Short side - right	10 cm in footing	2.11±2 %
SR-20 no1	YFLA-5-3L	Short side - right	20 cm in footing	2.11±2 %
SR45 no4	YFLA-5-3L	Short side - left	45 cm over footing	2.11±2 %
SR30 no4	YFLA-5-3L	Short side - left	30 cm over footing	2.11±2 %
SR15 no4	YFLA-5-3L	Short side - left	15 cm over footing	2.11±2 %
SR0 no4	YFLA-5-3L	Short side - left	Right on footing	2.11±2 %
SR-10 no4	YFLA-5-3L	Short side - left	10 cm in footing	2.11±2 %
SR-20 no4	YFLA-5-3L	Short side - left	20 cm in footing	2.11±2 %

Table 2.17 Properties of straingauges on transverse steel reinforcement.

Straingauges	Type of straingauge	Reinforcement position	Straingauge position	Gage factor
TR no1-2	FLA-3-11-3L	20cm over footing	Long side - right	2.10±1 %
TR no1-4	FLA-3-11-3L	20cm over footing	Short side - front	2.10±1 %
TR no2-3	FLA-3-11-3L	20cm over footing	Short side - rear	2.10±1 %
TR no3-4	FLA-3-11-3L	20cm over footing	Long side - left	2.10±1 %

In order to evaluate the effectiveness of the longitudinal FRP reinforcement and its interaction with longitudinal steel rebars, straingauges were glued on to the FRP reinforcement by following the same locations used for steel rebars. The locations of the straingauges of the first, second, third and fourth group specimens are shown in Figure 2.18, Figure 2.19 and Figure 2.20, respectively.

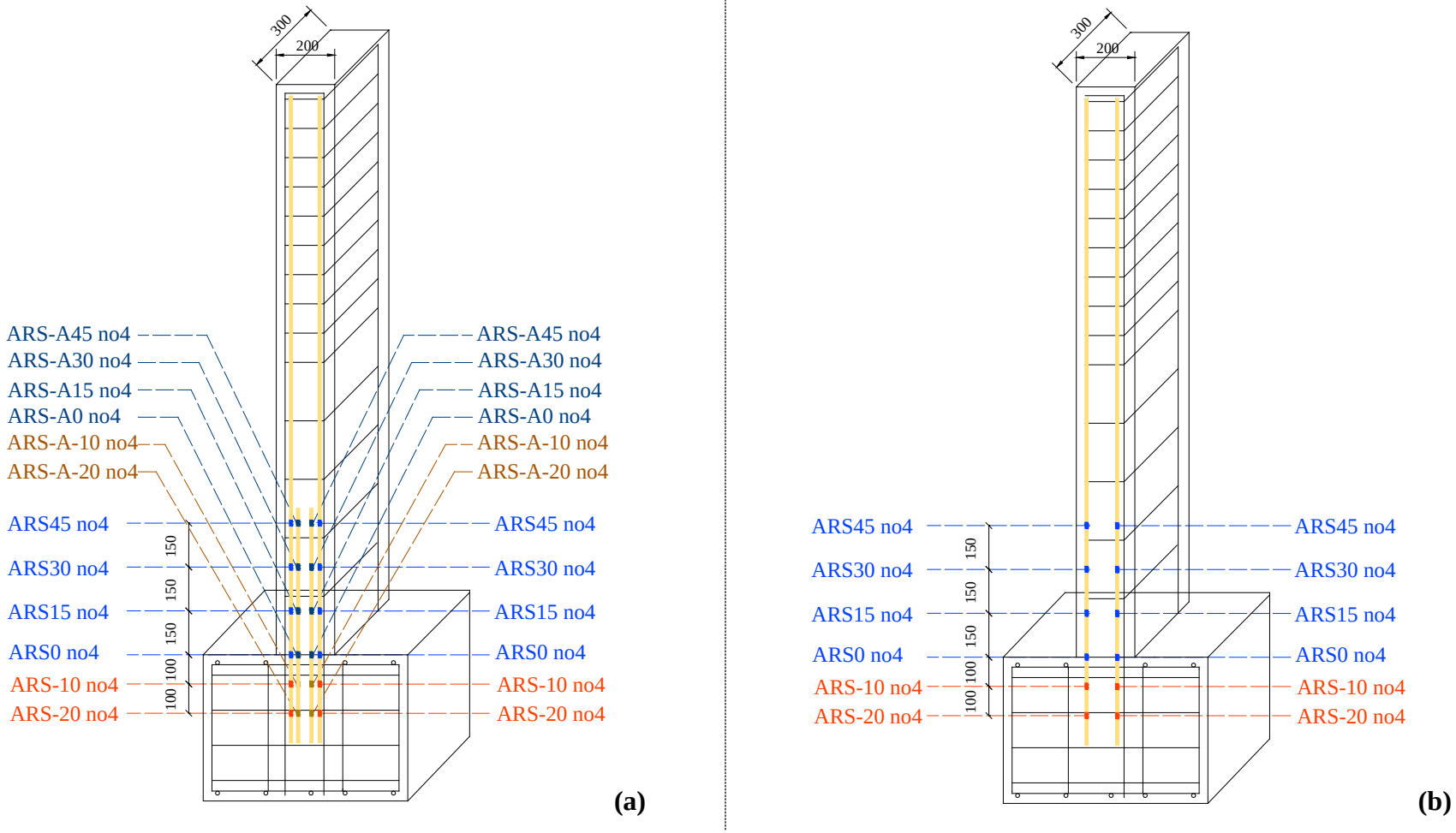

Figure 2.18 : Positions of the straingauges: (a)SD-N1-4ARS. (b)SD-N1-2ARS and SD-N1-2ARS-PB.

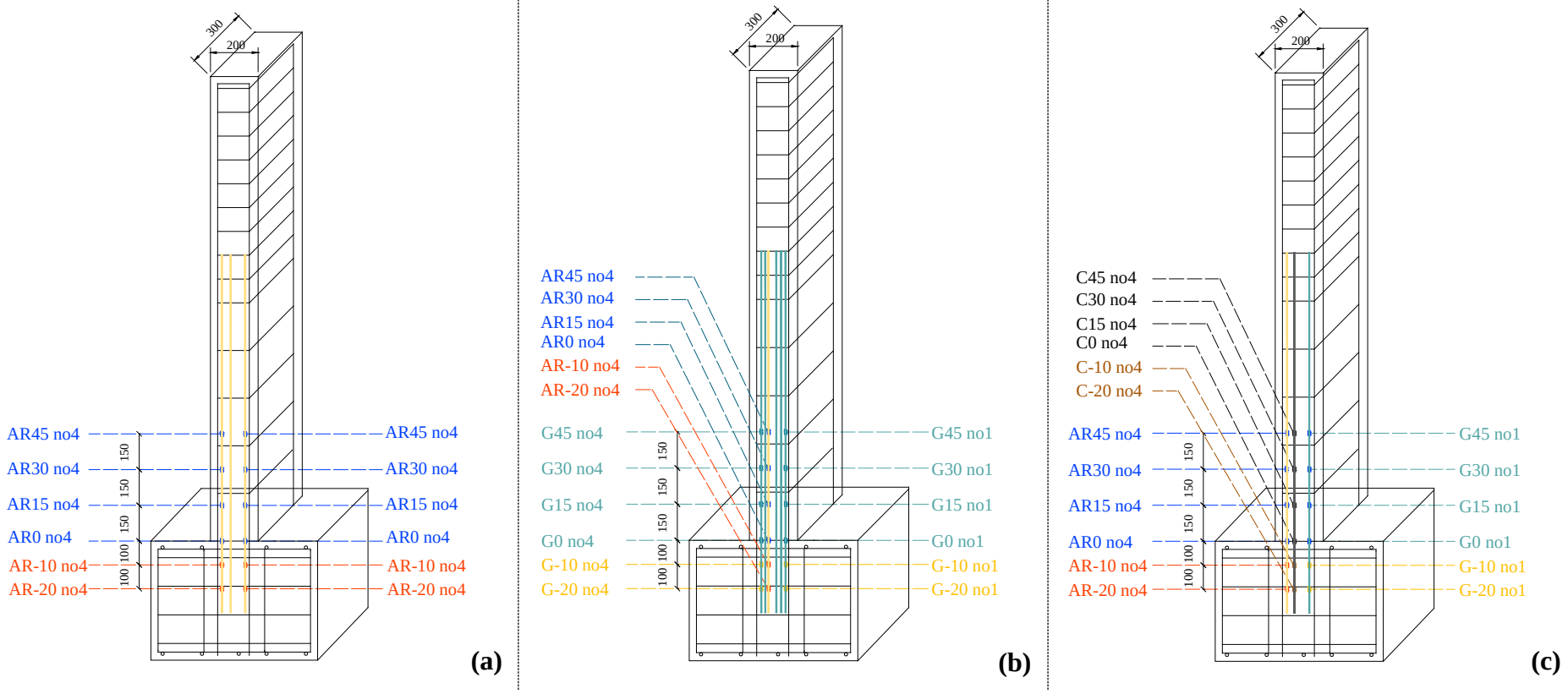

Figure 2.19 : Positions of the straingauges: (a)SD-N1-3AR. (b)SD-N1-1AR5G. (c)SD-N1-1AR1C1G.

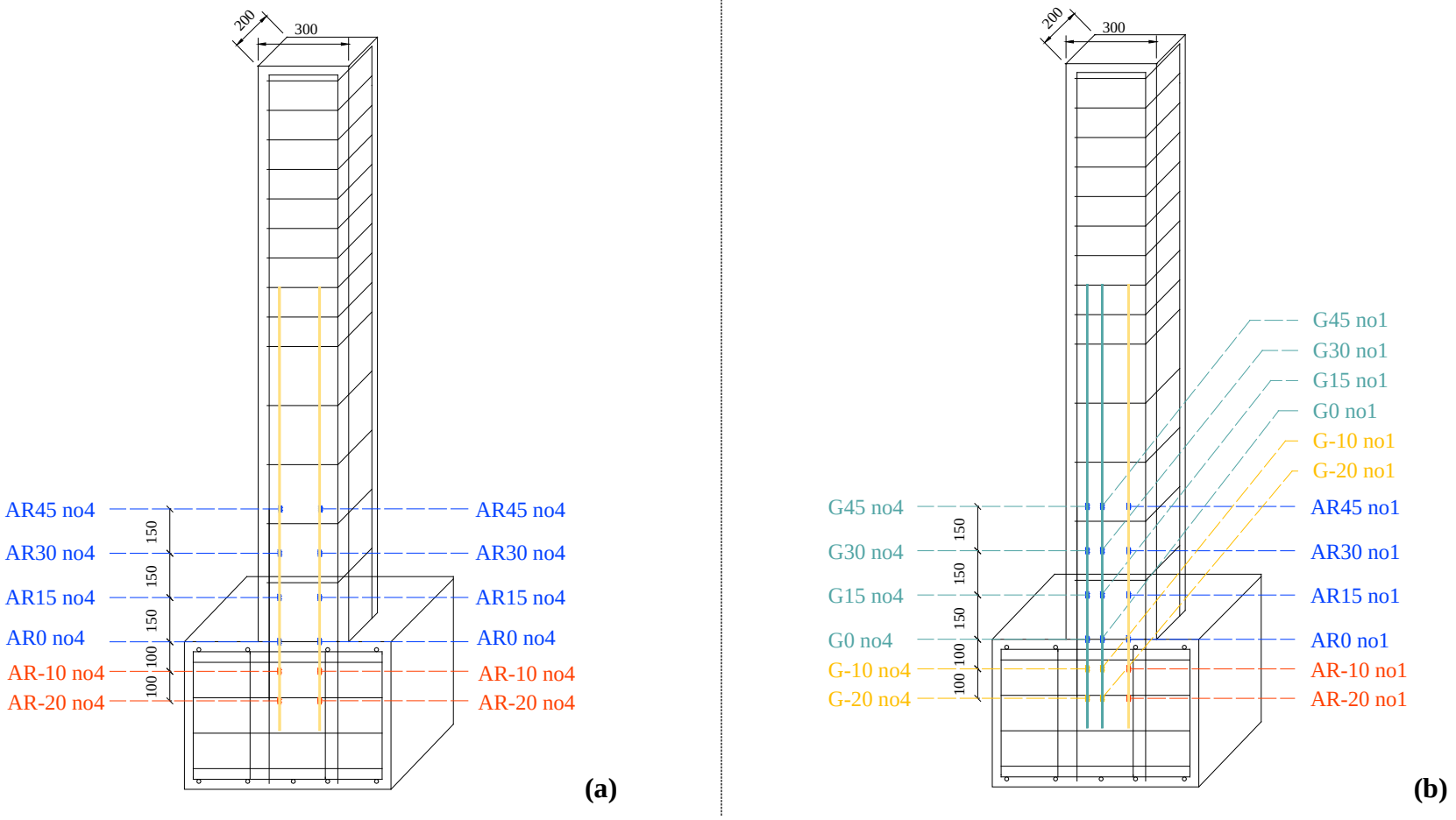

Figure 2.20 : Positions of the straingauges: (a)WD-N1-2AR, WD-N1-2AR-P1 and WD-N1-2AR-P2. (b)WD-N1-1AR2G.

Properties of straingauges used on longitudinal FRP reinforcement are presented in Table 2.18, Table 2.19, Table 2.20, Table 2.21, and Table 2.22.

Table 2.18 : Properties of straingauges on longitudinal FRP reinforcement in specimens SD-N1-2ARS and SD-N1-2ARS-PB.

Straingauge	Type of straingauge	FRP Reinforcement	Straingauge position	Gage factor
ARS45 no1	YFLA-5-3L	AFRP - right	45cm over footing	2.10±2 %
ARS30 no1	YFLA-5-3L	AFRP - right	30cm over footing	2.10±2 %
ARS15 no1	YFLA-5-3L	AFRP - right	15cm over footing	2.10±2 %
ARS0 no1	YFLA-5-3L	AFRP - right	Right on footing	2.10±2 %
ARS-10 no1	YFLA-5-3L	AFRP - right	10cm in footing	2.10±2 %
ARS-20 no1	YFLA-5-3L	AFRP - right	20cm in footing	2.10±2 %
ARS45 no4	YFLA-5-3L	AFRP - left	45cm over footing	2.10±2 %
ARS30 no4	YFLA-5-3L	AFRP - left	30cm over footing	2.10±2 %
ARS15 no4	YFLA-5-3L	AFRP - left	15cm over footing	2.10±2 %
ARS0 no4	YFLA-5-3L	AFRP - left	Right on footing	2.10±2 %
ARS-10 no4	YFLA-5-3L	AFRP - left	10cm in footing	2.10±2 %
ARS-20 no4	YFLA-5-3L	AFRP - left	20cm in footing	2.10±2 %

Table 2.19 : Properties of straingauges on longitudinal FRP reinforcement in specimen SD-N1-4ARS.

Straingauge	Type of straingauge	FRP Reinforcement	Straingauge position	Gage factor
ARS45 no1	YFLA-5-3L	AFRP - right	45cm over footing	2.10±2 %
ARS30 no1	YFLA-5-3L	AFRP - right	30cm over footing	2.10±2 %
ARS15 no1	YFLA-5-3L	AFRP - right	15cm over footing	2.10±2 %
ARS0 no1	YFLA-5-3L	AFRP - right	Right on footing	2.10±2 %
ARS-10 no1	YFLA-5-3L	AFRP - right	10cm in footing	2.10±2 %
ARS-20 no1	YFLA-5-3L	AFRP - right	20cm in footing	2.10±2 %
ARS45 no4	YFLA-5-3L	AFRP - left	45cm over footing	2.10±2 %
ARS30 no4	YFLA-5-3L	AFRP - left	30cm over footing	2.10±2 %
ARS15 no4	YFLA-5-3L	AFRP - left	15cm over footing	2.10±2 %
ARS0 no4	YFLA-5-3L	AFRP - left	Right on footing	2.10±2 %
ARS-10 no4	YFLA-5-3L	AFRP - left	10cm in footing	2.10±2 %
ARS-20 no4	YFLA-5-3L	AFRP - left	20cm in footing	2.10±2 %
ARS-A45 no1	YFLA-5-3L	AFRP anchor - right	45cm over footing	2.10±2 %
ARS-A30 no1	YFLA-5-3L	AFRP anchor - right	30cm over footing	2.10±2 %
ARS-A15 no1	YFLA-5-3L	AFRP anchor - right	15cm over footing	2.10±2 %
ARS-A0 no1	YFLA-5-3L	AFRP anchor - right	Right on footing	2.10±2 %
ARS-A-10 no1	YFLA-5-3L	AFRP anchor - right	10cm in footing	2.10±2 %
ARS-A-20 no1	YFLA-5-3L	AFRP anchor - right	20cm in footing	2.10±2 %
ARS-A45 no4	YFLA-5-3L	AFRP anchor - left	45cm over footing	2.10±2 %
ARS-A30 no4	YFLA-5-3L	AFRP anchor - left	30cm over footing	2.10±2 %
ARS-A15 no4	YFLA-5-3L	AFRP anchor - left	15cm over footing	2.10±2 %
ARS-A0 no4	YFLA-5-3L	AFRP anchor - left	Right on footing	2.10±2 %
ARS-A-10 no4	YFLA-5-3L	AFRP anchor - left	10cm in footing	2.10±2 %
ARS-A-20 no4	YFLA-5-3L	AFRP anchor - left	20cm in footing	2.10±2 %

Table 2.20 : Properties of straingauges on longitudinal FRP reinforcement in specimens SD-N1-3AR, WD-N1-2AR, WD-N1-2AR-P1 and WD-N1-2AR-P2.

Straingauge	Type of straingauge	FRP Reinforcement	Straingauge position	Gage factor
AR45 no1	YFLA-5-3L	AFRP - right	45cm over footing	2.10±2 %
AR30 no1	YFLA-5-3L	AFRP - right	30cm over footing	2.10±2 %
AR15 no1	YFLA-5-3L	AFRP - right	15cm over footing	2.10±2 %
AR0 no1	YFLA-5-3L	AFRP - right	Right on footing	2.10±2 %
AR-10 no1	YFLA-5-3L	AFRP - right	10cm in footing	2.10±2 %
AR-20 no1	YFLA-5-3L	AFRP - right	20cm in footing	2.10±2 %
AR45 no4	YFLA-5-3L	AFRP - left	45cm over footing	2.10±2 %
AR30 no4	YFLA-5-3L	AFRP - left	30cm over footing	2.10±2 %
AR15 no4	YFLA-5-3L	AFRP - left	15cm over footing	2.10±2 %
AR0 no4	YFLA-5-3L	AFRP - left	Right on footing	2.10±2 %
AR-10 no4	YFLA-5-3L	AFRP - left	10cm in footing	2.10±2 %
AR-20 no4	YFLA-5-3L	AFRP - left	20cm in footing	2.10±2 %

Table 2.21 : Properties of straingauges on longitudinal FRP reinforcement in specimens SD-N1-1AR5G and WD-N1-1AR2G.

Straingauge	Type of straingauge	FRP Reinforcement	Straingauge position	Gage factor
AR45 no4	YFLA-5-3L	AFRP - left	45cm over footing	2.10±2 %
AR30 no4	YFLA-5-3L	AFRP - left	30cm over footing	2.10±2 %
AR15 no4	YFLA-5-3L	AFRP - left	15cm over footing	2.10±2 %
AR0 no4	YFLA-5-3L	AFRP - left	Right on footing	2.10±2 %
AR-10 no4	YFLA-5-3L	AFRP - left	10cm in footing	2.10±2 %
AR-20 no4	YFLA-5-3L	AFRP - left	20cm in footing	2.10±2 %
G45 no1	YFLA-5-3L	GFRP - right	45cm over footing	2.10±2 %
G30 no1	YFLA-5-3L	GFRP - right	30cm over footing	2.10±2 %
G15 no1	YFLA-5-3L	GFRP - right	15cm over footing	2.10±2 %
G0 no1	YFLA-5-3L	GFRP - right	Right on footing	2.10±2 %
G-10 no1	YFLA-5-3L	GFRP - right	10cm in footing	2.10±2 %
G-20 no1	YFLA-5-3L	GFRP - right	20cm in footing	2.10±2 %
G45 no4	YFLA-5-3L	GFRP - left	45cm over footing	2.10±2 %
G30 no4	YFLA-5-3L	GFRP - left	30cm over footing	2.10±2 %
G15 no4	YFLA-5-3L	GFRP - left	15cm over footing	2.10±2 %
G0 no4	YFLA-5-3L	GFRP - left	Right on footing	2.10±2 %

Table 2.22 Properties of straingauges on longitudinal FRP reinforcement in specimen SD-N1-1AR1C1G.

Straingauge	Type of straingauge	FRP Reinforcement	Straingauge position	Gage factor
AR45 no4	YFLA-5-3L	AFRP - left	45cm over footing	2.10±2 %
AR30 no4	YFLA-5-3L	AFRP - left	30cm over footing	2.10±2 %
AR15 no4	YFLA-5-3L	AFRP - left	15cm over footing	2.10±2 %
AR0 no4	YFLA-5-3L	AFRP - left	Right on footing	2.10±2 %
AR-10 no4	YFLA-5-3L	AFRP - left	10cm in footing	2.10±2 %
AR-20 no4	YFLA-5-3L	AFRP - left	20cm in footing	2.10±2 %
G45 no1	YFLA-5-3L	GFRP - right	45cm over footing	2.10±2 %
G30 no1	YFLA-5-3L	GFRP - right	30cm over footing	2.10±2 %
G15 no1	YFLA-5-3L	GFRP - right	15cm over footing	2.10±2 %
G0 no1	YFLA-5-3L	GFRP - right	Right on footing	2.10±2 %
G-10 no1	YFLA-5-3L	GFRP - right	10cm in footing	2.10±2 %
G-20 no1	YFLA-5-3L	GFRP - right	20cm in footing	2.10±2 %
C45 no4	YFLA-5-3L	CFRP - left	45cm over footing	2.10±2 %
C30 no4	YFLA-5-3L	CFRP - left	30cm over footing	2.10±2 %
C15 no4	YFLA-5-3L	CFRP - left	15cm over footing	2.10±2 %
C0 no4	YFLA-5-3L	CFRP - left	Right on footing	2.10±2 %
C-10 no4	YFLA-5-3L	CFRP - left	10cm in footing	2.10±2 %
C-20 no4	YFLA-5-3L	CFRP - left	10cm in footing	2.10±2 %

2.4 Loading History

A displacement based loading history was used for all specimens. Reversed lateral displacements were applied for pushing and pulling cycles to the specimens to simulate the seismic loading. Drift ratios (d/L) were calculated as the ratio of the lateral displacement of the tip of the column (d), to the column length (L). Loading history of the specimens are shown in Figure 2.21. The loading history was composed of excursions at certain drift ratios ±0.0010 (±1.650 mm), ±0.0025 (±4.125 mm), ±0.0050 (±8.250 mm), ±0.0100 (±16.5 mm), ±0.0200 (±33.0 mm), ±0.0300 (±49.5 mm), ±0.0400 (±66 mm), ±0.0600 (±99 mm), ±0.0800 (±132 mm)), for pushing and pulling cycles.

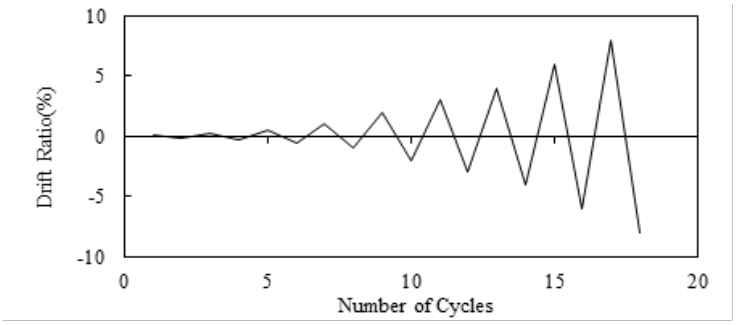

Figure 2.21 : Loading history of specimens.

3. SPECIMEN PREPARATION

Preparation of specimens were started at 08.10.2011 at ITU Structural and Earthquake Engineering Laboratory. After finishing steel reinforcement work, formwork and gluing of straingauges, concreting of footings and columns were finished at 02.11.2011.

3.1 Construction of Footings

Wooden formworks were prepared for the footings of specimens as first step of specimen manufacture. Afterwards, steel reinforcement cages were constructed and placed in the formworks. Construction phases of the footings are shown in Figure 3.1.

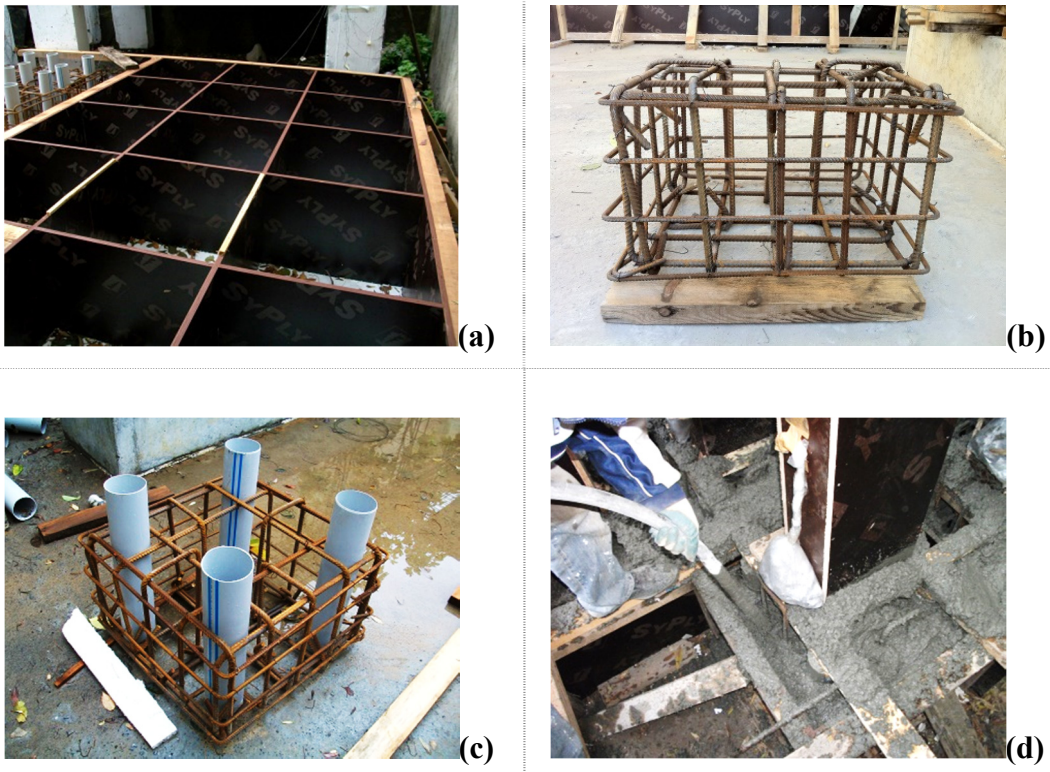

Figure 3.1 : Construction of footings: (a)Formwork. (b)Reinforcement cage. (c)PVC pipe installment. (d)Vibration during concreting.

Four PVC pipes, 70 mm in diameter, were placed in footing reinforcement cage in order to anchor the specimen to adaptor footing. The bottom extension of the four hooks, which were intended to be used in transportation of the specimens were placed under the reinforcement cage. Betonsa A.Ş. cast the concrete for the footing at 02.11.2011. Four standard cylinder specimens (150×300 mm) were taken for 28th day compressive strength tests, during the casting of concrete of footings. Electrical vibration equipment was used during concreting for better compaction. Curing was applied for seven days after casting of concrete. Specimens were cured with water twice a day, once in the morning and once in the evening.

3.2 Construction of Columns

Steel reinforcement cages were constructed and fixed on to the reinforcement cage of the footings. Straingauges were glued carefully as previously explained in details and wooden formworks were constructed and placed precisely (Figure 3.2). Concrete were placed in single step at 02.11.2011 including the footings.

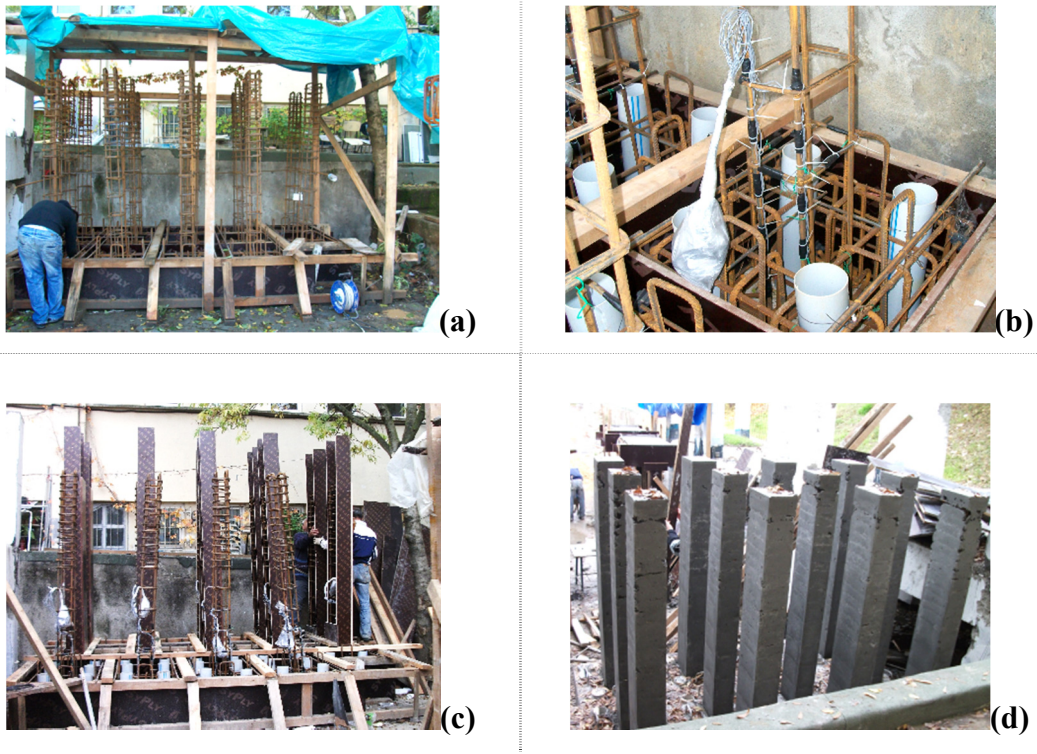

Figure 3.2 : Construction of columns: (a)Reinforcement cage. (b)Straingauges. (c)Formwork installation. (d)Overview of specimens after demolding.

Vibration was done for proper compaction of the concrete. 20 standard cylinder specimens were taken for 28th day and further compressive strength tests, during the casting of concrete. Six individual slump tests were done during concreting, the average value was obtained as 12.50 cm. Columns, and footings were cured by using water for seven days.

3.3 Retrofit of Specimens

In the scope of this study, 10 specimens were repaired and retrofitted systematically in İ.T.Ü. Structural Engineering and Earthquake Laboratory. As a part of the experimental study plan, three specimens were repaired and retrofitted by using different anchorage techniques to determine the most effective application method to be utilized for the remaining specimens. All columns, including the first group specimens, were repaired by following the same procedure, while retrofitting details varied depending on the type and kind of the FRP reinforcement.

As first step of repair application, loose concrete cover was removed from whole columns surfaces excluding footings by using hand held impact breakers (Figure 3.3).

Figure 3.3 : Removal of loose concrete cover by impact breaking.

Longitudinal reinforcement and transverse steel reinforcement were exposed completely and cleaned by using steel brushes. For the sake of simplicity and as a necessity of practice conical anchorage holes were dug right after removing the concrete cover, which makes easier to dig the holes on the footing near the column surface. Anchorage holes were dug 300 mm deep and approximately 100 mm wide at the top and 30 mm wide at the bottom along the column surface in the relevant direction (Figure 3.4).

Figure 3.4 : Anchorage holes on the two sides of the columns for embedding the longitudinal FRP reinforcement into the footing.

Exposed surfaces were cleaned by using high-pressure air and afterwards washed and saturated with clean water. Saturation with water was very critical to provide sufficient adhesion between structural repair mortar and concrete substrate by prevention quick loss of water in the fresh mortar, which is needed for hydration. MasterEmaco S 488, which is cement based, shrinkage compensated, high strength thixotropic repair mortar was applied to the column surfaces by using trowel. Application thickness varied between 20 – 30 mm depending on the substrate profile. Repair mortar was applied to cover the transverse reinforcement and create a sound substrate for bonding FRP longitudinal reinforcement (Figure 3.5).

Figure 3.5 : Levelling column surfaces with structural repair mortar.

3.3.1 First group specimens

Three specimens were retrofitted by utilizing AFRP strips in longitudinal direction as additional flexural reinforcement. AFRP strips were cut according to calculated geometry (42 mm x 2300 mm) and straingauges were glued as described in previous sections (Figure 3.6).

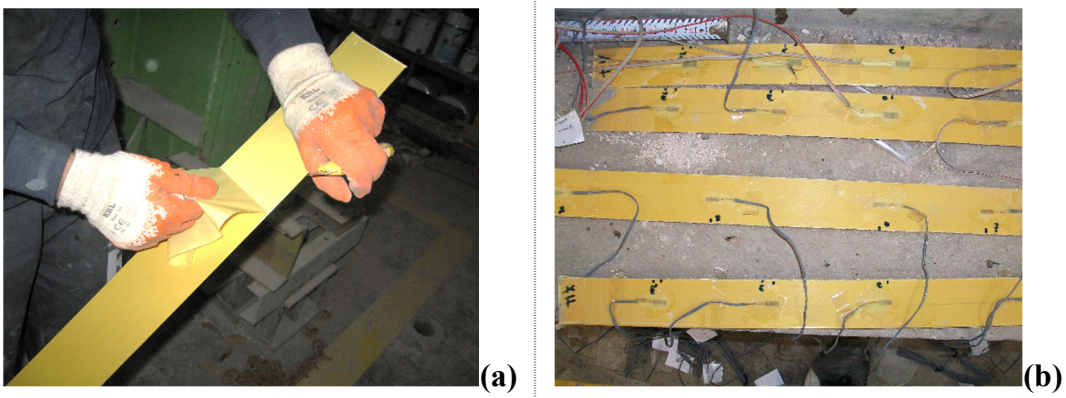

(a) **(b)**

Figure 3.6 : Preparation of AFRP reinforcement: (a)Removing peel ply on the AFRP strips. (b)Glued straingauges on the precut AFRP strips.

AFRP strips were bonded to the surfaces by using a high performance epoxy based pasty adhesive, which guarantees perfect load transfer between repair mortar and AFRP reinforcement (Figure 3.7).

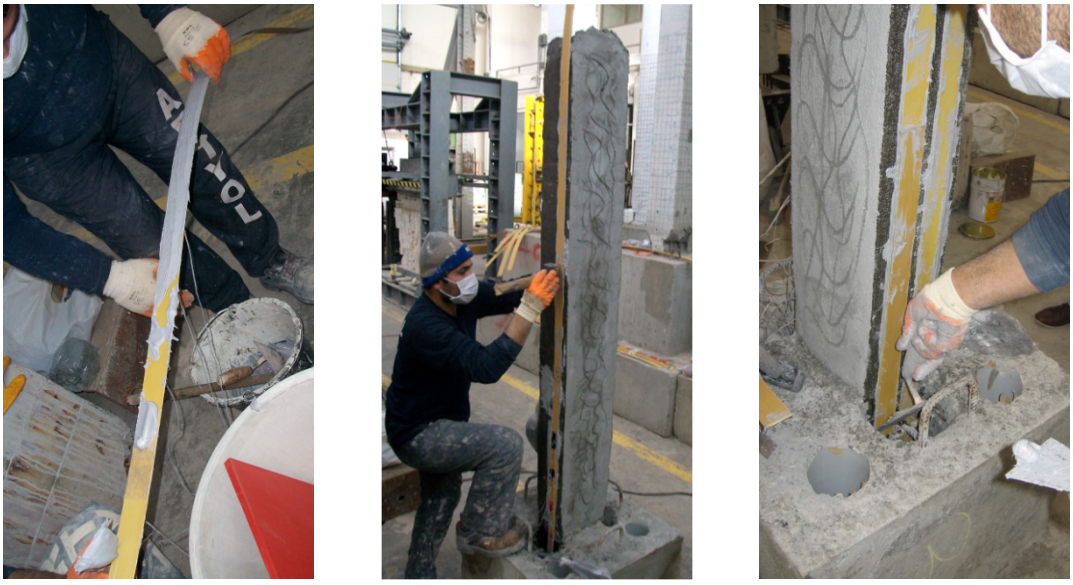

Figure 3.7 : Bonding AFRP strips on columns surfaces.

Differently from the specimens SD-N1-2ARS and SD-N1-2ARS-PB, 2 additional AFRP strips, which have the same geometry with longitudinal AFRP reinforcement were installed as additional anchorages in specimen SD-N1-4ARS (Figure 3.8).

Figure 3.8 : Embedding additional AFRP strips into anchorage holes.

An adhesive tape was used to create an isolated section on the AFRP strips, which would be stayed debonded in the anchorage hole for the specimen SD-N1-2ARS-PB (Figure 3.9).

Figure 3.9 : Partially isolated AFRP anchors.

Three-component, non-shrink epoxy grout was used to fill the anchorage holes and fix the anchorages structurally to the foundation (Figure 3.10).

Figure 3.10 : Filling anchorages holes with high performance epoxy grout.

After epoxy adhesive and epoxy grout fully cured (7 days at 23 ^{o}C), an epoxy based primer applied on to the columns surfaces and AFRP strips to create a structural bonding bridge between AFRPs and upcoming structural repair mortar. Whole columns surface was re-profilled with same structural repair mortar to obtain the original dimensions (200 mm x 300 mm) of the column cross section (Figure 3.11).

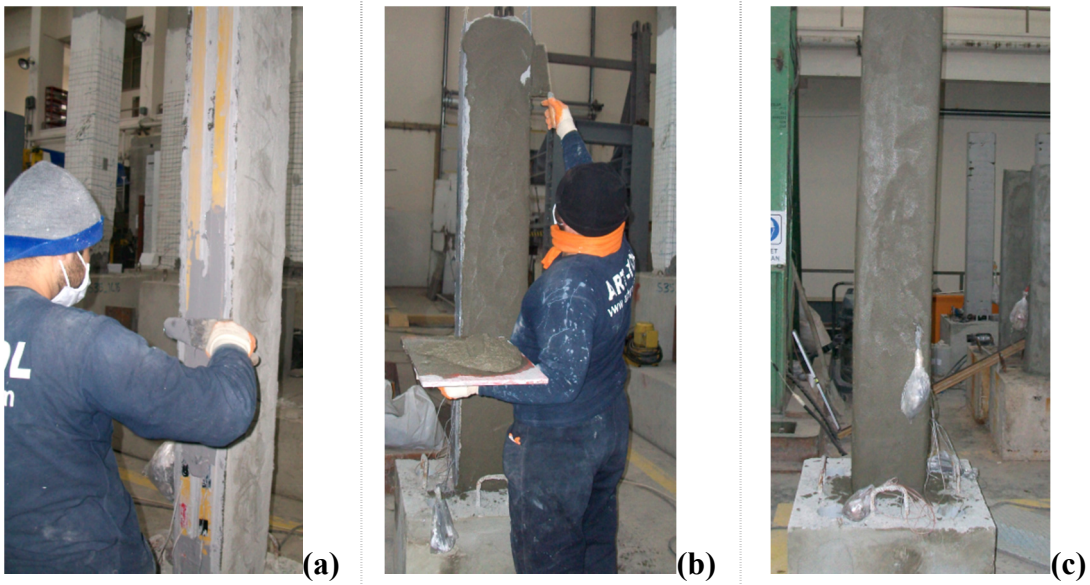

Figure 3.11 : Retfotting columns: (a)Applying epoxy primer on column surfaces. (b)Reprofilling column surface with SRM. (c)Reprofilled column prior to FRP confinement.

After levelling columns' surfaces with SRM and bring them back to their original dimensions, 7 days waited for curing of SRM. Specimens were wrapped with high strength type CFRP sheets in two layers by using a low viscous epoxy adhesive (Figure 3.12).

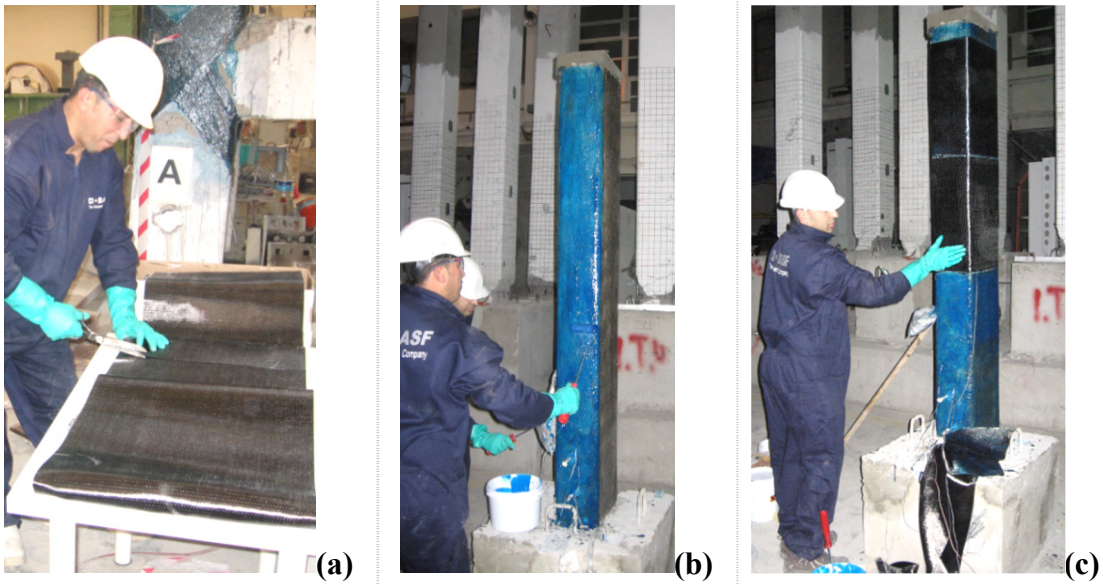

Figure 3.12 : Confinement: (a)Tailoring CFRP fabrics. (b)Applying epoxy adhesive onto the columns surface. (c)Wrapping column with CFRP fabric.

3.3.2 Second group specimens

Three specimens were retrofitted by utilizing aramid, glass and carbon FRP bars in longitudinal direction as additional flexural reinforcement. FRP bars were cut according to calculated geometry (1500 mm) and straingauges were glued as described in previous sections (Figure 3.13).

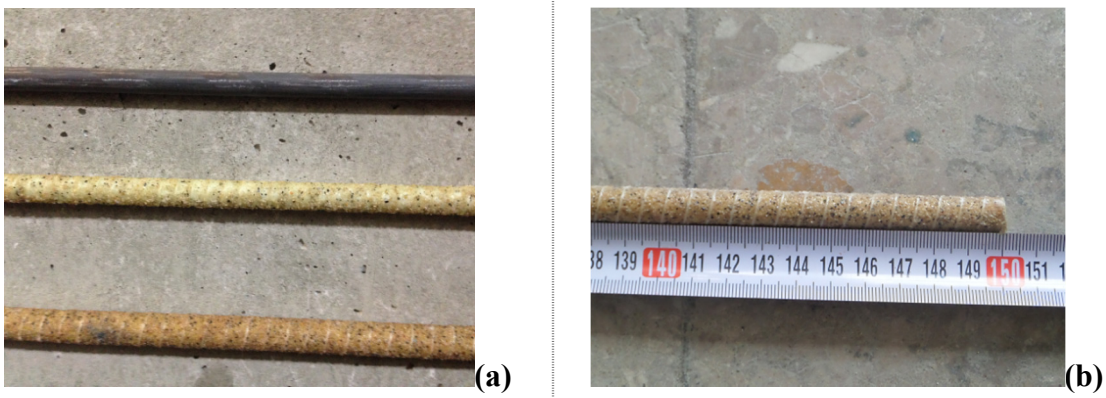

(a) (b)

Figure 3.13 : FRP reinforcement: (a)Carbon, glass and aramide FRP bars. (b)1500 mm long pre-cut AFRP bar.

FRP bars were bonded on to the surfaces by using an epoxy based adhesive, which guarantees perfect load transfer between repair mortar and AFRP reinforcement (Figure 3.14).

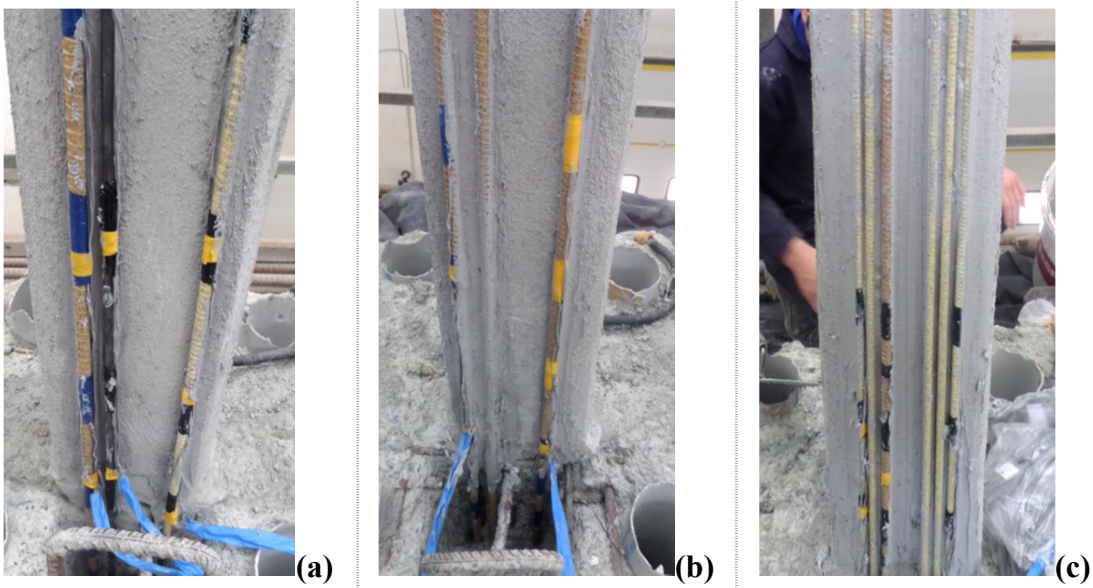

(a) (b) (c)

Figure 3.14 : Flexural retrofitting: (a)SD-N1-1AR1C1G. (b)SD-N1-3AR. (c)SD-N1-1AR5G.

Longitudinal FRP reinforcement were embedded directly into anchorage holes, which have the same geometry as the first group specimens. Anchors were designed to provide full bonding with epoxy grout, which fills the holes (Figure 3.15).

Figure 3.15 : Filling anchorages holes with high performance epoxy grout.

This anchoring method was chosen after evaluating the test results of first group specimens. Direct embedment of the longitudinal FRP reinforcement into the footing with full bonding was observed the most effiticent way of anchoring. After installing longitudinal FRP bars on the specimens, column surfaces were reprofilled with SRM and confined with CFRP sheets as it was done for first group specimens.

3.3.3 Third group specimens

Two pre-damaged specimens were repaired by using SRM and retrofitted by utilizing AFRP bars in longitudinal direction as additional flexural reinforcement (Figure 3.16).

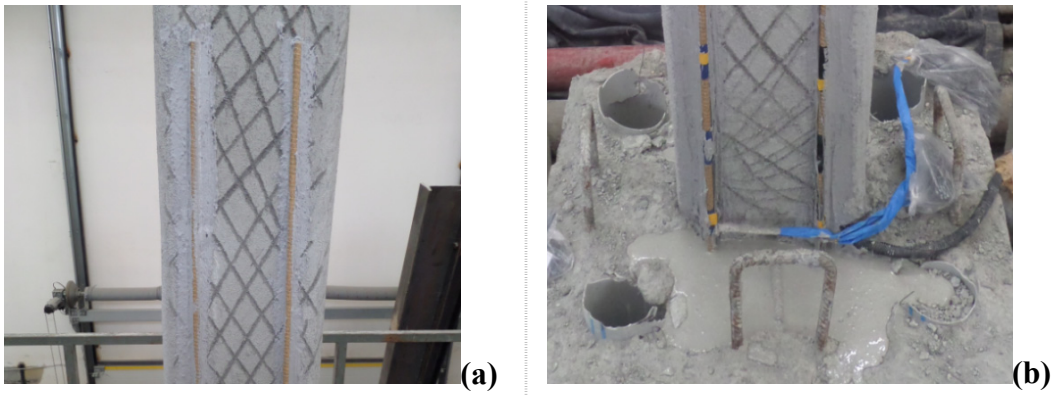

(a) **(b)**

Figure 3.16 : AFRP reinforcement: (a)Applied on the surface. (b)Anchored into footing.

AFRP bars were cut according to calculated geometry (1500 mm) and straingauges were glued as described in previous sections. AFRP bars were bonded to the relevant surfaces (long sides of the columns) by using a high performance epoxy based pasty adhesive (Figure 3.16a). Longitudinal FRP reinforcement were embedded directly into the conical holes, which were dug along the long sides of the columns (Figure 3.16b). Anchorages were designed and applied to provide full bonding with anchoring mortar (epoxy grout). After installing longitudinal FRP bars on the specimens, column surfaces were reprofilled with SRM and confined with CFRP sheets as it was done for first and second group specimens.

The remaining two specimens were repaired by using SRM and retrofitted by utilizing aramid and glass FRP bars in longitudinal direction as additional flexural reinforcement without any pre-damage conditiond. FRP bars were cut according to calculated geometry (1500 mm) and straingauges were glued as described in previous sections. FRP bars were bonded to the relevant surfaces (long sides of the columns) by using a high performance epoxy based pasty adhesive (Figure 3.17).

Figure 3.17 : Gluing AFRP and GFRP bars on to specimens WD-N1-1AR2G.

After gluing longitudinal FRP reinforcement, anchoring, reprofilling and confinement applications were done by using same materials and same methods, which were used for retrofitting of the previous specimens.

4. TEST RESULTS

4.1 Test Results of First Group Specimens

4.1.1 SD-N1-REF

No cracks were observed while loading to target displacements of ±1.65 mm (drift ratio 0.10 %).

First flexural crack was observed at the interface of the column and footing during loading to target displacement of 4.125 mm (drift ratio 0.25 %).

South and north views of the specimen SD-N1-REF at 0.25 % drift ratio is shown in Figure 4.1.

(a)

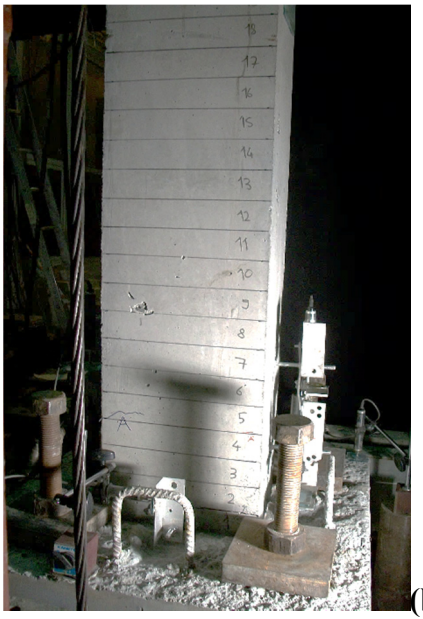

(b)

Figure 4.1 : Views of SD-N1-REF at 0.25 % drift ratio: (a)South. (b)North.

Further flexural cracks were observed 420, 570, 820 and 1020 mm above the footing during loading to target displacement of 8.25 mm (drift ratio 0.50 %). South and north views of the specimen SD-N1-REF at 0.50 % drift ratio is shown in Figure 4.2.

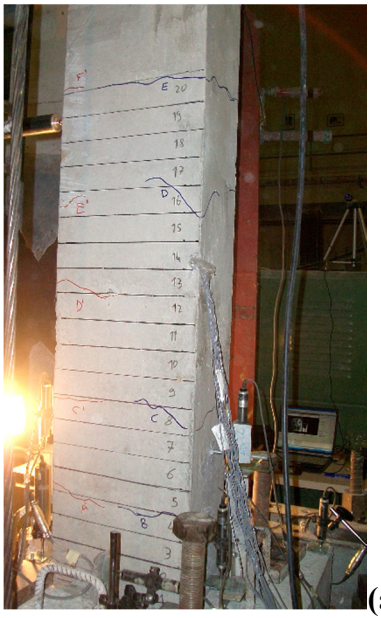
(a)

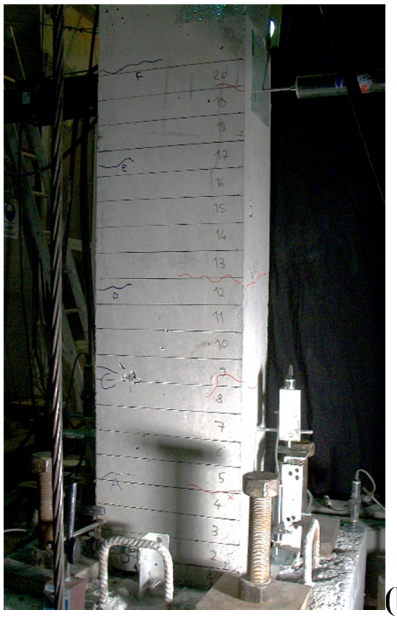
(b)

Figure 4.2 : Views of SD-N1-REF at 0.50 % drift ratio: (a)South. (b)North.

During loading to target displacement of 16.5 mm (drift ratio 1 %), flexural crack with a width of 0.6 mm formed at the column-footing interface. South and north views of the specimen SD-N1-REF at 1 % drift ratio is shown in Figure 4.3


(a)

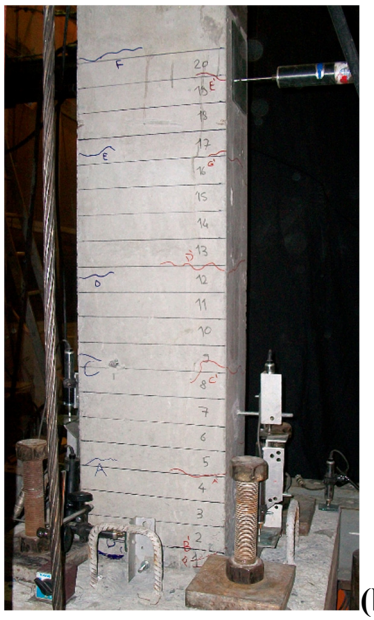
(b)

Figure 4.3 : Views of SD-N1-REF at 1 % drift ratio: (a)South. (b)North.

During loading to target displacement of 49.5 mm (drift ratio 3 %), longitudinal steel reinforcement started to yield, while stirrups were not yielded. At this point, concrete cover started to spall and the crack width at the column-footing interface reached to

2.5 mm. South and north views of the specimen SD-N1-REF at 1 % drift ratio is shown in Figure 4.4.

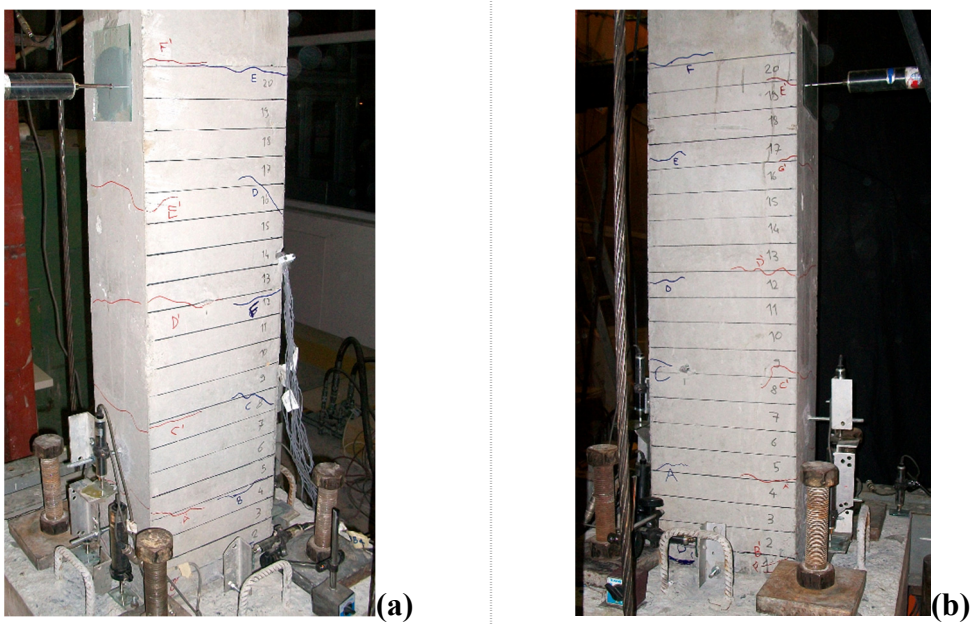

(a) (b)

Figure 4.4 : Views of SD-N1-REF at 3 % drift ratio: (a)South. (b)North.

As the testing progressed, concrete cover continued to spall and crushed at the column-footing interface. The major carck at this location continuted to widen and reached to 5 mm and 12 mm at the drift ratios 4 % and 6 % respectively. At the drift ratio 8 %, concrete cover and partially core were crushed as it is shown in Figure 4.5.

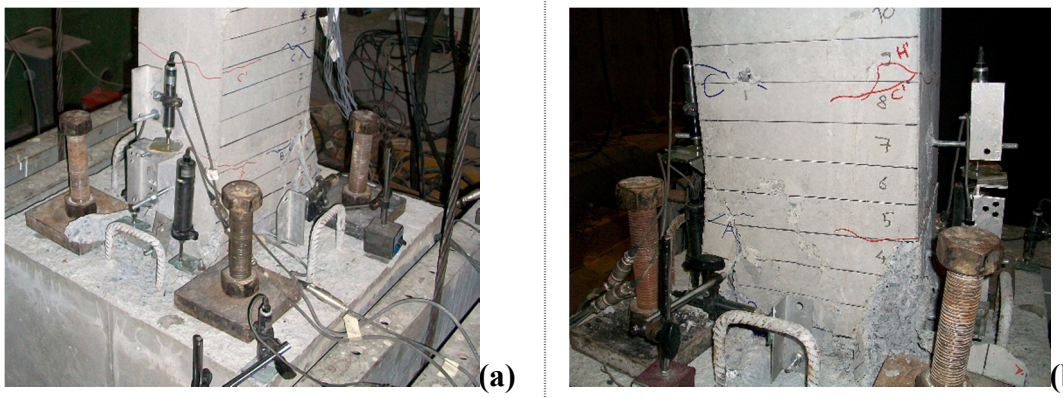

(a) (b)

Figure 4.5 : Views of SD-N1-REF at 8.00 % drift ratio: (a)South. (b)North.

Summary of the seismic behavior of specimen SD-N1-REF is shown in Table 4.1.

Table 4.1 : Summary of the seismic behavior of SD-N1-REF.

Drift ratio (%)	δ (mm/mm)	P (kN)	Observations
0.10	±1.65	4.15 / -5.60	No crack was observed
0.25	±4.125	8.20 / -10.65	First flexural crack was observed
0.50	±8.25	11.68 / -14.18	Further flexural cracks were observed
1.0	±16.5	14.65 / -18.35	Flexural crack at column-footing interface was observed
2.0	±33.0	19.60 / -24.08	Propagation of existing crack at column-footing interface was observed
3.0	±49.5	20.28 / -24.30	Crushing and spalling started at the concrete cover
4.0	±66.0	20.75 / -23.75	Propagation of existing cracks was observed
6.0	±99.0	18.43/ -21.23	Propagation of existing cracks was observed
8.0	±132.0	9.08 / -17.55	Vertical cracks were observed

Residual deformation was calculated as 118.1 mm when lateral load was absolute zero. Experimental and theoretical force-displacement relationships of SD-N1-REF is presented in Figure 4.6. First flexural crack, first yielding point of longitudinal steel reinforcement and maximum strain on the steel rebar are marked on the figure.

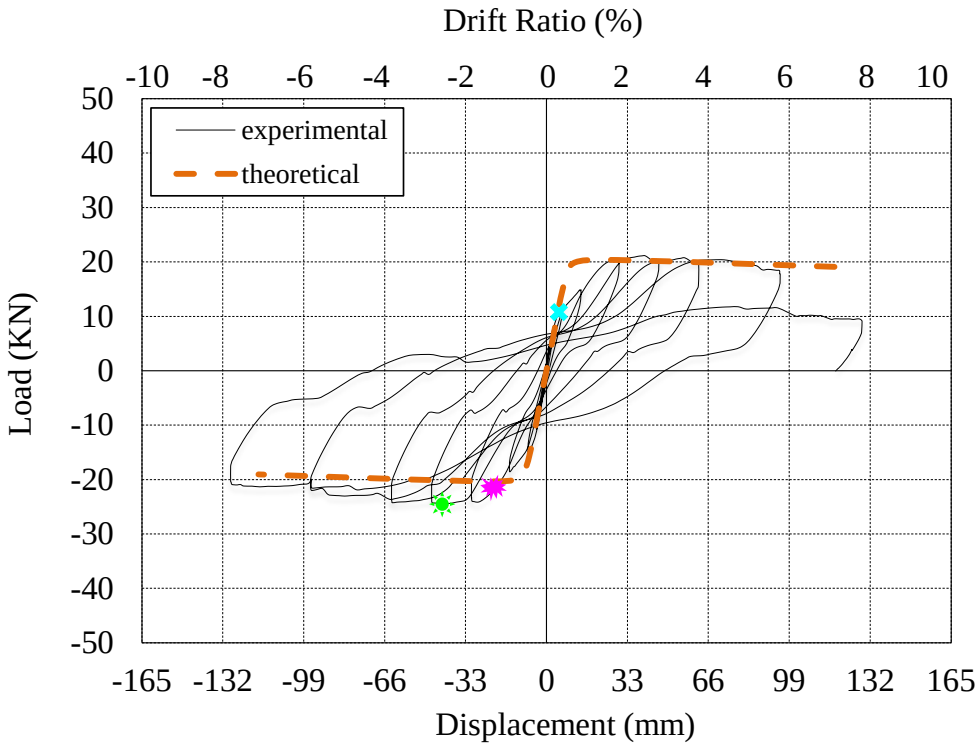

Figure 4.6 : Lateral load versus displacement for SD-N1-REF.

Moment-curvature relationships were obtained at different gage lengths at the potential plastic hinge zones to observe the distribution of damages, (Figure 4.7).

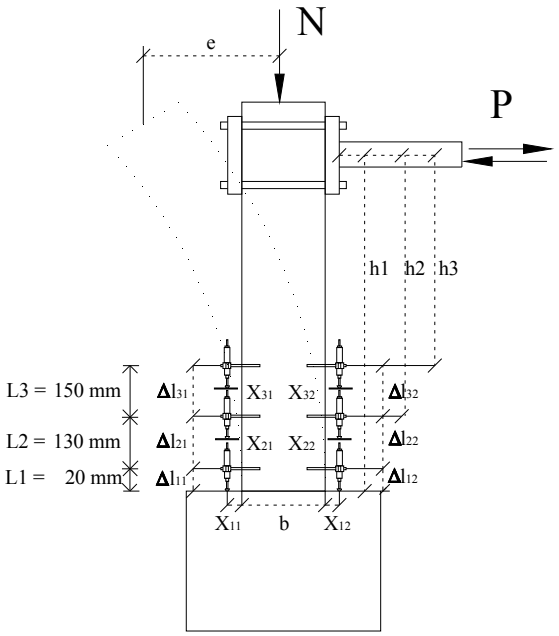

Figure 4.7 : Test setup with measurement system used in obtaining moment-curvature relationship (Göksu, 2012).

Moment-curvature relationships were calculated assuming that plane sections remain plain. Second-order effects are considered during the calculation of the moments in the selected sections by using equation 4.1 taking into account the second-order effects. In the equation, *P* is the applied lateral load, *H* is the height of the column, *N* is the axial load and *e* is the eccentricity due to horizontal displacement of the column, subjected to lateral load, *P*.

$$M = P \cdot H + N \cdot e \tag{4.1}$$

Average curvature values were determined in 20 mm, 150 mm and 300 mm above the footing for calculation of moment-curvature relationships. Curvatures were calculated by dividing the obtained strains from the LVDTs to the distance between the LVDTs as shown in equation (4.2).

$$x = \frac{\varepsilon_1 + \varepsilon_2}{b + X_{11} + X_{12}} \tag{4.2}$$

Distances between the concrete surfaces of the specimens and the LVDTs of the specimens are presented in Appendix B.

Experimental moment-curvature relationships obtained for critical sections of SD-N1-REF are presented in Figure 4.8.

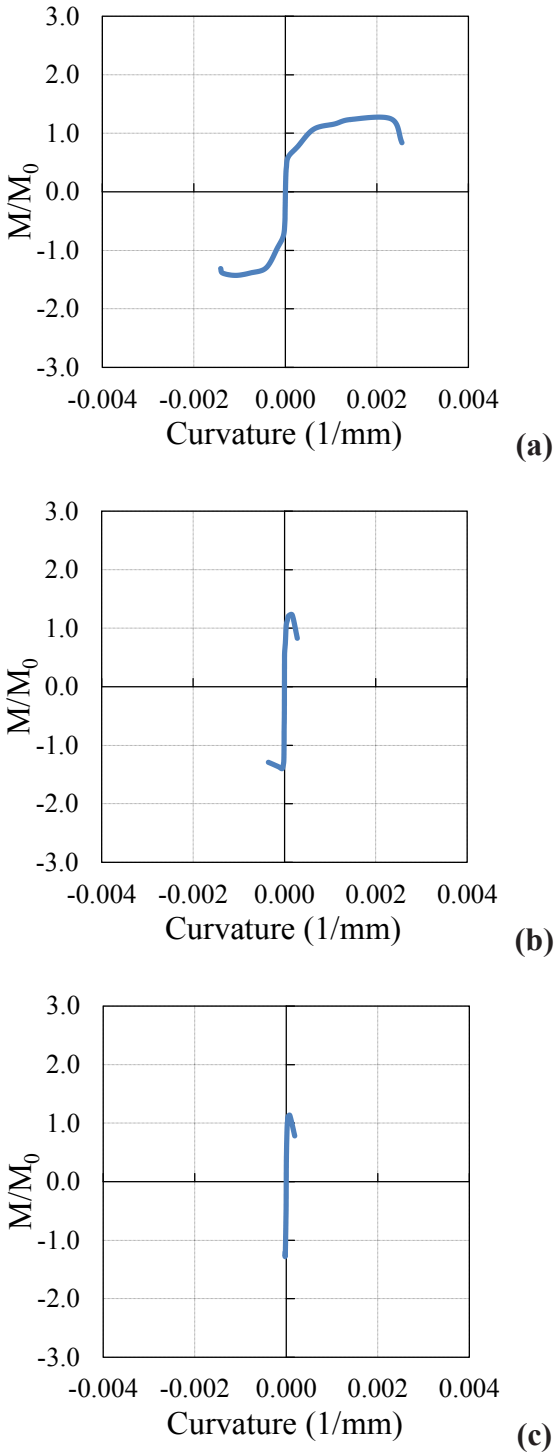

Figure 4.8 : Moment-curvature relationships obtained for gage lengths: (a)0 – 20 mm. (b)20 – 150 mm. (c)150 - 300 mm.

For the calculation of moment-curvature relationships, the average curvature values obtained for the ranges of 0-20 mm, 20-150 mm and 150-300 mm heights above the footing were taken into account. As seen from Figure 4.8, the curvature values of the member measured in 20-150 mm and 150-300 mm height above the support are in the order of 5.10^{-5} (1/mm), while the curvatures measured in 0-20 mm height are in the

order of 3.10^{-3} (1/mm). It is assessed by considering moment-curvature relationships that the damage was accumulated mainly in the first 20 mm height of the member from top of the footing, which was also confirmed with the damage pattern of the specimen.

According to the data from the straingauges on the longitudinal steel rebars of the SD-N1-REF, the maximum strain while pushing was 0.029, measured from the straingauge at +150 mm above the footing for F=-21.8 kN at -6 % drift ratio; the maximum strain while pulling was -0.0145, measured from the straingauge at +150 mm above the footing when F=16.1 kN at 6 % drift ratio. Average strain distribution of longitudinal steel rebars in different drift ratios are shown in Figure 4.9.

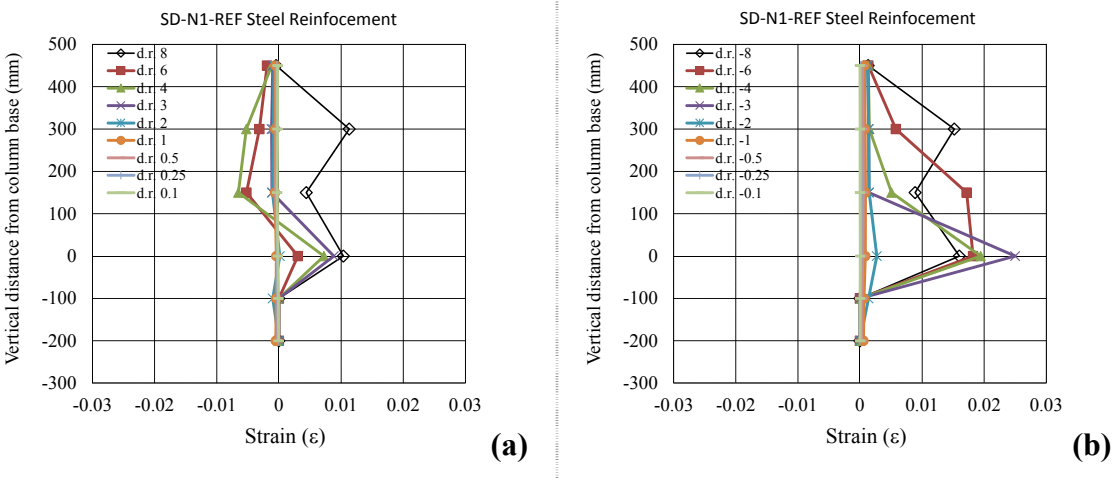

Figure 4.9 : Average strain distribution of longitudinal steel rebars of SD-N1-REF: (a)While pulling. b)While pushing.

4.1.2 SD-N1-2ARS

No cracks were observed while loading to target displacements of ±4.125 mm (drift ratio 0.25%).

First flexural crack was observed at the interface of the column and footing during loading to target displacement of 8.25 mm (drift ratio 0.50 %).

South and north views of the specimen SD-N1-2ARS at 0.50 % drift ratio is shown in Figure 4.10.

(a)

(b)

Figure 4.10 : Views of SD-N1-2ARS at 0.50 % drift ratio: (a)South. (b)North.

It was observed that all longitudinal steel reinforcement were yielded between 2 % and 3 % drift ratios, while stirrups were not yielded. While pushing towards -3 % drift ratio, a loud noice coming from the specimen was recorded with a sudden decrease in the lateral load. The reason of the sound was found as Fracture of the AFRP longitudinal reinforcement. This behaviour was repeated while pulling the column towards 3 % drift ratio. From this point forward, the specimen SD-N1-2ARS performed much similar to specimen SD-N1-REF in terms of load-displacement relation. No additional cracks were observed in further drift ratios, while the existing cracks at the column-footing interface were continously enlarged. At 8 % drift ratio the crack opening was measured 20 mm. South and north view of specimen SD-N1-2ARS after 8 % drift ratio are shown in Figure 4.11.

Residual deformation was calculated as 73.0 mm when lateral load was absolute zero. Until AFRP reinforcement fracture, measured lateral loads were significantly higher comparing to control specimen SD-N1-REF and the increase in the lateral load capacity was calculated as 38 % while pushing and 52 % while pulling compared to control specimen. AFRP reinforcement in both surfaces of the columns were fractured in the column – footing interface, where deformations were cumulated.


(a)


(b)

Figure 4.11 : Views of SD-N1-2ARS at 8 % drift ratio: (a)South. (b)North.

During the autopsy of the specimens, CFRP confinement was cut of in the first 60 cm height of the columns over footing and column surfaces was investigated for possible flexural cracks. It was seen that deformations were cumulated at the column-footing interface and no significant crack was observed through the column height. In order to confirm the Fracture pattern of the AFRP reinforcement, SRM cover around the core concrete was broken and AFRP strips were exposed. It was observed that both AFRP strips were ruptured in both sides of the column as seen in Figure 4.12.

Figure 4.12 : Fractured AFRP reinforcement in the specimen SD-N1-2ARS.

In order to confirm the continuous load transfer through the footing, epoxy grout filled in the anchorage holes were also broken in the first 10 cm depth. It was observed that

AFRP reinforcement were fully bonded in anchorage holes and no damage or slip was noticed.

Summary of the seismic behavior of specimen SD-N1-2ARS is shown in Table 4.2.

Table 4.2 : Summary of the seismic behavior of SD-N1-2ARS.

Drift ratio (%)	δ (mm/mm)	P (kN)	Observations
0.10	±1.65	4.90 / -5.40	No crack was observed
0.25	±4.125	8.95 / -9.58	No crack was observed
0.50	±8.25	13.73 / -14.45	First flexural crack at column-footing interface was observed
1.0	±16.5	19.03 / -20.98	Propagation of existing crack at column-footing interface was observed
2.0	±33.0	29.00 / -31	Propagation of existing crack at column-footing interface was observed
3.0	±49.5	32 / -33.75	AFRP reinforcement in tension Fractured and lateral load decreased to 22.65 kN
4.0	±66.0	22.85 / -28.13	Propagation of existing crack at column-footing interface was observed
6.0	±99.0	23.30/ -24.20	Propagation of existing crack at column-footing interface was observed
8.0	±132.0	22.40 / -23.48	Propagation of existing crack at column-footing interface was observed

Experimental and theoretical force-displacement relationships of SD-N1-2ARS is presented in Figure 4.13. First flexural crack, first yielding point of longitudinal steel reinforcement, maximum strain on the steel rebar and fracture of AFRP reinforcement are marked on the figure.

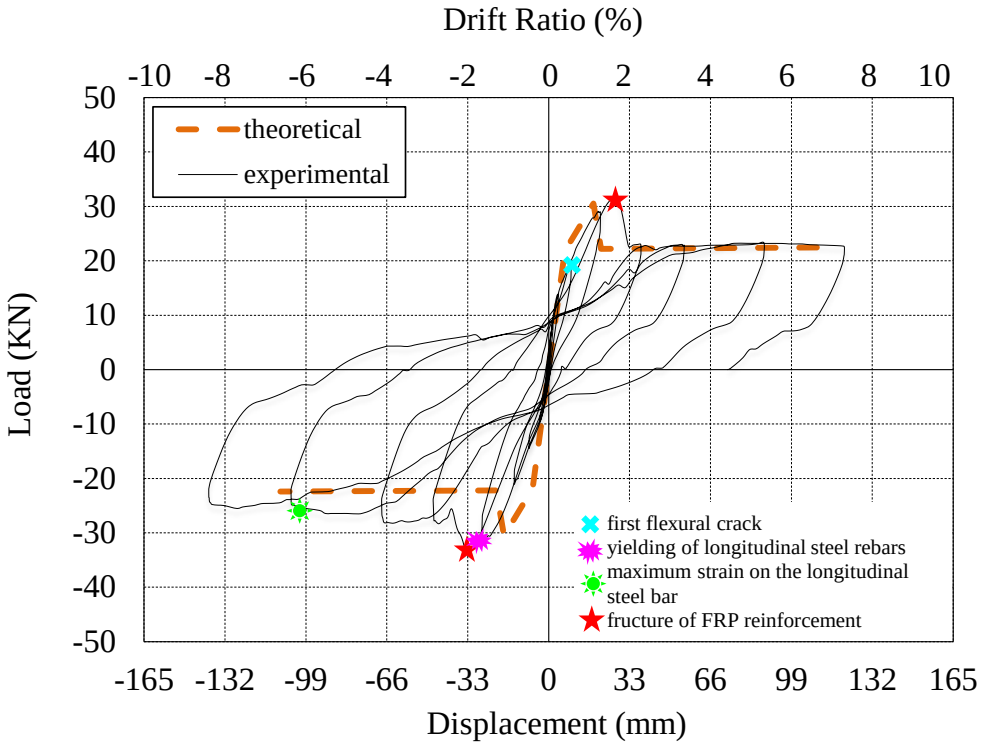

Figure 4.13 : Lateral load versus displacement for SD-N1-2ARS.

Experimental moment-curvature relationships obtained for critical sections of SD-N1-2ARS are presented in Figure 4.14

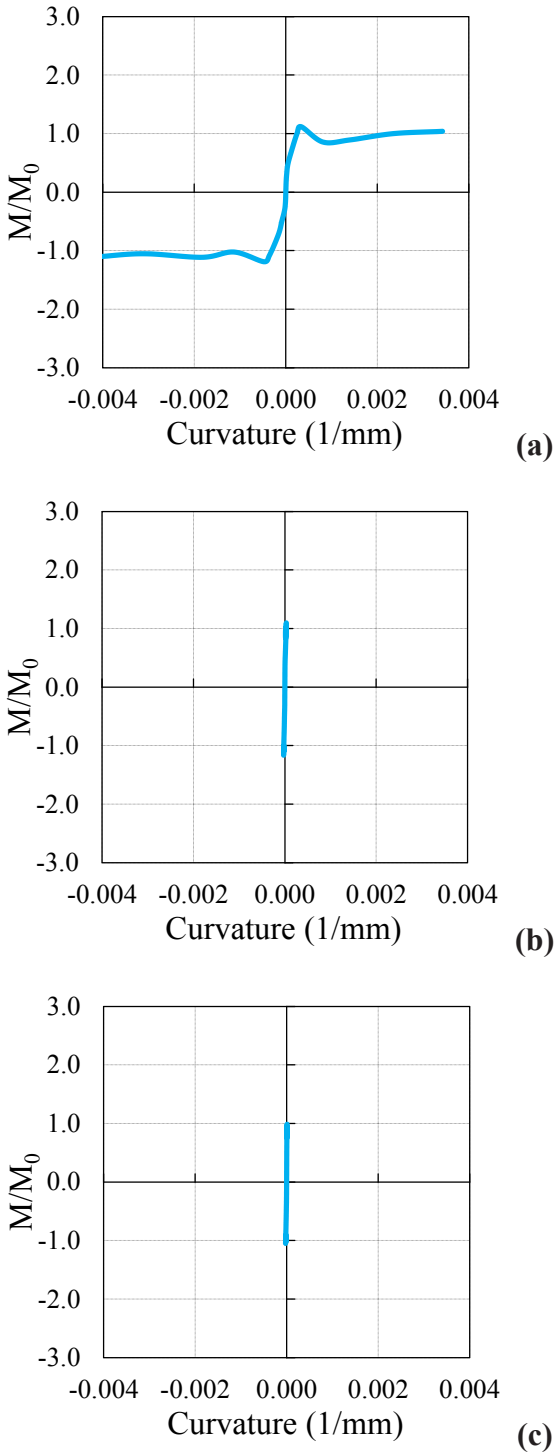

Figure 4.14 : Moment-curvature relationships obtained for gage lengths: (a)0 – 20 mm. (b)20 – 150 mm. (c)150 - 300 mm.

For the calculation of moment-curvature relationships, the average curvature values obtained for the ranges of 0-20 mm, 20-150 mm and 150-300 mm heights above the footing were taken into account. As seen from Figure 4.14, the curvature values of the

member measured in 20-150 mm and 150-300 mm height above the support are in the order of 5.10^{-5} (1/mm), while the curvatures measured in 0-20 mm height are in the order of 3.10^{-3} (1/mm). It is assessed by considering moment-curvature relationships that the damage was accumulated mainly in the first 20 mm height of the member from top of the footing, which was also confirmed with the damage pattern of the specimen.

Average strain distribution of longitudinal steel rebars and AFRP reinforcement in different drift ratios are shown in Figure 4.15 and Figure 4.16 respectively.

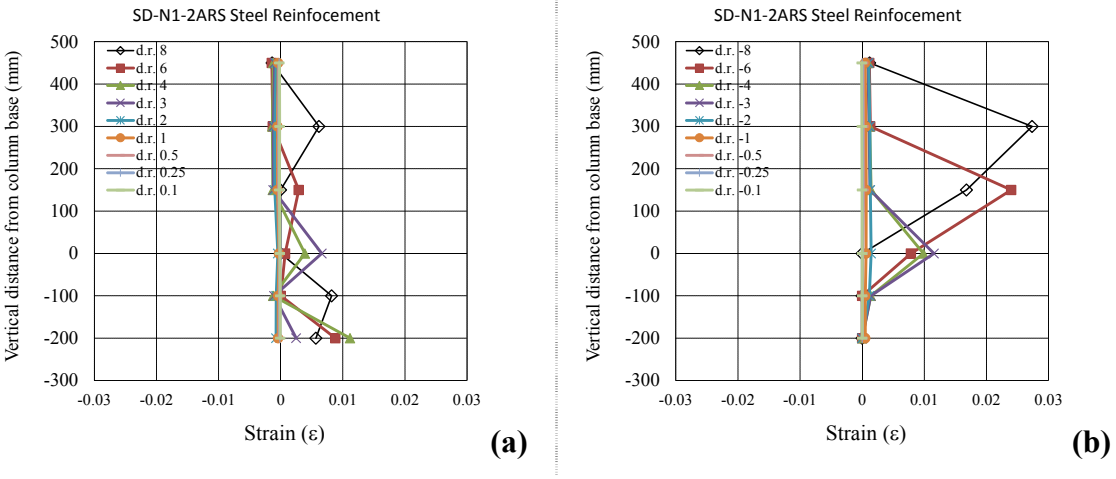

Figure 4.15 : Average strain distribution of longitudinal steel rebars of SD-N1-2ARS: (a)While pulling. (b)While pushing.

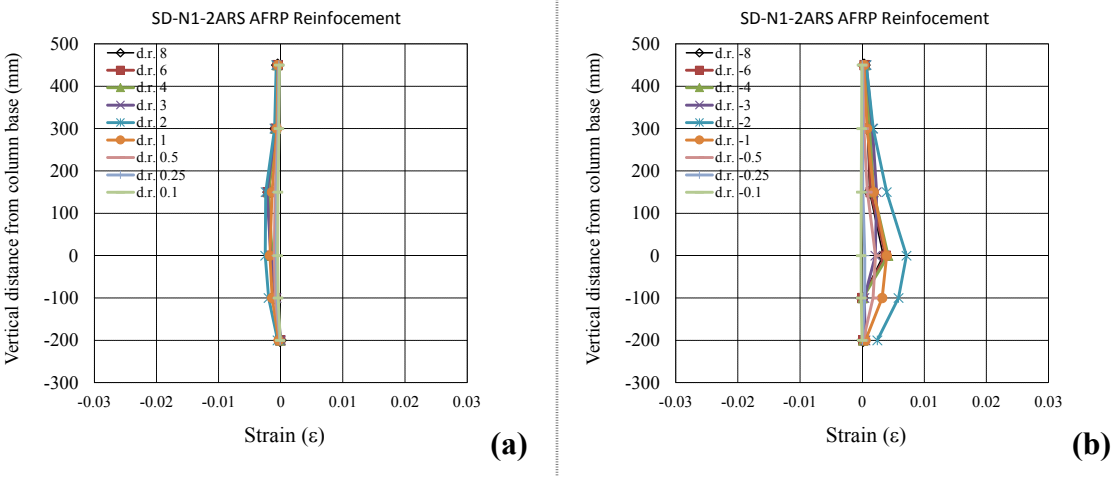

Figure 4.16 : Average strain distribution of longitudinal AFRP reinforcement of SD-N1-2ARS: (a)While pulling. (b)While pushing.

According to the data from the straingauges on the longitudinal steel rebars of the SD-N1-2ARS, the maximum strain while pushing was 0.0293, measured from the straingauge at +300 mm above the footing for F=-23.5 kN at -8 % drift ratio; the

maximum strain while pulling was -0.0145, measured from the straingauge at +300 mm above the footing when F=22.4 kN at 3 % drift ratio. Maximum strain at AFRP reinforcement was recorded as 0.01 at the column footing interface, while pushing through -3 % drift ratio at the lateral load -33.9 kN.

4.1.3 SD-N1-4ARS

No cracks were observed while loading to target displacements of ±4.125 mm (drift ratio 0.25%).

First flexural crack was observed at the interface of the column and footing during loading to target displacement of 8.25 mm (drift ratio 0.50 %).

South and north views of the specimen SD-N1-4ARS at 0.50 % drift ratio is shown in Figure 4.17.

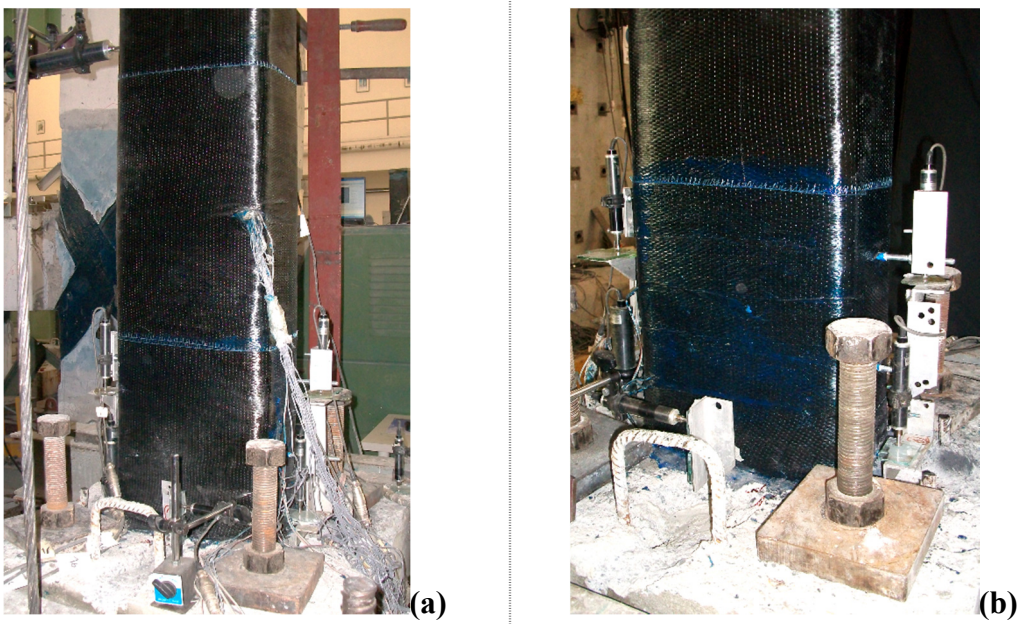

Figure 4.17 : Views of SD-N1-4ARS at 0.50 % drift ratio: (a)South. (b)North.

It was observed that all longitudinal steel reinforcement were yielded between 2 % and 3 % drift ratios, while stirrups were not yielded. While pushing towards -3 % drift ratio, a loud noice coming from the specimen was recorded with a sudden decrease in the lateral load. The reason of the sound was found as Fracture of the AFRP longitudinal reinforcement. This behaviour was repeated while pulling the column towards 3 % drift ratio. From this point forward, the specimen SD-N1-4ARS performed much similar to specimen SD-N1-REF in terms of load-displacement

relation. This behavior was very similar to specimen SD-N1-2ARS's behavior, except the lateral load level. Specimen SD-N1-4ARS was bared much higher lateral load up to this point compared to specimen SD-N1-2ARS. No additional cracks were observed in further drift ratios, while the existing cracks at the column-footing interface were continously enlarged. At 8 % drift ratio the crack opening was measured 25 mm. South and north view of specimen SD-N1-4ARS at 8 % drift ratio are shown in Figure 4.18.

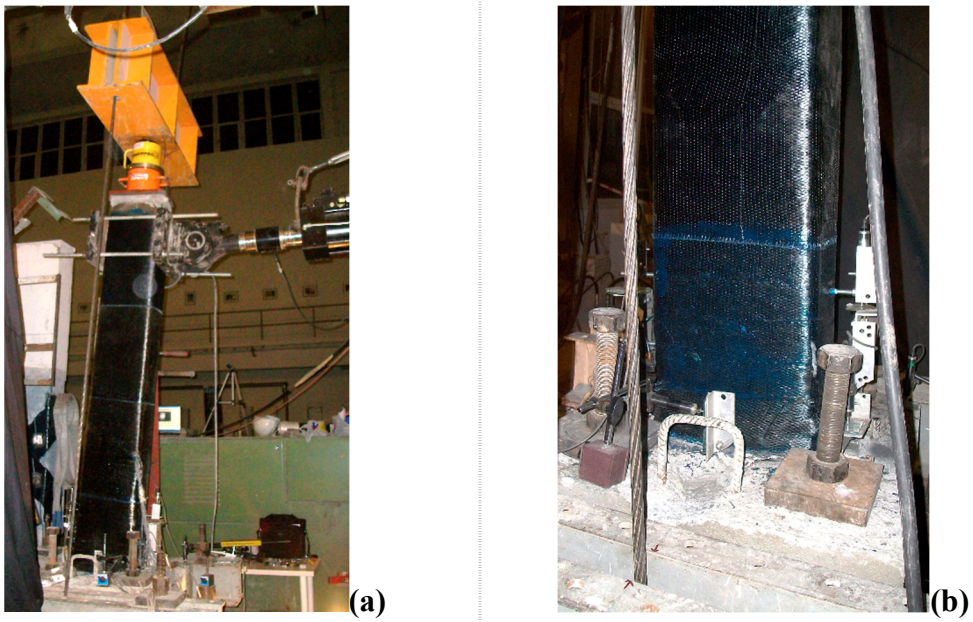

(a) **(b)**

Figure 4.18 : Views of SD-N1-4ARS at 8 % drift ratio: (a)South. (b)North.

Residual deformation was calculated as 60.3 mm when lateral load was absolute zero. Until AFRP reinforcement fracture, measured lateral loads were significantly higher comparing to control specimen SD-N1-REF and the retrofitted specimen SD-N1-2ARS and the increase in the lateral load capacity was calculated as 84 % while pushing and 95 % wile pulling compared to control specimen. Similar to specimen SD-N1-2ARS, AFRP reinforcement in both surfaces of the columns were fractured in the column – footing interface, where deformations were cumulated.

During the autopsy of the specimens, CFRP confinement was cut off in the first 60 cm height of the columns over footing and column surfaces was investigated for possible flexural cracks. It was seen that deformations were cumulated at the column-footing interface and no significant crack was observed through the column height. In order to confirm the Fracture pattern of the AFRP reinforcement, SRM cover around the core concrete was broken and AFRP strips were exposed. It was observed that both

AFRP strips used as longitudinal reinforcement and additional anchorage reinforcement were ruptured in both sides of the column as seen inFigure 4.19.

Figure 4.19 : Fractured AFRP longitudinal and anchorage reinforcement in the specimen SD-N1-4ARS.

It was also comfirmed that both longitudinal and additional anchorage AFRP reinforcement were fully bonded in anchorage holes and no damage or slip was noticed during the autopsy of the anchorage holes.

Summary of the seismic behavior of specimen SD-N1-4ARS is shown in Table 4.3.

Table 4.3 : Summary of the seismic behavior of SD-N1-4ARS.

Drift ratio (%)	δ (mm/mm)	P (kN)	Observations
0.10	±1.65	7.85 / -6.43	No crack was observed
0.25	±4.125	14.90 / -14.50	No crack was observed
0.50	±8.25	20.73 / -20.50	First flexural crack at column-footing interface was observed
1.0	±16.5	28.23 / -28.05	Propagation of existing crack at column-footing interface was observed
2.0	±33.0	37.70 / -40.28	Propagation of existing crack at column-footing interface was observed
3.0	±49.5	41.05 / -45.13	AFRP reinforcement in tension Fractured and lateral load decreased to -25.03 kN
4.0	±66.0	24.68 / -23.75	Propagation of existing crack at column-footing interface was observed
6.0	±99.0	22.53/ -24.63	Propagation of existing crack at column-footing interface was observed
8.0	±132.0	22.50 / -25.73	Propagation of existing crack at column-footing interface was observed

Experimental and theoretical force-displacement relationships of SD-N1-4ARS is presented in Figure 4.20. First flexural crack, first yielding point of longitudinal steel reinforcement, maximum strain on the steel rebar and fracture of AFRP reinforcement are marked on the figure.

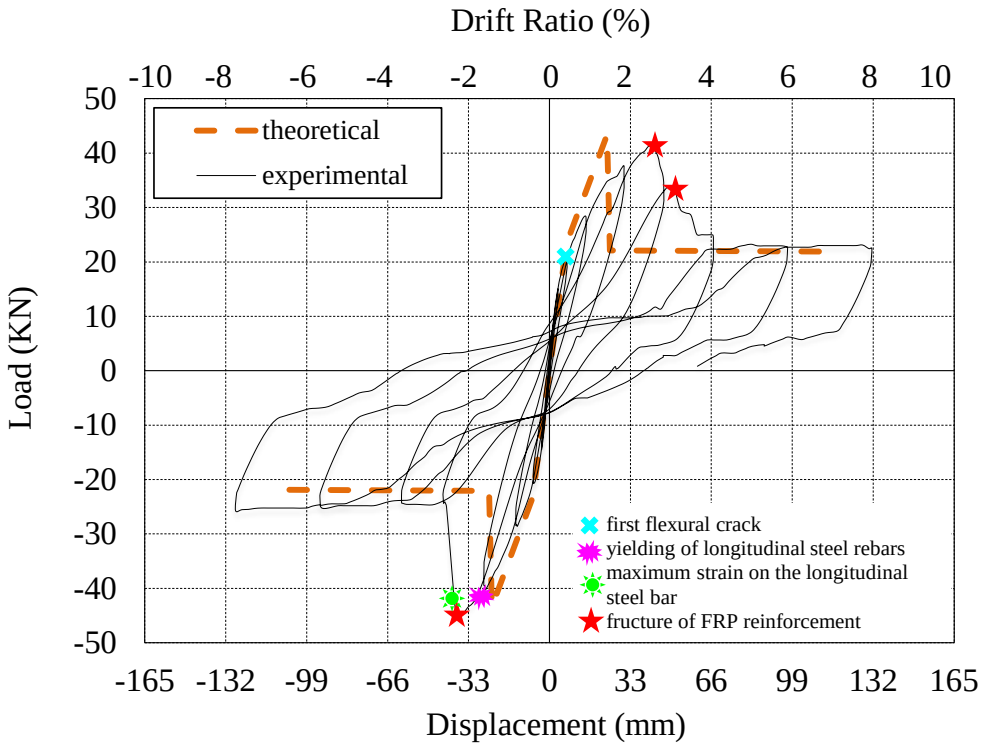

Figure 4.20 : Lateral load versus displacement for SD-N1-4ARS.

Experimental moment-curvature relationships obtained for critical sections of SD-N1-4ARS are presented in Figure 4.21. For the calculation of moment-curvature relationships, the average curvature values obtained for the ranges of 0-20 mm, 20-150 mm and 150-300 mm heights above the footing were taken into account. As seen in Figure 4.21, the curvature values of the member measured in 20-150 mm and 150-300 mm height above the support are in the order of 5.10^{-5} (1/mm), while the curvatures measured in 0-20 mm height are in the order of 3.10^{-3} (1/mm). It is assessed by considering moment-curvature relationships that the damage was accumulated mainly in the first 20 mm height of the member from top of the footing, which was also confirmed with the damage pattern of the specimen.

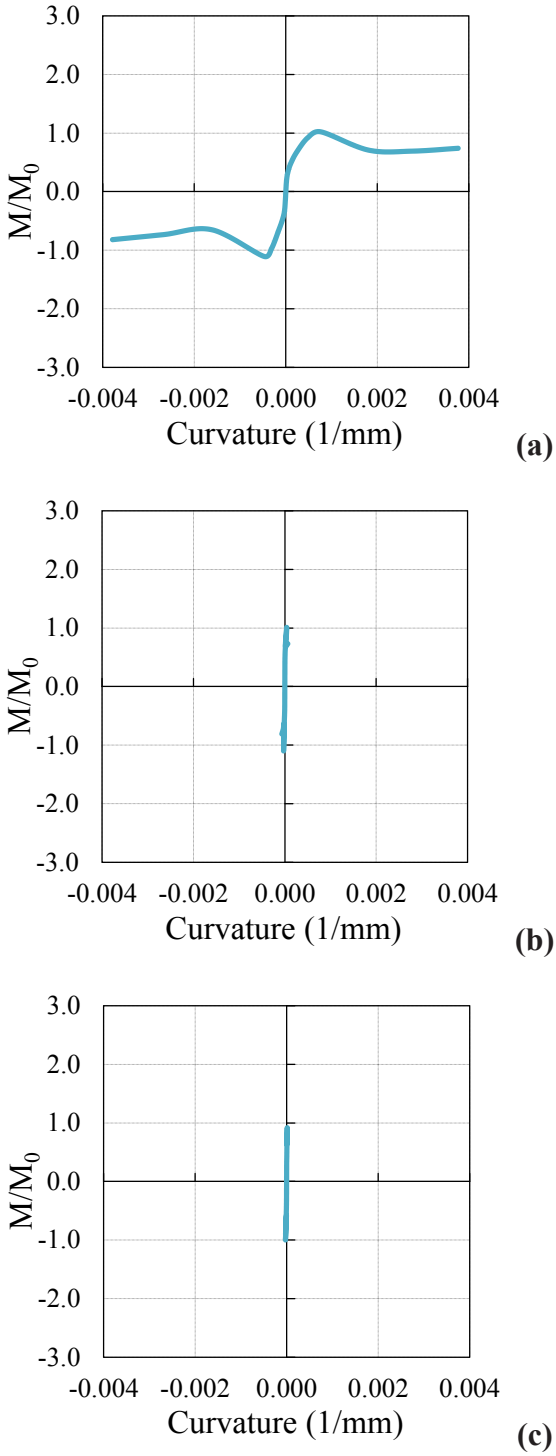

Figure 4.21 : Moment-curvature relationships obtained for gage lengths: (a)0 – 20 mm. (b)20 – 150 mm. (c)150 - 300 mm.

According to the data from the straingauges on the longitudinal steel rebars of the SD-N1-4ARS, the maximum strain while pushing was 0.0306, measured from the straingauge at the column-footing interface for F=-24.8 kN at -6 % drift ratio; the maximum strain while pulling was -0.0119, measured from the straingauge at +300 mm above the footing when F=23.0 kN at 8 % drift ratio. Maximum strain at

AFRP reinforcement was recorded as 0.0068 at the column-footing interface, while pushing through -2 % drift ratio at the lateral load -40.3 kN. Average strain distribution of longitudinal steel rebars, longitudinal AFRP reinforcement and anchorage AFRP reinforcement in different drift ratios are shown in Figure 4.22, Figure 4.23 and Figure 4.24 respectively.

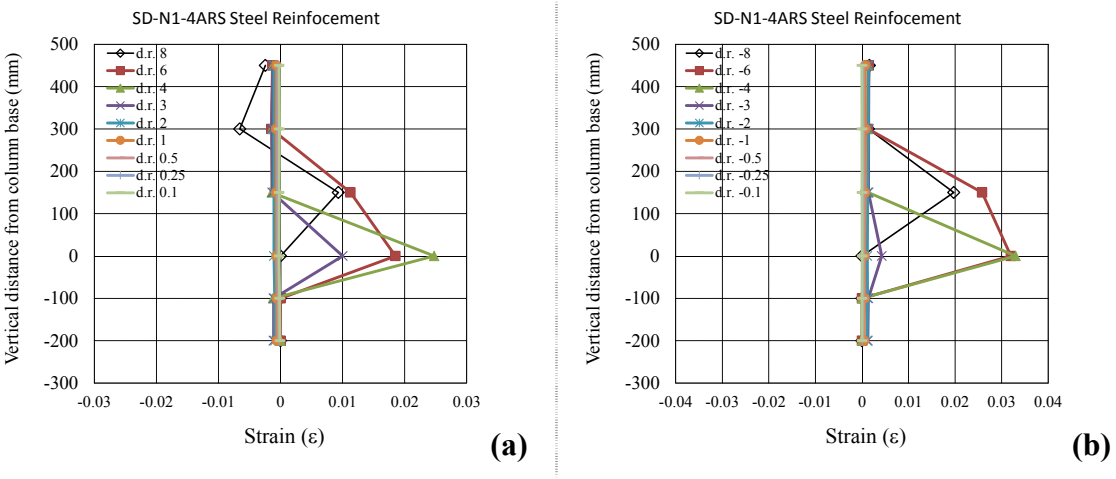

Figure 4.22 : Average strain distribution of longitudinal steel rebars of SD-N1-4ARS: (a)While pulling. (b)While pushing.

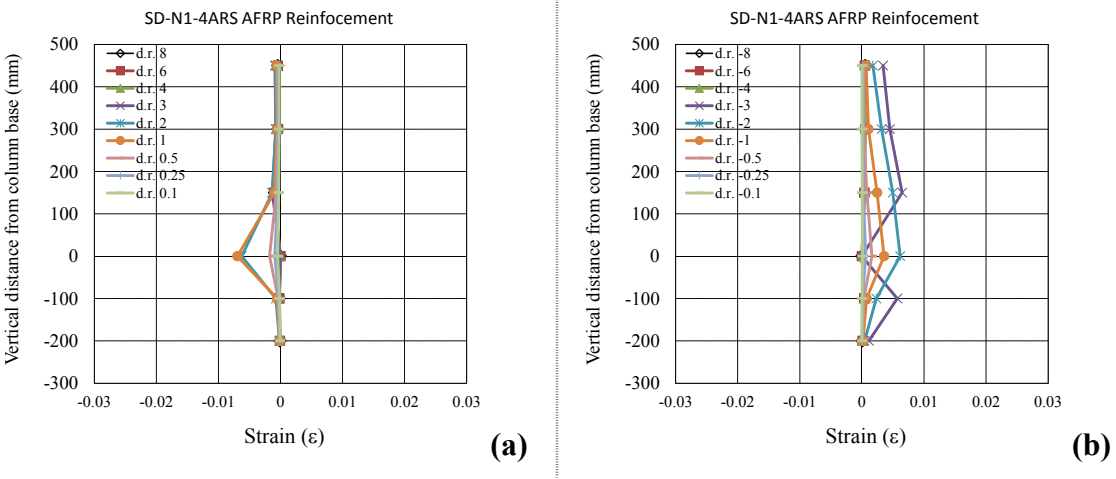

Figure 4.23 : Average strain distribution of longitudinal AFRP reinforcement of SD-N1-4ARS: (a)While pulling. (b)While pushing.

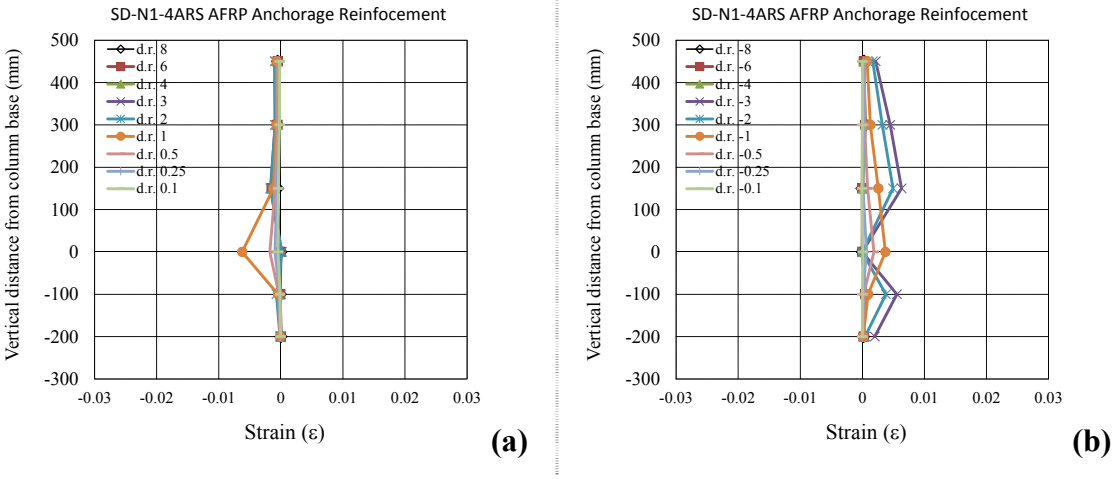

Figure 4.24 : Average strain distribution of longitudinal AFRP anchorage reinforcement of SD-N1-4ARS: (a)While pulling. (b)While pushing.

4.1.4 SD-N1-2ARS-PB

No cracks were observed while loading to target displacements of ±1.65 mm (drift ratio 0.10 %).

First flexural crack was observed at the interface of the column and footing during loading to target displacement of 4.125 mm (drift ratio 0.25 %).

South and north views of the specimen SD-N1-2ARS-PB at 0.25 % drift ratio is shown in Figure 4.25.

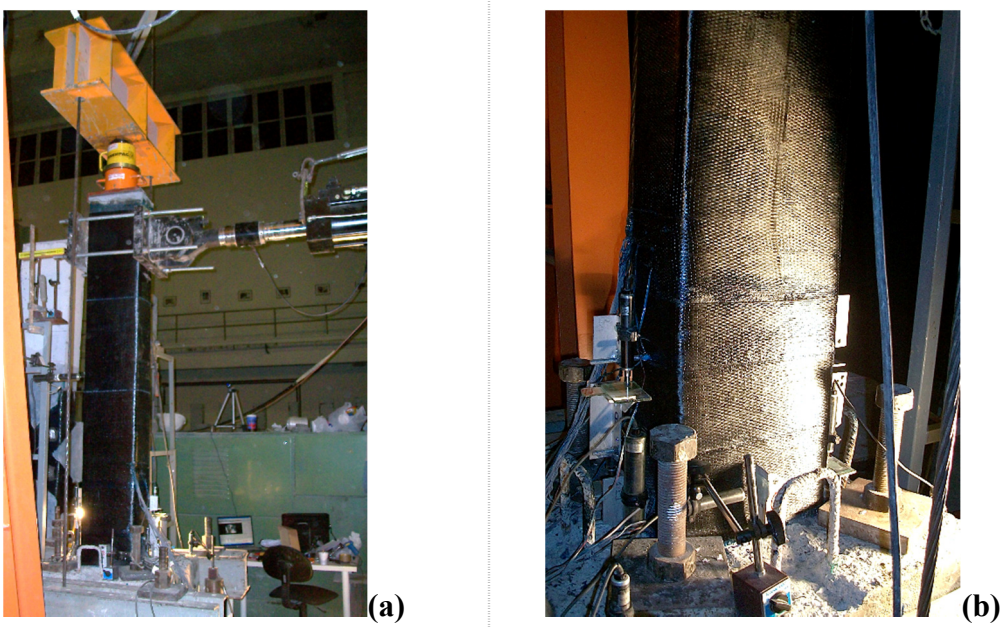

Figure 4.25 : Views of SD-N1-2ARS-PB at 0.25 % drift ratio: (a)South. (b)North.

It was observed that all longitudinal steel reinforcement were yielded between 2 % and 3 % drift ratios, while stirrups were not yielded. While pushing towards -3 % drift ratio, a loud noice coming from the specimen was recorded with a sudden decrease in the lateral load. The reason of the sound was found as Fracture of the AFRP longitudinal reinforcement. This behaviour was repeated while pulling the column towards 3 % drift ratio. From this point forward, the specimen SD-N1-2ARS-PB performed similar to specimen SD-N1-REF in terms of bared load but under different displacements. No additional cracks were observed in further drift ratios, while the existing cracks at the column-footing interface were continously enlarged. At 8 % drift ratio the crack opening was measured 21 mm. South and north view of specimen SD-N1-2ARS-PB at 8 % drift ratio are shown in Figure 4.26.

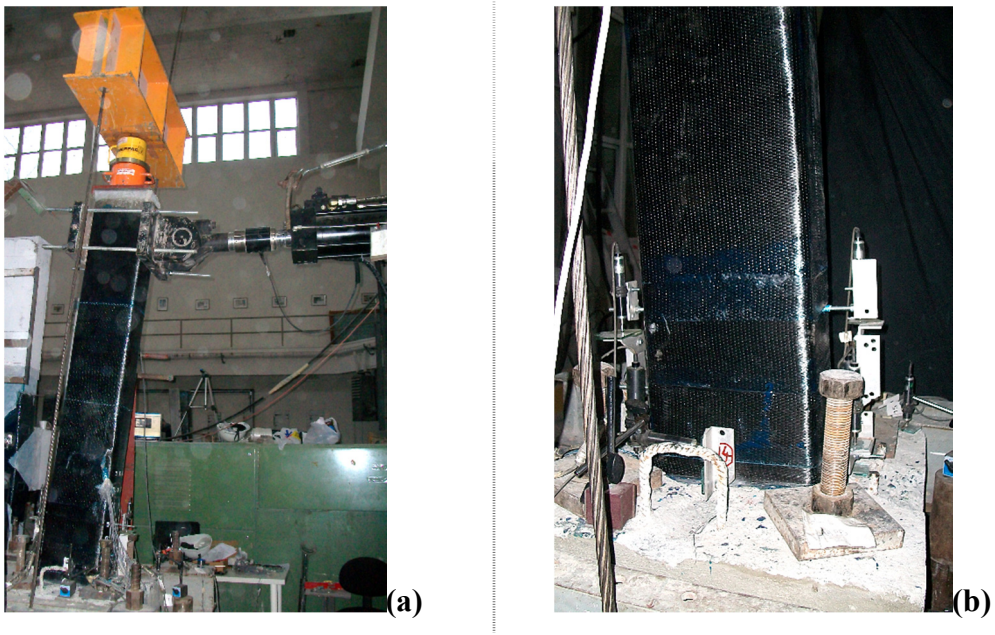

Figure 4.26 : Views of SD-N1-2ARS-PB at 8 % drift ratio: (a)South. (b)North.

During the autopsy of the specimens, CFRP confinement was cut off in the first 60 cm height of the columns over footing and column surfaces was investigated for possible flexural cracks. It was seen that deformations were cumulated at the column-footing interface and no significant crack was observed through the column height. In order to confirm the Fracture pattern of the AFRP reinforcement, SRM cover around the core concrete was broken and AFRP strips were exposed. It was observed that both AFRP strips were ruptured in both sides of the column as seen in Figure 4.27.

Figure 4.27 : Fractured AFRP reinforcement in the specimen SD-N1-2ARS-PB.

In order to confirm the continuous load transfer through the footing, epoxy grout filled in the anchorage holes were also broken in the first 10 cm depth. It was observed that AFRP reinforcement were fully bonded in anchorage holes and no damage or slip was noticed.

Summary of the seismic behavior of specimen SD-N1-2ARS-PB is shown in Table 4.2.

Table 4.4 : Summary of the seismic behavior of SD-N1-2ARS-PB.

Drift ratio (%)	δ (mm/mm)	P (kN)	Observations
0.10	±1.65	7.05 / -4.45	No crack was observed
0.25	±4.125	12.13 / -11.28	First flexural crack at column-footing interface was observed
0.50	±8.25	17.00 / -16.68	Propagation of existing crack at column-footing interface was observed
1.0	±16.5	22.83 / -22.38	Propagation of existing crack at column-footing interface was observed
2.0	±33.0	28.85 / -31.30	Propagation of existing crack at column-footing interface was observed
3.0	±49.5	32.83 / -34.55	AFRP reinforcement in tension Fractured and lateral load decreased to -27.98 kN
4.0	±66.0	20.45 / -25.35	Propagation of existing crack at column-footing interface was observed
6.0	±99.0	20.78/ -25.43	Propagation of existing crack at column-footing interface was observed
8.0	±132.0	19.55 / -24.93	Propagation of existing crack at column-footing interface was observed

Experimental and theoretical force-displacement relationships of SD-N1-2ARS-PB is presented in Figure 4.28. First flexural crack, first yielding point of longitudinal steel reinforcement, maximum strain on the steel rebar and fracture of AFRP reinforcement are marked on the figure.

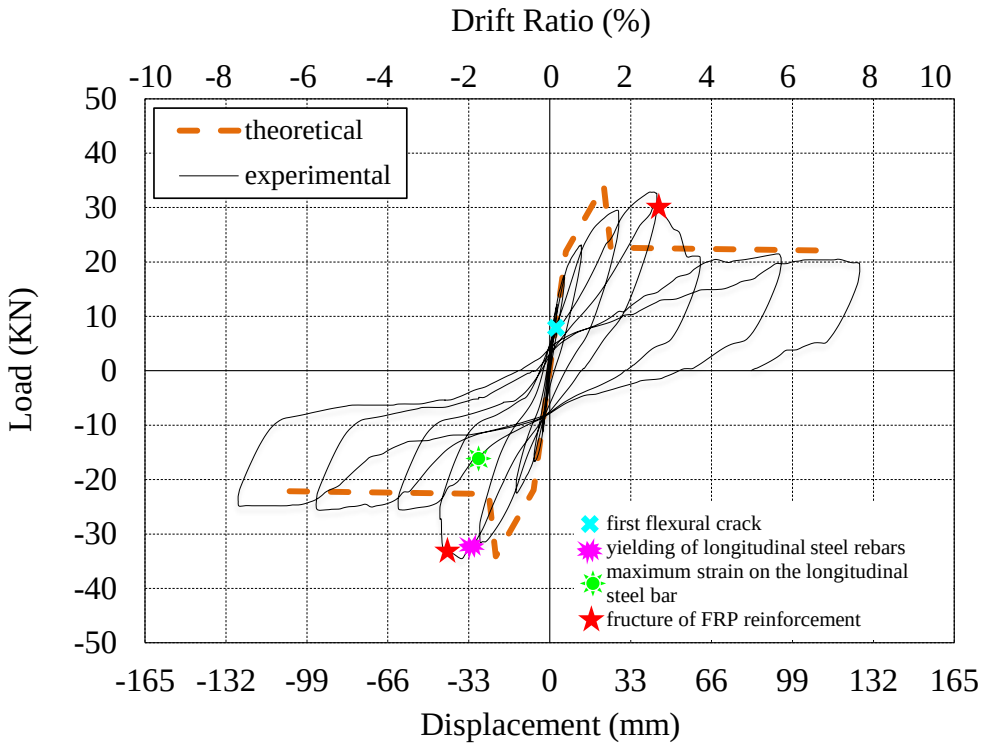

Figure 4.28 : Lateral load versus displacement for SD-N1-2ARS-PB.

Residual deformations were calculated as 13.2 mm and 82.1 mm while pushing and pulling respectively. Contribution of decomposed AFRP reinforcement to the behavior at larger drifts limited plastic residual deformations of the column SD-N1-2ARS-PB. As seen in Figure 4.28, marginal residual displacements remained after unloading branches in pulling direction up to 8 % drift ratio. Until AFRP reinforcement fracture, measured lateral loads were significantly higher comparing to control specimen SD-N1-REF and the increase in the lateral load capacity was calculated as 41 % while pushing and 56 % while pulling compared to control specimen.

Experimental moment-curvature relationships obtained for critical sections of SD-N1-2ARS-PB are presented in Figure 4.29.

For the calculation of moment-curvature relationships, the average curvature values obtained for the ranges of 0-20 mm, 20-150 mm and 150-300 mm heights above the footing were taken into account. As seen from Figure 4.29, the curvature values of the member measured in 20-150 mm and 150-300 mm height above the support are in the order of 5.10^{-5} (1/mm), while the curvatures measured in 0-20 mm height are in the order of 3.10^{-3} (1/mm). It is assessed by considering moment-curvature relationships

that the damage was accumulated mainly in the first 20 mm height of the member from top of the footing, which was also confirmed with the damage pattern of the specimen.

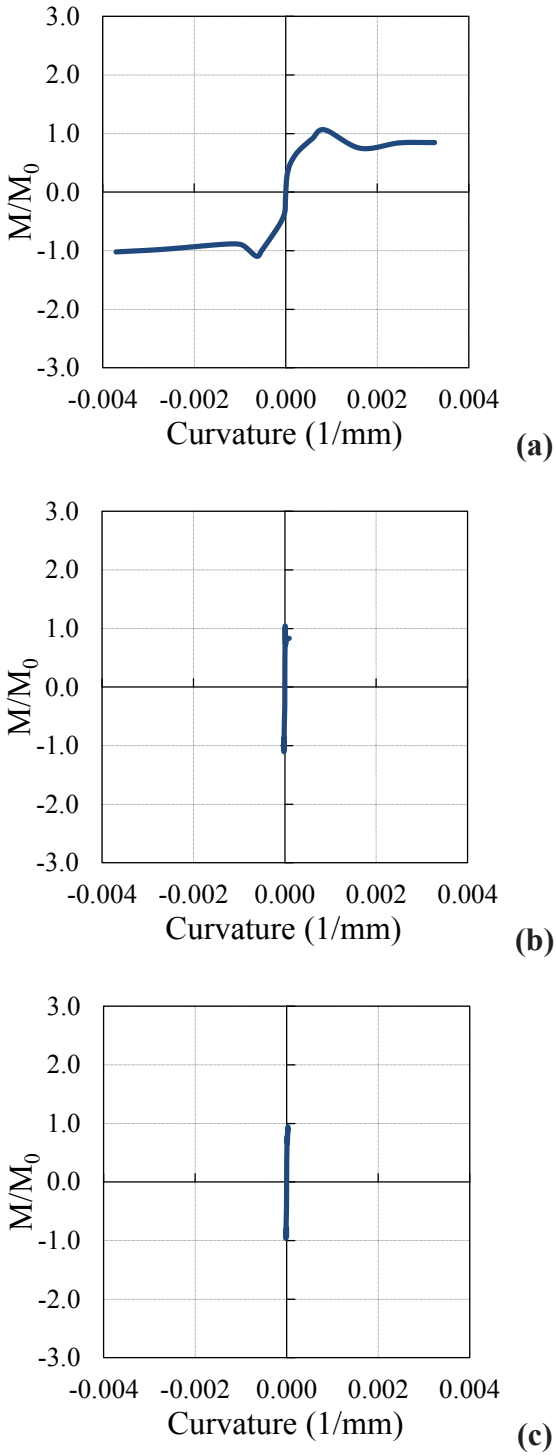

Figure 4.29 : Moment-curvature relationships obtained for gage lengths: (a)0 – 20 mm. (b)20 – 150 mm. (c)150 - 300 mm.

Average strain distribution of longitudinal steel rebars and AFRP reinforcement in different drift ratios are shown in Figure 4.30 and Figure 4.31 respectively.

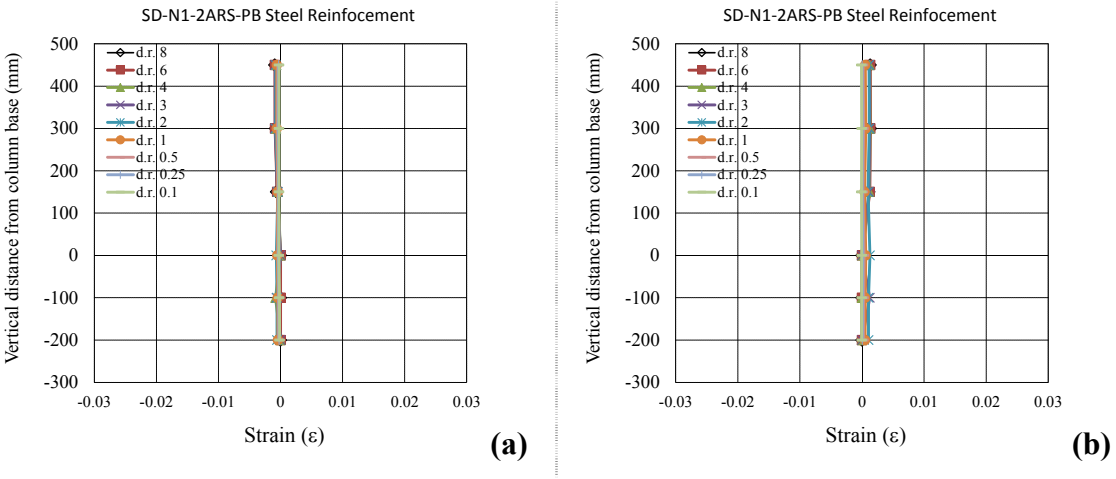

Figure 4.30 : Average strain distribution of longitudinal steel rebars of SD-N1-2ARS-PB: (a)While pulling. (b)While pushing.

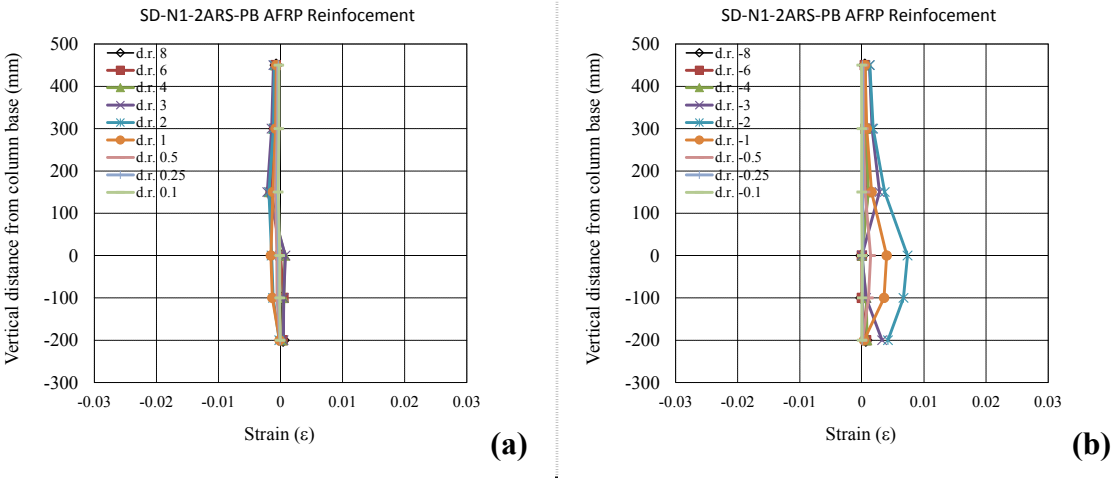

Figure 4.31 : Average strain distribution of longitudinal AFRP reinforcement of SD-N1-2ARS-PB: (a)While pulling. (b)While pushing.

According to the data from the straingauges on the longitudinal steel rebars of the SD-N1-2ARS-PB, the maximum strain while pushing was 0.0047, measured from the straingauge at column-footing interface for F=-33.5 kN at -3 % drift ratio; the maximum strain while pulling was -0.0013, measured from the straingauge at column-footing interface when F=28.9 kN at 2 % drift ratio. Maximum strain at AFRP reinforcement was recorded as 0.0125 at the column footing interface, while pushing through -3 % drift ratio at the lateral load -31.6 kN.

4.2 Test Results of Second Group Specimens

4.2.1 SD-N1-3AR

No cracks were observed while loading to target displacements of ±8.25 mm (drift ratio 0.50 %). First flexural crack was observed at the interface of the column and footing during loading to target displacement of 16.5 mm (drift ratio 1 %).

It was observed that all longitudinal steel reinforcement were yielded at 2 % drift ratio, while stirrups were not yielded. While pushing towards -3 % drift ratio, a loud noice coming from the specimen was recorded with a sudden decrease in the lateral load. The reason of the sound was found as Fracture of the AFRP longitudinal reinforcement. This behaviour was repeated while pulling the column towards 4 % drift ratio. From this point forward, the specimen SD-N1-3AR performed similar to specimen SD-N1-REF in terms of load-displacement relation. This behavior was very similar to specimen SD-N1-4ARS's behavior, except the deformations at the point, where AFRP reinforcement fractured. Specimen SD-N1-3AR reached larger deformations compared to specimen SD-N1-4ARS. No additional cracks were observed in further drift ratios, while the existing cracks at the column-footing interface were continously enlarged. At 8 % drift ratio the crack opening was measured 20 mm. South view of specimen SD-N1-3AR after 8 % drift ratio are shown in Figure 4.32.

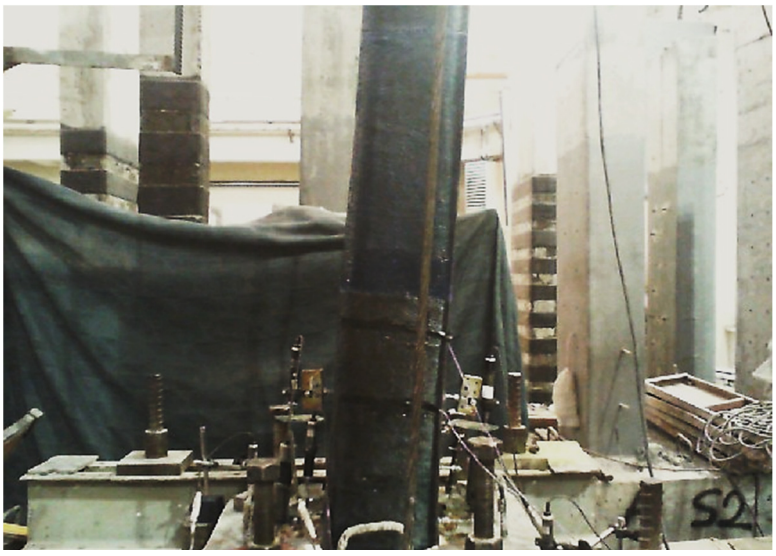

Figure 4.32 : South view of the specimen SD-N1-3AR at 8 % drift ratio.

Residual deformation was calculated as 70.0 mm when lateral load was absolute zero. Until AFRP reinforcement fracture, measured lateral loads were significantly higher comparing to control specimen SD-N1-REF and the increase in the lateral load capacity was calculated as 116 % while pushing and 123 % while pulling compared to control specimen. Similar to specimen SD-N1-2ARS and SD-N1-4ARS, AFRP reinforcement in both surfaces of the columns were fractured in the column-footing interface, where deformations were cumulated.

During the autopsy of the specimen, CFRP confinement was cut off in the first 60 cm height of the columns over footing and column surfaces was investigated for possible flexural cracks. It was seen that deformations were cumulated at the column-footing interface and no significant crack was observed through the column height. In order to confirm the Fracture pattern of the AFRP reinforcement, SRM cover around the core concrete was broken and AFRP bars were exposed. It was observed that all AFRP bars in both sides raptured as shown in Figure 4.33.

(a)

(b)

Figure 4.33 : Fractured AFRP longitudinal reinforcement in the specimen SD-N1-3AR: (a)East view. (b)West view.

Summary of the seismic behavior of specimen SD-N1-3AR is shown in Table 4.5.

Table 4.5 : Summary of the seismic behavior of SD-N1-3AR.

Drift ratio (%)	δ (mm/mm)	P (kN)	Observations
0.10	±1.65	4.40 / -4.02	No crack was observed
0.25	±4.125	8.38 / -9.10	No crack was observed
0.50	±8.25	13 / -16.25	No crack was observed
1.0	±16.5	19.99 / -27.09	First flexural crack at column-footing interface was observed
2.0	±33.0	36.17 / -40.63	Propagation of existing crack at column-footing interface was observed
3.0	±49.5	46.96 / -47.76	AFRP reinforcement in tension Fractured and lateral load decreased to 35.2 kN
4.0	±66.0	27.49 / -52.84	AFRP reinforcement in tension Fractured and lateral load decreased to 27.3 kN
6.0	±99.0	26.05/ -27.67	AFRP reinforcement in tension Fractured and lateral load decreased to -27.7 kN
8.0	±132.0	26.16 / -26.98	Propagation of existing crack at column-footing interface was observed

Experimental and theoretical force-displacement relationships of SD-N1-3AR is presented in Figure 4.34. First flexural crack, first yielding point of longitudinal steel reinforcement, fracture of AFRP reinforcement and maximum strain on the steel rebar are marked on the figure.

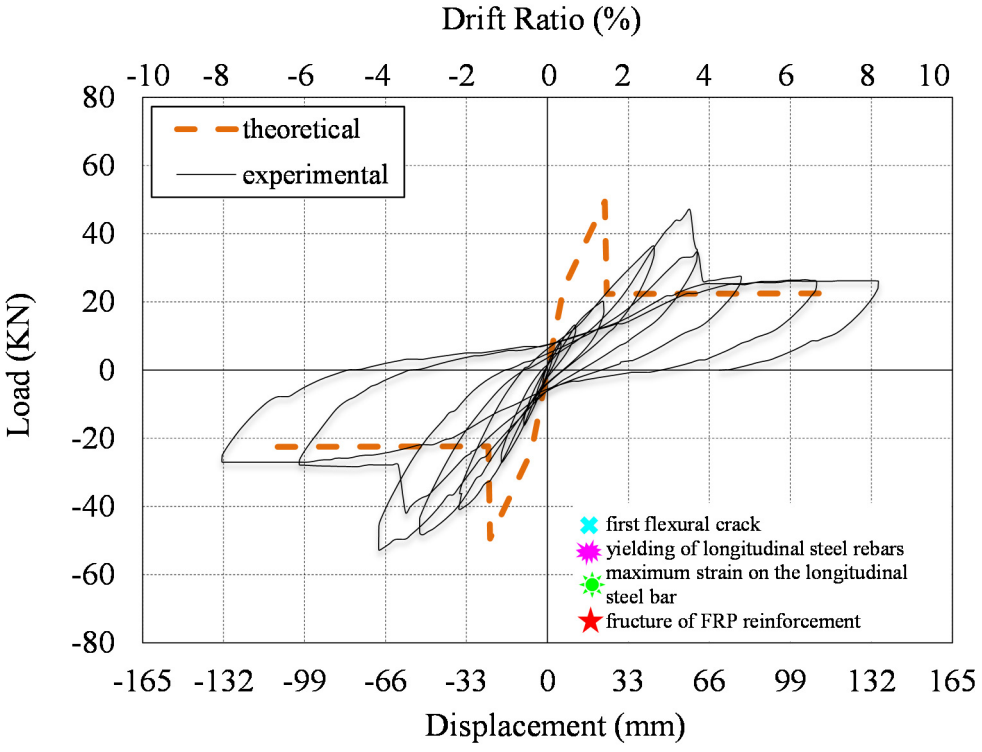

Figure 4.34 : Lateral load versus displacement for SD-N1-3AR.

Experimental moment-curvature relationships obtained for critical sections of SD-N1-3AR are presented in Figure 4.35. For the calculation of moment-curvature

relationships, the average curvature values obtained for the ranges of 0-20 mm, 20-150 mm and 150-300 mm heights above the footing were taken into account.

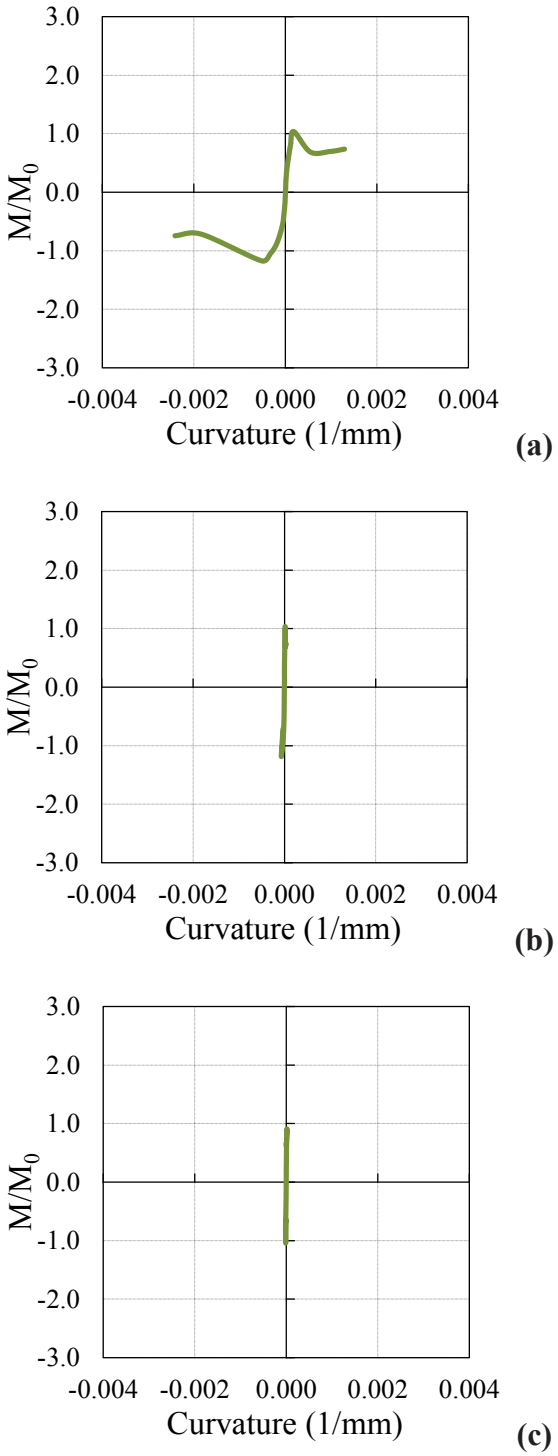

Figure 4.35 : Moment-curvature relationships obtained for: (a)0 - 20 mm. (b)20 - 150 mm. (c)150 - 300 mm gage lengths.

As seen from Figure 4.35, the curvature values of the member measured in 20-150 mm and 150-300 mm height above the support are in the order of 5.10^{-5} (1/mm), while the curvatures measured in 0-20 mm height are in the order of

3.10^{-3} (1/mm). It is assessed by considering moment-curvature relationships that the damage was accumulated mainly in the first 20 mm height of the member from top of the footing, which was also confirmed with the damage pattern of the specimen.

Average strain distribution of longitudinal steel rebars and longitudinal AFRP reinforcement in different drift ratios are shown in Figure 4.36 and Figure 4.37 respectively.

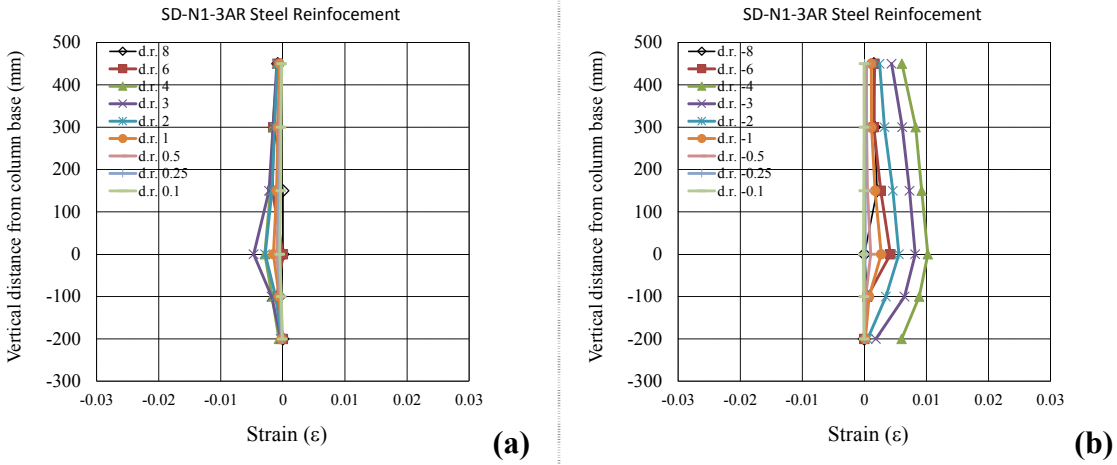

Figure 4.36 : Average strain distribution of longitudinal steel rebars of SD-N1-3AR: (a)While pulling. (b)While pushing.

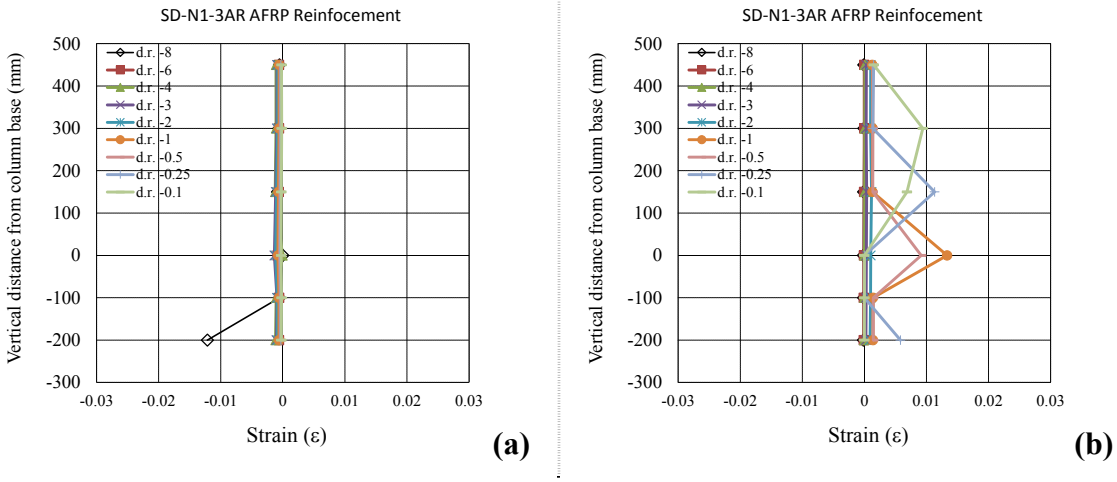

Figure 4.37 : Average strain distribution of longitudinal AFRP reinforcement of SD-N1-3AR: (a)While pulling. (b)While pushing.

According to the data from the straingauges on the longitudinal steel rebars of the SD-N1-3AR, the maximum strain while pushing was 0.0108, measured from the straingauge at the column-footing interface for F=-52.8 kN at -4 % drift ratio; the maximum strain while pulling was -0.0053, measured from the straingauge at the

column-footing interface when F=35.3 kN at 4 % drift ratio. Maximum strain at AFRP reinforcement was recorded as 0.0152 at the column-footing interface, while pulling through 4 % drift ratio at the lateral load 35.4 kN. This high strain value was observed right after the Fracture of the other AFRP bar in the vicinity, as a proof of load transfer between FRP reinforcement.

4.2.2 SD-N1-1AR5G

Test setup and general view of the specimen is shown in Figure 4.38.

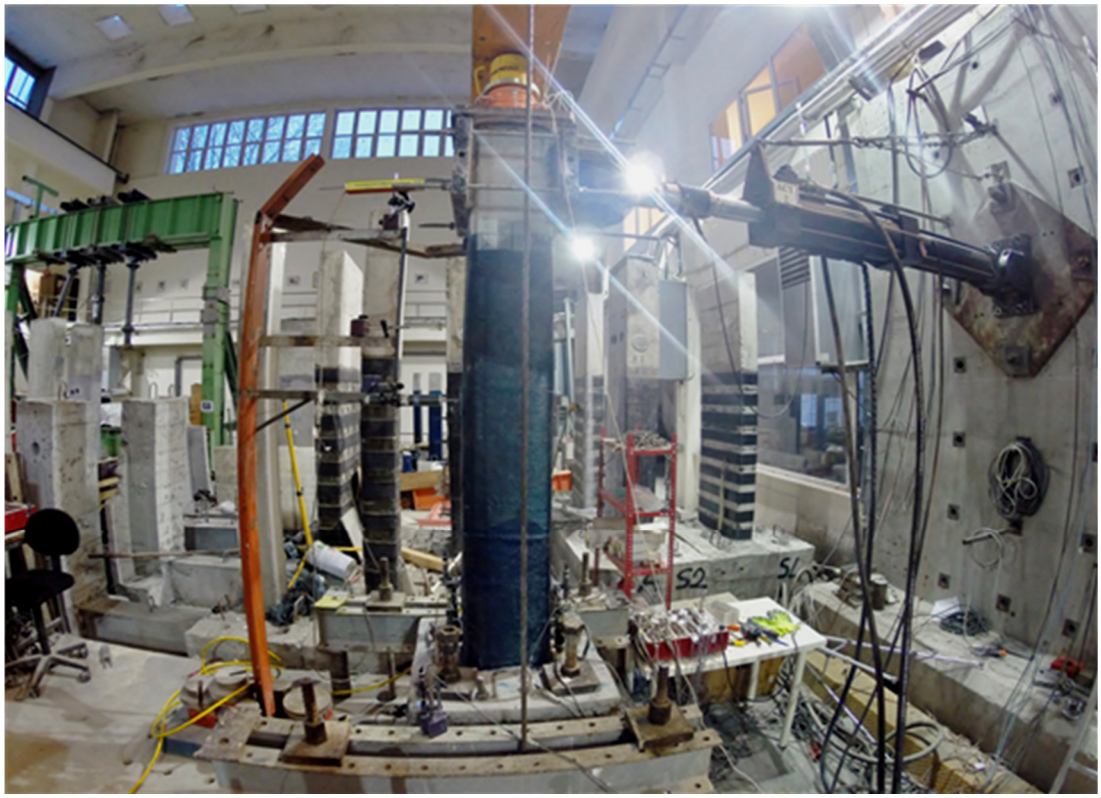

Figure 4.38 : South view of the specimen SD-N1-1AR5G prior to test.

No cracks were observed while loading to target displacements of ±8.25 mm (drift ratio 0.50 %). First flexural crack was observed at the interface of the column and footing during loading to target displacement of 16.5 mm (drift ratio 1 %). South, and north view of the specimen SD-N1-1AR5G after 1 % drift ratio are shown in Figure 4.39.

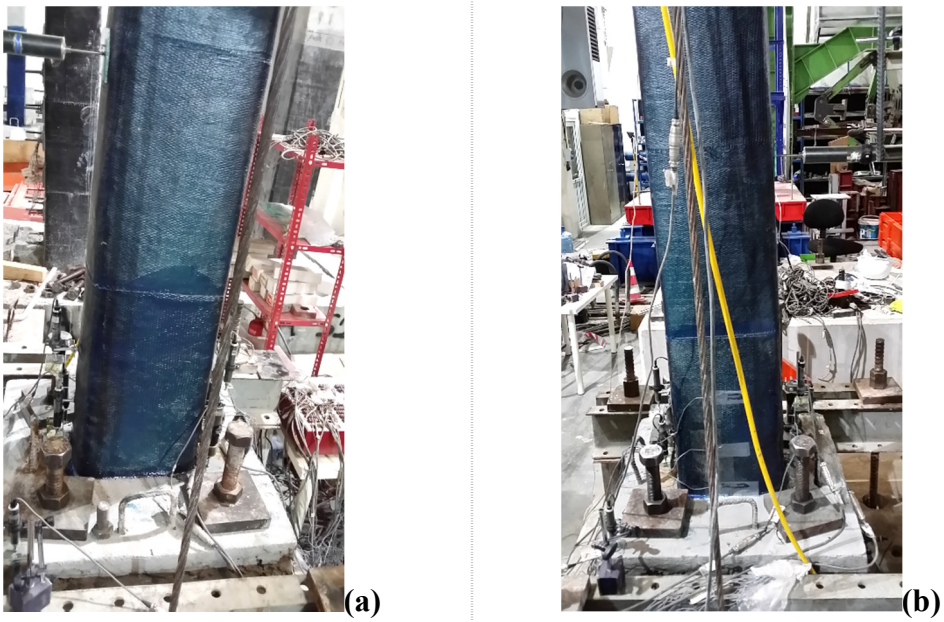

(a) (b)

Figure 4.39 : Views of SD-N1-1AR5G at 1 % drift ratio: (a)South. (b)North.

It was observed that all longitudinal steel reinforcement were yielded at 3 % drift ratio, while stirrups were not yielded. While pulling towards 6 % drift ratio, a loud noice coming from the specimen was recorded with a slight decrease in the lateral load. The reason of the sound was found as rupture of the AFRP longitudinal reinforcement. Even though AFRP reinforcement ruptured at 6 % drift ratio, lateral load continued to increase untill the end of the testing at 8 % drift ratio. This behavior could be explained with instant load transfer from ruptured AFRP bar to remaining GFRP bars and GFRP bars continued to bare lateral load. This unique behavior was observed because of unfractured GFRP reinforcement until the end of the test. Unlikely to previous retrofitted specimens, deformations were distributed along the height of the column in the first 1200 mm from the footing. Further cracks were observed on the column surface and finally a larger crack occurred at 1180 mm height, where almost longitudinal FRP reinforcement end (1200 mm). From this point on, increase in the lateral load slowed and plastic deformations were partially transferred from bottom of the column upto the point on the column surface, where FRP reinforcement have free ends. This was also confirmed during the autopsy of the specimen.

At 8 % drift ratio the crack opening at the bottom of the column was measured only 5 mm. South and north view of specimen SD-N1-1AR5G at 8 % drift ratio are shown in Figure 4.40.

(a)

(b)

Figure 4.40 : Views of SD-N1-1AR5G at 8 % drift ratio: (a)South. (b)North.

Residual deformation was calculated as 34.3 mm when lateral load was absolute zero. The increase in the lateral load capacity was calculated as 152 % while pushing and 207 % while pulling compared to control specimen. Similar to specimens SD-N1-2ARS, SD-N1-4ARS, and SD-N1-3AR, AFRP reinforcement in both surfaces of the columns were fractured in the column – footing interface, where deformations were partially cumulated upto 6 % drift ratio

During the autopsy of the specimen, CFRP confinement was cut off in the first 130 cm height of the columns over footing and column surfaces was investigated for possible flexural cracks. It was seen that deformations were cumulated in two sections: at the column-footing interface and at 1200 mm high from the footing, where FRP reinforcement end (Figure 4.41). SRM cover around the core concrete was broken and FRP bars were exposed. It was observed that AFRP bar on the north surface of the specimen raptured, while the one on the south surface was buckled under compression as shown in Figure 4.42.

Figure 4.41 : Cumulated damage at the free end of FRP reinforcement 120 cm above the footing.

(a)

(b)

Figure 4.42 : Fractured AFRP longitudinal reinforcement in the specimen SD-N1-1AR5G: (a)East view. (b)West view.

Summary of the seismic behavior of specimen SD-N1-1AR5G is shown in Table 4.6.

Table 4.6 : Summary of the seismic behavior of SD-N1-1AR5G.

Drift ratio (%)	δ (mm/mm)	P (kN)	Observations
0.10	±1.65	6.25 / -3.42	No crack was observed
0.25	±4.125	11.19 / -8.91	No crack was observed
0.50	±8.25	17.58 / -16.01	No crack was observed
1.0	±16.5	30.57 / -26.13	First flexural crack was observed
2.0	±33.0	44.20 / -41.92	Flexural crack at column-footing interface was observed
3.0	±49.5	52.12 / -51.07	Further flexural cracks were observed
4.0	±66.0	58.77 / -56.15	Propagation of existing cracks was observed
6.0	±99.0	63.01/ -61.84	AFRP reinforcement in tension fractured
8.0	±132.0	64.80 / -58.58	Flexural crack was observed on the column surface at +118 cm height where AFRP reinforcement end

Experimental and theoretical force-displacement relationships of SD-N1-1AR5G is presented in Figure 4.43. First flexural crack, first yielding point of longitudinal steel reinforcement, fracture of AFRP reinforcement and maximum strain on the steel rebar are marked on the figure.

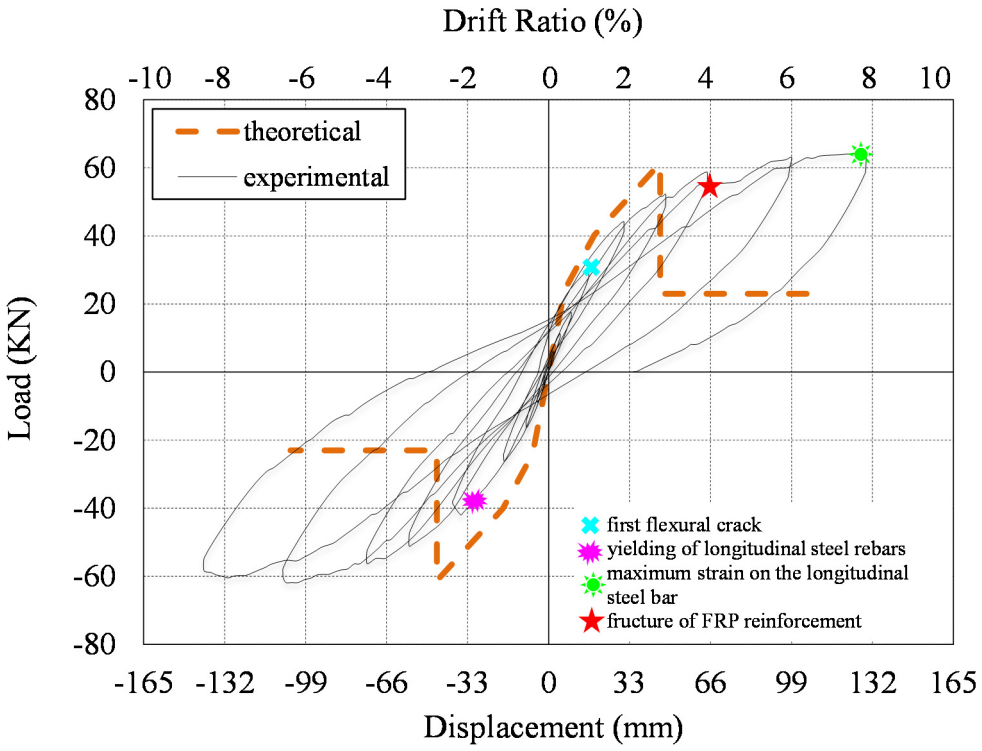

Figure 4.43 : Lateral load versus displacement for SD-N1-1AR5G.

Experimental moment-curvature relationships obtained for critical sections of SD-N1-1AR5G are presented in Figure 4.44.

For the calculation of moment-curvature relationships, the average curvature values obtained for the ranges of 0-20 mm, 20-150 mm and 150-300 mm heights above the footing were taken into account.

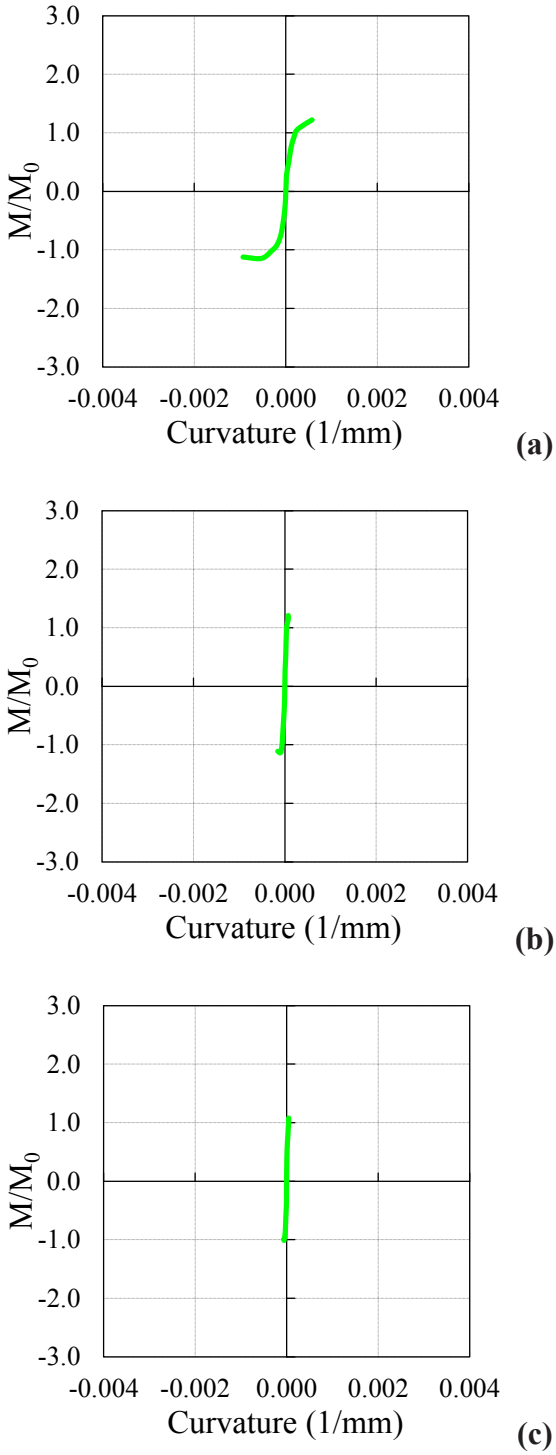

Figure 4.44 : Moment-curvature relationships obtained for gage lengths: (a)0 - 20 mm. (b)20 - 150 mm. (c)150 - 300 mm.

The curvature values of the member measured in 20-150 mm and 150-300 mm height above the support are in the order of 5.10^{-5} (1/mm), while the curvatures measured in

0-20 mm height are in the order of 3.10^{-3} (1/mm). It is assessed by considering moment-curvature relationships that the damage was partially accumulated in the first 20 mm height of the member from top of the footing, while an important part of the damage was accumulated at 1200 mm above footing, which was also confirmed with the damage pattern of the specimen.

According to the data from the straingauges on the longitudinal steel rebars of the SD-N1-1AR5G, the maximum strain while pushing was -0.0135, measured from the straingauge at 450 mm above footing for F=-58.2 kN at -8 % drift ratio; the maximum strain while pulling was 0.0290, measured from the straingauge at 150 mm above footing when F=62.9 kN at 8 % drift ratio. Maximum strain at AFRP reinforcement was recorded as 0.0089 at 300 mm above footing, while pushing through -6 % drift ratio at the lateral load -57.9 kN. Maximum strain at GFRP reinforcement was recorded as 0.0161 at 150 mm above footing, while pushing through -8 % drift ratio at the lateral load -59.9 kN. Average strain distribution of longitudinal steel rebars, longitudinal AFRP reinforcement and GFRP reinforcement in different drift ratios are shown in Figure 4.45, Figure 4.46 and Figure 4.47 respectively.

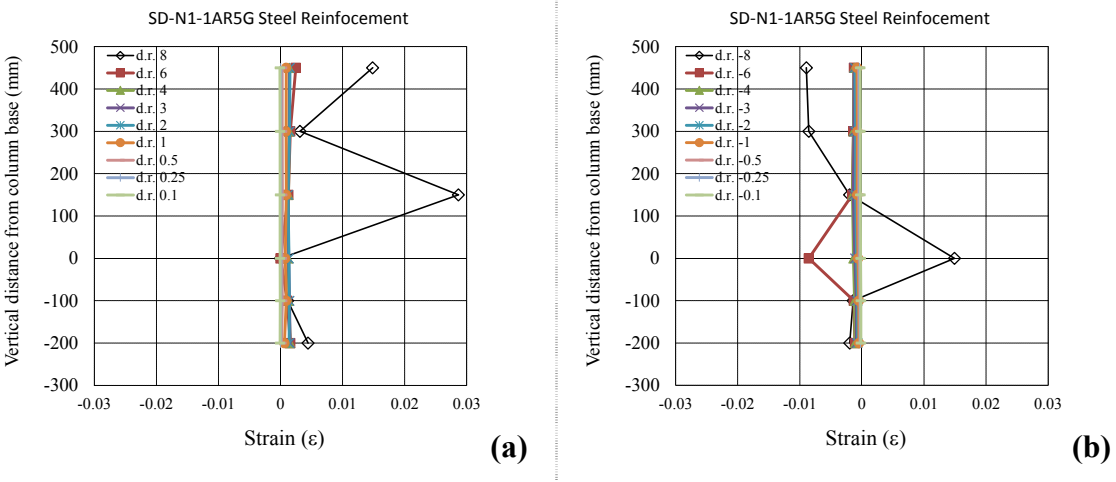

Figure 4.45 : Average strain distribution of longitudinal steel rebars of SD-N1-1AR5G: (a)While pulling. (b)While pushing.

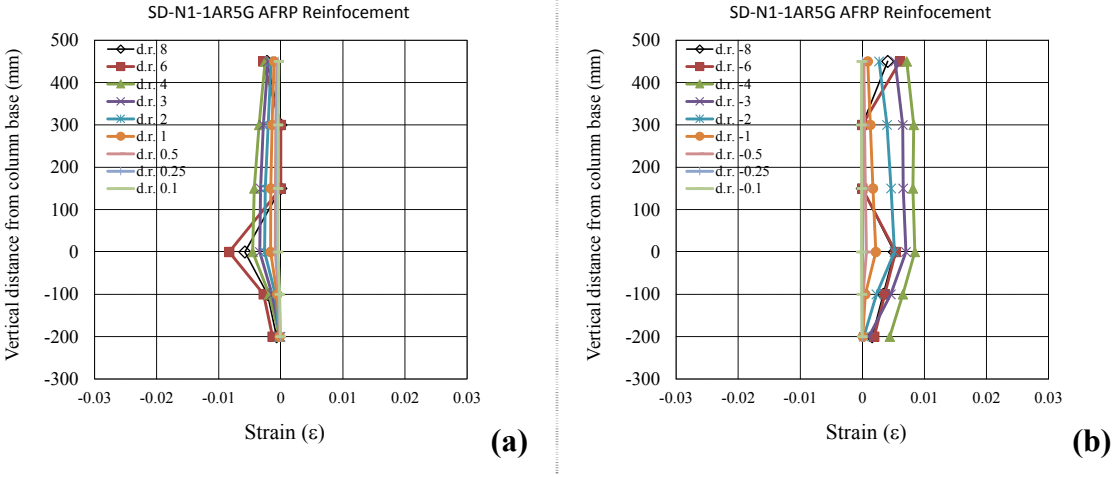

Figure 4.46 : Average strain distribution of longitudinal AFRP reinforcement of SD-N1-1AR5G: (a)While pulling. (b)While pushing.

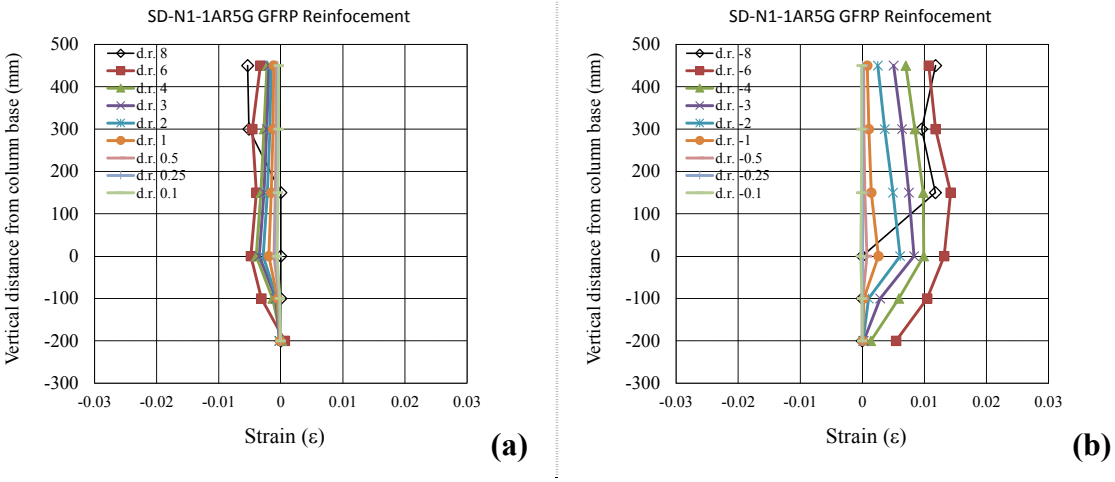

Figure 4.47 : Average strain distribution of longitudinal GFRP reinforcement of SD-N1-1AR5G: (a)While pulling. (b)While pushing.

4.2.3 SD-N1-1AR1C1G

Test setup and general view of the specimen is shown in Figure 4.48.

No cracks were observed while loading to target displacements of ±8.25 mm (drift ratio 0.50 %). First flexural crack was observed at the interface of the column and footing during loading to target displacement of 16.5 mm (drift ratio 1 %). South view of the specimen SD-N1-1AR1C1G at 1 % drift ratio is shown in Figure 4.49.

(a)

(b)

Figure 4.48 : Views of SD-N1-1AR1C1G prior to test: (a)West. (b)South.

Figure 4.49 : First flexural crack at 1% drift ratio.

It was observed that all longitudinal steel reinforcement were yielded at 3 % drift ratio, while stirrups were not yielded. While pushing towards -4 % drift ratio, a loud noice coming from the specimen was recorded with a slight decrease in the lateral load. This behaviour was repeated while pulling the column towards 4 % and 6 % drift ratios with a noticeable decrease in lateral load. The reason of the sound was found as rupture of the AFRP longitudinal reinforcement, while pushing and rupture of AFRP reinforcement at 4 % and GFRP reinforcement at 6 % drift ratio while pulling after autopsy of the specimen. This behavior could be explained with instant load transfer

from ruptured FRP reinforcement to remaining sound ones as already observed in specimen SD-N1-1AR1C1G. Unlikely to specimen SD-N1-1AR5G, deformations were cumulated at the column-footing interface. Further cracks were not observed on the column surface in the higher drift ratios.

At 8 % drift ratio the crack opening at the bottom of the column was measured 17 mm (Figure 4.50).

Figure 4.50 : Main crack at the specimen SD-N1-1AR1C1G at 8 % drift ratio.

Residual deformation was calculated as 99.1 mm when lateral load was absolute zero. The increase in the lateral load capacity was calculated as 82 % while pushing and 123 % while pulling compared to control specimen. Similar to specimens SD-N1-2ARS, SD-N1-4ARS, SD-N1-3AR and SD-N1-1AR5G, AFRP reinforcement in both surfaces of the columns were fractured in the column – footing interface, where deformations were concentrated.

During the autopsy of the specimen, CFRP confinement was cut off in the first 60 cm height of the columns over footing and column surfaces was investigated for possible flexural cracks. It was seen that deformations were cumulated at the column-footing interface and no significant crack was observed through the column height. In order to confirm the fracture pattern of the AFRP reinforcement, SRM cover around the core concrete was broken and AFRP bars were exposed. It was observed that AFRP and GFRP bars in one side raptured, while in the other side only AFRP reinforcement was buckled (Figure 4.51).

(a)

(b)

Figure 4.51 : Fractured longitudinal FRP reinforcement in the specimen SD-N1-1AR5G: (a)West view. (b)East view.

Summary of the seismic behavior of specimen SD-N1-1AR1C1G is shown in Table 4.7.

Table 4.7 : Summary of the seismic behavior of SD-N1-1AR1C1G.

Drift ratio (%)	δ (mm/mm)	P (kN)	Observations
0.10	±1.65	5.51 / -3.90	No crack was observed
0.25	±4.125	11.27 / -9.76	No crack was observed
0.50	±8.25	18.01 / -16.93	No crack was observed
1.0	±16.5	27.23 / -27.05	First flexural crack at column-footing interface was observed
2.0	±33.0	40.89 / -40.15	Propagation of existing crack at column-footing interface was observed
3.0	±49.5	47.11 / -43.44	Propagation of existing crack at column-footing interface was observed
4.0	±66.0	43.41 / -44.63	AFRP reinforcement in tension fractured and lateral load decreased to -38.3 kN
6.0	±99.0	43.44 / -36.68	Propagation of existing crack at column-footing interface was observed
8.0	±132.0	25.64 / -33.27	Propagation of existing crack at column-footing interface was observed

Experimental and theoretical force-displacement relationships of SD-N1-1AR1C1G is presented in Figure 4.52. First flexural crack, first yielding point of longitudinal steel reinforcement, fracture of AFRP reinforcement and maximum strain on the steel rebar are marked on the figure.

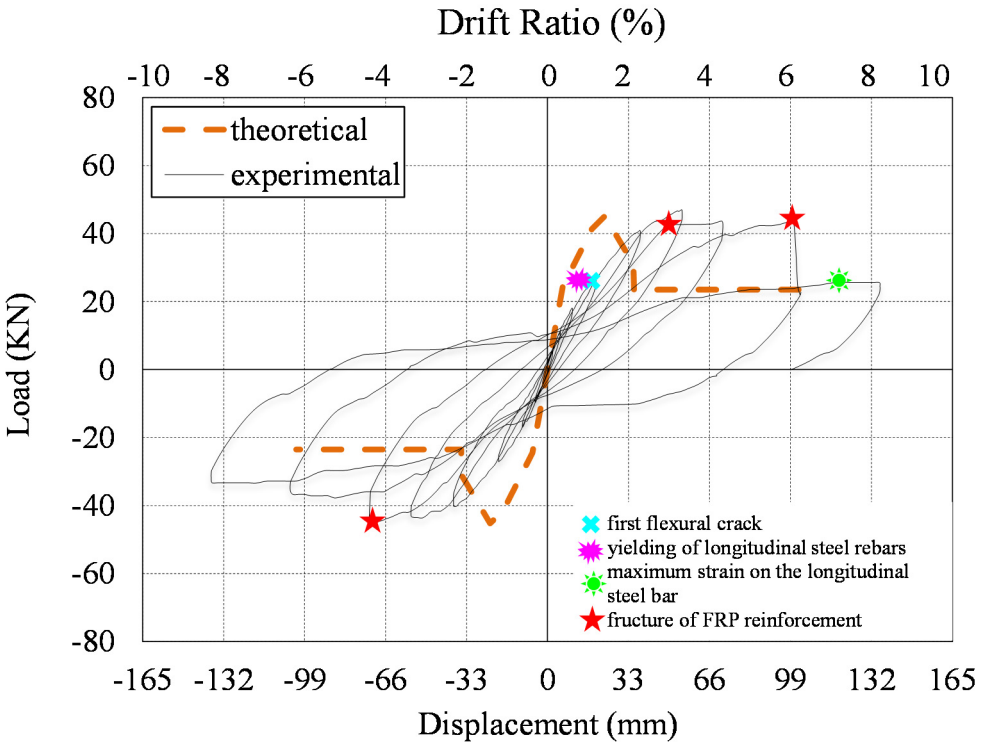

Figure 4.52 : Lateral load versus displacement for SD-N1-1AR1C1G.

Experimental moment-curvature relationships obtained for critical sections of SD-N1-1AR1C1G are presented in Figure 4.53. For the calculation of moment-curvature relationships, the average curvature values obtained for the ranges of 0-20 mm, 20-150 mm and 150-300 mm heights above the footing were taken into account.

The curvature values of the member measured in 20-150 mm and 150-300 mm height above the support are in the order of 5.10^{-5} (1/mm), while the curvatures measured in 0-20 mm height are in the order of 3.10^{-3} (1/mm). It is assessed by considering moment-curvature relationships that the damage was accumulated in the first 20 mm height of the member from top of the footing, which was also confirmed with the damage pattern of the specimen.

According to the data from the straingauges on the longitudinal steel rebars of the SD-N1-1AR1C1G, the maximum strain while pushing was -0.0025, measured from

the straingauge at 100mm in the footing for F=-26.1 kN at -8 % drift ratio; the maximum strain while pulling was 0.0295, measured from the straingauge at 300 mm above footing when F=25.7 kN at 8 % drift ratio.

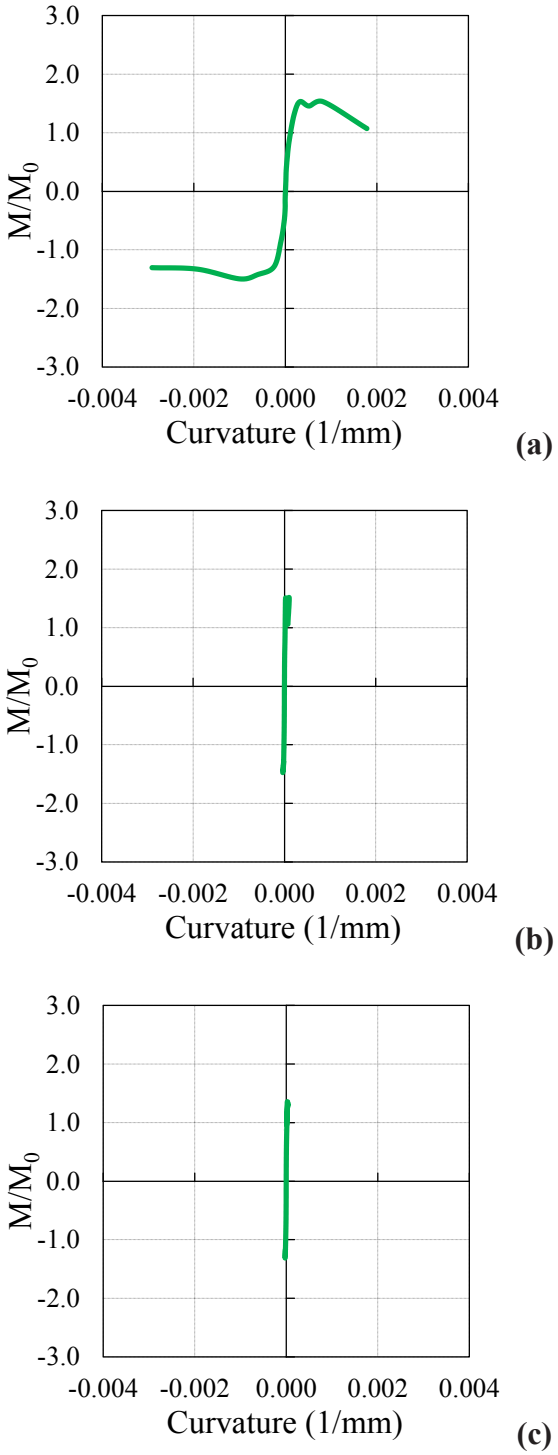

Figure 4.53 : Moment-curvature relationships obtained for: (a)0 - 20 mm. (b)20 - 150 mm. (c)150 - 300 mm gage lengths.

Maximum strain at AFRP reinforcement was recorded as 0.0081 at 300 mm above footing, while pushing through -4 % drift ratio at the lateral load -44.6 kN. Maximum

strain at GFRP reinforcement was recorded as 0.0137 at the column-footing interface, while pushing through -3 % drift ratio at the lateral load -43.0 kN. Maximum strain at CFRP reinforcement was recorded as 0.0075 at the column-footing interface, while pushing through -3 % drift ratio at the lateral load -43.6 kN. Strain distribution of longitudinal steel rebars, longitudinal AFRP, CFRP and GFRP reinforcement in different drift ratios are shown in Figure 4.54, Figure 4.55, Figure 4.56 and Figure 4.57 respectively.

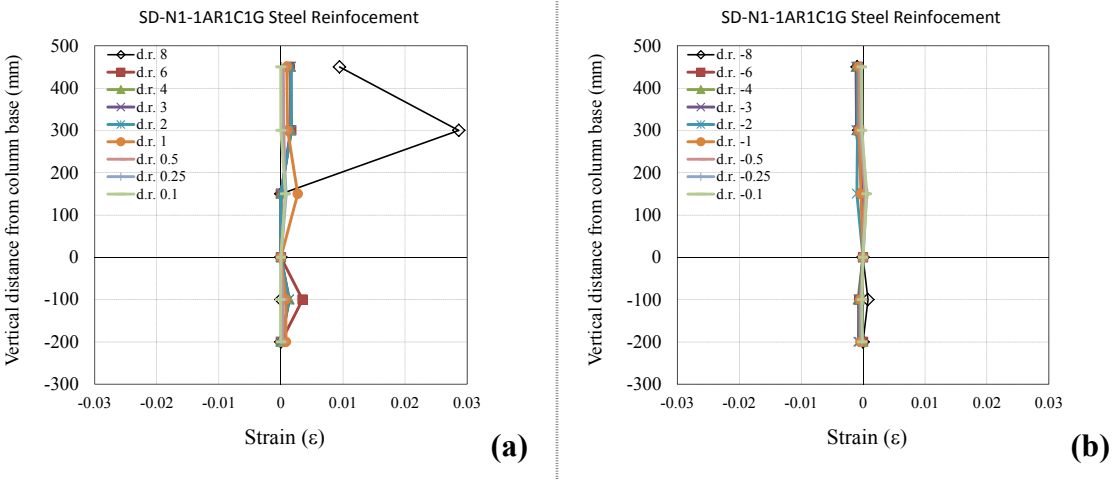

Figure 4.54 : Average strain distribution of longitudinal steel rebars of SD-N1-1AR1C1G: (a)While pulling. (b)While pushing.

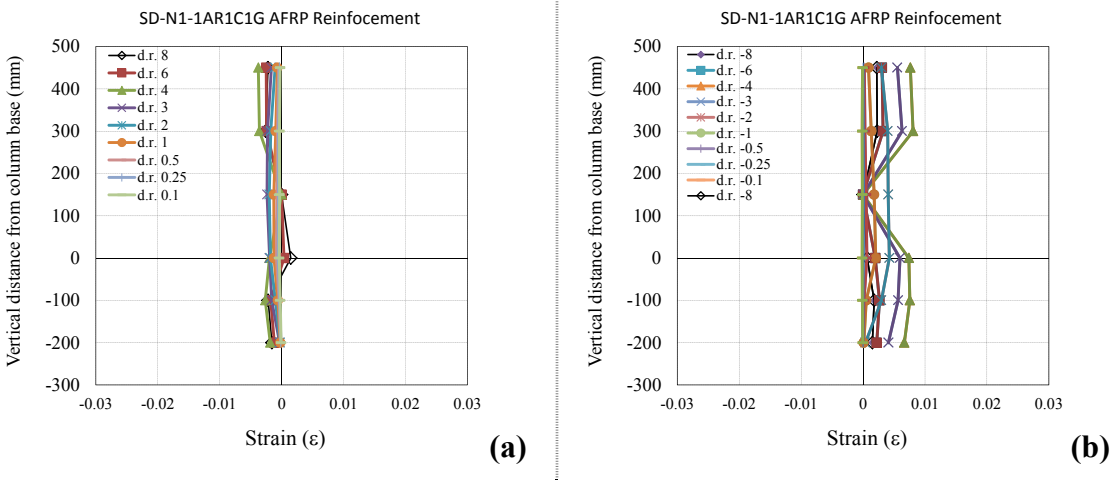

Figure 4.55 : Average strain distribution of longitudinal AFRP reinforcement of SD-N1-1AR1C1G: (a)While pulling. (b)While pushing.

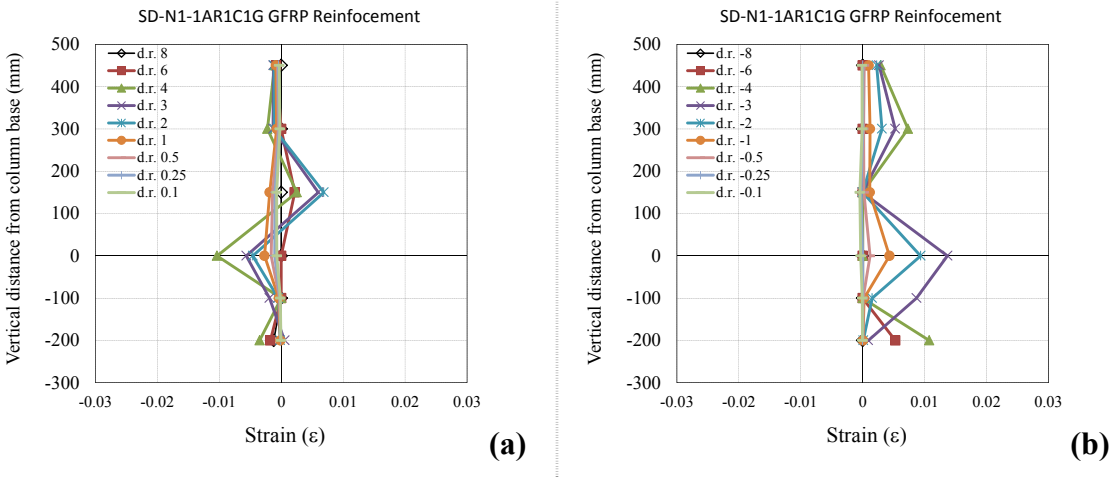

Figure 4.56 : Average strain distribution of longitudinal GFRP reinforcement of SD-N1-1AR1C1G: (a)While pulling. (b)While pushing.

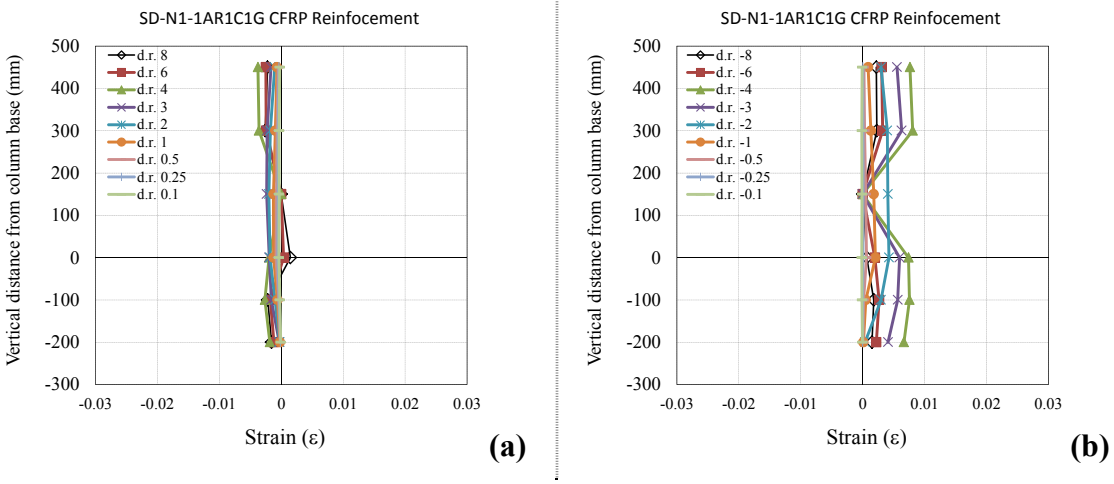

Figure 4.57 : Average strain distribution of longitudinal CFRP reinforcement of SD-N1-1AR1C1G: (a)While pulling. (b)While pushing.

4.3 Test Results of Third Group Specimens

4.3.1 WD-N1-P1

In order to represent the moderate damage for specimen WD-N1-P1, ±2 % drift ratio was targeted to achieve during the test under 120 kN constant axial load.

No cracks were observed while loading to target displacements of ±1.65 mm (drift ratio 0.10 %). First flexural crack was observed at the interface of the column and footing during loading to target displacement of 4.125 mm (drift ratio 0.25 %).

South and north views of the specimen WD-N1-P1 at 0.25 % drift ratio is shown in Figure 4.58.

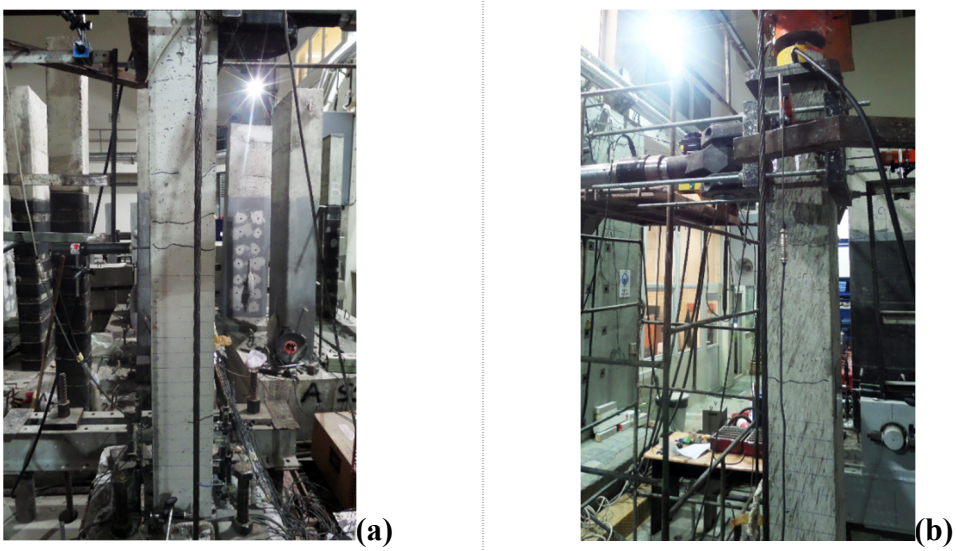

(a) (b)

Figure 4.58 : Views of WD-N1-P1 at 0.25 % drift ratio: (a)South. (b)North.

Further flexural cracks were observed along the column height during loading to target displacement of 8.25 mm (drift ratio 0.50 %). South and north view of the specimen WD-N1-P1 after 0.50 % drift ratio is shown in Figure 4.59.

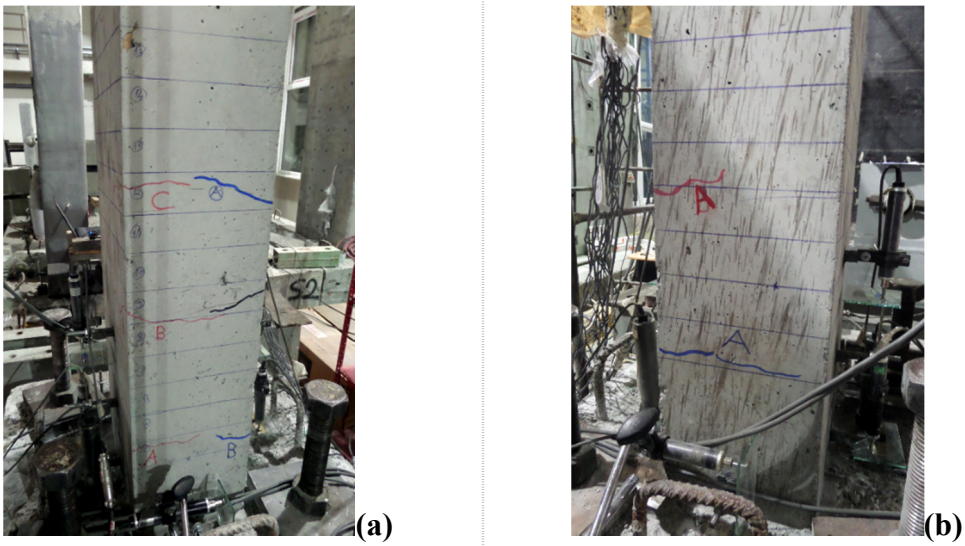

(a) (b)

Figure 4.59 : Views of WD-N1-P1 at 0.50 % drift ratio: (a)South. (b)North.

West and east view of the specimen WD-N1-P1 after 1 % drift ratio is shown in Figure 4.60.

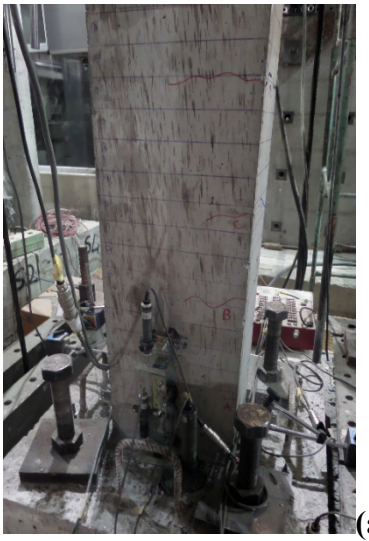

(a)

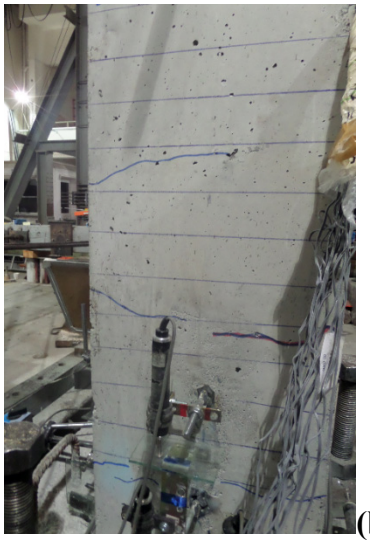

(b)

Figure 4.60 : Views of WD-N1-P1 at 1 % drift ratio: (a)West. (b)East.

During loading to target displacement of 33 mm (drift ratio 2 %), longitudinal steel reinforcement just came into the limit of yielding and eventually yielded for a quite limited time. At this point, the crack width at the column-footing interface reached to 1 mm (Figure 4.61).

Figure 4.61 : Major crack at the bottom of the column after 2 % drift ratio.

Summary of the seismic behavior of specimen WD-N1-P1 is shown in Table 4.8.

Table 4.8 : Summary of the seismic behavior of WD-N1-P1.

Drift ratio (%)	δ (mm/mm)	P (kN)	Observations
0.10	±1.65	1.40 / -1.78	No crack was observed
0.25	±4.125	2.83 / -3.28	First flexural crack at column-footing interface was observed
0.50	±8.25	4.80 / -5.35	Further flexural cracks were observed
1.0	±16.5	7.80 / -8.23	Propagation of existing cracks was observed
2.0	±33.0	10.93 / -11.58	Propagation of existing cracks was observed

Residual deformation was recorded as 9.7 mm at the end of the test. Experimental and theoretical force-displacement relationships of WD-N1-P1 are presented in Figure 4.62. First flexural crack, first yielding point of longitudinal steel reinforcement and maximum strain on the steel rebar are marked on the figure.

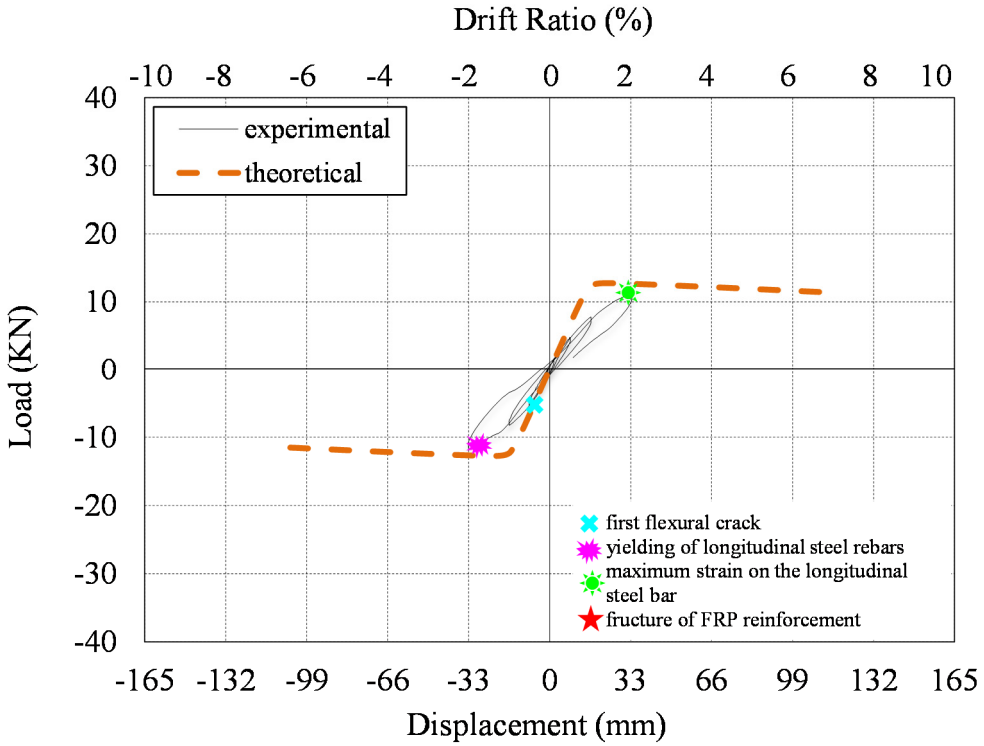

Figure 4.62 : Lateral load versus displacement for WD-N1-P1.

Experimental moment-curvature relationships obtained for critical sections of WD-N1-P1 are presented in Figure 4.63. For the calculation of moment-curvature relationships, the average curvature values obtained for the ranges of 0-20 mm, 20-150 mm and 150-300 mm heights above the footing were taken into account.

As seen from Figure 4.63, the curvature values of the member measured in 20-150 mm and 150-300 mm height above the support are in the order of 5.10^{-6} (1/mm), while the curvatures measured in 0-20 mm height are in the order of 3.10^{-4} (1/mm). It is assessed by considering moment-curvature relationships that the damage was accumulated mainly in the first 20 mm height of the member from top of the footing, which was also confirmed with the damage pattern of the specimen.

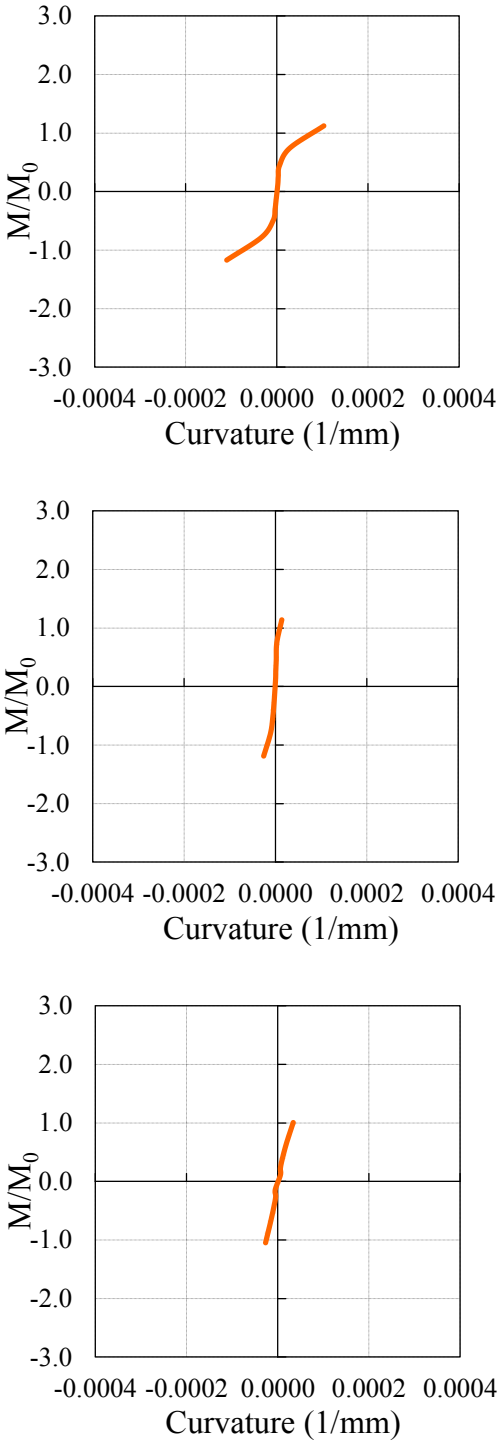

Figure 4.63 : Moment-curvature relationships obtained for gage lengths: (a)0 - 20 mm. (b)20 - 150 mm. (c)150 - 300 mm.

According to the data from the straingauges on the longitudinal steel rebars of the WD-N1-P1, the maximum strain while pushing was 0.0015, measured from the straingauge at the column-footing interface for F=-11.7 kN at -2 % drift ratio; the maximum strain while pulling was -0.0015, measured from the straingauge at +150

mm above the footing when F=11.0 kN at 2 % drift ratio. Average strain distribution of longitudinal steel rebars in different drift ratios are shown in Figure 4.64.

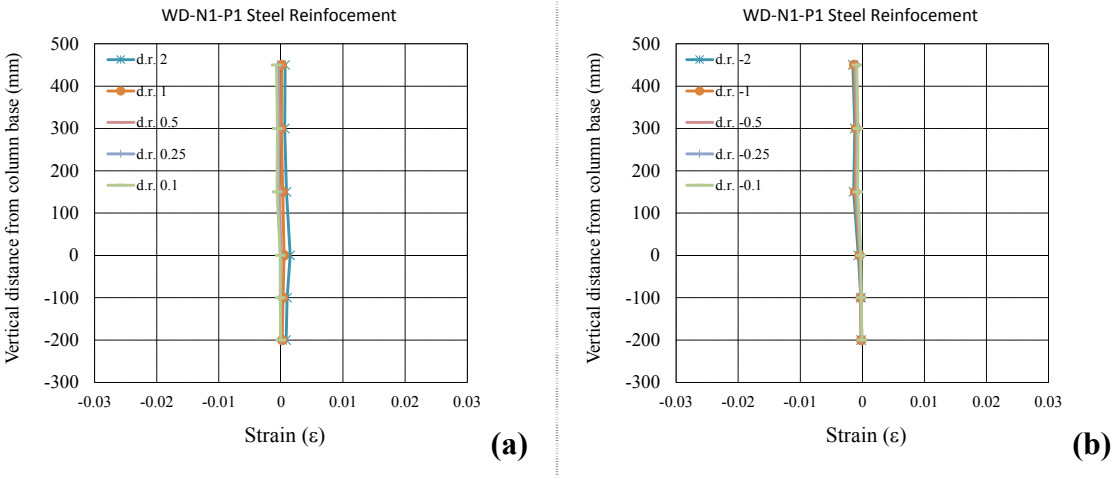

Figure 4.64 : Average strain distribution of longitudinal steel rebars of WD-N1-P1: (a)While pulling. (b)While pushing.

4.3.2 WD-N1-P2

The specimen WD-N1-P2 was selected to represent the the columns suffering from heavy damages. In order to create extensive damages, the specimen was tested up to ±4 % drift ratio under 120 kN constant axial load. South and north views of the specimen WD-N1-P2 prior to testing are shown in Figure 4.65.

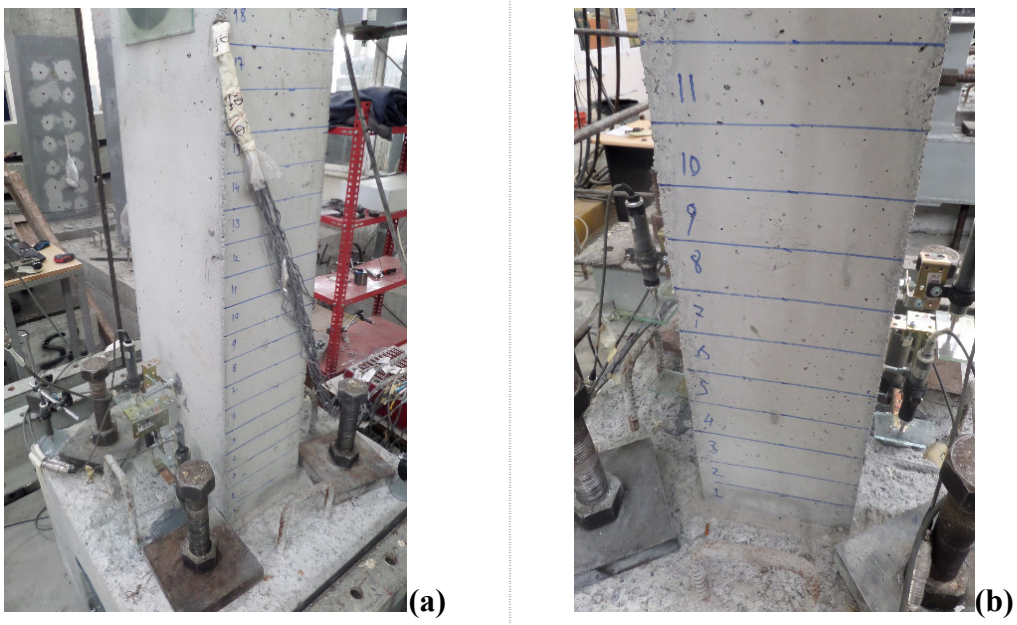

Figure 4.65 : Views of WD-N1-P2 prior to testing: (a)South. (b)North.

No cracks were observed while loading to target displacements of ±1.65 mm (drift ratio 0.10 %). First flexural crack was observed at the interface of the column and footing during loading to target displacement of 4.125 mm (drift ratio 0.25 %).

South and north views of the specimen WD-N1-P2 at 0.25 % drift ratio is shown in Figure 4.66.


(a)

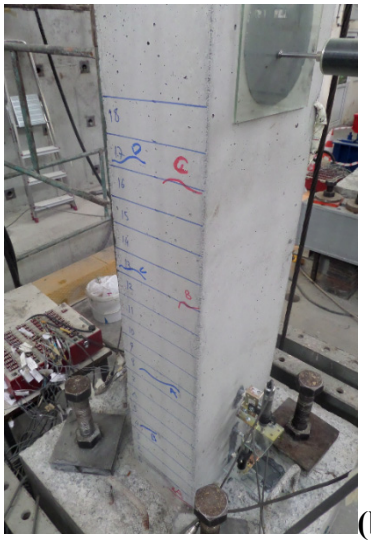
(b)

Figure 4.66 : Views of WD-N1-P2 at 0.25 % drift ratio: (a)South. (b)North.

Further flexural cracks were observed along the column height during loading to target displacement of 8.25 mm (drift ratio 0.50 %). South and north view of the specimen WD-N1-P2 after 0.50 % drift ratio is shown in Figure 4.67.

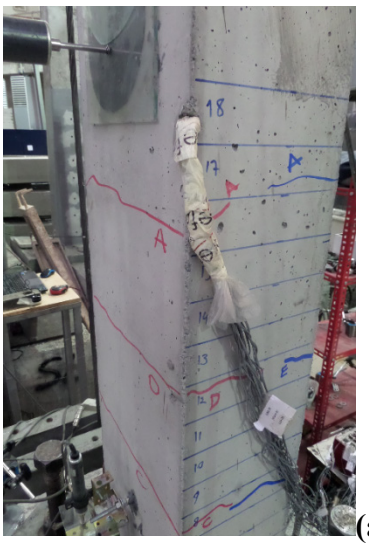
(a)

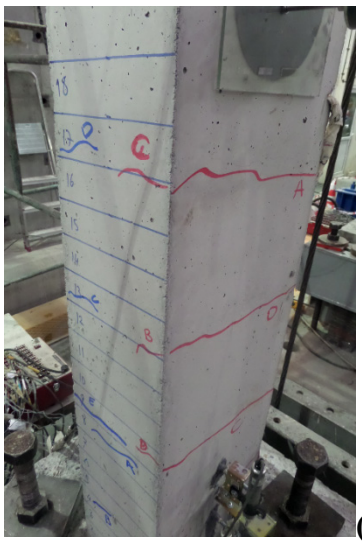
(b)

Figure 4.67 : Views of WD-N1-P2 at 0.50 % drift ratio: (a)South. (b)North.

South and north view of the specimen WD-N1-P2 after 1 % drift ratio is shown in Figure 4.68.

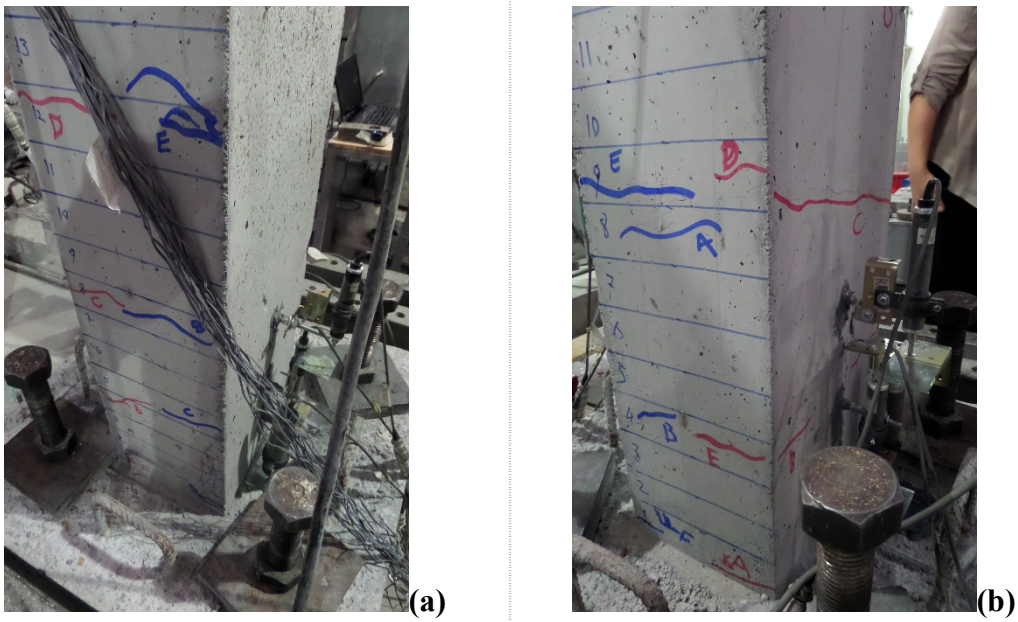

(a) (b)

Figure 4.68 : Views of WD-N1-P2 at 1 % drift ratio: (a)South. (b)North.

South and north view of the specimen WD-N1-P2 after 3 % drift ratio is shown in Figure 4.69.

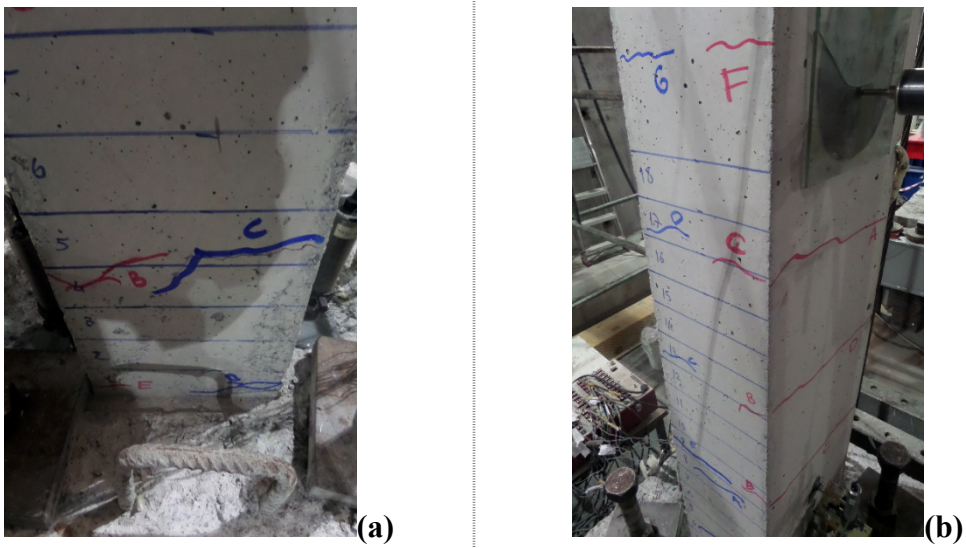

(a) (b)

Figure 4.69 : Views of WD-N1-P2 at 3 % drift ratio: (a)South. (b)North.

During loading to target displacement of 49.5 mm (drift ratio 3 %), longitudinal steel reinforcement started to yield, while stirrups were not yielded. At this point, existing

cracks opened wider and propogated along the cross section of the column. Besides, some new cracks occurred on the column surface at 100 cm above footing.

In the further steps of the test, concrete cover started to spall and locally crushed close to column-footing interface. Unlikely to previous specimens, it was observed that damage was accumulated 20 cm above the footing at the drift ratio 4 % (Figure 4.70).

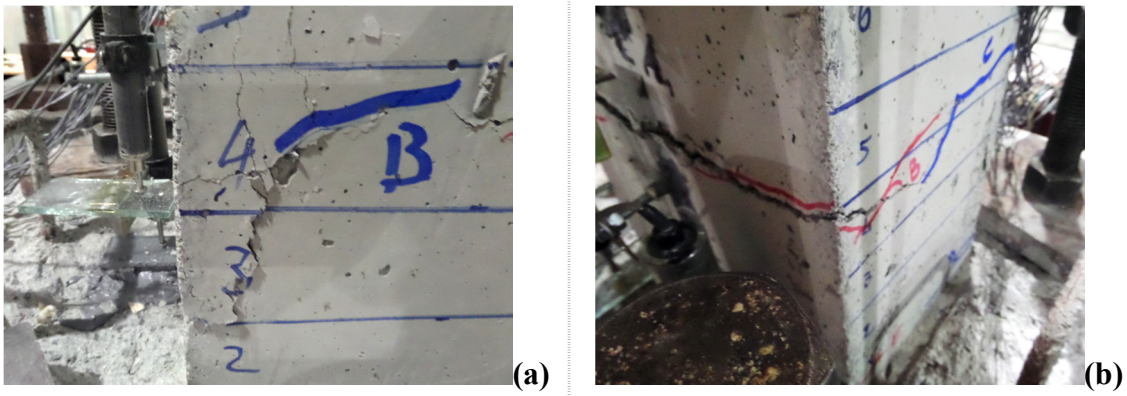

(a) **(b)**

Figure 4.70 : Damages at 4 % drift ratio: (a)Spalled concrete cover. (b)Accumulated damage 20 cm over footing.

Summary of the seismic behavior of specimen WD-N1-P2 is shown in Table 4.9.

Table 4.9 : Summary of the seismic behavior of WD-N1-P2.

Drift ratio (%)	δ (mm/mm)	P (kN)	Observations
0.10	±1.65	0.91 / -2.34	No crack was observed
0.25	±4.125	2.36 / -3.68	First flexural crack at column-footing interface was observed
0.50	±8.25	4.45 / -5.25	Further flexural cracks were observed
1.0	±16.5	7.79 / -8.05	Propagation of existing cracks was observed
2.0	±33.0	10.61 / -11.47	Propagation of existing cracks was observed
3.0	±49.5	12.32 / -12.76	Propagation of existing cracks was observed
4.0	±66.0	11.04 / -10.64	Crushing and spalling started at the concrete cover

Residual deformation was recorded as 22.1 mm at the end of the test. Experimental and theoretical force-displacement relationships of WD-N1-P2 are presented in Figure 4.71. First flexural crack, first yielding point of longitudinal steel reinforcement and maximum strain on the steel rebar are marked on the figure.

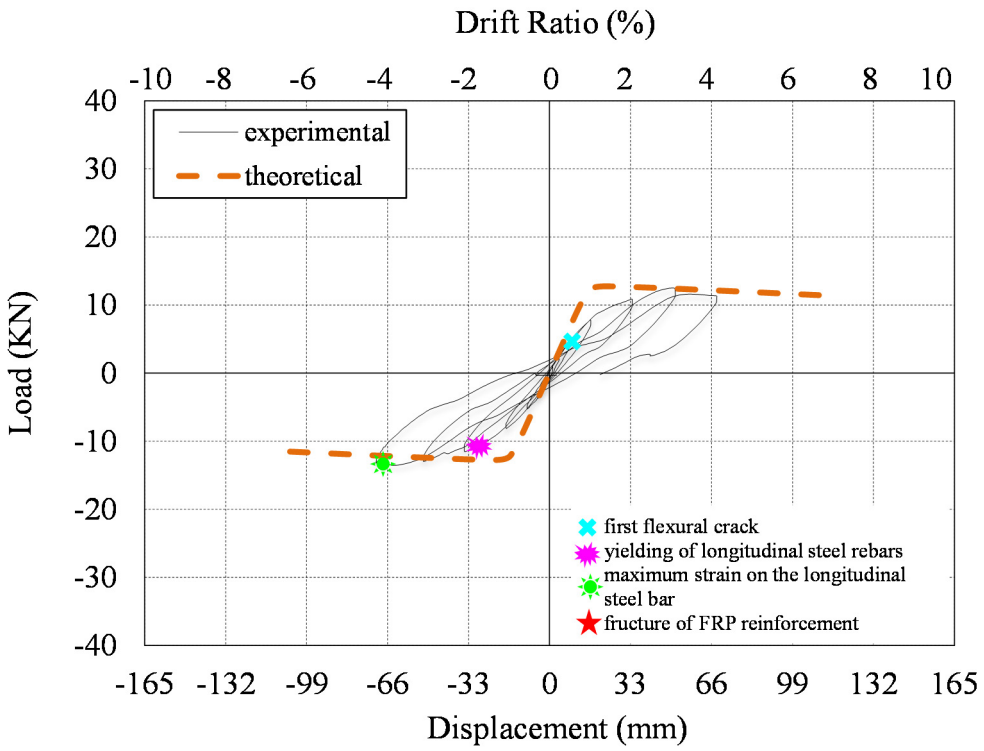

Figure 4.71 : Lateral load versus displacement for WD-N1-P2.

Experimental moment-curvature relationships obtained for critical sections of WD-N1-P2 are presented in Figure 4.72.

For the calculation of moment-curvature relationships, the average curvature values obtained for the ranges of 0-20 mm, 20-150 mm and 150-300 mm heights above the footing were taken into account. As seen from Figure 4.72, the curvature values of the member measured in 20-150 mm height above the support are in the order of 5.10^{-6} (1/mm), while the curvatures measured in 0-20 mm and 150-300 mm height are in the order of 3.10^{-4} (1/mm). It is assessed by considering moment-curvature relationships that the damage was accumulated mainly in the first 20 mm and 150-300 mm height of the member from top of the footing. This behavior is also confirmed by the damage pattern of the specimen, while a major crack was opened 200 mm above the footing because of accumulated damage exceptionally for specimen WD-N1-P2.

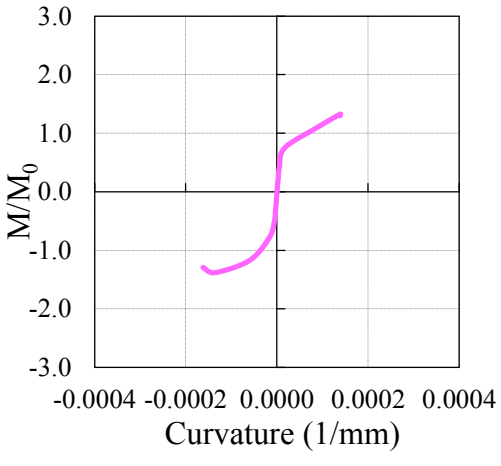

(a)

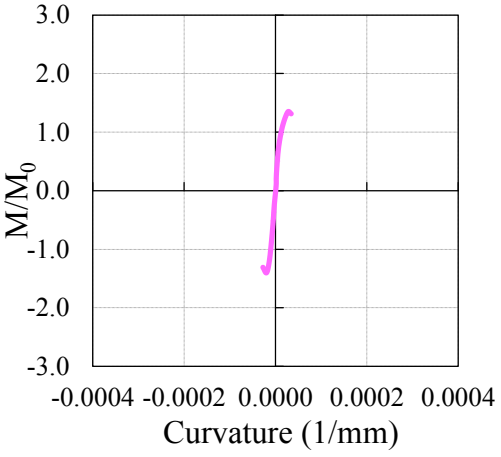

(b)

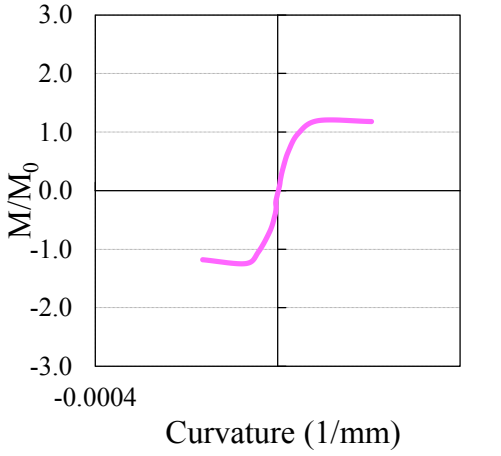

(c)

Figure 4.72 : Moment-curvature relationships obtained for gage lengths: (a)0 - 20 mm. (b)20 - 150 mm. (c)150 - 300 mm.

According to the data from the straingauges on the longitudinal steel rebars of the WD-N1-P2, the maximum strain while pushing was 0.0032, measured from the straingauge at +150 mm above the footing for F=-13.2 kN at -4 % drift ratio; the maximum strain while pulling was -0.0014, measured from the straingauge at +150 mm above the footing when F=11.5 kN at 4 % drift ratio. Average strain

distribution of longitudinal steel rebars in different drift ratios are shown in Figure 4.73.

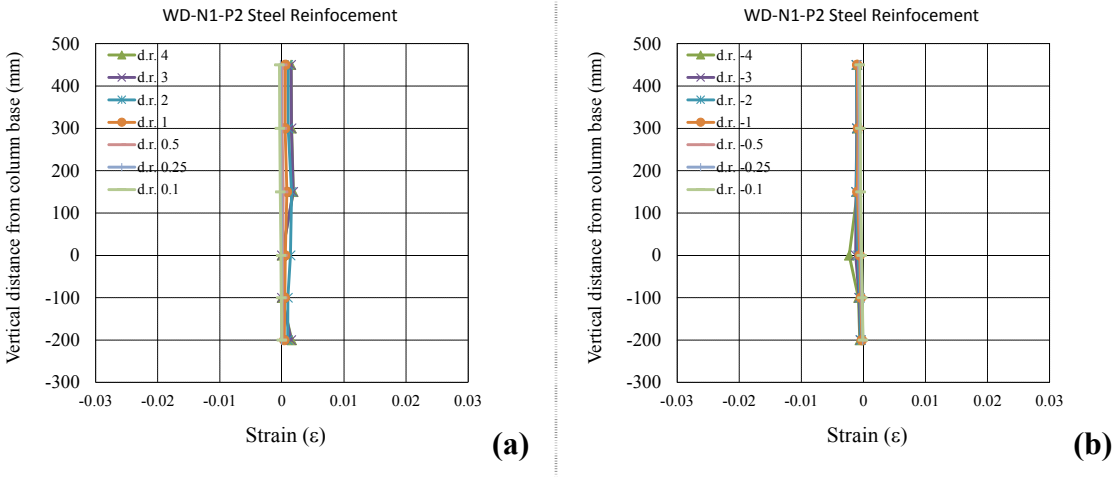

Figure 4.73 : Average strain distribution of longitudinal steel rebars of WD-N1-P2: (a)While pulling. (b)While pushing.

4.3.3 WD-N1-2AR-P1

Test setup and general view of the specimen is shown in Figure 4.74.

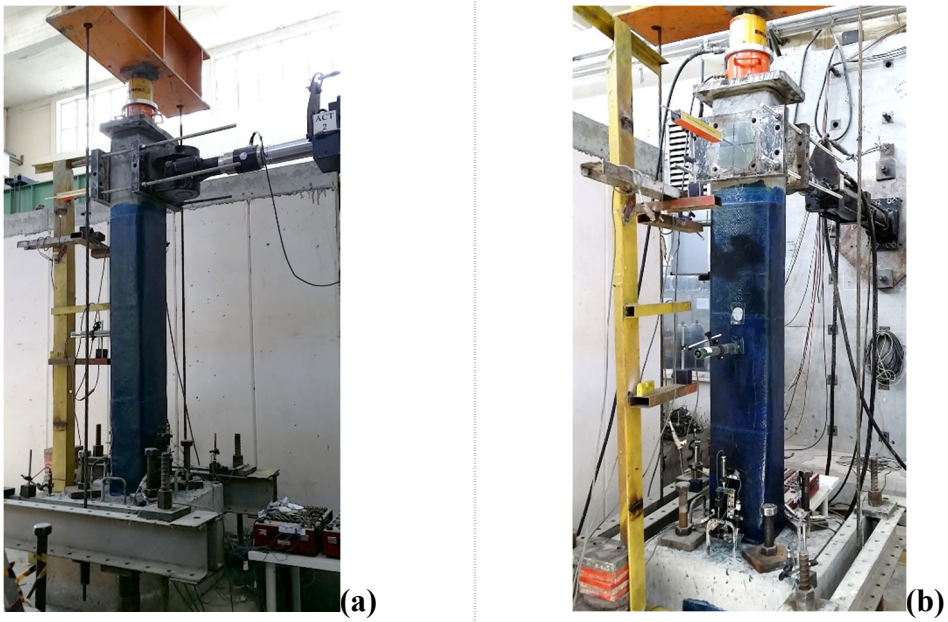

Figure 4.74 : Views of WD-N1-2AR-P1 prior to test: (a)Southeast. (b)West.

No cracks were observed while loading to target displacements of ±4.125 mm (drift ratio 0.25 %). First flexural crack was observed at the interface of the column and footing during loading to target displacement of 8.25 mm (drift ratio 0.50 %).

It was observed that longitudinal steel reinforcement started to yield at 2 % drift ratio, while stirrups were not yielded during the whole test. While pushing towards -4 % drift ratio, a loud noice coming from the specimen was recorded with a sudden decrease in the lateral load. The reason of the sound was found as fracture of the AFRP longitudinal reinforcement. This behaviour was repeated while pulling the column towards 4 % drift ratio with less decrease in the lateral load. From this point forward, the specimen WD-N1-2AR-P1 performed similar to specimen WD-N1-P2 in terms of load-displacement relation, while pulling, however it sustained a significant lateral load while pushing. This was confirmed with an unfractured AFRP contributing in pushing direction. No additional cracks were observed in further drift ratios, while the existing cracks at the column-footing interface were continously enlarged. At 8 % drift ratio the crack opening was measured 5 mm. South and north views of the specimen WD-N1-2AR-P1 at 8 % drift ratio is shown in Figure 4.75.

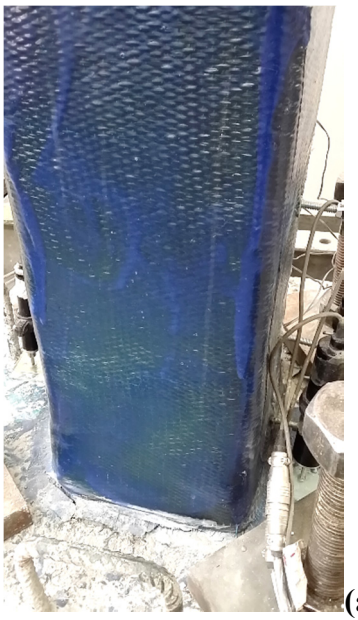
(a)


(b)

Figure 4.75 : Views of WD-N1-2AR-P1 at 8 % drift ratio: (a)South. (b)North.

Residual deformation was recorded as 87.5 mm when lateral load was absolute zero. Until AFRP reinforcement fracture, measured lateral loads were significantly higher comparing to specimen WD-N1-P1 and the increase in the lateral load capacity was calculated as 114 % while pushing and 94 % while pulling compared to specimen WD-N1-P2. Similar to previous retrofitted specimens, AFRP reinforcement in both surfaces of the columns were fractured (except one sound AFRP bar on east side of the column) in the column – footing interface, where deformations were cumulated.

During the autopsy of the specimen, CFRP confinement was cut of in the first 60 cm height of the columns over footing and column surfaces was investigated for possible flexural cracks. It was seen that deformations were cumulated at the column-footing interface and no significant crack was observed through the column height. In order to confirm the fracture pattern of the AFRP reinforcement, SRM cover around the core concrete was broken and AFRP bars were exposed. It was observed that three AFRP bars out of four raptured as shown in Figure 4.76.

(a)

(b)

Figure 4.76 : Fractured AFRP longitudinal reinforcement in the specimen WD-N1-2AR-P1: (a)East view. (b)West view.

Summary of the seismic behavior of specimen WD-N1-2AR-P1 is shown in Table 4.10.

Table 4.10 : Summary of the seismic behavior of WD-N1-2AR-P1.

Drift ratio (%)	δ (mm/mm)	P (kN)	Observations
0.10	±1.65	3.10 / -3.14	No crack was observed
0.25	±4.125	6.02 / -6.97	No crack was observed
0.50	±8.25	9.18 / -11.98	First flexural crack at column-footing interface was observed
1.0	±16.5	14.11 / -18.19	Propagation of existing crack at column-footing interface was observed
2.0	±33.0	20.49 / -25.67	Propagation of existing crack at column-footing interface was observed
3.0	±49.5	24.29 / -29.01	Propagation of existing crack at column-footing interface was observed
4.0	±66.0	14.69 / -25.39	AFRP reinforcement in tension fractured and lateral load decreased to 14.7 kN
6.0	±99.0	13.75 / -22.44	Propagation of existing crack at column-footing interface was observed
8.0	±132.0	13.40 / -23.05	Propagation of existing crack at column-footing interface was observed

Experimental and theoretical force-displacement relationships of WD-N1-2AR-P1 are presented in Figure 4.77. First flexural crack, first yielding point of longitudinal steel reinforcement and maximum strain on the steel rebar are marked on the figure.

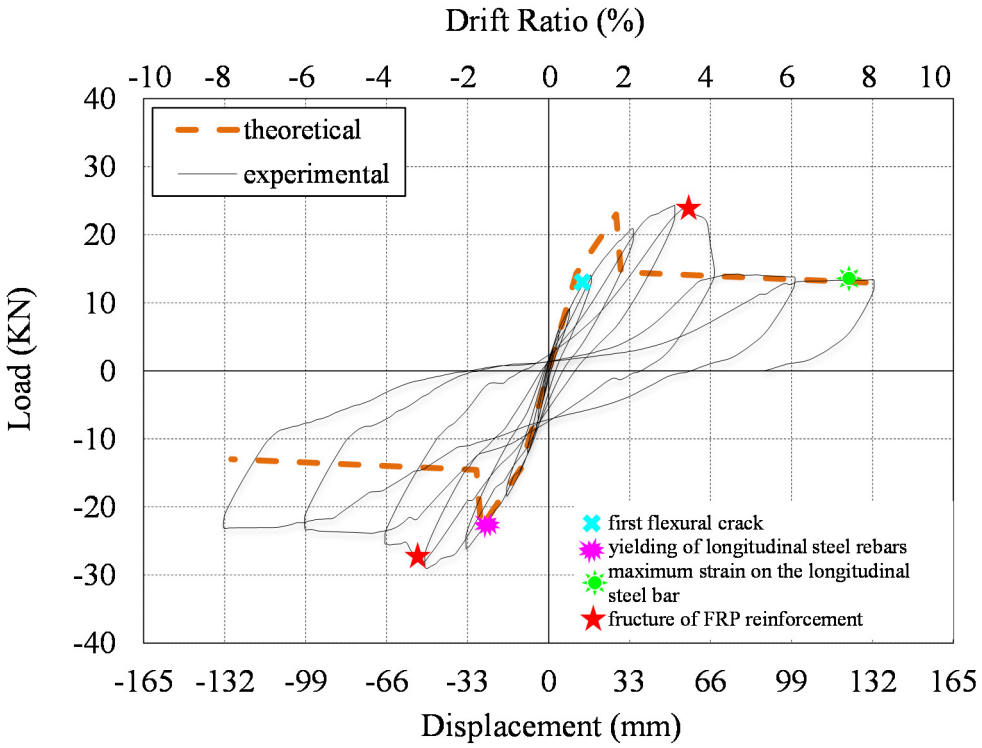

Figure 4.77 : Lateral load versus displacement for WD-N1-2AR-P1.

Experimental moment-curvature relationships obtained for critical sections of WD-N1-2AR-P1 are presented in Figure 4.78. For the calculation of moment-curvature relationships, the average curvature values obtained for the ranges

of 0-20 mm, 20-150 mm and 150-300 mm heights above the footing were taken into account.

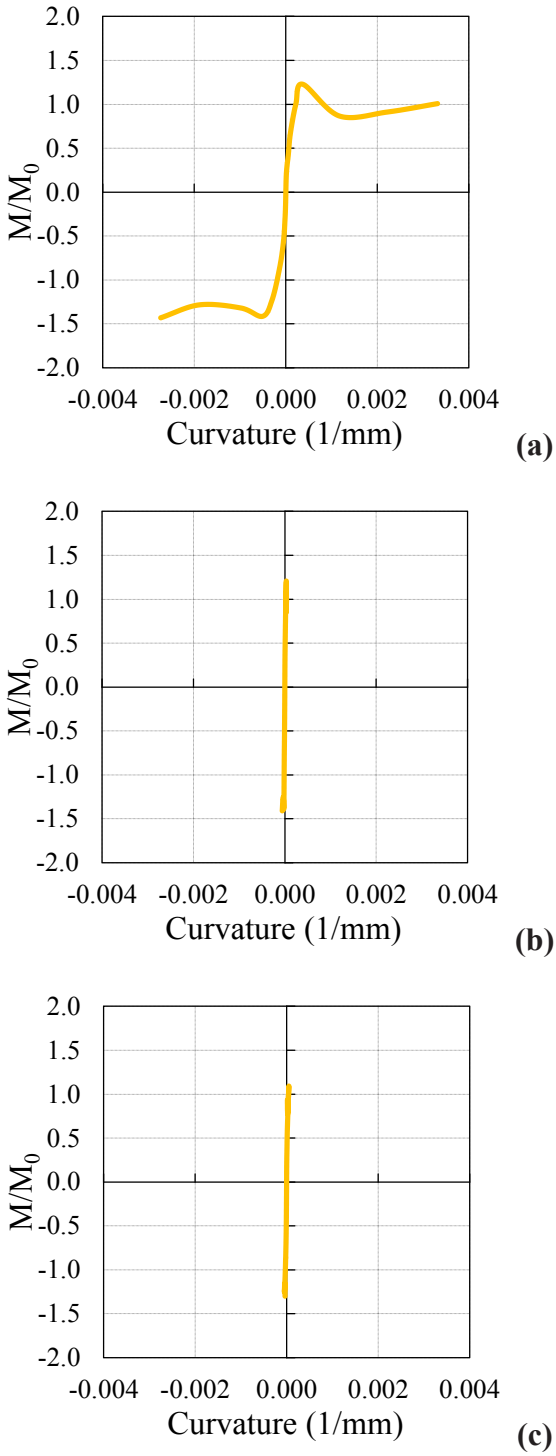

Figure 4.78 : Moment-curvature relationships obtained for gage lengths: (a)0 - 20 mm. (b)20 - 150 mm. (c)150 - 300 mm.

As seen from Figure 4.78, the curvature values of the member measured in 20-150 mm and 150-300 mm height above the support are in the order of 5.10^{-5} (1/mm), while the curvatures measured in 0-20 mm height are in the order of

3.10^{-3} (1/mm). It is assessed by considering moment-curvature relationships that the damage was accumulated mainly in the first 20 mm height of the member from top of the footing, which was also confirmed with the damage pattern of the specimen.

Average strain distribution of longitudinal steel rebars and longitudinal AFRP reinforcement in different drift ratios are shown in Figure 4.79 and Figure 4.80 respectively.

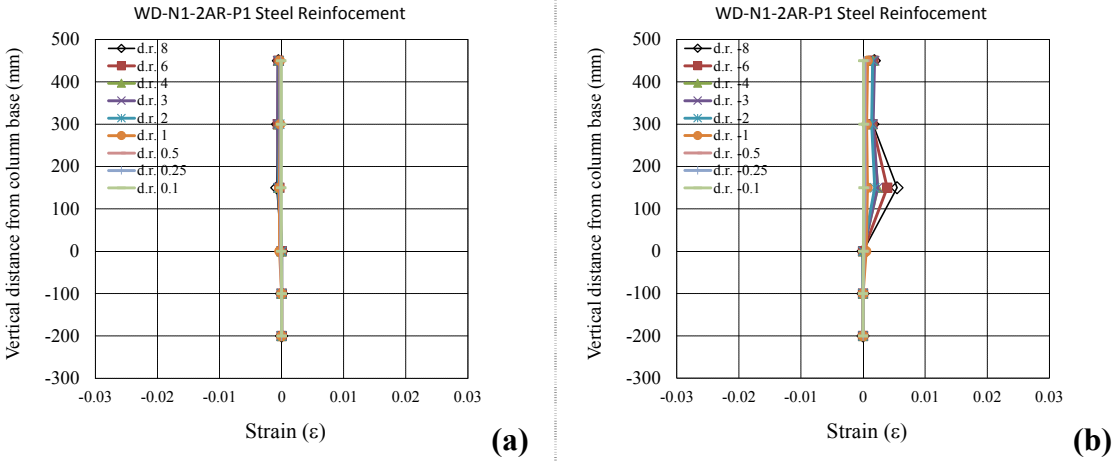

Figure 4.79 : Average strain distribution of longitudinal steel rebars of WD-N1-2AR-P1: (a)While pulling. (b)While pushing.

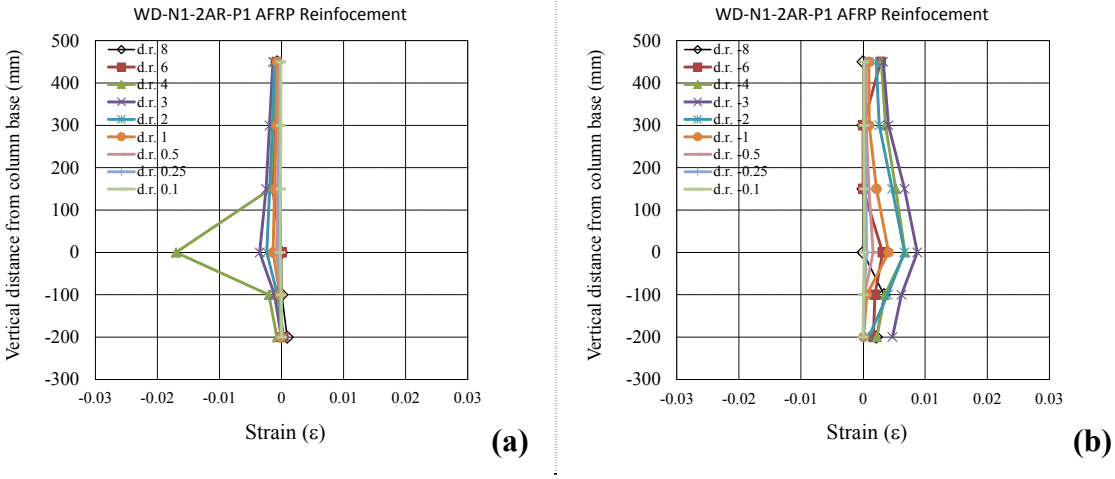

Figure 4.80 : Average strain distribution of AFRP longitudinal reinforcement of WD-N1-2AR-P1: (a)While pulling. (b)While pushing.

According to the data from the straingauges on the longitudinal steel rebars of the WD-N1-2AR-P1, the maximum strain while pushing was 0.0055, measured from the straingauge at 150 mm above footing for F=-23.1 kN at -8 % drift ratio; the maximum strain while pulling was -0.0014, measured from the straingauge at 150 mm above

footing when F=6.7 kN at 8 % drift ratio. Maximum strain at AFRP reinforcement was recorded as 0.0090 at the column-footing interface, while pushing through -4 % drift ratio at the lateral load -28.1 kN.

4.3.4 WD-N1-2AR-P2

No cracks were observed while loading to target displacements of ±8.25 mm (drift ratio 0.50 %). First flexural crack was observed at the interface of the column and footing during loading to target displacement of 16.50 mm (drift ratio 1 %).

It was observed that longitudinal steel reinforcement started to yield at 3 % drift ratio, while stirrups were not yielded during the whole test. While pushing towards -4 % drift ratio, a loud noise coming from the specimen was recorded with a sudden decrease in the lateral load. The reason of the sound was found as fracture of the AFRP longitudinal reinforcement. This behavior was repeated while pulling the column towards 4 % drift ratio with less decrease in the lateral load. Even though, lateral load decreased sharply, specimen WD-N1-2AR-P2 sustained significant lateral load, which is much higher (approximately 30 % in pushing and 50 % in pulling) than specimen WD-N1-P2 in further steps. No additional cracks were observed in further drift ratios, while the existing crack at the column-footing interface was continuously enlarged. At 8 % drift ratio the crack opening was measured 12 mm. South and north views of the specimen WD-N1-2AR-P2 at 8 % drift ratio is shown in Figure 4.81.

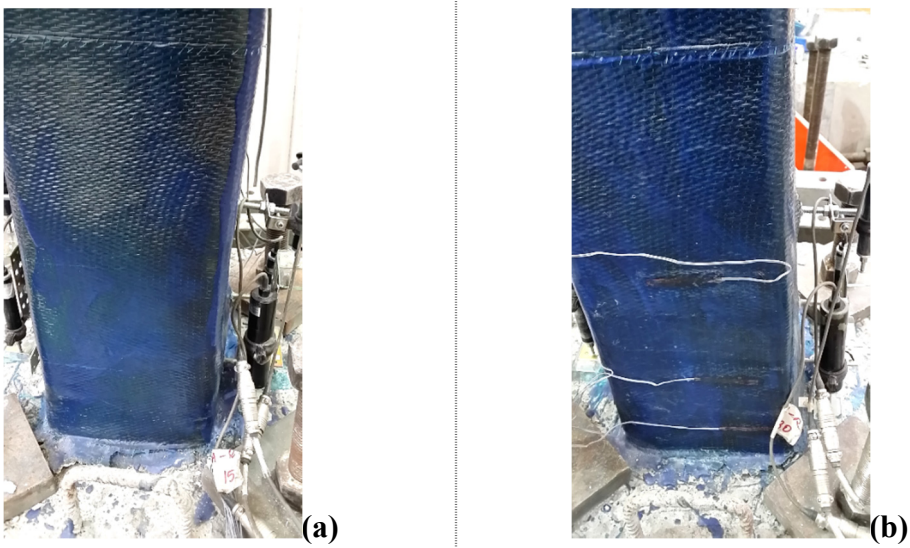

(a) **(b)**

Figure 4.81 : Views of WD-N1-2AR-P2 at 8 % drift ratio: (a)South. (b)North.

Residual deformation was recorded as 64.4 mm when lateral load was absolute zero. Until AFRP reinforcement fracture, increase in the lateral load capacity was calculated as 106 % while pushing and 128 % while pulling compared to specimen WD-N1-P2. Similar to previous retrofitted specimens, AFRP reinforcement in both surfaces of the columns were fractured (raptured in one side of the column, however buckled in the other side) in the column – footing interface, where deformations were cumulated.

During the autopsy of the specimen, CFRP confinement was cut off in the first 60 cm height of the columns over footing and column surfaces was investigated for possible flexural cracks. It was seen that deformations were cumulated at the column-footing interface and no significant crack was observed through the column height. In order to confirm the fracture pattern of the AFRP reinforcement, SRM cover around the core concrete was broken and AFRP bars were exposed. It was observed that two AFRP bars were raptured and remaining two were buckled as shown in Figure 4.82.

Summary of the seismic behavior of specimen WD-N1-2AR-P2 is shown in Table 4.11.

Table 4.11 : Summary of the seismic behavior of WD-N1-2AR-P2.

Drift ratio (%)	δ (mm/mm)	P (kN)	Observations
0.10	±1.65	4.40 / -2.76	No crack was observed
0.25	±4.125	8.52 / -6.28	No crack was observed
0.50	±8.25	12.14 / -10.31	No crack was observed
1.0	±16.5	17.35 / -15.61	First flexural crack at column-footing interface was observed
2.0	±33.0	24.18 / -23.30	Propagation of existing crack at column-footing interface was observed
3.0	±49.5	28.52 / -27.90	Propagation of existing crack at column-footing interface was observed
4.0	±66.0	26.70 / -27.15	AFRP reinforcement in tension fractured and lateral load decreased to -23.0 kN
6.0	±99.0	17.07 / -20.85	Propagation of existing crack at column-footing interface was observed
8.0	±132.0	16.24 / -20.64	Propagation of existing crack at column-footing interface was observed

Figure 4.82 : Fractured AFRP longitudinal reinforcement in the specimen WD-N1-2AR-P2: (a)East view. (b)West view.

Experimental and theoretical force-displacement relationships of WD-N1-2AR-P2 are presented in Figure 4.83.

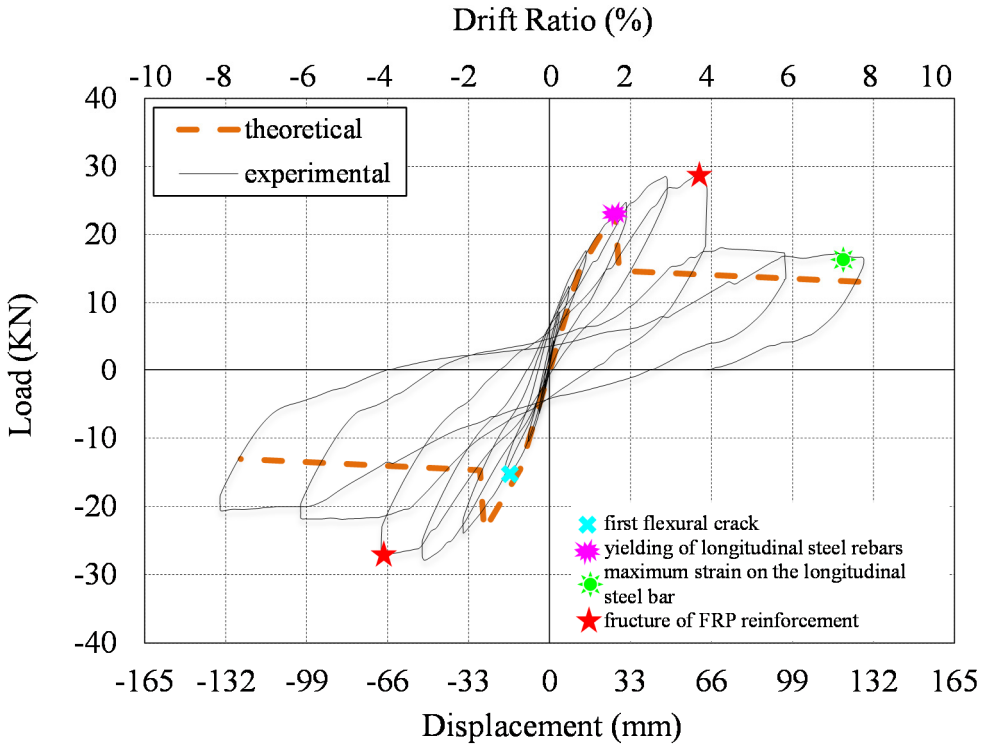

Figure 4.83 : Lateral load versus displacement for WD-N1-2AR-P2.

Experimental moment-curvature relationships obtained for critical sections of WD-N1-2AR-P2 are presented in Figure 4.84.

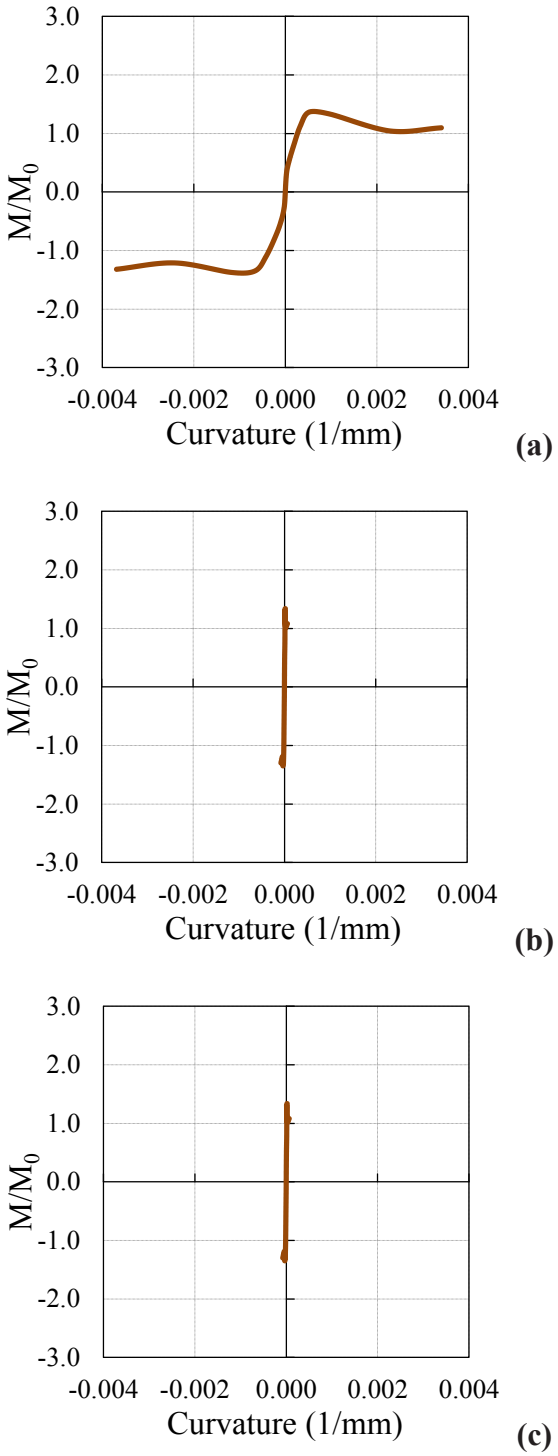

Figure 4.84 : Moment-curvature relationships obtained for gage lengths: (a)0 - 20 mm. (b)20 - 150 mm. (c)150 - 300 mm.

For the calculation of moment-curvature relationships, the average curvature values obtained for the ranges of 0-20 mm, 20-150 mm and 150-300 mm heights above the footing were taken into account. As seen from Figure 4.84, the curvature values of the

member measured in 20-150 mm and 150-300 mm height above the support are in the order of 5.10^{-5} (1/mm), while the curvatures measured in 0-20 mm height are in the order of 3.10^{-3} (1/mm). It is assessed by considering moment-curvature relationships that the damage was accumulated mainly in the first 20 mm height of the member from top of the footing, which was also confirmed with the damage pattern of the specimen.

Average strain distribution of longitudinal steel rebars and longitudinal AFRP reinforcement in different drift ratios are shown in Figure 4.85 and Figure 4.86 respectively.

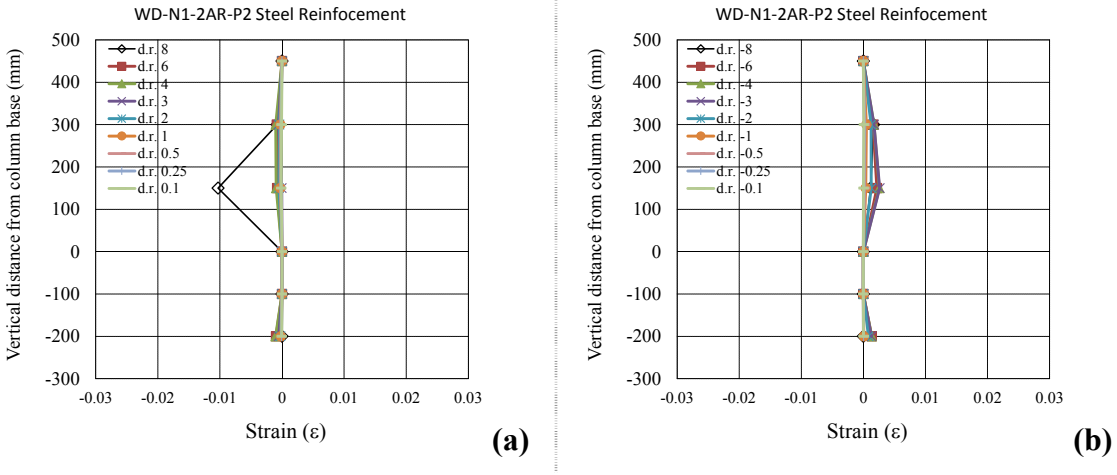

Figure 4.85 : Average strain distribution of longitudinal steel rebars of WD-N1-2AR-P2: (a)While pulling. (b)While pushing.

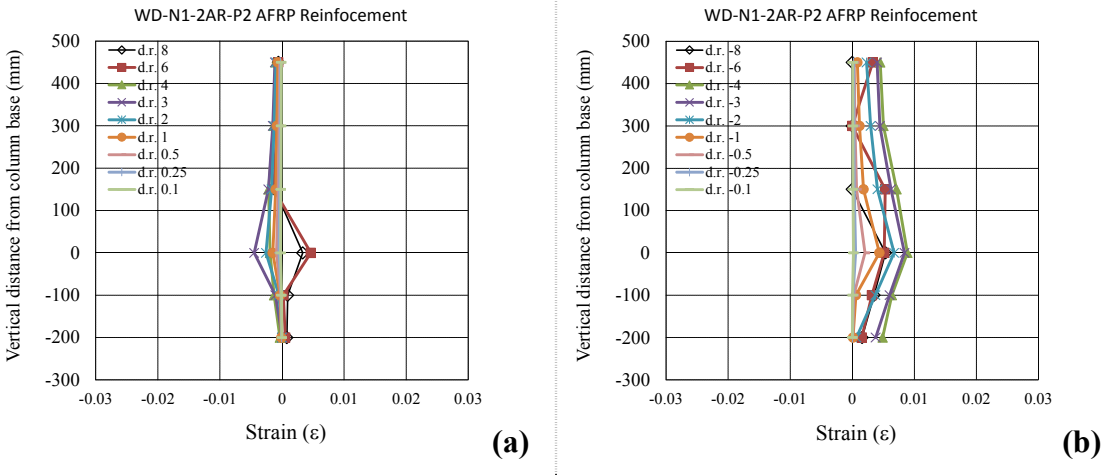

Figure 4.86 : Average strain distribution of AFRP longitudinal reinforcement of WD-N1-2AR-P2: (a)While pulling. (b)While pushing.

According to the data from the straingauges on the longitudinal steel rebars of the WD-N1-2AR-P2, the maximum strain while pushing was 0.0028, measured from the

straingauge at 200 mm in the footing for F=-20.1 kN at -8 % drift ratio; the maximum strain while pulling was -0.0132, measured from the straingauge at 150 mm above footing when F=7.9 kN at 8 % drift ratio. Maximum strain at AFRP reinforcement was recorded as 0.0114 at the column-footing interface, while pushing through -4 % drift ratio at the lateral load -27.2 kN.

4.3.5 WD-N1-2AR

No cracks were observed while loading to target displacements of ±4.125 mm (drift ratio 0.25 %). First flexural crack was observed at the interface of the column and footing during loading to target displacement of 8.25 mm (drift ratio 0.50 %). Southwest and north views of the specimen WD-N1-2AR at 8 % drift ratio are shown in Figure 4.87.

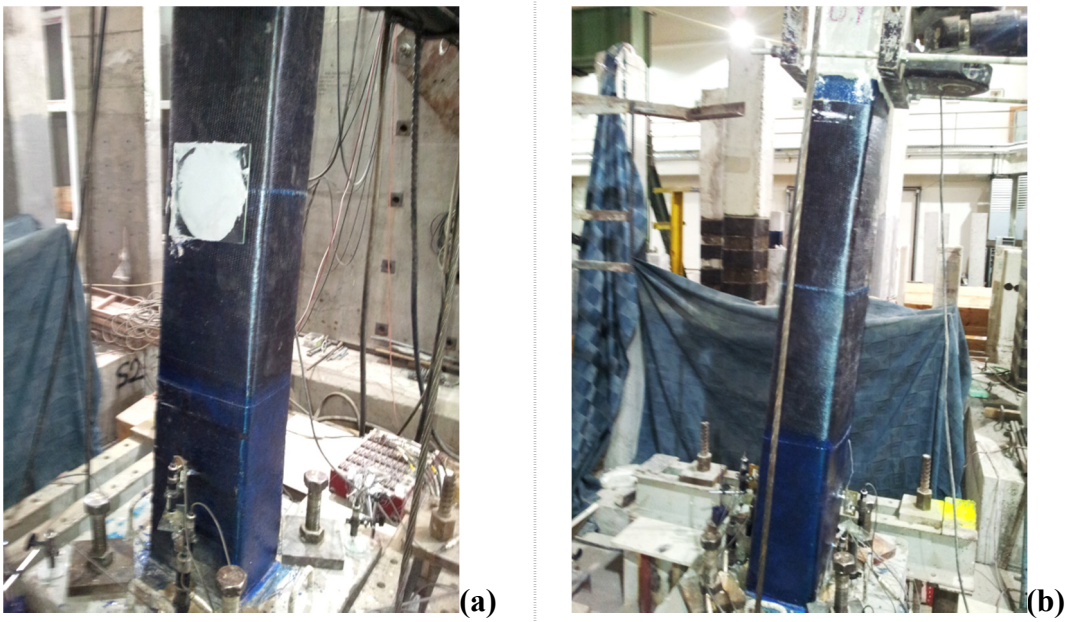

(a) **(b)**

Figure 4.87 : Views of WD-N1-2AR at 8 % drift ratio: (a)Southwest. (b)North.

It was observed that longitudinal steel reinforcement started to yield at 3 % drift ratio, while stirrups were not yielded during the whole test. While pulling towards 4 % drift ratio, a loud noise coming from the specimen was recorded with a sudden decrease in the lateral load. The reason of the sound was found as fracture of the AFRP longitudinal reinforcement located at west side of the column. Unlikely to previous specimens, FRP reinforcement fractured at only one side of the column, however the ones located at the other side continued to bare load until to the end of the test. No

additional cracks were observed in further drift ratios, while the existing crack at the column-footing interface was continuously enlarged.

Residual deformation was recorded as 103.9 mm when lateral load was absolute zero. Until AFRP reinforcement fracture, increase in the lateral load capacity was calculated as 110 % while pushing and 97 % while pulling compared to specimen WD-N1-P2.

Autopsy photos are shown in the Figure 4.88.

Figure 4.88 : Fractured AFRP longitudinal reinforcement in the specimen WD-N1-2AR: (a)East view. (b)West view.

During the autopsy of the specimen, CFRP confinement was cut off in the first 60 cm height of the columns over footing and column surfaces was investigated for possible flexural cracks. It was seen that deformations were cumulated at the column-footing interface and no significant crack was observed through the column height. In order to confirm the fracture pattern of the AFRP reinforcement, SRM cover around the core concrete was broken and AFRP bars were exposed. It was observed that two AFRP bars were raptured and remaining two were sound (Figure 4.88).

Summary of the seismic behavior of specimen WD-N1-2AR is shown in Table 4.12.

Table 4.12 : Summary of the seismic behavior of WD-N1-2AR.

Drift ratio (%)	δ mm/mm)	P (kN)	Observations
0.10	±1.65	3.75 / -2.93	No crack was observed
0.25	±4.125	6.74 / -7.04	No crack was observed
0.50	±8.25	9.73 / -11.74	First flexural crack at column-footing interface was observed
1.0	±16.5	14.43 / -16.75	Propagation of existing crack at column-footing interface was observed
2.0	±33.0	20.56 / -22.71	Propagation of existing crack at column-footing interface was observed
3.0	±49.5	24.71 / -25.80	Propagation of existing crack at column-footing interface was observed
4.0	±66.0	12.51 / -27.80	AFRP reinforcement in tension fractured and lateral load decreased to 12.5 kN
6.0	±99.0	12 / -23.38	Propagation of existing crack at column-footing interface was observed
8.0	±132.0	11.03 / -23.38	Propagation of existing crack at column-footing interface was observed

Experimental and theoretical force-displacement relationships of WD-N1-2AR are presented in Figure 4.89. First flexural crack, first yielding point of longitudinal steel reinforcement and maximum strain on the steel rebar are marked on the figure.

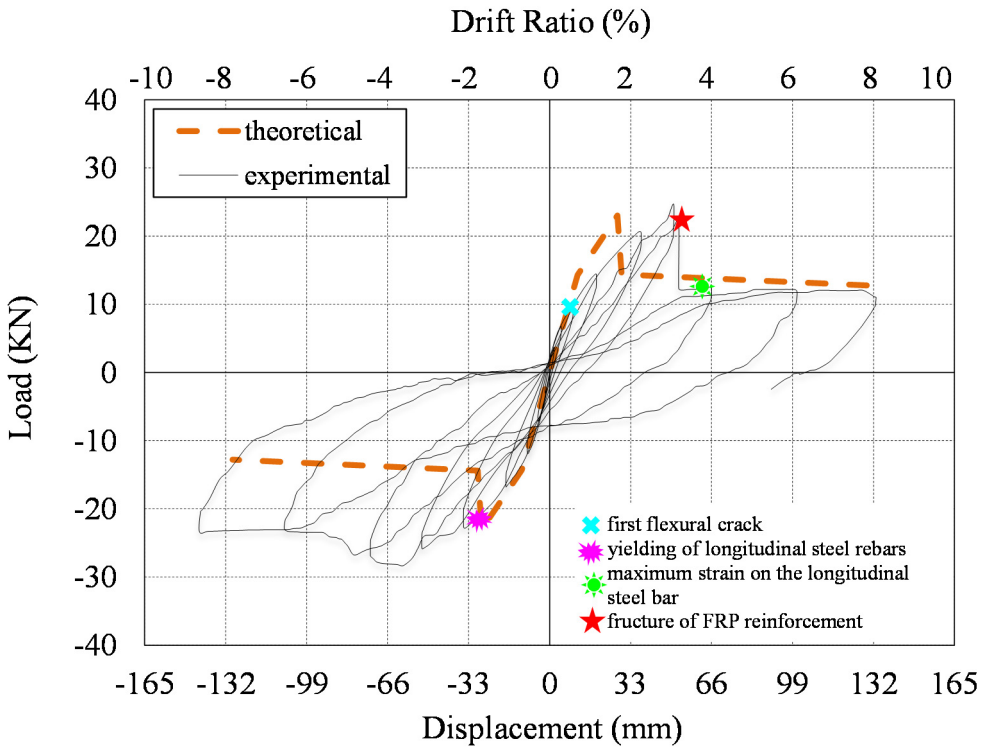

Figure 4.89 : Lateral load versus displacement for WD-N1-2AR.

Experimental moment-curvature relationships obtained for critical sections of WD-N1-2AR are presented in Figure 4.90. For the calculation of moment-curvature relationships, the average curvature values obtained for the ranges of 0-20 mm, 20-150 mm and 150-300 mm heights above the footing were taken into account.

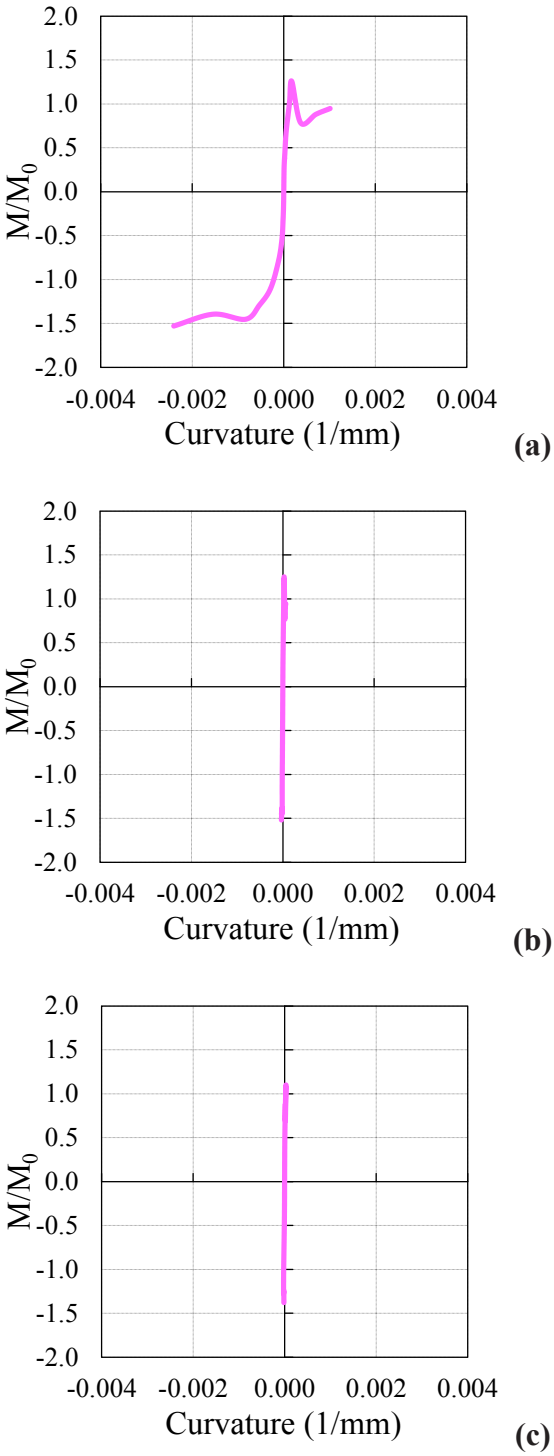

Figure 4.90 : Moment-curvature relationships obtained for gage lengths: (a)0 - 20 mm. (b)20 - 150 mm. (c)150 - 300 mm.

As seen in Figure 4.90, the curvature values of the member measured in 20-150 mm and 150-300 mm height above the support are in the order of 5.10^{-5} (1/mm), while the curvatures measured in 0-20 mm height are in the order of 3.10^{-3} (1/mm). It is assessed by considering moment-curvature relationships that the

damage was accumulated mainly in the first 20 mm height of the member from top of the footing, which was also confirmed with the damage pattern of the specimen.

Average strain distribution of longitudinal steel rebars and longitudinal AFRP reinforcement in different drift ratios are shown in Figure 4.91 and Figure 4.92 respectively.

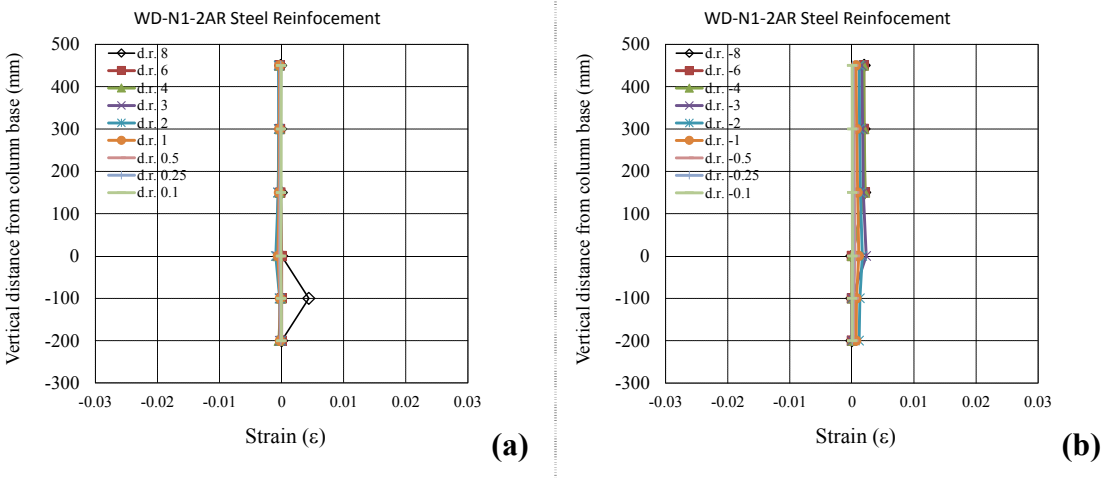

Figure 4.91 : Average strain distribution of longitudinal steel rebars of WD-N1-2AR: (a)While pulling. (b)While pushing.

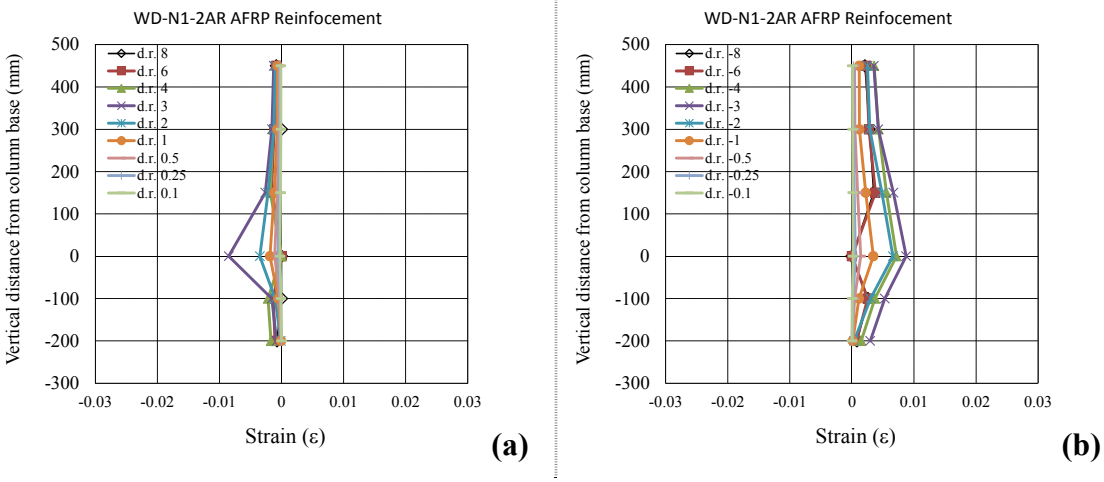

Figure 4.92 : Average strain distribution of AFRP longitudinal reinforcement of WD-N1-2AR: (a)While pulling. (b)While pushing.

According to the data from the straingauges on the longitudinal steel rebars of the WD-N1-2AR, the maximum strain while pushing was 0.0090, measured from the straingauge at 200 mm in the footing for F=-23.6 kN at -3 % drift ratio; the maximum strain while pulling was -0.0009, measured from the straingauge at the column-footing interface when F=20.6 kN at 2 % drift ratio. Maximum strain at AFRP reinforcement

was recorded as 0.0098 at the column-footing interface, while pushing through -4 % drift ratio at the lateral load -28.0 kN.

4.3.6 WD-N1-1AR2G

No cracks were observed while loading to target displacements of ±8.25 mm (drift ratio 0.50 %). First flexural crack was observed at the interface of the column and footing during loading to target displacement of 16.50 mm (drift ratio 1 %). South and north views of the specimen WD-N1-1AR2G at 8 % drift ratio is shown in Figure 4.93.

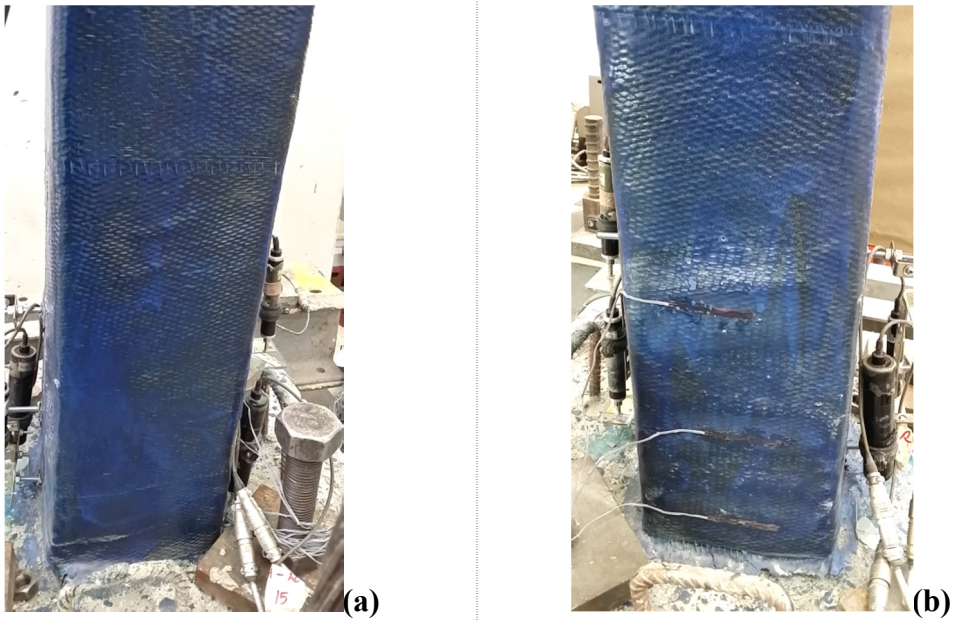

Figure 4.93 : Views of WD-N1-1AR2G at 8 % drift ratio: (a)South. (b)North.

It was observed that longitudinal steel reinforcement started to yield at 3 % drift ratio, while stirrups were not yielded during the whole test. While pulling towards 4 % drift ratio, a loud noise coming from the specimen was recorded with a marginal decrease in the lateral load. The reason of the sound was found as fracture of the AFRP longitudinal reinforcement located at west side of the column. Similar to specimen SD-N1-1AR5G, specimen sustained the lateral load level despite the fractured AFRP reinforcement. This could be explained by the significant contribution of the unfractured GFRP reinforcement in the cross section. No additional cracks were observed in further drift ratios, while the existing crack at the column-footing interface was continuously enlarged.

Residual deformation was recorded as 57.4 mm when lateral load was absolute zero. Until AFRP reinforcement fracture, increase in the lateral load capacity was calculated as 116 % in both loading directions (pushing and pulling) compared to specimen WD-N1-P2.

Autopsy photos are shown in the Figure 4.94.

(a)

(b)

Figure 4.94 : Fractured AFRP longitudinal reinforcement in the specimen WD-N1-1AR2G: (a)East view. (b)West view.

During the autopsy of the specimen, CFRP confinement was cut off in the first 60 cm height of the columns over footing and column surfaces was investigated for possible flexural cracks. It was seen that deformations were cumulated at the column-footing interface and no significant crack was observed through the column height. In order to confirm the fracture pattern of the AFRP reinforcement, SRM cover around the core concrete was broken and FRP bars were exposed. It was observed that two AFRP bars were raptured however; GFRP bars were sound as shown in Figure 4.94.

Summary of the seismic behavior of specimen WD-N1-1AR2G is shown in Table 4.13.

Table 4.13 : Summary of the seismic behavior of WD-N1-1AR2G.

Drift ratio (%)	δ (mm/mm)	P (kN)	Observations
0.10	±1.65	4.23 / -2.09	No crack was observed
0.25	±4.125	8.22 / -6.25	No crack was observed
0.50	±8.25	12.03 / -10.74	No crack was observed
1.0	±16.5	16.90 / -15.74	First flexural crack at column-footing interface was observed
2.0	±33.0	22.93 / -22.02	Propagation of existing crack at column-footing interface was observed
3.0	±49.5	27.01 / -26.24	Propagation of existing crack at column-footing interface was observed
4.0	±66.0	25.82 / -28.15	AFRP reinforcement in tension fractured but lateral load was not decreased
6.0	±99.0	25.06 / -26.71	Propagation of existing crack at column-footing interface was observed
8.0	±132.0	23.83 / -19.92	Propagation of existing crack at column-footing interface was observed

Experimental and theoretical force-displacement relationships of WD-N1-1AR2G are presented in Figure 4.95.

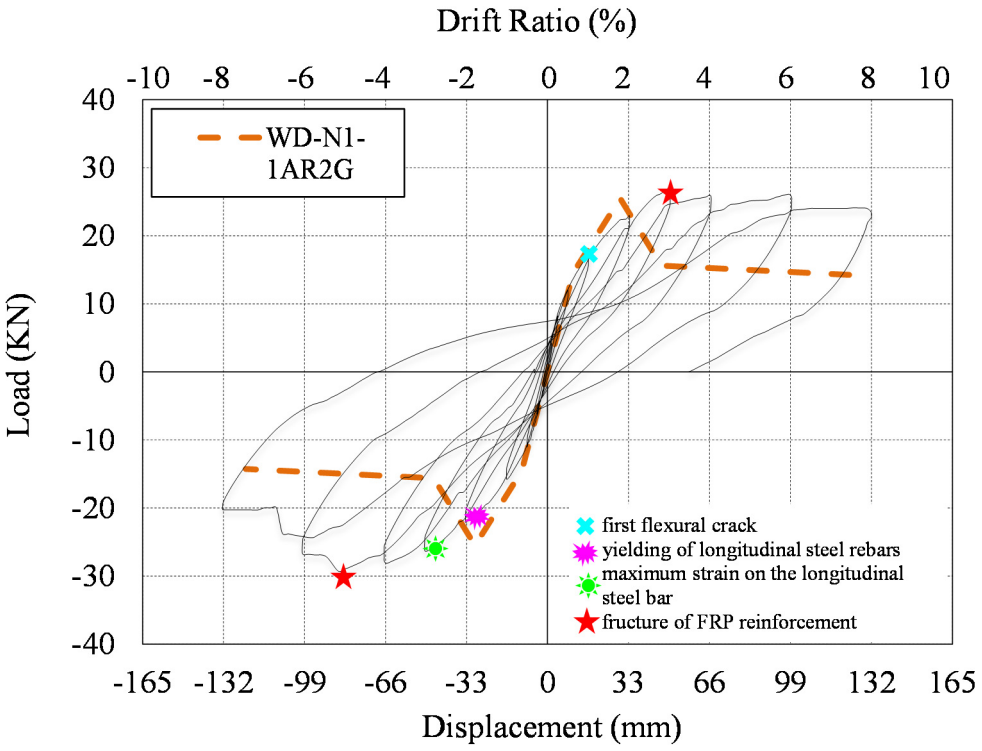

Figure 4.95 : Lateral load versus displacement for WD-N1-1AR2G.

Experimental moment-curvature relationships obtained for critical sections of WD-N1-1AR2G are presented in Figure 4.96. For the calculation of moment-curvature

relationships, the average curvature values obtained for the ranges of 0-20 mm, 20-150 mm and 150-300 mm heights above the footing were taken into account.

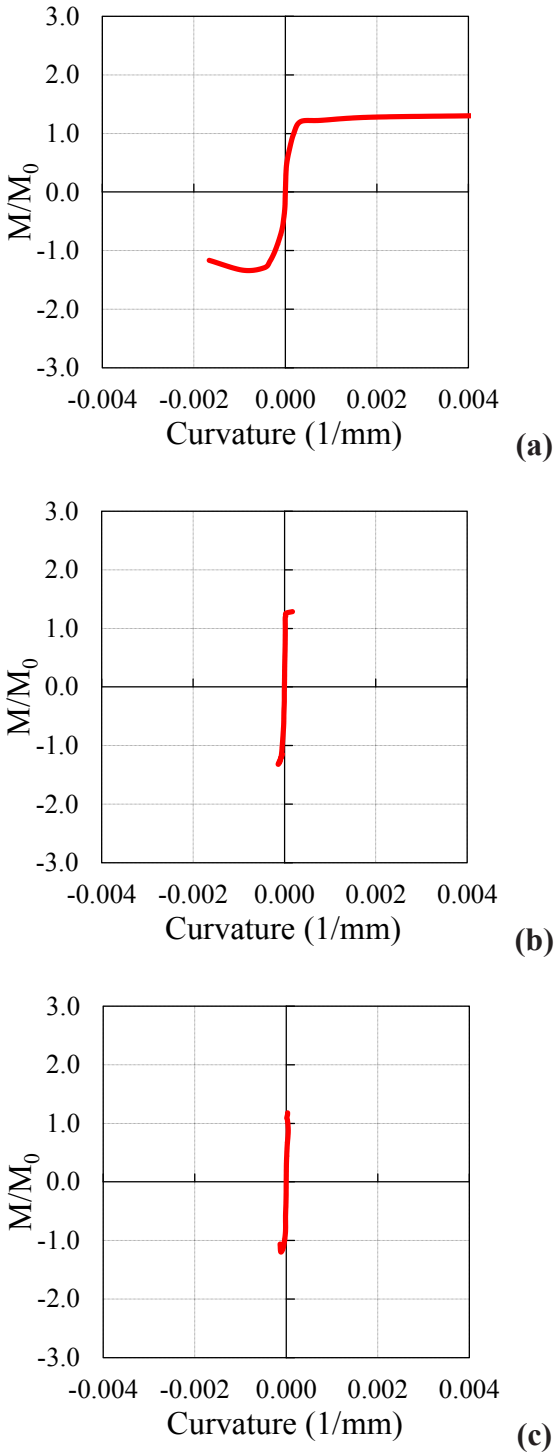

Figure 4.96 : Moment-curvature relationships obtained for gage lengths: (a)0 - 20 mm. (b)20 - 150 mm. (c)150 - 300 mm.

As seen in Figure 4.96, the curvature values of the member measured in 20-150 mm and 150-300 mm height above the support are in the order of 5.10^{-5} (1/mm), while the curvatures measured in 0-20 mm height are in the order of

3.10^{-3} (1/mm). It is assessed by considering moment-curvature relationships that the damage was accumulated mainly in the first 20 mm height of the member from top of the footing, which was also confirmed with the damage pattern of the specimen.

Average strain distribution of longitudinal steel rebars, longitudinal AFRP and GFRP reinforcement in different drift ratios are shown in Figure 4.97, Figure 4.98 and Figure 4.99 respectively.

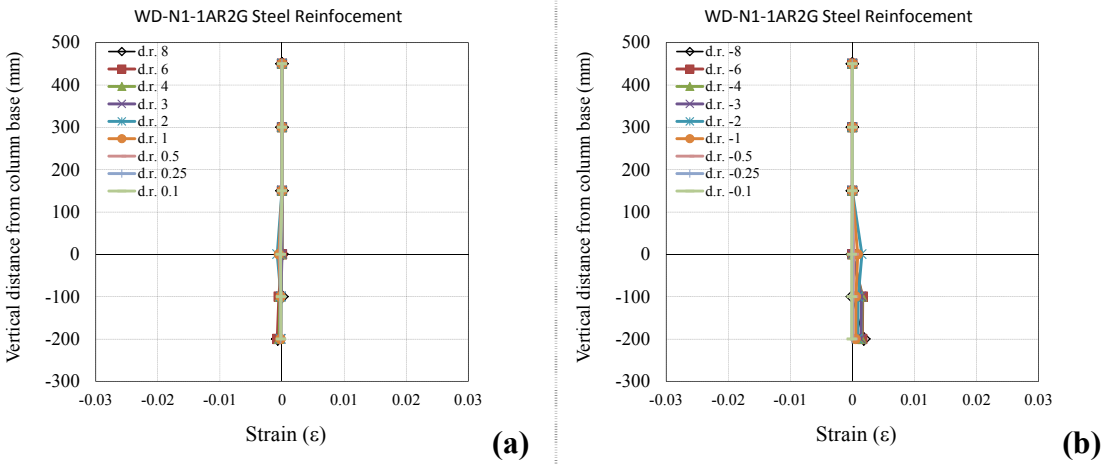

Figure 4.97 : Average strain distribution of longitudinal steel rebars of WD-N1-1AR2G: (a)While pulling. (b)While pushing.

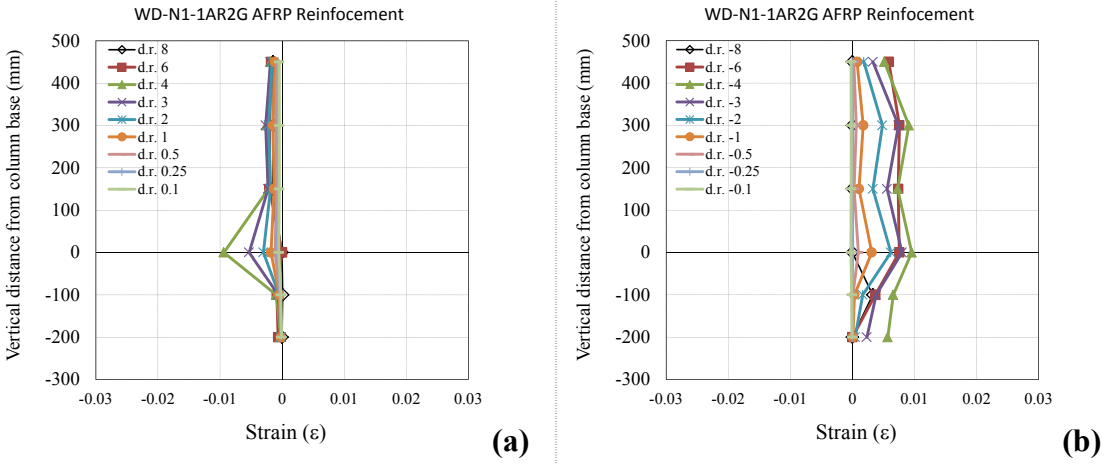

Figure 4.98 : Average strain distribution of AFRP longitudinal reinforcement of WD-N1-1AR2G: (a)While pulling. (b)While pushing.

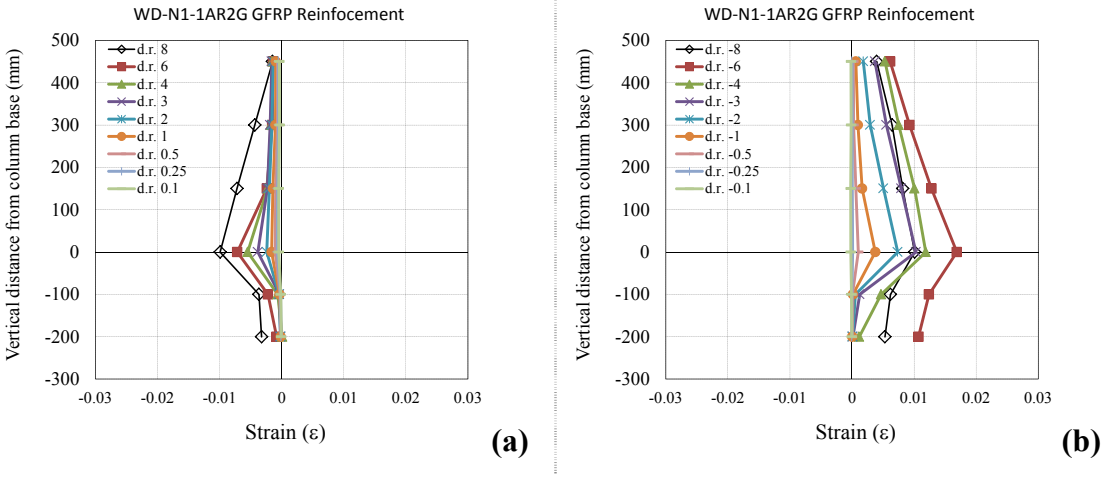

Figure 4.99 : Average strain distribution of GFRP longitudinal reinforcement of WD-N1-1AR2G: (a)While pulling. (b)While pushing.

According to the data from the straingauges on the longitudinal steel rebars of the WD-N1-1AR2G, the maximum strain while pushing was 0.0019, measured from the straingauge at the column-footing interface for F=-24.4 kN at -3 % drift ratio; the maximum strain while pulling was -0.001, measured from the straingauge at 200 mm in the footing when F=6.6 kN at 6 % drift ratio. Maximum strain at GFRP reinforcement was recorded as 0.02 at the column-footing interface, while pushing through -8 % drift ratio at the lateral load -23.7 kN, however, maximum strain recorded on AFRP reinforcement was only 0.013 at the same location at -6 % drift ratio and at -29.3 kN lateral load.

5. OVERALL EVALUATION OF TEST RESULTS

5.1 Lateral Load-Displacement Curves and Failure Modes

5.1.1 First group specimens

The hysteretic lateral load-displacement envelopes of first group specimens are presented in Figure 5.1 and Figure 5.2.

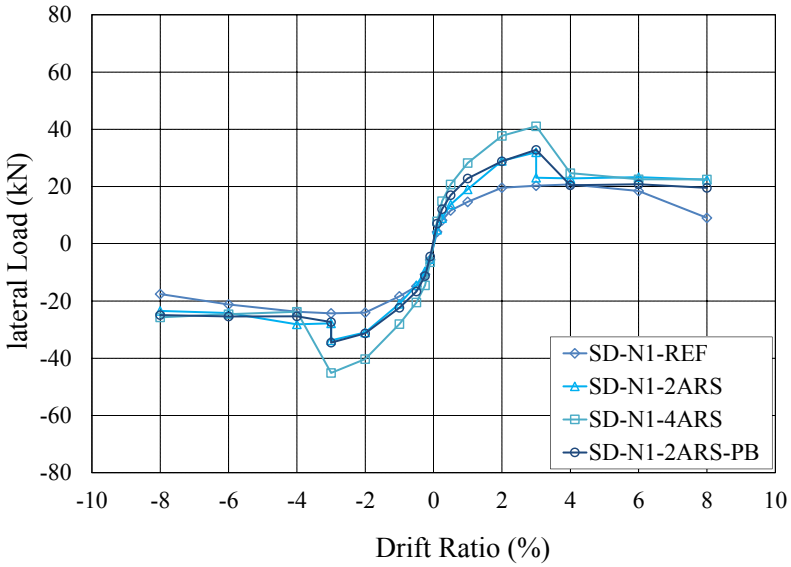

Figure 5.1 : The envelopes of load-displacement relationships of first group specimens.

As seen in Figure 5.2 and Table 5.1, the retrofitted specimens SD-N1-4ARS and SD-N1-2ARS-PB reached their theoretical capacities, while the reference column SD-N1-REF and retrofitted specimen SD-N1-2ARS are 11 % and 7 % behind their theoretical load capacities.

Table 5.1 : Summary of test results of the first group specimens.

Specimen	Peak Force (kN)		Theoretical Load Capacity	Degree of Strengthening $P_{max,\ specimen}$ / $P_{max,\ control}$	
	Push	Pull	kN	Push	Pull
SD-N1-REF	-24.5	21.1	20.4	n/a	n/a
SD-N1-2ARS	-33.8	32.0	30.5	1.38	1.52
SD-N1-4ARS	-45.1	41.3	43.4	1.84	1.95
SD-N1-2ARS-PB	-34.6	32.8	34.1	1.41	1.56

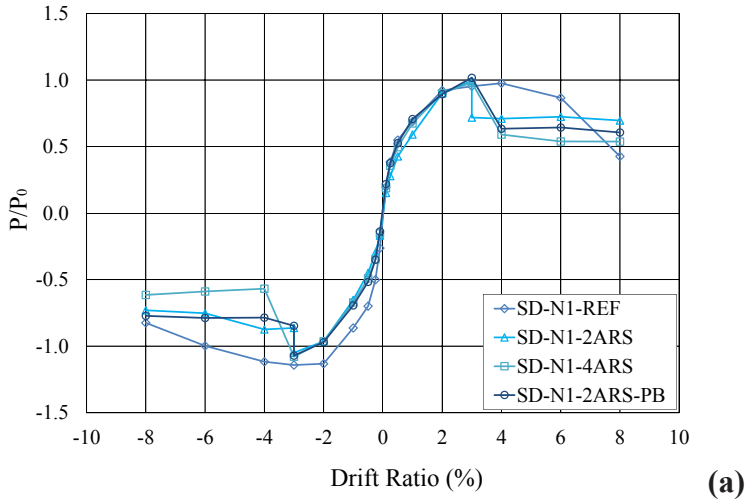

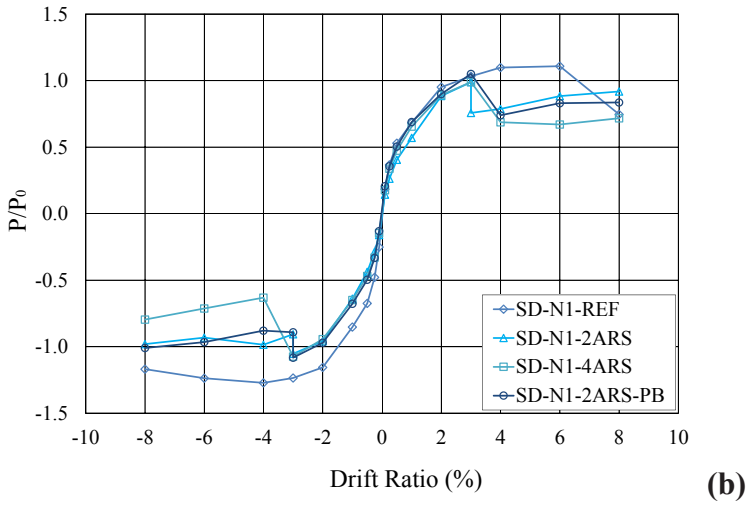

Figure 5.2 : Envelopes of the load-displacement curves for the first group specimens: (a)Without considering P-Δ effects. (b)Considering P-Δ effects.

Damage progression of the first group specimens is given in Table 5.2.

Table 5.2 : Damage progression of the first group specimens.

Damage Mechanisms	Specimens			
	SD-N1-REF	SD-N1-2ARS	SD-N1-4ARS	SD-N1-2ARS-PB
Yielding of longitudinal steel bars	2	3	3	3
Crushing of concrete cover	3	-	-	-
Spalling of concrete cover	-6	-	-	-
Fracture of FRP reinforcement	-	3	3	3

At 3 % drift ratio, the increase in strength was around 38 % with respect to control specimen SD-N1-REF (Table 5.1). The sudden remarkable loss of strength upon exceeding the drift ratio around 3 % was due to the rapture of AFRP reinforcement at the column-footing interface. Retrofitted specimen SD-N1-2ARS-PB behaved similar to the specimen SD-N1-2ARS in terms of maximum lateral load and fracture of AFRP

reinforcement around 3 % drift ratio. At this drift ratio, the improvement in strength was around 41 % with respect to the reference specimen. It was observed that, while pulling, both AFRP reinforcement under tension were raptured upon exceeding the drift ratio of 3 %. On the other hand, while pushing, only one AFRP reinforcement under tension fractured, whereas the other one did not fracture, instead, decomposed locally just above the isolated height. Decomposition was revealed with separation of the individual fibers after fracture of the epoxy matrix. Contribution of decomposed AFRP reinforcement to the behavior at larger drifts limited plastic residual deformations of the column SD-N1-2ARS-PB.

As seen in Figure 5.1, the column SD-N1-4ARS exhibited a remarkably superior performance with respect to the control specimen and the other retrofitted columns (SD-N1-2ARS and SD-N1-2ARS-PB) by bearing lateral loads, approximately 1.95 and 1.30 times the loads carried by the reference and other retrofitted columns, respectively. SD-N1-4ARS sustained its lateral load capacity until 3 % drift ratio, around where the AFRP reinforcement and AFRP anchorage reinforcement fractured at the same section. The higher flexural strength of the specimen SD-N1-4ARS is due to the contribution of additional AFRP anchorage reinforcement to the flexural capacity. Development length (700 mm) of the anchorage reinforcement was long enough to bring a full performance similar to longitudinal AFRP reinforcement under flexural loading.

The retrofitted columns behaved similar in terms of strength degradation after the rupture of FRP reinforcement as the specimens tested by Ilki and Kumbasar (2002), Bournas and Triantafillou (2009), and Vrettos et al. (2013), where the drift ratios at failure were approximately 2 %, 4 % and 2.5 %, respectively. It is also noted that all significant damage was accumulated at the base of the columns, since the columns were wrapped with CFRP sheets in transverse direction along the full height. Consequently, the crack width reached several centimeters at the intersection of the column and the footing. This type of damage may not be desired in case of seismic loading since the distribution of plastic deformations through the potential plastic hinge length is prevented due to presence of a rigid transverse CFRP reinforcement. The accumulation of an important part of plastic deformations only at the column-footing interface may significantly reduce the overall drift capacity of the column. Since high drift capacity is essential for a satisfactory seismic performance, this kind

of reduction in drift capacity should be avoided. This deficiency can be overcome by application of transverse FRP fabrics in strips allowing distribution of damage in the unconfined zones between transverse FRP strips.

5.1.2 Second group specimens

The hysteretic lateral load-displacement envelopes of second group specimens are presented in Figure 5.3 and Figure 5.4.

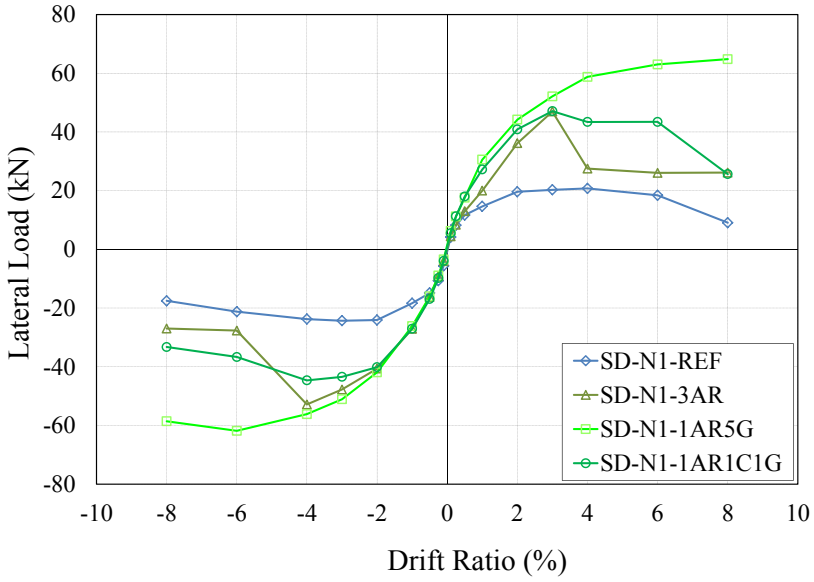

Figure 5.3 : The envelopes of load-displacement relationships of second group specimens.

As seen in Figure 5.4 and Table 5.3, all specimens reached their theoretical flexural capacities.

Table 5.3 : Summary of test results of the second group specimens and control specimen.

Specimen	Peak Force (kN)		Theoretical Load Capacity	Degree of Strengthening $P_{max,\ specimen}$ / $P_{max,\ control}$	
	Push	Pull	kN	Push	Pull
SD-N1-REF	-24.5	21.1	21.1	n/a	n/a
SD-N1-3AR	-52.8	47.0	49.4	2.16	2.23
SD-N1-1AR5G	-61.8	64.8	61.4	2.52	3.07
SD-N1-1AR1C1G	-44.6	47.1	45.2	1.82	2.23

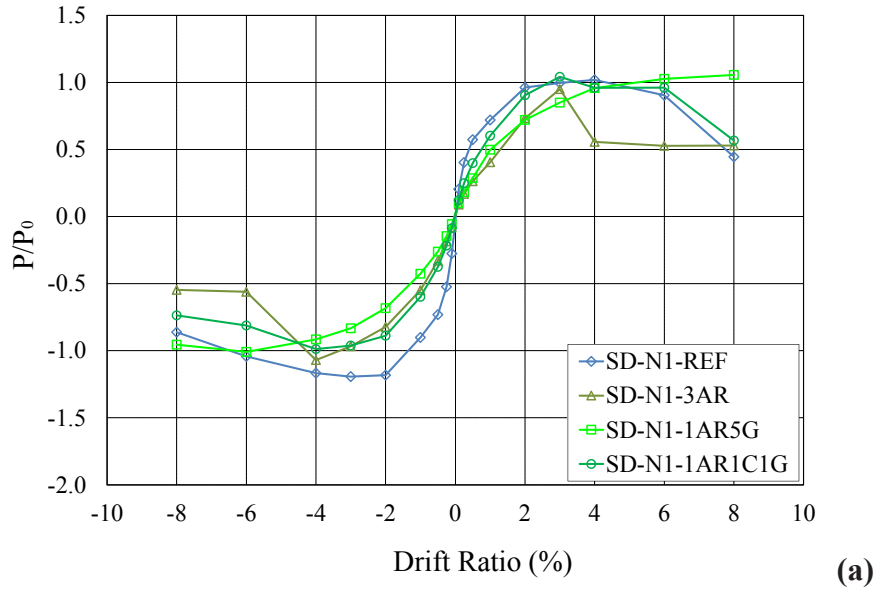

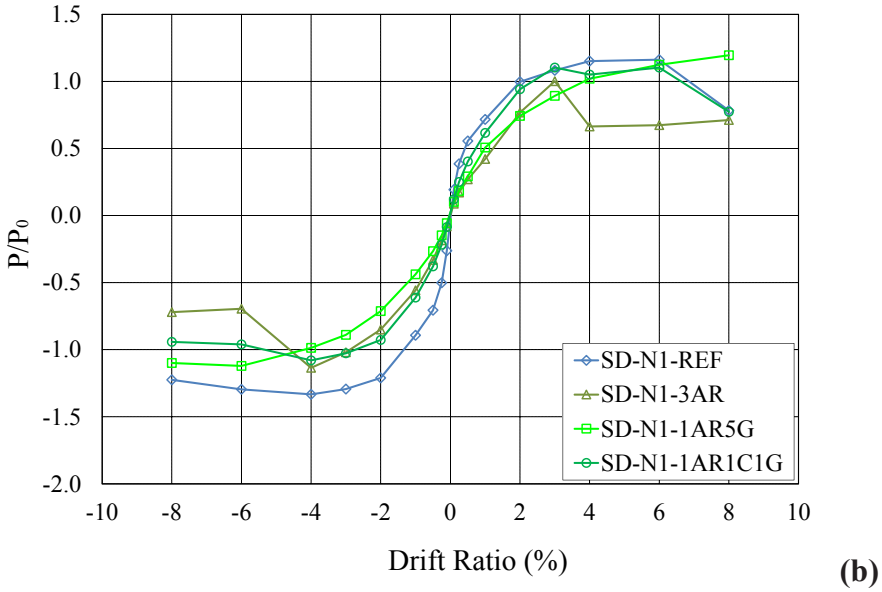

Figure 5.4 : Envelopes of the load-displacement curves for the second group specimens: (a)Without considering P-Δ effects. (b)Considering P-Δ effects.

Damage progression of the second group specimens is given in Table 5.4.

Table 5.4 : Damage progression of the second group specimens.

Damage Mechanisms	Specimens		
	SD-N1-3AR	SD-N1-1AR5G	SD-N1-1AR1C1G
Yielding of longitudinal steel bars	2	3	3
Crushing of concrete cover	-	-	-
Spalling of concrete cover	-	-	-
Fracture of FRP reinforcement	3	6	4

At 3 % drift ratio, the increase in strength of specimen SD-N1-3AR were around 116 % while pushing and 123 % while pulling with respect to control specimen

SD-N1-REF (Table 5.3). The sudden remarkable loss of strength upon exceeding the drift ratio around 3 % was due to the rapture of AFRP reinforcement at the column-footing interface. The specimen SD-N1-1AR1C1G behaved similar to the specimen SD-N1-3AR in terms of maximum lateral load while pushing but performed approximately 18 % less in terms of peak force while pulling. AFRP reinforcement fractured at 4 % drift ratio. At this drift ratio, the improvement in strength was around 82 % while pushing and 123 % while pulling with respect to control specimen SD-N1-REF (Table 5.3).

As seen in Figure 5.3, the column SD-N1-1AR5G exhibited a remarkably superior performance with respect to the control specimen and the other retrofitted columns by bearing lateral loads, approximately 2.52 and 3.07 times the loads carried by the reference, while pushing and pulling, respectively. Unlikely to previous retrofitted specimens, SD-N1-1AR5G sustained its lateral load capacity until 8 % drift ratio. The higher flexural strength even at large drift ratios could be explained with the outstanding contribution of GFRP reinforcement to the flexural capacity, although AFRP reinforcement fractured at 6 % drift ratio.

The specimen SD-N1-3AR behaved similar to first group specimens in terms of strength degradation after the rupture of AFRP reinforcement. Specimen SD-N1-1AR1C1G performed very limited strength degradation after rupture of AFRP reinforcement, while specimen SD-N1-1AR5G did not show strength degradation and reached peak force at 8 % drift ratio. It is also noted that all significant damage was accumulated at the base of the column SD-N1-3AR, similar to first group specimens. Consequently, the crack width reached several centimeters at the intersection of the column and the footing at the end of testing SD-N1-3AR. On the other hand, plastic deformations were distributed in the first 50 cm and 120 cm of the specimens SD-N1-1AR1C1G and SD-N1-1AR5G respectively. Due to the unfractured GFRP reinforcement and CFRP longitudinal reinforcement, stresses were distributed more homogenously along the column height. This type of damage is more preferred in case of seismic loading since the distribution of plastic deformations through a larger potential plastic hinge length is promoted by longitudinal FRP reinforcement even though the presence of rigid transverse CFRP reinforcement. Besides, high drift capacities of specimens SD-N1-1AR1C1G and SD-N1-1AR5G are essential for a satisfactory seismic performance.

5.1.3 Third group specimens

The hysteretic lateral load-displacement envelopes of third group specimens are presented in Figure 5.5 and Figure 5.6.

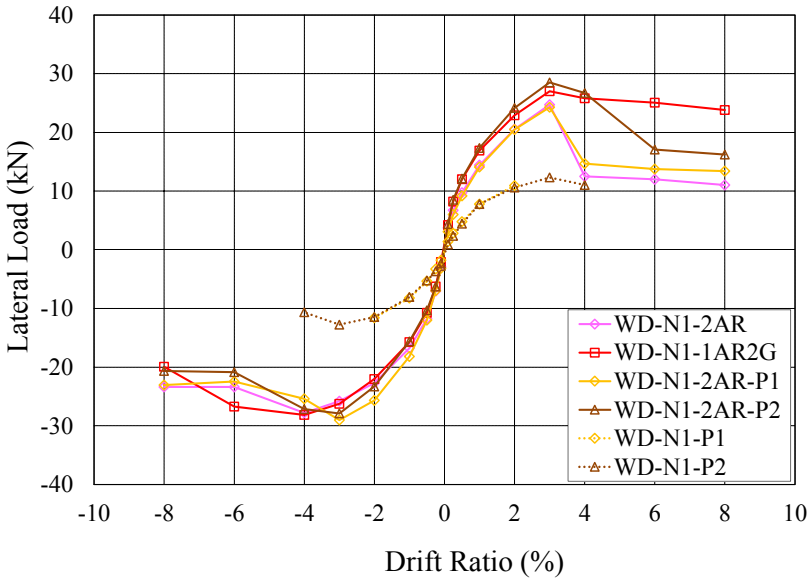

Figure 5.5 : The envelopes of load-displacement relationships of third group specimens.

As seen in Figure 5.6 and Table 5.5, all specimens, including non-retrofitted ones reached their theoretical flexural capacities.

Table 5.5 : Summary of test results of the third group specimens.

Specimen	Peak Force (kN)		Theoretical Load Capacity	Degree of Strengthening $P_{max,\ specimen}$ / $P_{max,\ control}$	
	Push	Pull	kN	Push	Pull
WD-N1-P1	-11.7	11.1	12.8	n/a	n/a
WD-N1-P2	-13.5	12.5	12.8	n/a	n/a
WD-N1-2AR-P1	-29.0	24.3	23.0	2.18	2.48
WD-N1-2AR-P2	-27.9	28.6	23.5	2.06	2.28
WD-N1-2AR	-28.4	24.7	23.0	2.10	1.97
WD-N1-1AR2G	-29.3	27.0	25.6	2.16	2.16

At 4 % drift ratio, the increase in strength of specimen WD-N1-2AR-P1 were around 118 % while pushing and 148 % while pulling with respect to control specimen WD-N1-P1 (Table 5.5). The sudden remarkable loss of strength upon exceeding the drift ratio around 4 % was due to the rapture of AFRP reinforcement at the column-footing interface. The specimen WD-N1-2AR-P2 behaved similar to the specimen WD-N1-2AR-P1 in terms of maximum lateral load while pushing but performed approximately 18 % more in terms of peak force while pulling. AFRP

reinforcement fractured at 4 % drift ratio. At this drift ratio, the improvement in strength was around 106 % while pushing and 128 % while pulling with respect to control specimen WD-N1-P2 (Table 5.5).

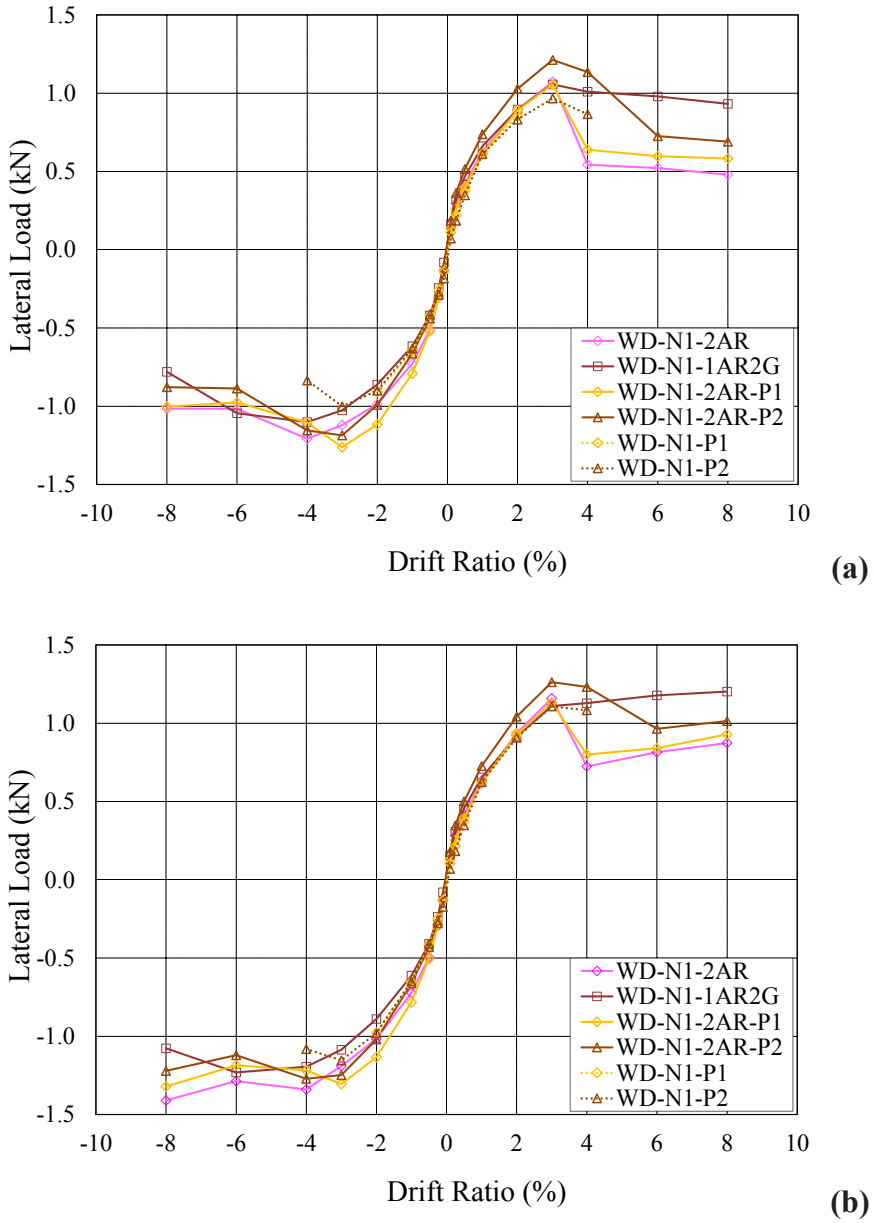

Figure 5.6 : Envelopes of the load-displacement curves for the third group specimens: (a)Without considering P-Δ effects. (b)Considering P-Δ effects.

Similar to the columns, which were retrofitted by hybrid utilization of the FRP reinforcement in second group specimens, the specimen WD-N1-1AR2G performed significantly higher than its theoretical capacity. This behavior also confirms the conservative calculations run by XTRACT software in case of hybrid FRP reinforced structural members.

Damage progression of the third group specimens is given in Table 5.6.

Table 5.6 : Damage progression of the retrofitted columns of the third group specimens.

Damage Mechanisms	Specimens			
	WD-N1-2AR-P1	WD-N1-2AR-P2	WD-N1-2AR	WD-N1-1AR2G
Yielding of longitudinal steel bars	2	3	3	3
Crushing of concrete cover	-	-	-	-
Spalling of concrete cover	-	-	-	-
Fracture of FRP reinforcement	4	4	4	4

At 4 % drift ratio, the increase in strength of specimen WD-N1-2AR were around 110 % while pushing and 97 % while pulling with respect to control specimen WD-N1-P2 (Table 5.5). The sudden remarkable loss of strength upon exceeding the drift ratio around -4 % was due to the rapture of AFRP reinforcement at the column-footing interface. Unlikely to other retrofitted specimens including AFRP reinforcement in entire testing program, AFRP reinforcement located on the western surface of the specimen WD-N1-2AR did not fracture and continued to bear lateral load until the end of the test. This behavior is clearly seen in the Figure 5.5. The specimen WD-N1-2R behaved similar to the specimen WD-N1-1AR2G in terms of maximum lateral load while pushing but performed approximately 9 % less in terms of peak force while pulling. It is also noted that all significant damage was accumulated at the base of the column WD-N1-2AR a similar to first and third group retrofitted specimens.

The specimens WD-N1-2AR-P1 and WD-N1-2AR-P2 behaved similar in terms of strength degradation after the rupture of AFRP reinforcement. Since the control specimens were tested up to limited drift ratios to represent the moderate and heavy damage states, a fair comparison with retrofitted specimens could not be done in terms of strength degradation. A rough estimation on behavior could be stated as being similar to the first group specimens' after fracture of AFRP reinforcement. It is also noted that all significant damage was accumulated at the base of the retrofitted columns, similar to first and second group specimens, since the columns were wrapped with CFRP sheets in transverse direction along almost full height. Eventually, the crack width reached several centimeters at the intersection of the column and the footing. As it has been stated before, this type of damage may not be desired in case of seismic loading. When compared to the specimen WD-N1-2AR, which was undamaged prior to retrofit application, pre-damaged specimens WD-N1-2AR-P1 and

WD-N1-2AR-P2 performed in the same level in terms of lateral load capacity. It could be concluded that pre-damage conditions did not show any negative effect on the performance of the retrofitted columns by using proposed technique.

AFRP reinforcement fractured at 4 % drift ratio while GFRP reinforcement did not fracture in specimen WD-N1-1AR2G similar to the previous specimens retrofitted with GFRP reinforcement. At this drift ratio, the improvement in strength was around 116 % in both pushing and pulling directions with respect to control specimen WD-N1-P2. The specimen WD-N1-1AR2G continued to bear significant amount of lateral load after rapture of AFRP reinforcement. Additionally, plastic deformations were distributed in the first 50 cm of the specimen WD-N1-1AR2G. Due to the unfractured GFRP reinforcement (up to 8 % drift ratio), stresses were distributed more homogenously along the column height. This type of damage is more preferred in case of seismic loading since the distribution of plastic deformations through a larger potential plastic hinge length is promoted by longitudinal FRP reinforcement even though the presence of rigid transverse CFRP reinforcement. Besides, high drift capacities of specimen WD-N1-1AR2G is essential for a satisfactory seismic performance.

5.2 Moment-Curvature Relationships

Average experimental moment-curvature relationships obtained for critical sections of columns. Second order effect is considered while calculating the experimental moment (M) and the theoretical moment capacity (M_0) was calculated per specimen, by using fiber analysis approach. For the calculation of experimental moment-curvature relationships, the average curvature values obtained along 0-20 mm, 20-150 mm, and 150-300 mm heights above the footing are taken into account.

5.2.1 First group specimens

Average experimental moment-curvature relationships obtained for critical sections of columns are presented in Figure 5.7.

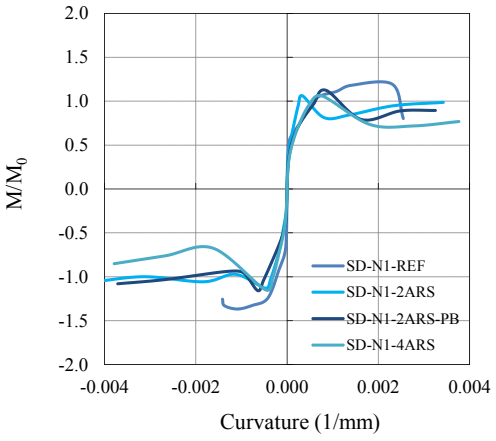

(a)

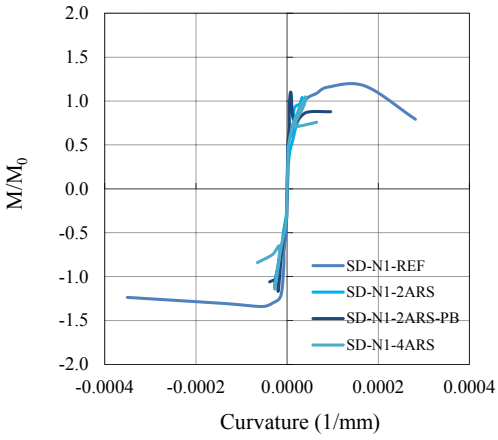

(b)

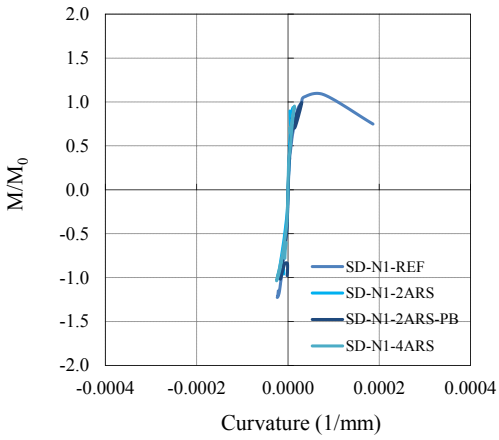

(c)

Figure 5.7 : Moment-curvature relationships of non-retrofitted specimens obtained for gage lengths: (a)0 - 20 mm. (b)20 - 150 mm. (c)150 - 300 mm.

As seen in Figure 5.7, for the first group specimens, the average curvature values of the column sections measured along 0-20 mm height were in the order of 4.5×10^{-3} (1/mm), while the curvatures measured in 20-150 mm height above the footing were in the order of 4.5×10^{-4} (1/mm). The curvature values of the columns measured along 150-300 mm height were even smaller. In agreement with these

measurements, the damage was also accumulated particularly in 20 mm height of the column from top of the footing. This conclusion is also supported by the autopsy after the tests, no concrete crushing and no additional cracking (other than the main damage at the interface of the column and the footing) were observed on the retrofitted columns. On the other hand, the deformations were distributed through the column height in case of the reference specimen SD-N1-REF.

5.2.2 Second group specimens

Average experimental moment-curvature relationships obtained for critical sections of columns are presented in Figure 5.8. As seen in Figure 5.8, for the second group specimens, the average curvature values of the column sections measured along 0-20 mm height were in the order of 2×10^{-3} (1/mm), while the curvatures measured in 20-150 mm height above the footing were in the order of 2×10^{-4} (1/mm). The curvature values of the columns measured along 150-300 mm height were even smaller (in the order of 1×10^{-4} (1/mm)). Even though the curvature values obtained for different sections are not in the same order, the difference is not that dramatic when compared to first group specimens. This behavior is clearer for the specimens SD-N1-1AR5G and SD-N1-1AR1C1G, which have relatively similar moment-curvature relationships obtanined in different sections. In agreement with these measurements, the damage was also accumulated particularly in 20 mm height of the specimen SD-N1-3AR from top of the footing, while deformations were distributed along the column height (first 500 mm) of the specimens SD-N1-1AR5G and SD-N1-1AR1C1G. This conclusion is also supported by the autopsy after the tests, no concrete crushing and no additional cracking (other than the main damage at the interface of the column and the footing) were observed on the specimen SD-N1-3AR, while several additional cracks apart from the main crack at the colum-footing interface were plotted on the specimens SD-N1-1AR5G and SD-N1-1AR1C1G.

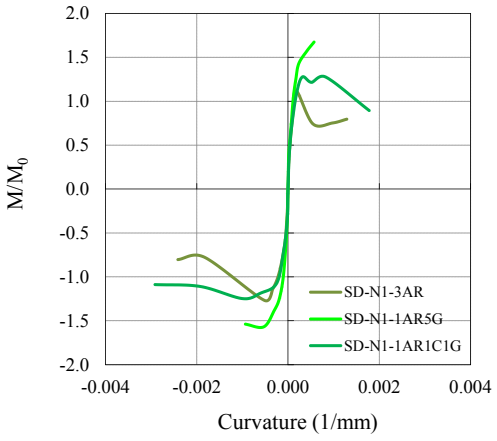

(a)

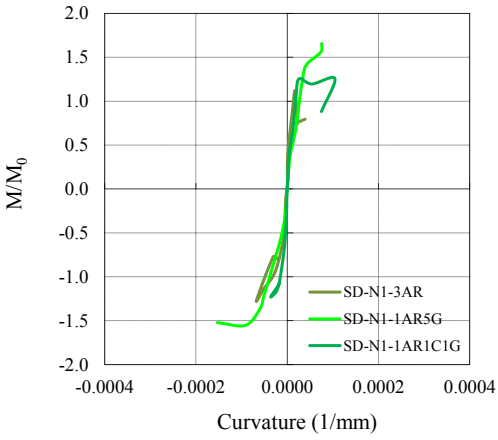

(b)

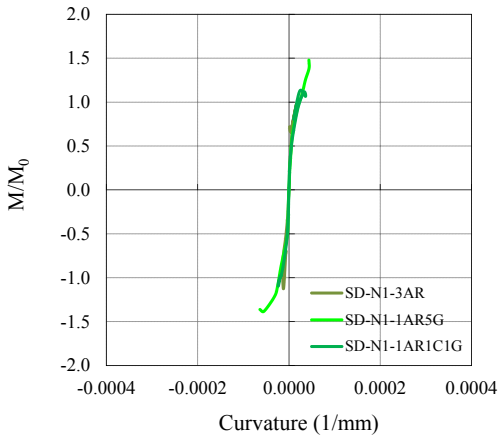

(c)

Figure 5.8 : Moment-curvature relationships of non-retrofitted specimens obtained for gage lengths: (a)0 - 20 mm. (b)20 - 150 mm. (c)150 - 300 mm.

5.2.3 Third group specimens

Since the non-retrofitted columns of the third group specimens were tested up to limited drift ratios, moment-curvature relationships are not comparable with the retrofitted columns in this group spesimens. Average experimental moment-curvature

relationships obtained for critical sections of non-retrofitted and retrofitted columns are given in Figure 5.9 and Figure 5.10 respectively.

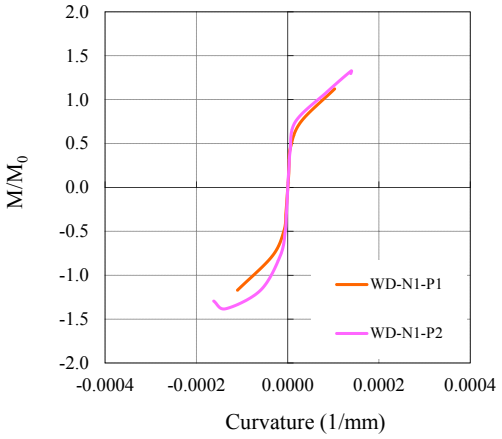

(a)

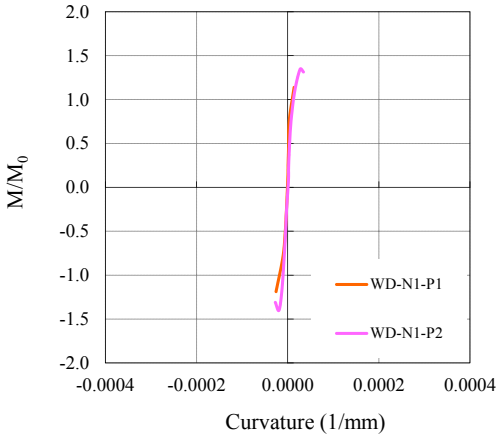

(b)

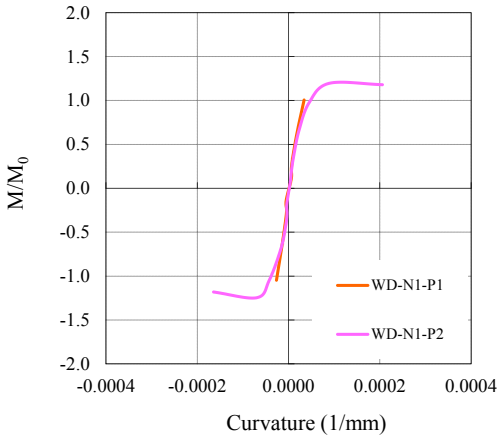

(c)

Figure 5.9 : Moment-curvature relationships of non-retrofitted specimens obtained for gage lengths: (a)0 - 20 mm. (b)20 - 150 mm. (c)150 - 300 mm.

As seen in Figure 5.9, for the non-retrofitted columns of the third group specimens, the average curvature values of the different column sections were in the order of between 0.5×10^{-4} - 2×10^{-4} (1/mm). In agreement with these measurements, the

deformations were not accumulated particularly in 20 mm height of the column from top of the footing but distributed along the column height similar to the control specimen SD-N1-REF, which was tested in its strong direction.

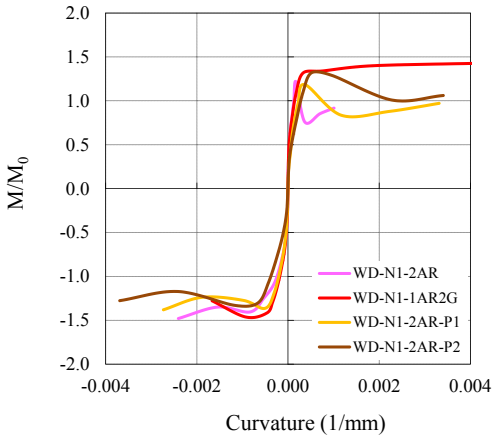

(a)

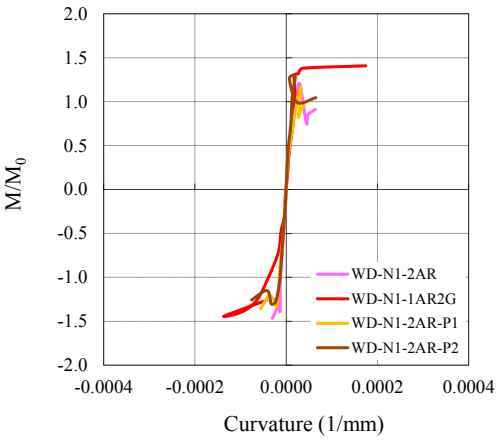

(b)

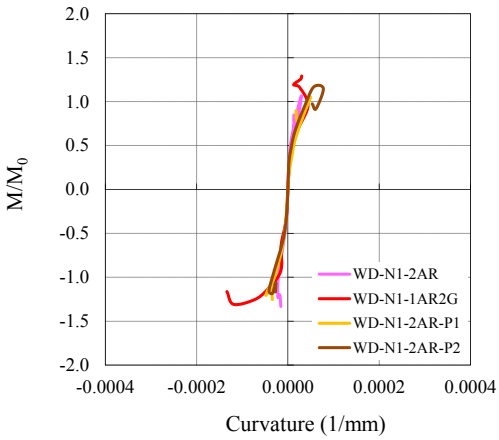

(c)

Figure 5.10 : Moment-curvature relationships of retrofitted specimens obtained for gage lengths: (a)0 - 20 mm. (b)20 - 150 mm. (c)150 - 300 mm.

On the other hand, pre-damaged columns performed significantly different after retrofitting. As seen in Figure 5.10, for the retrofitted columns of third group

specimens, the average curvature values of the column sections measured along 0-20 mm height were in the order of 4×10^{-3} (1/mm), while the curvatures measured in 20-150 mm and 150-300 mm height above the footing were in the order of 2×10^{-4} (1/mm). In agreement with these measurements, the deformations were accumulated particularly in 20 mm height of the column from top of the footing. This conclusion is also supported by the autopsy, where no concrete crushing and no additional cracking (other than the main crack at the interface of the column and the footing) were observed in these specimens.

Even though the curvature values obtained for different sections are not in the same order, the difference is not that dramatic when compared to first and third group specimens. This behavior is more clear for the specimen WD-N1-1AR2G, which has relatively similar moment-curvature relationships obtanined in different sections. In agreement with these measurements, the damage was also accumulated particularly in 20 mm height of the specimen WD-N1-2AR from top of the footing, while deformations were distributed along the column height (first 500 mm) of the specimen WD-N1-1AR2G. This conclusion is also supported by the autopsy after the tests, no concrete crushing and no additional cracking (other than the main damage at the interface of the column and the footing) were observed on the specimen WD-N1-2AR. On the other hand, several additional cracks apart from the main crack at the colum-footing interface were plotted along the columns height (first 500 mm) on the specimen WD-N1-1AR2G. This behavior could be explained with the contribution of the unfractured GFRP reinforcement used in these specimens via transferring tensile stresses uniformly along the column height even in high drift ratios, while deformations could not be distributed homogenously in the specimen retrofitted with only AFRP reinforcement due to rapture of FRP bars in relatively smaller drift ratios.

5.3 Strains of Steel and FRP Reinforcement

The strain values were obtained by making use of the straingauges on longitudinal and transverse steel, and longitudinal FRP reinforcement. Maximum strains measured on the longitudinal steel and FRP reinforcement are given in Table 5.7.

Table 5.7 : Maximum strains measured by using straingauges.

Specimen	Reinforcement			
	Steel	AFRP	GFRP	CFRP
SD-N1-REF	0.0290	-	-	-
SD-N1-2ARS	0.0293	0.0104	-	-
SD-N1-4ARS	0.0306	0.0068	-	-
SD-N1-2ARS-PB	0.0047	0.0125	-	-
SD-N1-3AR	0.0108	0.0152		-
SD-N1-1AR5G	0.0290	0.0089	0.0161	-
SD-N1-1AR1C1G	0.0295	0.0081	0.0137	0.0075
WD-N1-P1	0.0015	-	-	-
WD-N1-P2	0.0032	-	-	-
WD-N2-P1	0.0014	-	-	-
WD-N1-2AR-P1	0.0055	0.0090	-	-
WD-N1-2AR-P2	0.0028	0.0114	-	-
WD-N1-2AR	0.0090	0.0098	-	-
WD-N1-1AR2G	0.019	0.0128	0.0201	-

The efficiency of FRP reinforcement on flexural capacity can also be seen through the measured strains of longitudinal FRP reinforcement. The maximum strains of longitudinal AFRP strips and bars in tension vary between 0.0068 – 0.0152 right before the rupture of the AFRP reinforcement. These wide range of values correspond to approximately 30 % - 63 % of design rupture strain of AFRP reinforcement, while ACI 440-2R-08 (2008) recommends to reduce ε_{fu} by using a factor of 0.70 for NSM application technique under monotonic flexural loading.

GFRP bars performed as the most efficient FRP reinforcement in enhancing flexural behavior of the specimens. The maximum strains of longitudinal GFRP strips and bars in tension vary between 0.0137 – 0.0201 right before the rupture of the AFRP reinforcement. These wide ranges of values correspond to approximately 49 % - 72 % of design rupture strain of GFRP reinforcement. Although GFRP bars performed much higher strains under tension when compared to AFRP reinforcement, still it does not fully comply with the recommendation of ACI 440-2R-08 (2008).

Although the studied method, DSE is not identical with NSM technique, still NSM is the most relevant flexural retrofitting method, which could be considered as a reference. Based on this assumption, it could be concluded that the recommended reduction factor for NSM FRP applications by ACI 440-2R-08 (2008) is not valid for DSE FRP applications in reversed cyclic loading. Besides, the clear difference in efficiency between AFRP and GFRP reinforcement points the effect of the type of FRP on flexural behavior under cyclic loading. Similar to different environmental reduction factors depending on the type of FRP, strain reduction factors used for flexural design shall be reconsidered and tailored according to FRP reinforcement

types (e.g. Carbon, glass, aramid or basalt). Since CFRP reinforcement was used only in one specimen, existing data is not enough to make clear conclusions on the effectivenessof the CFRP reinforcing bars. The maximum strain of CFRP bar in tension was measured as 0.0075, which refers to 50 % of the rupture strain.

5.3.1 Strain of steel reinforcement

Average strain values, which were obtained by using straingauges on longitudinal steel reinforcement, are given for first group specimens in Figure 5.11.

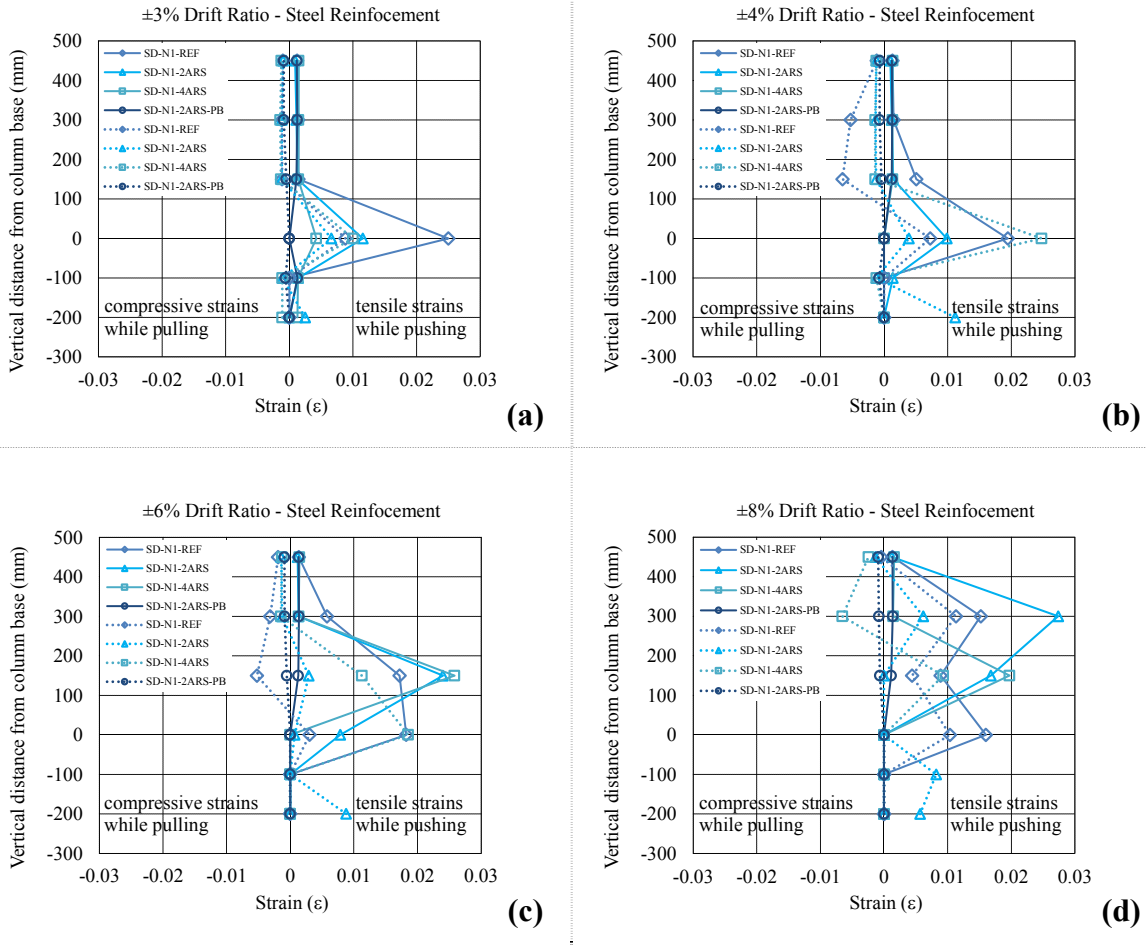

Figure 5.11 : Average strain distribution of longitudinal steel rebars of first group specimens at different drift ratios: (a)±3 %. (b)±4 %. (c)±6 %. (d)±8 %.

The longitudinal steel bars of the column SD-N1-REF yielded at drift ratio of 2 %, while that of retrofitted columns in first group specimens yielded at drift ratio around 3 % right after the columns experienced strength degradation due to rupture of AFRP reinforcement. Since longitudinal steel reinforcing bars already reached their yield strain at around 3 % drift ratio before rupture of AFRP reinforcement, the brittle failure

of the column was avoided, which is desired for better seismic behavior. Drift ratios exceeding 3 % may only be expected if substandard RC structures are subjected to severe earthquakes. As it could be seen in Figure 5.11, strains of longitudinal steel bars did not reach tensile strain corresponding to strain hardening. Besides, none of the transeverse steel reinforcing bars yielded (strains were in the range of 0.00004 and 0.0006) and no damage was observed on CFRP confinement due to relatively low level of applied axial load (20 % axial load capacity of the specimen) and shear stresses. Average strain values, which were obtained by using straingauges on longitudinal steel reinforcement, are given for second group specimens in Figure 5.12.

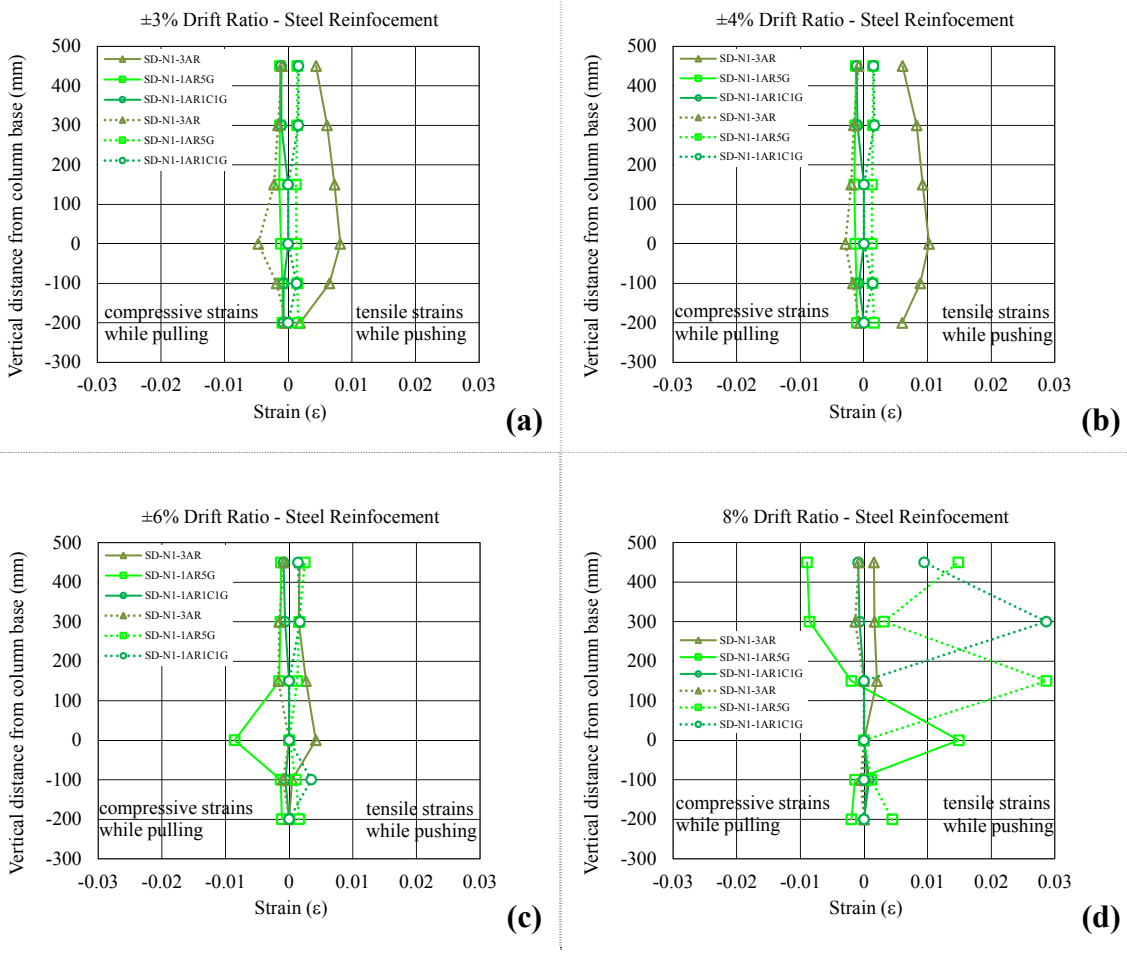

Figure 5.12 : Average strain distribution of longitudinal steel rebars of second group specimens at different drift ratios: (a)±3 %. (b)±4 %. (c)±6 %. (d)±8 %.

When compared to first group specimen, strain values measured by straingauges were not consistent in general for second group specimens. Some straingauges were damaged during the repair and retrofitting applications. In the light of existing measurements, it could be noted that longitudinal steel reinforcement started yielding

at around ±3 % drift ratio, while transverse steel reinforcement did not yield at all during the test. Since the longitudinal steel reinforcement yielded before fracture of FRP reinforcement, brittle failure of the columns was avoided. Average strain values, which were obtained on longitudinal steel reinforcement, are given for the pre-damaged columns of the third group specimens in Figure 5.13.

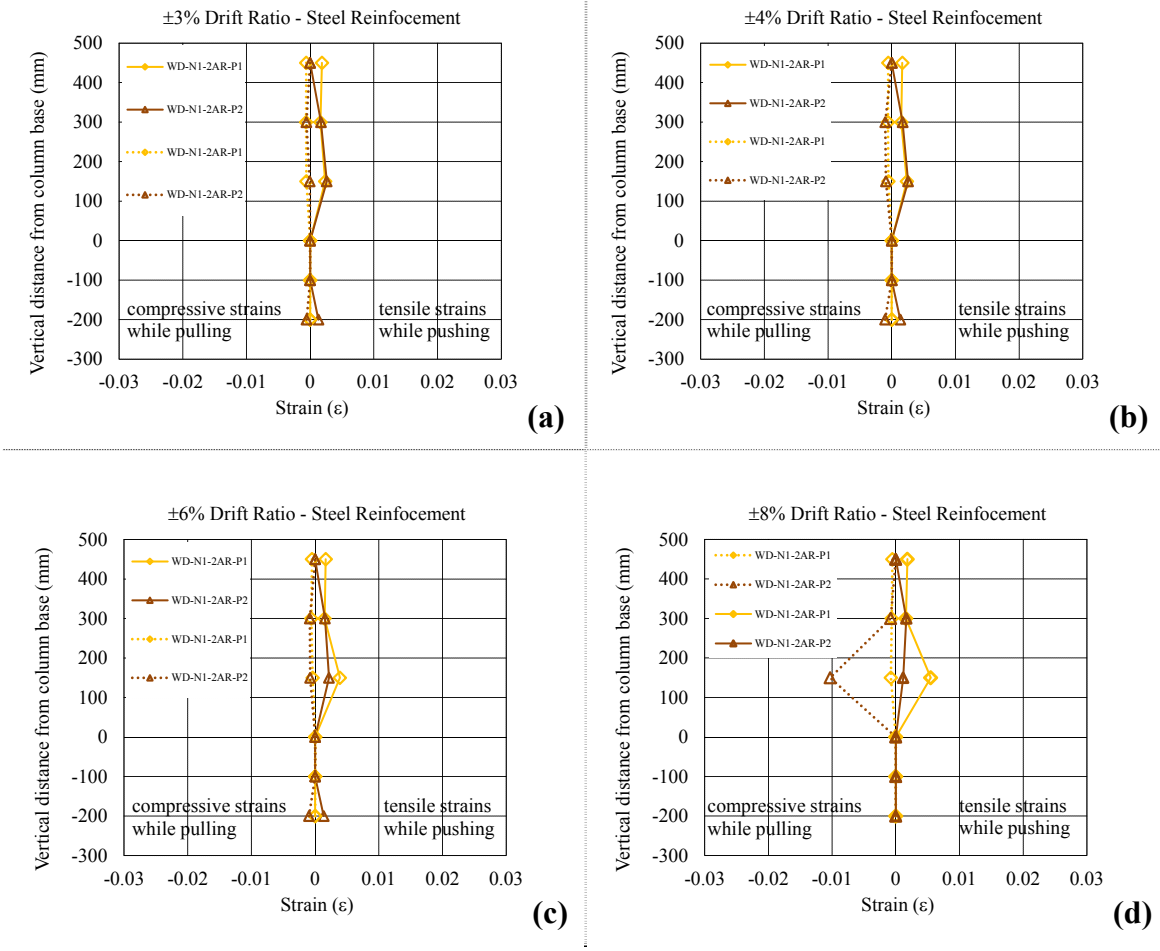

Figure 5.13 : Average strain distribution of longitudinal steel rebars of third group specimens at different drift ratios: (a)±3 %. (b)±4 %. (c)±6 %. (d)±8 %.

Since the specimen WD-N1-P1 was tested up to ±2 % drift ratio, average strain values have not been given in this section. According to measurements, longitudinal steel reinforcement started yielding around ±1 % drift ratio, while yielding was started at ±2 % drift ratio for the specimen WD-N1-P2, which was tested up to ±4 %. In all three non-retrofitted specimens, transverse steel reinforcement did not yield during the tests similar to first and second group specimens. Straingauges located at the column footing interface, which is the most cricital section were damaged partially during the pre-damaging tests and partially during the repair and retrofitting applications.

Therefore, no readings from these sensors were recorded during the tests. But the measurements at 150 mm above the footing were quite consistent and provided enough data to make healty assessment. According to measurements at this point, longitudinal steel reinforcement started yielding before ±3 % drift ratio, while transverse steel reinforcement did not yield at all during the test similar to first and second group specimens. Since the longitudinal steel reinforcement yielded before fracture of FRP reinforcement for all two retrofitted specimen, brittle failure of the columns was avoided. Average strain values, which were obtained on longitudinal steel reinforcement, are given for the undamaged columns of the third group specimens in Figure 5.14.

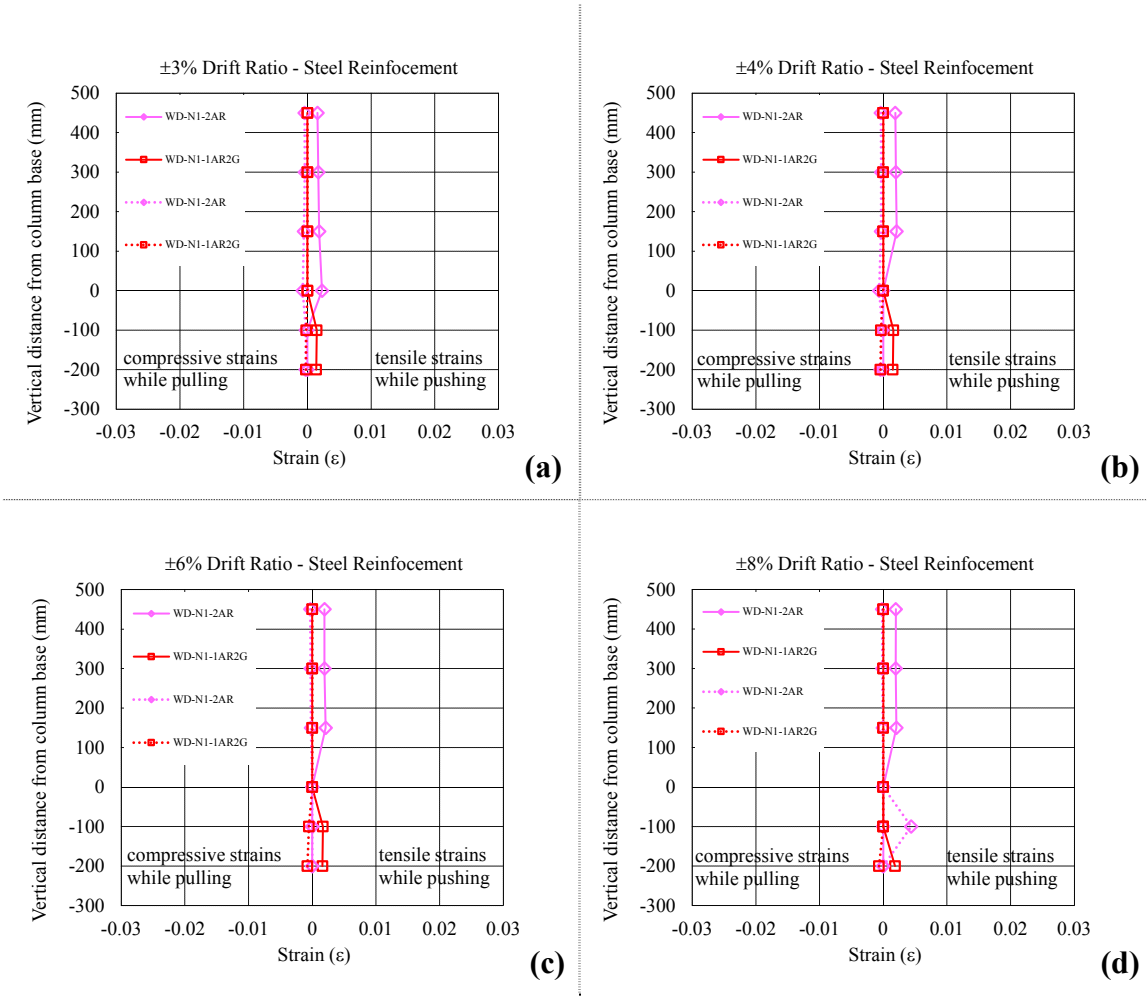

Figure 5.14 : Average strain distribution of longitudinal steel rebars of third group specimens at different drift ratios: (a)±3 %. (b)±4 %. (c)±6 %. (d)±8 %.

In the light of existing measurements, it could be noted that longitudinal steel reinforcement started yielding at around ±3 % drift ratio, while transverse steel reinforcement did not yield at all during the test. Since the longitudinal steel

reinforcement yielded before fracture of FRP reinforcement, brittle failure of the columns was avoided similar to other retrofitted specimens.

5.3.2 Strain of AFRP reinforcement

Average strain values, which were obtained by using straingauges on longitudinal AFRP reinforcement, are given for first group specimens in Figure 5.15.

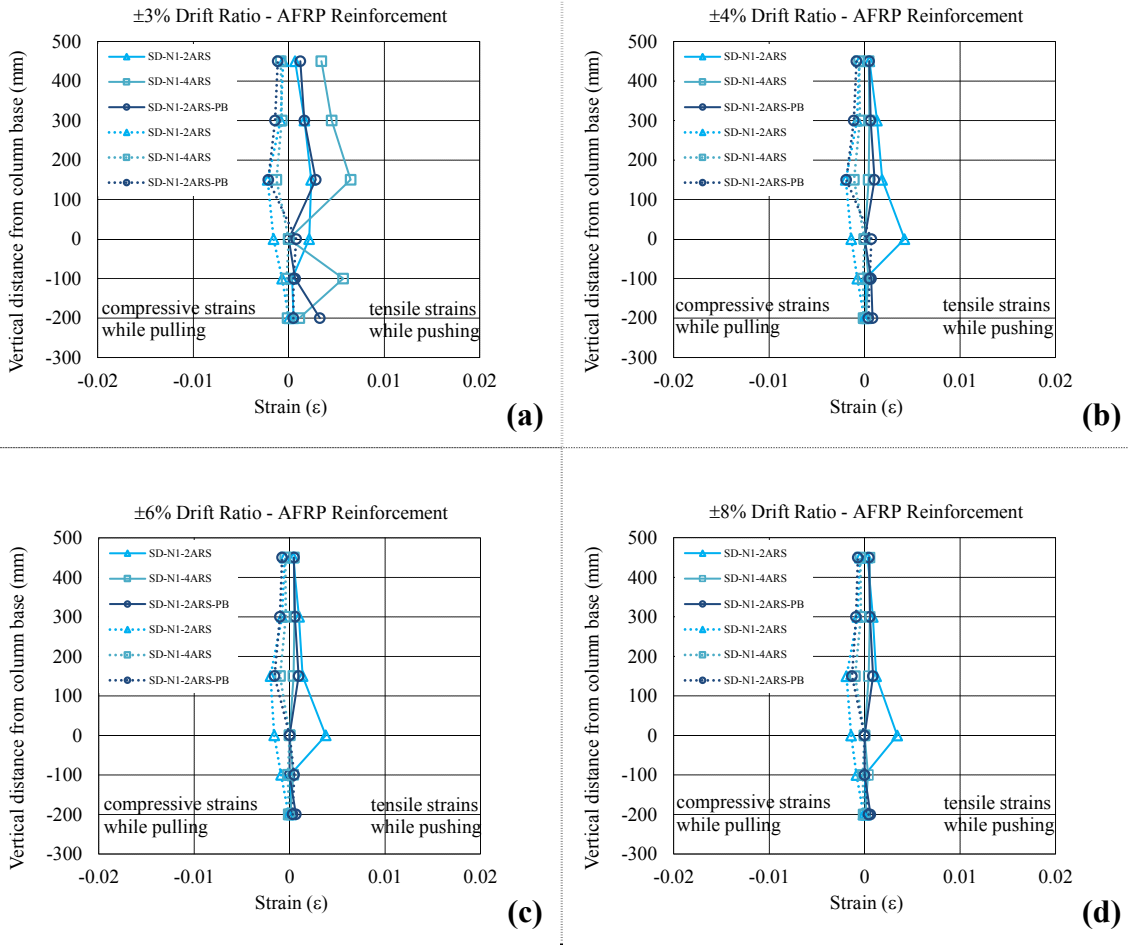

Figure 5.15 : Average strain distribution of longitudinal AFRP reinforcement of first group specimens at different drift ratios: (a)±3 %. (b)±4 %. (c)±6 %. (d)±8 %.

As it could beseen in Figure 5.11 and Figure 5.15 right after the rupture of the AFRP reinforcement around 3 % drift ratio, the strains decreased within the AFRP reinforcement, and corresponding stresses were transferred to the longitudinal steel reinforcement. The strains of steel rebars increased remarkably along the measured height as seen in Figure 5.11a, Figure 5.11b and Figure 5.11c. Besides, compressive strains measured on AFRP strips were very limited when compared to tensile strains measured up to 3 % drift ratio before rupture (Figure 5.15a).

Average strain values, which were obtained by using straingauges on longitudinal AFRP reinforcement, are given for second group specimens in Figure 5.16.

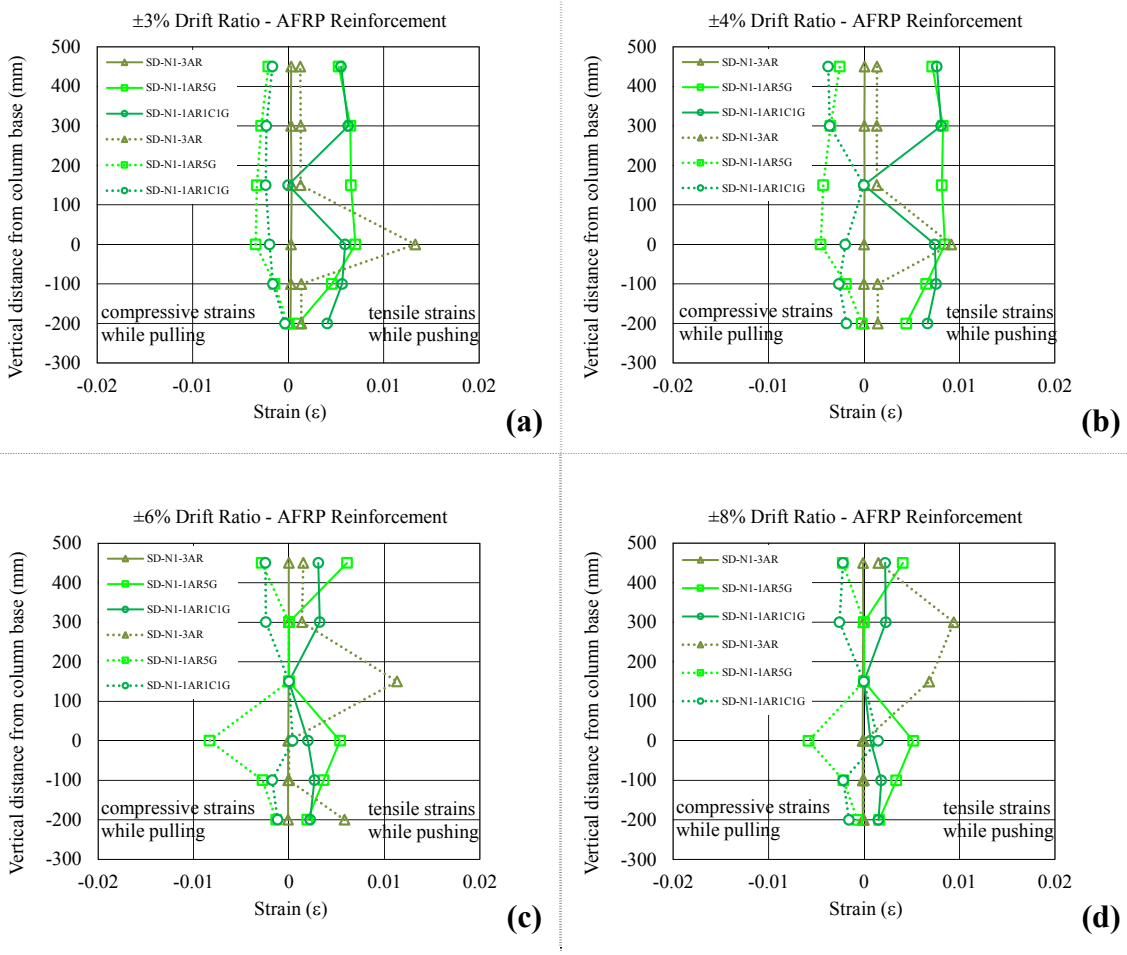

Figure 5.16 : Average strain distribution of longitudinal AFRP reinforcement of second group specimens at different drift ratios: (a)±3 %. (b)±4 %. (c)±6 %. (d)±8 %.

As seen in the Figure 5.16, measured strains on AFRP reinforcement used in specimen SD-N1-3AR are not logic to make some conclusions. It would be due to damaged straingauges prior to testing. On the other hand, strain data obtained from the straingauges installed in specimens SD-N1-1AR5G and SD-N1-1AR1C1G are reliable and inline with the relevant load-displacement relations. Since the AFRP reinforcement raptured around 4 % drift ratio, strains were transferred to GFRP reinforcement in the cross section of the columns SD-N1-1AR5G and SD-N1-1AR1C1G.

Average strain values, which were obtained by using straingauges on longitudinal AFRP reinforcement, are given for the pre-damaged columns of the third group specimens in Figure 5.17.

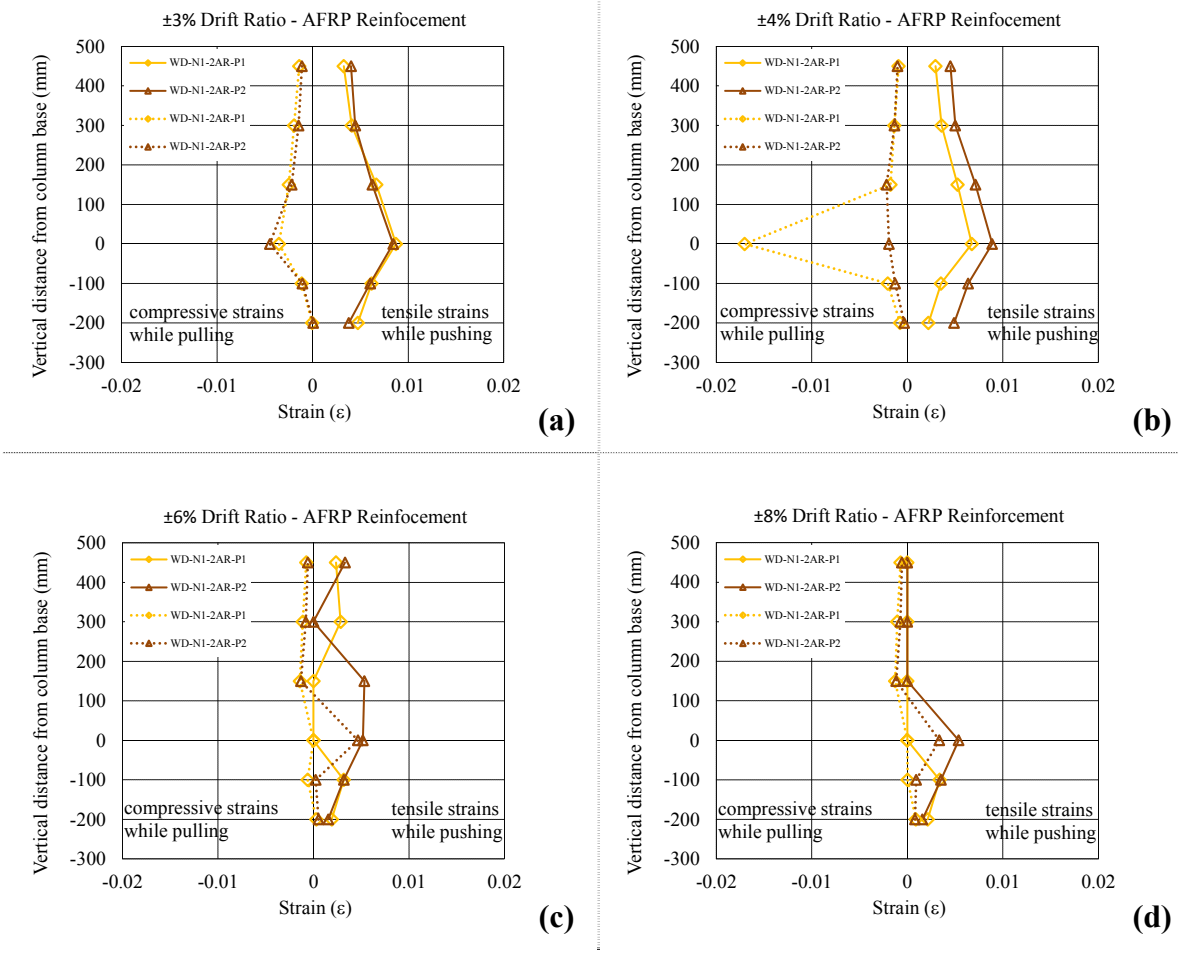

Figure 5.17 : Average strain distribution of longitudinal AFRP reinforcement of third group specimens at different drift ratios: (a)±3 %. (b)±4 %. (c)±6 %. (d)±8 %.

As it is seen in Figure 5.17, maximum strains (between 0.008 and 0.012) were measured at 4 % drift ratios since the retrofitted columns of third group specimens reached their lateral load capacity at this point. Besides, AFRP reinforcement contributed to the load bearing capacity of the columns by performing significant strains under compression stresses up to 4 % drift ratio, moment of rupture. On the other hand, contribution of FRP reinforcement under compression stresses are neglected during the theoretical modelling of the specimens due to risk of buckling.

Average strain values, which were obtained by using straingauges on longitudinal AFRP reinforcement, are given for undamaged columns of third group specimens in Figure 5.18.

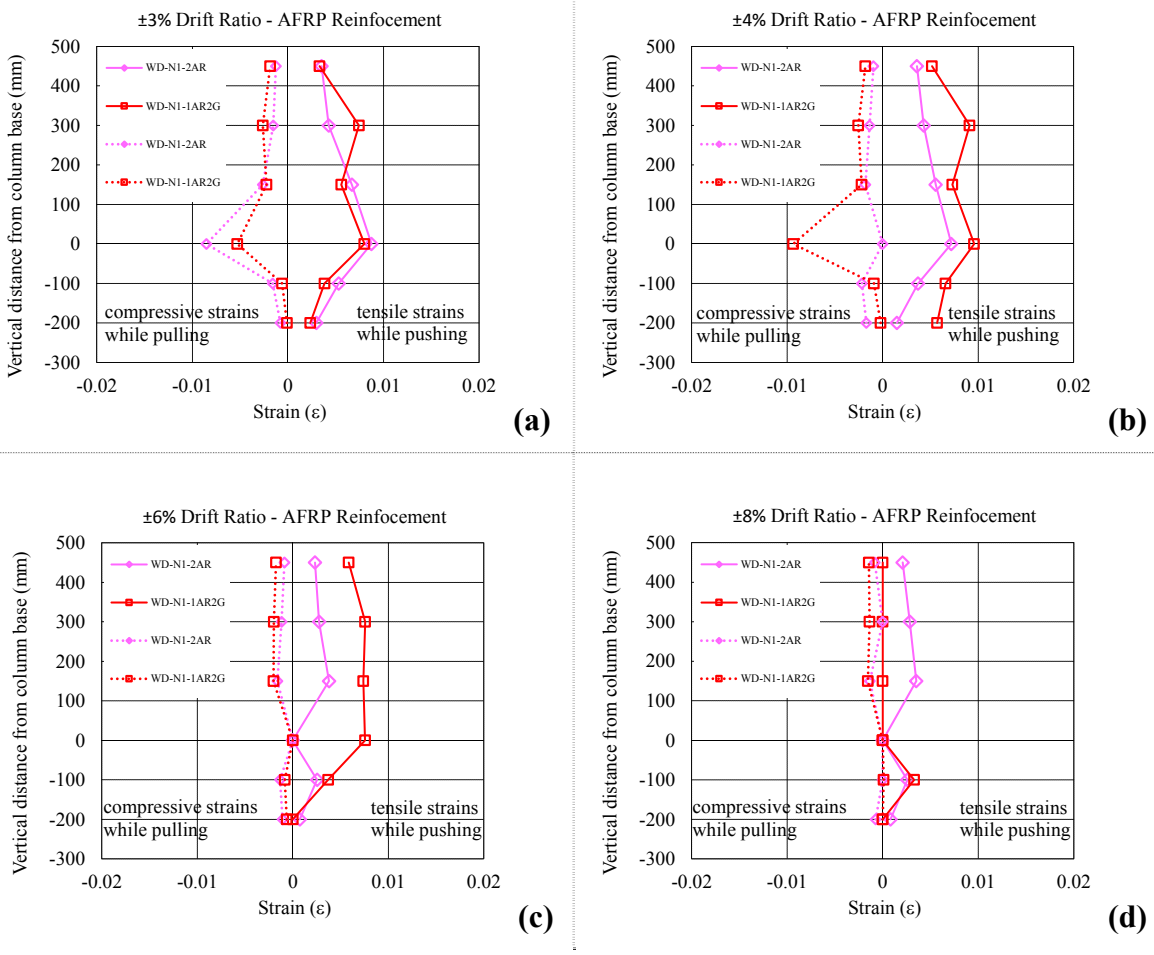

Figure 5.18 : Average strain distribution of longitudinal AFRP reinforcement of third group specimens at different drift ratios: (a)±3 %. (b)±4 %. (c)±6 %. (d)±8 %.

5.3.3 Strain of GFRP reinforcement

Average strain values, which were obtained by using straingauges on longitudinal GFRP reinforcement, are given for first group specimens in Figure 5.19.

As seen in Figure 5.19, GFRP reinforcement performed far better than AFRP reinforcement in terms of strain capaticities during the tests. Besides, GFRP bars reached their ultimate strains around ±6 % drift ratio. Furthermore, the homogenous distribution of the deformations along the first 50 cm height of the columns, which retrofitted with GFRP reinforcement, is also confirmed with the linear strain profile of the GFRP bars as seen in Figure 5.19. This behavior also proves the efficiency of the GFRP bars in enhancing cyclic flexural behavior of the substandard RC columns. Similar to AFRP bars, measured strains under compression are limited when compared to strains under tensile stresses. Thus, neglecting the contribution of FRP

reinforcement under compression does not have a significant impact on theoretical calculations of the flexural capacities.

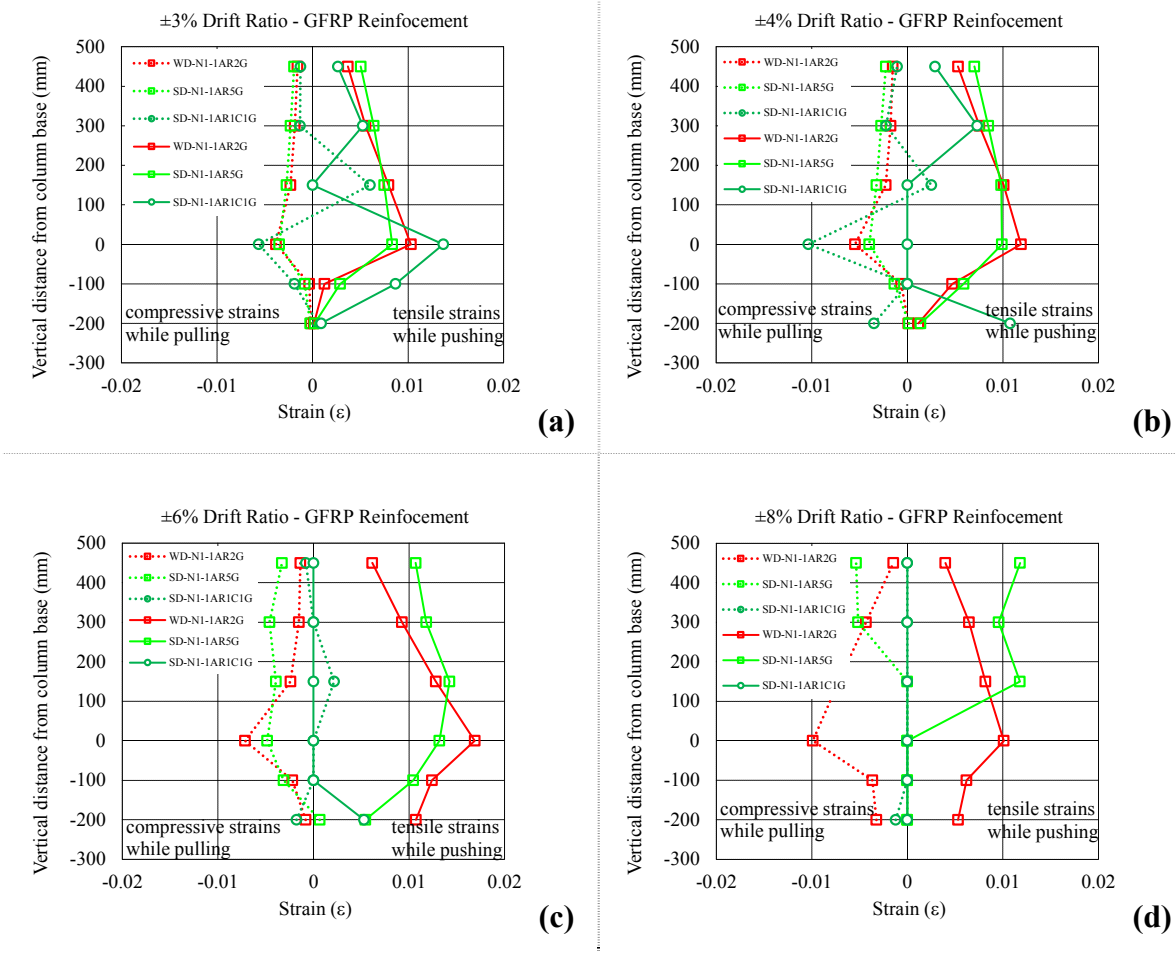

Figure 5.19 : Average strain distribution of longitudinal GFRP reinforcement at different drift ratios: (a)±3 %. (b)±4 %. (c)±6 %. (d)±8 %.

5.3.4 Strain of CFRP reinforcement

Average strain values, which were obtained by using straingauges on longitudinal CFRP reinforcement, are given for first group specimens in Figure 5.20.

As shown in Figure 5.20, CFRP reinforcement did not perform better than AFRP and GFRP reinforcement in terms of strain capaticity under tensile stresses during the tests. Therefore, efficiency of CFRP reinforcement in enhancing flexural behavior of the columns under cyclic lateral loading is limited. It should be noted that, this conclusion is made based on the test results of a single specimen in which CFRP reinforcement was utilized. In order to make more solid statements, further research should be done on utilizing CFRP reinforcement in flexural retrofitting of columns. Additionally,

similar to AFRP and GFRP bars, measured strains under compression are limited when compared to strains under tensile stresses.

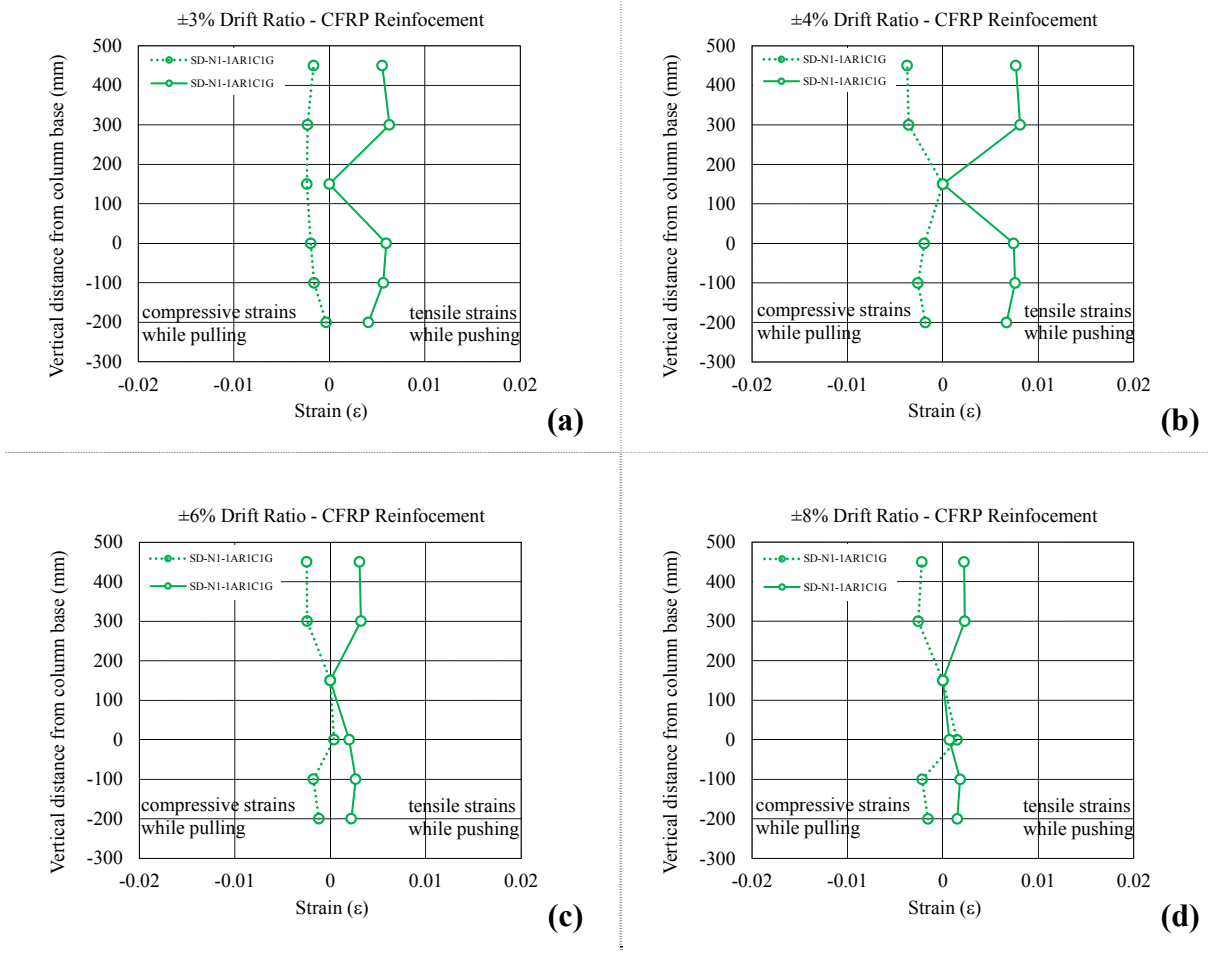

Figure 5.20 : Average strain distribution of longitudinal CFRP reinforcement at different drift ratios: (a)±3 %. (b)±4 %. (c)±6 %. (d)±8 %.

5.4 Energy Dissipation Capacities

Energy dissipation capacities of the tested specimens are calculated as the areas enclosed by the load-displacement hysteresis loops and presented in Figure 5.21.

As seen in Figure 5.21, the specimens, in which GFRP reinforcement is utilized for retrofitting, performed much higher energy dissipation capacity regardless the loading direction. This behavior could be explained with remarkable contribution of GFRP bars to the flexural strength at even in high drift ratios where AFRP reinforcement fractured at relatively small drift ratios.

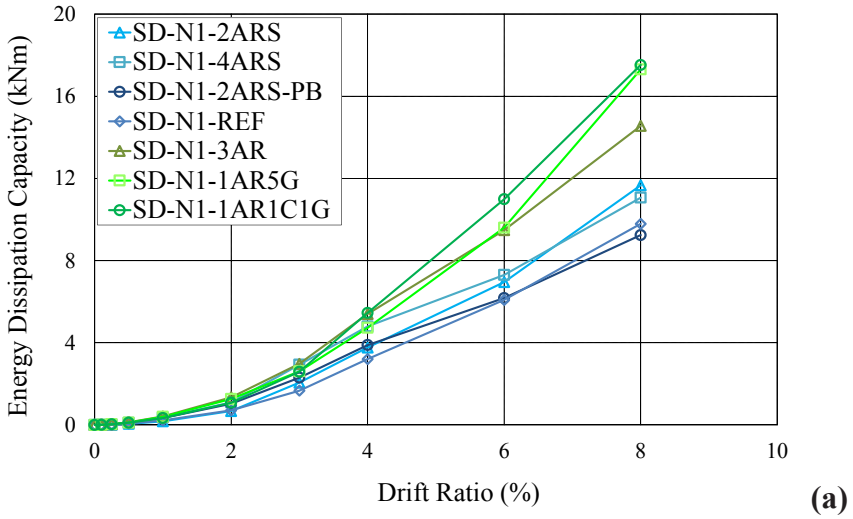

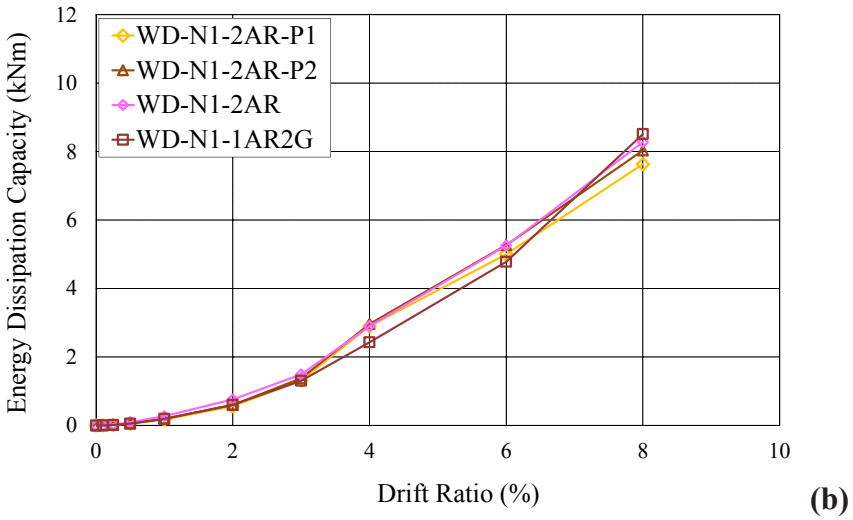

Figure 5.21 : Energy dissipation capacities of the specimens tested in: (a)Strong direction. (b)Weak direction.

In the first group specimens, the column SD-N1-4ARS shows the highest energy dissipation capacity until the rupture of the AFRP reinforcement due to its higher lateral load capacity with respect to other columns. Energy dissipation capacity of the specimen SD-N1-2ARS is higher than the specimen SD-N1-2ARS-PB due to larger elastic deformations along the embedded unbonded length of AFRP reinforcement in case of specimen SD-N1-2ARS-PB. After the rupture of the AFRP reinforcement, energy dissipation capacities of the columns SD-N1-2ARS and SD-N1-4ARS are approximately same, since the columns behave like the reference column SD-N1-REF in terms of sustained lateral load. The dissipated energy is significantly less for column SD-N1-2ARS-PB due to elastic behavior of unbonded AFRP reinforcement.

In the second group specimens, the column SD-N1-3AR shows the highest energy dissipation capacity until the 4 % drift ratio due to its higher lateral load capacity with respect to other specimens. After rupture of the AFRP reinforcement at around 4 % drift ratio, SD-N1-3AR started to behave similar to reference column SD-N1-REF, which resulted with relatively less energy dissipation in the further loading loading steps. From this point on, the specimen SD-N1-1AR1C1G showed the highest energy dissipation capacity, while specimen SD-N1-1AR5G almost caught it at the final loading cycle. Despite the limited plastic deformations due to unfractured GFRP reinforcement utilized in specimen SD-N1-1AR5G, high lateral load capacity lead to high energy dissipation capacity even at 8 % drift ratio. Besides, lateral load capacity of the specimen SD-N1-1AR1C1G decreased dramatically after the fracture of FRP reinforcement at 6 % drift ratio, which resulted significant loss in energy dissipation from this point forward.

In the third and fourth group specimens, the columns, which were retrofitted by using GFRP reinforcement showed much higher energy dissipation capacity as expected. It should be noted that there is not any significant negative impact of pre-damage conditions of the third group specimens was noticed on the energy dissipation capacities. This observation is very valuable, when the effectiveness of this retrofitting technique is considered for the pre-damaged columns in case of seismic loading.

5.5 Residual Displacements

The ratios of residual plastic displacements (δ_{res}) to the target displacements (δ_{un}) at each drift ratio are presented in Figure 5.22.

Residual deformations are limited up to 3 % drift ratio due to the elastic behavior of the columns. After 3 % drift ratio as seen from the Figure 5.22a, δ_{res} of the specimen SD-N1-1AR5G is far less than δ_{res} of the other specimens. Elastic behavior due to the unfractured GFRP bars limited the residual deformations in all drift ratios**.**

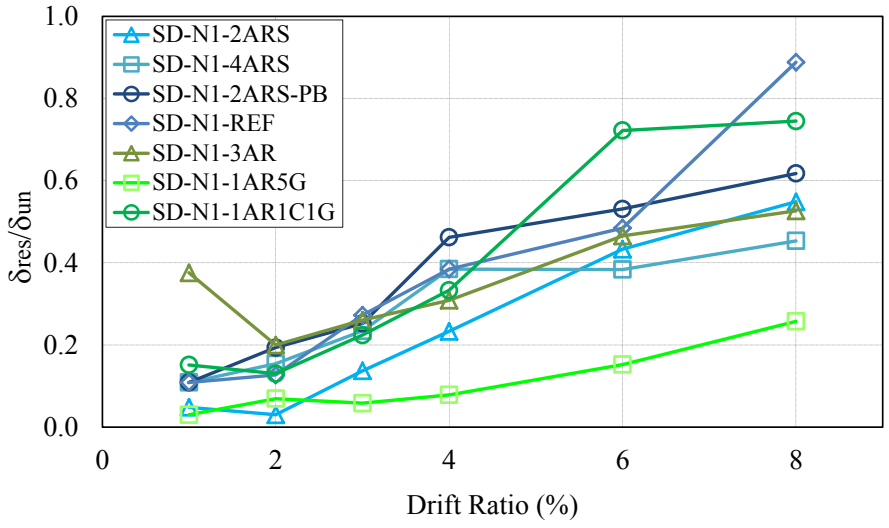

(a)

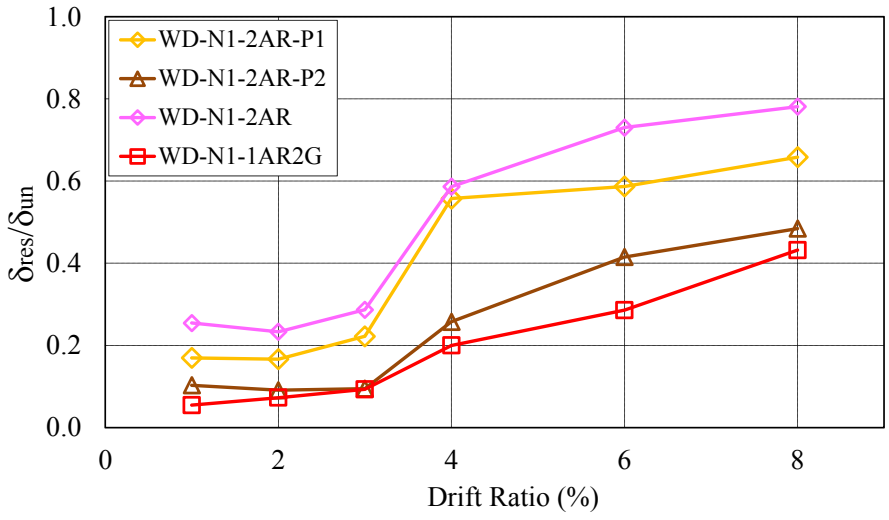

(b)

Figure 5.22 : Residual displacements of the specimens tested in: (a)Strong direction. (b)Weak direction.

Similar to the specimens tested in strong direction, residual displacements of the columns tested in weak direction are limited up to 3 % drift ratio due to the elastic behviour of the specimens. After this point, residual displacements increase due to the fracture of longitudinal AFRP reinforcement at around 4 % drift ratio, while sound GFRP reinforcement contributed to the elastic behavior of the specimen WD-N1-1AR2G up to 6 % drift ratio and limited the residual deformations.

6. ANALYTICAL STUDY

In the analytical study, the observed behavioral characteristics of the retrofitted sub-standard RC columns were taken into account in the nonlinear analyses of a typical RC building standing on sub-standard columns to investigate the effectiveness of the proposed retrofitting technique to improve the seismic bahaviour of the structures.

For studying the effectiveness of the proposed technique on the flexural performance of sub-standard RC columns, fiber element approach and plastic hinge concept were utilized during nonlinear analysis of the hypothetical building.

6.1 Building Selected for Analytical Study

For assessing the effectiveness of the proposed retrofitting technique on the seismic performance of the existing RC buildings, a numerical study is carried out on a typical low story, old RC building (> 30 years old) with poor quality materials, poor construction practice and without seismic design concepts. The seismic performance of the building both before and after retrofitting were examined through nonlinear pushover analysis considering with TSDC (2007).

The architectural and structural plans of the hypothetical building are presented in Figure 6.1 and Figure 6.2 respectively.

Hypothetical building was designed to have three stories with two symmetrical flats (in X direction) in each floor. As it is seen on the architectural plan, building has a full symmetry in X-axis, however, it is not totally symmetrical in Y axis. Although the structural system has full symmetry in both directions, loading is not symmetrical due to the non-symmetrical architectural plan of the building. The effect of non-symmetrical loading will be seen later in seismic analysis of the building.

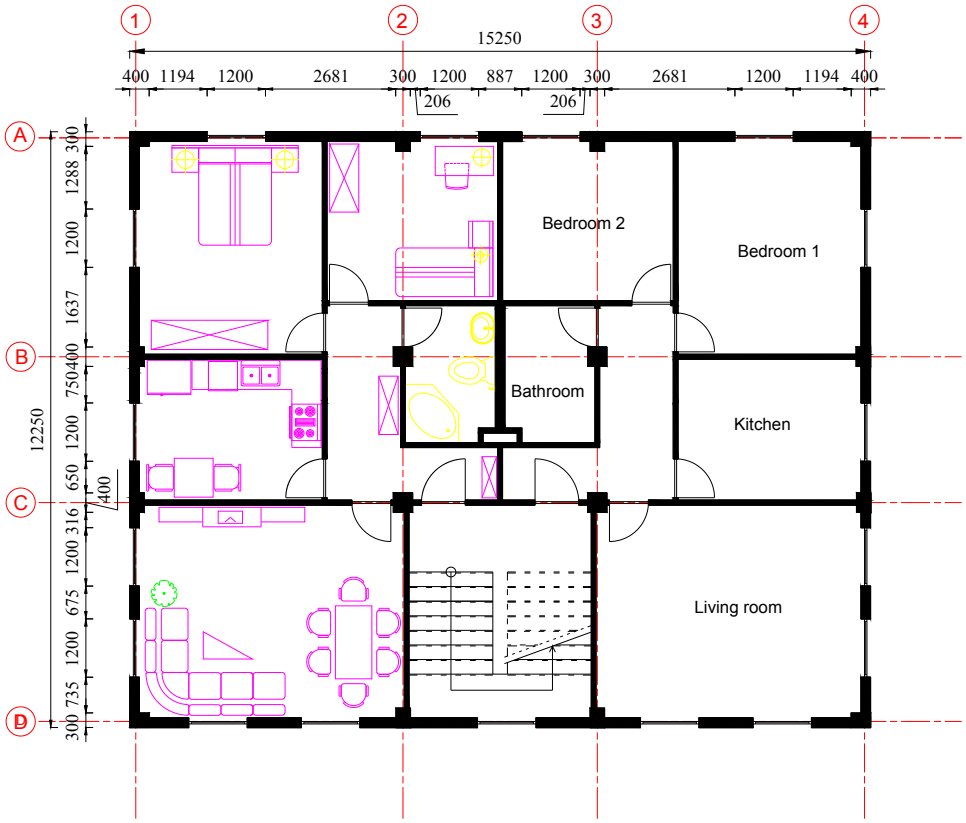

Figure 6.1 : Architectural plan of the building.

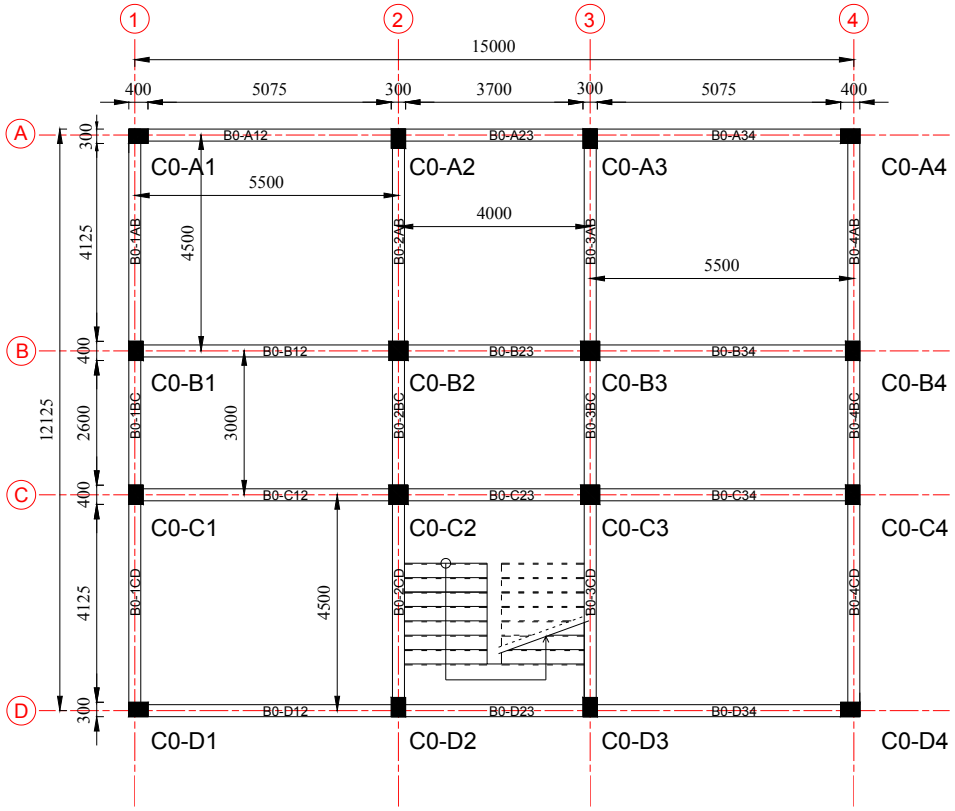

Figure 6.2 : Structural plan of the building.

Structural system of the building consists of columns in three different dimensions, which are identically located in each story. Although the column reinforcement schemes are the same for ground and first floor, smaller reinforcing bars were selected for second floor due to low capacity demand at top floor. Reinforcement schemes of the columns and the beams are given in the Figure 6.3, Figure 6.4 and Figure 6.5.

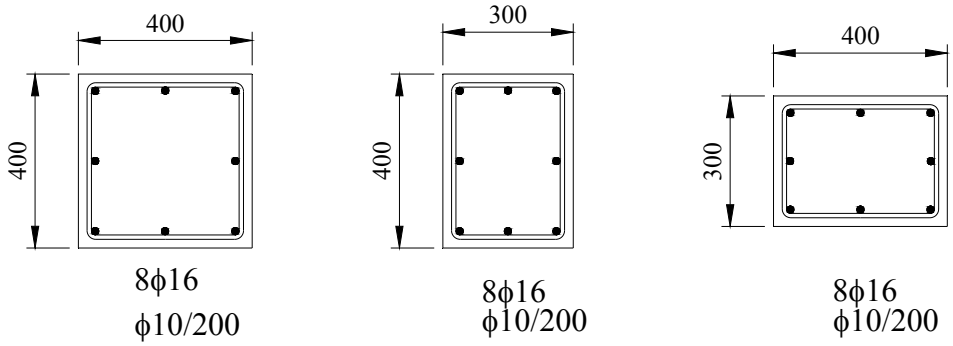

Figure 6.3 : Reinfocement scheme of the columns at the ground and first floors.

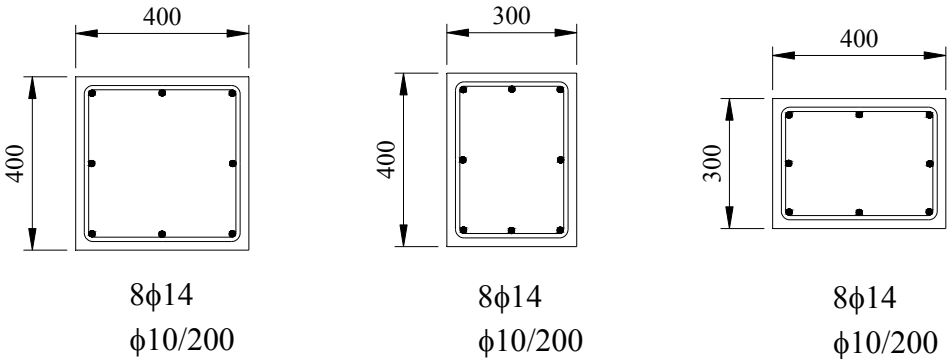

Figure 6.4 : Reinfocement scheme of the columns at the second floor.

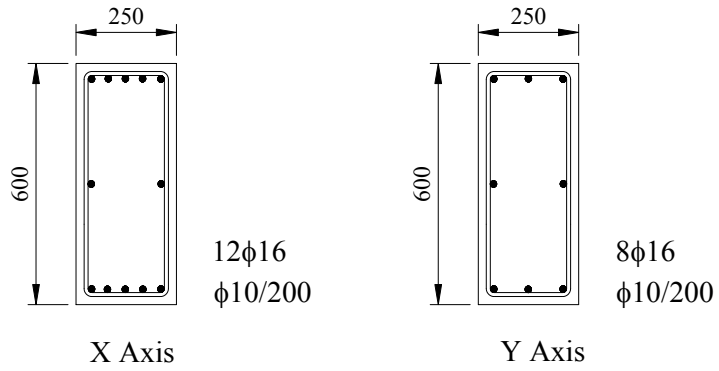

Figure 6.5 : Reinfocement scheme of the beams both in X and Y axis directions.

The subjected dead and live loads are determined considering the Turkish code of design loads for buildings, TS 498 (1997). The list of the construction materials and the considered loads are given in Appendix D.

Based on the loading data given in Appendix D, both dead and live loads subjected to slabs and transferred to the beams are calculated for all three floors and the list of the loads, which are considered for nonlinear analysis are given in in Appendix D.

6.2 Seismic Characteristics of the Building

As the selected building aimed to represent the existing building stock with poor seismic performance, compressive strength of the concrete was assumed 12 MPa and the steel reinforcement was selected as smooth bars in S220 type for both longitudinal and transverse reinforcement. As it is seen in Figure 6.3 and Figure 6.4, longitudinal reinforcement in the columns has a dimeter of 16 mm at ground and first floors while it is 14 mm at second floor.

The modal analysis of the building is done by using the structural analysis program called SAP 2000 (2015). The periods of structure for x and y directions are determined as 0.41 and 0.37 seconds, respectively. The results of the modal analysis are given in the Table 6.1.

Table 6.1 : Parameters calculated by modal analysis.

Parameter	Data	Unit
Period in X axis	0.41	s
Period in Y axis	0.37	s
Mass participation factor in X direction	0.9187	-
Mass participation factor in X direction	0.9270	-
ϕ_{11}	0.0750	m
ϕ_{21}	0.1329	m
ϕ_{31}	0.1559	m
ϕ_{12}	0.0779	m
ϕ_{22}	0.1348	m
ϕ_{32}	0.1572	m

The RC building to analyze is selected on the highest seismic risk zone described by TSDC (2007). The design horizontal acceleration is stated as 0.4g for this high risk zone and the seismic load reduction factor is taken as 1. Additionally, overall weight of the structure is calculated as 6,941 kN under “G+0.3Q” load combination, where G, Q and 0.3 are dead load, live load and live load participation factor, respectively stated by TSDC (2007).

6.3 Non-Linear Analysis of the Building

6.3.1 Moment-curvature and moment-rotation relationships

Pushover analysis is a static, nonlinear procedure, based on deformation, which requires moment-rotation relationships of each structural element of the building. For determining moment-rotation relationships, analytical model of hypothetical structure is analyzed under dead and live loads to determine the axial load levels of columns. Calculated and design axial loads (used for moment-rotation relationships) for the columns at ground, first and second floors are given in Table 6.2, Table 6.3 and Table 6.4 respectively.

Table 6.2 : Properties of the columns at ground floor.

Column notation	Dimension (mm)	Plastic hinge length - X (mm)	Plastic hinge length - Y (mm)	Axial load Calculated (kN)	Axial load design (kN)	Axial load level (%)
C0-A1	400×300	200	150	324	324	26
C0-A4	400×300	200	150	324	324	26
C0-A2	300×400	150	200	447	450	37
C0-A3	300×400	150	200	450	450	37
C0-B1	300×400	150	200	410	450	34
C0-B4	300×400	150	200	410	450	34
C0-B2	400×400	200	200	583	587	36
C0-B3	400×400	200	200	586	587	36
C0-C1	300×400	150	200	389	450	32
C0-C4	300×400	150	200	389	450	32
C0-C2	400×400	200	200	587	587	36
C0-C3	400×400	200	200	584	587	36
C0-D1	400×300	200	150	301	324	25
C0-D4	400×300	200	150	301	324	25
C0-D2	300×400	150	200	428	450	35
C0-D3	300×400	150	200	426	450	35

Table 6.3 : Properties of the columns at first floor.

Column notation	Dimension (mm)	Plastic hinge length - X (mm)	Plastic hinge length - Y (mm)	Axial load Calculated (kN)	Axial load design (kN)	Axial load level (%)
C1-A1	400×300	200	150	189	190	15
C1-A4	400×300	200	150	190	190	15
C1-A2	300×400	150	200	261	263	21
C1-A3	300×400	150	200	263	263	21
C1-B1	300×400	150	200	239	263	20
C1-B4	300×400	150	200	239	263	20
C1-B2	400×400	200	200	349	351	21
C1-B3	400×400	200	200	350	351	21
C1-C1	300×400	150	200	230	263	19
C1-C4	300×400	150	200	230	263	19
C1-C2	400×400	200	200	351	351	21
C1-C3	400×400	200	200	349	351	21
C1-D1	400×300	200	150	178	190	15
C1-D4	400×300	200	150	178	190	15
C1-D2	300×400	150	200	252	263	21
C1-D3	300×400	150	200	251	263	20

Table 6.4 : Properties of the columns at second floor.

Column notation	Dimension (mm)	Plastic hinge length - X (mm)	Plastic hinge length - Y (mm)	Axial load calculated (kN)	Axial load design (kN)	Axial load level (%)
C2-A1	400×300	200	150	53	53	4
C2-A4	400×300	200	150	53	53	4
C2-A2	300×400	150	200	76	76	6
C2-A3	300×400	150	200	76	76	6
C2-B1	300×400	150	200	69	76	6
C2-B4	300×400	150	200	69	76	6
C2-B2	400×400	200	200	117	117	7
C2-B3	400×400	200	200	117	117	7
C2-C1	300×400	150	200	71	76	6
C2-C4	300×400	150	200	71	76	6
C2-C2	400×400	200	200	116	117	7
C2-C3	400×400	200	200	116	117	7
C2-D1	400×300	200	150	52	53	4
C2-D4	400×300	200	150	52	53	4
C2-D2	300×400	150	200	76	76	6
C2-D3	300×400	150	200	76	76	6

For the sake of simplicity, the calculated axial loads for the columns are equalized when they are in similar levels and noted as design axial loads for calculating moment-curvature relationships. The moment-curvature relationships of the columns are obtained through a fiber-analysis approach using the XTRACT computer programme. The cross-sections of the columns consist of steel reinforcement, cover concrete and confined concrete. Material models, which are pre-defined in XTRACT are used to determine the nonlinear load-deformation capacity of materials in the column cross section for analytical model. The material models proposed by Mander (1988) are already considered by XTRACT to determine the stress – strain relationships in the cross sections.

Moment – curvature relationships of the columns at all floors are given in Appendix D. Plastic hinge length of the columns are assumed as the half of the effective depth of the column cross sections as recommended by TSDC (2007) in calculation of the moment – rotation relationships. Additionally, the calculated moment – relationhips for the columns are idealized as described by FEMA 273 (1997), which is already defined by structural analysis program SAP 2000 as default pattern for the moment – rotation relationship of plastic hinges, Figure 6.6.

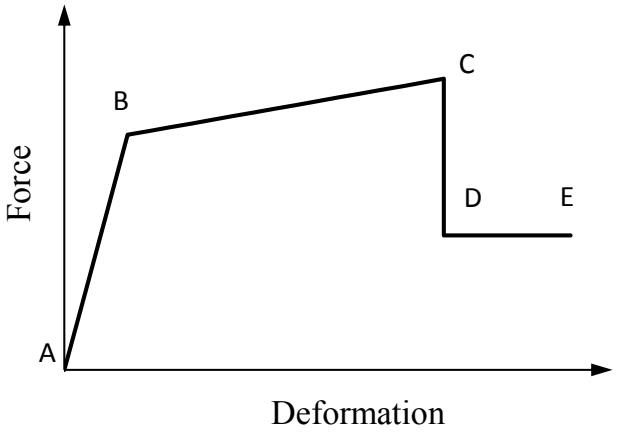

Figure 6.6 : Generalized force – deformation relationship for plastic hinges stated by FEMA 273 (1997).

Calculated and idealized moment – rotation relationships of the columns in dimensions 300x400 are given in Figure 6.7, Figure 6.8 and Figure 6.9.

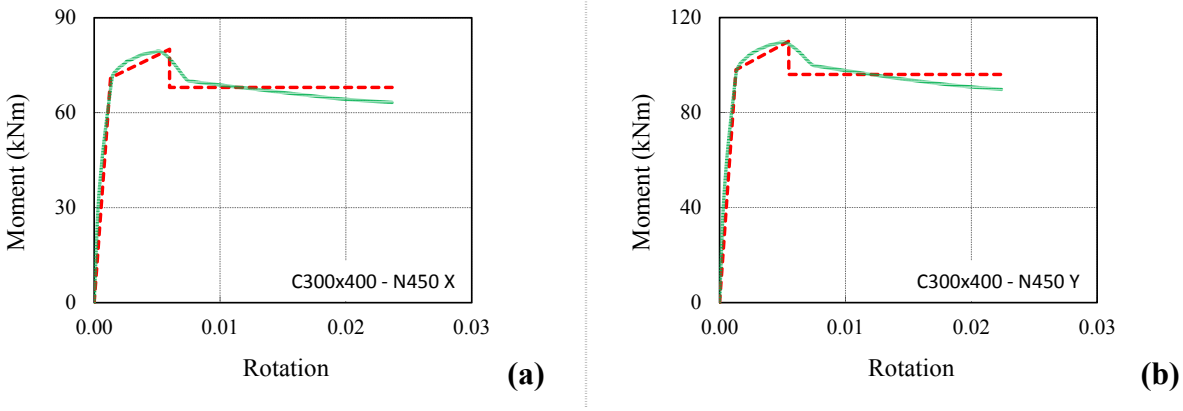

Figure 6.7 : Moment – rotation relationships of the column 300x400 at ground floor: (a)In X axis. (b)In Y axis.

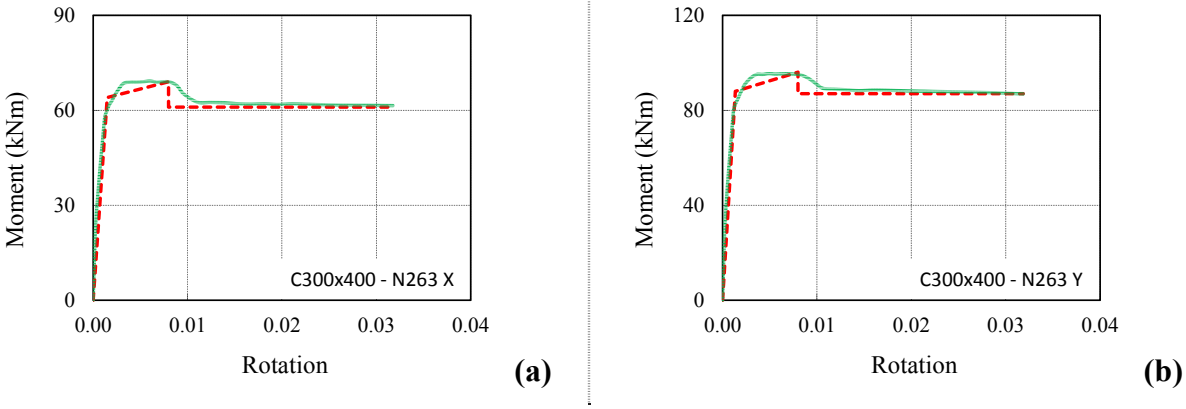

Figure 6.8 : Moment – rotation relationships of the column 300x400 at first floor: (a)In X axis. (b)In Y axis.

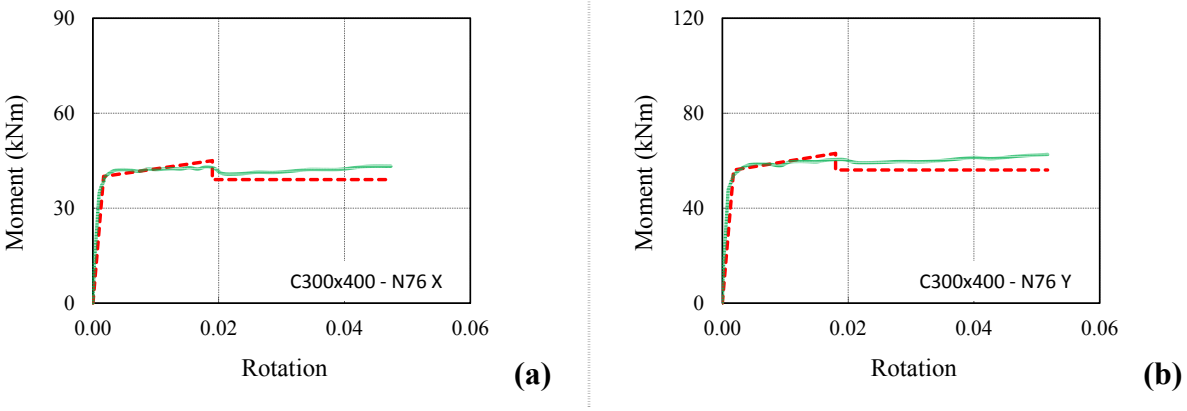

Figure 6.9 : Moment – rotation relationships of the column 300x400 at second floor: (a)In X axis. (b)In Y axis.

Calculated and idealized moment – rotation relationships of the columns in dimensions 400x300 are given in Figure 6.10, Figure 6.11 and Figure 6.12.

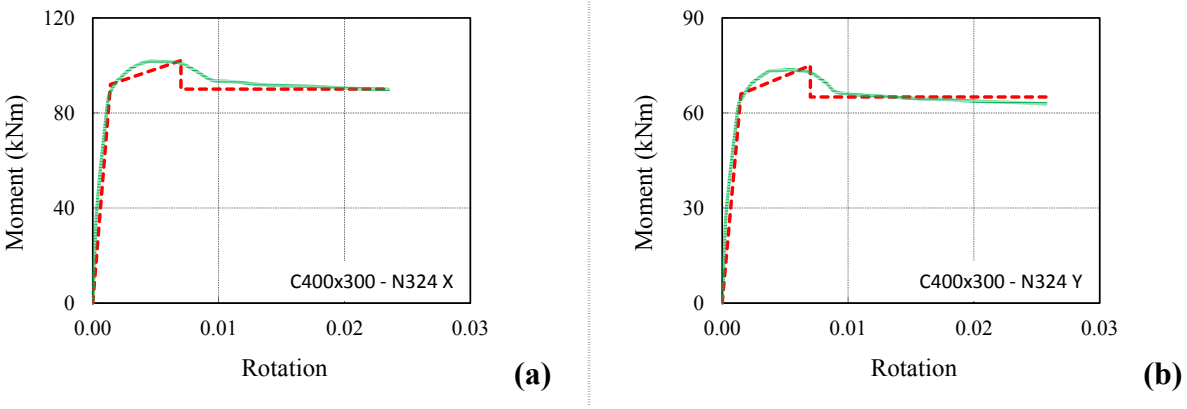

Figure 6.10 : Moment – rotation relationships of the column 400x300 at ground floor: (a)In X axis. (b)In Y axis.

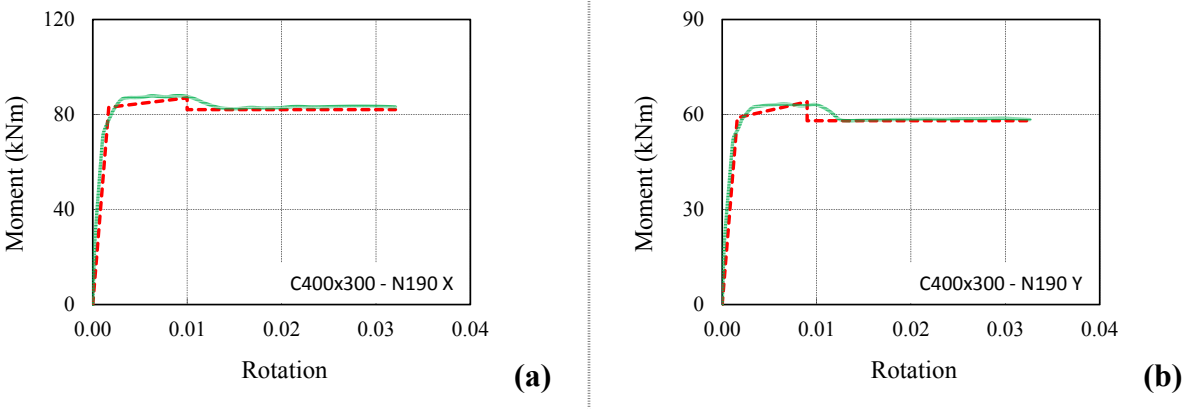

Figure 6.11 : Moment – rotation relationships of the column 400x300 at first floor: (a)In X axis. (b)In Y axis.

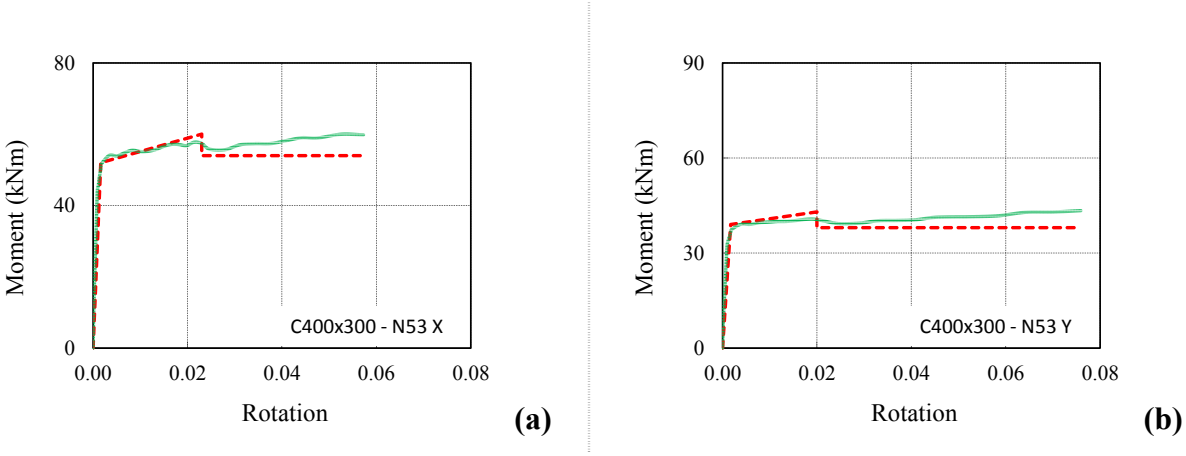

Figure 6.12 : Moment – rotation relationships of the column 400x300 at second floor: (a)In X axis. (b)In Y axis.

Calculated and idealized moment – rotation relationships of the columns in dimensions 400x400 are given in Figure 6.13, Figure 6.14 and Figure 6.15. Since these columns are fully symmetrical moment – rotation relationships are identical in each axis.

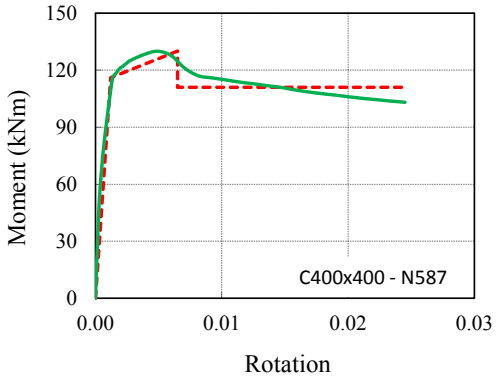

Figure 6.13 : Moment – rotation relationships of the column 400x400 at ground floor.

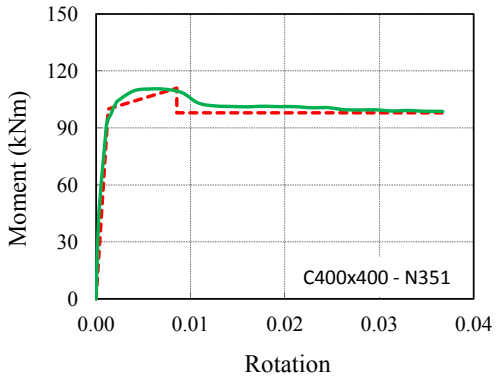

Figure 6.14 : Moment – rotation relationships of the column 400x300 at first floor.

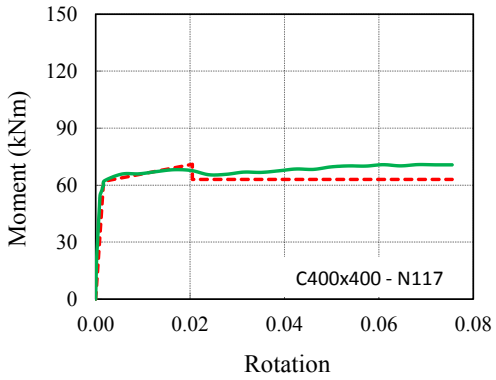

Figure 6.15 : Moment – rotation relationships of the column 400x300 at second floor.

6.3.2 Pushover analysis of the building

Pushover analyses is carried out in each axis to examine the nonlinear behavior of the hypothetical building having sub-standard columns by using the structural analysis computer program SAP 2000. The analysis proceeds with the lateral loads representing seismic loading in a static manner. The lateral-load distribution through the height of the structure is determined by considering the relevant mode shape and the mass distribution as stated by TSDC (2007). Since the beams have much higher flexural capacity when compared to columns, they are assumed to behave elastically throughout the loading. The parameters considered for calculation of the seismic performance level of the building is given in Table 6.5.

Table 6.5 : Parameters considered for calculation of the seismic performance level of the building.

Parameter	Value	Unit
Earthquake risk zone according to TSDC (2007)	1 (highest risk zone)	-
Design horizontal acceleration, A_0	0.40 g	m/s^2
Soil class	Z1	-
Building importance factor, I	1	-
Gravitational acceleration, g	9.81	m/s^2
Mass of the ground floor, m_1	289.6	kNs^2/m
Mass of the first floor, m_2	289.6	kNs^2/m
Mass of the second floor, m_3	128.4	kNs^2/m

Base shear – top displacement relationships of the building are calculated in both directions by using nonlinear – static pushover analysis. Modal capacity diagram (modal displacement – modal acceleration) is calculated by using base shear – top displacement diagram by using equation (6.1), equation (6.2) and equation (6.3).

$$a_1^{(i)} = \frac{V_{x1}^{(i)}}{M_{x1}} \tag{6.1}$$

In equation 6.1, $a_1^{(i)}$ represents modal acceleration at $(i)^{th}$ step at the first mode, $V_{x1}^{(i)}$ represents base shear force at $(i)^{th}$ step for the first mode, $M_{x1}^{(i)}$ represents the effective modal mass for the first mode for an earthquake in "*x*" direction. $M_{x1}^{(i)}$ is obtained as follows;

$$M_{x1}^{(i)} = \frac{\left(\sum_{N=1}^{n} m_N \phi_{N1}^{(i)}\right)^2}{\sum_{N=1}^{n} m_N \phi_{N1}^{(i)2}} \tag{6.2}$$

In equation 6.2, m_N represents lumped story mass, $\phi_{N1}^{(i)}$ represents N^{th} component of the mode shape vector for the first mode.

$$d_1^i = \frac{u_{xN1}^{(i)}}{\Phi_{xN1}\Gamma_{x1}} \tag{6.3}$$

In equation 6.3, $d_1^{(i)}$ represents modal displacement, $U_{xN1}^{(i)}$ represents top displacement in x direction, Φ_{xN1} represents the mode shape vector for the first mode at N^{th} story at the $(i)^{th}$ step in the x direction, Γ_{x1} represents participation factor for the first mode. Γ_{x1} is obtained as follows;

$$\Gamma_{x1} = \frac{L_{x1}}{M_1} \tag{6.4}$$

L_{x1} and M_1 are obtained as shown in equation 6.5 and equation 6.6 respectively;

$$L_{x1} = \sum_{i=1}^{N} m_i \Phi_{xi1} \tag{6.5}$$

$$M_1 = \sum_{i=1}^{N} m_i \, \Phi_{xi1}^2 \tag{6.6}$$

Elastic demand spectrum is calculated by using elastic design acceleration spectrum for calculating elastic spectral displacement demand. Elastic design acceleration spectrum is obtained by using equation (6.7), equation (6.8) and equation (6.9).

$$S(T)=1+1.5\,(T/T_A) \quad 0\leq T\leq T_A$$

$$S(T)=2.5 \qquad T_A \leq T\leq T_B \tag{6.7}$$

$$S(T)=2.5(T_B/T)^{0.8} \qquad T_B\leq T$$

In equation 6.7, S(T) represents spectrum coefficient, T represents period of the building for the first mode. Depending on the elastic design acceleration spectrum, elastic demand spectrum is obtained by using equation (6.8) and equation (6.9).

$$S_{ae1}(T)=A(T)g$$
$$A(T)=A_0\, I\, S(T) \tag{6.8}$$

$$S_{de1}(T)=\frac{S_{ae1}}{\left(\omega_1^{(1)}\right)^2}$$
$$\omega_1^2=\frac{2\pi}{T_1^{(1)}} \tag{6.9}$$

In equation 6.8, S_{ae1} represents elastic spectral acceleration for the first mode for an earthquake in "x" direction, A(T) represents spectral acceleration coefficient, A_0 represents effective ground acceleration coefficient and I represent building importance factor. In equation 6.9, S_{de1} represents linear elastic spectral displacement for the first mode for an earthquake in "x" direction and ω_1 represents circular frequency for the first mode.

Modal capacity diagram and elastic demand spectrum are combined in a single diagram for determining elastic spectral displacement demand. A linear line, which is the initial tangent of the modal capacity diagram extended long enough to intersect with the elastic demand spectrum. The spectral displacement at this intersection point is taken into account to calculate the inelastic spectral displacement demand as shown by equation (6.10).

$$S_{di1}=C_{R1}\,S_{de1}$$

$$C_{R1}=1 \qquad T1\geq T_B$$

$$C_{R1}=\frac{1+(R_{y1})\frac{T_B}{T_1^{(1)}}}{R_{y1}} \qquad T1<T_B \tag{6.10}$$

In equation 6.10, S_{di1} represents nonlinear spectral displacement demand for the first mode for an earthquake in "x" direction, C_{R1} represents spectral displacement amplification factor for the first mode of the building for an earthquake in "x" direction, R_{y1} represents load reduction factor for the first mode for an earthquake in "x" direction.

The top displacement demand of the building is calculated by using equation (6.11).

$$u_{xN1}^{(p)} = \Phi_{xN1}\Gamma_{x1}S_{di1} \tag{6.11}$$

After calculation of the top displacement demand, pushover analysis through SAP 2000 computer program are repeated for both directions and plastic rotation demands (Θ_p) of the columns are obtained. These values are divided by plastic hinge length (L_p) of the corresponding column and plastic curvature demands (χ_p) are calculated as shown in equation (6.12).

$$\chi_p = \frac{\theta_p}{L_p} \tag{6.12}$$

Total curvature demand (χ_T) was calculating by summing the plastic curvature demand and the yield curvature (χ_y) value obtained from moment-curvature relationship by using cross section analysis program XTRACT as seen in the equation (6.13).

$$\chi_T = \chi_p + \chi_y \tag{6.13}$$

Strain demands are determined from detailed moment-curvature relationships containing strain and stress values.

TSDC (2007) states minimum damage limit (MN), safety limit (GV) and collapsing limit (GC) as limit conditions on the cross-section of the ductile reinforced concrete members, Figure 6.16. Minimum damage limit refers the end of the elastic behavior

of the structural element, safety limit stands for the point, where structural element starts failing in strength and collapsing limit defines the limit of the behavior before collapsing.

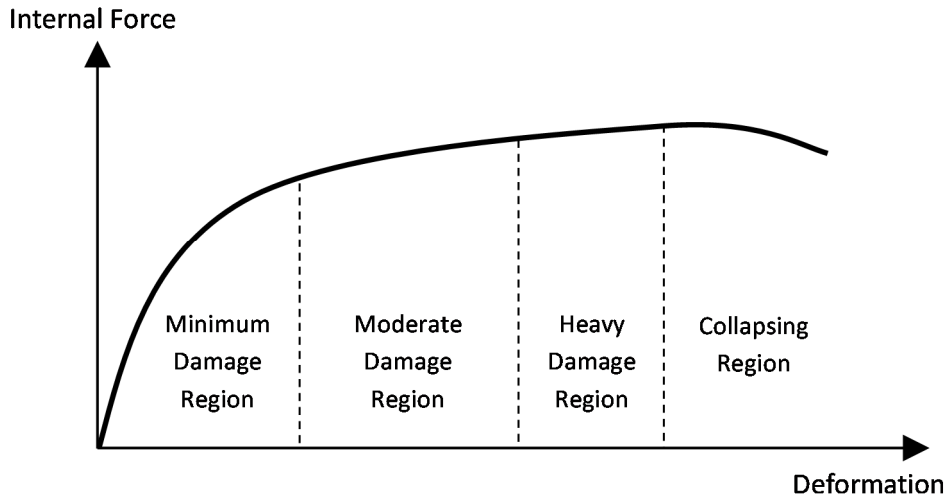

Figure 6.16 : Damage regions of the reinforced concrete sections according to TSDC (2007).

Strain limits for MN is taken as the upper bounds of the concrete strain in the outmost fiber of the section (unconfined concrete cover), while strain limits for GV and GC are taken as the upper bounds of the concrete strain in the outmost fiber of core area surrounded by transverse reinforcement. In performance levels GV and GC, the strain limit for core concrete depends on the confinement conditions of the structural elements. In Table 6.6, ρ_s and ρ_{sm} represent the existing and the required volumetric ratio of transverse reinforcement of columns, respectively.

Table 6.6 : Strain limits for each performance level defined by TSDC (2007).

Damage Limits	Upper limit for reinforcement strain (ε_s)	Upper limit for concrete strain in case of sufficient transverse reinforcement detailing (ε_c)	Upper limit for concrete strain (ε_c)
MN	0.010	0.0035	0.0035
GV	0.040	$0.0035 + 0.010\ (\rho_s/\rho_{sm}) \leq 0.0135$	0.0035
GC	0.060	$0.0040 + 0.014\ (\rho_s/\rho_{sm}) \leq 0.0180$	0.0040

It should be noted that these strain limits for confined concrete are valid when transverse reinforcement details are in accordance with the seismic detailing required by TSDC (2007). In case of non-conformance with TSDC (2007) requirements, ρ_s has to be considered as 0 and the strain limits have to be calculated accordingly.

Modal capacity diagrams and elastic demand spectrums for the building are obtained for 5 % damping ratio for both X and Y directions as shown in Figure 6.17 and Figure 6.18 respectively.

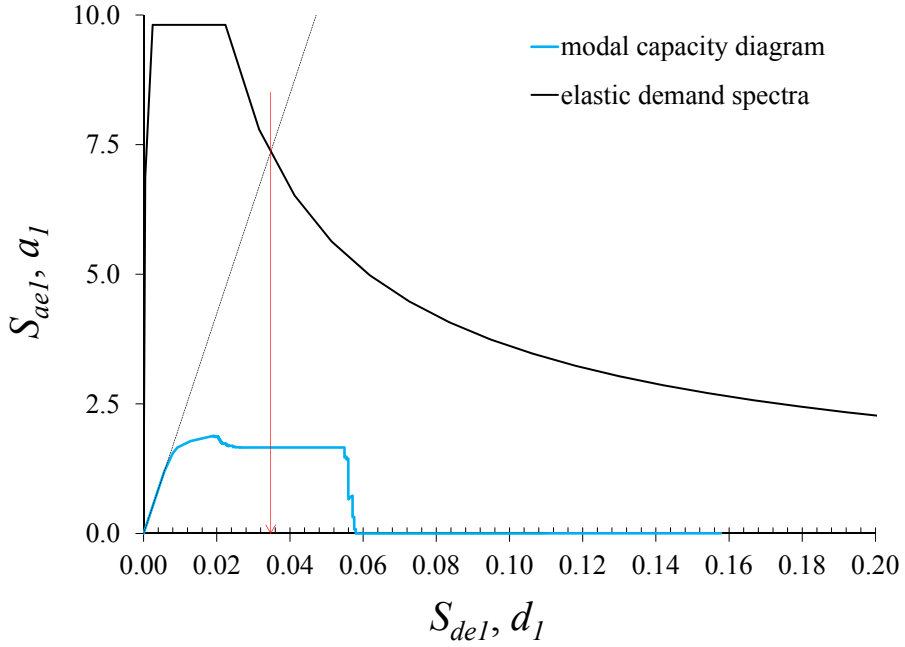

Figure 6.17 : Modal capacity diagram and elastic demand spectrum in X direction.

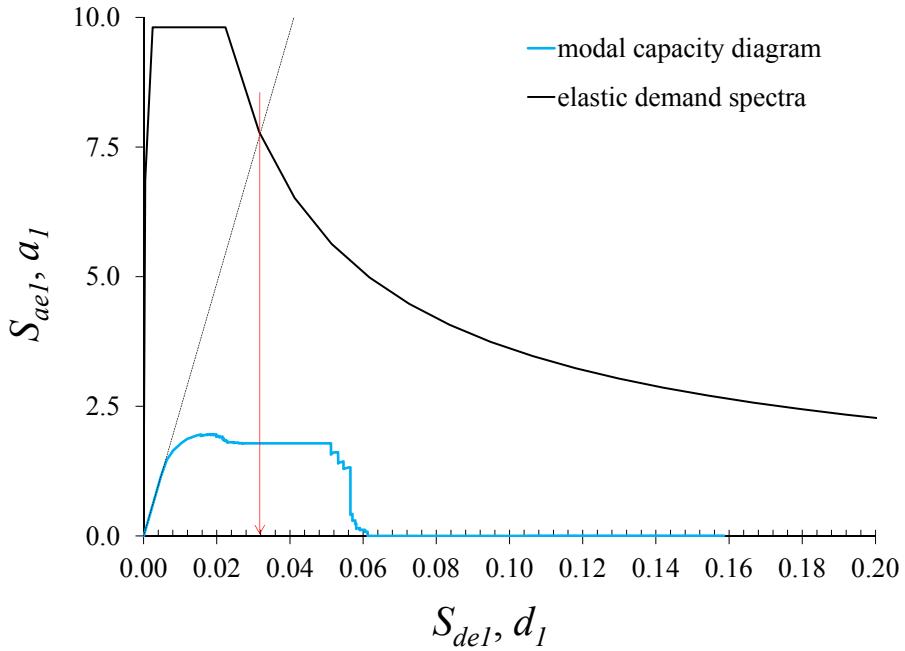

Figure 6.18 : Modal capacity diagram and elastic demand spectrum in X direction.

The periods of the building in both directions (T_1=0.41 s, T_2=0.37 s) are higher than T_B=0.3 s, CR is taken as 1 as recommended by TSDC, (2007), and therefore nonlinear spectral displacements in both directions (S_{di}) become equal to linear spectral

displacements (S_{de1}). The target displacements (U_{xN1} and U_{yN1}) are found as 0.044 m and 0.040 m in X and Y directions respectively.

The base shear capacity curves of the building are shown in shown in Figure 6.19.

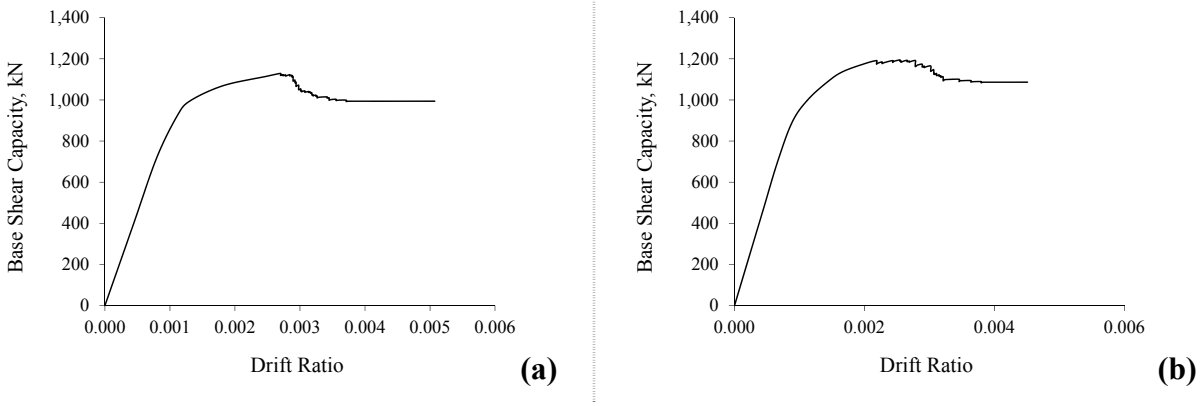

Figure 6.19 : Capacity curve of the building: (a)In X axis. (b)In Y axis.

Total curvature demands of the columns were calculated by summing elastic and plastic curvature, which are found in the pushover analysis by SAP 2000 and cross section analysis by XTRACT computer programs. The total curvature demands of the columns are given for X and Y directions in the Table 6.7 and Table 6.8 respectively.

Table 6.7 : Total curvature demands of the columns of the non-retrofitted building in X direction.

Story	Column notation	Pushover direction	Hinge	Plastic Rotation θ_p	Plastic Hinge length L_p (m)	Plastic Curvature χ_p (1/m)	Elastic Curvature χ_y (1/m)	Total Curvature χ_T (1/m)
Ground	C0-A2	X	C1-X0	0.01172	0.150	0.07810	0.00975	0.08785
Ground	C0-A3	X	C1-X0	0.01165	0.150	0.07769	0.00975	0.08744
Ground	C0-B1	X	C1-X0	0.01184	0.150	0.07895	0.00975	0.08870
Ground	C0-B4	X	C1-X0	0.01199	0.150	0.07991	0.00975	0.08966
Ground	C0-C1	X	C1-X0	0.01206	0.150	0.08037	0.00975	0.09012
Ground	C0-C4	X	C1-X0	0.01218	0.150	0.08119	0.00975	0.09094
Ground	C0-D2	X	C1-X0	0.01257	0.150	0.08379	0.00975	0.09354
Ground	C0-D3	X	C1-X0	0.01250	0.150	0.08336	0.00975	0.09311
Ground	C0-A1	X	C2-X0	0.01181	0.200	0.05906	0.00613	0.06519
Ground	C0-A4	X	C2-X0	0.01191	0.200	0.05957	0.00613	0.06570
Ground	C0-D1	X	C2-X0	0.01263	0.200	0.06316	0.00613	0.06929
Ground	C0-D4	X	C2-X0	0.01274	0.200	0.06372	0.00613	0.06985
Ground	C0-B2	X	C3-X0	0.01239	0.200	0.06197	0.00678	0.06875
Ground	C0-B3	X	C3-X0	0.01229	0.200	0.06147	0.00678	0.06825
Ground	C0-C2	X	C3-X0	0.01259	0.200	0.06297	0.00678	0.06975
Ground	C0-C3	X	C3-X0	0.01252	0.200	0.06258	0.00678	0.06936
1	C1-A2	X	C1-X1	0.00079	0.150	0.00529	0.00821	0.01350
1	C1-A3	X	C1-X1	0.00011	0.150	0.00072	0.00821	0.00893
1	C1-B1	X	C1-X1	0.00000	0.150	0.00000	0.00821	0.00821
1	C1-B4	X	C1-X1	0.00050	0.150	0.00331	0.00821	0.01152
1	C1-C1	X	C1-X1	0.00000	0.150	0.00000	0.00821	0.00821
1	C1-C4	X	C1-X1	0.00059	0.150	0.00395	0.00821	0.01215
1	C1-D2	X	C1-X1	0.00166	0.150	0.01109	0.00821	0.01929
1	C1-D3	X	C1-X1	0.00087	0.150	0.00581	0.00821	0.01402
1	C1-A1	X	C2-X1	0.00000	0.200	0.00000	0.00541	0.00541
1	C1-A4	X	C2-X1	0.00000	0.200	0.00000	0.00541	0.00541
1	C1-D1	X	C2-X1	0.00000	0.200	0.00000	0.00541	0.00541
1	C1-D4	X	C2-X1	0.00038	0.200	0.00188	0.00541	0.00729
1	C1-B2	X	C3-X1	0.00115	0.200	0.00574	0.00575	0.01149
1	C1-B3	X	C3-X1	0.00018	0.200	0.00090	0.00575	0.00665
1	C1-C2	X	C3-X1	0.00127	0.200	0.00633	0.00575	0.01208
1	C1-C3	X	C3-X1	0.00047	0.200	0.00235	0.00575	0.00810
2	C2-A2	X	C1-X2	0.00012	0.150	0.00079	0.00660	0.00739
2	C2-A3	X	C1-X2	0.00000	0.150	0.00000	0.00660	0.00660
2	C2-B1	X	C1-X2	0.00000	0.150	0.00000	0.00660	0.00660
2	C2-B4	X	C1-X2	0.00012	0.150	0.00080	0.00660	0.00740
2	C2-C1	X	C1-X2	0.00000	0.150	0.00000	0.00660	0.00660
2	C2-C4	X	C1-X2	0.00015	0.150	0.00102	0.00660	0.00762
2	C2-D2	X	C1-X2	0.00062	0.150	0.00416	0.00660	0.01076
2	C2-D3	X	C1-X2	0.00009	0.150	0.00061	0.00660	0.00721
2	C2-A1	X	C2-X2	0.00000	0.200	0.00000	0.00456	0.00456
2	C2-A4	X	C2-X2	0.00000	0.200	0.00000	0.00456	0.00456
2	C2-D1	X	C2-X2	0.00000	0.200	0.00000	0.00456	0.00456
2	C2-D4	X	C2-X2	0.00000	0.200	0.00000	0.00456	0.00456
2	C2-B2	X	C3-X2	0.00035	0.200	0.00175	0.00465	0.00640
2	C2-B3	X	C3-X2	0.00000	0.200	0.00000	0.00465	0.00465
2	C2-C2	X	C3-X2	0.00041	0.200	0.00207	0.00465	0.00671
2	C2-C3	X	C3-X2	0.00000	0.200	0.00000	0.00465	0.00465

Table 6.8 : Total curvature demands of the columns of the non-retrofitted building in Y direction.

Story	Column notation	Pushover direction	Hinge	Plastic Rotation θ_p	Plastic Hinge length L_p (m)	Plastic Curvature χ_p (1/m)	Elastic Curvature χ_y (1/m)	Total Curvature χ_T (1/m)
Ground	C0-A2	Y	C1-Y0	0.01106	0.200	0.05528	0.00669	0.06197
Ground	C0-A3	Y	C1-Y0	0.01036	0.200	0.05181	0.00669	0.05850
Ground	C0-B1	Y	C1-Y0	0.01210	0.200	0.06050	0.00669	0.06719
Ground	C0-B4	Y	C1-Y0	0.00945	0.200	0.04726	0.00669	0.05395
Ground	C0-C1	Y	C1-Y0	0.01214	0.200	0.06071	0.00669	0.06739
Ground	C0-C4	Y	C1-Y0	0.00947	0.200	0.04735	0.00669	0.05403
Ground	C0-D2	Y	C1-Y0	0.01101	0.200	0.05503	0.00669	0.06171
Ground	C0-D3	Y	C1-Y0	0.01031	0.200	0.05157	0.00669	0.05826
Ground	C0-A1	Y	C2-Y0	0.01191	0.150	0.07941	0.00870	0.08811
Ground	C0-A4	Y	C2-Y0	0.00927	0.150	0.06177	0.00870	0.07047
Ground	C0-D1	Y	C2-Y0	0.01181	0.150	0.07874	0.00870	0.08744
Ground	C0-D4	Y	C2-Y0	0.00921	0.150	0.06137	0.00870	0.07007
Ground	C0-B2	Y	C3-Y0	0.01126	0.200	0.05632	0.00678	0.06310
Ground	C0-B3	Y	C3-Y0	0.01055	0.200	0.05273	0.00678	0.05951
Ground	C0-C2	Y	C3-Y0	0.01131	0.200	0.05655	0.00678	0.06333
Ground	C0-C3	Y	C3-Y0	0.01059	0.200	0.05296	0.00678	0.05974
1	C1-A2	Y	C1-Y1	0.00001	0.200	0.00007	0.00581	0.00588
1	C1-A3	Y	C1-Y1	0.00000	0.200	0.00000	0.00581	0.00581
1	C1-B1	Y	C1-Y1	0.00132	0.200	0.00662	0.00581	0.01243
1	C1-B4	Y	C1-Y1	0.00000	0.200	0.00000	0.00581	0.00581
1	C1-C1	Y	C1-Y1	0.00189	0.200	0.00945	0.00581	0.01526
1	C1-C4	Y	C1-Y1	0.00000	0.200	0.00000	0.00581	0.00581
1	C1-D2	Y	C1-Y1	0.00000	0.200	0.00000	0.00581	0.00581
1	C1-D3	Y	C1-Y1	0.00000	0.200	0.00000	0.00581	0.00581
1	C1-A1	Y	C2-Y1	0.00119	0.150	0.00795	0.00767	0.01561
1	C1-A4	Y	C2-Y1	0.00000	0.150	0.00000	0.00767	0.00767
1	C1-D1	Y	C2-Y1	0.00003	0.150	0.00020	0.00767	0.00787
1	C1-D4	Y	C2-Y1	0.00000	0.150	0.00000	0.00767	0.00767
1	C1-B2	Y	C3-Y1	0.00076	0.200	0.00382	0.00575	0.00957
1	C1-B3	Y	C3-Y1	0.00024	0.200	0.00120	0.00575	0.00695
1	C1-C2	Y	C3-Y1	0.00125	0.200	0.00627	0.00575	0.01202
1	C1-C3	Y	C3-Y1	0.00065	0.200	0.00324	0.00575	0.00899
2	C2-A2	Y	C1-Y2	0.00000	0.200	0.00000	0.00470	0.00470
2	C2-A3	Y	C1-Y2	0.00000	0.200	0.00000	0.00470	0.00470
2	C2-B1	Y	C1-Y2	0.00015	0.200	0.00077	0.00470	0.00547
2	C2-B4	Y	C1-Y2	0.00000	0.200	0.00000	0.00470	0.00470
2	C2-C1	Y	C1-Y2	0.00059	0.200	0.00296	0.00470	0.00766
2	C2-C4	Y	C1-Y2	0.00000	0.200	0.00000	0.00470	0.00470
2	C2-D2	Y	C1-Y2	0.00000	0.200	0.00000	0.00470	0.00470
2	C2-D3	Y	C1-Y2	0.00000	0.200	0.00000	0.00470	0.00470
2	C2-A1	Y	C2-Y2	0.00024	0.150	0.00157	0.00643	0.00800
2	C2-A4	Y	C2-Y2	0.00000	0.150	0.00000	0.00643	0.00643
2	C2-D1	Y	C2-Y2	0.00000	0.150	0.00000	0.00643	0.00643
2	C2-D4	Y	C2-Y2	0.00000	0.150	0.00000	0.00643	0.00643
2	C2-B2	Y	C3-Y2	0.00000	0.200	0.00000	0.00465	0.00465
2	C2-B3	Y	C3-Y2	0.00000	0.200	0.00000	0.00465	0.00465
2	C2-C2	Y	C3-Y2	0.00035	0.200	0.00175	0.00465	0.00639
2	C2-C3	Y	C3-Y2	0.00005	0.200	0.00025	0.00465	0.00489

After calculation of the total curvature values of the columns in both directions, the corresponding strain values of the reinforcing steel, cover concrete and core concrete are determined by using the detailed moment – curvature relationships given in Appendix D and compared with the strain limits of the TSDC (2007) listed in Table 6.6.

The damage regions for the columns of the non-retrofitted building are given in Table 6.9 and Table 6.10.

Table 6.9 : Damage regions for the columns of the non-retrofitted building in X direction.

Story	Column notation	Pushover direction	Hinge	Steel rebar	Unconfined concrete	Confined concrete	Damage region
				ε_s	ε_c	ε_{cc}	
Ground	C0-A2	X	C1-X0	0.0102	0.0109	0.0092	Collapsing
Ground	C0-A3	X	C1-X0	0.0102	0.0109	0.0092	Collapsing
Ground	C0-B1	X	C1-X0	0.0109	0.0118	0.0099	Collapsing
Ground	C0-B4	X	C1-X0	0.0109	0.0118	0.0099	Collapsing
Ground	C0-C1	X	C1-X0	0.0109	0.0118	0.0099	Collapsing
Ground	C0-C4	X	C1-X0	0.0109	0.0118	0.0099	Collapsing
Ground	C0-D2	X	C1-X0	0.0109	0.0118	0.0099	Collapsing
Ground	C0-D3	X	C1-X0	0.0109	0.0118	0.0099	Collapsing
Ground	C0-A1	X	C2-X0	0.0139	0.0087	0.0074	Collapsing
Ground	C0-A4	X	C2-X0	0.0139	0.0087	0.0074	Collapsing
Ground	C0-D1	X	C2-X0	0.0151	0.0094	0.0080	Collapsing
Ground	C0-D4	X	C2-X0	0.0151	0.0094	0.0080	Collapsing
Ground	C0-B2	X	C3-X0	0.0129	0.0113	0.0098	Collapsing
Ground	C0-B3	X	C3-X0	0.0129	0.0113	0.0098	Collapsing
Ground	C0-C2	X	C3-X0	0.0129	0.0113	0.0098	Collapsing
Ground	C0-C3	X	C3-X0	0.0129	0.0113	0.0098	Collapsing
1	C1-A2	X	C1-X1	0.0020	0.0013	0.0011	MN
1	C1-A3	X	C1-X1	0.0011	0.0010	0.0008	MN
1	C1-B1	X	C1-X1	0.0008	0.0008	0.0007	MN
1	C1-B4	X	C1-X1	0.0017	0.0012	0.0010	MN
1	C1-C1	X	C1-X1	0.0008	0.0008	0.0007	MN
1	C1-C4	X	C1-X1	0.0017	0.0012	0.0010	MN
1	C1-D2	X	C1-X1	0.0026	0.0016	0.0012	MN
1	C1-D3	X	C1-X1	0.0020	0.0013	0.0011	MN
1	C1-A1	X	C2-X1	0.0008	0.0007	0.0007	MN
1	C1-A4	X	C2-X1	0.0008	0.0007	0.0007	MN
1	C1-D1	X	C2-X1	0.0008	0.0007	0.0007	MN
1	C1-D4	X	C2-X1	0.0014	0.0009	0.0009	MN
1	C1-B2	X	C3-X1	0.0026	0.0015	0.0012	MN
1	C1-B3	X	C3-X1	0.0011	0.0009	0.0008	MN
1	C1-C2	X	C3-X1	0.0026	0.0015	0.0012	MN
1	C1-C3	X	C3-X1	0.0017	0.0011	0.0010	MN
2	C2-A2	X	C1-X2	0.0011	0.0006	0.0000	MN
2	C2-A3	X	C1-X2	0.0009	0.0005	0.0000	MN
2	C2-B1	X	C1-X2	0.0009	0.0005	0.0000	MN
2	C2-B4	X	C1-X2	0.0011	0.0006	0.0000	MN
2	C2-C1	X	C1-X2	0.0009	0.0005	0.0000	MN
2	C2-C4	X	C1-X2	0.0011	0.0006	0.0000	MN
2	C2-D2	X	C1-X2	0.0019	0.0008	0.0000	MN
2	C2-D3	X	C1-X2	0.0011	0.0006	0.0000	MN
2	C2-A1	X	C2-X2	0.0009	0.0004	0.0004	MN
2	C2-A4	X	C2-X2	0.0009	0.0004	0.0004	MN
2	C2-D1	X	C2-X2	0.0009	0.0004	0.0004	MN
2	C2-D4	X	C2-X2	0.0009	0.0004	0.0004	MN
2	C2-B2	X	C3-X2	0.0014	0.0006	0.0005	MN
2	C2-B3	X	C3-X2	0.0011	0.0006	0.0004	MN
2	C2-C2	X	C3-X2	0.0016	0.0007	0.0005	MN
2	C2-C3	X	C3-X2	0.0011	0.0006	0.0004	MN

Table 6.10 : Damage regions for the columns of the non-retrofitted building in Y direction.

Story	Column notation	Pushover direction	Hinge	Steel rebar ε_s	Unconfined concrete ε_c	Confined concrete ε_{cc}	Damage region
Ground	C0-A2	Y	C1-Y0	0.0105	0.0102	0.0090	Collapsing
Ground	C0-A3	Y	C1-Y0	0.0105	0.0102	0.0090	Collapsing
Ground	C0-B1	Y	C1-Y0	0.0112	0.0111	0.0098	Collapsing
Ground	C0-B4	Y	C1-Y0	0.0092	0.0086	0.0075	Collapsing
Ground	C0-C1	Y	C1-Y0	0.0112	0.0111	0.0098	Collapsing
Ground	C0-C4	Y	C1-Y0	0.0092	0.0086	0.0075	Collapsing
Ground	C0-D2	Y	C1-Y0	0.0105	0.0102	0.0090	Collapsing
Ground	C0-D3	Y	C1-Y0	0.0098	0.0094	0.0083	Collapsing
Ground	C0-A1	Y	C2-Y0	0.0125	0.0086	0.0069	Collapsing
Ground	C0-A4	Y	C2-Y0	0.0102	0.0070	0.0056	Collapsing
Ground	C0-D1	Y	C2-Y0	0.0125	0.0086	0.0069	Collapsing
Ground	C0-D4	Y	C2-Y0	0.0102	0.0070	0.0056	Collapsing
Ground	C0-B2	Y	C3-Y0	0.0119	0.0104	0.0090	Collapsing
Ground	C0-B3	Y	C3-Y0	0.0109	0.0094	0.0081	Collapsing
Ground	C0-C2	Y	C3-Y0	0.0119	0.0104	0.0090	Collapsing
Ground	C0-C3	Y	C3-Y0	0.0109	0.0094	0.0081	Collapsing
1	C1-A2	Y	C1-Y1	0.0006	0.0007	0.0006	MN
1	C1-A3	Y	C1-Y1	0.0006	0.0007	0.0006	MN
1	C1-B1	Y	C1-Y1	0.0017	0.0012	0.0010	MN
1	C1-B4	Y	C1-Y1	0.0006	0.0007	0.0006	MN
1	C1-C1	Y	C1-Y1	0.0023	0.0015	0.0012	MN
1	C1-C4	Y	C1-Y1	0.0006	0.0007	0.0006	MN
1	C1-D2	Y	C1-Y1	0.0006	0.0007	0.0006	MN
1	C1-D3	Y	C1-Y1	0.0006	0.0007	0.0006	MN
1	C1-A1	Y	C2-Y1	0.0026	0.0014	0.0010	MN
1	C1-A4	Y	C2-Y1	0.0009	0.0007	0.0006	MN
1	C1-D1	Y	C2-Y1	0.0011	0.0009	0.0007	MN
1	C1-D4	Y	C2-Y1	0.0009	0.0007	0.0006	MN
1	C1-B2	Y	C3-Y1	0.0024	0.0009	0.0007	MN
1	C1-B3	Y	C3-Y1	0.0016	0.0007	0.0005	MN
1	C1-C2	Y	C3-Y1	0.0024	0.0009	0.0007	MN
1	C1-C3	Y	C3-Y1	0.0022	0.0008	0.0006	MN
2	C2-A2	Y	C1-Y2	0.0006	0.0004	0.0003	MN
2	C2-A3	Y	C1-Y2	0.0006	0.0004	0.0003	MN
2	C2-B1	Y	C1-Y2	0.0009	0.0005	0.0004	MN
2	C2-B4	Y	C1-Y2	0.0006	0.0004	0.0003	MN
2	C2-C1	Y	C1-Y2	0.0011	0.0006	0.0004	MN
2	C2-C4	Y	C1-Y2	0.0006	0.0004	0.0003	MN
2	C2-D2	Y	C1-Y2	0.0006	0.0004	0.0003	MN
2	C2-D3	Y	C1-Y2	0.0006	0.0004	0.0003	MN
2	C2-A1	Y	C2-Y2	0.0014	0.0006	0.0005	MN
2	C2-A4	Y	C2-Y2	0.0009	0.0004	0.0003	MN
2	C2-D1	Y	C2-Y2	0.0009	0.0004	0.0003	MN
2	C2-D4	Y	C2-Y2	0.0009	0.0004	0.0003	MN
2	C2-B2	Y	C3-Y2	0.0011	0.0006	0.0004	MN
2	C2-B3	Y	C3-Y2	0.0011	0.0006	0.0004	MN
2	C2-C2	Y	C3-Y2	0.0014	0.0006	0.0005	MN
2	C2-C3	Y	C3-Y2	0.0011	0.0006	0.0004	MN

As it is clearly seen from the strain values for the columns given in Table 6.9 and Table 6.10, all the columns at the ground floor collapse in both X and Y direction. Under these circumstances, this building is assumed to be in collapsing condition according to TSDC (2007) and endangers the human life safety.

6.4 Non-Linear Analysis of the Retrofitted Building

As expected, the hypothetical building performs poorly during the pushover analysis and the building collapses in the ground floor. In order to overcome this vital collapsing problem and enhance the seismic behaviour of the building the proposed retrofitting method is utilized and the behavior of the retrofitted building studied through pushover analysis.

6.4.1 Retrofitting of the columns

The hypothetical building is selected to represent the existing building stock of many developing countries, with low quality materials, poor seismic design and poor construction practice. Due to low material quality and relatively old age of the structure, it is also assumed that there should be already carbonation induced corrosion damages, which is generally seen as cracks and delaminated poor concrete cover around the corroded reinforcing bars. Under these circumstances, corrosion repairs prior to the retrofitting with FRPs are inevitable as explained in previous chapters. Therefore, the proposed method in this study will be followed including the corrosion repairs by using structural repair mortars.

Retrofitting procedure starts with the corrosion repairs, which is replacing the entire poor concrete cover with the structural repair mortar within the original dimensions of the column. This corrosion repairs is applied to all columns in the entire building regardless the level of need for capacity increase. Afterwards, the columns at the ground floor selected to be retrofitted by longitudinal GFRP bars to ensure a significant enhancement in the flexural capacity. GFRP bars are selected due to their good performance observed in the experimental part of this study. Besides, GFRP bars are the most cost effective option in pultruded FRP reinforcement. In addition to the longitudinal GFRP reinforcement, the columns at the ground floor are assumed to be confined with two layers of CFRP, which was already used in the experimental phase to ensure the sufficient shear strength and enhanced ductility for better seismic performance.

The columns in the first floor are also assumed to be retrofitted with the same approach followed for the ground floor but this time GFRP bars, which are smaller in diameter

are selected as longitudinal reinforcement. The increase in the total flexural capacity of the columns at each story is aimed to be proportional with the applied earthquake loads. Due to this fact, the capacity increase in the first and second floor columns were limited by avoiding GFRP bars for retrofitting the columns with dimensions 300x400 and 400x300. CFRP sheets are utilized as additional reinforcement for confinement for these columns instead of GFRP longitudinal reinforcement. The retrofitting details for the columns are shown in Figure 6.20, Figure 6.21 and Figure 6.22.

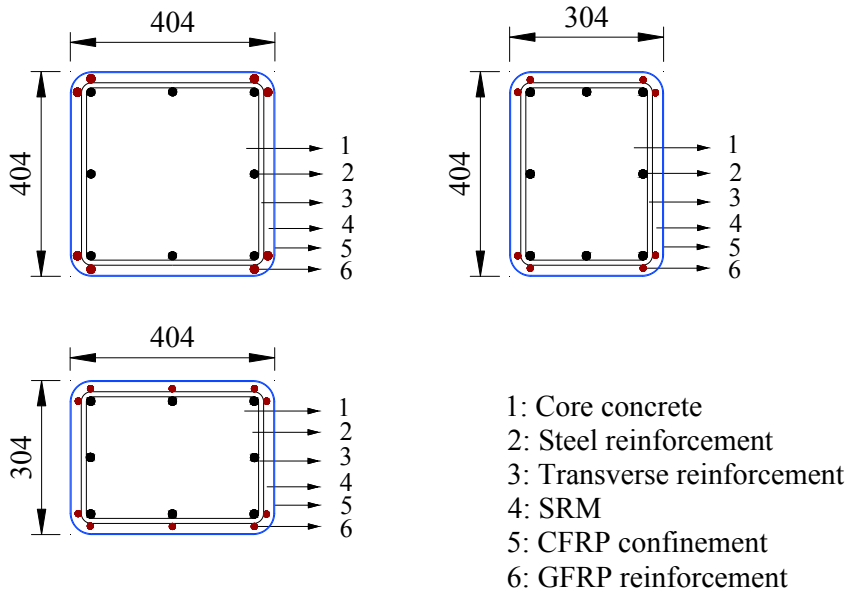

Figure 6.20 : Retrofitting details for the columns at ground floor.

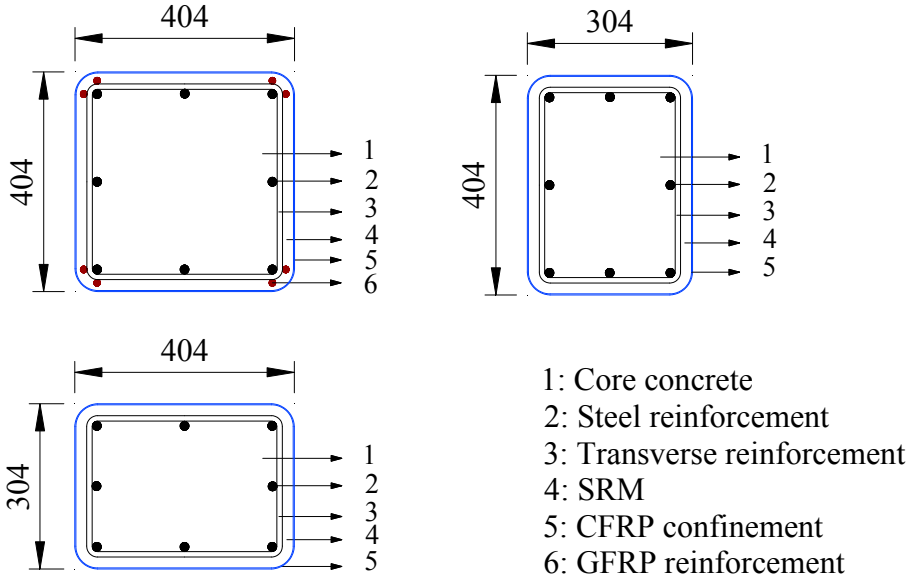

Figure 6.21 : Retrofitting details for the columns at first floor.

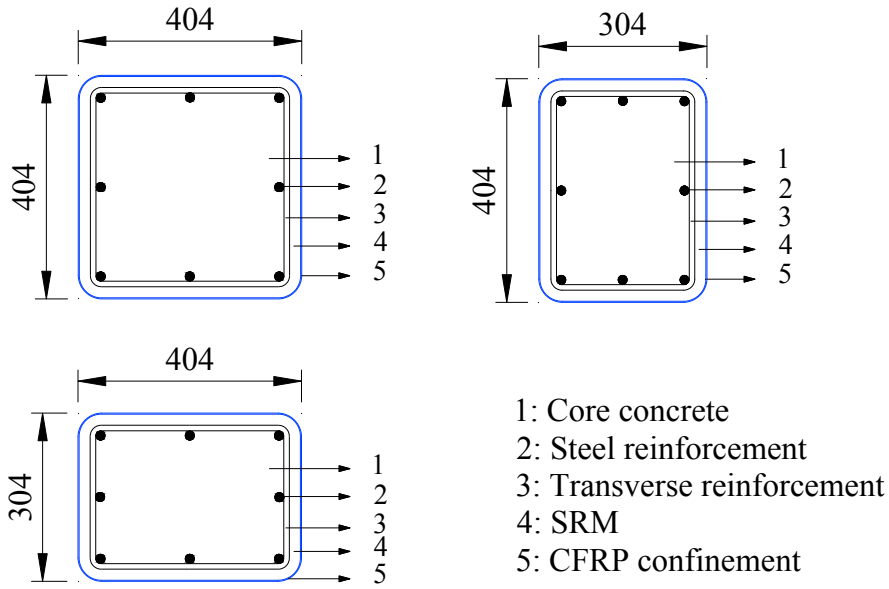

Figure 6.22 : Retrofitting details for the columns at second floor.

Reinforcement details of the retrofitted columns are given in the Table 6.11.

Table 6.11 : Retrofitting details of the columns.

Column Dimension	Story	Confinement	Number of CFRP layers	Longitudinal FRP reinforcement	Diameter of FRP reinforcement	Quantity of FRP reinforcement
300x400	Ground	CFRP	2	GFRP bars	16mm	8
400x300	Ground	CFRP	2	GFRP bars	12mm	10
400x400	Ground	CFRP	2	GFRP bars	12mm	8
300x400	1	CFRP	2	-	-	-
400x300	1	CFRP	2	-	-	-
400x400	1	CFRP	2	GFRP bars	12mm	8
300x400	2	CFRP	2	-	-	-
400x300	2	CFRP	2	-	-	-
400x400	2	CFRP	2	-	-	-

6.4.2 Moment-curvature and moment-rotation relationships

The moment – curvature relationships and local deformation characteristics are determined through moment-curvature relationships obtained by following the same fiber analysis approach with the non-retrofitted columns. In the moment-curvature analysis, longitudinal steel rebars are assumed to behave in an elasto-plastic manner with strain hardening. Longitudinal FRP reinforcement are taken into account as linear elastic material in tension and their possible contribution in compression is neglected. Buckling and debonding of FRP reinforcement during cyclic loading is intended to be prevented by structural repair mortar and CFRP confinement. The environmental reduction factor, C_E, is taken as 0.75 as recommended by ACI 440-2R-08 (2008) for

GFRP reinforcement. Strength reduction factor ϕ, stated by ACI 318M-14 (2014) is considered as 0.90 and eventually an additional strength reduction factor is considered as 0.60 in the light of the findings in the experimental part of this study. The design rupture strain of AFRP reinforcement (ε_{fu}) is calculated as shown in equation 6.14, where ε_{fu}^* is the manufacturer declared ultimate strain for GFRP bar.

$$\varepsilon_{fu} = 0.60\ C_E\ \phi\ \varepsilon_{fu}^* \tag{6.14}$$

The model proposed by TSDC (2007), which is used to obtain the stress-strain relationship of CFRP confined concrete and structural repair mortar is shown in equation (6.15), equation (6.16), equation (6.17) and equation (6.18).

$$f_{cc} = f_{cm}\left(1 + 2.4\left(\frac{f_l}{f_{cm}}\right)\right) \geq 1.2 f_{cm} \tag{6.15}$$

$$f_l = \frac{1}{2}\kappa_a\ \rho_f\ \varepsilon_f\ E_f \tag{6.16}$$

$$\kappa_a = \begin{bmatrix} 1 & Circular\ cross-section \\ \left(\frac{b}{h}\right) & Elliptical\ cross-section \\ 1 - \frac{(b-2r_c)^2 + (h-2r_c)^2}{3bh} & Rectangular\ cross-section \end{bmatrix} \tag{6.17}$$

$$\varepsilon_{cc} = 0.002\ (1 + 15(f_l/f_{cm})^{0.75}) \tag{6.18}$$

It should be noted that the contribution of stirrups to the confinement of the core concrete is not considered. The reason is poor detailing of the transverse reinforcement, which does not conform the seismic design requirements of TSDC (2007). Material properties of the retrofitted sections are given in the Table 6.12.

Table 6.12 : Material properties of the retrofitted columns.

Cross Section	Concrete		SRM		GFRP
	Ultimate strain (ε_{cc})	Ultimate stress (f_{cc})	Ultimate strain (ε_{cc})	Ultimate stress (f_{cc})	Ultimate strain (ε_{fu})
300x400	0.0128	19.33 MPa	0.0070	40.39 MPa	0.011
400x300	0.0128	19.33 MPa	0.0070	40.39 MPa	0.011
400x400	0.0115	18.25 MPa	0.0065	39.31 MPa	0.011

Neither geometry, nor the dead loads are not changed during the application of the proposed retrofitting technique, the results (axial loads of the columns) of the previous analyses done for non-retrofitted building are used as relevant input for determining moment-rotation relationships.

The moment-curvature relationships of the columns are obtained through the same fiber-analysis approach by using the XTRACT computer programme. The cross-sections of the columns consist of steel reinforcement, cover concrete, confined concrete, GFRP and CFRP reinforcement. Material models for confined concrete and confined SRM and steel reinforcement are determined considering TSDC (2007). Stress – strain relationships for concrete and SRM are give in Figure 6.23.

Moment – curvature relationships of the columns at all floors are given in Appendix D.

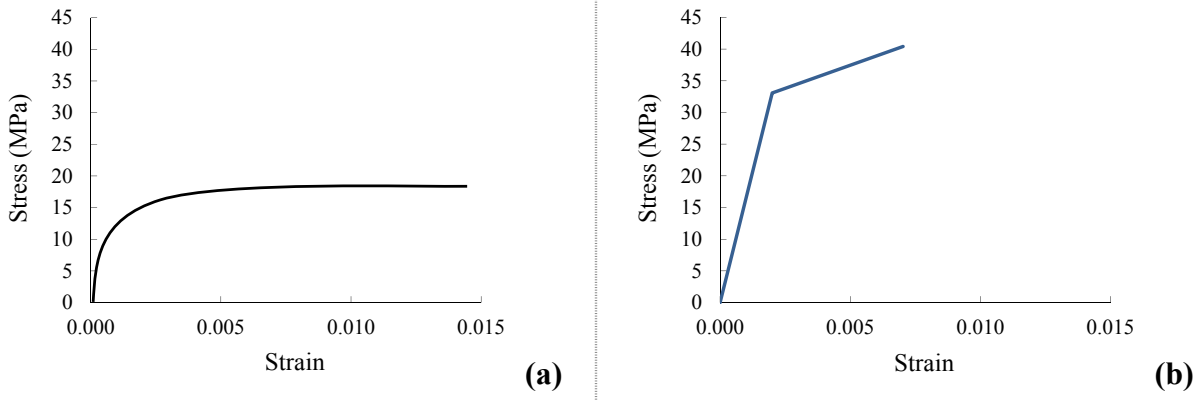

Figure 6.23 : Stress – strain relationship: (a)Concrete. (b)SRM.

Calculated and idealized moment – rotation relationships of the retrofitted columns in dimensions 300x400 are given in Figure 6.24, Figure 6.25 and Figure 6.26.

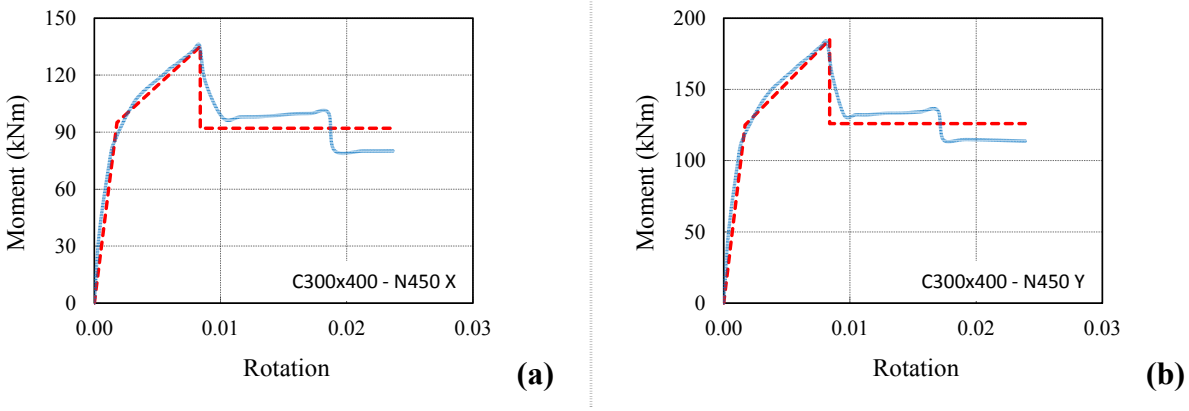

Figure 6.24 : Moment – rotation relationships of the column 300x400 at ground floor: (a)In X axis. (b)In Y axis.

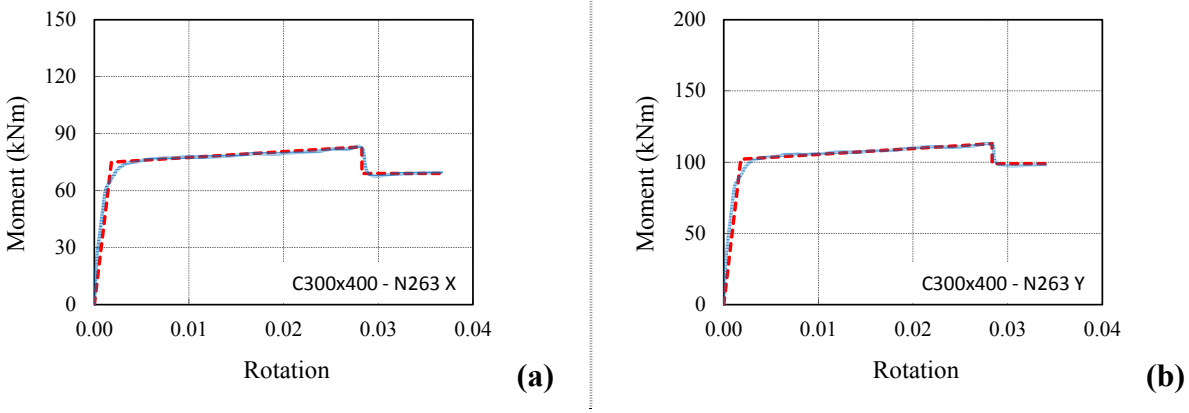

Figure 6.25 : Moment – rotation relationships of the column 300x400 at first floor: (a)In X axis. (b)In Y axis.

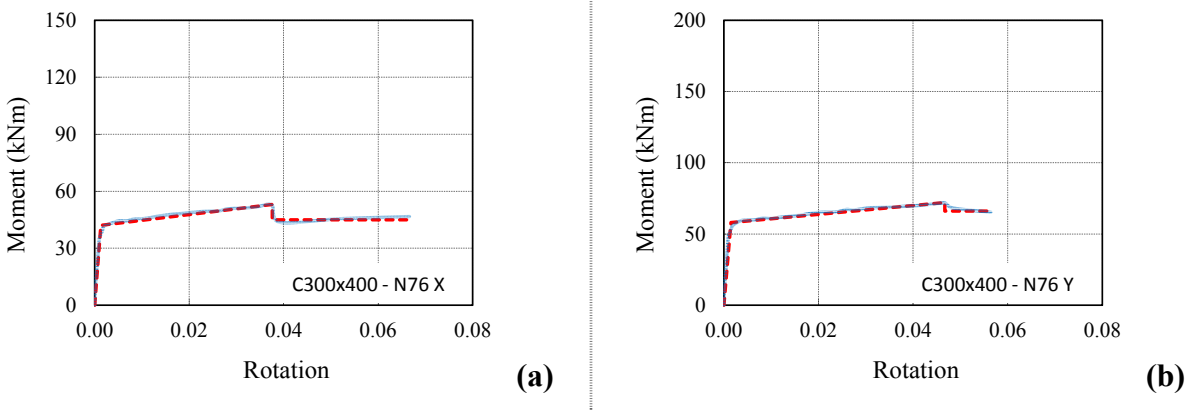

Figure 6.26 : Moment – rotation relationships of the column 300x400 at second floor: (a)In X axis. (b)In Y axis.

Calculated and idealized moment – rotation relationships of the retrofitted columns in dimensions 400x300 are given in Figure 6.27, Figure 6.28 and Figure 6.29.

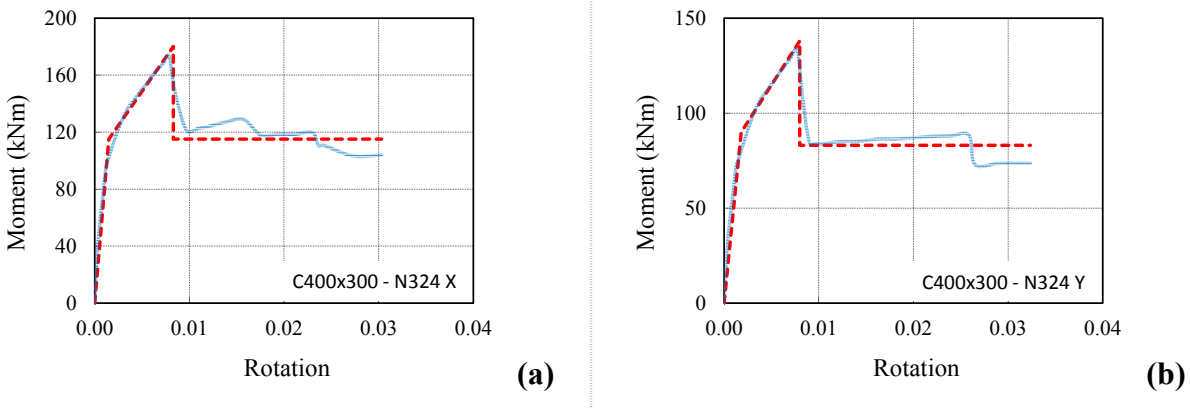

Figure 6.27 : Moment – rotation relationships of the column 400x300 at ground floor: (a)In X axis. (b)In Y axis.

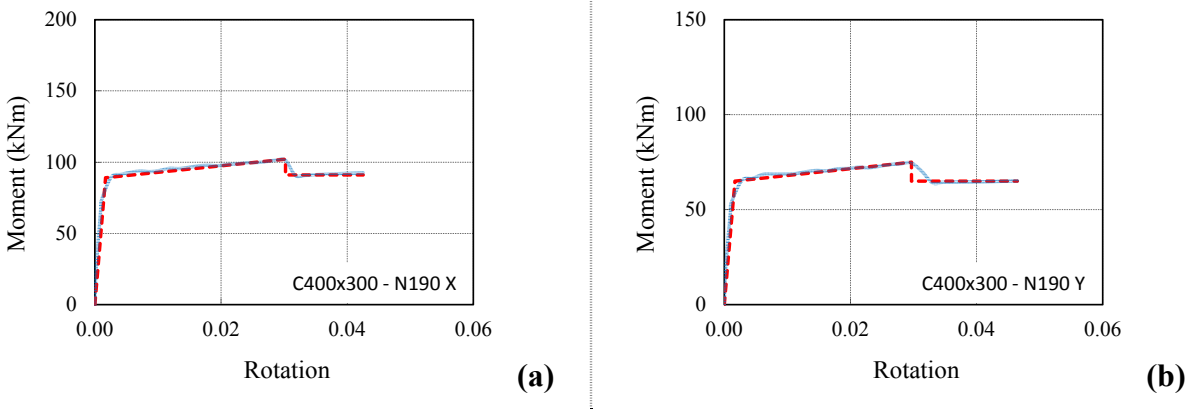

Figure 6.28 : Moment – rotation relationships of the column 400x300 at first floor: (a)In X axis. (b)In Y axis.

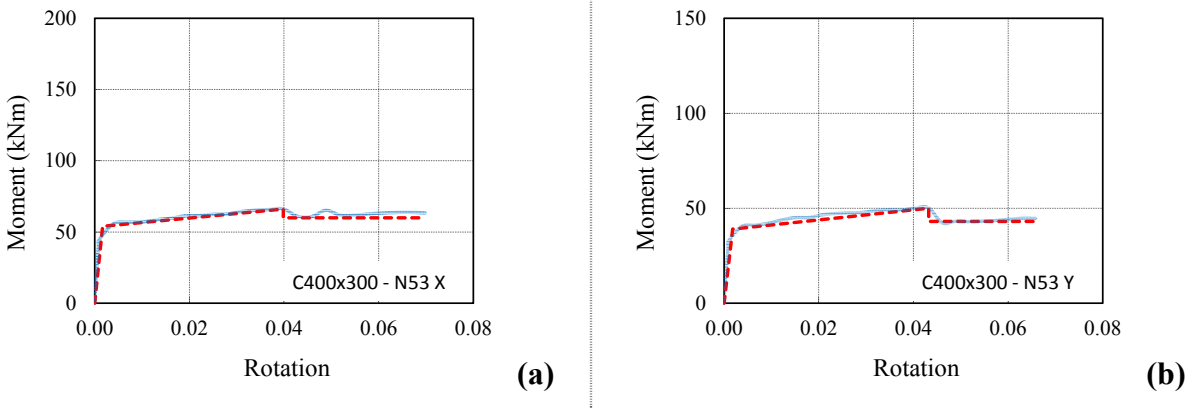

Figure 6.29 : Moment – rotation relationships of the column 400x300 at second floor: (a)In X axis. (b)In Y axis.

Calculated and idealized moment – rotation relationships of the retrofitted columns in dimensions 400x400 are given in Figure 6.30, Figure 6.31 and Figure 6.32. Since these

columns are fully symmetrical moment – rotation relationships are identical in each axis.

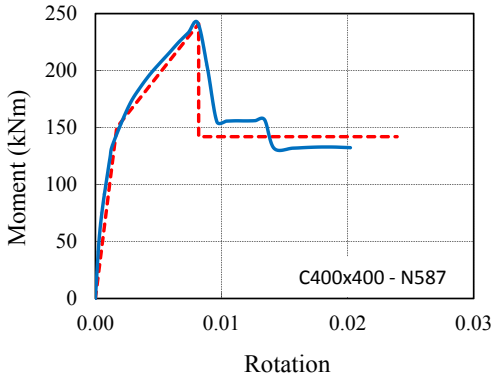

Figure 6.30 : Moment – rotation relationships of the column 400x400 at ground floor.

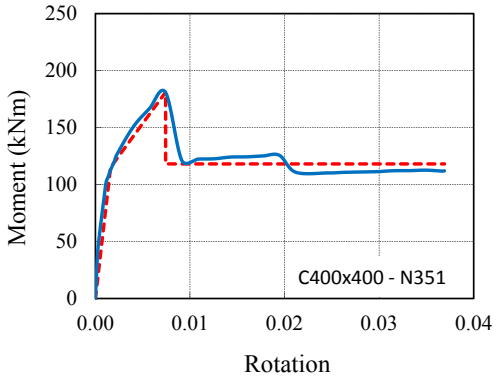

Figure 6.31 : Moment – rotation relationships of the column 400x300 at first floor.

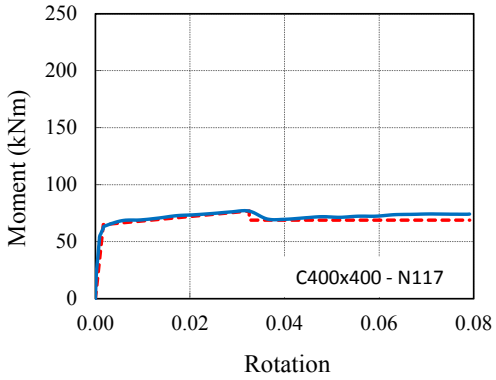

Figure 6.32 : Moment–rotation relationships of the column 400x300 at second floor.

6.4.3 Pushover analysis of the retrofitted building

Pushover analyses is carried out based on the modal analysis results of the non-retrofitted building, due to the negligible difference with the results of the analysed retrofitted building. Beams are assumed to behave elastically throughout the loading.

Strain limits for FRP confined elements given by TSDC (2007) differ from the values stated for the non-retrofitted elements. The ultimate strain value calculated in the Equation 6.18 is assummed the strain limit for collapsing region (GC), 75 % of this value is stated as the limit for significant damage (GV) and 0.004 is assumed as the strain limit for minimum damage region (MN) for the outmost fiber of the cross section of the element. Strain limits for the longitudinal steel reinforcement remains as it stated for non-confined sections. Strain limits for the CFRP confined sections are given in the Table 6.13.

Table 6.13 : Strain limits for each performance level defined by TSDC (2007).

Damage Limits	Upper limit for reinforcement strain (ε_s)	Upper limit for concrete strain for 400x400 sections (ε_{cc})	Upper limit for concrete strain for 300x400 and 400x300 sections (ε_{cc})
MN	0.010	0.004	0.004
GV	0.040	0.0087	0.0096
GC	0.060	0.0115	0.0128

Modal capacity diagrams and elastic demand spectrums for the building are obtained for 5 % damping ratio for both X and Y directions as shown in Figure 6.33 and Figure 6.34 respectively.

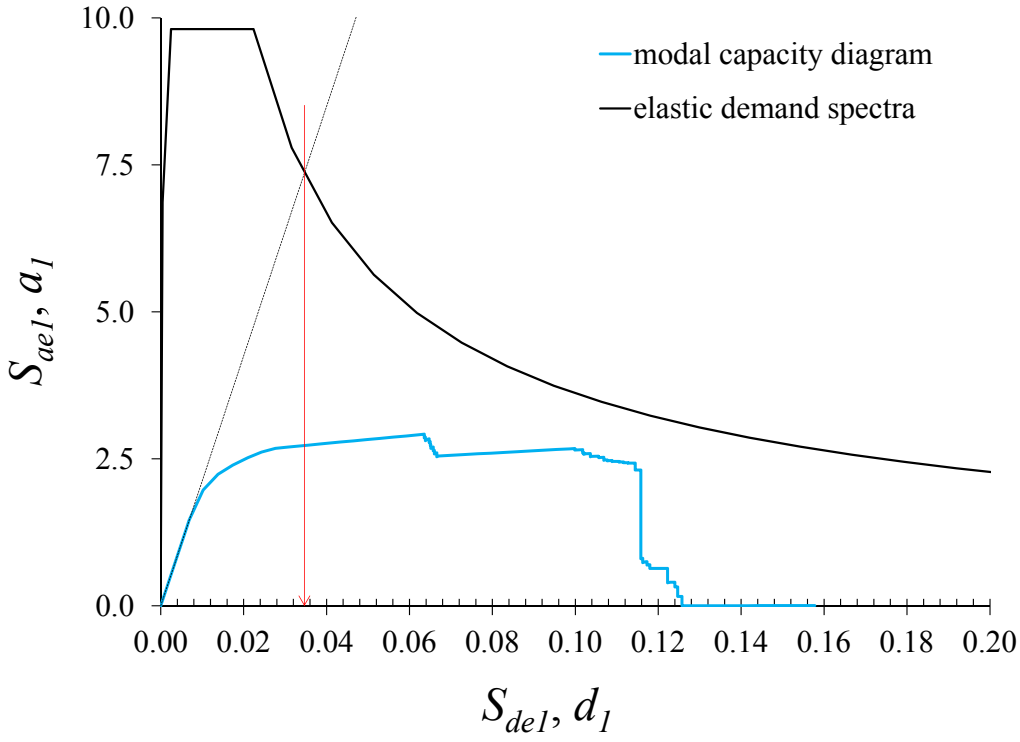

Figure 6.33 : Modal capacity diagram and elastic demand spectrum in X direction.

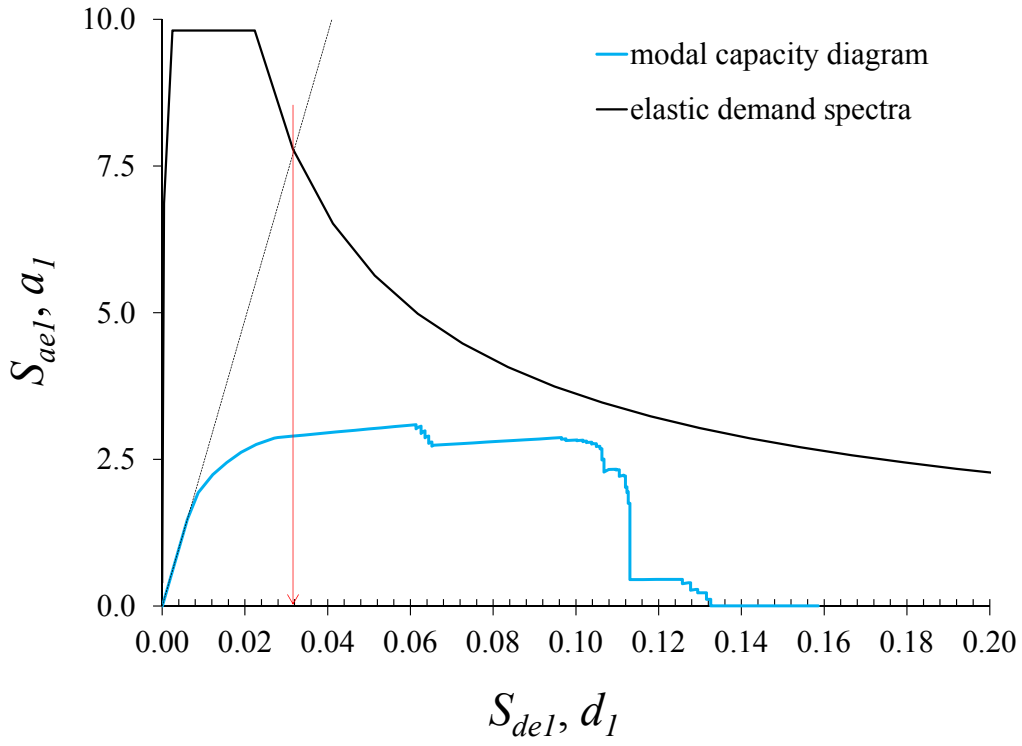

Figure 6.34 : Modal capacity diagram and elastic demand spectrum in X direction.

The base shear capacity curves of both non-retrofitted and retrofitted building are shown in shown in Figure 6.35.

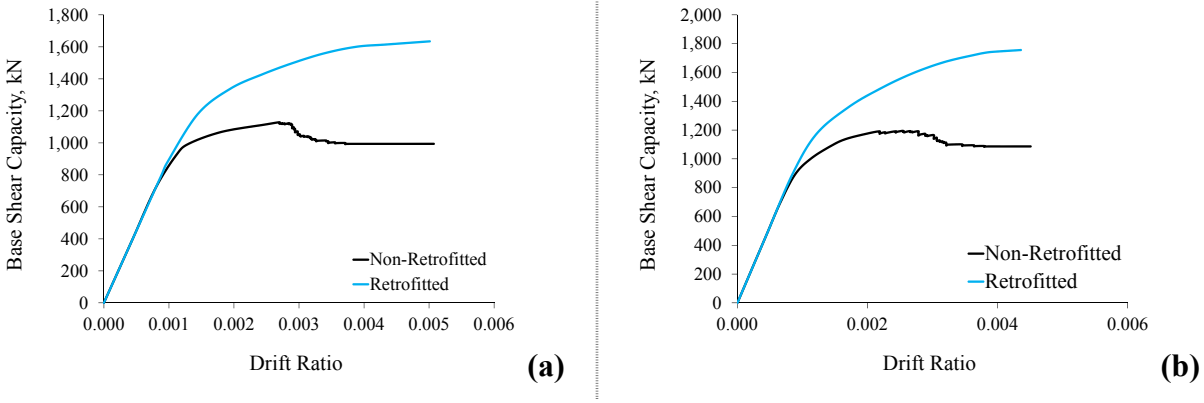

Figure 6.35 : Capacity curves of the building before and after retrofitting: (a)In X axis. (b)In Y axis.

As it is clearly seen on the capacity curves, retrofitting increases the base shear capacity of the building significantly.

Total curvature demands of the retrofitted columns are calculated by summing elastic and plastic curvature, which are found in the pushover analysis by SAP 2000 and cross

section analysis by XTRACT computer programs. The total curvature demands of the columns are given for X and Y directions in the Table 6.14 and Table 6.15 respectively.

Table 6.14 : Total curvature demands of the columns of the retrofitted building in X direction.

Story	Column notation	Pushover direction	Hinge	Plastic Rotation θ_p	Plastic Hinge length L_p (m)	Plastic Curvature χ_p (1/m)	Elastic Curvature χ_y (1/m)	Total Curvature χ_T (1/m)
Ground	C0-A2	X	C1-X0	0.00256	0.150	0.01707	0.00923	0.02631
Ground	C0-A3	X	C1-X0	0.00240	0.150	0.01603	0.00923	0.02526
Ground	C0-B1	X	C1-X0	0.00252	0.150	0.01678	0.00923	0.02601
Ground	C0-B4	X	C1-X0	0.00284	0.150	0.01890	0.00923	0.02813
Ground	C0-C1	X	C1-X0	0.00282	0.150	0.01878	0.00923	0.02801
Ground	C0-C4	X	C1-X0	0.00308	0.150	0.02053	0.00923	0.02976
Ground	C0-D2	X	C1-X0	0.00374	0.150	0.02492	0.00923	0.03415
Ground	C0-D3	X	C1-X0	0.00358	0.150	0.02389	0.00923	0.03312
Ground	C0-A1	X	C2-X0	0.00252	0.200	0.01262	0.00606	0.01868
Ground	C0-A4	X	C2-X0	0.00281	0.200	0.01403	0.00606	0.02009
Ground	C0-D1	X	C2-X0	0.00368	0.200	0.01841	0.00606	0.02446
Ground	C0-D4	X	C2-X0	0.00394	0.200	0.01968	0.00606	0.02573
Ground	C0-B2	X	C3-X0	0.00341	0.200	0.01704	0.00653	0.02356
Ground	C0-B3	X	C3-X0	0.00325	0.200	0.01624	0.00653	0.02277
Ground	C0-C2	X	C3-X0	0.00367	0.200	0.01835	0.00653	0.02487
Ground	C0-C3	X	C3-X0	0.00356	0.200	0.01778	0.00653	0.02430
1	C1-A2	X	C1-X1	0.00335	0.150	0.02235	0.00792	0.03027
1	C1-A3	X	C1-X1	0.00235	0.150	0.01567	0.00792	0.02359
1	C1-B1	X	C1-X1	0.00048	0.150	0.00319	0.00792	0.01111
1	C1-B4	X	C1-X1	0.00265	0.150	0.01769	0.00792	0.02561
1	C1-C1	X	C1-X1	0.00087	0.150	0.00579	0.00792	0.01371
1	C1-C4	X	C1-X1	0.00283	0.150	0.01885	0.00792	0.02677
1	C1-D2	X	C1-X1	0.00452	0.150	0.03015	0.00792	0.03807
1	C1-D3	X	C1-X1	0.00357	0.150	0.02379	0.00792	0.03171
1	C1-A1	X	C2-X1	0.00000	0.200	0.00000	0.00532	0.00532
1	C1-A4	X	C2-X1	0.00178	0.200	0.00889	0.00532	0.01421
1	C1-D1	X	C2-X1	0.00081	0.200	0.00405	0.00532	0.00937
1	C1-D4	X	C2-X1	0.00272	0.200	0.01362	0.00532	0.01894
1	C1-B2	X	C3-X1	0.00324	0.200	0.01621	0.00558	0.02179
1	C1-B3	X	C3-X1	0.00226	0.200	0.01130	0.00558	0.01688
1	C1-C2	X	C3-X1	0.00340	0.200	0.01699	0.00558	0.02257
1	C1-C3	X	C3-X1	0.00263	0.200	0.01317	0.00558	0.01875
2	C2-A2	X	C1-X2	0.00590	0.150	0.03931	0.00643	0.04575
2	C2-A3	X	C1-X2	0.00486	0.150	0.03241	0.00643	0.03885
2	C2-B1	X	C1-X2	0.00331	0.150	0.02207	0.00643	0.02851
2	C2-B4	X	C1-X2	0.00555	0.150	0.03701	0.00643	0.04345
2	C2-C1	X	C1-X2	0.00361	0.150	0.02403	0.00643	0.03047
2	C2-C4	X	C1-X2	0.00565	0.150	0.03764	0.00643	0.04407
2	C2-D2	X	C1-X2	0.00655	0.150	0.04367	0.00643	0.05010
2	C2-D3	X	C1-X2	0.00562	0.150	0.03745	0.00643	0.04389
2	C2-A1	X	C2-X2	0.00267	0.200	0.01334	0.00447	0.01781
2	C2-A4	X	C2-X2	0.00492	0.200	0.02458	0.00447	0.02905
2	C2-D1	X	C2-X2	0.00344	0.200	0.01721	0.00447	0.02168
2	C2-D4	X	C2-X2	0.00549	0.200	0.02746	0.00447	0.03193
2	C2-B2	X	C3-X2	0.00592	0.200	0.02959	0.00453	0.03412
2	C2-B3	X	C3-X2	0.00481	0.200	0.02405	0.00453	0.02858
2	C2-C2	X	C3-X2	0.00599	0.200	0.02997	0.00453	0.03450
2	C2-C3	X	C3-X2	0.00508	0.200	0.02540	0.00453	0.02993

Table 6.15 : Total curvature demands of the columns of theretrofitted building in Y direction.

Story	Column notation	Pushover direction	Hinge	Plastic Rotation θ_p	Plastic Hinge length L_p (m)	Plastic Curvature χ_p (1/m)	Elastic Curvature χ_y (1/m)	Total Curvature χ_T (1/m)
Ground	C0-A2	Y	C1-Y0	0.00347	0.200	0.01736	0.00666	0.02401
Ground	C0-A3	Y	C1-Y0	0.00258	0.200	0.01288	0.00666	0.01954
Ground	C0-B1	Y	C1-Y0	0.00486	0.200	0.02429	0.00666	0.03094
Ground	C0-B4	Y	C1-Y0	0.00147	0.200	0.00733	0.00666	0.01399
Ground	C0-C1	Y	C1-Y0	0.00492	0.200	0.02460	0.00666	0.03126
Ground	C0-C4	Y	C1-Y0	0.00153	0.200	0.00764	0.00666	0.01429
Ground	C0-D2	Y	C1-Y0	0.00333	0.200	0.01665	0.00666	0.02331
Ground	C0-D3	Y	C1-Y0	0.00244	0.200	0.01219	0.00666	0.01884
Ground	C0-A1	Y	C2-Y0	0.00430	0.150	0.02865	0.00853	0.03719
Ground	C0-A4	Y	C2-Y0	0.00108	0.150	0.00719	0.00853	0.01572
Ground	C0-D1	Y	C2-Y0	0.00413	0.150	0.02756	0.00853	0.03609
Ground	C0-D4	Y	C2-Y0	0.00087	0.150	0.00577	0.00853	0.01431
Ground	C0-B2	Y	C3-Y0	0.00365	0.200	0.01826	0.00653	0.02478
Ground	C0-B3	Y	C3-Y0	0.00279	0.200	0.01395	0.00653	0.02047
Ground	C0-C2	Y	C3-Y0	0.00372	0.200	0.01862	0.00653	0.02514
Ground	C0-C3	Y	C3-Y0	0.00284	0.200	0.01421	0.00653	0.02074
1	C1-A2	Y	C1-Y1	0.00230	0.200	0.01151	0.00563	0.01714
1	C1-A3	Y	C1-Y1	0.00131	0.200	0.00655	0.00563	0.01218
1	C1-B1	Y	C1-Y1	0.00479	0.200	0.02393	0.00563	0.02956
1	C1-B4	Y	C1-Y1	0.00081	0.200	0.00404	0.00563	0.00966
1	C1-C1	Y	C1-Y1	0.00534	0.200	0.02671	0.00563	0.03234
1	C1-C4	Y	C1-Y1	0.00131	0.200	0.00654	0.00563	0.01217
1	C1-D2	Y	C1-Y1	0.00128	0.200	0.00641	0.00563	0.01203
1	C1-D3	Y	C1-Y1	0.00029	0.200	0.00143	0.00563	0.00705
1	C1-A1	Y	C2-Y1	0.00434	0.150	0.02893	0.00748	0.03641
1	C1-A4	Y	C2-Y1	0.00052	0.150	0.00344	0.00748	0.01092
1	C1-D1	Y	C2-Y1	0.00322	0.150	0.02143	0.00748	0.02891
1	C1-D4	Y	C2-Y1	0.00000	0.150	0.00000	0.00748	0.00748
1	C1-B2	Y	C3-Y1	0.00311	0.200	0.01554	0.00558	0.02112
1	C1-B3	Y	C3-Y1	0.00216	0.200	0.01080	0.00558	0.01638
1	C1-C2	Y	C3-Y1	0.00358	0.200	0.01792	0.00558	0.02350
1	C1-C3	Y	C3-Y1	0.00264	0.200	0.01318	0.00558	0.01876
2	C2-A2	Y	C1-Y2	0.00342	0.200	0.01710	0.00460	0.02170
2	C2-A3	Y	C1-Y2	0.00280	0.200	0.01398	0.00460	0.01857
2	C2-B1	Y	C1-Y2	0.00472	0.200	0.02362	0.00460	0.02821
2	C2-B4	Y	C1-Y2	0.00228	0.200	0.01140	0.00460	0.01599
2	C2-C1	Y	C1-Y2	0.00526	0.200	0.02631	0.00460	0.03091
2	C2-C4	Y	C1-Y2	0.00278	0.200	0.01389	0.00460	0.01849
2	C2-D2	Y	C1-Y2	0.00231	0.200	0.01157	0.00460	0.01616
2	C2-D3	Y	C1-Y2	0.00169	0.200	0.00847	0.00460	0.01307
2	C2-A1	Y	C2-Y2	0.00483	0.150	0.03217	0.00626	0.03843
2	C2-A4	Y	C2-Y2	0.00240	0.150	0.01603	0.00626	0.02229
2	C2-D1	Y	C2-Y2	0.00365	0.150	0.02434	0.00626	0.03060
2	C2-D4	Y	C2-Y2	0.00137	0.150	0.00916	0.00626	0.01542
2	C2-B2	Y	C3-Y2	0.00385	0.200	0.01926	0.00453	0.02379
2	C2-B3	Y	C3-Y2	0.00323	0.200	0.01615	0.00453	0.02068
2	C2-C2	Y	C3-Y2	0.00440	0.200	0.02198	0.00453	0.02651
2	C2-C3	Y	C3-Y2	0.00377	0.200	0.01886	0.00453	0.02339

After calculation of the total curvature values of the retrofitted columns in both directions, the corresponding strain values of the reinforcing steel, cover concrete and core concrete are determined by using the detailed moment – curvature relationships are given in Appendix D and are compared with the strain limits for the FRP confined sections stated by TSDC (2007) listed in Table 6.13.

The damage regions for the columns of the retrofitted building are given in Table 6.16 and Table 6.17.

Table 6.16 : Damage regions for the columns of the retrofitted building in X direction.

Story	Column notation	Pushover direction	Hinge	Steel rebar ε_s	Cover concrete ε_c	Core concrete ε_{cc}	Damage region
Ground	C0-A2	X	C1-X0	0.004	0.0024	0.0019	MN
Ground	C0-A3	X	C1-X0	0.004	0.0024	0.0019	MN
Ground	C0-B1	X	C1-X0	0.004	0.0024	0.0019	MN
Ground	C0-B4	X	C1-X0	0.004	0.0027	0.0021	MN
Ground	C0-C1	X	C1-X0	0.004	0.0027	0.0021	MN
Ground	C0-C4	X	C1-X0	0.004	0.0027	0.0021	MN
Ground	C0-D2	X	C1-X0	0.006	0.0031	0.0024	MN
Ground	C0-D3	X	C1-X0	0.005	0.0029	0.0023	MN
Ground	C0-A1	X	C2-X0	0.004	0.0022	0.0018	MN
Ground	C0-A4	X	C2-X0	0.004	0.0022	0.0018	MN
Ground	C0-D1	X	C2-X0	0.006	0.0027	0.0022	MN
Ground	C0-D4	X	C2-X0	0.006	0.0027	0.0022	MN
Ground	C0-B2	X	C3-X0	0.005	0.0030	0.0025	MN
Ground	C0-B3	X	C3-X0	0.005	0.0030	0.0025	MN
Ground	C0-C2	X	C3-X0	0.005	0.0030	0.0025	MN
Ground	C0-C3	X	C3-X0	0.005	0.0030	0.0025	MN
1	C1-A2	X	C1-X1	0.005	0.0017	0.0012	MN
1	C1-A3	X	C1-X1	0.004	0.0015	0.0011	MN
1	C1-B1	X	C1-X1	0.002	0.0011	0.0009	MN
1	C1-B4	X	C1-X1	0.004	0.0015	0.0011	MN
1	C1-C1	X	C1-X1	0.002	0.0012	0.0009	MN
1	C1-C4	X	C1-X1	0.005	0.0017	0.0012	MN
1	C1-D2	X	C1-X1	0.007	0.0020	0.0012	MN
1	C1-D3	X	C1-X1	0.006	0.0018	0.0012	MN
1	C1-A1	X	C2-X1	0.001	0.0008	0.0007	MN
1	C1-A4	X	C2-X1	0.003	0.0013	0.0010	MN
1	C1-D1	X	C2-X1	0.001	0.0008	0.0007	MN
1	C1-D4	X	C2-X1	0.003	0.0013	0.0010	MN
1	C1-B2	X	C3-X1	0.005	0.0019	0.0015	MN
1	C1-B3	X	C3-X1	0.003	0.0014	0.0011	MN
1	C1-C2	X	C3-X1	0.005	0.0019	0.0015	MN
1	C1-C3	X	C3-X1	0.003	0.0014	0.0011	MN
2	C2-A2	X	C1-X2	0.010	0.0015	0.0001	MN
2	C2-A3	X	C1-X2	0.007	0.0014	0.0001	MN
2	C2-B1	X	C1-X2	0.005	0.0011	0.0000	MN
2	C2-B4	X	C1-X2	0.007	0.0014	0.0001	MN
2	C2-C1	X	C1-X2	0.005	0.0011	0.0000	MN
2	C2-C4	X	C1-X2	0.007	0.0014	0.0001	MN
2	C2-D2	X	C1-X2	0.010	0.0015	0.0001	MN
2	C2-D3	X	C1-X2	0.007	0.0014	0.0001	MN
2	C2-A1	X	C2-X2	0.001	0.0005	0.0004	MN
2	C2-A4	X	C2-X2	0.006	0.0011	0.0007	MN
2	C2-D1	X	C2-X2	0.006	0.0011	0.0007	MN
2	C2-D4	X	C2-X2	0.006	0.0011	0.0007	MN
2	C2-B2	X	C3-X2	0.009	0.0014	0.0007	MN
2	C2-B3	X	C3-X2	0.009	0.0014	0.0007	MN
2	C2-C2	X	C3-X2	0.009	0.0014	0.0007	MN
2	C2-C3	X	C3-X2	0.009	0.0014	0.0007	MN

Table 6.17 : Damage regions for the columns of the retrofitted building in Y direction.

Story	Column notation	Pushover direction	Hinge	Steel rebar ε_s	Unconfined concrete ε_c	Confined concrete ε_{cc}	Damage region
Ground	C0-A2	Y	C1-Y0	0.005	0.0030	0.0025	MN
Ground	C0-A3	Y	C1-Y0	0.004	0.0024	0.0021	MN
Ground	C0-B1	Y	C1-Y0	0.007	0.0037	0.0031	MN
Ground	C0-B4	Y	C1-Y0	0.003	0.0019	0.0016	MN
Ground	C0-C1	Y	C1-Y0	0.007	0.0037	0.0031	MN
Ground	C0-C4	Y	C1-Y0	0.003	0.0019	0.0016	MN
Ground	C0-D2	Y	C1-Y0	0.005	0.0030	0.0025	MN
Ground	C0-D3	Y	C1-Y0	0.004	0.0024	0.0021	MN
Ground	C0-A1	Y	C2-Y0	0.006	0.0028	0.0021	MN
Ground	C0-A4	Y	C2-Y0	0.002	0.0015	0.0012	MN
Ground	C0-D1	Y	C2-Y0	0.006	0.0028	0.0021	MN
Ground	C0-D4	Y	C2-Y0	0.002	0.0014	0.0011	MN
Ground	C0-B2	Y	C3-Y0	0.005	0.0030	0.0025	MN
Ground	C0-B3	Y	C3-Y0	0.004	0.0025	0.0021	MN
Ground	C0-C2	Y	C3-Y0	0.005	0.0030	0.0025	MN
Ground	C0-C3	Y	C3-Y0	0.004	0.0025	0.0021	MN
1	C1-A2	Y	C1-Y1	0.004	0.0015	0.0012	MN
1	C1-A3	Y	C1-Y1	0.003	0.0013	0.0011	MN
1	C1-B1	Y	C1-Y1	0.008	0.0021	0.0015	MN
1	C1-B4	Y	C1-Y1	0.002	0.0012	0.0010	MN
1	C1-C1	Y	C1-Y1	0.008	0.0021	0.0015	MN
1	C1-C4	Y	C1-Y1	0.003	0.0013	0.0011	MN
1	C1-D2	Y	C1-Y1	0.003	0.0013	0.0011	MN
1	C1-D3	Y	C1-Y1	0.001	0.0010	0.0008	MN
1	C1-A1	Y	C2-Y1	0.006	0.0016	0.0016	MN
1	C1-A4	Y	C2-Y1	0.001	0.0008	0.0008	MN
1	C1-D1	Y	C2-Y1	0.003	0.0013	0.0013	MN
1	C1-D4	Y	C2-Y1	0.001	0.0008	0.0008	MN
1	C1-B2	Y	C3-Y1	0.002	0.0008	0.0006	MN
1	C1-B3	Y	C3-Y1	0.002	0.0008	0.0006	MN
1	C1-C2	Y	C3-Y1	0.002	0.0008	0.0006	MN
1	C1-C3	Y	C3-Y1	0.002	0.0008	0.0006	MN
2	C2-A2	Y	C1-Y2	0.005	0.0011	0.0008	MN
2	C2-A3	Y	C1-Y2	0.005	0.0011	0.0008	MN
2	C2-B1	Y	C1-Y2	0.008	0.0013	0.0008	MN
2	C2-B4	Y	C1-Y2	0.002	0.0008	0.0006	MN
2	C2-C1	Y	C1-Y2	0.008	0.0013	0.0008	MN
2	C2-C4	Y	C1-Y2	0.005	0.0011	0.0008	MN
2	C2-D2	Y	C1-Y2	0.002	0.0008	0.0006	MN
2	C2-D3	Y	C1-Y2	0.002	0.0008	0.0006	MN
2	C2-A1	Y	C2-Y2	0.005	0.0011	0.0006	MN
2	C2-A4	Y	C2-Y2	0.001	0.0005	0.0004	MN
2	C2-D1	Y	C2-Y2	0.005	0.0011	0.0006	MN
2	C2-D4	Y	C2-Y2	0.001	0.0005	0.0004	MN
2	C2-B2	Y	C3-Y2	0.002	0.0008	0.0006	MN
2	C2-B3	Y	C3-Y2	0.002	0.0008	0.0006	MN
2	C2-C2	Y	C3-Y2	0.002	0.0008	0.0006	MN
2	C2-C3	Y	C3-Y2	0.002	0.0008	0.0006	MN

As it is seen from Table 6.16 and Table 6.17, all the columns in all floors are positioned in minimum damage limit for both X and Y direction, which means that building conforms “immediate occupancy” performance level. When compared to non-retrofitted form of the building, which stays in collapsing region, the proposed technique showed an outstanding efficiency in terms of improving the seismic behavior of poorly designed and constructed buildings.

7. CONCLUSIONS AND RECOMMENDATIONS

In this study, the effects of using DSE (Deep Surface Embedded) FRP longitudinal reinforcement for the flexural retrofit of substandard RC columns are investigated. Three groups of specimens were subjected to reversed cyclic lateral loads under constant axial load.

7.1 First Group Specimens

Goksu et al. (2012), which is the precursor of this experimental study reported premature failure of the FRP anchorages in the column footing interface. In the light of this experience, it is aimed to design the FRP anchorages avoiding premature failures and maximize the efficiency of the material. Therefore, three specimens were selected to investigate the most efficient anchorage technique for longitudinal FRP reinforcement. These columns belonging to first group specimens were retrofitted in their strong direction by utilizing embedded AFRP strips in longitudinal direction and one column remained unretrofitted as control specimen. In order to determine the most efficient anchorage technique for the embedded FRP reinforcement into the footing, three different type of anchorage detail were applied to the specimens. Longitudinal AFRP reinforcement were directly embedded into the anchorage holes directly by using an epoxy grout in specimens SD-N1-2ARS and SD-N1-4ARS, while 2 additional AFRP strips in the same geometry were embedded into the anchorage holes along with existing longitudinal AFRP reinforcement in the specimen SD-N1-4ARS to further enhance the anchorage performance. Apart from the first two specimens, a partially bonded anchorage system is designed for the specimen SD-N1-2ARS-PB to prevent the cumulation of deformations at the column – footing interface. An adhesive tape was used to create an isolated section on the AFRP strips, which would be stayed debonded in the anchorage hole during the test. The aim of creating an unbonded section just at the column – footing intersection is to distribute the strains in a wide area on the AFRP strip and avoid the premature fracture due to concentrated deformations at the column-footing intersection. Conical holes were dug on the

footings to anchor the longitudinal AFRP reinforcement for all three specimens. All specimens in this group were subjected to lateral loads under 120 kN constant axial load (approximately 20 % of axial load capacity of unretrofitted specimen) up to 8 % drift ratio.

The reference column reached its theoretical flexural capacity, and exhibited a ductile behavior as foreseen during design. The retrofitted columns (SD-N1-2ARS, SD-N1-4ARS, SD-N1-2ARS-PB) failed due to the rupture of AFRP reinforcement at around 3 % drift ratio. At this drift ratio, the enhancement in strength (while pushing) was around 38 %, 84 % and 41 % for the columns SD-N1-2ARS, SD-N1-4ARS and SD-N1-2ARS-PB, respectively, with respect to the reference column SD-N1-REF. After AFRP reinforcement were fractured at around 3 % drift ratio, the columns still resisted significant lateral loads due to contribution of longitudinal steel reinforcement until extremely large drift ratios (~6 % to 8 %). The column SD-N1-4ARS exhibited a remarkably better performance with respect to other specimens due to additional AFRP anchorage reinforcement, which performed far beyond a load transferring anchorage but mostly as an additional longitudinal reinforcement. The sustained full composite action between the existing embedded AFRP reinforcements and the additional AFRP anchorages led to transfer loads efficiently in to the footing until both AFRP reinforcement fracture. This behavior is also confirmed with the theoretical lateral load capacities, where the individual AFRP anchorages are taken into account as additional longitudinal reinforcement. When compared with the column SD-N1-2ARS, the proposed anchorage type used for the column SD-N1-2ARS-PB, limited the residual plastic deformations, while did not affect the lateral load capacity adversely. Depending on these results, direct embedment of the longitudinal FRP reinforcement into the footing was selected as the most effective anchorage technique, which would be applied for the remaining specimens in the test program.

7.2 Second Group Specimens

In order to investigate the effect of the different types of the FRP reinforcement on the flexural strength development, pultruded bars were used in retrofitting the second group specimens instead of strips. Additionally, combining different kinds of FRP reinforcement (aramid, glass and carbon) was also investigated in this group of specimens. Three specimens were retrofitted with different kinds of longitudinal FRP

reinforcement in different configuration by using the determined anchoring technique, which was used in specimen SD-N1-2ARS. In order to compare the effect of type and the kind of FRP reinforcement, axial load kept same as first group specimens.

All three specimens reached their theoretical flexural capacity, while specimens SD-N1-1AR5G and SD-N1-1AR1C1G reached strengths approximately 50 % and 20 % more than their theoretical capacities respectively. SD-N1-3AR and SD-N1-1AR1C1G failed due to the rupture of AFRP reinforcement at around 3 % and 4 % drift ratios respectively. At these drift ratios, the enhancement in strength (while pushing) was around 116 % for SD-N1-3AR and 82 % for SD-N1-1AR1C1G, with respect to the reference column SD-N1-REF. Similar to the first group specimens, after rupture of AFRP reinforcement, specimens behaved similar to reference column. On the other hand, the column SD-N1-1AR5G exhibited an extraordinary performance with respect to other specimens in terms of strength and deformation capacity. SD-N1-1AR5G beared very high lateral loads, approximately 2.52 and 3.07 times the loads carried by the reference, while pushing and pulling, respectively. Moreover, it sustained its lateral load capacity until 8 % drift ratio, which can be explained with the significant contribution of GFRP reinforcement to the flexural capacity, although AFRP reinforcement fractured at 6 % drift ratio. This outstanding contribution of the GFRP reinforcement is quite promosing for improving the seismic performance of the columns even under severe earthquake loading, which may also require high displacement demands.

7.3 Third Group Specimens

Two columns were tested to achive a certain level of damage, then repaired and retrofitted (with AFRP bars) in their weak direction and eventually, re-tested under same conditions, in order to investigate the efficiency of the proposed technique in structural members with different levels of predamage conditions. The specimen WD-N1-P1 was tested untill achieving ±2 % drift ratio to represent the moderate damage, while the specimen WD-N1-P2 was tested untill ±4 % drift ratio, which could be considered for representing heavy damage conditions.

Both specimens reached their theoretical flexural capacity both before and after retrofitting. Retrofitted specimens failed at 4 % drift ratio due to the rupture of AFRP reinforcement at the column-footing intersection. At this drift ratio, the enhancement

in strength (while pushing) was around 148 % for WD-N1-2AR-P1 and 106 % for WD-N1-2AR-P2, with respect to the pre-damaged specimens WD-N1-P1 and WD-N1-P2 respectively.

An additional specimen was retrofitted identically to the pre-damaged specimens in order to investigate the efficiency of the proposed retrofitting technique comparatively on damaged and non-damaged specimens. One final specimen was retrofitted by hybrid utilization of AFRP and GFRP bars and tested in weak direction to further investigate the hybrid use of FRP reinforcement in flexural retrofitting.

Both undamaged specimens reached their theoretical flexural capacity, which proves the accuracy of the design approach for calculating the actual capacities of the columns. When compared to the reference specimen, which is actually the specimen tested for representing heavy damage case (WD-N1-P2), the undamaged retrofitted specimens significantly performed better. Specimen WD-N1-2AR failed at 4 % drift ratio due to the rupture of AFRP reinforcement and at this drift ratio, the enhancement in strength (while pushing) was around 110 % when compared to reference specimen. The column retrofitted with hybrid FRP reinforcement sustained maximum lateral load at relatively higher drift ratios, which is a similar behaviour already observed in the second group specimens with hybrid FRP reinforcement. At this drift ratio, the enhancement in strength (while pushing) was around 116 % for the specimen WD-N1-1AR2G when compared to reference specimen (WD-N1-P2).

7.4 Conclusions

A significant enhancement in the flexural strength of the substandard column specimens was achieved by the proposed retrofitting technique. There were no significant difference in ultimate lateral load capacities evaluated between different types (strip vs bar) of FRP reinforcement used in retrofitting. On the other hand, different kind of FRP reinforcement had different influence on the flexural performance of the columns. Since the rupture of FRP reinforcement defines the behavior and ultimate strength of the specimen, GFRP reinforcement sustains tensile stresses upto very high drift ratios when compared to AFRP reinforcement. Despite the very low elasticity modulus of GFRP bars, they were much more effective than AFRP reinforcement in terms of deformation capacity under reversed cyclic loading.

Besides, the columns retrofitted with GFRP reinforcement beared much higher lateral loads when compared with the specimens retrofitted only with AFRP reinforcement.

As the longitudinal FRP reinforcement ratio increased, the lateral load capacity of the columns was also increased proportionally. Besides, it has been also proven that moderate or even heavy pre-damage conditions do not have a considerable impact on flexural behavior of the columns when they are retrofitted with the proposed technique, DSE FRP (Deep Surface Embedded FRP). These promising results should be supported with further investigation in this specific area and the positive results should be confirmed for utilizing the technique in pre-damaged structures due to seismis actions or damaged with other reasons. With this way, many structures, which have been moderately or even heavily damaged, could be retrofitted and continue to service safely. Therefore, massive costs for demolishing and reconstruction of many heavily damaged structures could be avoided.

Although, direct embedment of the longitudinal FRP reinforcement into the footing was the preferred anchorage technique in this study, the results showed that partially bonded anchorages could be utilized to limit the residual displacement and corresponding damage. On the other hand, the price of limited residual displacement providedby partially debonded anchorages is a remarkable decrease in the ductility enhancement.

It was assessed that the predicted results through theoretical modelling satisfactorily captured the test results by means of lateral load and deformation capacities, particularly, when the actual rupture strains of FRP reinforcement measured by straingaguges are considered as the rupture strain of the FRP reinforcement during theoretical calculations. However, this conclusion does not valid for the specimens retrofitted with hbyrid FRP reinforcement. Since GFRP bars did not fracture during the tests, their ultimate rupture strains are considered during the theoretical calculations and the calculated lateral load capacities were in agreement with the test results.

Besides, the experimentally measured rupture strain of AFRP reinforcement was observed to vary between 30 % - 63 % of design rupture strain of AFRP reinforcement. GFRP bars performed as the most efficient FRP reinforcement in enhancing flexural behavior of the specimens. The maximum strains of longitudinal GFRP strips and bars

in tension vary between 0.0137 – 0.0201 right before the rupture of the AFRP reinforcement. These wide ranges of values correspond to approximately 49 % - 72 % of design rupture strain of GFRP reinforcement. GFRP bars, which performed much higher strains under tension when compared to AFRP reinforcement, still it does not fully comply with while ACI 440-2R-08 (2008) recommends to reduce ε_{fu} by using a factor of 0.70 for NSM application technique under monotonic flexural loading. Therefore, the strain reduction factor (70 %) recommended by ACI 440-2R-08 (2008) for NSM applications under monotonic loading conditions may lead to unconservative predictions of lateral load-deformation capacity for the proposed retrofitting technique, DSE FRP in this study under cyclic loading conditions. Although there are not any significant difference observed in the deformation capacities of the FRP reinforcement in different shapes (strip and bar), different kind of FRP material (aramid, glass and carbon) exhibit different deformation capacities. In order to increase the accuracy of the design approach, strain reduction factor should be tailored according to material type of FRP reinforcement. Additionally, the contribution of the FRP reinforcement under compression was limited as also confirmed with the measureremements done with straingauges. Therefore, neglecting the contribution of FRP reinforcement under compression during the theoretical lateral load capacity calculations does not have a significant impact on the accuracy of the theoretical modelling.

Energy dissipation capacities were increased significantly by the proposed retrofitting technique in this study. Exceptionally, only one specimen, SD-N1-2ARS-PB performed slightly worse than reference column due to elastic behavior of unbonded AFRP reinforcement. In general, the specimens with higher lateral load capacity also performed higher energy dissipation capacities. The specimens containing GFRP reinforcement performed remarkably better due to higher deforation capacities and sustained lateral loads up to very high drift ratios, where the specimens not containing GFRP reinforcement exhibited limited energy dissipation after rupture of AFRP reinforcement in relatively early drift ratios.

Retrofitting the individual reinforced concrete members and improving the seismic behavior of these elements is an important step in seismic rehabilitation of the structures. However, more importantly, the efficiency of the retrofitting method can be determined by evaluating the overall seismic performance of the retrofitted

structure. The traditional CFRP confinement also contributes to improvement of the flexural strength and ductility in case of reversed cyclic loading but many times due to the limited increase on the flexural capacity and high plastic deformations, the structure can lose its functionality and cannot turn back in to the service after severe earthquakes. This means a huge impact on the deomistic economy and on the public services when public buildings (e.g. schools, hospitals, state offices) are considered. The primary aim of this study is to develop a retrofitting method not only increases the flexural capacity of the substandard columns under reversed cyclic loading but also limiting the plastic deformations bring the structure to immediate occupancy performance level stated by TSDC (2007), in most of the cases. In the analytical part of the study, it has been proved that the proposed technique, DSE FRP is not only effective to improve the cyclic flexural capacity of the substandard columns but also preserves the functionality of the structure by limiting the plastic deformations even under high seismic loading.

Clearly, further investigations are also needed to accurately identify the theoretical seismic behavior of the columns retrofitted by using the proposed DSE technique under cyclic loading conditions. Altough the lateral load capacities and elastic deformations could be calculated more accurately, the theoretical plastic deformations were way behind the experimental results, which leads to strong question marks on the assumed plastic hinge lengths (h/2). Further studies are needed to clarify the plastic hinge behavior of the FRP retrofitted elements under reversed cyclic loading. Particularly, the effect of different kinds of FRP reinforcement on the flexural behaviour is needed to be investigated.

REFERENCES

ACI 318M-14 (2014). Metric Building Code Requirements for Structural Concrete and Commentary. *American Concrete Institute 318*, Farmington Hills, MI, USA.

ACI 355.1R-91 (1991). State-of-the-art report on anchorage to concrete. *American Concrete Institute 355*, Farmington Hills, MI, USA.

ACI 440.2R-08 (2008). Guide for design and construction of externally bonded FRP systems for strengthening concrete structures. *American Concrete Institute 440*, Farmington Hills, MI, USA.

Antonopoulos, C. P., and Triantafillou, T. C. (2003). Experimental investigation of FRP-strengthened RC beam-column joints. *ASCE, Journal of Composites for Construction*, *7* (1), 39–49.

ASCE/SEI 41/06 (2007). Seismic rehabilitation of existing buildings. *American Society of Civil Engineers*, Reston, Virginia, USA.

ASTM D3039 (1993). Standard test method tensile properties of polymer matrix composite materials. *American Society for Testing and Materials*, Philadelphia, USA.

Badawi, M., and Soudki, K. (2009). Fatigue behavior of RC beams strengthened with NSM CFRP rods. *ASCE, Journal of Composites for Construction*, *13* (5), 415-421.

Bakis, C. E., Bank, L.C., Brown, V.L., Cosenza, E, Davalos, J.F., Lesko, J.J., Machida, A., Rizkalla, S.H., and Triantafillou, T.C. (2002). Fiber-reinforced polymer composites for construction-State-of-the-Art Review. *ASCE, Journal of Composites for Construction*, *6* (2), 73-87.

Bank, L.C. (2013). Progressive Failure and Ductility of FRP Composites for Construction: Review. *ASCE, Journal of Composites for Construction*, *17*(3), 406-419.

Barros, J.A.O. and Dias, S.J.E. (2006). Near surface mounted CFRP laminates for shear strengthening of concrete beams. *Cement & Concrete Composites*, *28*, 276–292.

Barros, J.A.O., Ferreira, D.R.S.M., Fortes, A.S., and Dias, S.J.E. (2006). Assessing the effectiveness of embedding CFRP laminates in the near surface for structural strengthening. *Construction and Building Materials, 20* (7), 478–491.

Barros, J.A.O., Varma, R.K., Sena-Cruz, J.M., Azevedo, A.F.M. (2008). Near surface mounted CFRP strips for the flexural strengthening of RC columns: Experimental and numerical research. *Engineering Structures, 30,* 3412-3425.

Bilotta, A., Ceroni, F., Barros, J., Costa, I., Palmieri, A., Szabó, Z., Nigro, E., Matthys, S., Balazs, G., and Pecce, M. (2015). Bond of NSM FRP-Strengthened Concrete: Round Robin Test Initiative. *ASCE, Journal of Composites for Construction*, 10.1061/(ASCE)CC.1943-561400579, 04015026.

Bournas, D.A., and Triantafillou, T.C. (2009). Flexural strengthening of reinforced concrete columns with near surface mounted FRP or stainless steel. *ACI*, *Structural Journal*, *106* (4), 495-505.

Bournas D.A., and Triantafillou, T.C. (2011). Bond strength of lap spliced bars in concrete confined with composite jackets. *ASCE*, *Journal of Composites for Construction*, *15* (2), 156-167.

Bousias, S.N., Triantafillou, T.C., Fardis, M.N., Spathis, L., and O'Regan, B.A. (2004). Fiber-reinforced polymer retrofitting of rectangular reinforced concrete columns with or without corrosion. *ACI*, *Structural Journal*, *101* (4), 512-520.

Castro, E.K., Melo, G.S., and Nagato, Y. (2007). Flexural strengthening of RC "t" beams with near surface mounted (NSM) FRP reinforcement. *Proc. Int. Symposium on FRP Reinforcement of Concrete Structures (FRPRCS-8)*, Patras, Greece, 16-18 July.

CEB-FIB. (2001). Externally bonded FRP reinforcement for RC structures. *International federation for structural concrete*-Technical report, Lausanne, Switzerland.

Ceroni, F. (2010). Experimental performances of RC beams strengthened with FRP materials. *Construction and Building Materials, 24* (9), 1547-1559.

Chang, S., Li, Y., and Loh, C. (2004). Experimental study of seismic behaviors of as-built and carbon fiber reinforced plastics repaired reinforced concrete bridge columns. *ASCE, Journal of Bridge Engineering*, *9* (4), 391-402.

Chikh, N., Foret, G., Bousalem, B. and Firas, S. (2008). Analysis of reinforced concrete members strengthened with near-surface-mounted CFRP. *11DBMC Proc. Int. Conf. on Durability of Building Materials and Components*, Istanbul-Turkey, 11-14 May.

CNR-DT 200/2004 (2004). Guide for the design and construction of externally bonded FRP systems for strengthening existing structures. *National research council, advisory committee on technical recommendations for construction* - Rome, Italy.

De Lorenzis, L., and Nanni, A. (2002). Bond between near surface mounted fiber reinforced polymer rods and concrete in structural strengthening. *ACI*, *Structural Journal*, *99* (2), 123-132.

De Lorenzis, L., Lundgren, K., and Rizzo, A. (2004). Anchorage length of near-surface mounted fiber reinforced polymer bars for concrete strengthening-experimental investigation and numerical modelling. *ACI*, *Structural Journal*, *101* (2), 269-278.

De Lorenzis, L., and Teng, J.G. (2006). Near-surface mounted FRP reinforcement: An emerging technique for strengthening structures. *Composites: PartB*, *38*, 119-143.

Demir, C., Darılmaz, K., Ilki, A. (2015). Cyclic Stress–Strain Relationships of FRP Confined Concrete Members. *Arabian Journal for Science and Engineering*, *40*, 363-379.

Demirtaş, B. (2008). *The Effect of Corrosion on Reinforced Concrete Columns in regard of Seismic Performance.* (Masters' dissertation). Istanbul Technical University, Istanbul, Turkey.

Ehsani, M. R. (1993). Glass Fiber Reinforcing Bars. *Alternative Materials for the Reinforcement and Prestressing of Concrete*. J. L. Clarke, Blackie Academic & Professional, London, pp. 35-54

El-Maaddawy, T.A., and El-Dieb, A.S. (2011). Near-surface-mounted composite system for repair and strengthening of reinforced concrete columns subjected to axial load and biaxial bending. *ASCE*, *Journal of Composites for Construction*, *15* (4), 602-614.

El-Hacha, R., and Rizkalla, S.H. (2004). Near-surface-mounted fiber-reinforced polymer reinforcement for flexural strengthening of concrete structures. *ACI*, *Structural Journal*, *101* (5), 717-726.

Eurocode 8-Part 3 (2005). Assessment and retrofitting of buildings, *European Committee for Standardization*. Brussels, Belgium.

EN 1504-3 (2005). Products and systems for the protection and repair of concrete structures - Definitions, requirements, quality control and evaluation of conformity - Part 3: Structural and non-structural repair. *European Committee for Standardization*, Brussels, Belgium.

EN 1504-4 (2004). Products and systems for the protection and repair of concrete structures - Definitions, requirements, quality control and evaluation of conformity - Part 4: Structural bonding. *European Committee for Standardization*, Brussels, Belgium.

EN 1504-6 (2006). Products and systems for the protection and repair of concrete structures - Definitions, requirements, quality control and evaluation of conformity - Part 6: Anchoring of Reinforcing Steel Bars. *European Committee for Standardization*, Brussels, Belgium.

Fahmy, M.F.M. and Wu, Z. (2012). Retrofitting of existing RC square bridge columns using basalt FRP rebars. *CICE 2012*, Rome.

Faustino, P. and Chastre C. (2015). Flexural Strengthening of Columns with CFRP Composites and Stainless Steel: Cyclic Behavior. *ASCE Journal of Structural Engineering*. doi: 10.1061/(ASCE)ST.1943-541X.0001400.

FEMA 273 (1997). NEHRP Guidelines for the Seismic Rehabilitation of Buildings. *Federal Emergency Management Agency*, Washington, DC.

Garcia, R., Hajirasouliha, I., and Pilakoutas, K. (2010). Seismic behaviour of deficient RC frames strengthened with CFRP composites. *Engineering Structures*, *32* (10), 3075-3085.

Goksu, C. (2012). *Seismic behavior of RC columns with corroded plain and deformed reinforcing bars*. (Doctoral dissertation). Istanbul Technical University, Istanbul, Turkey.

Goksu, C., Polat, A., and Ilki, A. (2012). Attempt for seismic retrofit of existing sub-standard RC members under reversed cyclic flexural effects. *ASCE, Journal of Composites for Construction*, *16* (3), 286-299.

Hassan, T.K., and Rizkalla, S.H. (2004). Bond mechanism of near-surface-mounted fiber-reinforced polymer bars for flexural strengthening of concrete structures. *ACI*, *Structural Journal*, *101* (6), 830-839.

Iacobucci, R. D., Sheikh A.S., Bayrak O. (2003). Retrofit of square concrete columns with carbon fiber-reinforced polymer for seismic resistance. *ACI*, *Structural Journal*, *100* (6), 785-794.

Ilki, A., and Kumbasar, N. (2002). The behavior of damaged reinforced concrete members strengthened by carbon fiber reinforced polymer composites." *Technical Journal of Turkish Chamber of Civil Engineers*, *13* (1), 2597-2616.

Ilki, A., Peker O., Karamuk E., Demir, C., and Kumbasar, N. (2008). FRP retrofit of low and medium strength circular and rectangular reinforced concrete columns. *ASCE, Journal of Materials in Civil Engineering, 20* (2), 169-188.

Ilki, A., Demir C., Bedirhanoglu I., and Kumbasar, N. (2009). Seismic retrofit of brittle and low-strength RC columns using fiber reinforced polymer and cementitious composites. *Advances in Structural Engineering*, *12* (3), 325-347.

Ilki, A., Bedirhanoglu I., and Kumbasar, N. (2011). Behavior of FRP retrofitted joints built with plain bars and low-strength concrete. *ASCE*, *Journal of Composites for Construction, 15* (3), 312-326.

Jirawattanasomkul, T., Zhang, D.W., and Ueda, T. (2013). Prediction of the post-peak behavior of reinforced concrete columns with and without FRP-jacketing. *Engineering Structures*, *56*, 1511-1526.

Kaya, E., Kütan, C., Sheikh, S., and İlki, A. (2016). Flexural Retrofit of Support Regions of Reinforced Concrete Beams with Anchored FRP Ropes Using NSM and ETS Methods under Reversed Cyclic Loading. *ASCE, Journal of Composites for Construction*, 10.1061/(ASCE)CC. 1943-5614.0000732, 04016072.

Lam, L., and Teng, J. G. (2003). Design-oriented stress-strain model for FRP-confined concrete. *Construction in Building Materials*, *17* (6-7), 471-489.

Li, X., Lv, H.L., Zhang, G.C., Sha, S.Y., and Zhou, S.C. (2013). Seismic retrofitting of rectangular reinforced concrete columns using fiber composites for enhanced flexural strength. *Journal of Reinforced Plastics and Composites*, *32* (9) 619–630.

Liu, I. S. T., Oehlers, D. J., and Seracino, R. (2006). Tests on the ductility of reinforced concrete beams retrofitted with FRP and steel near-surface-

mounted plates. *ASCE, Journal of Composites for Construction*, *10* (2), 106-114.

Mallick, P. K. (1988). Fiber Reinforced Composites, Materials, Manufacturing, and Design. *Marcell Dekker, Inc*., New York, 469.

Matamoros, A.B. and Sozen, M.A. (2003). Drift limits of high-strength concrete columns subjected to load reversals. *ASCE, Journal of Structural Engineering*, *129* (3), 297-313.

Memon M.S. and Sheikh, S.A. (2005). Seismic resistance of square concrete columns retrofitted with glass fiber-reinforced polymer. *ACI, Structural Journal*, *102* (5), 774-783.

Nanni, A., Alkhrdaji, T., Chen, G., Barker, M., Yang, X., and Mayo, R. (1999). Overview of testing to failure program of a highway bridge strengthened with FRP composites. *Proc. Fourth Int. Symposium on FRP for Reinforcement of Concrete Structures*, Baltimore, November, 69-80.

Nordin, H., and Täljsten, B. (2006). Concrete beams strengthened with prestressed near surface mounted CFRP. *ASCE, Journal of Composites for Construction*, *10* (1), 60-68.

Parvin, A., Brighton, D. (2014). FRP Composites Strengthening of Concrete Columns under Various Loading Conditions. *Polymers*, *6*, 1040-1056.

Perrone, M., Barros, J.A.P. and Aprile, A. (2009). CFRP based strengthening technique to increase the flexural and energy dissipation capacities of RC columns. *ASCE, Journal of Composites for Construction.* doi: 10.1061/(ASCE)CC.1943-561400031, 372-383.

Pessiki, S., Harries, K.A., Kestner, J.T., Sause, R., and Ricles, J.M. (2001). Axial behavior of reinforced concrete columns confined with FRP jackets. *ASCE, Journal of Composites for Construction*, *5* (4), 237-245.

Prota, A., Nanni, A., Manfredi, G., and Cosenza, E. (2004). Selective upgrade of underdesigned reinforced concrete beam-column joints using carbon fiber polymers. *ACI, Structural Journal*, *101* (5), 699-707.

Sena Cruz, J.M., Barros, J.A.O., Gettu, R., and Azevedo, A.F.M. (2006). Bond behavior of near surface mounted CFRP laminate strips under monotonic and cyclic loading. *ASCE, Journal of Composites for Construction*, *10* (4), 295-303.

Seible, F., Priestley, M.J., Hegemier G.A., and Innamorato, D. (1997). Seismic retrofit of RC columns with continuous carbon fiber jackets. *ASCE, Journal of Composites for Construction*, *1* (2), 52-62.

Seracino, R., Raizal Saifulnaz, M. R., and Oehlers, D. J. (2007). Generic debonding resistance of EB and NSM plate-to-concrete joints. *ASCE, Journal of Composites for Construction*, *11* (1), 62-70.

Sharaky, I.A., Torres, L., Comas, J., Barris, C. (2013). Flexural response of reinforced concrete (RC) beams strengthened with near surface mounted (NSM) fibre reinforced polymer (FRP) bars. *Composite Structures*, *109*, 8-22.

Sheikh, S. and Yau, G. (2002). Seismic behavior of concrete columns confined with steel and fiber-reinforced polymers. *ACI, Structural Journal*, *99* (1), 72-80.

Teng, J.G., De Lorenzis, L., Wang, B., Li, R., Wong, T.N., Lam, L. (2006). Debonding failures of RC beams strengthened with near surface mounted CFRP strips. *ASCE, Journal of Composites for Construction*, *10* (2), 92-105.

TSDC. (2007). Regulations for buildings to be constructed in earthquake prone areas. *Turkish Seismic Design Code*, Ankara, Turkey.

Tsonos, A.G. (2007). Effectiveness of CFRP-jackets in post-earthquake and pre-earthquake retrofitting of beam-column subassemblages. *Structural Engineering and Mechanics*, *27* (4), 393-408.

TS EN 12390-3 (2003). Testing hardened concrete-Part 3: Compressive strength of test specimens. *Turkish Standards Institute*, Ankara, Turkey.

TS-EN 196-1 (2009). Methods of testing cement-Part 1: Determination of strength. *Turkish Standards Institute*, Ankara, Turkey.

TS 708 (1996). Steel bars for concrete. *Turkish Standards Institute*, Ankara, Turkey.

Vrettos, I., Kefela, E., and Triantafillou, T.C. (2013). Innovative flexural strengthening of reinforced concrete columns using carbon-fiber anchors. *ACI, Structural Journal*, *110* (1), 63-70.

Xiao, Y. (2004). Applications of FRP composites in concrete columns. *Advances in Structural Engineering, 7* (4), 335-343.

XTRACT (2011). Cross-sectional structural analysis of components. *Imbsen & Associates Inc.,* Sacramento, USA.

Wang, Z., Wang, D., Smith, S.T., and Lu, D. (2011). CFRP-confined square RC columns. I: Experimental investigation. *ASCE, Journal of Composites for Construction*, *16* (2), 150-160.

Wu, W. P. (1990). *Thermomechanical Properties of Fiber Reinforced Plastic (FRP) Bars.* (Doctoral dissertation*)*. West Virginia University, Morgantown, W.Va., 292.

APPENDICES

APPENDIX A: Reinforcing Cage of the Specimens
APPENDIX B: Locations of the LVDTs
APPENDIX C: Strain Distribution of the Reinforcement
APPENDIX D: Detailed Input and Output of the Analytical Study

APPENDIX A

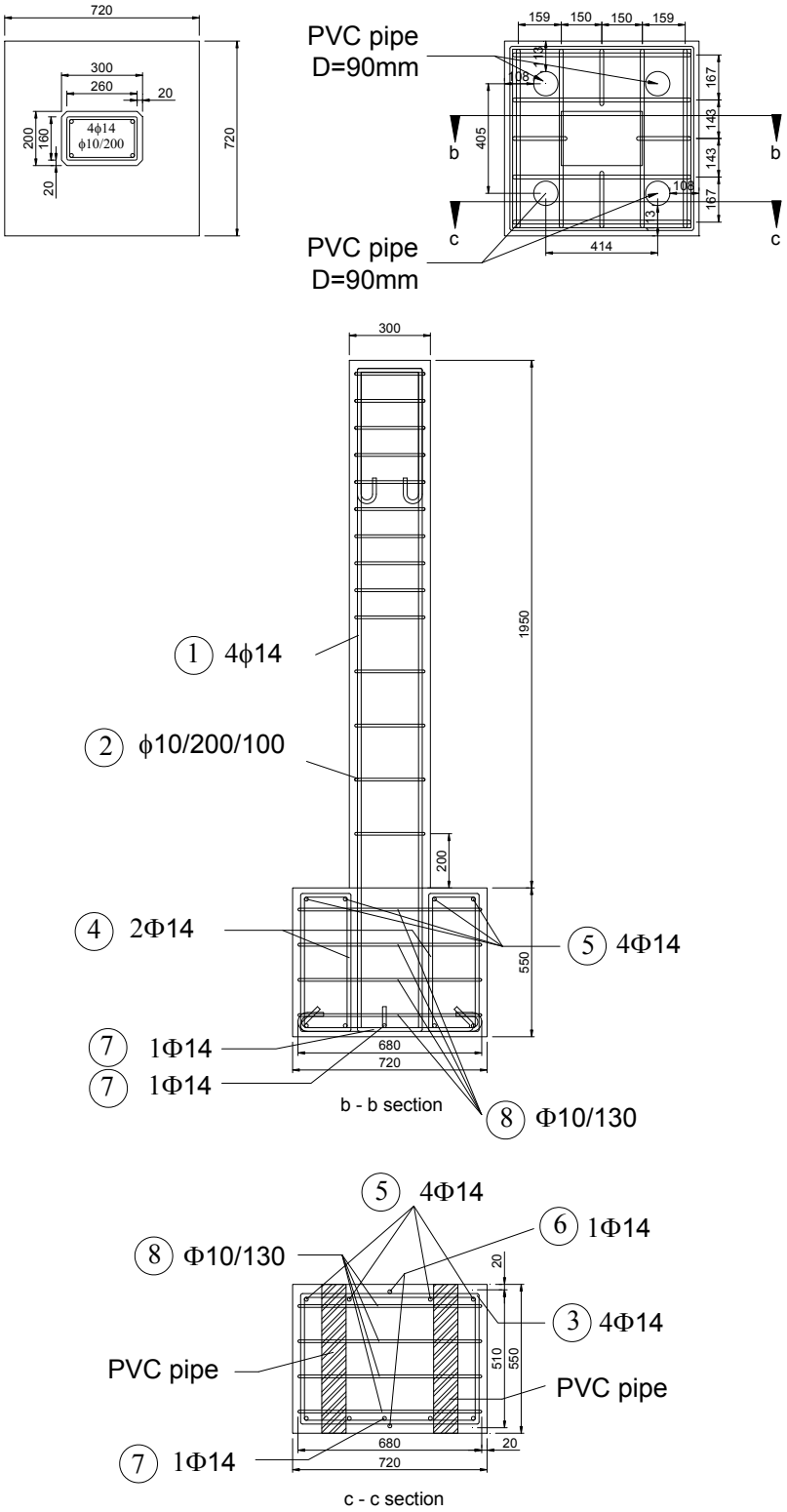

Figure A.1 : Reinforcing cage of the specimens.

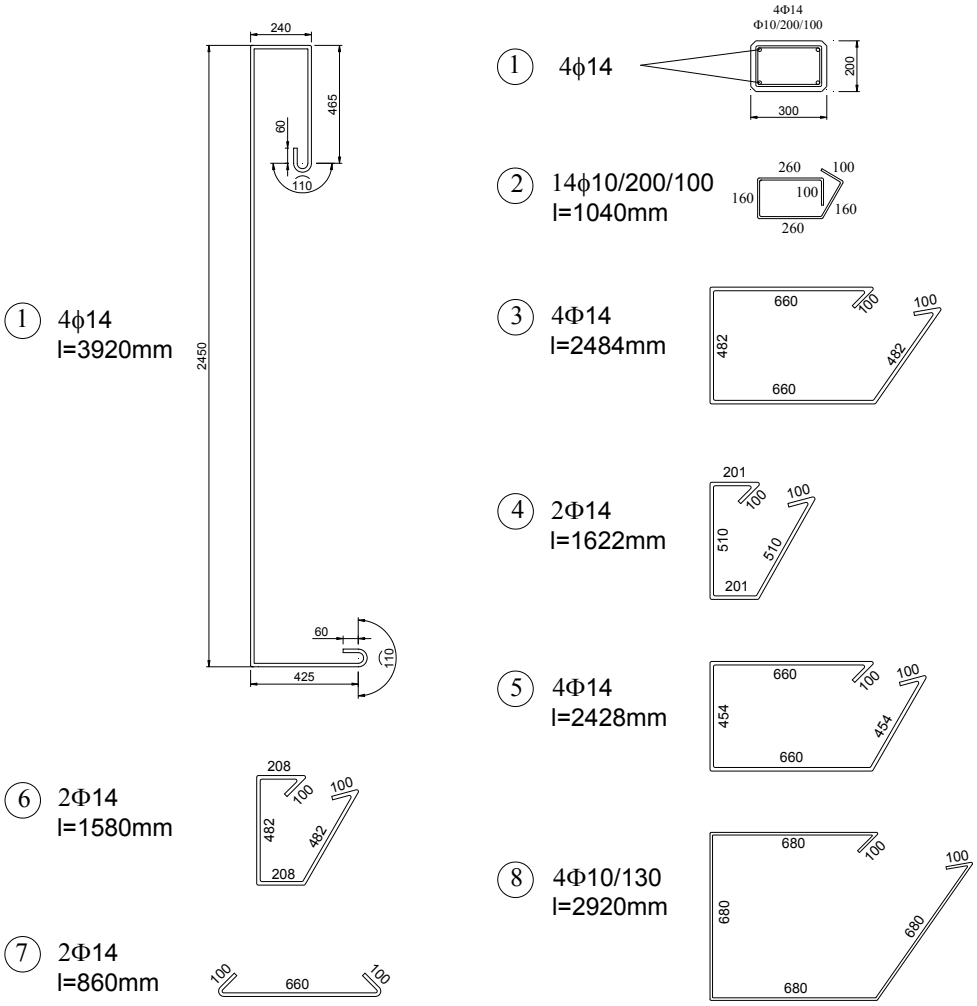

Figure A.2 : Details of the Reinforcing cage of the specimens.

APPENDIX B

Table B.1 : Distances between the column surfaces and the LVDTs.

Specimen	Distances (mm)					
	X_{12}	X_{22}	X_{32}	X_{11}	X_{21}	X_{31}
SD-N1-REF	51	45	51	45	56	61
SD-N1-2ARS	38	45	48	37	43	55
SD-N1-4ARS	44	43	56	35	46	56
SD-N1-2ARS-PB	45	46	61	33	56	63
SD-N1-3AR	85	33	82	95	35	80
SD-N1-1AR5G	35	37	58	24	45	54
SD-N1-1AR1C1G	35	45	55	25	35	47
WD-N1-P1	72	75	60	60	60	55
WD-N1-P2	38	38	82	36	52	80
WD-N1-2AR-P1	41	65	75	44	58	62
WD-N1-2AR-P2	50	58	83	40	60	78
WD-N1-2AR	80	35	87	85	40	85
WD-N1-1AR2G	26	50	55	39	55	56

Table B.2 : Vertical distances between the LVDTs.

Specimen	Distances (mm)						
	Δ_{12}	Δ_{22}	Δ_{32}	Δ_{11}	Δ_{21}	Δ_{31}	h_1
SD-N1-REF	20	134	139	20	110	162	1714
SD-N1-2ARS	20	125	150	20	115	160	1710
SD-N1-4ARS	20	139	144	20	69	153	1732
SD-N1-2ARS-PB	20	130	155	20	130	144	1705
SD-N1-3AR	20	105	150	80	105	150	1720
SD-N1-1AR5G	30	115	148	45	120	150	1700
SD-N1-1AR1C1G	23	129	153	39	114	162	1665
WD-N1-P1	35	102	160	32	137	144	1728
WD-N1-P2	74	88	122	74	84	128	1726
WD-N1-2AR-P1	25	125	150	25	125	145	1710
WD-N1-2AR-P2	20	122	144	23	122	148	1678
WD-N1-2AR	27	135	176	62	120	160	1715
WD-N1-1AR2G	30	120	140	30	120	145	1654

APPENDIX C

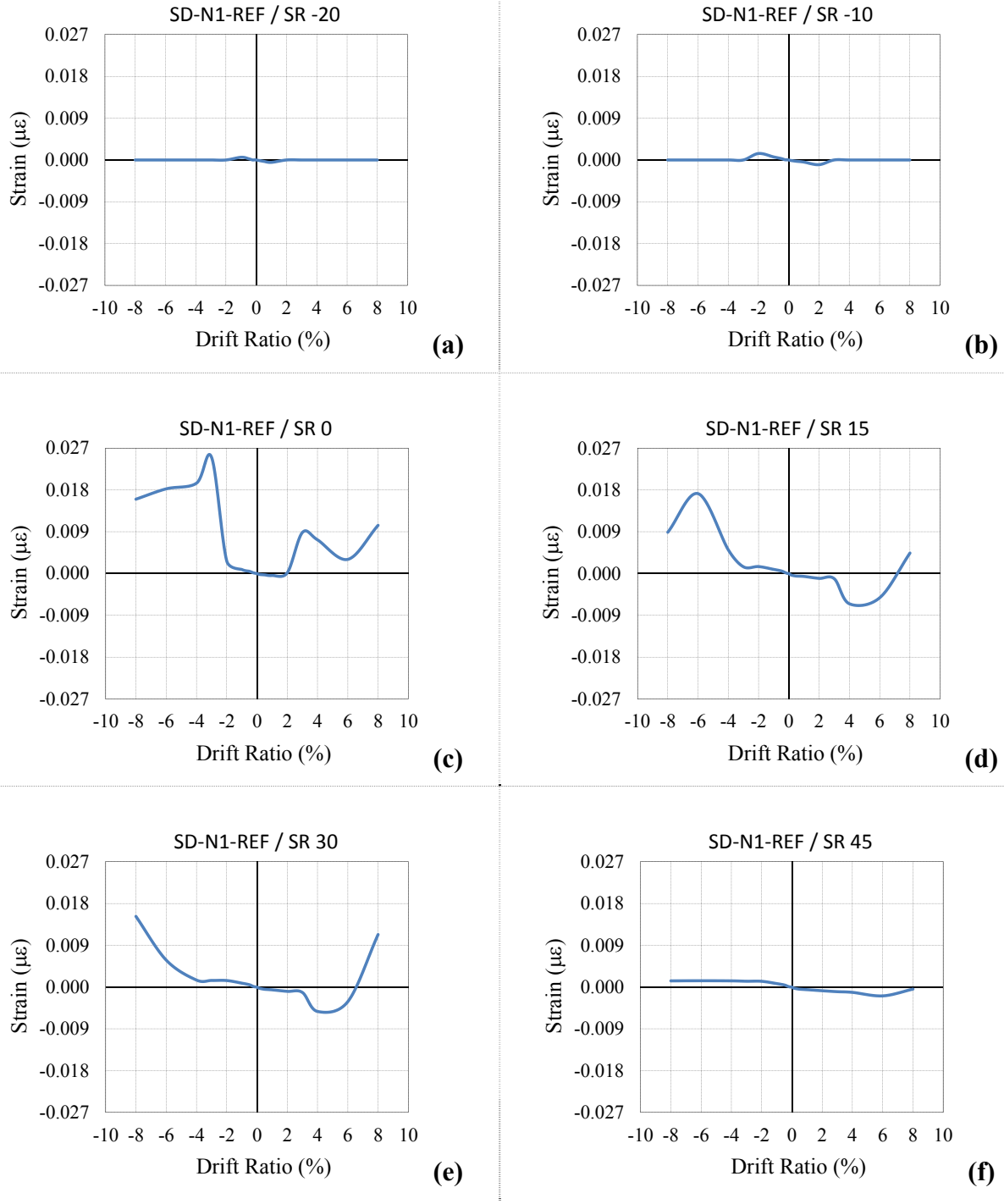

Figure C.1 : Average strain distribution of longitudinal steel reinforcement of specimen SD-N1-REF: (a)At -20 cm. (b)At -10 cm. (c)At 0 cm. (d)At 15 cm. (e)At 30 cm. (f)At 45 cm.

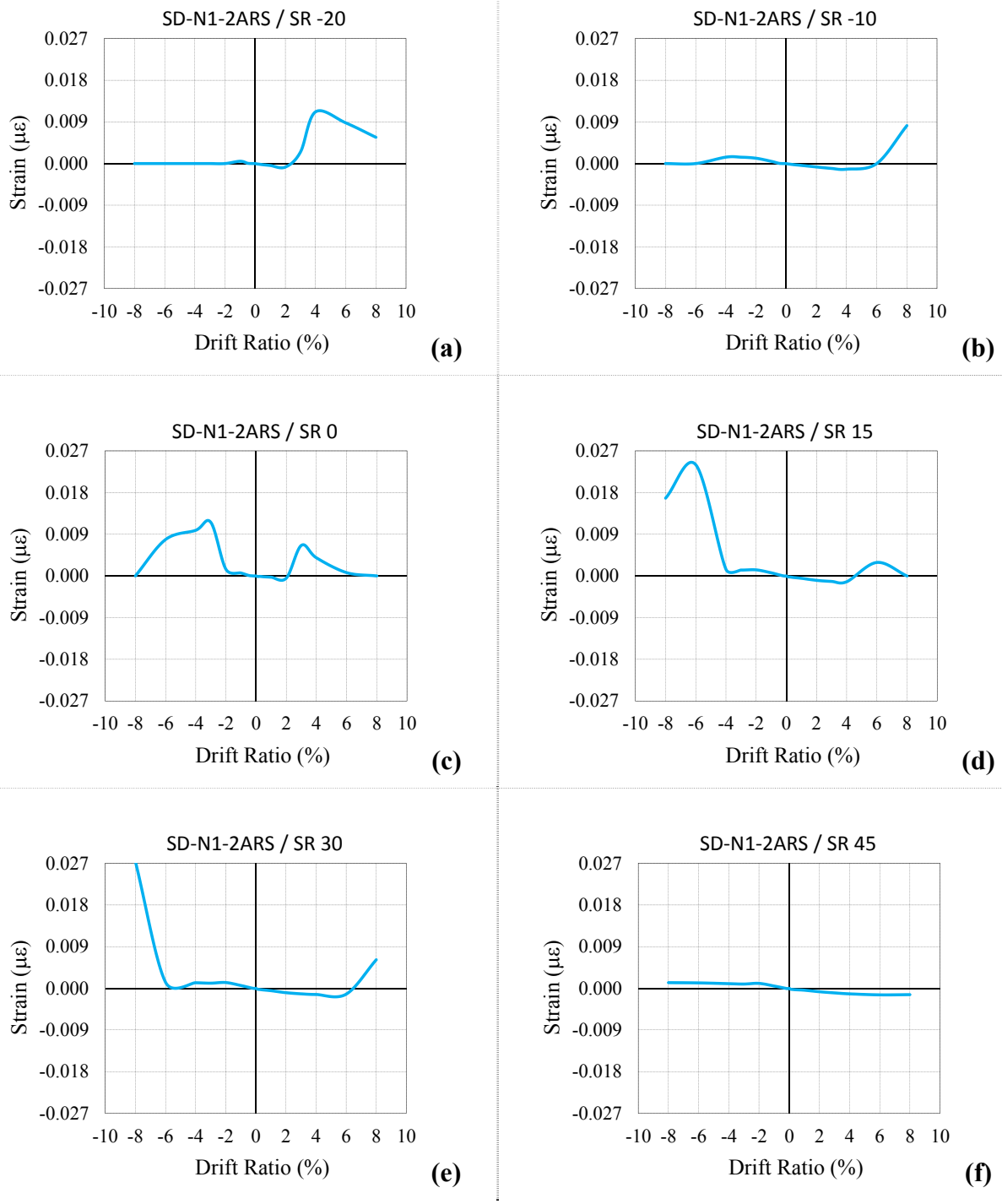

Figure C.2 : Average strain distribution of longitudinal steel reinforcement of specimen SD-N1-2ARS: (a)At -20 cm. (b)At -10 cm. (c)At 0 cm. (d)At 15 cm. (e)At 30 cm. (f)At 45 cm.

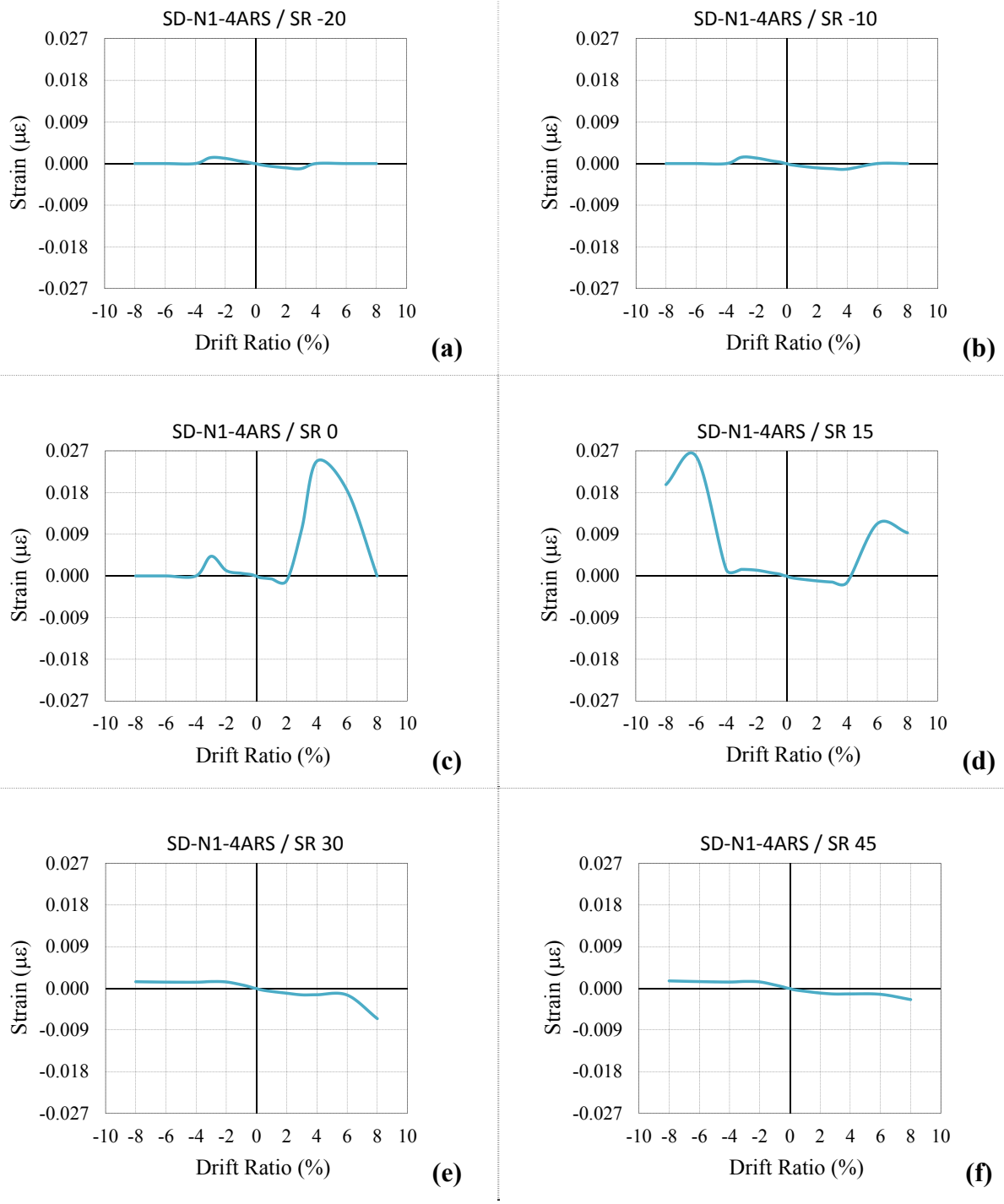

Figure C.3 : Average strain distribution of longitudinal steel reinforcement of specimen SD-N1-4ARS: (a)At -20 cm. (b)At -10 cm. (c)At 0 cm. (d)At 15 cm. (e)At 30 cm. (f)At 45 cm.

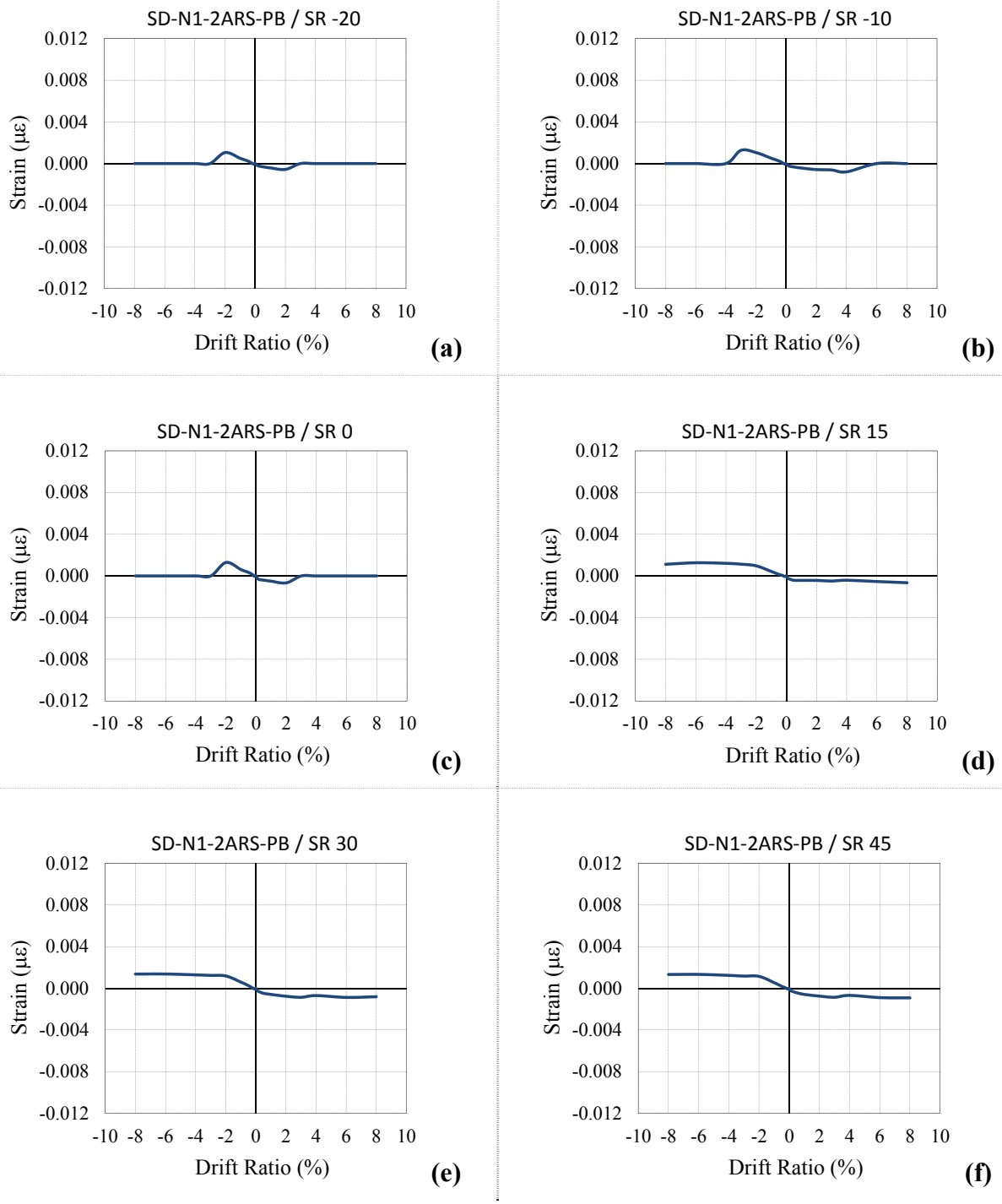

Figure C.4 : Average strain distribution of longitudinal steel reinforcement of specimen SD-N1-2ARS-PB: (a)At -20 cm. (b)At -10 cm. (c)At 0 cm. (d)At 15 cm. (e)At 30 cm. (f)At 45 cm.

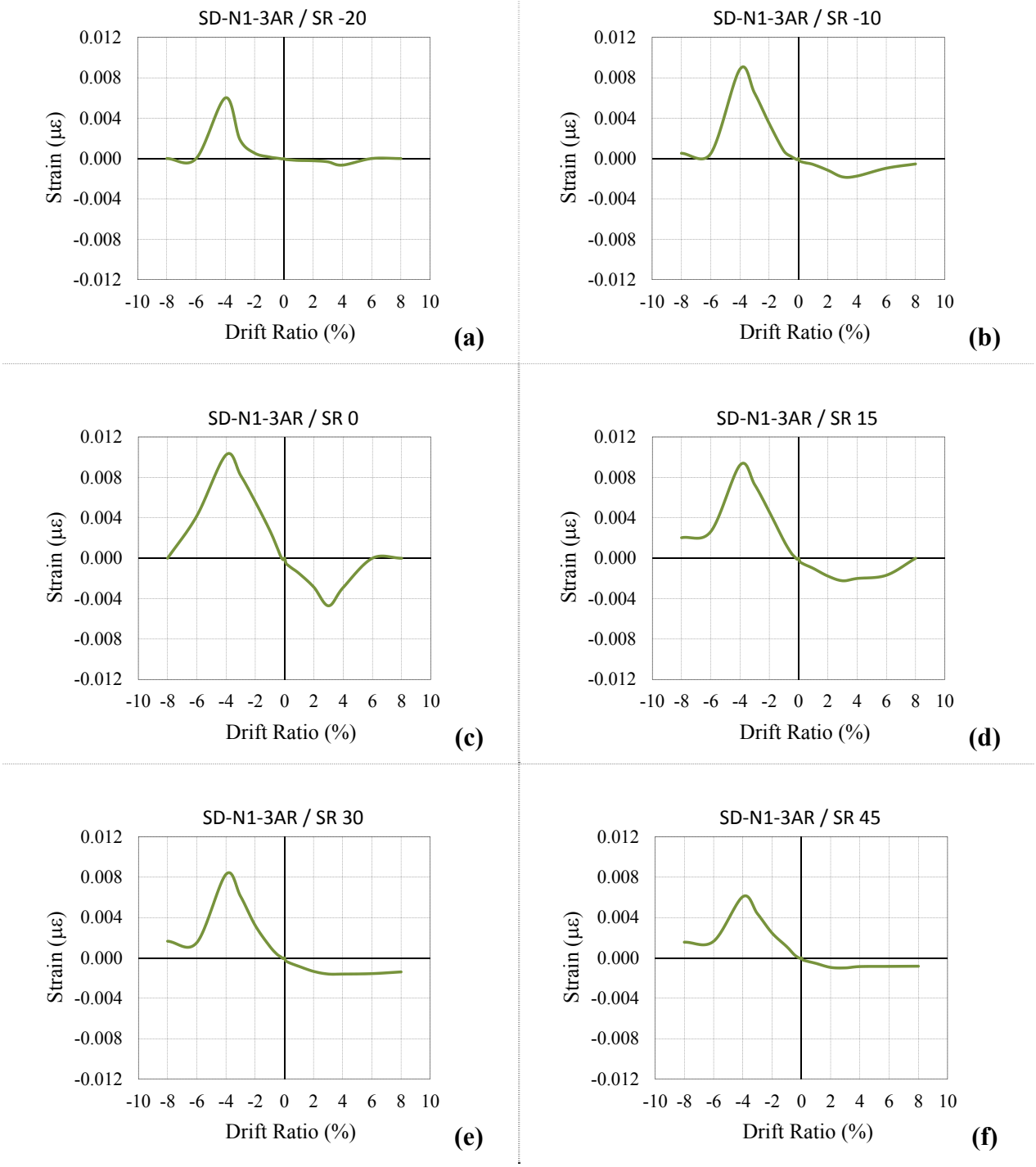

Figure C.5 : Average strain distribution of longitudinal steel reinforcement of specimen SD-N1-3AR: (a)At -20 cm. (b)At -10 cm. (c)At 0 cm. (d)At 15 cm. (e)At 30 cm. (f)At 45 cm.

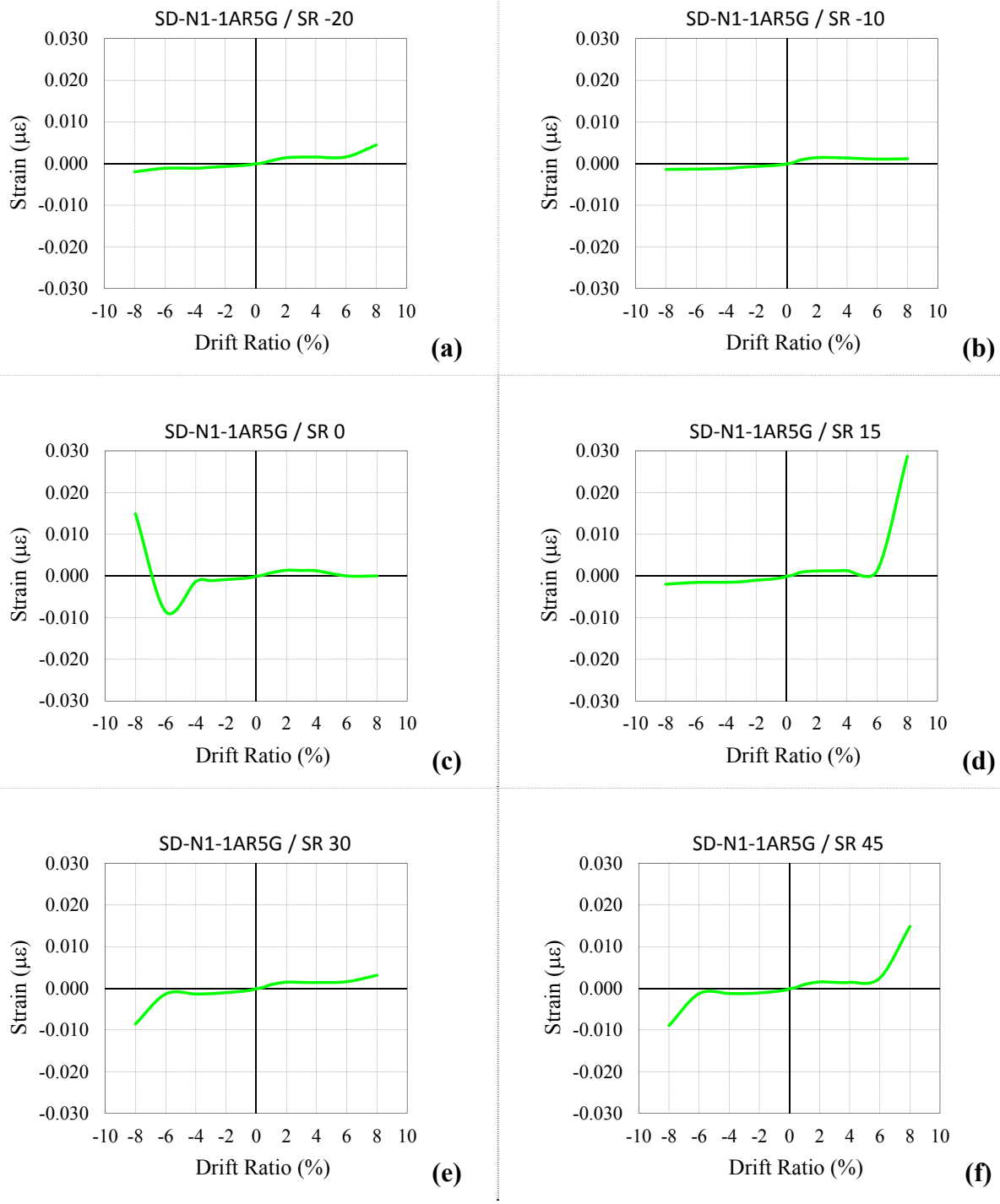

Figure C.6 : Average strain distribution of longitudinal steel reinforcement of specimen SD-N1-1AR5G: (a)At -20 cm. (b)At -10 cm. (c)At 0 cm. (d)At 15 cm. (e)At 30 cm. (f)At 45 cm.

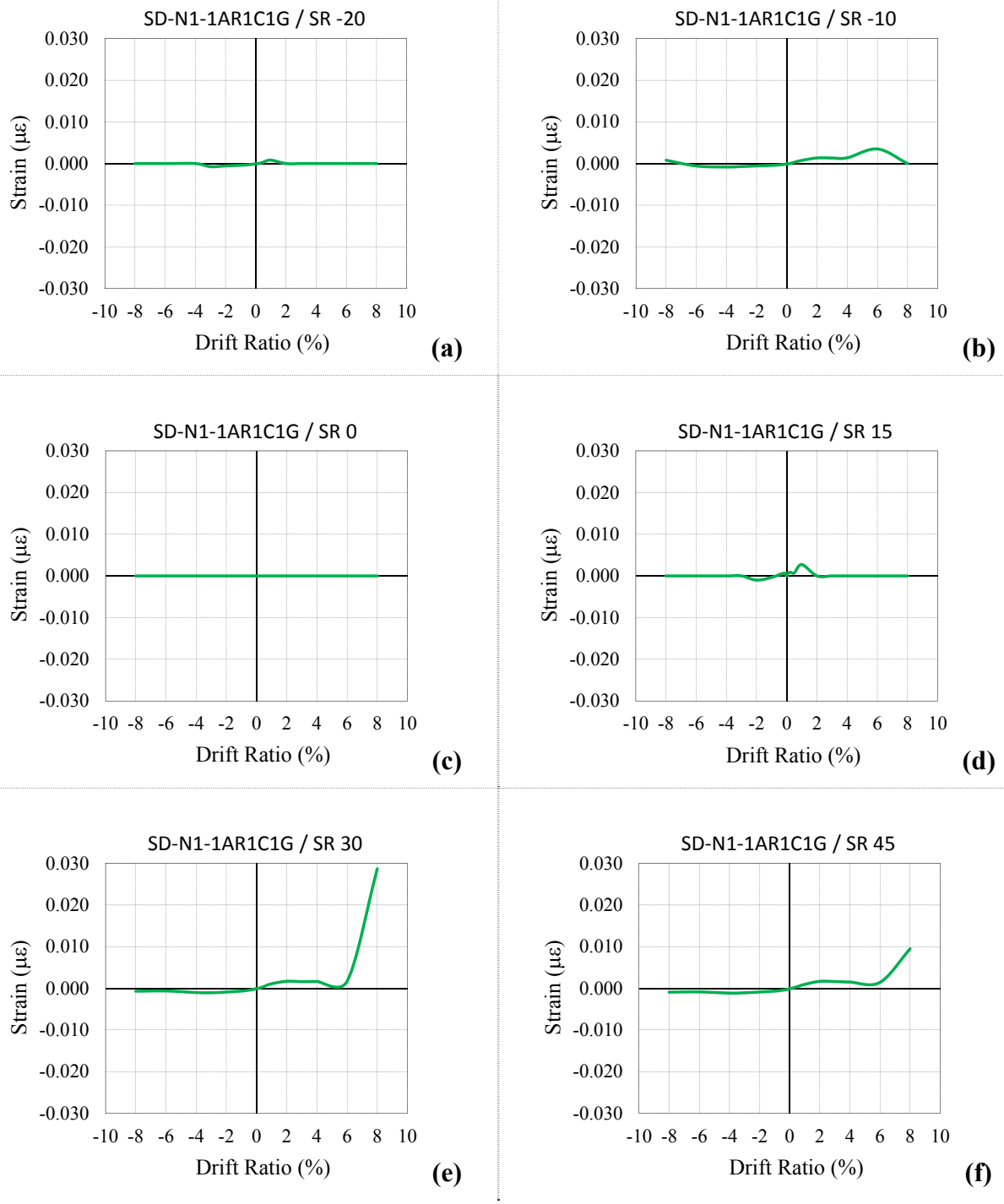

Figure C.7 : Average strain distribution of longitudinal steel reinforcement of specimen SD-N1-1AR1C1G: (a)At -20 cm. (b)At -10 cm. (c)At 0 cm. (d)At 15 cm. (e)At 30 cm. (f)At 45 cm.

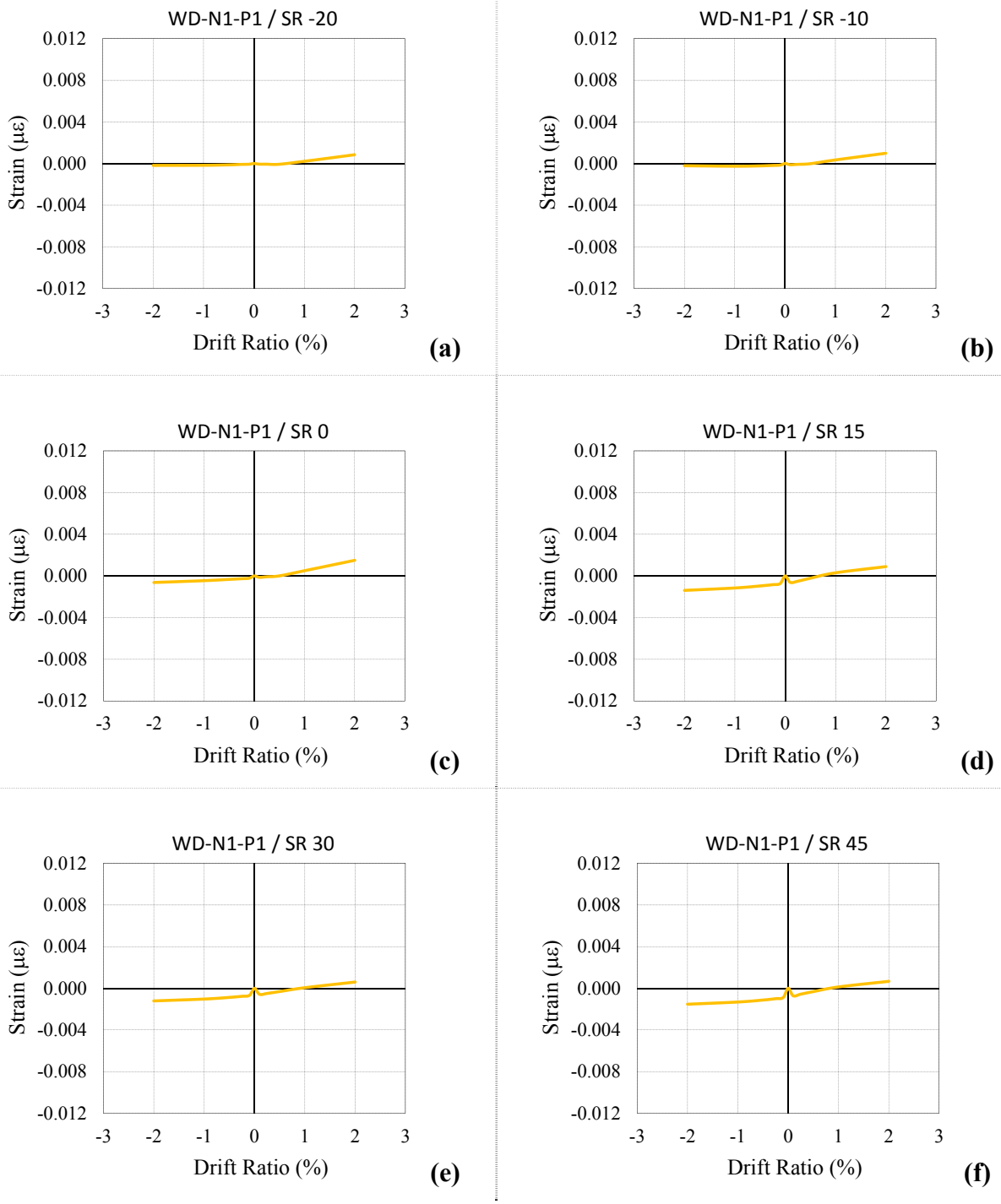

Figure C.8 : Average strain distribution of longitudinal steel reinforcement of specimen WD-N1-P1: (a)At -20 cm. (b)At -10 cm. (c)At 0 cm. (d)At 15 cm. (e)At 30 cm. (f)At 45 cm.

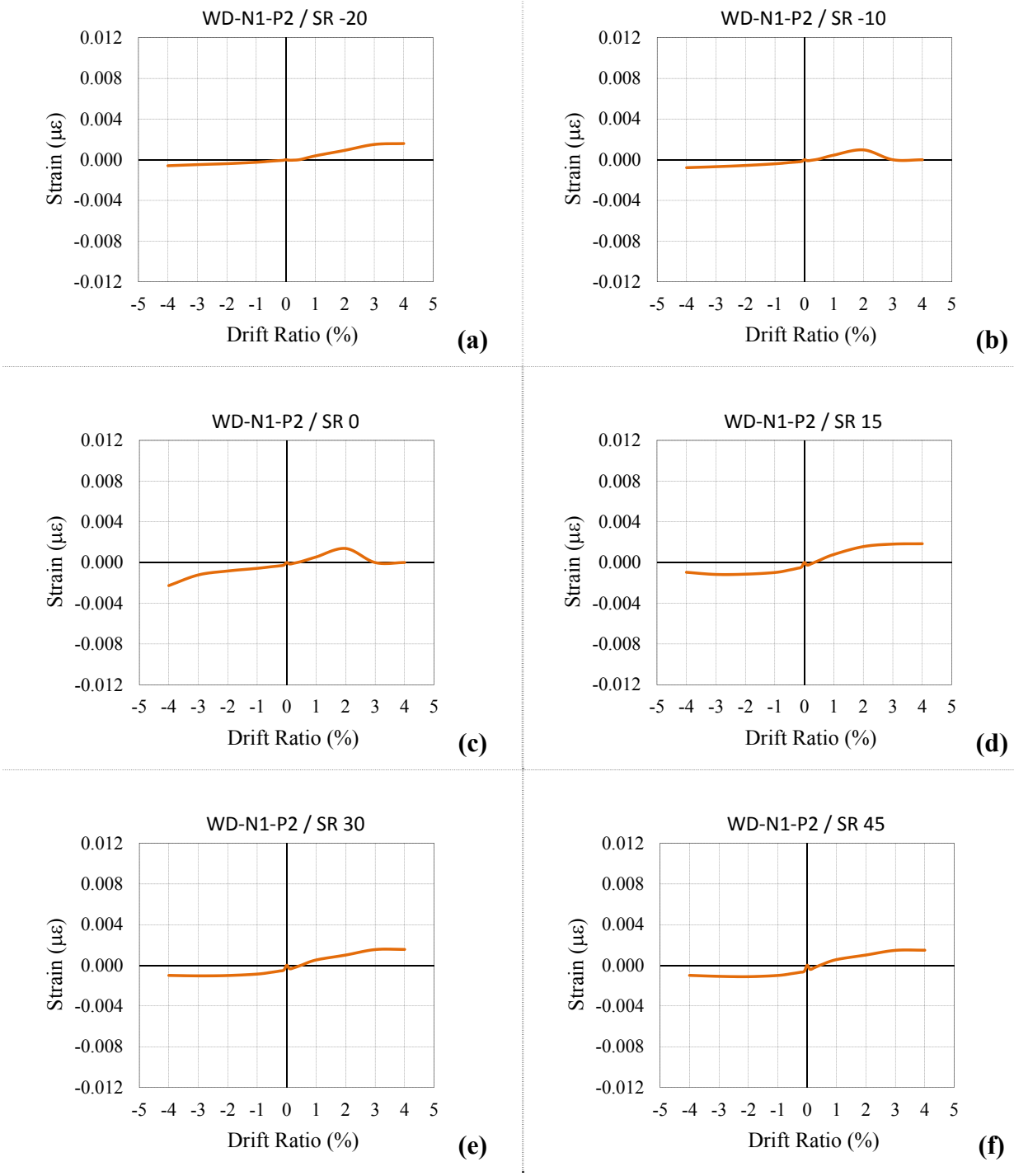

Figure C.9 : Average strain distribution of longitudinal steel reinforcement of specimen WD-N1-P2: (a)At -20 cm. (b)At -10 cm. (c)At 0 cm. (d)At 15 cm. (e)At 30 cm. (f)At 45 cm.

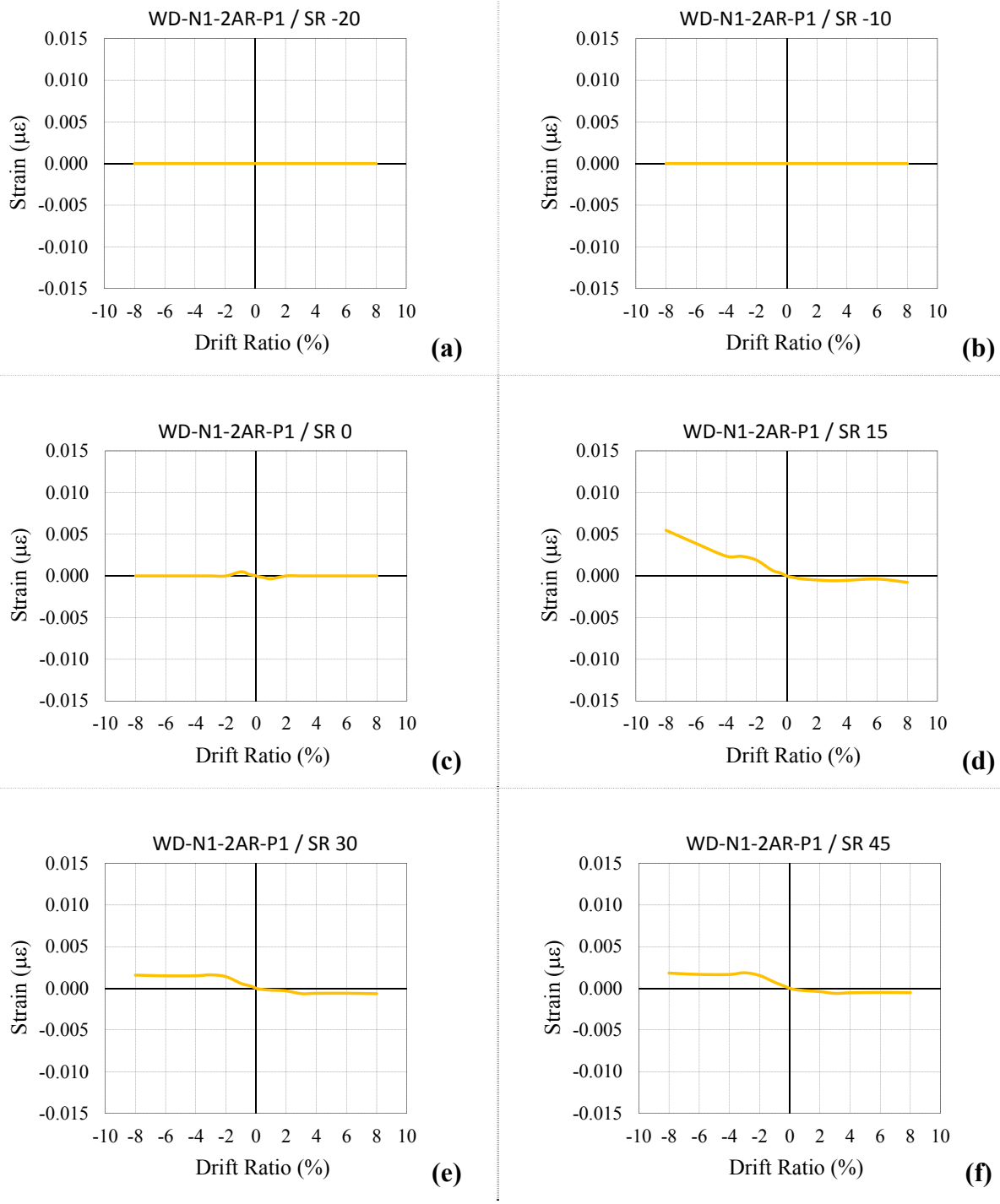

Figure C.10 : Average strain distribution of longitudinal steel reinforcement of specimen WD-N1-2AR-P1: (a)At -20 cm. (b)At -10 cm. (c)At 0 cm. (d)At 15 cm. (e)At 30 cm. (f)At 45 cm.

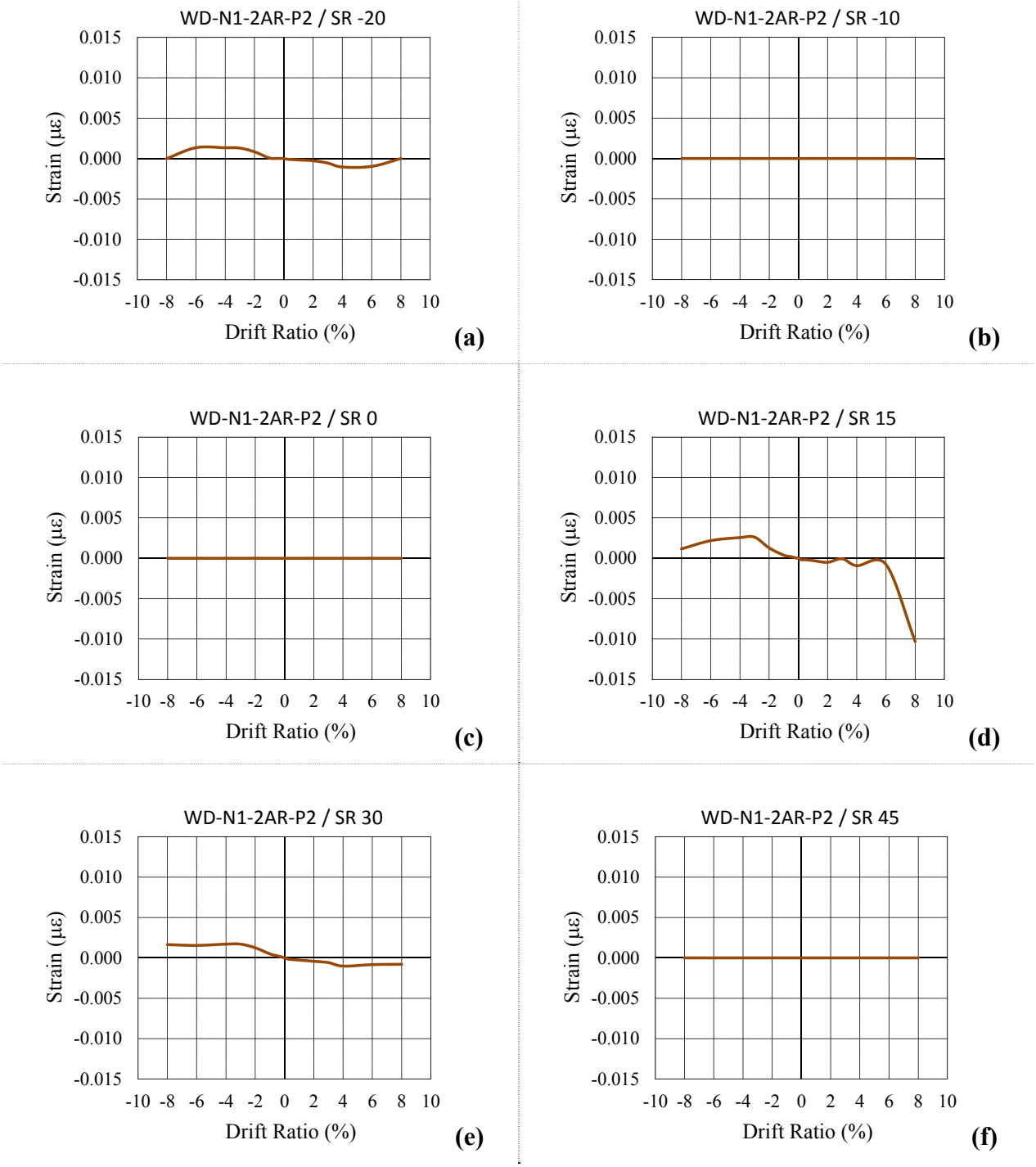

Figure C.11 : Average strain distribution of longitudinal steel reinforcement of specimen WD-N1-2AR-P2: (a)At -20 cm. (b)At -10 cm. (c)At 0 cm. (d)At 15 cm. (e)At 30 cm. (f)At 45 cm.

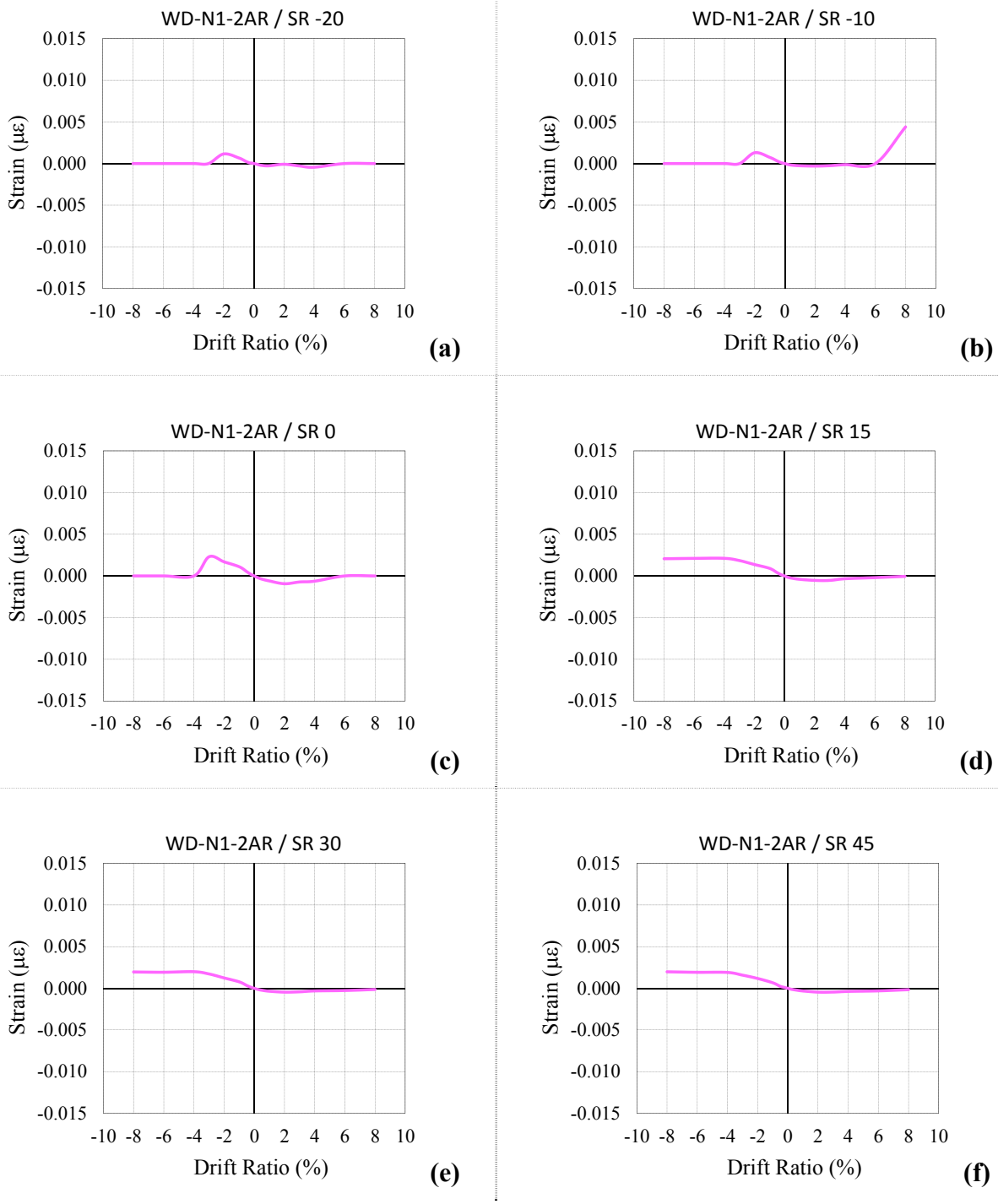

Figure C.12 : Average strain distribution of longitudinal steel reinforcement of specimen WD-N1-2AR: (a)At -20 cm. (b)At -10 cm. (c)At 0 cm. (d)At 15 cm. (e)At 30 cm. (f)At 45 cm.

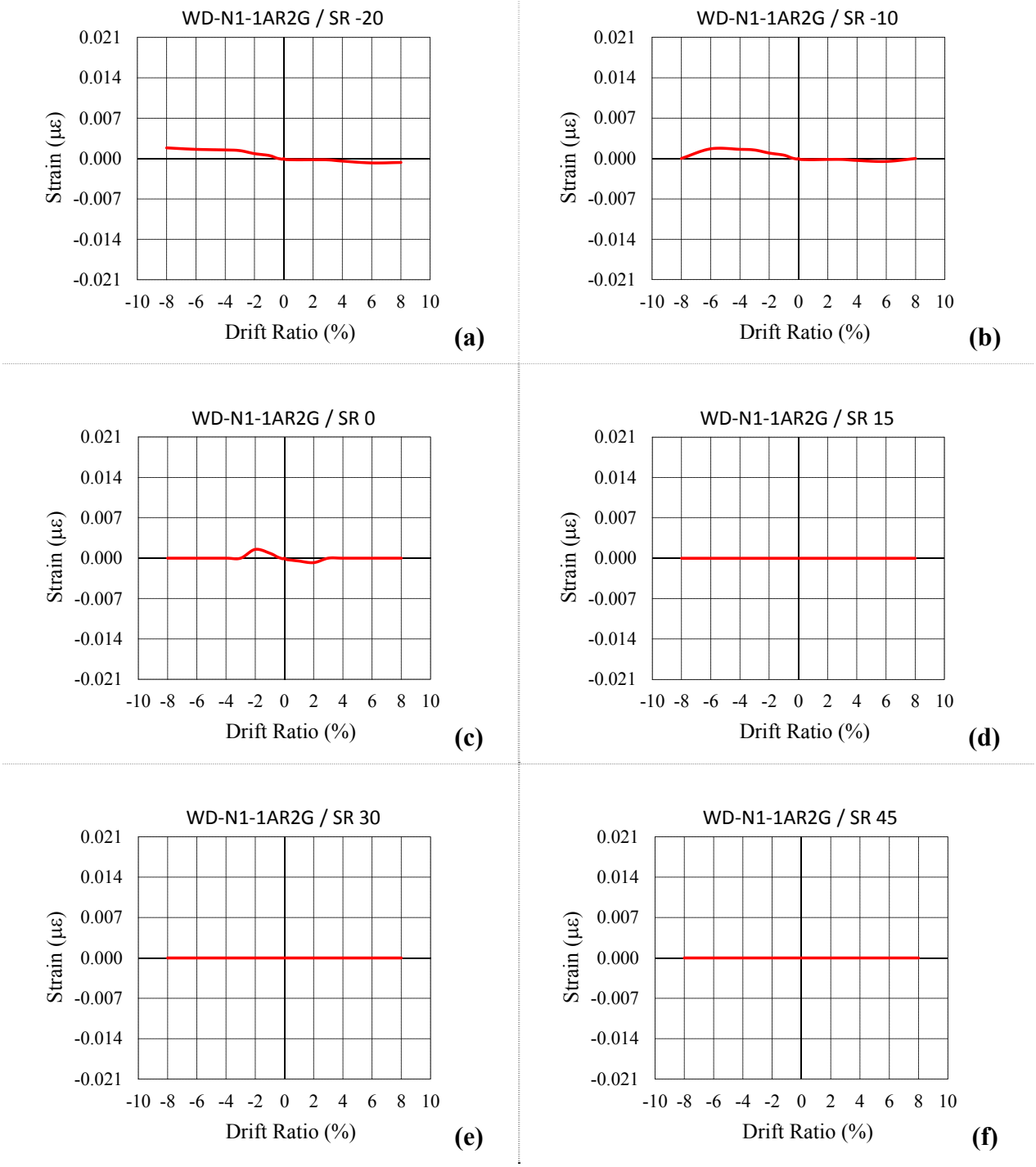

Figure C.13 : Average strain distribution of longitudinal steel reinforcement of specimen WD-N1-1AR2G: (a)At -20 cm. (b)At -10 cm. (c)At 0 cm. (d)At 15 cm. (e)At 30 cm. (f)At 45 cm.

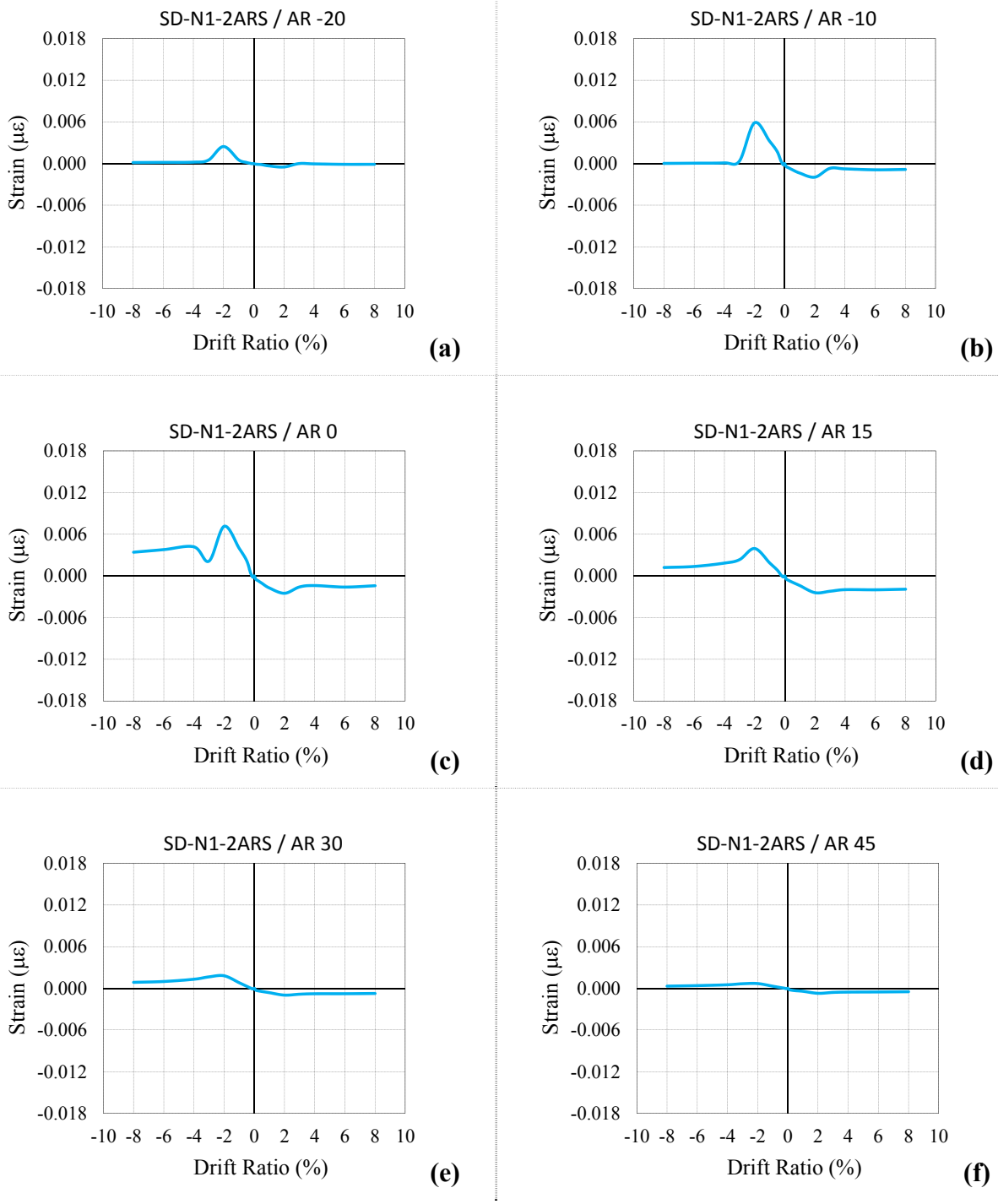

Figure C.14 : Average strain distribution of longitudinal AFRP reinforcement of specimen SD-N1-2ARS: (a)At -20 cm. (b)At -10 cm. (c)At 0 cm. (d)At 15 cm. (e)At 30 cm. (f)At 45 cm.

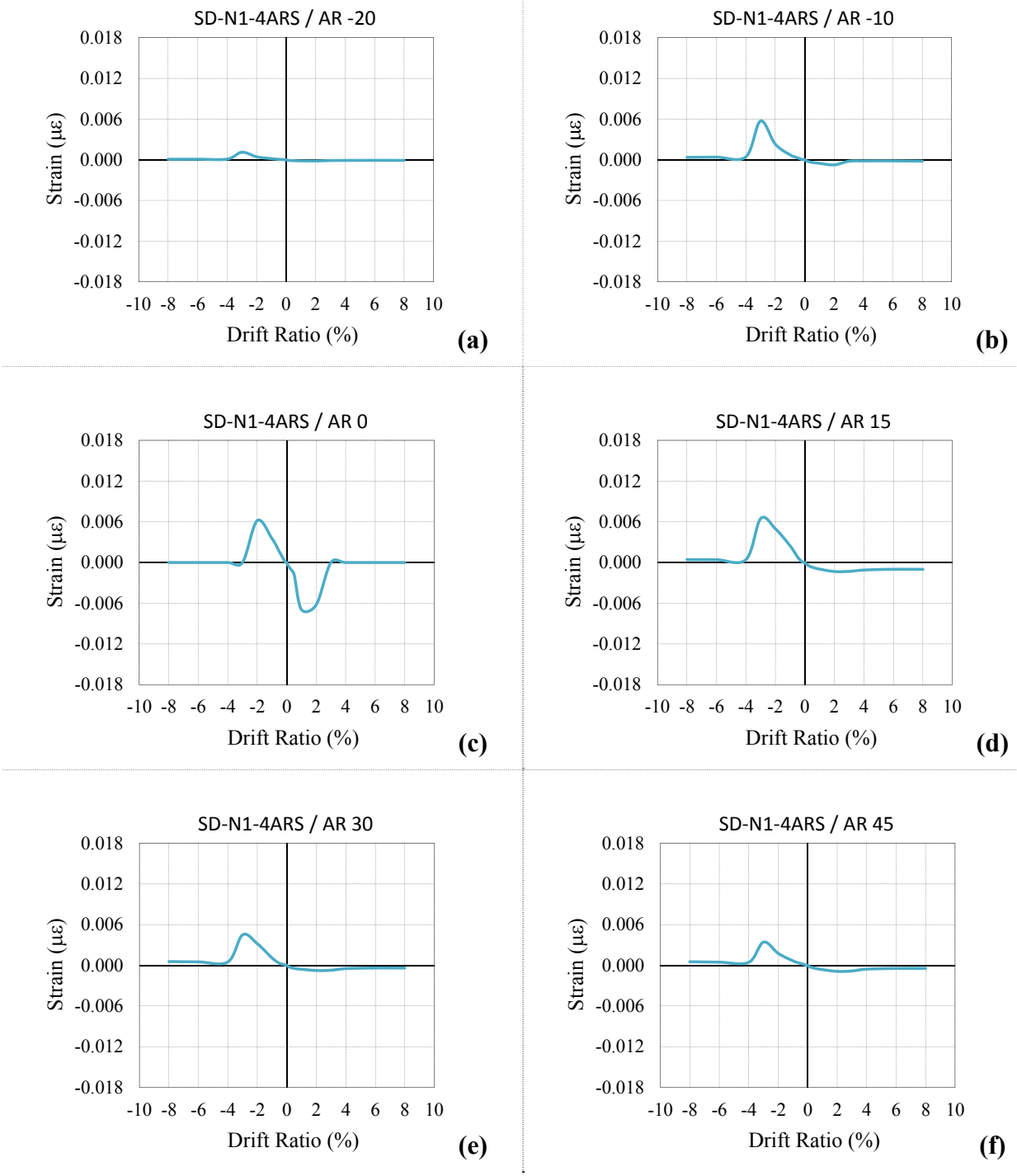

Figure C.15 : Average strain distribution of longitudinal AFRP reinforcement of specimen SD-N1-4ARS: (a)At -20 cm. (b)At -10 cm. (c)At 0 cm. (d)At 15 cm. (e)At 30 cm. (f)At 45 cm.

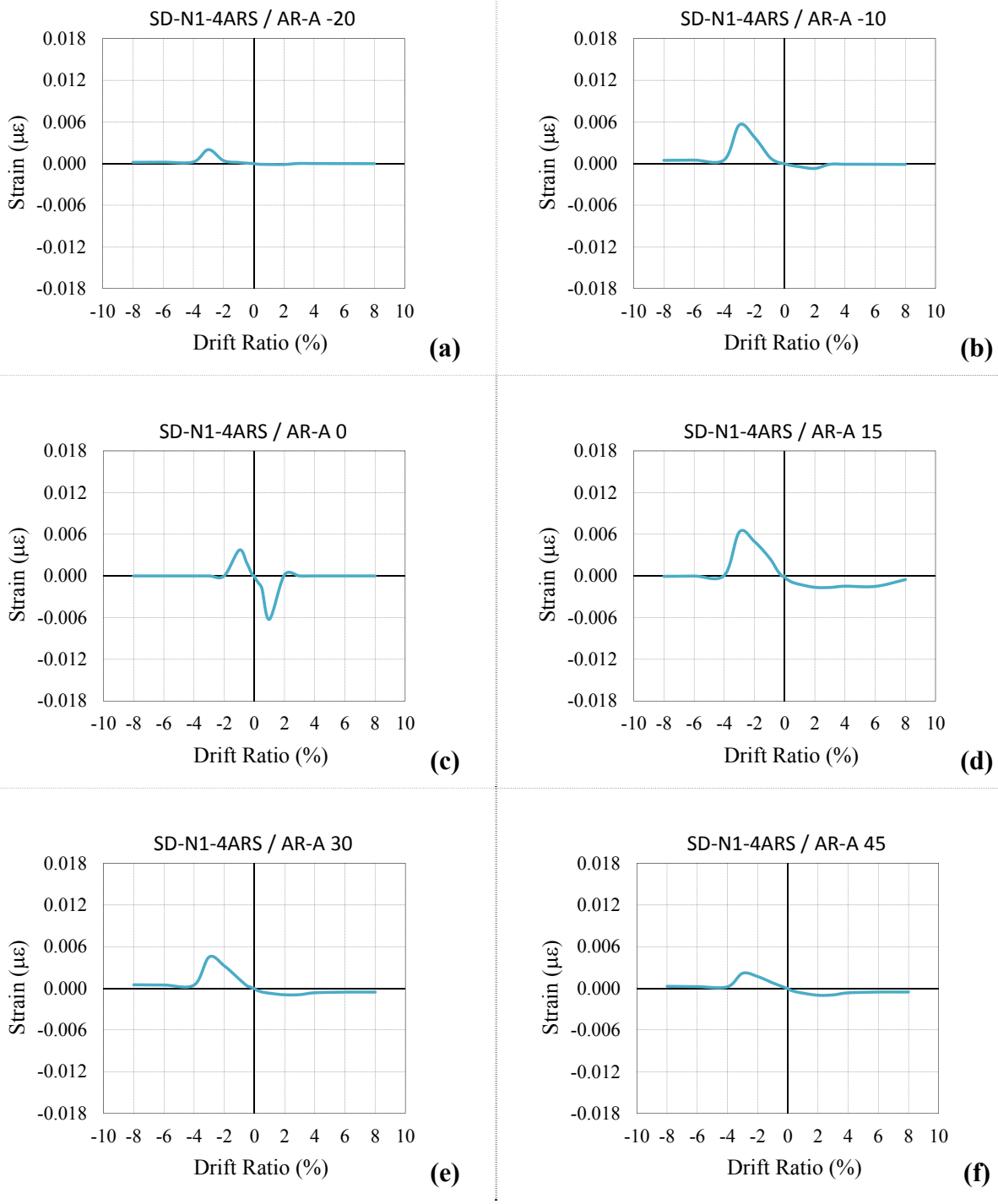

Figure C.16 : Average strain distribution of AFRP anchorage reinforcement of specimen SD-N1-4ARS: (a)At -20 cm. (b)At -10 cm. (c)At 0 cm. (d)At 15 cm. (e)At 30 cm. (f)At 45 cm.

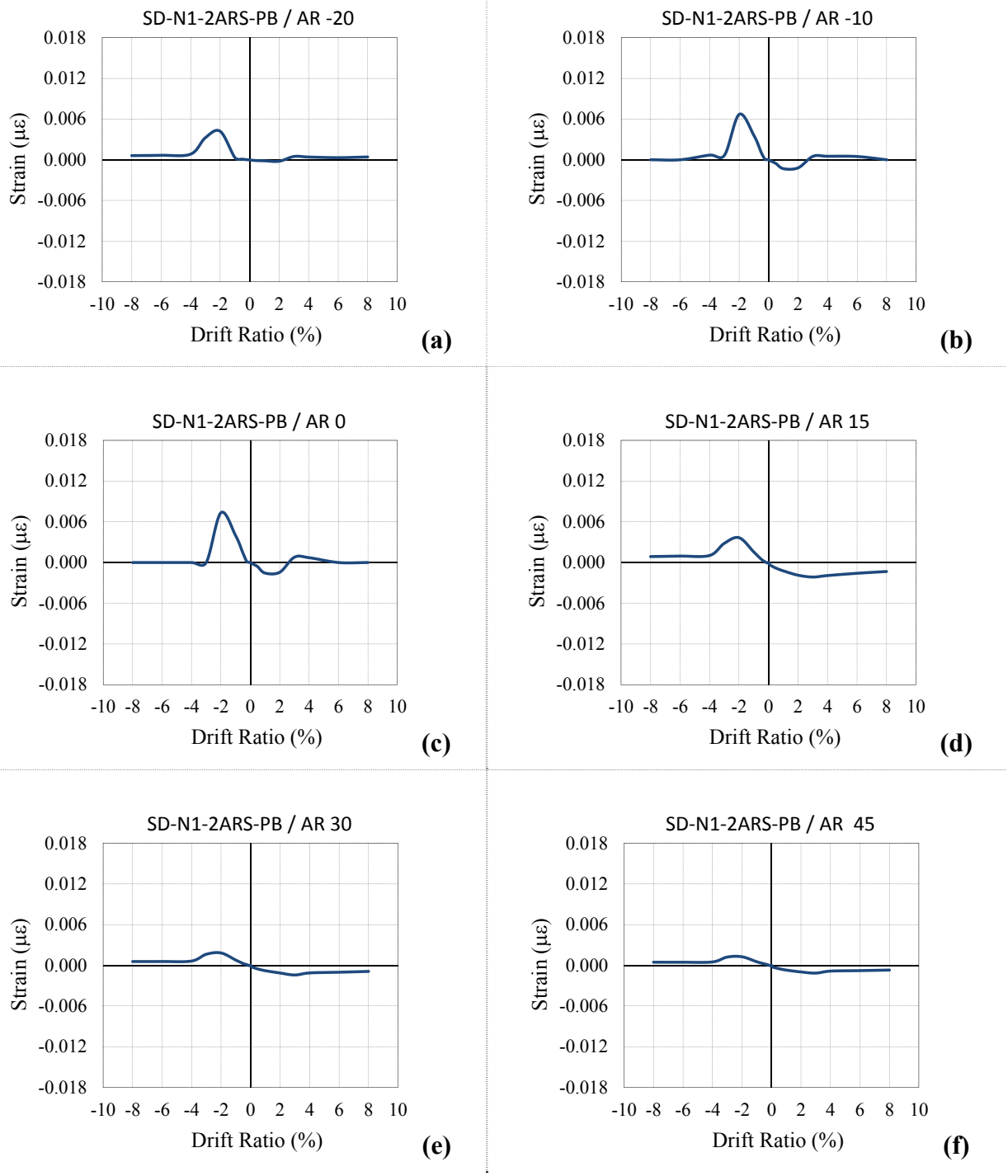

Figure C.17 : Average strain distribution of longitudinal AFRP reinforcement of specimen SD-N1-2ARS-PB: (a)At -20 cm. (b)At -10 cm. (c)At 0 cm. (d)At 15 cm. (e)At 30 cm. (f)At 45 cm.

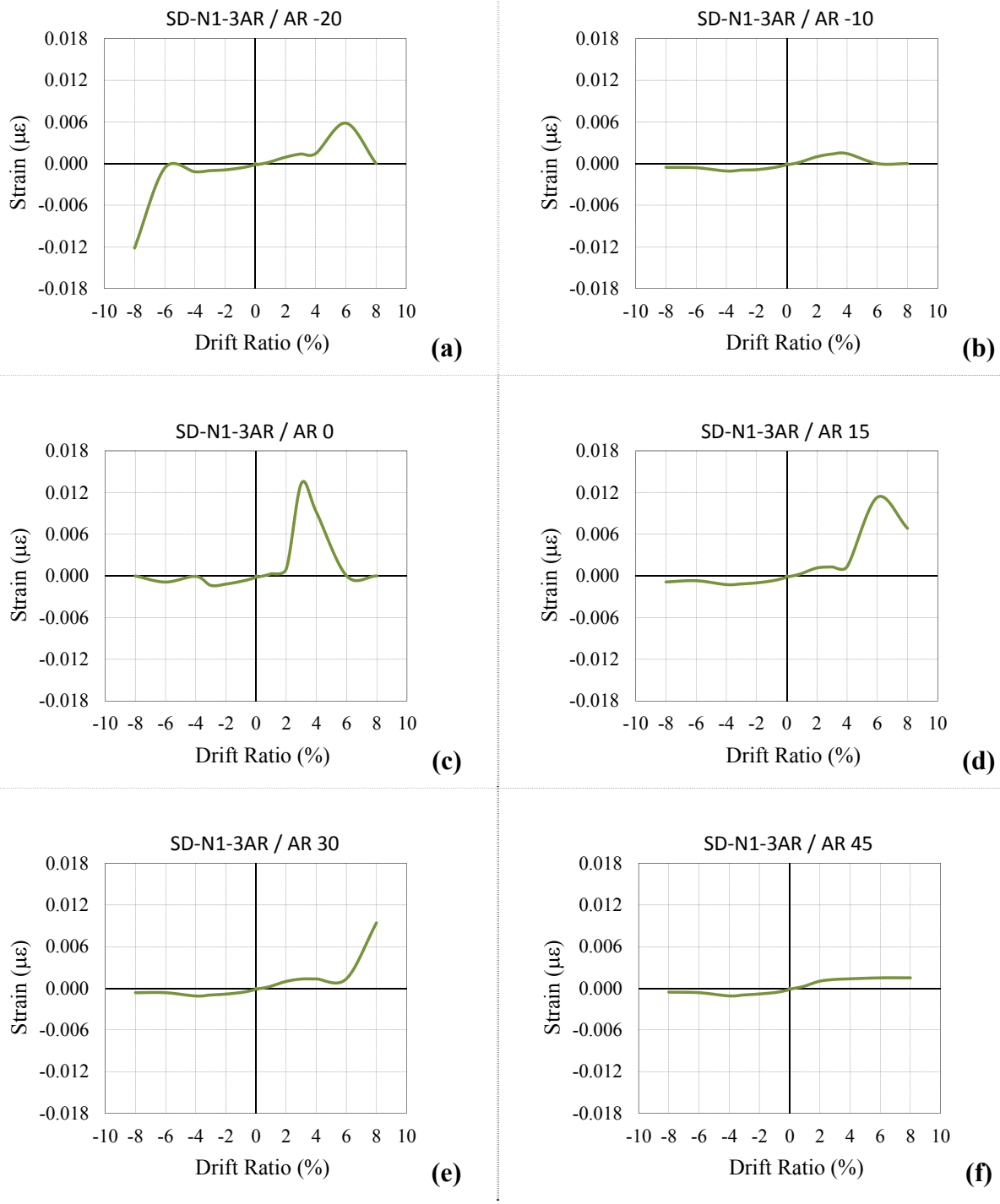

Figure C.18 : Average strain distribution of longitudinal AFRP reinforcement of specimen SD-N1-3AR: (a)At -20 cm. (b)At -10 cm. (c)At 0 cm. (d)At 15 cm. (e)At 30 cm. (f)At 45 cm.

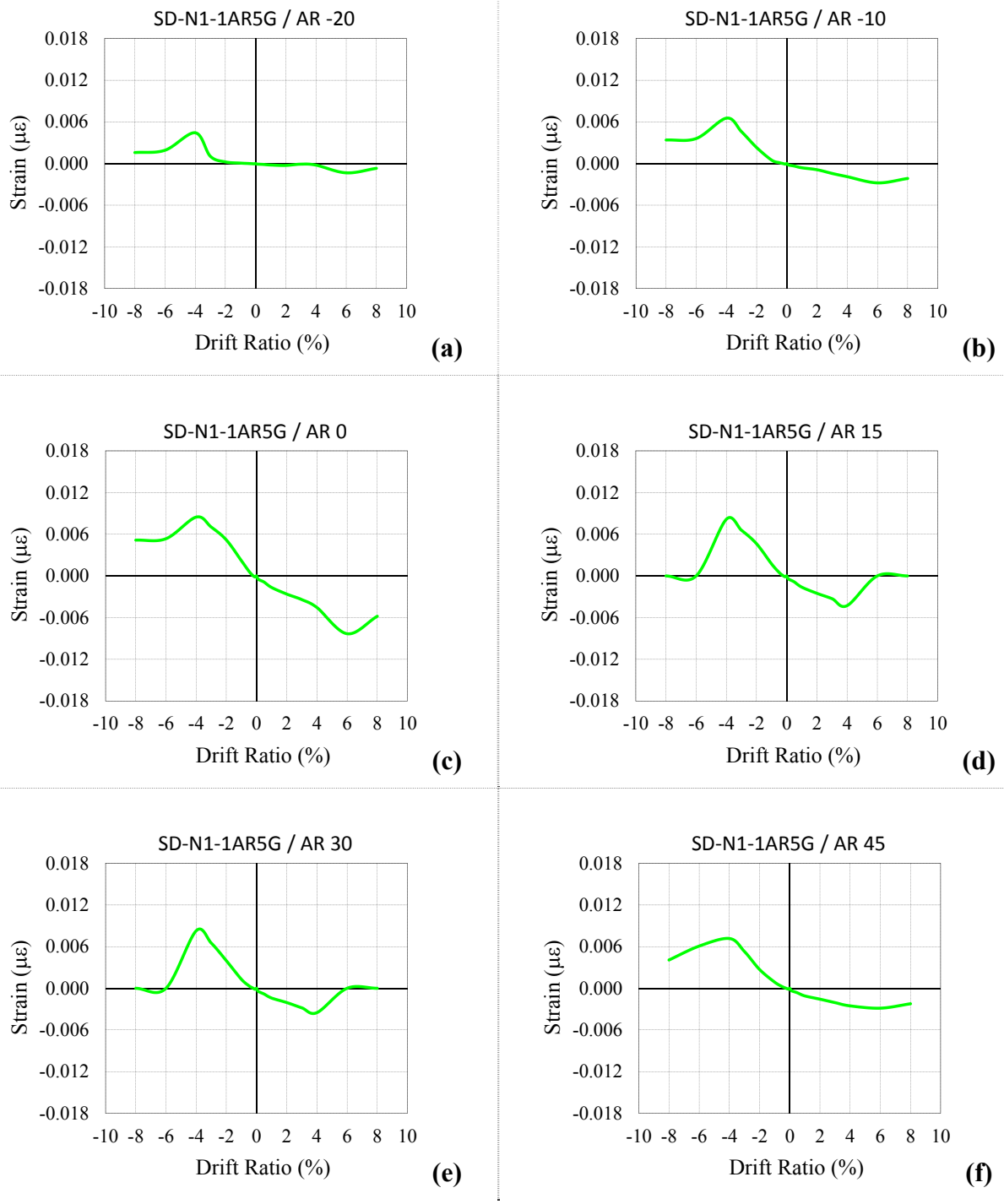

Figure C.19 : Average strain distribution of longitudinal AFRP reinforcement of specimen SD-N1-1AR5G: (a)At -20 cm. (b)At -10 cm. (c)At 0 cm. (d)At 15 cm. (e)At 30 cm. (f)At 45 cm.

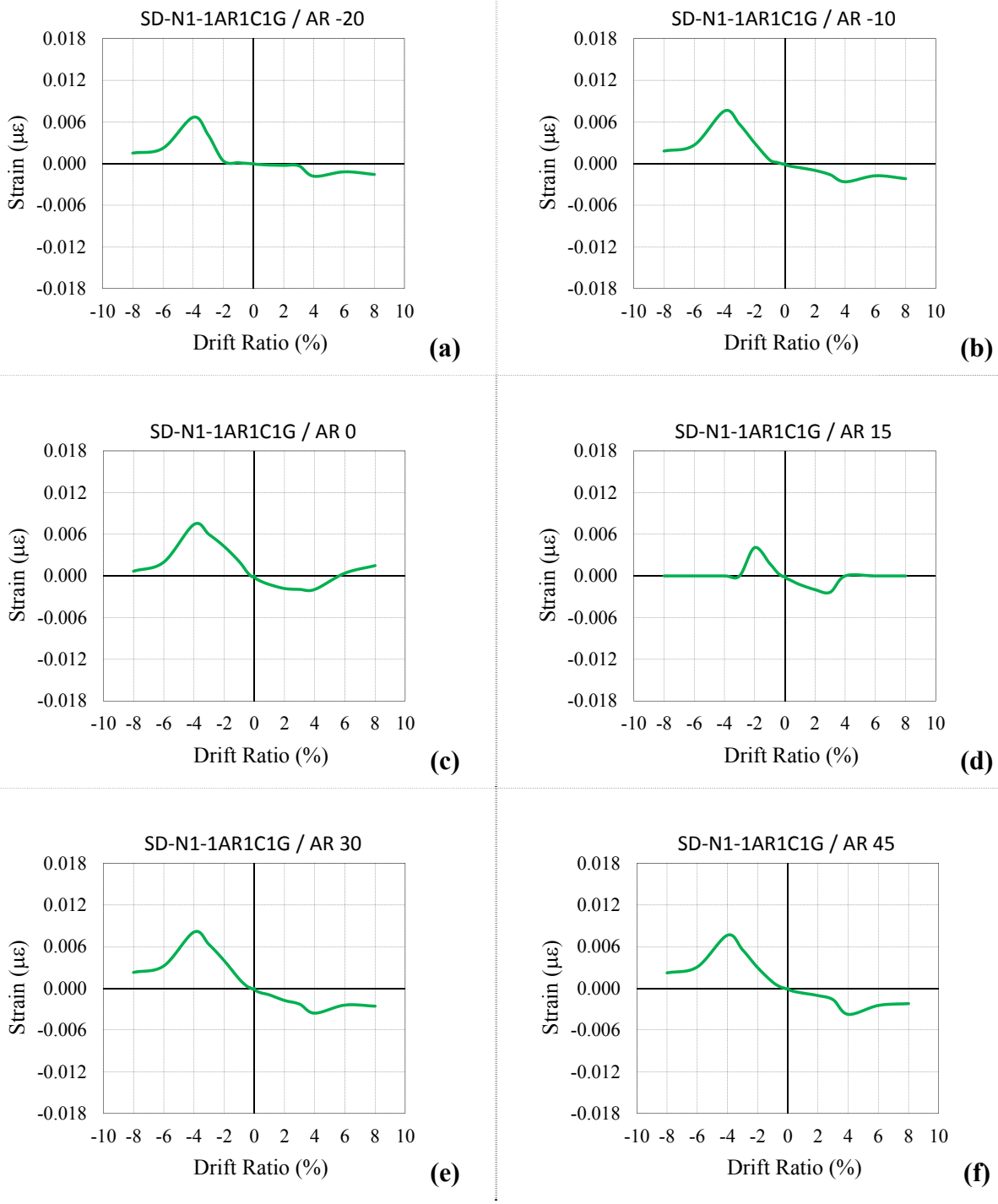

Figure C.20 : Average strain distribution of longitudinal AFRP reinforcement of specimen SD-N1-1AR1C1G: (a)At -20 cm. (b)At -10 cm. (c)At 0 cm. (d)At 15 cm. (e)At 30 cm. (f)At 45 cm.

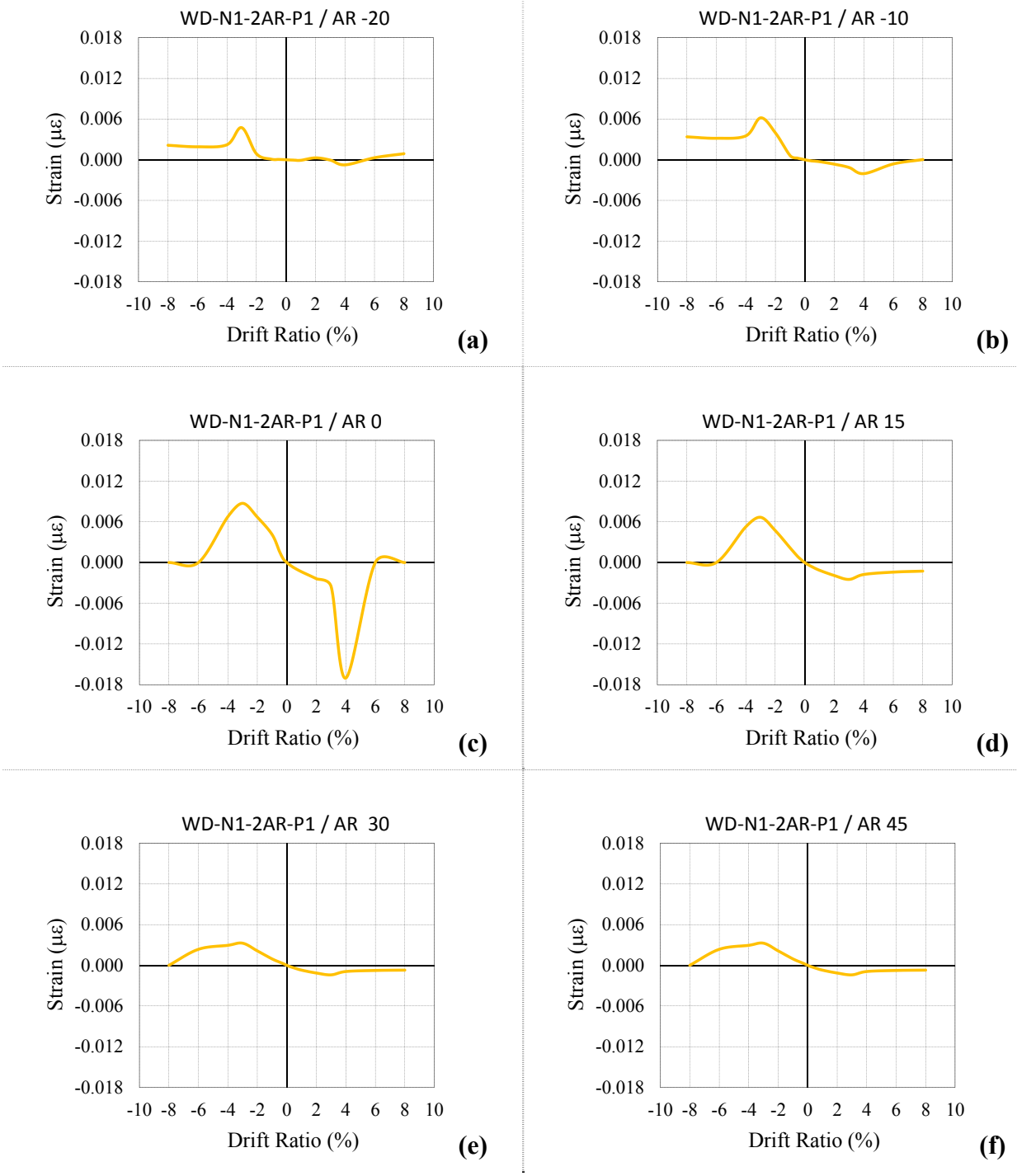

Figure C.21 : Average strain distribution of longitudinal AFRP reinforcement of specimen WD-N1-2AR-P1: (a)At -20 cm. (b)At -10 cm. (c)At 0 cm. (d)At 15 cm. (e)At 30 cm. (f)At 45 cm.

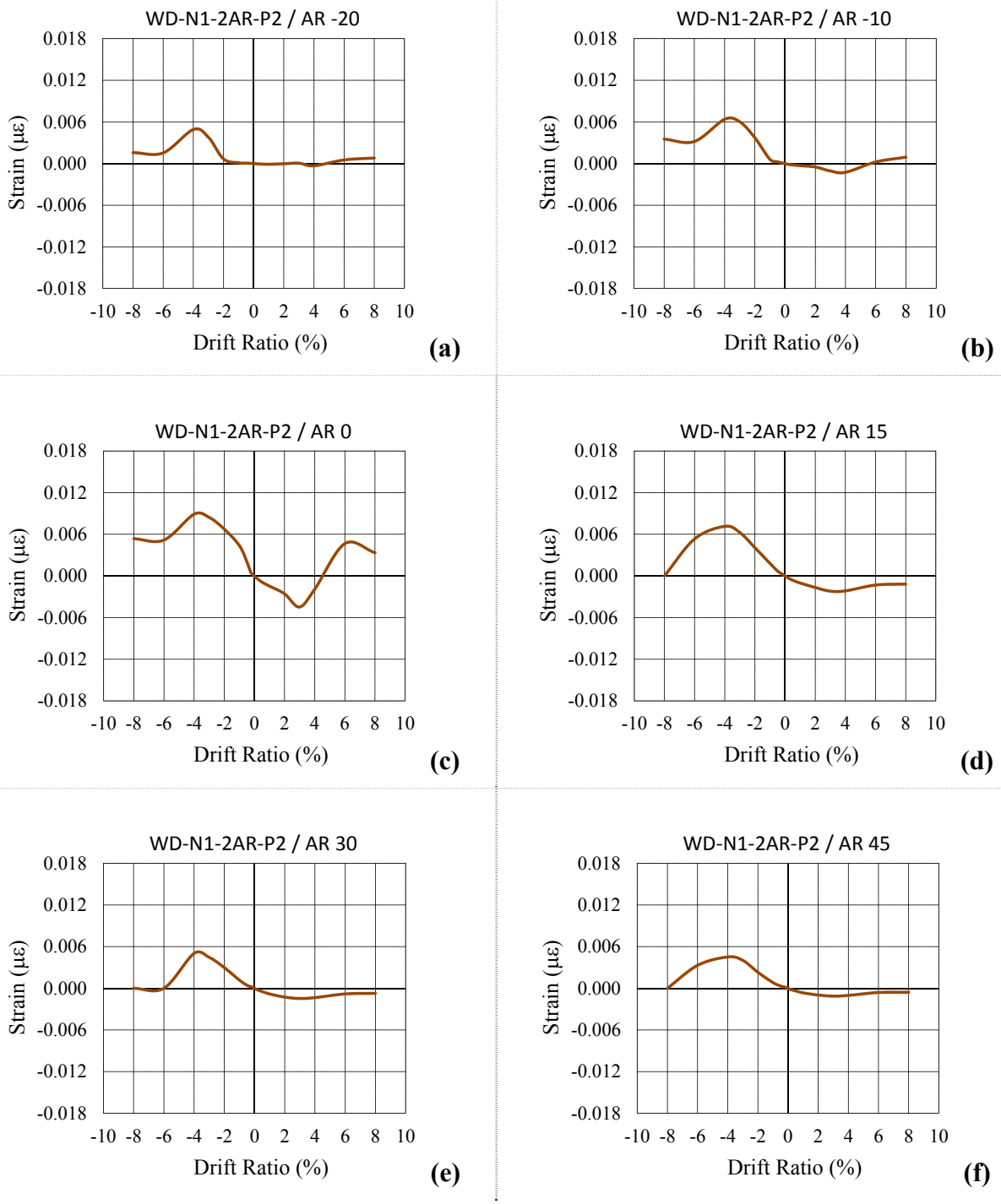

Figure C.22 : Average strain distribution of longitudinal AFRP reinforcement of specimen WD-N1-2AR-P2: (a)At -20 cm. (b)At -10 cm. (c)At 0 cm. (d)At 15 cm. (e)At 30 cm. (f)At 45 cm.

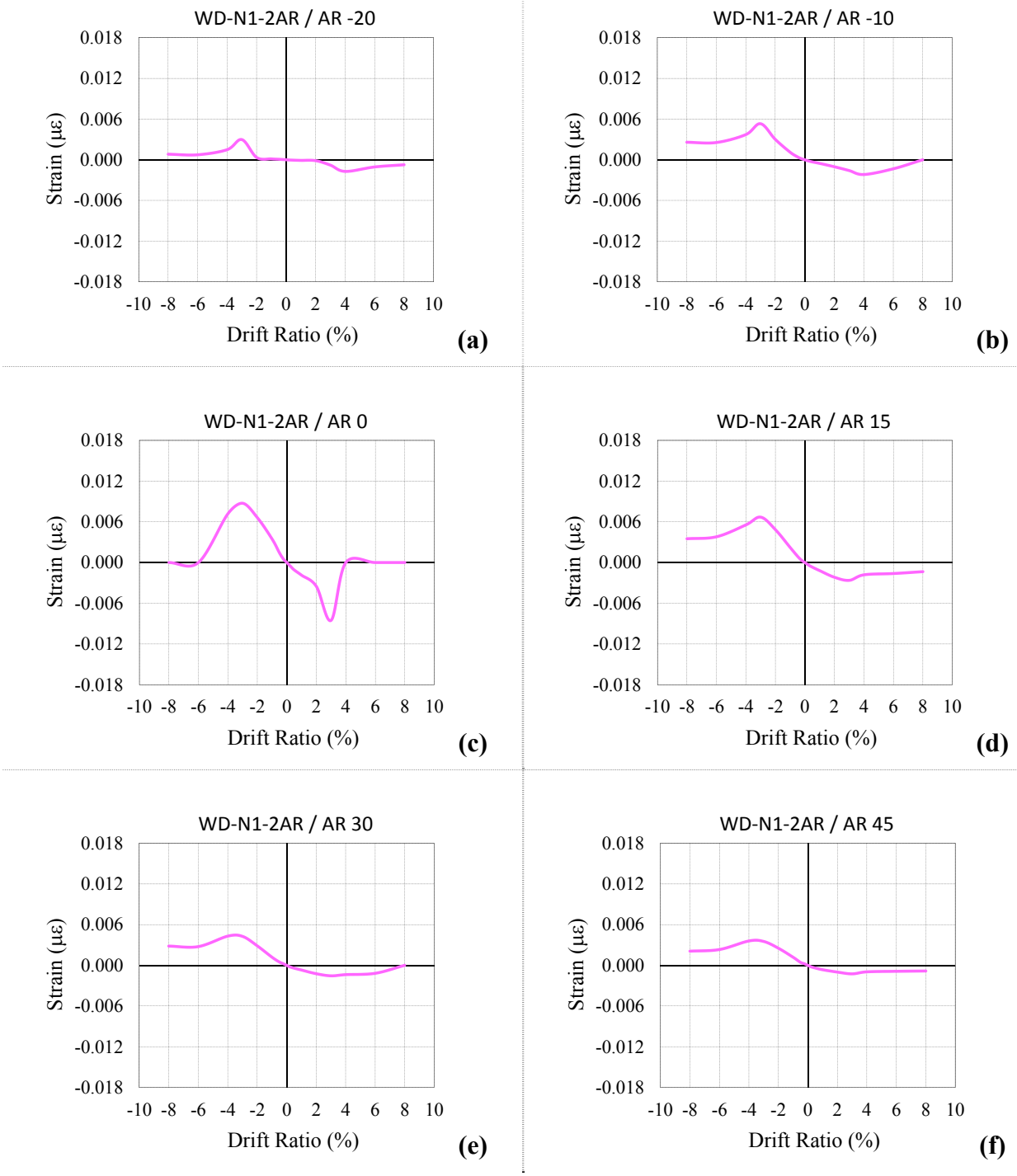

Figure C.23 : Average strain distribution of longitudinal AFRP reinforcement of specimen WD-N1-2AR: (a)At -20 cm. (b)At -10 cm. (c)At 0 cm. (d)At 15 cm. (e)At 30 cm. (f)At 45 cm.

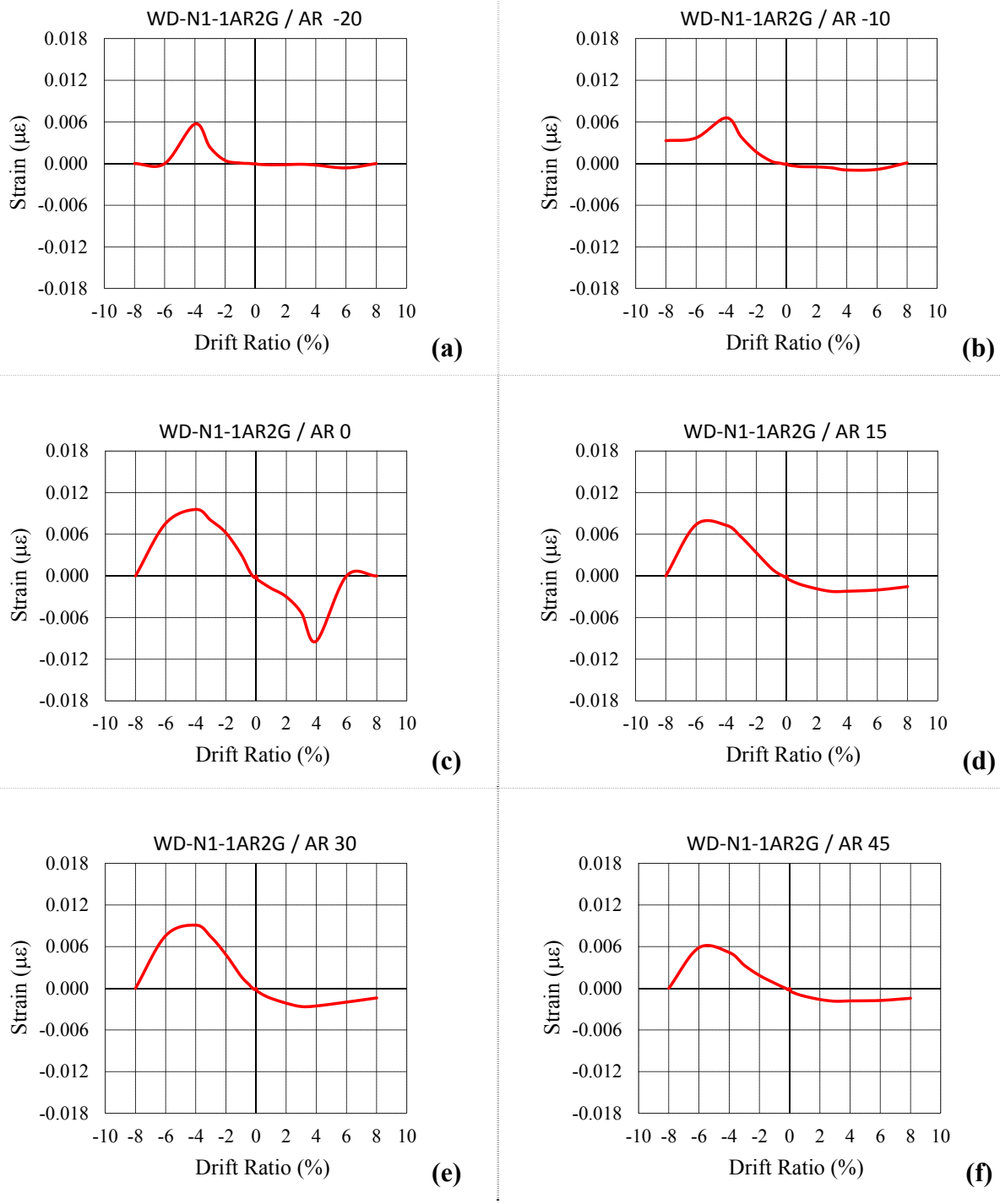

Figure C.24 : Average strain distribution of longitudinal AFRP reinforcement of specimen WD-N1-1AR2G: (a)At -20 cm. (b)At -10 cm. (c)At 0 cm. (d)At 15 cm. (e)At 30 cm. (f)At 45 cm.

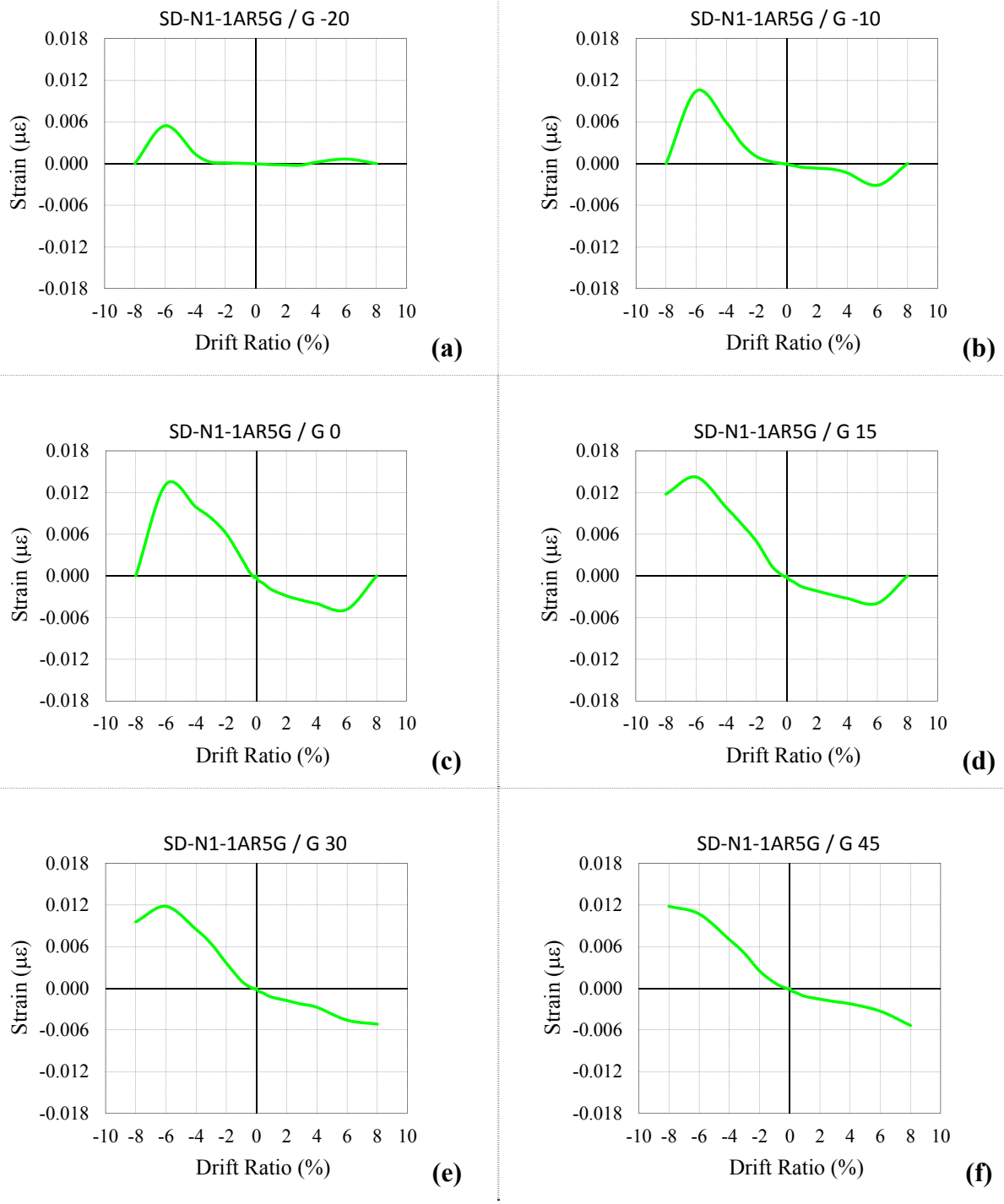

Figure C.25 : Average strain distribution of longitudinal GFRP reinforcement of specimen SD-N1-1AR5G: (a)At -20 cm. (b)At -10 cm. (c)At 0 cm. (d)At 15 cm. (e)At 30 cm. (f)At 45 cm.

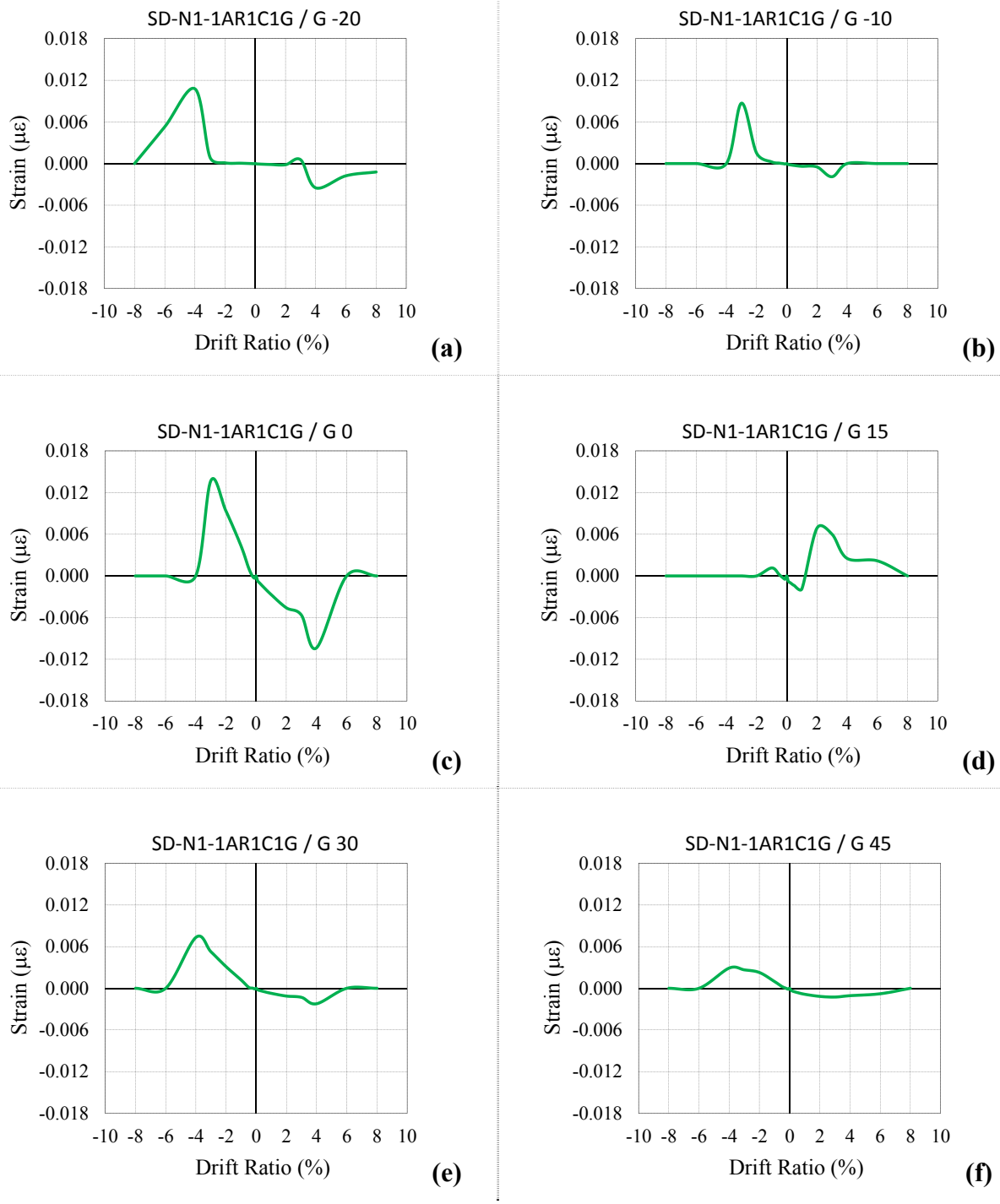

Figure C.26 : Average strain distribution of longitudinal GFRP reinforcement of specimen SD-N1-1AR1C1G: (a)At -20 cm. (b)At -10 cm. (c)At 0 cm. (d)At 15 cm. (e)At 30 cm. (f)At 45 cm.

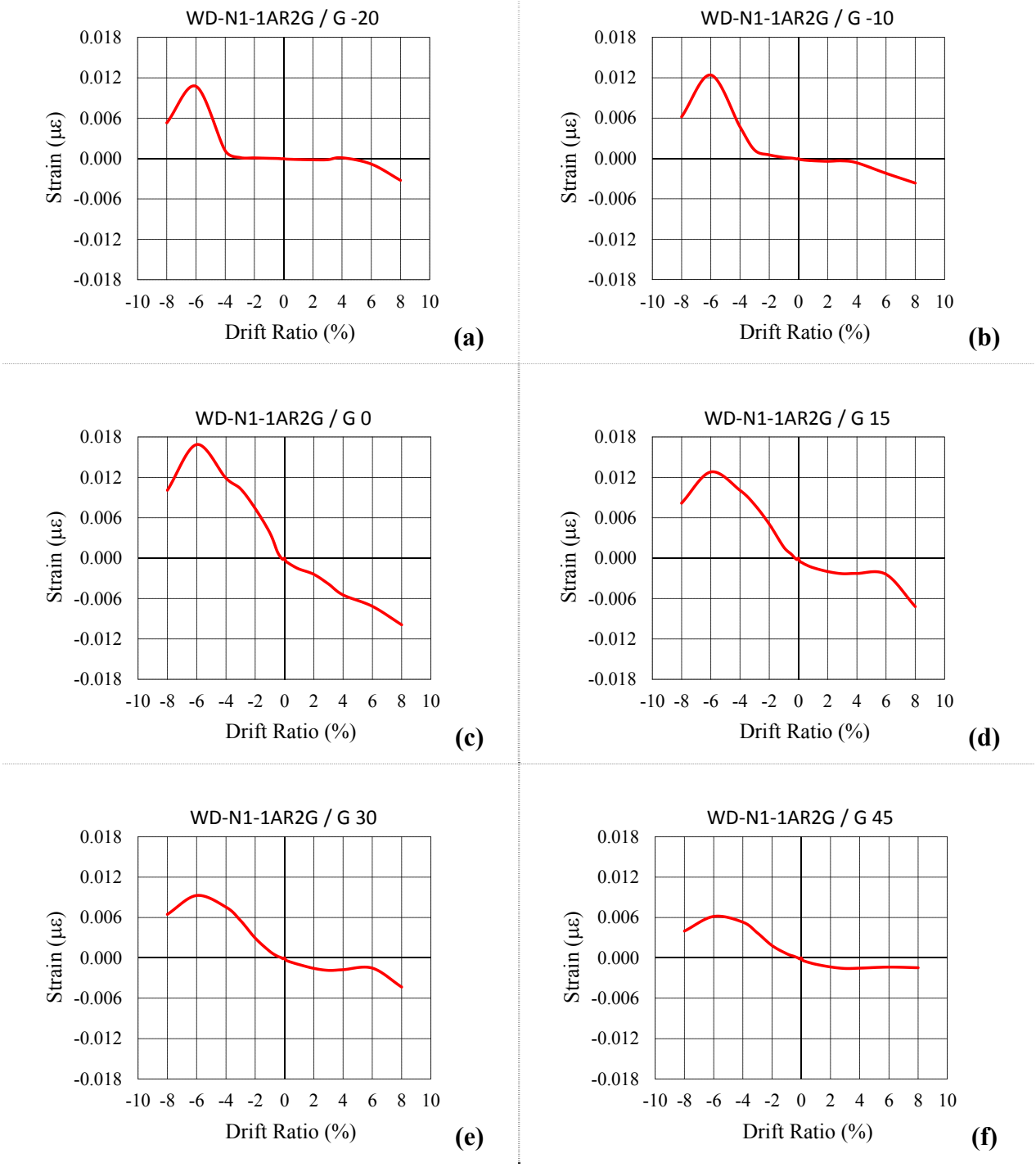

Figure C.27 : Average strain distribution of longitudinal GFRP reinforcement of specimen WD-N1-1AR2G: (a)At -20 cm. (b)At -10 cm. (c)At 0 cm. (d)At 15 cm. (e)At 30 cm. (f)At 45 cm.

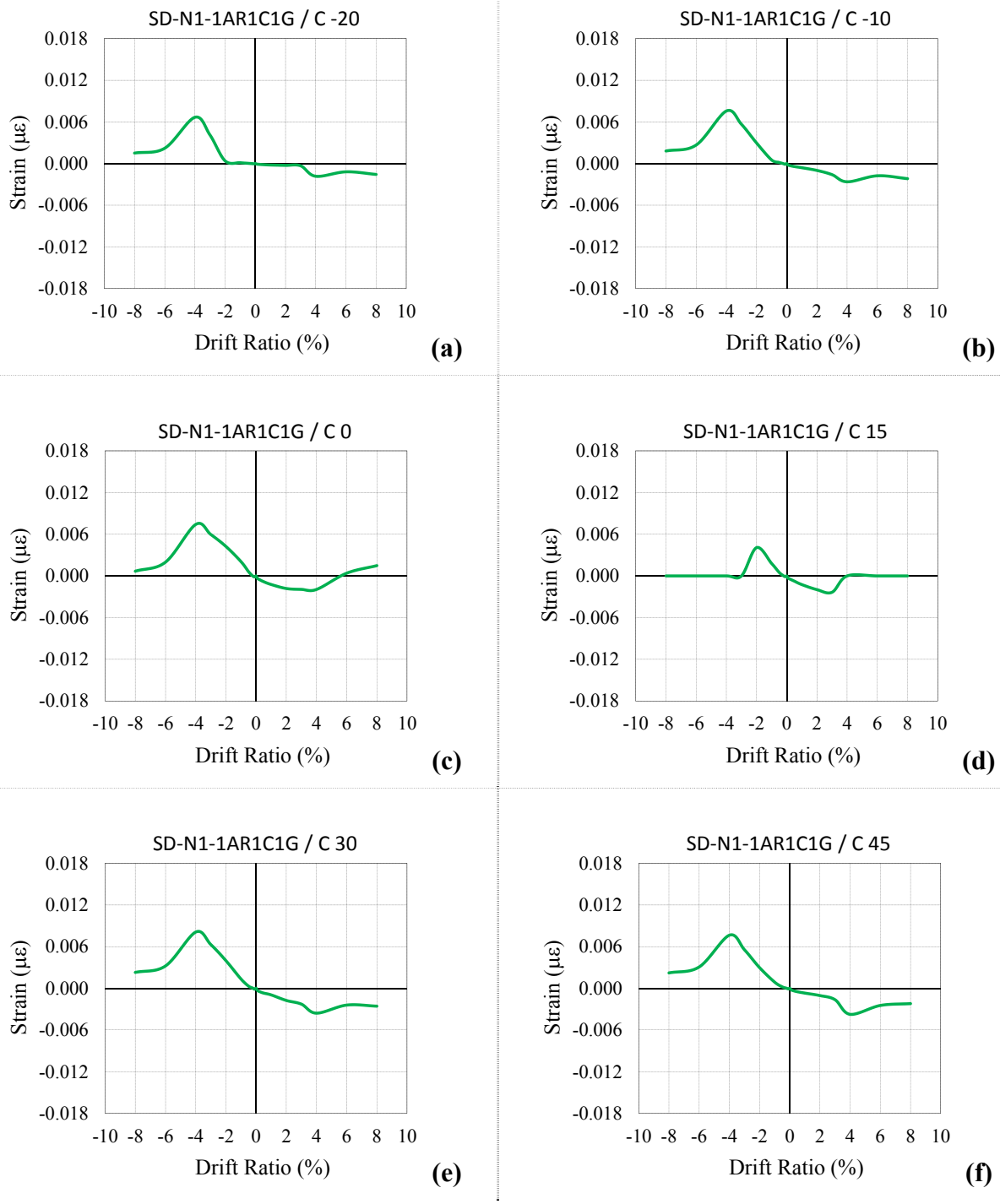

Figure C.28 : Average strain distribution of longitudinal CFRP reinforcement of specimen SD-N1-1AR1C1G: (a)At -20 cm. (b)At -10 cm. (c)At 0 cm. (d)At 15 cm. (e)At 30 cm. (f)At 45 cm.

APPENDIX D

Table D.1 : Characteristics of the construction materials used in the building.

Materials	Density (kN/m^3)	Thickness (m)	Weight (kN/m^2)
Reinforced Concrete	25	-	-
Render for walls	20	0.020	-
Brick mortar	20	0.010	-
Levelling mortar on slabs	16	0.050	-
PVC Flooring	16	0.002	-
Roofing	-	-	0.38
Brick-Exterior	19	0.200	-
Brick-Interior	17	0.100	-

Table D.2 : Dead loads and live loads subjected to the construction elements.

Elements	Height (m)	Width (m)	Depth (m)	Weight	Live Load	Snow Load	Unit
Walls - Exterior	2.4	-	0.20	11.52	-	-	kN/m
Walls - Interior	2.4	-	0.10	6.48	-	-	kN/m
Columns-40x40	3.0	0.40	0.40	12.00	-	-	kN
Columns-30x40	3.0	0.30	0.40	9.00	-	-	kN
Beams-25x60	-	0.25	0.60	3.75	-	-	kN/m
Slabs - Floors	-	-	0.12	3.83	2.00	-	kN/m^2
Slabs - Roof	-	-	0.10	2.88	1.50	0.75	kN/m^2
Stairs	-	-	0.18	4.50	3.50	-	kN/m^2

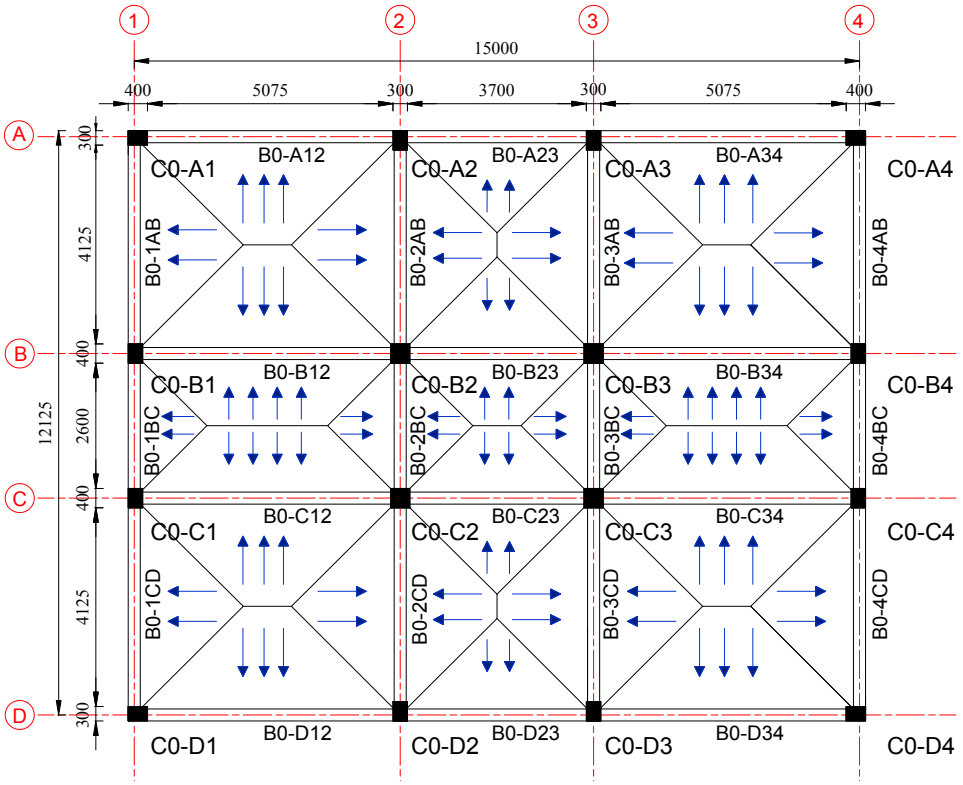

Figure D.1 : Load transfer from slabs to the beams at ground floor.

Table D.3 : Loading details for the beams at ground and first floors.

Beam	Axis	Own Gravity (kN/m)	Loads from Slabs (kN/m)	Loads from Walls (kN/m)	Total Dead Load (kN/m)	Total Live Load (kN/m)
B0-A12	X	3.75	8.63	11.52	23.90	3.20
B0-A34	X	3.75	8.63	11.52	23.90	3.20
B0-D12	X	3.75	6.14	11.52	21.41	3.20
B0-D34	X	3.75	6.14	11.52	21.41	3.20
B0-B12	X	3.75	14.27	6.48	24.50	5.46
B0-B34	X	3.75	14.27	6.48	24.50	5.46
B0-C12	X	3.75	11.78	6.48	22.01	5.46
B0-C34	X	3.75	11.78	6.48	22.01	5.46
B0-A23	X	3.75	8.90	11.52	24.17	2.50
B0-B23	X	3.75	17.08	0.00	20.83	4.53
B0-C23	X	3.75	13.80	6.48	24.03	6.50
B0-D23	X	3.75	5.63	11.52	20.90	4.38
B0-1AB	Y	3.75	7.41	11.52	22.68	2.75
B0-4AB	Y	3.75	7.41	11.52	22.68	2.75
B0-2AB	Y	3.75	17.24	0.00	20.99	5.51
B0-3AB	Y	3.75	17.24	0.00	20.99	5.51
B0-1BC	Y	3.75	4.18	11.52	19.45	1.67
B0-4BC	Y	3.75	4.18	11.52	19.45	1.67
B0-2BC	Y	3.75	10.88	6.48	21.11	3.33
B0-3BC	Y	3.75	10.88	6.48	21.11	3.33
B0-1CD	Y	3.75	5.27	11.52	20.54	2.75
B0-4CD	Y	3.75	5.27	11.52	20.54	2.75
B0-2CD	Y	3.75	11.48	6.48	21.71	7.58
B0-3CD	Y	3.75	11.48	6.48	21.71	7.58

Table D.4 : Loading details for the beams at second floor (roof).

Beam	Axis	Own Gravity (kN/m)	Loads from Slabs (kN/m)	Loads from Walls (kN/m)	Total Dead Load (kN/m)	Total Live Load (kN/m)
B2-A12	X	3.75	4.61	0.00	8.36	3.61
B2-A34	X	3.75	4.61	0.00	8.36	3.61
B2-D12	X	3.75	4.61	0.00	8.36	3.61
B2-D34	X	3.75	4.61	0.00	8.36	3.61
B2-B12	X	3.75	7.86	0.00	11.61	6.14
B2-B34	X	3.75	7.86	0.00	11.61	6.14
B2-C12	X	3.75	7.86	0.00	11.61	6.14
B2-C34	X	3.75	7.86	0.00	11.61	6.14
B2-A23	X	3.75	3.60	0.00	7.35	2.81
B2-D23	X	3.75	3.60	0.00	7.35	2.81
B2-B23	X	3.75	6.53	0.00	10.28	5.10
B2-C23	X	3.75	6.53	0.00	10.28	5.10
B2-1AB	Y	3.75	3.09	0.00	6.84	3.09
B2-4AB	Y	3.75	3.09	0.00	6.84	3.09
B2-1CD	Y	3.75	3.09	0.00	6.84	3.09
B2-4CD	Y	3.75	3.09	0.00	6.84	3.09
B2-2AB	Y	3.75	6.20	0.00	9.95	6.20
B2-3AB	Y	3.75	6.20	0.00	9.95	6.20
B2-2CD	Y	3.75	6.20	0.00	9.95	6.20
B2-3CD	Y	3.75	6.20	0.00	9.95	6.20
B2-1BC	Y	3.75	1.88	0.00	5.63	1.88
B2-4BC	Y	3.75	1.88	0.00	5.63	1.88
B2-2BC	Y	3.75	3.75	0.00	7.50	3.75
B2-3BC	Y	3.75	3.75	0.00	7.50	3.75

Table D.5 : Moment – Curvature relationship of non-retrofitted column 400x400 under 587 kN axial load for both X and Y directions.

Moment (N)	Curvature (1/m)	Max. S220 Strain	Max. S220 Stress (N/mm^2)	Min. Cover Strain (kN/m)	Min. Cover Stress (N/mm^2)	Min. Core Strain (kN/m)	Min. Core Stress (N/mm^2)
0	0.000000	0.000	0	-0.0002	-3	-0.0002	-3.3
46,850	0.001359	0.000	0	-0.0005	-7	-0.0005	-6.2
72,200	0.002717	0.000	50	-0.0007	-9	-0.0007	-8.0
89,070	0.004076	0.001	105	-0.0009	-10	-0.0008	-9.3
103,300	0.005435	0.001	162	-0.0011	-11	-0.0010	-10.2
115,800	0.006794	0.001	220	-0.0013	-11	-0.0012	-10.9
118,300	0.008152	0.001	220	-0.0015	-12	-0.0013	-11.4
120,700	0.009511	0.002	220	-0.0017	-12	-0.0015	-11.9
122,100	0.010870	0.002	220	-0.0018	-12	-0.0016	-12.2
123,500	0.012230	0.002	220	-0.0020	-12	-0.0017	-12.5
124,900	0.013590	0.003	220	-0.0022	-12	-0.0019	-12.7
128,100	0.019030	0.004	220	-0.0029	-12	-0.0025	-13.2
129,900	0.024480	0.005	220	-0.0037	-11	-0.0032	-13.3
127,700	0.029920	0.006	220	-0.0046	-7	-0.0040	-13.2
121,000	0.035370	0.007	220	-0.0057	-2	-0.0049	-12.9
117,000	0.040810	0.008	220	-0.0067	0	-0.0058	-12.5
115,900	0.046250	0.009	220	-0.0076	0	-0.0066	-12.2
114,800	0.051700	0.010	220	-0.0085	0	-0.0074	-11.9
113,700	0.057140	0.011	220	-0.0094	0	-0.0081	-11.7
112,800	0.062590	0.012	220	-0.0104	0	-0.0090	-11.4
111,800	0.068030	0.013	220	-0.0113	0	-0.0098	-11.1
110,900	0.073480	0.014	220	-0.0123	0	-0.0107	-10.9
109,600	0.078920	0.014	220	-0.0138	0	-0.0121	-10.5
108,500	0.084370	0.015	220	-0.0148	0	-0.0130	-10.3
107,600	0.089810	0.016	221	-0.0159	0	-0.0140	-10.1
106,800	0.095250	0.017	222	-0.0171	0	-0.0150	-9.8
105,900	0.100700	0.018	222	-0.0183	0	-0.0161	-9.6
105,100	0.106100	0.018	223	-0.0194	0	-0.0171	-9.5
104,400	0.111600	0.019	224	-0.0205	0	-0.0181	-9.3
103,700	0.117000	0.020	225	-0.0216	0	-0.0190	-9.2
103,100	0.122500	0.021	226	-0.0227	0	-0.0200	-9.0

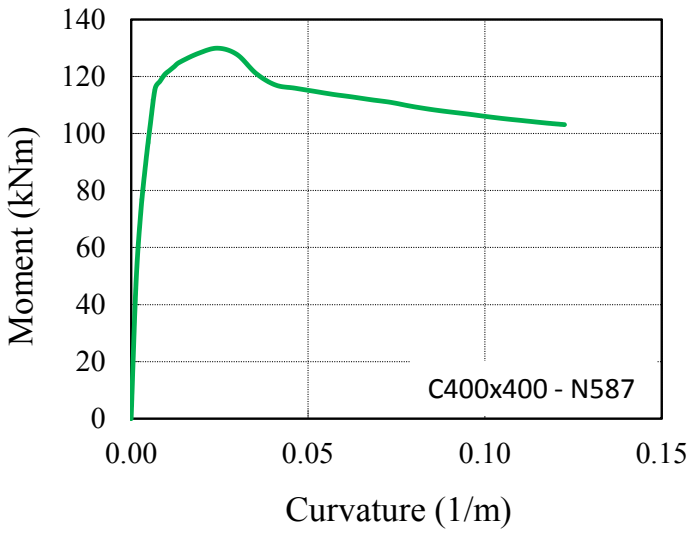

Figure D.2 : Moment – Curvature relationship of non-retrofitted column 400x400 under 587 kN axial load for both X and Y directions.

Table D.6 : Moment – Curvature relationship for non-retrofitted column 400x400 under 351 kN axial load for both X and Y directions.

Moment (N)	Curvature (1/m)	Max. S220 Strain	Max. S220 Stress (N/mm^2)	Min. Cover Strain (kN/m)	Min. Cover Stress (N/mm^2)	Min. Core Strain (kN/m)	Min. Core Stress (N/mm^2)
0	0.000000	0.000	0	-0.0001	-2	-0.0001	-2.0
37,510	0.001146	0.000	14	-0.0003	-5	-0.0003	-4.5
55,070	0.002293	0.000	62	-0.0005	-7	-0.0005	-6.1
68,480	0.003439	0.001	115	-0.0006	-8	-0.0006	-7.3
80,990	0.004586	0.001	167	-0.0008	-9	-0.0007	-8.3
92,630	0.005732	0.001	219	-0.0009	-10	-0.0008	-9.2
95,470	0.006878	0.001	220	-0.0010	-11	-0.0009	-9.6
97,540	0.008025	0.002	220	-0.0011	-11	-0.0010	-10.0
100,600	0.009171	0.002	220	-0.0013	-11	-0.0011	-10.5
102,400	0.010320	0.002	220	-0.0014	-11	-0.0011	-10.8
104,200	0.011460	0.003	220	-0.0015	-12	-0.0012	-11.1
109,500	0.020010	0.005	220	-0.0022	-12	-0.0018	-12.6
110,500	0.028550	0.007	220	-0.0030	-12	-0.0024	-13.1
110,300	0.037090	0.009	220	-0.0037	-11	-0.0029	-13.3
108,500	0.045630	0.012	220	-0.0046	-7	-0.0036	-13.2
103,100	0.054170	0.013	220	-0.0059	0	-0.0047	-12.9
101,600	0.062710	0.015	220	-0.0069	0	-0.0056	-12.6
101,300	0.071250	0.017	222	-0.0079	0	-0.0063	-12.3
101,100	0.079800	0.019	224	-0.0089	0	-0.0071	-12.0
101,400	0.088340	0.021	226	-0.0099	0	-0.0080	-11.7
101,200	0.096880	0.023	228	-0.0110	0	-0.0088	-11.4
101,200	0.105400	0.025	230	-0.0121	0	-0.0098	-11.1
100,600	0.114000	0.028	232	-0.0130	0	-0.0105	-10.9
100,700	0.122500	0.029	233	-0.0143	0	-0.0116	-10.6
99,640	0.131000	0.030	234	-0.0162	0	-0.0133	-10.2
99,460	0.139600	0.032	236	-0.0176	0	-0.0145	-9.9
99,510	0.148100	0.034	237	-0.0188	0	-0.0156	-9.7
98,920	0.156700	0.036	239	-0.0199	0	-0.0164	-9.6
99,170	0.165200	0.037	240	-0.0213	0	-0.0176	-9.4
98,780	0.173800	0.039	242	-0.0223	0	-0.0185	-9.2
98,730	0.182300	0.041	243	-0.0238	0	-0.0198	-9.0
98,650	0.183600	0.041	243	-0.0240	0	-0.0200	-9.0

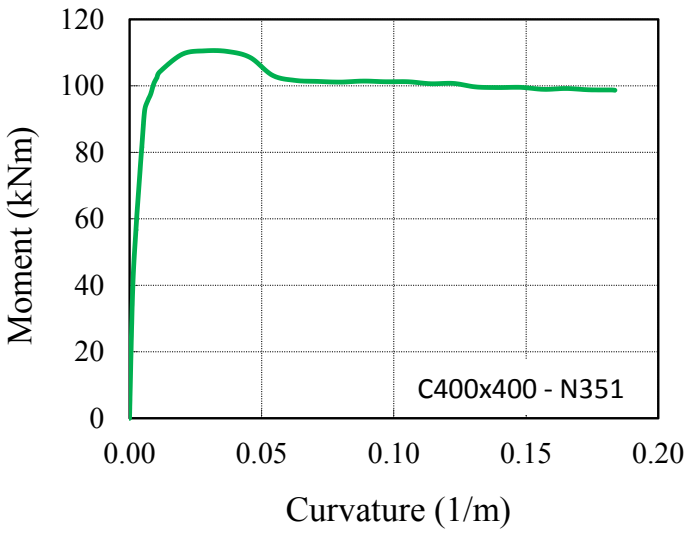

Figure D.3 : Moment – Curvature relationship of non-retrofitted column 400x400 under 351 kN axial load for both X and Y directions.

Table D.7 : Moment – Curvature relationship for non-retrofitted column 400x400 under 117 kN axial load for both X and Y directions.

Moment (N)	Curvature (1/m)	Max. S220 Strain	Max. S220 Stress (N/mm^2)	Min. Cover Strain (kN/m)	Min. Cover Stress (N/mm^2)	Min. Core Strain (kN/m)	Min. Core Stress (N/mm^2)
0	0.000000	0.000	0	0.0000	-1	0.0000	-0.7
19,820	0.000929	0.000	30	-0.0002	-3	-0.0002	-2.5
28,840	0.001858	0.000	77	-0.0003	-4	-0.0002	-3.5
37,870	0.002786	0.001	124	-0.0004	-5	-0.0003	-4.5
46,200	0.003715	0.001	172	-0.0005	-6	-0.0004	-5.3
54,440	0.004644	0.001	220	-0.0006	-7	-0.0004	-6.1
56,020	0.005573	0.001	220	-0.0006	-8	-0.0005	-6.5
57,100	0.006502	0.002	220	-0.0007	-8	-0.0005	-6.9
58,890	0.007430	0.002	220	-0.0007	-9	-0.0006	-7.3
59,830	0.008359	0.002	220	-0.0008	-9	-0.0006	-7.6
62,260	0.009288	0.002	220	-0.0009	-10	-0.0007	-8.0
65,810	0.027740	0.008	220	-0.0016	-12	-0.0010	-10.3
65,950	0.046180	0.014	220	-0.0023	-12	-0.0013	-11.4
67,130	0.064630	0.020	225	-0.0030	-12	-0.0016	-12.1
68,110	0.083080	0.026	230	-0.0036	-11	-0.0018	-12.5
67,670	0.101500	0.032	236	-0.0042	-10	-0.0020	-12.8
65,460	0.120000	0.036	239	-0.0069	0	-0.0043	-13.1
65,690	0.138400	0.041	243	-0.0080	0	-0.0049	-12.8
66,840	0.156900	0.047	248	-0.0091	0	-0.0057	-12.6
66,690	0.175300	0.052	252	-0.0102	0	-0.0063	-12.3
67,510	0.193800	0.058	256	-0.0113	0	-0.0071	-12.0
68,480	0.212200	0.063	260	-0.0125	0	-0.0079	-11.7
68,270	0.230700	0.068	263	-0.0136	0	-0.0085	-11.5
69,570	0.249100	0.074	267	-0.0149	0	-0.0094	-11.2
70,100	0.267600	0.079	270	-0.0161	0	-0.0102	-11.0
70,010	0.286000	0.085	273	-0.0171	0	-0.0109	-10.8
70,750	0.304500	0.090	276	-0.0185	0	-0.0118	-10.6
70,130	0.322900	0.091	277	-0.0240	0	-0.0169	-9.5
70,790	0.341400	0.101	282	-0.0207	0	-0.0132	-10.2
70,680	0.359800	0.101	282	-0.0269	0	-0.0190	-9.1
70,660	0.377600	0.106	284	-0.0283	0	-0.0200	-9.0

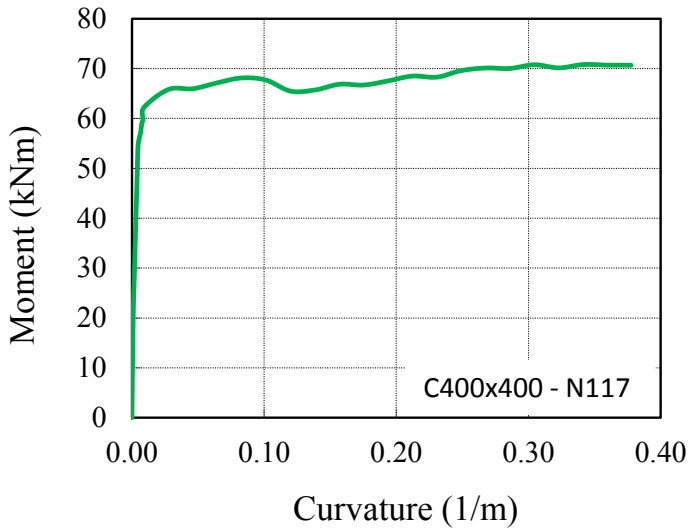

Figure D.4 : Moment – Curvature relationship of non-retrofitted column 400x400 under 117 kN axial load for both X and Y directions.

Table D.8 : Moment – Curvature relationship for non-retrofitted column 300x400 under 450 kN axial load for X direction.

Moment (N)	Curvature (1/m)	Max. S220 Strain	Max. S220 Stress (N/mm^2)	Min. Cover Strain (kN/m)	Min. Cover Stress (N/mm^2)	Min. Core Strain (kN/m)	Min. Core Stress (N/mm^2)
0	0.000000	0.000	0	-0.0002	-3	-0.0002	-3.2
28,440	0.001950	0.000	0	-0.0005	-7	-0.0005	-6.2
43,340	0.003900	0.000	52	-0.0007	-9	-0.0007	-8.0
54,020	0.005850	0.001	107	-0.0010	-10	-0.0008	-9.3
63,300	0.007800	0.001	162	-0.0012	-11	-0.0010	-10.3
71,570	0.009750	0.001	220	-0.0014	-12	-0.0012	-11.0
73,250	0.011700	0.001	220	-0.0016	-12	-0.0013	-11.6
74,460	0.013650	0.002	220	-0.0018	-12	-0.0015	-12.0
75,260	0.015600	0.002	220	-0.0020	-12	-0.0016	-12.4
76,310	0.017550	0.002	220	-0.0022	-12	-0.0018	-12.7
76,680	0.019500	0.003	220	-0.0023	-12	-0.0019	-12.9
77,580	0.022510	0.003	220	-0.0027	-12	-0.0022	-13.2
78,350	0.025510	0.004	220	-0.0030	-11	-0.0025	-13.4
78,740	0.028520	0.004	220	-0.0033	-11	-0.0027	-13.5
79,090	0.031520	0.004	220	-0.0037	-11	-0.0030	-13.6
79,410	0.034530	0.005	220	-0.0040	-10	-0.0033	-13.6
78,390	0.037540	0.005	220	-0.0044	-8	-0.0037	-13.6
76,670	0.040540	0.006	220	-0.0048	-6	-0.0040	-13.5
74,530	0.043550	0.006	220	-0.0053	-4	-0.0044	-13.4
72,130	0.046560	0.006	220	-0.0058	-1	-0.0048	-13.3
70,170	0.049560	0.006	220	-0.0063	0	-0.0053	-13.2
69,860	0.052570	0.007	220	-0.0067	0	-0.0056	-13.1
69,560	0.055580	0.007	220	-0.0071	0	-0.0059	-13.0
69,330	0.058580	0.007	220	-0.0075	0	-0.0063	-12.8
68,920	0.064590	0.008	220	-0.0083	0	-0.0070	-12.6
68,450	0.070610	0.009	220	-0.0092	0	-0.0077	-12.4
68,010	0.076620	0.010	220	-0.0100	0	-0.0084	-12.2
67,620	0.082630	0.010	220	-0.0109	0	-0.0092	-11.9
67,170	0.088640	0.011	220	-0.0118	0	-0.0099	-11.7
66,530	0.097660	0.012	220	-0.0131	0	-0.0111	-11.4
65,510	0.112700	0.014	220	-0.0152	0	-0.0129	-11.0
64,510	0.127700	0.015	220	-0.0174	0	-0.0148	-10.6
63,790	0.142800	0.017	222	-0.0196	0	-0.0167	-10.2
63,240	0.157800	0.019	223	-0.0218	0	-0.0185	-9.9

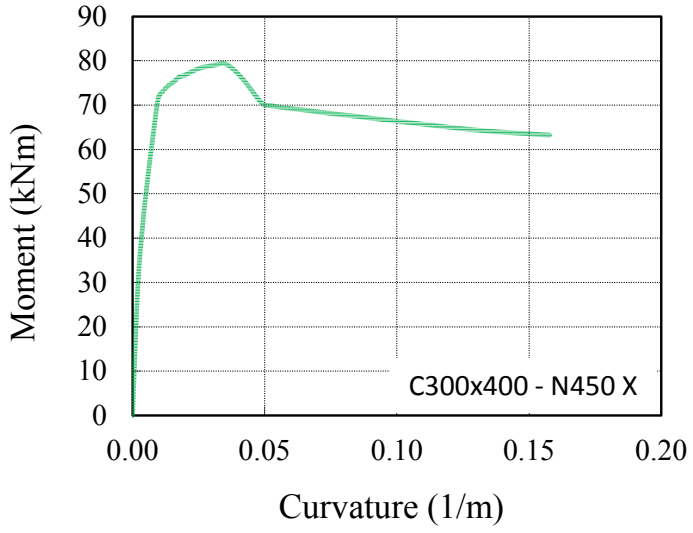

Figure D.5 : Moment – Curvature relationship of non-retrofitted column 300x400 under 450 kN axial load for X direction.

Table D.9 : Moment – Curvature relationship for non-retrofitted column 300x400 under 263 kN axial load for both X direction.

Moment (N)	Curvature (1/m)	Max. S220 Strain	Max. S220 Stress (N/mm^2)	Min. Cover Strain (kN/m)	Min. Cover Stress (N/mm^2)	Min. Core Strain (kN/m)	Min. Core Stress (N/mm^2)
0	0.000000	0.000	0	-0.0001	-2	-0.0001	-1.9
22,410	0.001643	0.000	15	-0.0003	-5	-0.0003	-4.5
33,150	0.003286	0.000	64	-0.0005	-7	-0.0004	-6.1
42,110	0.004929	0.001	116	-0.0007	-8	-0.0006	-7.3
50,110	0.006571	0.001	168	-0.0008	-10	-0.0007	-8.3
57,810	0.008214	0.001	220	-0.0010	-10	-0.0008	-9.2
59,900	0.009857	0.001	220	-0.0011	-11	-0.0009	-9.8
61,770	0.011500	0.002	220	-0.0012	-11	-0.0010	-10.2
62,900	0.013140	0.002	220	-0.0013	-11	-0.0011	-10.6
64,330	0.014790	0.002	220	-0.0015	-12	-0.0012	-10.9
65,610	0.016430	0.003	220	-0.0016	-12	-0.0012	-11.2
68,390	0.021190	0.003	220	-0.0020	-12	-0.0015	-12.1
68,850	0.025950	0.004	220	-0.0023	-12	-0.0017	-12.6
68,870	0.030710	0.005	220	-0.0026	-12	-0.0019	-12.9
69,000	0.035480	0.006	220	-0.0029	-12	-0.0022	-13.1
69,220	0.040240	0.007	220	-0.0032	-11	-0.0024	-13.3
68,850	0.045000	0.008	220	-0.0035	-11	-0.0026	-13.4
69,010	0.049760	0.009	220	-0.0038	-11	-0.0028	-13.5
68,870	0.054520	0.010	220	-0.0042	-10	-0.0031	-13.6
67,710	0.059290	0.010	220	-0.0047	-7	-0.0035	-13.6
65,120	0.064050	0.011	220	-0.0055	-2	-0.0042	-13.5
62,570	0.073570	0.012	220	-0.0067	0	-0.0052	-13.2
62,500	0.083100	0.014	220	-0.0076	0	-0.0059	-13.0
62,380	0.092620	0.015	220	-0.0086	0	-0.0067	-12.7
62,050	0.102100	0.017	222	-0.0094	0	-0.0073	-12.5
61,950	0.111700	0.018	223	-0.0103	0	-0.0080	-12.3
62,060	0.121200	0.020	224	-0.0113	0	-0.0088	-12.0
61,820	0.130700	0.021	226	-0.0122	0	-0.0095	-11.8
62,060	0.140200	0.023	227	-0.0132	0	-0.0103	-11.6
61,850	0.154500	0.025	229	-0.0146	0	-0.0114	-11.3
61,650	0.168800	0.027	231	-0.0159	0	-0.0125	-11.1
61,600	0.183100	0.029	233	-0.0174	0	-0.0136	-10.8
61,560	0.197400	0.032	235	-0.0188	0	-0.0148	-10.6
61,470	0.211700	0.034	237	-0.0203	0	-0.0159	-10.4

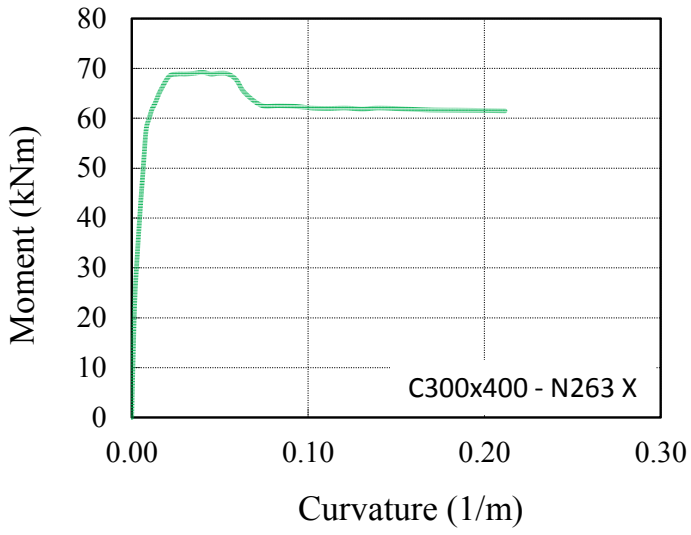

Figure D.6 : Moment – Curvature relationship of non-retrofitted column 300x400 under 263 kN axial load for X direction.

Table D.10 : Moment – Curvature relationship for non-retrofitted column 300x400 under 76 kN axial load for X direction.

Moment (N)	Curvature (1/m)	Max. S220 Strain	Max. S220 Stress (N/mm^2)	Min. Cover Strain (kN/m)	Min. Cover Stress (N/mm^2)	Min. Core Strain (kN/m)	Min. Core Stress (N/mm^2)
0	0.000000	0.000	0	0.0000	-1	0.0000	-0.6
11,380	0.001320	0.000	32	-0.0002	-3	-0.0001	-2.3
17,410	0.002641	0.000	79	-0.0003	-4	-0.0002	-3.4
23,040	0.003961	0.001	127	-0.0004	-5	-0.0003	-4.3
29,070	0.005282	0.001	173	-0.0005	-7	-0.0004	-5.3
34,510	0.006602	0.001	220	-0.0006	-8	-0.0004	-6.1
35,960	0.007922	0.001	220	-0.0007	-8	-0.0005	-6.6
37,150	0.009243	0.002	220	-0.0007	-9	-0.0005	-7.0
37,810	0.010560	0.002	220	-0.0008	-9	-0.0006	-7.3
38,730	0.011880	0.002	220	-0.0009	-10	-0.0006	-7.7
40,000	0.013200	0.002	220	-0.0009	-10	-0.0007	-8.1
41,800	0.022100	0.004	220	-0.0013	-11	-0.0008	-9.2
42,140	0.031000	0.006	220	-0.0016	-12	-0.0009	-9.9
42,000	0.039900	0.008	220	-0.0019	-12	-0.0011	-10.5
41,650	0.048800	0.010	220	-0.0021	-12	-0.0011	-10.9
42,290	0.057700	0.012	220	-0.0025	-12	-0.0013	-11.4
42,150	0.066600	0.014	220	-0.0028	-12	-0.0014	-11.7
42,350	0.075500	0.016	221	-0.0030	-11	-0.0015	-12.0
42,450	0.084390	0.018	223	-0.0033	-11	-0.0016	-12.3
42,340	0.093290	0.020	225	-0.0036	-11	-0.0017	-12.4
42,770	0.102200	0.022	227	-0.0039	-11	-0.0018	-12.7
42,330	0.111100	0.024	229	-0.0042	-10	-0.0019	-12.8
43,040	0.120000	0.026	230	-0.0046	-7	-0.0022	-13.1
42,510	0.128900	0.028	232	-0.0049	-6	-0.0023	-13.3
40,890	0.137800	0.029	233	-0.0062	0	-0.0034	-13.6
40,830	0.155600	0.032	236	-0.0075	0	-0.0043	-13.5
41,320	0.173400	0.036	239	-0.0086	0	-0.0050	-13.3
41,240	0.191200	0.039	242	-0.0093	0	-0.0054	-13.1
41,620	0.209000	0.043	245	-0.0104	0	-0.0061	-12.9
42,160	0.226800	0.047	248	-0.0114	0	-0.0067	-12.7
42,180	0.244600	0.050	251	-0.0122	0	-0.0072	-12.5
42,240	0.262400	0.054	253	-0.0131	0	-0.0077	-12.4
43,130	0.289100	0.059	257	-0.0146	0	-0.0087	-12.1
43,210	0.315800	0.065	261	-0.0160	0	-0.0095	-11.8

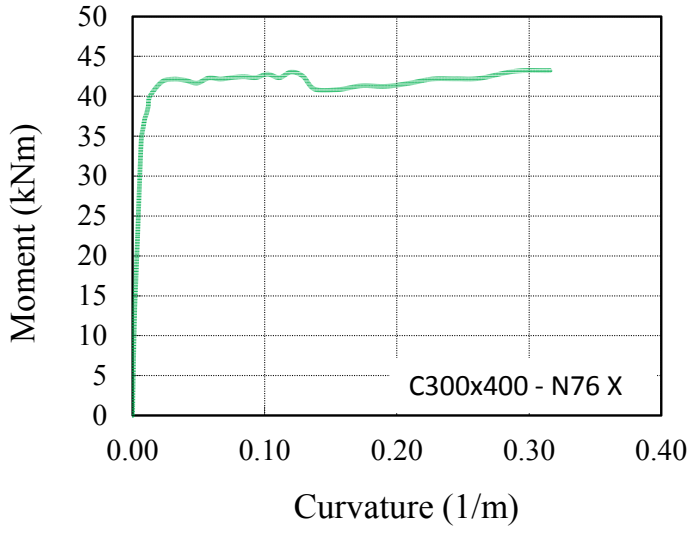

Figure D.7 : Moment – Curvature relationship of non-retrofitted column 300x400 under 76 kN axial load for X direction.

Table D.11 : Moment – Curvature relationship for non-retrofitted column 300x400 under 450 kN axial load for Y direction.

Moment (N)	Curvature (1/m)	Max. S220 Strain	Max. S220 Stress (N/mm^2)	Min. Cover Strain (kN/m)	Min. Cover Stress (N/mm^2)	Min. Core Strain (kN/m)	Min. Core Stress (N/mm^2)
0	0.000000	0.000	0	-0.0002	-3	-0.0002	-3.2
36,620	0.001337	0.000	0	-0.0005	-7	-0.0004	-6.1
57,610	0.002675	0.000	48	-0.0007	-9	-0.0007	-8.0
72,380	0.004012	0.001	102	-0.0009	-10	-0.0008	-9.2
85,130	0.005350	0.001	158	-0.0011	-11	-0.0010	-10.2
96,980	0.006687	0.001	213	-0.0013	-11	-0.0012	-11.0
100,300	0.008025	0.001	220	-0.0015	-12	-0.0013	-11.6
101,800	0.009362	0.002	220	-0.0017	-12	-0.0015	-12.0
103,100	0.010700	0.002	220	-0.0019	-12	-0.0016	-12.4
104,400	0.012040	0.002	220	-0.0020	-12	-0.0018	-12.7
105,200	0.013370	0.003	220	-0.0022	-12	-0.0019	-12.9
106,500	0.015520	0.003	220	-0.0025	-12	-0.0022	-13.2
107,400	0.017660	0.003	220	-0.0028	-12	-0.0024	-13.4
108,400	0.019810	0.004	220	-0.0031	-11	-0.0027	-13.5
108,800	0.021950	0.004	220	-0.0034	-11	-0.0030	-13.6
109,500	0.024100	0.005	220	-0.0038	-11	-0.0033	-13.6
109,500	0.026240	0.005	220	-0.0041	-10	-0.0036	-13.6
108,200	0.028380	0.006	220	-0.0045	-8	-0.0039	-13.5
106,500	0.030530	0.006	220	-0.0049	-6	-0.0043	-13.5
104,400	0.032670	0.006	220	-0.0054	-3	-0.0047	-13.4
102,000	0.034820	0.007	220	-0.0058	-1	-0.0051	-13.3
100,000	0.036960	0.007	220	-0.0062	0	-0.0054	-13.1
99,510	0.039110	0.007	220	-0.0066	0	-0.0058	-13.0
99,110	0.041250	0.008	220	-0.0070	0	-0.0061	-12.9
98,410	0.045540	0.008	220	-0.0078	0	-0.0068	-12.7
97,690	0.049830	0.009	220	-0.0086	0	-0.0075	-12.4
97,030	0.054110	0.010	220	-0.0094	0	-0.0083	-12.2
96,310	0.058400	0.011	220	-0.0102	0	-0.0090	-12.0
95,650	0.062690	0.011	220	-0.0111	0	-0.0098	-11.7
94,610	0.069120	0.012	220	-0.0124	0	-0.0109	-11.4
93,130	0.079840	0.014	220	-0.0145	0	-0.0128	-11.0
91,760	0.090570	0.016	221	-0.0166	0	-0.0147	-10.6
90,650	0.101300	0.017	222	-0.0187	0	-0.0166	-10.2
89,740	0.112000	0.019	224	-0.0209	0	-0.0185	-9.9

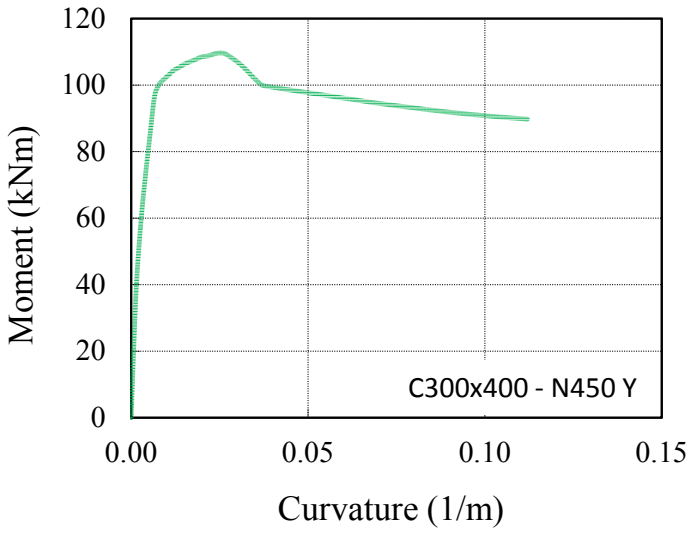

Figure D.8 : Moment – Curvature relationship of non-retrofitted column 300x400 under 450 kN axial load for Y direction.

Table D.12 : Moment – Curvature relationship for non-retrofitted column 300x400 under 263 kN axial load for Y direction.

Moment (N)	Curvature (1/m)	Max. S220 Strain	Max. S220 Stress (N/mm^2)	Min. Cover Strain (kN/m)	Min. Cover Stress (N/mm^2)	Min. Core Strain (kN/m)	Min. Core Stress (N/mm^2)
0	0.000000	0.000	0	-0.0001	-2	-0.0001	-1.9
29,860	0.001168	0.000	16	-0.0003	-5	-0.0003	-4.5
45,110	0.002335	0.000	65	-0.0005	-7	-0.0005	-6.2
57,590	0.003503	0.001	116	-0.0007	-8	-0.0006	-7.4
69,020	0.004671	0.001	169	-0.0008	-9	-0.0007	-8.5
79,830	0.005838	0.001	220	-0.0010	-10	-0.0008	-9.3
82,880	0.007006	0.001	220	-0.0011	-11	-0.0009	-9.9
84,850	0.008173	0.002	220	-0.0012	-11	-0.0010	-10.3
86,980	0.009341	0.002	220	-0.0013	-11	-0.0011	-10.7
88,840	0.010510	0.002	220	-0.0014	-12	-0.0012	-11.0
90,780	0.011680	0.003	220	-0.0015	-12	-0.0013	-11.4
93,580	0.014880	0.003	220	-0.0019	-12	-0.0016	-12.2
95,070	0.018090	0.004	220	-0.0022	-12	-0.0018	-12.7
95,080	0.021300	0.005	220	-0.0025	-12	-0.0020	-13.0
95,430	0.024510	0.006	220	-0.0028	-12	-0.0022	-13.2
95,240	0.027720	0.007	220	-0.0030	-11	-0.0024	-13.4
95,330	0.030930	0.008	220	-0.0033	-11	-0.0027	-13.5
95,380	0.034140	0.009	220	-0.0036	-11	-0.0029	-13.6
95,250	0.037340	0.009	220	-0.0039	-11	-0.0031	-13.6
95,040	0.040550	0.010	220	-0.0042	-10	-0.0033	-13.6
94,150	0.043760	0.011	220	-0.0046	-7	-0.0037	-13.6
92,670	0.046970	0.012	220	-0.0051	-5	-0.0041	-13.5
90,730	0.050180	0.012	220	-0.0057	-2	-0.0046	-13.4
89,190	0.053390	0.013	220	-0.0062	0	-0.0051	-13.2
88,890	0.059800	0.014	220	-0.0071	0	-0.0059	-13.0
88,580	0.066220	0.016	221	-0.0079	0	-0.0065	-12.8
88,250	0.072640	0.017	222	-0.0086	0	-0.0071	-12.6
88,590	0.079050	0.019	223	-0.0095	0	-0.0079	-12.3
88,540	0.085470	0.020	225	-0.0104	0	-0.0086	-12.1
88,210	0.095100	0.022	227	-0.0115	0	-0.0096	-11.8
87,910	0.111100	0.026	230	-0.0136	0	-0.0113	-11.3
87,690	0.127200	0.029	233	-0.0158	0	-0.0131	-10.9
87,360	0.143200	0.033	236	-0.0181	0	-0.0151	-10.5
86,860	0.159300	0.035	238	-0.0216	0	-0.0183	-10.0

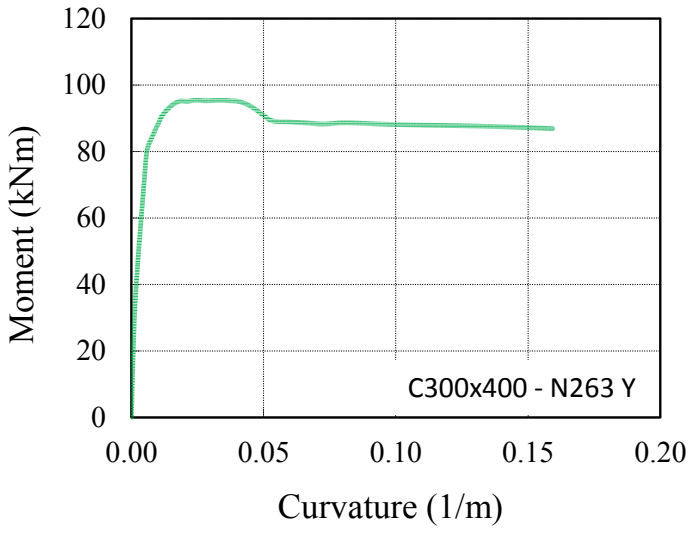

Figure D.9 : Moment – Curvature relationship of non-retrofitted column 300x400 under 263 kN axial load for Y direction.

Table D.13 : Moment – Curvature relationship for non-retrofitted column 300x400 under 76 kN axial load for Y direction.

Moment (N)	Curvature (1/m)	Max. S220 Strain	Max. S220 Stress (N/mm^2)	Min. Cover Strain (kN/m)	Min. Cover Stress (N/mm^2)	Min. Core Strain (kN/m)	Min. Core Stress (N/mm^2)
0	0.000000	0.000	0	0.0000	-1	0.0000	-0.6
15,570	0.000939	0.000	32	-0.0002	-3	-0.0002	-2.4
23,590	0.001879	0.000	79	-0.0003	-4	-0.0002	-3.5
31,490	0.002818	0.001	127	-0.0004	-5	-0.0003	-4.5
39,500	0.003758	0.001	174	-0.0005	-6	-0.0004	-5.4
47,550	0.004697	0.001	220	-0.0006	-8	-0.0005	-6.3
49,120	0.005636	0.001	220	-0.0006	-8	-0.0005	-6.8
50,330	0.006576	0.002	220	-0.0007	-9	-0.0006	-7.2
52,020	0.007515	0.002	220	-0.0008	-9	-0.0006	-7.6
52,990	0.008455	0.002	220	-0.0008	-9	-0.0006	-7.9
54,120	0.009394	0.002	220	-0.0009	-10	-0.0007	-8.3
57,170	0.016720	0.005	220	-0.0012	-11	-0.0009	-9.7
58,530	0.024050	0.007	220	-0.0016	-12	-0.0011	-10.5
58,630	0.031380	0.009	220	-0.0018	-12	-0.0012	-11.0
58,430	0.038720	0.012	220	-0.0021	-12	-0.0013	-11.4
57,800	0.046050	0.014	220	-0.0023	-12	-0.0014	-11.7
59,390	0.053380	0.016	221	-0.0026	-12	-0.0015	-12.1
59,660	0.060710	0.019	224	-0.0029	-12	-0.0016	-12.4
59,600	0.068040	0.021	226	-0.0032	-11	-0.0017	-12.6
59,530	0.075370	0.023	228	-0.0034	-11	-0.0018	-12.7
60,180	0.082700	0.026	230	-0.0037	-11	-0.0020	-12.9
60,420	0.090030	0.028	232	-0.0040	-11	-0.0021	-13.1
60,360	0.097360	0.030	234	-0.0045	-8	-0.0025	-13.4
59,300	0.104700	0.032	236	-0.0051	-5	-0.0029	-13.6
59,080	0.112000	0.034	237	-0.0063	0	-0.0039	-13.5
59,240	0.126700	0.038	240	-0.0074	0	-0.0048	-13.3
59,630	0.141300	0.042	244	-0.0084	0	-0.0054	-13.1
59,510	0.156000	0.046	248	-0.0091	0	-0.0058	-13.0
59,860	0.170700	0.050	251	-0.0104	0	-0.0069	-12.7
60,600	0.185300	0.053	253	-0.0124	0	-0.0085	-12.1
61,300	0.200000	0.058	256	-0.0135	0	-0.0093	-11.9
60,860	0.214600	0.062	259	-0.0144	0	-0.0099	-11.7
61,940	0.236600	0.068	263	-0.0162	0	-0.0113	-11.4
62,570	0.258600	0.074	267	-0.0180	0	-0.0126	-11.0

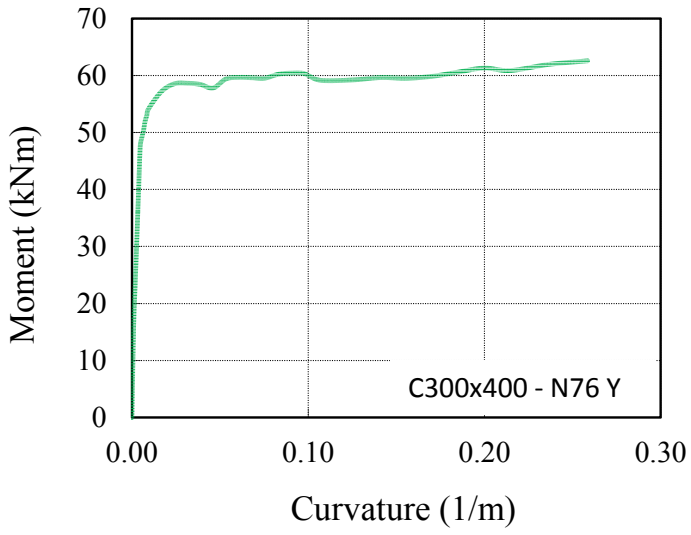

Figure D.10 : Moment – Curvature relationship of non-retrofitted column 300x400 under 76 kN axial load for Y direction.

Table D.14 : Moment – Curvature relationship for non-retrofitted column 400x300 under 324 kN axial load for X direction.

Moment (N)	Curvature (1/m)	Max. S220 Strain	Max. S220 Stress (N/mm^2)	Min. Cover Strain (kN/m)	Min. Cover Stress (N/mm^2)	Min. Core Strain (kN/m)	Min. Core Stress (N/mm^2)
0	0.000000	0.000	0	-0.0001	-2	-0.0001	-2.3
32,820	0.001231	0.000	11	-0.0004	-6	-0.0004	-5.1
49,780	0.002463	0.000	60	-0.0006	-8	-0.0005	-6.8
62,760	0.003694	0.001	114	-0.0007	-9	-0.0007	-8.1
74,910	0.004925	0.001	167	-0.0009	-10	-0.0008	-9.1
86,050	0.006157	0.001	220	-0.0011	-11	-0.0010	-10.0
89,540	0.007388	0.001	220	-0.0012	-11	-0.0011	-10.5
91,850	0.008619	0.002	220	-0.0013	-11	-0.0012	-10.9
93,740	0.009851	0.002	220	-0.0015	-12	-0.0013	-11.3
94,730	0.011080	0.002	220	-0.0016	-12	-0.0014	-11.7
96,150	0.012310	0.003	220	-0.0018	-12	-0.0015	-12.0
98,540	0.015010	0.003	220	-0.0021	-12	-0.0018	-12.6
100,100	0.017710	0.004	220	-0.0024	-12	-0.0020	-13.0
101,200	0.020410	0.005	220	-0.0027	-12	-0.0023	-13.3
101,700	0.023100	0.005	220	-0.0030	-11	-0.0025	-13.4
101,600	0.025800	0.006	220	-0.0033	-11	-0.0028	-13.5
101,600	0.028500	0.007	220	-0.0036	-11	-0.0030	-13.6
101,400	0.031200	0.007	220	-0.0038	-11	-0.0032	-13.6
101,200	0.033890	0.008	220	-0.0041	-10	-0.0034	-13.6
100,200	0.036590	0.008	220	-0.0045	-8	-0.0038	-13.6
98,670	0.039290	0.009	220	-0.0049	-6	-0.0041	-13.5
97,020	0.041990	0.010	220	-0.0054	-3	-0.0045	-13.4
93,740	0.047380	0.010	220	-0.0064	0	-0.0054	-13.1
93,320	0.052780	0.012	220	-0.0072	0	-0.0061	-12.9
92,910	0.058170	0.013	220	-0.0080	0	-0.0068	-12.7
92,200	0.063570	0.014	220	-0.0087	0	-0.0074	-12.5
91,740	0.068960	0.015	220	-0.0094	0	-0.0080	-12.3
91,550	0.074360	0.016	221	-0.0103	0	-0.0087	-12.1
91,340	0.079750	0.017	222	-0.0112	0	-0.0095	-11.8
91,210	0.085150	0.018	223	-0.0121	0	-0.0103	-11.6
90,840	0.093240	0.020	225	-0.0133	0	-0.0113	-11.3
90,390	0.101300	0.022	226	-0.0144	0	-0.0123	-11.1
90,130	0.109400	0.023	228	-0.0157	0	-0.0134	-10.9
89,890	0.117500	0.025	229	-0.0170	0	-0.0145	-10.6

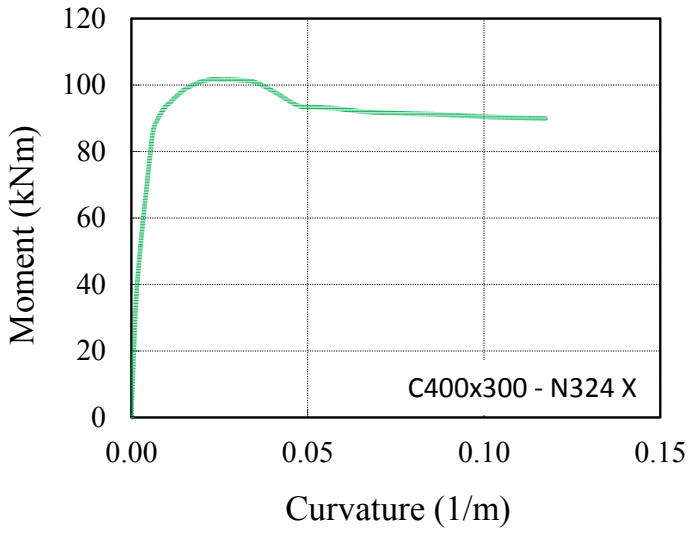

Figure D.11 : Moment – Curvature relationship of non-retrofitted column 400x300 under 324 kN axial load for X direction.

Table D.15 : Moment – Curvature relationship for non-retrofitted column 400x300 under 190 kN axial load for X direction.

Moment (N)	Curvature (1/m)	Max. S220 Strain	Max. S220 Stress (N/mm^2)	Min. Cover Strain (kN/m)	Min. Cover Stress (N/mm^2)	Min. Core Strain (kN/m)	Min. Core Stress (N/mm^2)
0	0.000000	0.000	0	-0.0001	-1	-0.00009	-1.4
25,570	0.001083	0.000	22	-0.0003	-4	-0.00025	-3.8
38,540	0.002165	0.000	70	-0.0004	-6	-0.00037	-5.3
49,990	0.003248	0.001	120	-0.0006	-7	-0.00049	-6.5
61,150	0.004331	0.001	169	-0.0007	-9	-0.00060	-7.6
71,160	0.005414	0.001	220	-0.0008	-9	-0.00071	-8.4
74,090	0.006496	0.001	220	-0.0009	-10	-0.00079	-9.0
76,090	0.007579	0.002	220	-0.0010	-10	-0.00086	-9.4
78,010	0.008662	0.002	220	-0.0011	-11	-0.00093	-9.8
79,740	0.009744	0.002	220	-0.0012	-11	-0.00099	-10.2
81,660	0.010830	0.003	220	-0.0013	-11	-0.00106	-10.5
86,140	0.014870	0.004	220	-0.0016	-12	-0.00129	-11.4
87,070	0.018910	0.005	220	-0.0019	-12	-0.00151	-12.1
87,120	0.022950	0.006	220	-0.0022	-12	-0.00171	-12.5
87,300	0.026990	0.007	220	-0.0025	-12	-0.00191	-12.8
87,820	0.031030	0.008	220	-0.0028	-12	-0.00214	-13.1
87,610	0.035070	0.009	220	-0.0031	-11	-0.00232	-13.3
87,410	0.039110	0.011	220	-0.0033	-11	-0.00249	-13.4
87,840	0.043150	0.012	220	-0.0036	-11	-0.00273	-13.5
87,860	0.047190	0.013	220	-0.0039	-11	-0.00294	-13.6
87,330	0.051230	0.014	220	-0.0042	-9	-0.00316	-13.6
86,220	0.055270	0.015	220	-0.0046	-7	-0.00346	-13.6
84,780	0.059320	0.016	221	-0.0054	-3	-0.00416	-13.5
82,820	0.067400	0.017	222	-0.0066	0	-0.00517	-13.2
82,410	0.075480	0.020	224	-0.0073	0	-0.00573	-13.0
82,950	0.083560	0.022	226	-0.0082	0	-0.00646	-12.8
82,660	0.091640	0.024	228	-0.0090	0	-0.00705	-12.6
82,880	0.099720	0.026	230	-0.0098	0	-0.00773	-12.4
83,410	0.107800	0.028	232	-0.0108	0	-0.00852	-12.1
83,130	0.115900	0.030	234	-0.0115	0	-0.00909	-11.9
83,250	0.124000	0.032	235	-0.0124	0	-0.00980	-11.7
83,590	0.136100	0.035	238	-0.0138	0	-0.01093	-11.4
83,580	0.148200	0.038	240	-0.0151	0	-0.01200	-11.2
83,140	0.160300	0.039	242	-0.0179	0	-0.01451	-10.6

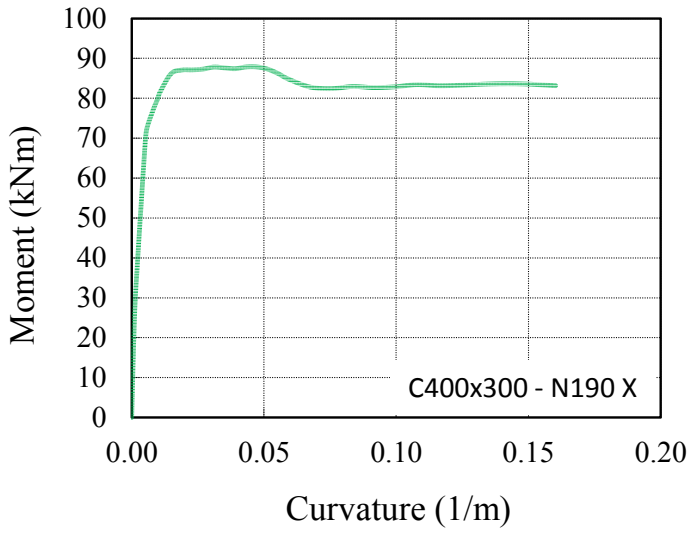

Figure D.12 : Moment – Curvature relationship of non-retrofitted column 400x300 under 190 kN axial load for X direction.

Table D.16 : Moment – Curvature relationship for non-retrofitted column 400x300 under 53 kN axial load for X direction.

Moment (N)	Curvature (1/m)	Max. S220 Strain	Max. S220 Stress (N/mm^2)	Min. Cover Strain (kN/m)	Min. Cover Stress (N/mm^2)	Min. Core Strain (kN/m)	Min. Core Stress (N/mm^2)
0	0.000000	0.000	0	0.0000	0	0.0000	-0.4
12,920	0.000913	0.000	36	-0.0001	-2	-0.0001	-2.0
20,840	0.001826	0.000	82	-0.0002	-4	-0.0002	-3.0
28,870	0.002739	0.001	128	-0.0003	-5	-0.0003	-4.0
36,800	0.003652	0.001	174	-0.0004	-6	-0.0004	-5.0
44,150	0.004564	0.001	220	-0.0005	-7	-0.0004	-5.8
45,410	0.005477	0.001	220	-0.0006	-8	-0.0005	-6.2
47,510	0.006390	0.002	220	-0.0006	-8	-0.0005	-6.7
48,890	0.007303	0.002	220	-0.0007	-9	-0.0006	-7.1
50,430	0.008216	0.002	220	-0.0008	-9	-0.0006	-7.5
51,750	0.009129	0.002	220	-0.0008	-10	-0.0006	-7.9
54,080	0.017280	0.005	220	-0.0012	-11	-0.0008	-9.3
53,890	0.025430	0.008	220	-0.0015	-12	-0.0009	-9.9
54,810	0.033580	0.010	220	-0.0018	-12	-0.0011	-10.6
55,500	0.041730	0.013	220	-0.0021	-12	-0.0012	-11.2
55,110	0.049880	0.015	220	-0.0024	-12	-0.0013	-11.5
55,190	0.058030	0.018	223	-0.0026	-12	-0.0014	-11.8
55,670	0.066180	0.021	225	-0.0029	-12	-0.0016	-12.2
56,520	0.074330	0.023	228	-0.0032	-11	-0.0017	-12.5
57,130	0.082490	0.026	230	-0.0035	-11	-0.0018	-12.7
57,110	0.090640	0.028	233	-0.0038	-11	-0.0019	-12.8
56,780	0.098790	0.031	235	-0.0040	-11	-0.0020	-12.9
57,730	0.106900	0.034	237	-0.0044	-9	-0.0022	-13.2
57,390	0.115100	0.036	239	-0.0047	-7	-0.0023	-13.3
55,810	0.123200	0.037	240	-0.0064	0	-0.0038	-13.6
55,630	0.139500	0.042	244	-0.0073	0	-0.0044	-13.4
57,040	0.155800	0.047	248	-0.0083	0	-0.0051	-13.3
57,340	0.172100	0.052	252	-0.0092	0	-0.0056	-13.1
57,370	0.188400	0.057	256	-0.0100	0	-0.0061	-12.9
58,190	0.204700	0.062	259	-0.0111	0	-0.0068	-12.7
59,000	0.221000	0.066	262	-0.0121	0	-0.0075	-12.4
58,910	0.237400	0.071	265	-0.0129	0	-0.0080	-12.3
59,950	0.261800	0.078	270	-0.0147	0	-0.0092	-11.9
59,810	0.286300	0.084	273	-0.0177	0	-0.0118	-11.2

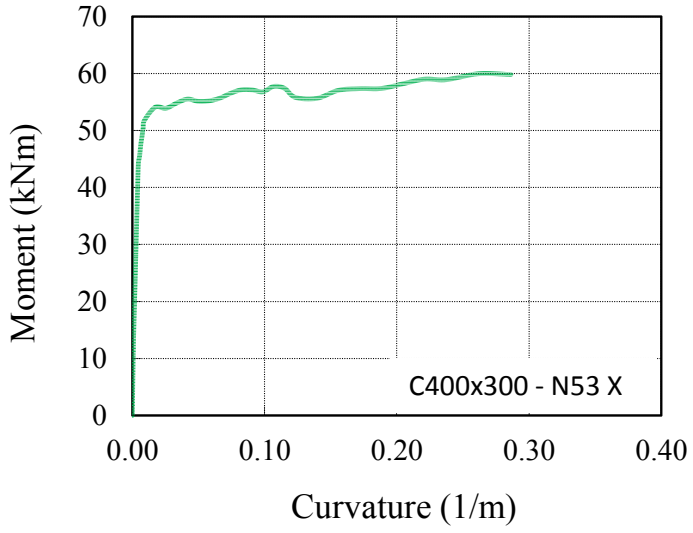

Figure D.13 : Moment – Curvature relationship of non-retrofitted column 400x300 under 53 kN axial load for X direction.

Table D.17 : Moment – Curvature relationship for non-retrofitted column 400x300 under 324 kN axial load for Y direction.

Moment (N)	Curvature (1/m)	Max. S220 Strain	Max. S220 Stress (N/mm^2)	Min. Cover Strain (kN/m)	Min. Cover Stress (N/mm^2)	Min. Core Strain (kN/m)	Min. Core Stress (N/mm^2)
0	0.000000	0.000	0	-0.0001	-2	-0.0001	-2.3
24,770	0.001743	0.000	10	-0.0004	-6	-0.0004	-5.1
36,640	0.003485	0.000	61	-0.0006	-8	-0.0005	-6.7
46,200	0.005228	0.001	113	-0.0008	-9	-0.0007	-8.0
54,770	0.006971	0.001	167	-0.0009	-10	-0.0008	-9.1
62,620	0.008713	0.001	220	-0.0011	-11	-0.0009	-9.9
64,690	0.010460	0.001	220	-0.0013	-11	-0.0010	-10.4
66,400	0.012200	0.002	220	-0.0014	-12	-0.0011	-10.8
67,960	0.013940	0.002	220	-0.0015	-12	-0.0012	-11.2
69,350	0.015680	0.002	220	-0.0017	-12	-0.0013	-11.6
70,160	0.017430	0.003	220	-0.0018	-12	-0.0015	-11.9
71,850	0.021280	0.003	220	-0.0022	-12	-0.0017	-12.5
73,170	0.025130	0.004	220	-0.0025	-12	-0.0020	-13.0
73,350	0.028980	0.005	220	-0.0028	-12	-0.0022	-13.2
73,510	0.032830	0.005	220	-0.0031	-11	-0.0025	-13.4
73,670	0.036680	0.006	220	-0.0035	-11	-0.0027	-13.5
73,340	0.040530	0.007	220	-0.0037	-11	-0.0029	-13.6
73,110	0.044380	0.007	220	-0.0040	-10	-0.0031	-13.6
72,290	0.048240	0.008	220	-0.0045	-8	-0.0035	-13.6
70,730	0.052090	0.008	220	-0.0049	-6	-0.0038	-13.6
68,990	0.055940	0.009	220	-0.0055	-3	-0.0043	-13.5
66,700	0.059790	0.009	220	-0.0062	0	-0.0050	-13.3
65,940	0.067490	0.010	220	-0.0070	0	-0.0056	-13.1
65,560	0.075190	0.011	220	-0.0078	0	-0.0062	-12.9
65,310	0.082900	0.013	220	-0.0086	0	-0.0069	-12.6
65,020	0.090600	0.014	220	-0.0095	0	-0.0077	-12.4
64,680	0.098300	0.015	220	-0.0104	0	-0.0083	-12.2
64,380	0.106000	0.016	221	-0.0114	0	-0.0092	-11.9
64,320	0.113700	0.017	222	-0.0123	0	-0.0100	-11.7
63,990	0.125300	0.018	223	-0.0137	0	-0.0111	-11.4
63,630	0.136800	0.020	225	-0.0150	0	-0.0121	-11.1
63,410	0.148400	0.022	226	-0.0164	0	-0.0133	-10.9
63,160	0.159900	0.023	228	-0.0177	0	-0.0145	-10.6
62,910	0.171500	0.025	229	-0.0192	0	-0.0157	-10.4

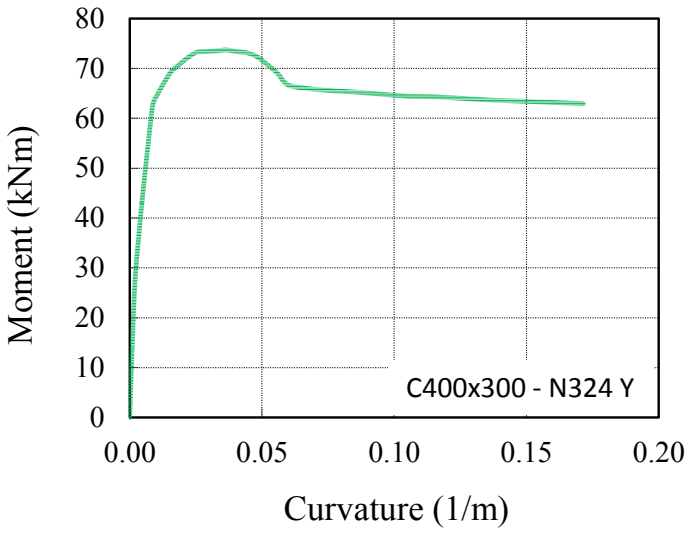

Figure D.14 : Moment – Curvature relationship of non-retrofitted column 400x300 under 324 kN axial load for Y direction.

Table D.18 : Moment – Curvature relationship for non-retrofitted column 400x300 under 190 kN axial load for Y direction.

Moment (N)	Curvature (1/m)	Max. S220 Strain	Max. S220 Stress (N/mm^2)	Min. Cover Strain (kN/m)	Min. Cover Stress (N/mm^2)	Min. Core Strain (kN/m)	Min. Core Stress (N/mm^2)
0	0.000000	0.000	0	-0.0001	-1	-0.0001	-1.4
18,950	0.001535	0.000	22	-0.0003	-4	-0.0002	-3.7
28,460	0.003071	0.000	70	-0.0004	-6	-0.0004	-5.2
36,480	0.004606	0.001	122	-0.0006	-8	-0.0005	-6.3
44,690	0.006141	0.001	170	-0.0007	-9	-0.0006	-7.4
51,990	0.007677	0.001	220	-0.0009	-10	-0.0007	-8.3
53,850	0.009212	0.001	220	-0.0010	-10	-0.0008	-8.9
54,950	0.010750	0.002	220	-0.0011	-11	-0.0008	-9.3
56,480	0.012280	0.002	220	-0.0012	-11	-0.0009	-9.7
58,260	0.013820	0.002	220	-0.0013	-11	-0.0010	-10.1
59,270	0.015350	0.003	220	-0.0014	-11	-0.0010	-10.4
62,060	0.020960	0.004	220	-0.0017	-12	-0.0012	-11.2
62,620	0.026570	0.005	220	-0.0019	-12	-0.0014	-11.7
62,940	0.032190	0.006	220	-0.0022	-12	-0.0016	-12.2
63,080	0.037800	0.007	220	-0.0025	-12	-0.0017	-12.6
63,280	0.043410	0.008	220	-0.0028	-12	-0.0020	-12.9
63,090	0.049020	0.009	220	-0.0031	-11	-0.0021	-13.1
62,750	0.054630	0.011	220	-0.0034	-11	-0.0022	-13.2
62,870	0.060240	0.012	220	-0.0037	-11	-0.0024	-13.4
63,110	0.065850	0.013	220	-0.0041	-10	-0.0027	-13.5
62,190	0.071460	0.014	220	-0.0046	-7	-0.0032	-13.6
60,640	0.077070	0.015	220	-0.0052	-4	-0.0036	-13.6
58,490	0.082680	0.015	220	-0.0060	0	-0.0043	-13.5
58,040	0.088290	0.016	221	-0.0065	0	-0.0047	-13.4
58,180	0.099510	0.018	223	-0.0074	0	-0.0054	-13.2
58,280	0.110700	0.020	225	-0.0083	0	-0.0060	-13.0
58,390	0.122000	0.022	227	-0.0091	0	-0.0066	-12.7
58,420	0.133200	0.024	229	-0.0100	0	-0.0072	-12.5
58,540	0.144400	0.026	230	-0.0108	0	-0.0078	-12.3
58,450	0.155600	0.028	232	-0.0116	0	-0.0084	-12.2
58,640	0.166800	0.030	234	-0.0126	0	-0.0091	-11.9
58,680	0.183700	0.033	237	-0.0139	0	-0.0102	-11.6
58,740	0.200500	0.036	239	-0.0153	0	-0.0112	-11.4
58,400	0.217300	0.037	240	-0.0183	0	-0.0138	-10.8

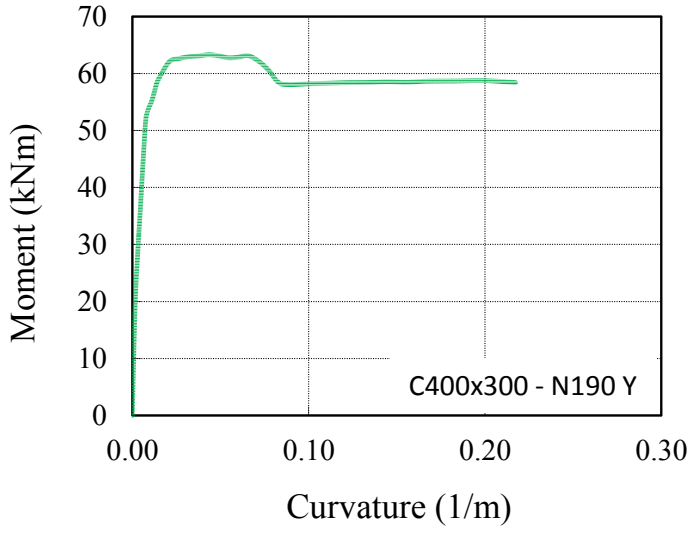

Figure D.15 : Moment – Curvature relationship of non-retrofitted column 400x300 under 190 kN axial load for Y direction.

Table D.19 : Moment – Curvature relationship for non-retrofitted column 400x300 under 53 kN axial load for Y direction.

Moment (N)	Curvature (1/m)	Max. S220 Strain	Max. S220 Stress (N/mm^2)	Min. Cover Strain (kN/m)	Min. Cover Stress (N/mm^2)	Min. Core Strain (kN/m)	Min. Core Stress (N/mm^2)
0	0.000000	0.000	0	0.0000	0	0.0000	-0.4
9,869	0.001290	0.000	35	-0.0002	-2	-0.0001	-2.0
15,370	0.002579	0.000	83	-0.0002	-4	-0.0002	-2.9
21,450	0.003869	0.001	128	-0.0003	-5	-0.0003	-4.0
26,970	0.005159	0.001	175	-0.0004	-6	-0.0003	-4.8
32,430	0.006449	0.001	220	-0.0005	-7	-0.0004	-5.7
33,730	0.007738	0.001	220	-0.0006	-8	-0.0005	-6.1
34,740	0.009028	0.002	220	-0.0007	-8	-0.0005	-6.5
35,520	0.010320	0.002	220	-0.0007	-9	-0.0005	-6.8
36,570	0.011610	0.002	220	-0.0008	-9	-0.0006	-7.2
37,430	0.012900	0.002	220	-0.0009	-10	-0.0006	-7.5
39,080	0.025870	0.005	220	-0.0013	-11	-0.0008	-8.9
39,050	0.038850	0.008	220	-0.0017	-12	-0.0009	-9.8
39,580	0.051830	0.011	220	-0.0021	-12	-0.0011	-10.6
39,750	0.064810	0.014	220	-0.0025	-12	-0.0012	-11.1
39,960	0.077780	0.017	222	-0.0029	-12	-0.0013	-11.6
39,990	0.090760	0.020	225	-0.0033	-11	-0.0015	-11.9
40,250	0.103700	0.023	227	-0.0037	-11	-0.0016	-12.3
40,610	0.116700	0.026	230	-0.0042	-9	-0.0018	-12.7
40,670	0.129700	0.028	232	-0.0047	-7	-0.0021	-13.1
40,130	0.142700	0.031	235	-0.0053	-4	-0.0024	-13.3
39,540	0.155600	0.034	237	-0.0060	0	-0.0028	-13.5
39,230	0.168600	0.036	239	-0.0075	0	-0.0041	-13.5
39,450	0.194600	0.041	243	-0.0087	0	-0.0047	-13.4
40,200	0.220500	0.046	248	-0.0100	0	-0.0055	-13.1
40,270	0.246500	0.052	252	-0.0112	0	-0.0061	-12.9
40,480	0.272400	0.057	256	-0.0124	0	-0.0068	-12.7
41,230	0.298400	0.062	259	-0.0142	0	-0.0080	-12.3
41,390	0.324400	0.067	263	-0.0158	0	-0.0091	-11.9
41,440	0.350300	0.072	266	-0.0173	0	-0.0101	-11.7
41,740	0.389200	0.080	271	-0.0193	0	-0.0113	-11.4
42,850	0.428200	0.088	275	-0.0214	0	-0.0126	-11.0
42,940	0.467100	0.096	279	-0.0234	0	-0.0138	-10.8
43,370	0.506000	0.104	283	-0.0254	0	-0.0150	-10.5

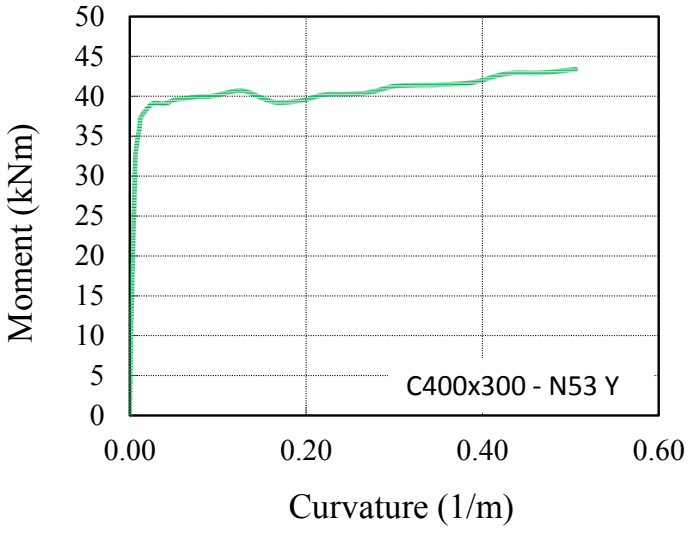

Figure D.16 : Moment – Curvature relationship of non-retrofitted column 400x300 under 53 kN axial load for Y direction.

Table D.20 : Moment – Curvature relationship of retrofitted column 400x400 under 587 kN axial load for both X and Y directions.

Moment (N)	Curvature (1/m)	Max. S220 Strain	Max. S220 Stress (N/mm^2)	Min. Cover Strain (kN/m)	Min. Cover Stress (N/mm^2)	Min. Core Strain (kN/m)	Min. Core Stress (N/mm^2)
0	0.000000	0.000	0	0.000	-4	-0.0002	-3.2
23,870	0.000658	0.000	0	0.000	-6	-0.0003	-4.7
46,960	0.001316	0.000	0	0.000	-8	-0.0004	-6.1
63,340	0.001974	0.000	22	-0.001	-10	-0.0005	-7.1
75,930	0.002632	0.000	48	-0.001	-11	-0.0006	-8.0
86,940	0.003291	0.000	75	-0.001	-13	-0.0007	-8.7
96,760	0.003949	0.001	104	-0.001	-15	-0.0008	-9.3
106,300	0.004607	0.001	133	-0.001	-16	-0.0009	-9.9
115,800	0.005265	0.001	161	-0.001	-18	-0.0009	-10.4
124,900	0.005923	0.001	190	-0.001	-19	-0.0010	-10.9
133,100	0.006581	0.001	220	-0.001	-20	-0.0011	-11.3
154,400	0.010360	0.002	220	-0.002	-27	-0.0014	-12.9
172,600	0.014140	0.003	220	-0.002	-33	-0.0017	-14.1
185,600	0.017930	0.004	220	-0.003	-34	-0.0021	-15.2
196,800	0.021710	0.005	220	-0.003	-34	-0.0025	-16.0
206,300	0.025490	0.006	220	-0.003	-35	-0.0029	-16.6
215,400	0.029270	0.007	220	-0.004	-36	-0.0032	-17.0
224,800	0.033050	0.007	220	-0.004	-36	-0.0037	-17.4
233,100	0.036830	0.008	220	-0.005	-37	-0.0040	-17.6
241,700	0.040610	0.009	220	-0.005	-38	-0.0045	-17.8
202,700	0.044400	0.011	220	-0.005	-37	-0.0040	-17.6
155,100	0.048180	0.013	220	-0.004	-36	-0.0032	-17.0
155,600	0.051960	0.014	220	-0.005	-37	-0.0034	-17.2
155,900	0.055740	0.015	220	-0.005	-37	-0.0036	-17.3
155,800	0.059520	0.016	221	-0.005	-37	-0.0037	-17.4
156,000	0.063300	0.017	222	-0.005	-38	-0.0039	-17.5
156,800	0.067080	0.018	223	-0.006	-38	-0.0041	-17.6
131,700	0.070870	0.017	222	-0.008	0	-0.0069	-18.3
157,800	0.074650	0.020	225	-0.006	-39	-0.0044	-17.8
131,900	0.078430	0.019	224	-0.009	0	-0.0075	-18.3
132,700	0.085990	0.021	225	-0.010	0	-0.0082	-18.2
132,900	0.093550	0.022	227	-0.011	0	-0.0088	-18.2
132,300	0.101100	0.024	229	-0.012	0	-0.0097	-18.1
131,700	0.112500	0.027	231	-0.013	0	-0.0110	-18.0

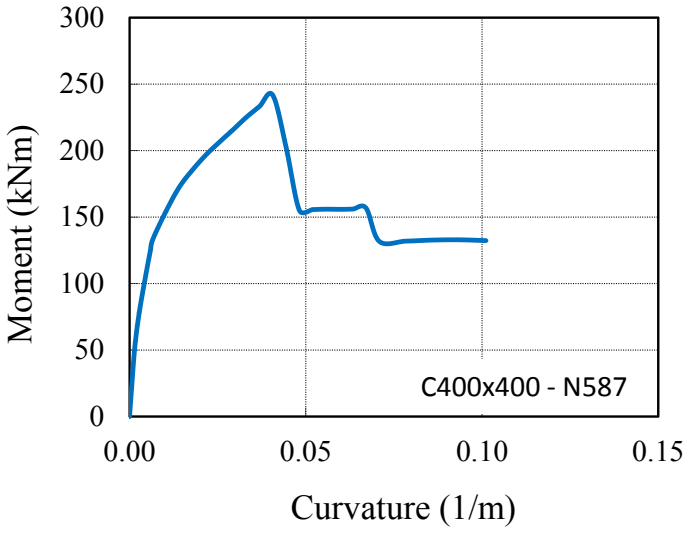

Figure D.17 : Moment – Curvature relationship of retrofitted column 400x400 under 587 kN axial load for both X and Y directions

Table D.21 : Moment – Curvature relationship for retrofitted column 400x400 under 351 kN axial load for both X and Y directions.

Moment (N)	Curvature (1/m)	Max. S220 Strain	Max. S220 Stress (N/mm^2)	Min. Cover Strain (kN/m)	Min. Cover Stress (N/mm^2)	Min. Core Strain (kN/m)	Min. Core Stress (N/mm^2)
0	0.000000	0.000	0	0.000	-2	-0.0001	-2.0
38,110	0.001130	0.000	13	0.000	-6	-0.0003	-4.5
57,160	0.002261	0.000	62	0.000	-8	-0.0004	-6.1
72,580	0.003391	0.001	114	-0.001	-11	-0.0006	-7.3
87,340	0.004522	0.001	167	-0.001	-13	-0.0007	-8.3
101,700	0.005652	0.001	220	-0.001	-15	-0.0008	-9.2
106,900	0.006783	0.001	220	-0.001	-17	-0.0009	-9.7
112,200	0.007913	0.002	220	-0.001	-18	-0.0009	-10.3
116,600	0.009044	0.002	220	-0.001	-20	-0.0010	-10.7
120,800	0.010170	0.002	220	-0.001	-21	-0.0011	-11.0
126,100	0.011300	0.003	220	-0.001	-23	-0.0011	-11.4
150,300	0.019910	0.005	220	-0.002	-32	-0.0015	-13.3
166,500	0.028510	0.008	220	-0.003	-34	-0.0019	-14.8
180,700	0.037110	0.010	220	-0.003	-35	-0.0025	-15.9
121,100	0.045710	0.014	220	-0.003	-34	-0.0016	-13.8
122,300	0.054310	0.016	221	-0.003	-35	-0.0018	-14.5
122,600	0.062910	0.019	224	-0.003	-35	-0.0020	-14.8
124,100	0.071510	0.022	226	-0.004	-35	-0.0021	-15.3
124,300	0.080110	0.024	229	-0.004	-36	-0.0023	-15.5
125,100	0.088710	0.027	231	-0.004	-36	-0.0024	-15.9
125,600	0.097310	0.030	234	-0.005	-37	-0.0026	-16.1
110,800	0.105900	0.029	233	-0.009	0	-0.0065	-18.2
110,200	0.123100	0.033	237	-0.010	0	-0.0076	-18.3
110,700	0.131700	0.036	239	-0.011	0	-0.0082	-18.2
111,000	0.140300	0.038	241	-0.012	0	-0.0087	-18.2
111,300	0.148900	0.040	243	-0.012	0	-0.0092	-18.2
112,100	0.157500	0.043	245	-0.013	0	-0.0098	-18.1
112,200	0.166100	0.045	247	-0.014	0	-0.0102	-18.1
112,600	0.174700	0.048	248	-0.015	0	-0.0108	-18.0
111,800	0.183300	0.050	250	-0.015	0	-0.0115	-17.9
112,000	0.184500	0.050	250	-0.016	0	-0.0115	-17.9

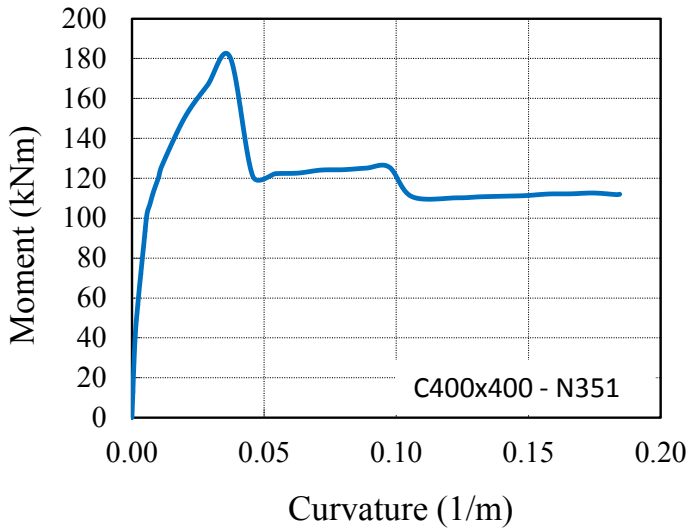

Figure D.18 : Moment – Curvature relationship of retrofitted column 400x400 under 351 kN axial load for both X and Y directions.

Table D.22 : Moment – Curvature relationship for retrofitted column 400x400 under 117 kN axial load for both X and Y directions.

Moment (N)	Curvature (1/m)	Max. S220 Strain	Max. S220 Stress (N/mm^2)	Min. Cover Strain (kN/m)	Min. Cover Stress (N/mm^2)	Min. Core Strain (kN/m)	Min. Core Stress (N/mm^2)
0	0.000000	0.000	0	0.0000	-1	0.0000	-0.7
20,050	0.000918	0.000	29	-0.0002	-3	-0.0002	-2.5
29,660	0.001836	0.000	75	-0.0003	-5	-0.0002	-3.5
37,950	0.002755	0.001	124	-0.0004	-6	-0.0003	-4.4
46,490	0.003673	0.001	172	-0.0004	-7	-0.0004	-5.1
54,800	0.004591	0.001	220	-0.0005	-9	-0.0004	-5.9
56,510	0.005509	0.001	220	-0.0006	-10	-0.0005	-6.3
58,290	0.006427	0.002	220	-0.0006	-11	-0.0005	-6.6
60,080	0.007345	0.002	220	-0.0007	-11	-0.0005	-6.9
61,390	0.008264	0.002	220	-0.0007	-12	-0.0006	-7.2
63,480	0.009182	0.002	220	-0.0008	-13	-0.0006	-7.5
68,520	0.028360	0.009	220	-0.0014	-22	-0.0007	-8.8
69,110	0.047540	0.015	220	-0.0017	-28	-0.0007	-8.2
70,770	0.066730	0.022	226	-0.0021	-33	-0.0006	-7.9
72,850	0.085910	0.028	232	-0.0025	-34	-0.0007	-8.1
73,660	0.105100	0.034	238	-0.0030	-35	-0.0007	-8.7
74,800	0.124300	0.041	243	-0.0036	-35	-0.0008	-9.5
76,170	0.143500	0.047	248	-0.0041	-36	-0.0010	-10.4
76,890	0.162600	0.053	253	-0.0046	-37	-0.0011	-11.0
69,930	0.181800	0.056	255	-0.0089	0	-0.0049	-18.0
69,720	0.201000	0.062	259	-0.0097	0	-0.0053	-18.1
70,880	0.220200	0.068	263	-0.0107	0	-0.0059	-18.2
71,970	0.239400	0.073	267	-0.0117	0	-0.0064	-18.2
71,430	0.258500	0.079	270	-0.0129	0	-0.0072	-18.3
72,410	0.277700	0.085	273	-0.0139	0	-0.0078	-18.2
72,420	0.296900	0.091	277	-0.0148	0	-0.0083	-18.2
73,740	0.316100	0.096	280	-0.0158	0	-0.0089	-18.2
74,040	0.335300	0.102	282	-0.0168	0	-0.0094	-18.1
74,360	0.354400	0.108	285	-0.0177	0	-0.0099	-18.1
74,190	0.373600	0.114	287	-0.0192	0	-0.0110	-18.0
74,120	0.392800	0.120	289	-0.0200	0	-0.0114	-17.9
74,270	0.395600	0.120	290	-0.0202	0	-0.0115	-17.9

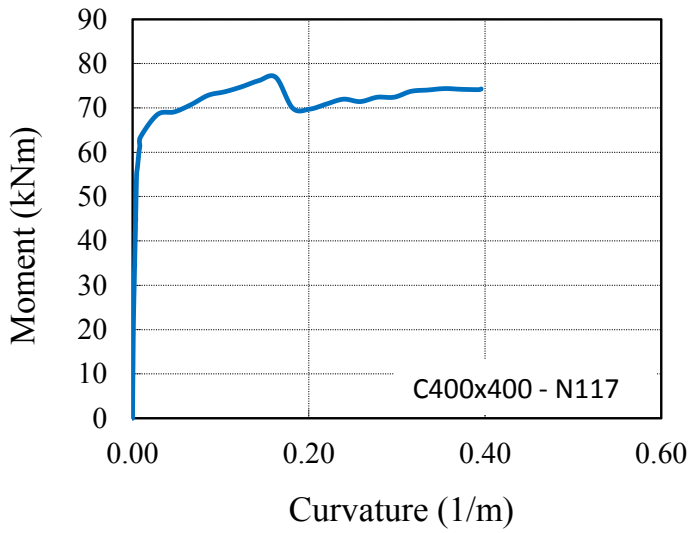

Figure D.19 : Moment – Curvature relationship of retrofitted column 400x400 under 117 kN axial load for both X and Y directions.

Table D.23 : Moment – Curvature relationship for retrofitted column 300x400 under 450 kN axial load for X direction.

Moment (N)	Curvature (1/m)	Max. S220 Strain	Max. S220 Stress (N/mm^2)	Min. Cover Strain (kN/m)	Min. Cover Stress (N/mm^2)	Min. Core Strain (kN/m)	Min. Core Stress (N/mm^2)
0	0.000000	0.000	0	0.000	-3	-0.0002	-3.2
28,600	0.001842	0.000	0	0.000	-8	-0.0004	-6.1
45,520	0.003685	0.000	48	-0.001	-12	-0.0006	-7.9
58,480	0.005527	0.001	104	-0.001	-15	-0.0008	-9.3
70,270	0.007370	0.001	161	-0.001	-18	-0.0009	-10.4
81,180	0.009212	0.001	220	-0.001	-21	-0.0011	-11.3
85,740	0.011050	0.001	220	-0.001	-23	-0.0012	-11.8
90,240	0.012900	0.002	220	-0.002	-25	-0.0012	-12.3
94,040	0.014740	0.002	220	-0.002	-27	-0.0013	-12.9
97,950	0.016580	0.002	220	-0.002	-30	-0.0014	-13.3
101,200	0.018420	0.003	220	-0.002	-32	-0.0015	-13.7
106,500	0.021520	0.003	220	-0.002	-33	-0.0017	-14.3
110,100	0.024620	0.004	220	-0.002	-34	-0.0019	-15.0
113,000	0.027710	0.004	220	-0.003	-34	-0.0021	-15.6
115,600	0.030810	0.005	220	-0.003	-34	-0.0023	-16.0
118,100	0.033910	0.006	220	-0.003	-35	-0.0024	-16.4
120,700	0.037000	0.006	220	-0.003	-35	-0.0026	-16.8
123,600	0.040100	0.007	220	-0.004	-36	-0.0028	-17.1
125,700	0.043200	0.007	220	-0.004	-36	-0.0030	-17.3
128,200	0.046290	0.008	220	-0.004	-36	-0.0032	-17.6
130,500	0.049390	0.008	220	-0.004	-37	-0.0034	-17.8
133,100	0.052480	0.009	220	-0.005	-37	-0.0036	-18.0
135,700	0.055580	0.009	220	-0.005	-37	-0.0038	-18.2
116,400	0.058680	0.010	220	-0.005	-37	-0.0033	-17.7
97,470	0.067970	0.013	220	-0.004	-37	-0.0029	-17.3
98,020	0.077260	0.015	220	-0.005	-37	-0.0031	-17.5
98,140	0.086540	0.017	222	-0.005	-38	-0.0033	-17.7
98,690	0.095830	0.019	224	-0.005	-38	-0.0035	-17.9
99,580	0.105100	0.021	226	-0.006	-39	-0.0037	-18.1
99,840	0.114400	0.023	228	-0.006	-39	-0.0039	-18.3
100,100	0.123700	0.025	229	-0.007	-40	-0.0040	-18.4
80,370	0.126800	0.021	225	-0.012	0	-0.0092	-19.3
80,050	0.142300	0.023	228	-0.013	0	-0.0105	-19.2
80,090	0.157800	0.026	230	-0.015	0	-0.0115	-19.2

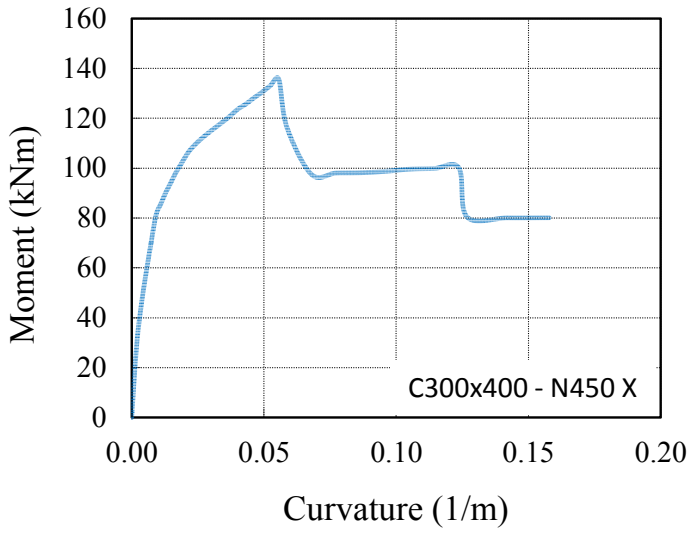

Figure D.20 : Moment – Curvature relationship of retrofitted column 300x400 under 450 kN axial load for X direction.

Table D.24 : Moment – Curvature relationship for retrofitted column 300x400 under 263 kN axial load for both X direction.

Moment (N)	Curvature (1/m)	Max. S220 Strain	Max. S220 Stress (N/mm^2)	Min. Cover Strain (kN/m)	Min. Cover Stress (N/mm^2)	Min. Core Strain (kN/m)	Min. Core Stress (N/mm^2)
0	0.000000	0.000	0	0.000	-2	-0.0001	-1.9
22,460	0.001574	0.000	13	0.000	-6	-0.0003	-4.4
33,400	0.003148	0.000	62	0.000	-8	-0.0004	-5.9
42,600	0.004721	0.001	115	-0.001	-10	-0.0005	-7.1
51,920	0.006295	0.001	166	-0.001	-13	-0.0006	-8.1
60,260	0.007869	0.001	220	-0.001	-15	-0.0007	-9.0
62,850	0.009443	0.001	220	-0.001	-17	-0.0008	-9.5
64,640	0.011020	0.002	220	-0.001	-18	-0.0009	-9.9
67,040	0.012590	0.002	220	-0.001	-20	-0.0009	-10.3
68,440	0.014160	0.002	220	-0.001	-21	-0.0010	-10.6
70,740	0.015740	0.003	220	-0.001	-22	-0.0010	-11.0
73,630	0.020820	0.004	220	-0.002	-26	-0.0011	-11.6
74,840	0.025900	0.005	220	-0.002	-28	-0.0012	-11.9
75,370	0.030980	0.006	220	-0.002	-30	-0.0012	-12.1
76,250	0.036060	0.007	220	-0.002	-33	-0.0012	-12.2
76,760	0.041150	0.008	220	-0.002	-33	-0.0013	-12.5
76,950	0.046230	0.010	220	-0.002	-33	-0.0013	-12.7
77,260	0.051310	0.011	220	-0.002	-34	-0.0014	-12.9
77,180	0.056390	0.012	220	-0.003	-34	-0.0014	-13.1
77,520	0.061470	0.013	220	-0.003	-34	-0.0015	-13.4
77,680	0.066560	0.014	220	-0.003	-34	-0.0015	-13.7
77,660	0.076720	0.016	221	-0.003	-35	-0.0016	-14.0
77,820	0.081800	0.018	223	-0.003	-35	-0.0017	-14.2
78,340	0.097050	0.021	226	-0.004	-36	-0.0018	-14.6
79,500	0.112300	0.024	229	-0.004	-36	-0.0019	-15.1
79,370	0.127500	0.028	232	-0.005	-37	-0.0020	-15.3
80,090	0.142800	0.031	235	-0.005	-38	-0.0021	-15.7
80,760	0.158000	0.035	238	-0.006	-38	-0.0023	-16.0
81,900	0.168200	0.037	240	-0.006	-39	-0.0024	-16.3
81,850	0.178400	0.039	242	-0.006	-39	-0.0025	-16.4
82,440	0.188500	0.042	244	-0.006	-40	-0.0026	-16.6
68,650	0.193600	0.036	239	-0.013	0	-0.0093	-19.3
68,880	0.213900	0.040	242	-0.015	0	-0.0102	-19.3
69,570	0.244400	0.046	247	-0.017	0	-0.0116	-19.1

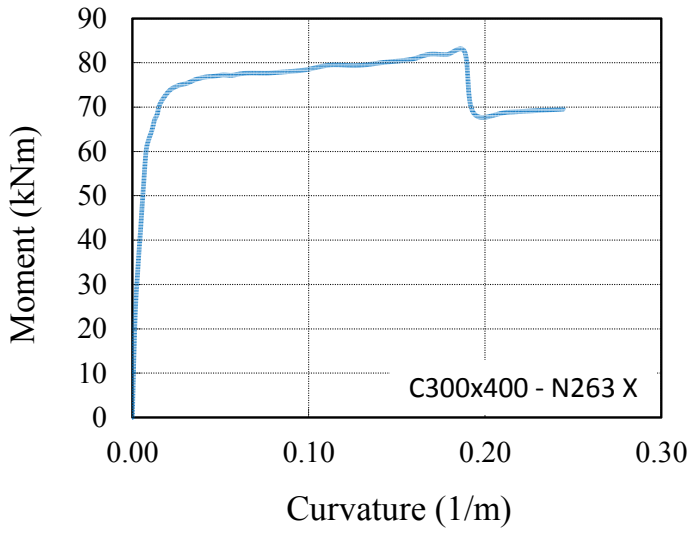

Figure D.21 : Moment – Curvature relationship of retrofitted column 300x400 under 263 kN axial load for X direction.

Table D.25 : Moment – Curvature relationship for retrofitted column 300x400 under 76 kN axial load for X direction.

Moment (N)	Curvature (1/m)	Max. S220 Strain	Max. S220 Stress (N/mm^2)	Min. Cover Strain (kN/m)	Min. Cover Stress (N/mm^2)	Min. Core Strain (kN/m)	Min. Core Stress (N/mm^2)
0	0.000000	0.000	0	0.0000	-1	0.0000	-0.6
11,220	0.001297	0.000	32	-0.0002	-3	-0.0001	-2.3
17,250	0.002595	0.000	79	-0.0003	-4	-0.0002	-3.3
23,240	0.003892	0.001	126	-0.0004	-6	-0.0003	-4.2
29,150	0.005190	0.001	173	-0.0005	-8	-0.0004	-5.0
34,900	0.006487	0.001	220	-0.0006	-9	-0.0004	-5.8
36,400	0.007784	0.001	220	-0.0006	-10	-0.0005	-6.2
37,780	0.009082	0.002	220	-0.0007	-11	-0.0005	-6.6
38,540	0.010380	0.002	220	-0.0007	-12	-0.0005	-6.8
40,200	0.011680	0.002	220	-0.0008	-13	-0.0006	-7.2
41,660	0.012970	0.002	220	-0.0009	-14	-0.0006	-7.6
43,220	0.023750	0.005	220	-0.0011	-19	-0.0006	-8.1
44,420	0.034530	0.007	220	-0.0014	-22	-0.0006	-8.1
44,390	0.045310	0.010	220	-0.0015	-25	-0.0006	-7.7
45,450	0.056090	0.013	220	-0.0017	-29	-0.0006	-7.5
45,530	0.066870	0.015	220	-0.0019	-32	-0.0005	-7.2
46,030	0.077650	0.018	223	-0.0021	-33	-0.0005	-7.1
46,820	0.088430	0.020	225	-0.0024	-34	-0.0006	-7.2
47,370	0.099210	0.023	227	-0.0026	-34	-0.0006	-7.2
47,930	0.110000	0.025	230	-0.0029	-34	-0.0006	-7.7
48,210	0.120800	0.028	232	-0.0031	-35	-0.0007	-8.2
48,640	0.131500	0.030	234	-0.0034	-35	-0.0007	-8.9
48,970	0.142300	0.033	236	-0.0037	-36	-0.0008	-9.4
49,380	0.153100	0.035	238	-0.0040	-36	-0.0009	-10.0
49,530	0.163900	0.038	240	-0.0043	-36	-0.0009	-10.4
49,610	0.174700	0.040	242	-0.0046	-37	-0.0010	-10.8
50,510	0.185400	0.042	244	-0.0049	-37	-0.0011	-11.4
50,960	0.196200	0.045	246	-0.0052	-38	-0.0012	-11.9
51,010	0.207000	0.047	248	-0.0055	-38	-0.0012	-12.2
51,760	0.228600	0.052	252	-0.0061	-39	-0.0014	-13.0
52,670	0.250100	0.057	256	-0.0066	-40	-0.0014	-13.3
43,700	0.260900	0.057	256	-0.0097	0	-0.0043	-18.6
45,530	0.347100	0.074	267	-0.0149	0	-0.0078	-19.3
46,660	0.444100	0.094	278	-0.0191	0	-0.0100	-19.3

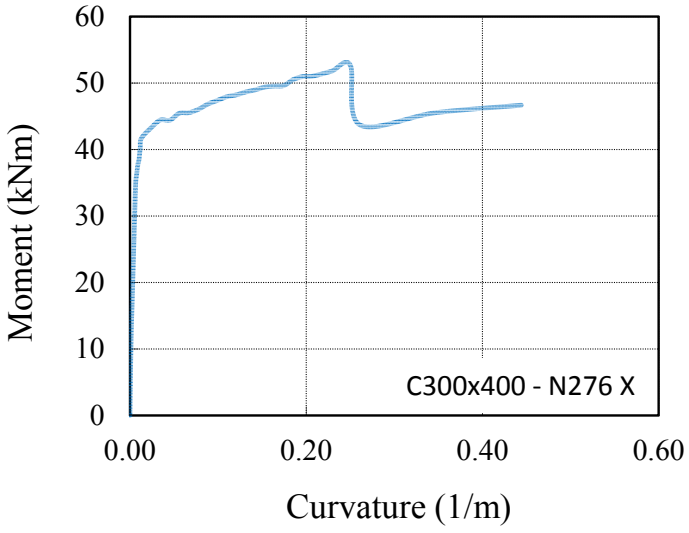

Figure D.22 : Moment – Curvature relationship of retrofitted column 300x400 under 76 kN axial load for X direction.

Table D.26 : Moment – Curvature relationship for retrofitted column 300x400 under 450 kN axial load for Y direction.

Moment (N)	Curvature (1/m)	Max. S220 Strain	Max. S220 Stress (N/mm^2)	Min. Cover Strain (kN/m)	Min. Cover Stress (N/mm^2)	Min. Core Strain (kN/m)	Min. Core Stress (N/mm^2)
0	0.000000	0.000	0	0.000	-3	-0.0002	-3.2
37,420	0.001311	0.000	0	0.000	-8	-0.0004	-6.1
60,690	0.002622	0.000	50	-0.001	-11	-0.0006	-8.0
78,530	0.003933	0.001	104	-0.001	-14	-0.0008	-9.4
94,740	0.005244	0.001	161	-0.001	-17	-0.0009	-10.5
110,100	0.006555	0.001	220	-0.001	-20	-0.0011	-11.5
116,400	0.007866	0.001	220	-0.001	-23	-0.0012	-12.1
121,400	0.009177	0.002	220	-0.002	-25	-0.0013	-12.7
125,900	0.010490	0.002	220	-0.002	-27	-0.0014	-13.2
130,700	0.011800	0.002	220	-0.002	-29	-0.0015	-13.7
134,900	0.013110	0.003	220	-0.002	-32	-0.0016	-14.1
141,800	0.015420	0.003	220	-0.002	-33	-0.0018	-14.8
147,300	0.017740	0.004	220	-0.002	-34	-0.0021	-15.5
151,900	0.020050	0.004	220	-0.003	-34	-0.0023	-16.1
155,400	0.022360	0.005	220	-0.003	-34	-0.0025	-16.5
159,200	0.024670	0.006	220	-0.003	-35	-0.0027	-16.9
162,600	0.026990	0.006	220	-0.003	-35	-0.0029	-17.2
166,500	0.029300	0.007	220	-0.004	-36	-0.0031	-17.5
169,900	0.031610	0.007	220	-0.004	-36	-0.0033	-17.8
173,000	0.033930	0.008	220	-0.004	-36	-0.0035	-18.0
176,900	0.036240	0.008	220	-0.005	-37	-0.0038	-18.2
180,300	0.038550	0.009	220	-0.005	-37	-0.0040	-18.4
183,300	0.040870	0.009	220	-0.005	-38	-0.0042	-18.5
158,700	0.043180	0.011	220	-0.005	-37	-0.0039	-18.3
131,600	0.047810	0.013	220	-0.004	-37	-0.0034	-17.8
132,200	0.052430	0.014	220	-0.005	-37	-0.0036	-18.1
132,200	0.057060	0.015	220	-0.005	-37	-0.0038	-18.2
133,200	0.064000	0.017	222	-0.005	-38	-0.0041	-18.4
133,400	0.070940	0.019	224	-0.006	-39	-0.0043	-18.6
134,200	0.077870	0.021	226	-0.006	-39	-0.0046	-18.7
135,200	0.084810	0.023	228	-0.007	-40	-0.0049	-18.9
114,400	0.087130	0.021	225	-0.010	0	-0.0085	-19.3
114,800	0.096380	0.023	228	-0.011	0	-0.0092	-19.3
113,700	0.119500	0.028	232	-0.014	0	-0.0118	-19.1

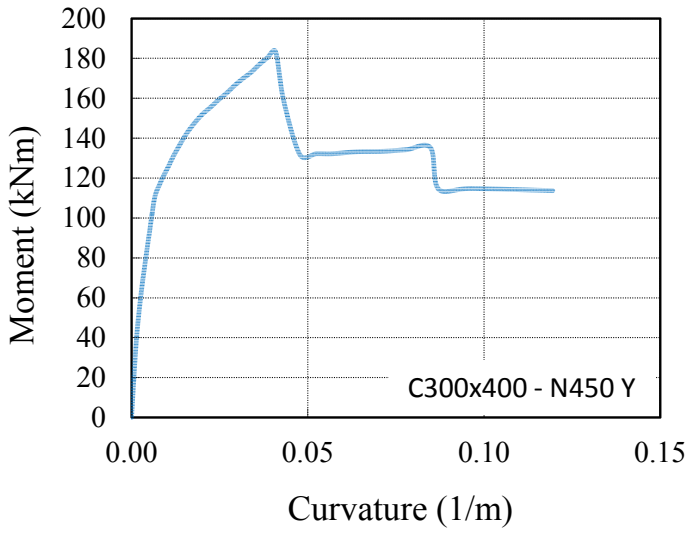

Figure D.23 : Moment – Curvature relationship of retrofitted column 300x400 under 450 kN axial load for Y direction.

Table D.27 : Moment – Curvature relationship for retrofitted column 300x400 under 263 kN axial load for Y direction.

Moment (N)	Curvature (1/m)	Max. S220 Strain	Max. S220 Stress (N/mm^2)	Min. Cover Strain (kN/m)	Min. Cover Stress (N/mm^2)	Min. Core Strain (kN/m)	Min. Core Stress (N/mm^2)
0	0.000000	0.000	0	0.000	-2	-0.0001	-1.9
29,860	0.001125	0.000	15	0.000	-5	-0.0003	-4.4
45,230	0.002250	0.000	63	0.000	-8	-0.0004	-6.0
58,090	0.003376	0.001	115	-0.001	-10	-0.0006	-7.2
70,640	0.004501	0.001	167	-0.001	-13	-0.0007	-8.3
82,300	0.005626	0.001	220	-0.001	-15	-0.0008	-9.2
85,930	0.006751	0.001	220	-0.001	-16	-0.0008	-9.8
88,320	0.007876	0.002	220	-0.001	-18	-0.0009	-10.2
90,740	0.009001	0.002	220	-0.001	-19	-0.0010	-10.6
93,200	0.010130	0.002	220	-0.001	-20	-0.0010	-11.0
96,240	0.011250	0.003	220	-0.001	-22	-0.0011	-11.4
100,900	0.014780	0.004	220	-0.002	-25	-0.0012	-12.2
102,400	0.018310	0.005	220	-0.002	-28	-0.0013	-12.6
103,400	0.021840	0.006	220	-0.002	-30	-0.0014	-12.9
103,700	0.025370	0.007	220	-0.002	-32	-0.0014	-13.1
104,300	0.028900	0.008	220	-0.002	-33	-0.0015	-13.3
105,300	0.032420	0.009	220	-0.002	-33	-0.0015	-13.7
105,300	0.035950	0.010	220	-0.002	-34	-0.0016	-14.0
105,700	0.039480	0.012	220	-0.002	-34	-0.0017	-14.3
105,100	0.043010	0.013	220	-0.003	-34	-0.0017	-14.3
105,900	0.046540	0.014	220	-0.003	-34	-0.0018	-14.7
105,800	0.050070	0.015	220	-0.003	-34	-0.0018	-14.8
106,100	0.053600	0.016	221	-0.003	-35	-0.0019	-15.0
107,100	0.060650	0.018	223	-0.003	-35	-0.0021	-15.5
107,000	0.071240	0.022	226	-0.004	-36	-0.0022	-15.9
108,000	0.078300	0.024	228	-0.004	-36	-0.0024	-16.3
108,300	0.088880	0.027	231	-0.004	-37	-0.0026	-16.6
109,900	0.099470	0.030	234	-0.005	-37	-0.0028	-17.0
110,800	0.110100	0.034	237	-0.005	-38	-0.0030	-17.3
110,400	0.120600	0.037	240	-0.006	-38	-0.0030	-17.4
111,400	0.131200	0.041	243	-0.006	-39	-0.0032	-17.7
112,200	0.141800	0.044	246	-0.006	-39	-0.0034	-17.9
98,550	0.145300	0.039	242	-0.012	0	-0.0094	-19.3
98,290	0.170000	0.045	247	-0.015	0	-0.0115	-19.2

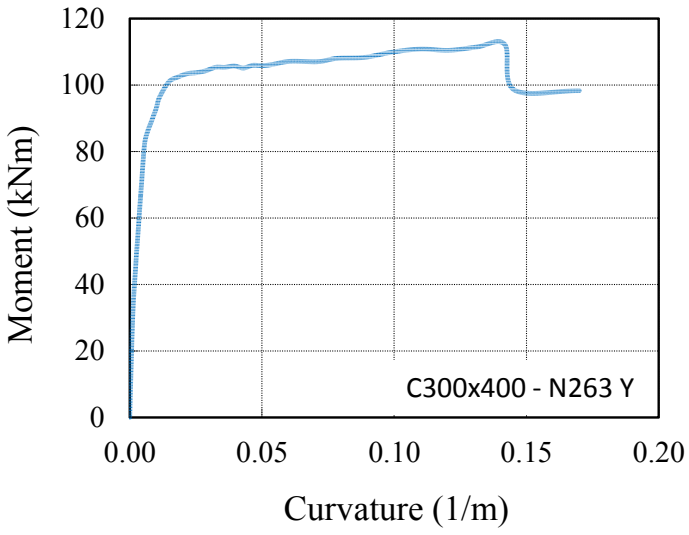

Figure D.24 : Moment – Curvature relationship of retrofitted column 300x400 under 263 kN axial load for Y direction.

Table D.28 : Moment – Curvature relationship for retrofitted column 300x400 under 76 kN axial load for Y direction.

Moment (N)	Curvature (1/m)	Max. S220 Strain	Max. S220 Stress (N/mm^2)	Min. Cover Strain (kN/m)	Min. Cover Stress (N/mm^2)	Min. Core Strain (kN/m)	Min. Core Stress (N/mm^2)
0	0.000000	0.000	0	0.0000	-1	0.0000	-0.6
15,310	0.000924	0.000	32	-0.0002	-3	-0.0002	-2.3
23,280	0.001847	0.000	79	-0.0003	-4	-0.0002	-3.4
31,420	0.002770	0.001	126	-0.0004	-6	-0.0003	-4.3
39,780	0.003694	0.001	172	-0.0005	-7	-0.0004	-5.3
47,770	0.004617	0.001	220	-0.0005	-9	-0.0004	-6.1
49,920	0.005541	0.001	220	-0.0006	-10	-0.0005	-6.6
51,320	0.006464	0.002	220	-0.0007	-11	-0.0005	-7.0
53,070	0.007388	0.002	220	-0.0007	-12	-0.0006	-7.4
54,410	0.008311	0.002	220	-0.0008	-13	-0.0006	-7.7
55,940	0.009235	0.002	220	-0.0008	-14	-0.0006	-8.0
59,150	0.017260	0.005	220	-0.0011	-18	-0.0008	-9.1
59,680	0.025280	0.008	220	-0.0013	-22	-0.0008	-9.4
59,950	0.033300	0.010	220	-0.0015	-25	-0.0008	-9.5
61,170	0.041320	0.013	220	-0.0017	-28	-0.0008	-9.7
60,860	0.049340	0.016	221	-0.0018	-30	-0.0008	-9.4
61,520	0.057360	0.018	223	-0.0020	-33	-0.0008	-9.3
62,050	0.065380	0.021	226	-0.0022	-33	-0.0008	-9.4
62,610	0.073400	0.024	228	-0.0024	-34	-0.0008	-9.6
63,220	0.081430	0.026	231	-0.0025	-34	-0.0008	-9.8
64,180	0.089450	0.029	233	-0.0028	-34	-0.0009	-10.3
64,970	0.097470	0.032	235	-0.0030	-35	-0.0010	-10.8
65,360	0.105500	0.034	238	-0.0033	-35	-0.0011	-11.2
65,310	0.113500	0.037	240	-0.0035	-35	-0.0011	-11.5
65,740	0.121500	0.039	242	-0.0037	-36	-0.0012	-11.9
67,170	0.129600	0.042	244	-0.0040	-36	-0.0013	-12.4
66,870	0.137600	0.045	246	-0.0042	-36	-0.0013	-12.6
68,310	0.153600	0.050	250	-0.0046	-37	-0.0014	-13.3
68,930	0.177700	0.058	256	-0.0053	-38	-0.0016	-14.0
69,810	0.201700	0.066	262	-0.0060	-39	-0.0018	-14.7
71,340	0.225800	0.074	267	-0.0067	-40	-0.0020	-15.3
71,680	0.233800	0.076	268	-0.0069	-40	-0.0021	-15.5
68,260	0.241800	0.078	269	-0.0081	0	-0.0031	-17.4
65,240	0.282000	0.086	274	-0.0139	0	-0.0080	-19.3

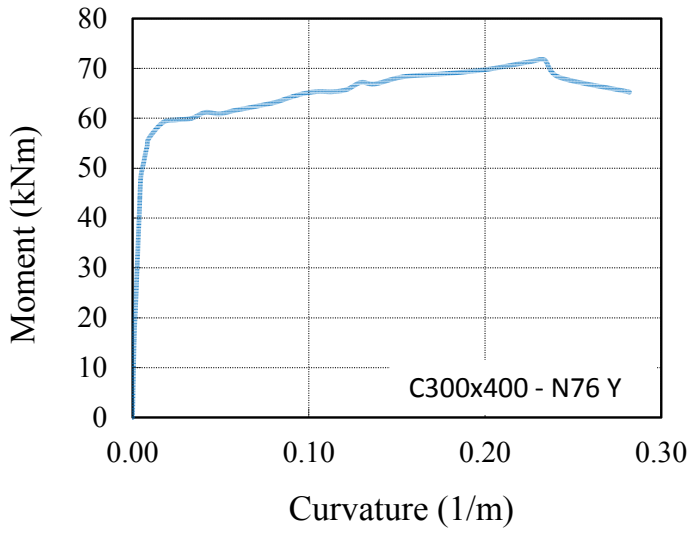

Figure D.25 : Moment – Curvature relationship of retrofitted column 300x400 under 76 kN axial load for Y direction.

Table D.29 : Moment – Curvature relationship for retrofitted column 400x300 under 324 kN axial load for X direction.

Moment (N)	Curvature (1/m)	Max. S220 Strain	Max. S220 Stress (N/mm^2)	Min. Cover Strain (kN/m)	Min. Cover Stress (N/mm^2)	Min. Core Strain (kN/m)	Min. Core Stress (N/mm^2)
0	0.000000	0.000	0	-0.0001	-2	-0.0001	-2.3
33,010	0.001199	0.000	10	-0.0004	-6	-0.0004	-5.0
51,850	0.002399	0.000	58	-0.0006	-9	-0.0005	-6.8
67,230	0.003598	0.001	111	-0.0007	-12	-0.0006	-8.1
81,700	0.004798	0.001	165	-0.0009	-15	-0.0008	-9.3
95,670	0.005997	0.001	220	-0.0010	-17	-0.0009	-10.2
101,500	0.007197	0.001	220	-0.0012	-19	-0.0010	-10.9
106,100	0.008396	0.002	220	-0.0013	-21	-0.0011	-11.4
111,300	0.009596	0.002	220	-0.0014	-23	-0.0012	-11.9
115,800	0.010800	0.002	220	-0.0015	-24	-0.0012	-12.4
120,300	0.011990	0.003	220	-0.0016	-26	-0.0013	-12.8
130,200	0.015030	0.003	220	-0.0019	-31	-0.0016	-13.8
137,900	0.018060	0.004	220	-0.0022	-33	-0.0018	-14.6
143,000	0.021100	0.005	220	-0.0024	-34	-0.0020	-15.3
148,600	0.024130	0.006	220	-0.0027	-34	-0.0022	-15.9
153,500	0.027160	0.007	220	-0.0030	-35	-0.0025	-16.5
159,000	0.030200	0.007	220	-0.0034	-35	-0.0027	-17.0
163,900	0.033230	0.008	220	-0.0037	-36	-0.0030	-17.4
168,400	0.036260	0.009	220	-0.0040	-36	-0.0033	-17.7
173,300	0.039300	0.010	220	-0.0044	-37	-0.0035	-18.0
148,800	0.042330	0.011	220	-0.0041	-36	-0.0032	-17.7
121,300	0.048400	0.013	220	-0.0038	-36	-0.0028	-17.1
122,500	0.054470	0.015	220	-0.0042	-36	-0.0031	-17.5
124,100	0.060530	0.017	222	-0.0046	-37	-0.0034	-17.8
127,200	0.069640	0.019	224	-0.0053	-38	-0.0038	-18.3
128,800	0.078740	0.022	227	-0.0059	-39	-0.0043	-18.5
117,900	0.087840	0.026	230	-0.0054	-38	-0.0035	-18.0
118,500	0.096940	0.029	233	-0.0057	-39	-0.0037	-18.1
118,500	0.106000	0.032	235	-0.0061	-39	-0.0038	-18.3
119,600	0.115100	0.034	238	-0.0065	-40	-0.0041	-18.4
110,600	0.118200	0.028	233	-0.0136	0	-0.0111	-19.2
110,600	0.121200	0.029	233	-0.0139	0	-0.0113	-19.2
103,300	0.136400	0.035	238	-0.0132	0	-0.0104	-19.2
103,900	0.151500	0.039	242	-0.0147	0	-0.0115	-19.2

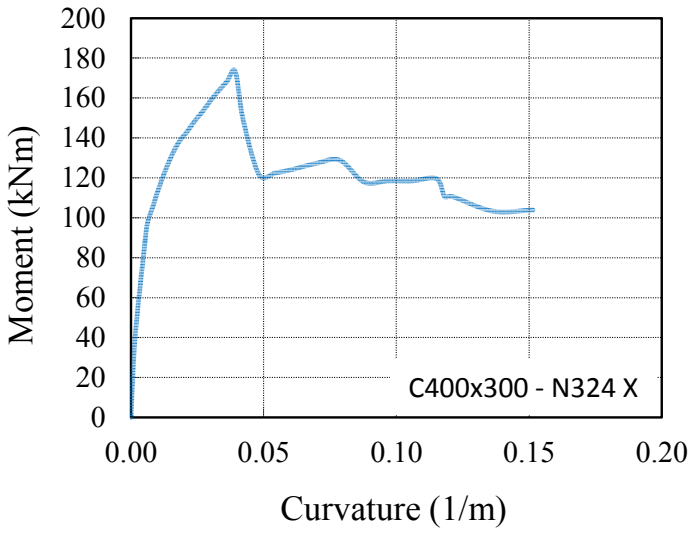

Figure D.26 : Moment – Curvature relationship of retrofitted column 400x300 under 324 kN axial load for X direction.

Table D.30 : Moment – Curvature relationship for retrofitted column 400x300 under 190 kN axial load for X direction.

Moment (N)	Curvature (1/m)	Max. S220 Strain	Max. S220 Stress (N/mm^2)	Min. Cover Strain (kN/m)	Min. Cover Stress (N/mm^2)	Min. Core Strain (kN/m)	Min. Core Stress (N/mm^2)
0	0.000000	0.000	0	-0.0001	-1	-0.0001	-1.4
16,090	0.000528	0.000	0	-0.0002	-3	-0.0002	-2.7
25,380	0.001056	0.000	21	-0.0003	-4	-0.0002	-3.7
32,180	0.001584	0.000	45	-0.0003	-6	-0.0003	-4.4
38,580	0.002112	0.000	69	-0.0004	-7	-0.0004	-5.1
44,800	0.002640	0.000	93	-0.0005	-8	-0.0004	-5.8
50,630	0.003169	0.001	118	-0.0005	-9	-0.0005	-6.3
56,050	0.003697	0.001	144	-0.0006	-10	-0.0005	-6.8
62,060	0.004225	0.001	169	-0.0007	-11	-0.0006	-7.4
67,840	0.004753	0.001	194	-0.0007	-12	-0.0006	-7.9
73,340	0.005281	0.001	220	-0.0008	-13	-0.0007	-8.3
89,460	0.012960	0.003	220	-0.0013	-22	-0.0010	-11.1
91,430	0.020640	0.006	220	-0.0016	-26	-0.0012	-11.8
92,840	0.028320	0.008	220	-0.0018	-30	-0.0012	-12.3
93,880	0.036000	0.011	220	-0.0020	-33	-0.0013	-12.6
93,390	0.043680	0.013	220	-0.0023	-33	-0.0014	-12.9
94,190	0.051360	0.016	221	-0.0025	-34	-0.0014	-13.3
95,640	0.059050	0.018	223	-0.0028	-34	-0.0016	-13.8
95,500	0.066730	0.021	225	-0.0030	-35	-0.0016	-14.1
96,370	0.074410	0.023	228	-0.0033	-35	-0.0017	-14.4
97,390	0.082090	0.026	230	-0.0035	-35	-0.0018	-14.8
97,820	0.089770	0.028	232	-0.0038	-36	-0.0019	-15.0
97,510	0.097450	0.031	235	-0.0040	-36	-0.0019	-15.1
98,350	0.105100	0.033	237	-0.0042	-36	-0.0020	-15.3
98,800	0.112800	0.036	239	-0.0044	-37	-0.0021	-15.5
99,600	0.120500	0.038	241	-0.0047	-37	-0.0022	-15.7
99,720	0.128200	0.041	243	-0.0049	-37	-0.0022	-15.9
100,400	0.135900	0.043	245	-0.0051	-38	-0.0023	-16.1
101,400	0.143500	0.046	247	-0.0054	-38	-0.0024	-16.3
101,200	0.151200	0.048	249	-0.0056	-38	-0.0024	-16.4
90,680	0.158900	0.045	247	-0.0114	0	-0.0081	-19.3
90,710	0.166600	0.047	248	-0.0124	0	-0.0089	-19.3
91,560	0.181900	0.051	251	-0.0135	0	-0.0097	-19.3
92,450	0.212700	0.060	258	-0.0157	0	-0.0113	-19.2

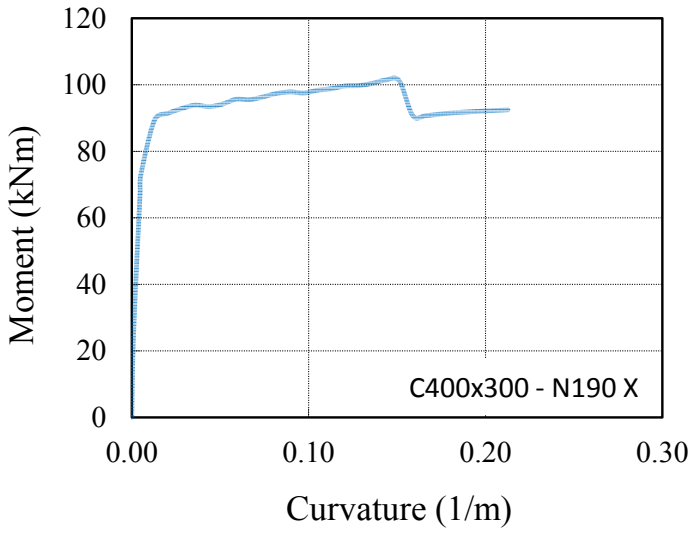

Figure D.27 : Moment – Curvature relationship of retrofitted column 400x300 under 190 kN axial load for X direction.

Table D.31 : Moment – Curvature relationship for retrofitted column 400x300 under 53 kN axial load for X direction.

Moment (N)	Curvature (1/m)	Max. S220 Strain	Max. S220 Stress (N/mm^2)	Min. Cover Strain (kN/m)	Min. Cover Stress (N/mm^2)	Min. Core Strain (kN/m)	Min. Core Stress (N/mm^2)
0	0.000000	0.000	0	0.0000	0	0.0000	-0.4
8,805	0.000451	0.000	13	-0.0001	-2	-0.0001	-1.4
13,000	0.000902	0.000	35	-0.0001	-2	-0.0001	-2.0
17,390	0.001353	0.000	57	-0.0002	-3	-0.0002	-2.6
20,970	0.001805	0.000	81	-0.0002	-4	-0.0002	-3.0
24,840	0.002256	0.001	105	-0.0003	-5	-0.0002	-3.5
29,370	0.002707	0.001	126	-0.0003	-5	-0.0003	-4.0
33,360	0.003158	0.001	150	-0.0004	-6	-0.0003	-4.5
37,240	0.003609	0.001	173	-0.0004	-7	-0.0003	-4.9
40,980	0.004060	0.001	197	-0.0005	-8	-0.0004	-5.3
44,410	0.004511	0.001	220	-0.0005	-8	-0.0004	-5.6
55,620	0.019490	0.006	220	-0.0011	-18	-0.0007	-8.6
56,800	0.034470	0.011	220	-0.0015	-24	-0.0008	-9.0
56,900	0.049450	0.016	221	-0.0017	-29	-0.0007	-8.7
58,500	0.064440	0.021	226	-0.0020	-33	-0.0007	-8.6
59,480	0.079420	0.026	230	-0.0024	-34	-0.0007	-9.0
61,180	0.094400	0.031	235	-0.0028	-34	-0.0008	-9.8
61,440	0.109400	0.036	239	-0.0032	-35	-0.0009	-10.5
62,400	0.124400	0.041	243	-0.0037	-35	-0.0011	-11.3
62,610	0.139300	0.045	247	-0.0041	-36	-0.0012	-11.8
64,240	0.154300	0.050	251	-0.0045	-37	-0.0013	-12.6
65,270	0.169300	0.055	254	-0.0050	-37	-0.0014	-13.2
65,720	0.184300	0.060	258	-0.0054	-38	-0.0015	-13.7
66,120	0.199300	0.065	261	-0.0058	-39	-0.0016	-14.1
60,960	0.214200	0.066	262	-0.0096	0	-0.0052	-19.0
60,760	0.229200	0.071	265	-0.0102	0	-0.0054	-19.0
65,180	0.244200	0.079	270	-0.0080	0	-0.0029	-17.2
61,820	0.259200	0.081	271	-0.0116	0	-0.0062	-19.2
61,730	0.274200	0.085	274	-0.0121	0	-0.0064	-19.2
62,610	0.289100	0.090	276	-0.0129	0	-0.0069	-19.3
63,330	0.304100	0.094	279	-0.0136	0	-0.0073	-19.3
63,710	0.319100	0.098	281	-0.0149	0	-0.0082	-19.3
63,780	0.334100	0.103	283	-0.0155	0	-0.0086	-19.3
63,380	0.349100	0.108	285	-0.0160	0	-0.0088	-19.3

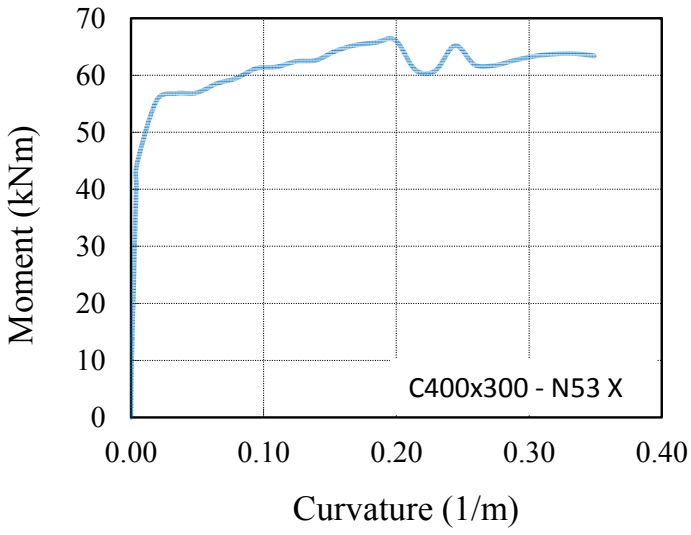

Figure D.28 : Moment – Curvature relationship of retrofitted column 400x300 under 53 kN axial load for X direction.

Table D.32 : Moment – Curvature relationship for retrofitted column 400x300 under 324 kN axial load for Y direction.

Moment (N)	Curvature (1/m)	Max. S220 Strain	Max. S220 Stress (N/mm^2)	Min. Cover Strain (kN/m)	Min. Cover Stress (N/mm^2)	Min. Core Strain (kN/m)	Min. Core Stress (N/mm^2)
0	0.000000	0.000	0	-0.0001	-2	-0.0001	-2.3
24,970	0.001689	0.000	9	-0.0004	-6	-0.0004	-5.0
38,580	0.003378	0.000	59	-0.0006	-9	-0.0005	-6.7
50,150	0.005067	0.001	111	-0.0007	-12	-0.0006	-8.0
61,050	0.006756	0.001	164	-0.0009	-15	-0.0008	-9.1
71,730	0.008445	0.001	219	-0.0011	-18	-0.0009	-10.1
75,870	0.010130	0.001	220	-0.0012	-19	-0.0010	-10.7
79,860	0.011820	0.002	220	-0.0013	-21	-0.0010	-11.2
83,800	0.013510	0.002	220	-0.0014	-23	-0.0011	-11.6
87,490	0.015200	0.002	220	-0.0015	-25	-0.0012	-12.0
91,660	0.016890	0.003	220	-0.0016	-27	-0.0013	-12.4
100,400	0.021210	0.004	220	-0.0019	-31	-0.0015	-13.4
107,000	0.025530	0.004	220	-0.0022	-33	-0.0016	-14.1
111,600	0.029860	0.005	220	-0.0025	-34	-0.0019	-14.9
115,900	0.034180	0.006	220	-0.0028	-34	-0.0021	-15.5
120,600	0.038500	0.007	220	-0.0031	-35	-0.0023	-16.1
124,800	0.042830	0.008	220	-0.0034	-35	-0.0026	-16.6
129,300	0.047150	0.008	220	-0.0038	-36	-0.0028	-17.1
133,600	0.051470	0.009	220	-0.0041	-36	-0.0031	-17.5
104,900	0.055800	0.011	220	-0.0036	-35	-0.0024	-16.4
84,250	0.060120	0.012	220	-0.0030	-35	-0.0018	-14.7
83,970	0.064440	0.013	220	-0.0032	-35	-0.0018	-14.8
83,780	0.068760	0.014	220	-0.0033	-35	-0.0019	-14.9
84,970	0.081730	0.017	222	-0.0038	-36	-0.0021	-15.5
85,140	0.094700	0.020	225	-0.0042	-36	-0.0022	-15.9
86,350	0.107700	0.023	227	-0.0047	-37	-0.0025	-16.4
86,360	0.120600	0.026	230	-0.0050	-38	-0.0026	-16.6
87,030	0.133600	0.029	233	-0.0054	-38	-0.0026	-16.7
87,720	0.146600	0.032	235	-0.0057	-38	-0.0027	-16.9
88,020	0.159500	0.035	238	-0.0061	-39	-0.0028	-17.0
88,370	0.172500	0.038	240	-0.0064	-40	-0.0029	-17.2
72,840	0.176800	0.032	236	-0.0131	0	-0.0095	-19.3
73,580	0.194100	0.035	238	-0.0144	0	-0.0104	-19.2
73,600	0.215700	0.039	242	-0.0158	0	-0.0114	-19.2

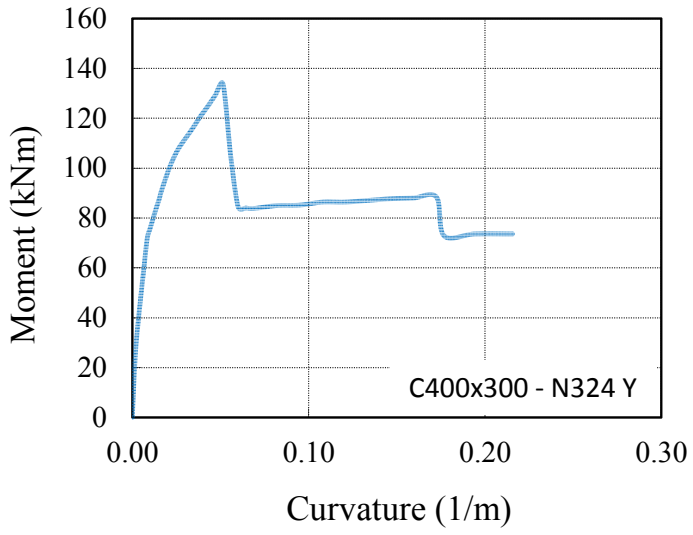

Figure D.29 : Moment – Curvature relationship of retrofitted column 400x300 under 324 kN axial load for Y direction.

Table D.33 : Moment – Curvature relationship for retrofitted column 400x300 under 190 kN axial load for Y direction.

Moment (N)	Curvature (1/m)	Max. S220 Strain	Max. S220 Stress (N/mm^2)	Min. Cover Strain (kN/m)	Min. Cover Stress (N/mm^2)	Min. Core Strain (kN/m)	Min. Core Stress (N/mm^2)
0	0.000000	0.000	0	-0.0001	-1	-0.0001	-1.4
12,240	0.000741	0.000	0	-0.0002	-3	-0.0002	-2.7
19,080	0.001482	0.000	20	-0.0003	-5	-0.0002	-3.7
24,060	0.002222	0.000	44	-0.0003	-6	-0.0003	-4.4
28,510	0.002963	0.000	68	-0.0004	-7	-0.0004	-5.0
32,970	0.003704	0.000	93	-0.0005	-8	-0.0004	-5.6
37,190	0.004445	0.001	118	-0.0005	-9	-0.0005	-6.2
41,210	0.005186	0.001	144	-0.0006	-10	-0.0005	-6.7
45,440	0.005927	0.001	169	-0.0007	-11	-0.0005	-7.2
49,490	0.006667	0.001	195	-0.0007	-12	-0.0006	-7.6
53,590	0.007408	0.001	220	-0.0008	-13	-0.0006	-8.1
65,340	0.018610	0.003	220	-0.0013	-22	-0.0010	-10.6
66,440	0.029810	0.006	220	-0.0016	-27	-0.0010	-11.0
68,590	0.041010	0.009	220	-0.0019	-32	-0.0011	-11.4
68,730	0.052210	0.011	220	-0.0022	-33	-0.0011	-11.6
68,740	0.063410	0.014	220	-0.0024	-34	-0.0011	-11.7
68,910	0.074610	0.016	221	-0.0027	-34	-0.0012	-12.1
69,920	0.085810	0.019	224	-0.0031	-35	-0.0013	-12.7
70,600	0.097010	0.021	226	-0.0034	-35	-0.0014	-13.1
70,400	0.108200	0.024	228	-0.0037	-36	-0.0015	-13.4
71,480	0.119400	0.026	231	-0.0040	-36	-0.0016	-13.9
71,700	0.130600	0.029	233	-0.0043	-36	-0.0017	-14.2
72,270	0.141800	0.032	235	-0.0047	-37	-0.0017	-14.5
72,080	0.153000	0.034	238	-0.0050	-37	-0.0018	-14.7
72,840	0.164200	0.037	240	-0.0053	-38	-0.0019	-15.0
73,720	0.175400	0.039	242	-0.0056	-38	-0.0020	-15.4
74,180	0.186600	0.042	244	-0.0059	-39	-0.0021	-15.6
74,540	0.197800	0.044	246	-0.0063	-39	-0.0022	-15.8
70,060	0.209000	0.046	247	-0.0076	0	-0.0033	-17.7
64,090	0.220200	0.044	246	-0.0123	0	-0.0078	-19.3
64,400	0.231400	0.046	247	-0.0129	0	-0.0082	-19.3
64,480	0.242600	0.049	249	-0.0134	0	-0.0085	-19.3
64,690	0.276200	0.055	254	-0.0159	0	-0.0102	-19.3
65,150	0.309800	0.061	259	-0.0177	0	-0.0113	-19.2

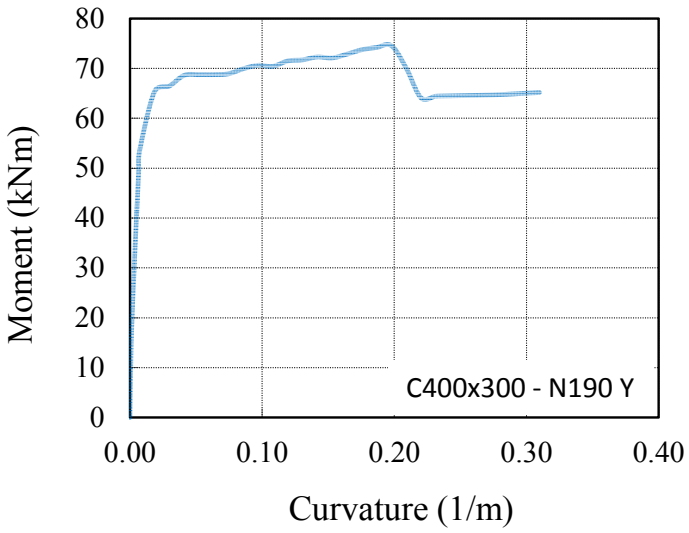

Figure D.30 : Moment – Curvature relationship of retrofitted column 400x300 under 190 kN axial load for Y direction.

Table D.34 : Moment – Curvature relationship for retrofitted column 400x300 under 53 kN axial load for Y direction.

Moment (N)	Curvature (1/m)	Max. S220 Strain	Max. S220 Stress (N/mm^2)	Min. Cover Strain (kN/m)	Min. Cover Stress (N/mm^2)	Min. Core Strain (kN/m)	Min. Core Stress (N/mm^2)
0	0.000000	0.000	0	0.0000	0	0.0000	-0.4
6,635	0.000630	0.000	12	-0.0001	-2	-0.0001	-1.4
9,807	0.001259	0.000	34	-0.0002	-2	-0.0001	-2.0
12,540	0.001889	0.000	57	-0.0002	-3	-0.0002	-2.4
15,120	0.002518	0.000	81	-0.0002	-4	-0.0002	-2.8
18,310	0.003148	0.001	104	-0.0003	-5	-0.0002	-3.3
21,400	0.003777	0.001	126	-0.0003	-6	-0.0003	-3.8
23,840	0.004407	0.001	150	-0.0004	-6	-0.0003	-4.1
26,610	0.005036	0.001	174	-0.0004	-7	-0.0003	-4.5
30,070	0.005666	0.001	195	-0.0005	-8	-0.0004	-5.1
32,730	0.006295	0.001	219	-0.0005	-9	-0.0004	-5.4
40,450	0.025100	0.005	220	-0.0011	-18	-0.0006	-7.5
41,060	0.043900	0.010	220	-0.0014	-24	-0.0005	-7.0
42,130	0.062700	0.014	220	-0.0018	-29	-0.0005	-6.5
43,840	0.081500	0.019	224	-0.0021	-33	-0.0004	-6.1
45,070	0.100300	0.023	228	-0.0025	-34	-0.0005	-6.3
45,110	0.119100	0.027	232	-0.0029	-34	-0.0005	-6.4
46,520	0.137900	0.032	235	-0.0035	-35	-0.0006	-8.0
47,180	0.156700	0.036	239	-0.0040	-36	-0.0008	-9.0
47,560	0.175500	0.040	243	-0.0045	-37	-0.0009	-9.9
47,720	0.194300	0.045	246	-0.0049	-37	-0.0009	-10.1
48,690	0.213100	0.049	250	-0.0053	-38	-0.0009	-10.4
49,210	0.231900	0.054	253	-0.0057	-38	-0.0009	-10.2
49,080	0.250700	0.058	256	-0.0059	-39	-0.0008	-9.2
50,120	0.269500	0.062	259	-0.0064	-39	-0.0008	-9.6
50,080	0.288300	0.067	263	-0.0066	-40	-0.0007	-8.7
42,360	0.307100	0.068	263	-0.0106	0	-0.0043	-18.6
43,120	0.325900	0.072	266	-0.0112	0	-0.0045	-18.7
42,930	0.344700	0.076	268	-0.0118	0	-0.0047	-18.8
43,160	0.363500	0.080	271	-0.0124	0	-0.0049	-18.9
43,500	0.382300	0.085	273	-0.0129	0	-0.0051	-18.9
44,120	0.401100	0.089	276	-0.0136	0	-0.0053	-19.0
44,650	0.419900	0.093	278	-0.0142	0	-0.0056	-19.1
44,570	0.438700	0.094	278	-0.0181	0	-0.0091	-19.3

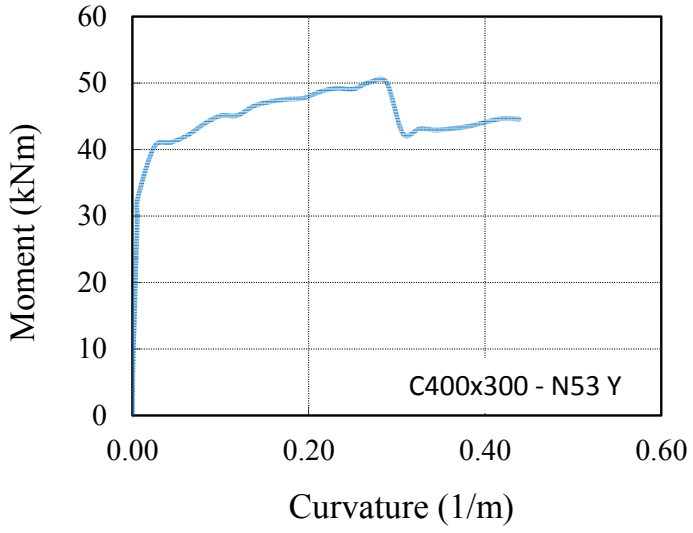

Figure D.31 : Moment – Curvature relationship of retrofitted column 400x300 under 53 kN axial load for Y direction.

Table D.35 : Idealized moment – rotation relationship for non-retrofitted column 300x400 in X direction.

Performance Point	Axial Load 450 kN		Axial Load 263 kN		Axial Load 76 kN	
	M (kNm)	θ	M (kN/m)	θ	M (kNm)	θ
A	0	0	0	0	0	0
B	71	0.00130	64.0	0.00150	40.0	0.00170
C	80	0.00600	69.0	0.00800	45.0	0.01900
D	68	0.00600	61.0	0.00800	39.0	0.01900
E	68	0.02367	61.0	0.03176	39.0	0.04737

Table D.36 : Idealized moment – rotation relationship for retrofitted column 300x400 in X direction.

Performance Point	Axial Load 450 kN		Axial Load 263 kN		Axial Load 76 kN	
	M (kNm)	θ	M (kN/m)	θ	M (kNm)	θ
A	0	0	0	0	0	0
B	95.0	0.00180	75.0	0.00180	42.0	0.00130
C	135.0	0.00840	83.0	0.02828	53.0	0.03757
D	92.0	0.00840	69.0	0.02828	45.0	0.03757
E	92.0	0.02367	69.0	0.03666	45.0	0.06662

Table D.37 : Idealized moment – rotation for non-retrofitted column 300x400 in Y direction.

Performance Point	Axial Load 450 kN		Axial Load 263 kN		Axial Load 76 kN	
	M (kNm)	θ	M (kN/m)	θ	M (kNm)	θ
A	0	0	0	0	0	0
B	98.0	0.00130	88	0.00135	56	0.00180
C	110.0	0.00550	96	0.00800	63	0.01800
D	96.0	0.00550	87	0.00800	56	0.01800
E	96.0	0.02240	87	0.03186	56	0.05172

Table D.38 : Idealized moment – rotation for retrofitted column 300x400 in Y direction.

Performance Point	Axial Load 450 kN		Axial Load 263 kN		Axial Load 76 kN	
	M (kNm)	θ	M (kN/m)	θ	M (kNm)	θ
A	0	0	0	0	0	0
B	125.0	0.00170	102	0.00180	58.0	0.00150
C	185.0	0.00840	113	0.02836	72.0	0.04670
D	126.0	0.00840	99	0.02836	66.0	0.04670
E	126.0	0.02390	99	0.03400	66.0	0.05640

Table D.39 : Idealized moment – rotation relationship for non-retrofitted column 400x300 in X direction.

Performance Point	Axial Load 324 kN		Axial Load 190 kN		Axial Load 53 kN	
	M (kNm)	θ	M (kN/m)	θ	M (kNm)	θ
A	0	0	0	0	0	0
B	92.0	0.00140	83.0	0.00170	52	0.00164
C	102.0	0.00700	87.0	0.01000	60	0.02300
D	90.0	0.00700	82.0	0.01000	54	0.02300
E	90.0	0.02350	82.0	0.03206	54	0.05726

Table D.40 : Idealized moment – rotation relationship for retrofitted column 400x300 in X direction.

Performance Point	Axial Load 324 kN		Axial Load 190 kN		Axial Load 53 kN	
	M (kNm)	θ	M (kN/m)	θ	M (kNm)	θ
A	0	0	0	0	0	0
B	115.0	0.00150	89	0.00170	54	0.00170
C	180.0	0.00830	102	0.03024	66	0.03986
D	115.0	0.00830	91	0.03024	60	0.03986
E	115.0	0.03030	91	0.04254	60	0.06982

Table D.41 : Idealized moment – rotation relationship for non-retrofitted column 400x300 in Y direction.

Performance Point	Axial Load 324 kN		Axial Load 190 kN		Axial Load 53 kN	
	M (kNm)	θ	M (kN/m)	θ	M (kNm)	θ
A	0	0	0	0	0	0
B	66.0	0.00150	59.0	0.00160	39	0.00172
C	75.0	0.00700	64.0	0.00900	43	0.02000
D	65.0	0.00700	58.0	0.00900	38	0.02000
E	65.0	0.02573	58.0	0.03260	38	0.07590

Table D.42 : Idealized moment – rotation relationship for retrofitted column 400x300 in Y direction.

Performance Point	Axial Load 324 kN		Axial Load 190 kN		Axial Load 53 kN	
	M (kNm)	θ	M (kN/m)	θ	M (kNm)	θ
A	0	0	0	0	0	0
B	90.0	0.00180	65	0.00170	39.0	0.00180
C	138.0	0.00800	75	0.02967	50.0	0.04325
D	83.0	0.00800	65	0.02967	43.0	0.04325
E	83.0	0.03236	65	0.04647	43.0	0.06581

Table D.43 : Idealized moment – rotation relationship for non-retrofitted column 400x400 in X and Y directions.

Performance Point	Axial Load 587 kN		Axial Load 351 kN		Axial Load 117 kN	
	M (kNm)	θ	M (kN/m)	θ	M (kNm)	θ
A	0	0	0	0	0	0
B	116.0	0.00120	100.0	0.00130	62	0.00170
C	130.0	0.00650	111.0	0.00855	71	0.02050
D	111.0	0.00650	98.0	0.00855	63	0.02050
E	111.0	0.02450	98.0	0.03672	63	0.07552

Table D.44 : Idealized moment – rotation relationship for retrofitted column 400x400 in X and Y directions.

Performance Point	Axial Load 587 kN		Axial Load 351 kN		Axial Load 117 kN	
	M (kNm)	θ	M (kN/m)	θ	M (kNm)	θ
A	0	0	0	0	0	0
B	150.0	0.00170	115.0	0.00160	65.0	0.00170
C	241.0	0.00820	181.0	0.00742	77.0	0.03252
D	142.0	0.00820	118.0	0.00742	69.0	0.03252
E	142.0	0.02392	118.0	0.03690	69.0	0.07912

CURRICULUM VITAE

Name Surname : Engin Cüneyt Seyhan

Place and Date of Birth : Amasya/Turkey 1979

E-Mail : ecseyhan@yahoo.com

EDUCATION :

- **B.Sc.** : 2003, Istanbul Technical University, Civil Engineering Faculty, Civil Engineering
- **B.Sc.** : 2004, Istanbul Technical University, Faculty of Management, Management Engineering
- **M.Sc.** : 2006, Istanbul Technical University, Institute of Science and Technology, Structural Engineering

PROFESSIONAL EXPERIENCE AND REWARDS:

- 2003 Top graduates, İ.T.Ü. Civil Engineering Faculty, Graduation rank: 3
- 2003 Top graduates, İ.T.Ü. Civil Engineering Department, Graduation rank: 2
- 2004 – 2006 Degussa Construction Chemicals Turkey, Product Specialist, Concrete Repair&Strengthening and Flooring Systems.
- 2006 – 2011 BASF Construction Chemicals Turkey, Product Manager, Concrete Repair&Strengthening.
- 2011 – BASF Construction Chemicals, Europe (Germany), Regional Product Manager, Concrete Repair&Strengthening&Protection and Performance Grouts.

PUBLICATIONS AND PRESENTATIONS ON THE THESIS:

- **Seyhan E.C.**, Goksu C., Uzunhasanoglu A., İlki A., 2015. Seismic Behavior of Substandard RC Columns Retrofitted with Embedded Aramid Fiber Reinforced Polymer (AFRP) Reinforcement, *Polymers*, *7*, 2535–2557. doi:10.3390/polym7121527.

- Goksu C., Uzunhasanoglu A., **Seyhan E.C.**, and Ilki A., 2013. Seismic Retrofit of Sub-Standard RC Columns with Embedded Aramid FRP Reinforcement. *Second Conference on Smart Monitoring, Assessment and Rehabilitation of Civil Structures*, September 9-11, 2013 Istanbul, Turkey.

OTHER PRESENTATIONS:

- Yılmaz A.D., **Seyhan E.C.**, 2005. Case Histories On Repair&Strengthening. *Earthquake Symposium*, March 23-25, 2005 Kocaeli, Turkey.
- **Seyhan E.C.**, 2006. Corrosion Inhibition Technologies. *Structural Repair and Strengthening Symposium*, December 7-8, 2006 Denizli, Turkey.
- İlki A., **Seyhan E.C.**, Kumbasar N. 2007. Pull-Out Behavior Of Chemically Bonded Deformed Bars Typically Used During Structural Retrofitting. *Ninth Canadian Conference on Earthquake Engineering*, June 26-29, 2007 Ottawa, Ontario, Canada.
- **Seyhan E.C.**, 2007. Utilization of Ready-Packed Mortars In Repair Of Historic Buildings. *Symposium On Strengthening And Preserving Historical Buildings And Cultural Heritage*, September 27-29, 2007 Ankara, Turkey.
- Gürbüz T., **Seyhan E.C.**, İlki A., Kumbasar N., 2007. Behavior Of The Chemical Anchors Used In Structural Retrofitting Under Axial Tensile Loads. *6. National Earthquake Engineering Conference*, Volume 1, 649-659, Istanbul, Turkey.
- **Seyhan E.C.**, 2007. Repair&Retrofitting Systems. *International Earthquake Symposium*, October 22-24, 2007 Kocaeli, Turkey.